Curriculum Vitae of Ralf Cuntze

comprising Family, Career, essential Scientific Findings & Personal Pictures

Prof. Dr.-Ing. habil. Ralf Cuntze VDI, Ralf_Cuntze@t-online.de

Retired from industry, MAN-Technologie, and from Composites United

Engineer and hobby scientist: This was my LIFE.

application-oriented with a touch for material modelling and with the hope to be some bridge-builder between mechanical and civil engineering (construction).

Hobbies: exploring the world, nature photography, gardening, mountaineering, cyclamen breeding, etc.

Father of 'Failure-Mode-Concept' + 'Generic' material number

1939 born Sept 8 in Erfurt, Thuringia. Survived bombing at Erfurt and a machine gun fire at the war's end

1964: Dipl.-Ing. Civil Engineering CE (construction, ***TU Hannover***). 1968: Dr.-Ing. in Structural Dynamics (CE) on 'Structural Vibrations of deep beams'. 1978: Dr.-Ing. habil., Venia Legendi in Mechanics of Lightweight Structures (CE, TU-Munich)

1980-1983: Lecturer at *Universität der Bundeswehr München*: on 'Fracture Mechanics' in the construction faculty and 1990-2002 on 'Composite Lightweight Design' in the aerospace faculty

1987: Full professorship 'Lightweight Construction', *not started in favor of industry*

1998: Honorary professorship at Universität der Bundeswehr München

1968-1970: Finite Element Analysis -programming (***DFVLR*** at the airport Essen/Mühlheim)

1970-2004: to ***MAN - Neue Technologie*** (München, Augsburg) instead of being ***DLR***-Postdoc at Stanford University. Headed the Main Department 'Structural and Thermal Analysis'. Thereby facing 50 years of life with Fibers: CarbonF, AramidF, GlassF, BF (bor), Bs(basalt)F.

*Theoretical fields of work: structural dynamics, finite element analysis, rotor dynamics, structural reliability, partial/deterministic safety concepts, material modeling and model validation, fatigue, fracture mechanics, design development 'philosophy' & design verification

*Mechanical Engineering applications at ***MAN****:* ARIANE 1-5 launcher family (design of different parts of the launcher stages, inclusively Booster), propellant motor cases MAGE, IRIS, Cryogenic Tanks, High Pressure Vessels, Heat Exchanger in Solar Towers (GAST Almeria) and Solar Field, Wind Energy Rotors (GROWIAN Ø103 m, WKA 60, AEROMAN. MAN bus, SR 240, Wendelstein VII. Probably the first world-wide wind energy conferences organized in 1979, 1980 with Dr. Windheim), Space Antennas, IRAM antenna, SOFIA telescope (2003), Automated Transfer Vehicle (Jules Verne, supplying the space station ISS), Crew Rescue Vehicle (CMC application) for ISS, Carbon and Steel Gas-Ultra-Centrifuges for Uranium enrichment. Filament winding theory, Material Databank etc.

*Civil Engineering applications: Supermarket statics, armoring plans, pile foundation, 5th German climbing garden (1980 designed, concreted and natural stone-bricked)

1971-2010*:* Co-author in ASMIEG-WG of ***ESA/ESTEC***-Structural Materials Handbook, Co-author and first convener of the ESA-Buckling Handbook and co-author in Working Groups WGs for ESA-Standards 'Structural Analysis', 'High Pressure Vessels' (metals and composites) and 'Safety Factors'

1972–2015, ***IASB***: Luftfahrt-Technisches Handbuch HSB 'Fundamentals and Methods for Aeronautical Design and Analyses'. Author and Co-author of numerous HSB sheets and about 2006-2008 co-

transfer with co-translation of the HSB aerospace structural handbook into its present English version.

1980-2011: **Surveyor/Advisor** for German BMFT (MATFO, MATEC), BMBF (LuFo) and DFG

1980-2006: **VDI Guideline 2014**, co-author of Parts 1 and 2, Beuth Verlag '*Development of Fiber-reinforced Plastic Components';* Part 3 *'Analysis*', editor/convener/co-author

1986 and 1889: One week **FRP-lecture** on composite design in Pretoria, SA

2000-2013: World-Wide-Failure-Exercises **WWFE** on Uni-directional fiber-reinforced materials (UD) strength: WWFE-I (*2D stress states)* non-funded winner against institutes of the world, WWFE-II (*3D states*) top-ranked

2009-2021 linked to ***Carbon Composites e.V***. at Augsburg, later ***Composites United CU e.V.*** and to TUDALIT Dresden. Since 2011 working on the light weight material Fiber-reinforced (polymer) Carbon Concrete. **Founded and headed the working groups**: (1) 2009: 'Engineering' linked to the WG Non-Destructive Testing and the WG Connection Technologies, mechanical engineering. (2) 2010: 'Composite Fatigue'. In 2010 the author held an event that was excellently attended by international speakers. (3) 2011: 'Design Dimensioning (*Auslegung, Bemessung*) and Design Verification (*Nachweis*)' mainly for carbon concrete. This working group was the foundation stone for the later specialist network ***CU Construction***, aiming at *"Fiber-based lightweight construction*". (4) 2017: 'Automated fabrication in construction including serial production' *("3D-Print")*. (5) 2020, 2021: Forum 'Carbon concrete for practice' at the well-known 'Ulm Concrete Days'

2010: Founder of the Germany-wide Working Group BeNa to base fatigue life prediction 'embedded lamina-wise' in order to become more general in future fatigue life design

2019: *__GLOSSAR__ "Fachbegriffe für Kompositbauteile - *technical terms for composite parts*". Springer 2019. Edited at suggestion of carbon concrete colleagues to improve mutual understanding

2022: **Life-Work Cuntze - a compilation from the author's papers, presentations, published and non-published design sheets and project works in industry* (850 Pages, more design work-related)

2023: **Design of Composites using Failure-Mode-Concept-based tools - from Failure Model Validation to Design Verification*. Mechanics of Composite Materials, Vol. 59, No. 2, May, 2023, pp. 263-282. **Minimum Test Effort-based Derivation of Constant-Fatigue-Life curves, displayed for the brittle UD composite materials*. Mechanics of Composite Materials, Springer, Advanced Structured Materials, Vol.199, 107–146, draft. *Cuntze R and Kappel E: *Benefits, applying Tsai's Ideas 'Trace', 'Double-Double' and 'Omni Failure Envelope' to Multiply UD-ply composed Laminates? * UD-Strength Failure criteria: Which one should I take*? * Elaboration on Finite Fracture Mechanics.

* such marked p*reprints, drafts are fully open for the public and are downloadable from*
https://www.carbon-connected.de/Group/Prof.Ralf.Cuntze or from Research Gate

1) *The presented novel scientific ideas invite for discussion.*
2) *The author's research works were never funded, seldom supported.*
3) *The author asks for forgiveness in advance for inaccuracies, due to missing proofreaders. Of course, the text content in the scientific chapters would have deserved a revision and harmonization, but the author hopes to become 86 this year.*

For me, this document collects all available memories, which were relevant for me during life and which may be of interest for family, friends and scientific partners. The document comprises results of the author's never funded, non-supported research work performed in his vacant time at industry and as retired person.

He assumes no liability for damages resulting from application.

Me, Home, School and University - *Time before contracted Working at University, MAN-Technologie and Composites United, Contracts ESA/ESTEC and Airbus*

Guess 1939: " ***Birth of son Ralf*** in the first week of World War-II was one of the few rays of hope".

2024: The author after the yearly 'pilgrimage', 27 miles. To and from the monasteries Kloster Indersdorf (home) ↔ Kloster Scheyern.

STRENGTH is still his Life !

"Anyone who stops learning is old, whether at twenty or beyond eighty.
Anyone who keeps learning stays young.
The greatest thing in life is to keep your mind young". *Henry Ford*

Movings

Erfurt → 1945 Heimboldshausen (house of the Grandparents, below right 1947; left 1939, with my parents) → 1953 Harnrode → 1959 Hannover → 1968 Mühlheim-Ruhr → 1970 Dachau → 1976 Markt Indersdorf.

1966, married Jutta Leonhardt (*no children*); in 2012 wife Jutta moved to another place; 2013, meeting Maria Hasler; 2015, divorced from first wife and marriage of Maria.

Me: Becoming older and older and a little more wise

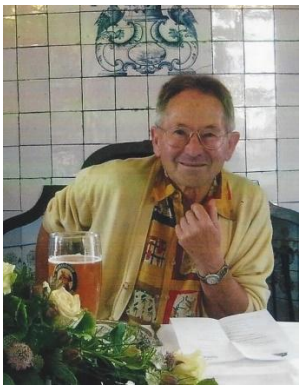

2024

Family, at Home, School

The Ancestors:

A very old family.
A Cuntze was privy councilor to the Roman-German King Wenzel.
A captain Friedrich Cuntze took part in a crusade with Emperor Friedrich III (crowned in 1452). For this he received a coat of arms and the so-called letter nobility 'von'. (Wiener Wappensammlung, Folio 247, 37. Teil).
The two branches of the family have less than 100 members worldwide.

Mother of father.
GrandDad passed away before my birth (Hofgeismar)

Father

Mother , 1936

Parents of mother
(Heimboldshausen)

After the war
Happy with her two sons
(3 girls and 2 sons).
See pictures later

Mother parents:

During the war
happy with the second daughter.

The first daughter terribly died from pulmonary tuberculosis (at that time a person got nothing to drink !)

Impressed statement of

Terrible World War I

Mother's father was saved from freezing to death in the Carpathians.
He said to me
"*My feeling was inner peace and warmth*".

After 25 years the same happened again.

Penny farthing1929

On a motor bike with his brother 1930

The father, celebrating a festivity in his small town of Hofgeismar

Father
Semester trip 1932 of
civil engineer students

No engineering work after studies,
1931 → 1935 !

During this time, he worked again as a bricklayer for a relative and for other small companies, at maximum at the technician and not the engineering level

1935-1945, now continually working as a Civil Engineer at "Eisenbetonbau Erfurt".
Before 1939 it became 'normal' for getting jobs in construction industry.

Living at Erfurt during World War II.
When the bombers had planted their 'Christmas trees' in the sky, it was time to run to the bunker as quickly as possible, if there was a bunker at all ('father's' one).

Because of his eyes, Papa was not fit for war, he built industrial plants and bunkers

The first independent steps:

Comment of the relatives:
"He's going to be a professor one day." This requires Strength *R* + Effort *Eff* ! **see later**

Potatoe collecting at Cuntze's acre , 1941

On dad's motor bike

Traveling in Dad's company car, 1942

And the traditional yearly Cuntze-Family Festivities

Family festivity in the fifties

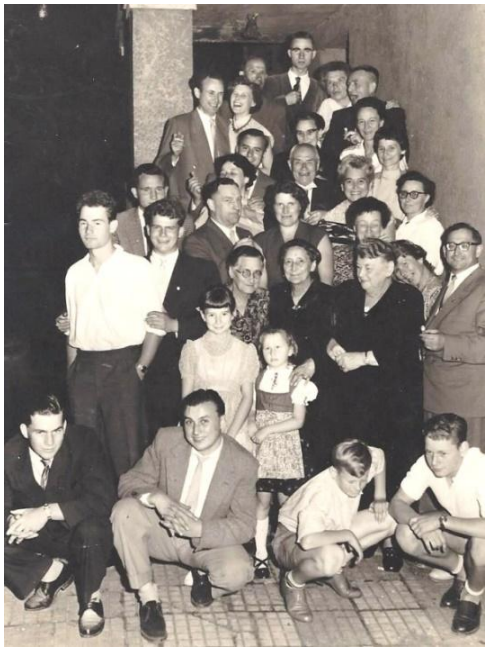

in front: my generation

Grandma's 90 years birthday

Dad and son

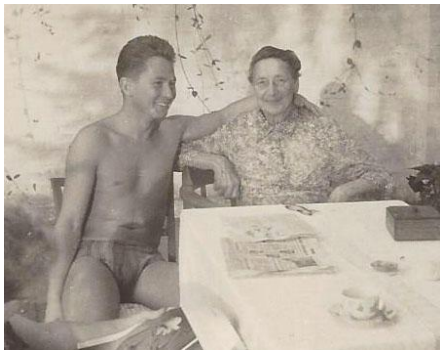

Grandma and grandson

Son and mum

and later

1960 Visit of my Grandma and of my North-Tyrol friend Alois, who looked for a job

* During war II urban bomb victims had been quartered in the countryside, which means into grandpa's house.
March 30: The mother was shot dead like my grandma (right), the daughter survived and went directly back to her home city.

March 30, 1945
Most impressive life experience

Katharina Koch
Memorial plaque
(see Burnt memories)

Burnt Memories:

1944: Dreams

*Finally getting a ball as a gift. Realized 3 years later at Christmas

* A dream with a net descending over me. (symbolically became true):Descending plane over the house crashing behind the house in Erfurt on a free field in front of a hospital.

* Running to the nearest bunker when the so-called 'Christmas trees' enlightened the sky over Erfurt. We were allowed to take this bunker, which had not yet been released, because dad happened to be the construction responsible here

* Relocation of the prisoners of war towards the Americans. March of these unfortunates over the Werra bridge and then through Heimboldshausen further west.

1945:

US Army advances over the Werra border into Thuringia: Target shooting at individual buildings from a mountain. This causes us to flee to the opposite and supposed safe side.

After the German Werwolf blowed up the Werra bridge directly before the arrival of a US reconnaissance tank, the civilians lined up on the hemp were covered with a machine gun fire. Aunt shot in the head, grandmother shot in the stomach, *see memorial plaque on the right*.

Concerning me: I ran 200 m further to my parents into the forest and we were not shot dead on March 30, 1945, because 'our' machine gun salvo was 20 cm too high. There was one elder man with us, who wanted to get up to pee. I can still hear my dad yelling "*Ship in your pants*!"

We then surrendered to a US officer with a white flag. The fact that there were still 4 people in the forest was probably reported by the same tank gunner who had previously shot other civilians dead.

Despite all the bitterness: *We were all happy to leave that time behind us.*

* Refugees from Sudetenland: In 1945 and 1946 two families = 8 persons had to be quartered. After repairing the damage caused by shelling and a huge explosion of a train.

* The smell of an extinguished candle still immediately creates this memory: In the basement, candles are burning, I'm lying on a potato sack, at a distance of 5 m from the air one US tank after the other rattles by, upstairs the grandma lies bleeding to death after her shot in the stomach

* On April 3, 1945, a German Me Bf109 G-8 fighter attacked a German train with tankers. This was in Heimboldshausen, now behind the US border line, and was to be destroyed according to the German command. However, the American forces that had occupied Heimboldshausen on March 31 had already set up shop near Heimboldshausen station. The German fighter plane had no bombs on board and attacked the train only with on-board weapons. Parts of the exploding tanks or hit by US anti-aircraft machine guns then crashed the plane with the pilot at the first houses of Röhrigshof, the engine landed in the entrance of a classmate. At that time, my father was sitting on top of the roof repairing the grenade impact of March 31st. He was lucky, he didn't fly off the roof.

* Each pupil had to take a piece of wood with him on his footpath to school so that the elementary school in the neighboring village, which had not been destroyed, could be heated.

1946:

* The desire to finally get a pair of long pants. This was done years later with trousers made of the fabric of a military coat. This in order to finally no longer have to wear the girly long stockings, which were held with elastic bands.

After the WW-II:

I remember: War and war-captivity were spoken about, but the Hitler era was not discussed. Every homecoming of a prisoner of war was a great village event.

After the war, Heimboldshausen was still the crossing point of a line from Russian-occupied Thuringia to Hesse and then back to Thuringia and further from the route of the inner-Hessian district railway to the district town of Bad Hersfeld. In my grandfather's general store, the train drivers from Thuringia shopped. This offered the opportunity to have the machines of my uncle's paint factory in Erfurt transported to his new workplace, namely the town Hanau, which had been completely bombed. You 'only' had to load a wagon in Erfurt, attach it and decouple it in Heimboldshausen. The new beginning in the West was secured and successful.

Despite of being just a child: With the end of the WWII troubles I felt peace.
And despite everything: I had a very nice childhood.

Supply of Clothing & Food: Situation during war and after

Ausstellende Behörde: Gemeinde Heimboldshausen

Bezugschein I № 7507

für ein Paar Straßenschuhe für Frauen

An den — die Helene Bünger
(Vor- und Zuname)

wohnhaft in Heimboldshausen, (Ort) Nr. 95 (Straße)

von Beruf ....., geboren am 14.3.12 in Heimboldshausen (Geburtsort)

darf innerhalb von drei Monaten vom Tage der Ausfertigung dieses Bezugscheins an ein Paar Straßenschuhe abgegeben werden.

Die Ware darf nur unter gleichzeitiger Aushändigung dieses auf der Rückseite mit einer Empfangsbescheinigung des Bezugsberechtigten versehenen Scheins ausgegeben werden. Wird die Ware durch einen Vertreter oder einen Beauftragten bezogen, so hat dieser die Empfangsbescheinigung zu vollziehen. Andere als die obenbezeichnete Ware darf nicht abgegeben werden. Der Bezugschein ist nicht übertragbar. Jeder Mißbrauch ist strafbar.

Für die Entwertung und Registrierung des Bezugscheins nach der Warenausgabe gelten besondere Vorschriften.

(Dienstsiegel) Gemeinde Heimboldshausen

Heimboldshausen den 24. 11. 1944

Im Auftrage: Adolf

Ausgabe März 1944

Druck: A. Bernecker, Melsungen

Cloth Card 1944
(within 3 months of the issuance of this voucher, a pair of street shoes is available

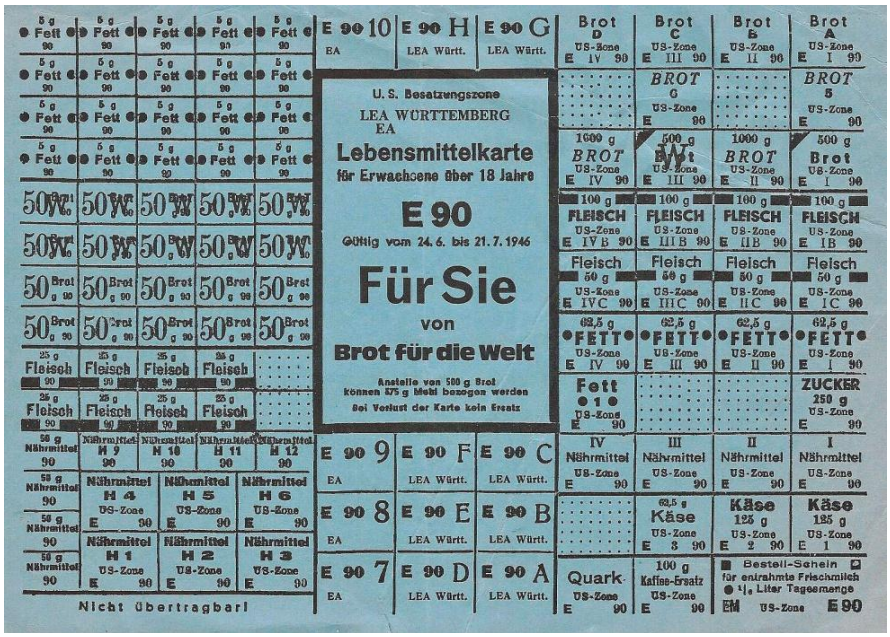

U. S. Besatzungszone
LEA WÜRTTEMBERG
EA

Lebensmittelkarte
für Erwachsene über 18 Jahre

E 90
Gültig vom 24. 6. bis 21. 7. 1946

Für Sie
von
Brot für die Welt

Anstelle von 500 g Brot können 375 g Mehl bezogen werden
Bei Verlust der Karte kein Ersatz

Nicht übertragbar!

Food Ration Card

after the 2nd World War
1946 (as in the 2nd war)

Dad's second run for a job

In 1944 after finalizing a construction, built by the company 'Eisenbetonbau Erfurt' he was working for

The march of those involved in the construction following the Nazi leaders

Großhessisches Staatsministerium
Der Minister für Wiederaufbau
und politische Befreiung.
Der öffentliche Kläger bei der Spruchkammer
Hersfeld

Hersfeld, d. 11.3.47
(Datum)

Aktenzeichen: He/21738

Auf Grund der Angaben in Ihrem Meldebogen sind Sie von dem Gesetz zur Befreiung von Nationalsozialismus und Militarismus vom 5. 3. 1946 nicht betroffen.

Der öffentliche Kläger:

An Herrn ~~/Frau/Frl.~~
Werner Cuntze
in Heinboldshausen
Dorfstrasse 95

Formblatt 11 — Mitteilung an Nichtbetroffene —

De-Nazification receipt, 1947

With the receipt of above certificate, one became again a recognized citizen with all rights and obligations.

Very decisive for a new job!

Dad was now able to find work as a civil engineer in the potash mine, 1949

In the nearby salt mine, he was now able to supervise large construction sites again. This was his life.

My uncle Rudi was a 'Soft Nazi'. In the Russian-occupied zone, it was therefore possible for him to work!! Of course, he also needed things from home. We brought these things (me too, because at childs it was not so 'easy to shoot') with the handcart to the border 4 km away. (How could one manage this without a smartphone?). When my uncle later wanted to go home, he was sentenced and then sat in the prison of Hofgeismar. There, we children (when I visited grandma) brought food to the prison with the usual cooking utensils of the soldiers at that time, a so-called approximately 'bretzel-shaped Henkelmann', which I always had with me for receiving the school meal). I experienced something like this again in Ladakh in 1981, however there the relatives lived 10 km away from the prison and not just a few hundred meters. My uncle was guarded by a warden with a rifle, but this was no problem for the warden to go with the prisoner at his exit time to a newly opened pub.

I remember that in 1946 there was excitement again: Suddenly soldiers of the Red Army appeared again with, among other things, Panje horses, they had probably mistakenly oriented themselves on old maps. This would have meant that the place where we wanted to build our new house would not have become western territory. The US Army tanks, however, quickly put an end to this exciting situation.

Dad the biker: The 'new' life approaches the former life

1938

1950

Me:

1956
This was the
great time
to learn shorthand

School at Heringen-Werra

(left**) Class 1957.** Entrance examination 1950 (*64 pupils*), Abitur 1959 *(just 9 pupils left at exams)* (right) **about 2012.** Our strict, fantastic class teacher Hans-Heinrich Bähr; Ralf , Kurt

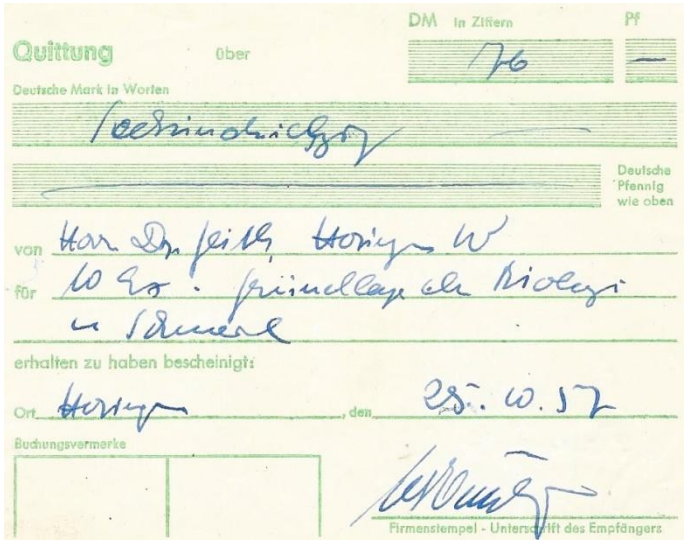

Books had to be privately paid

Class trip

art teacher Gulitz

Class , trip to the island of Sylt.
1958

Our strong, however beloved teacher H.H. Bähr, who finally married a class mate (left)

.. and later class meetings

Building a new home, 1952/1953

My dad's drawing

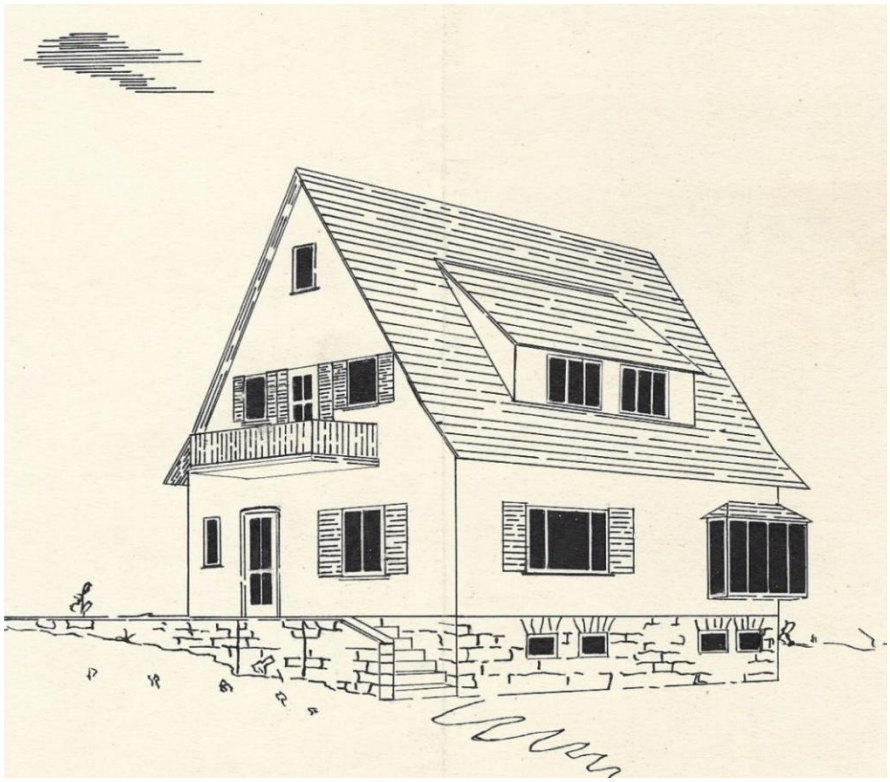

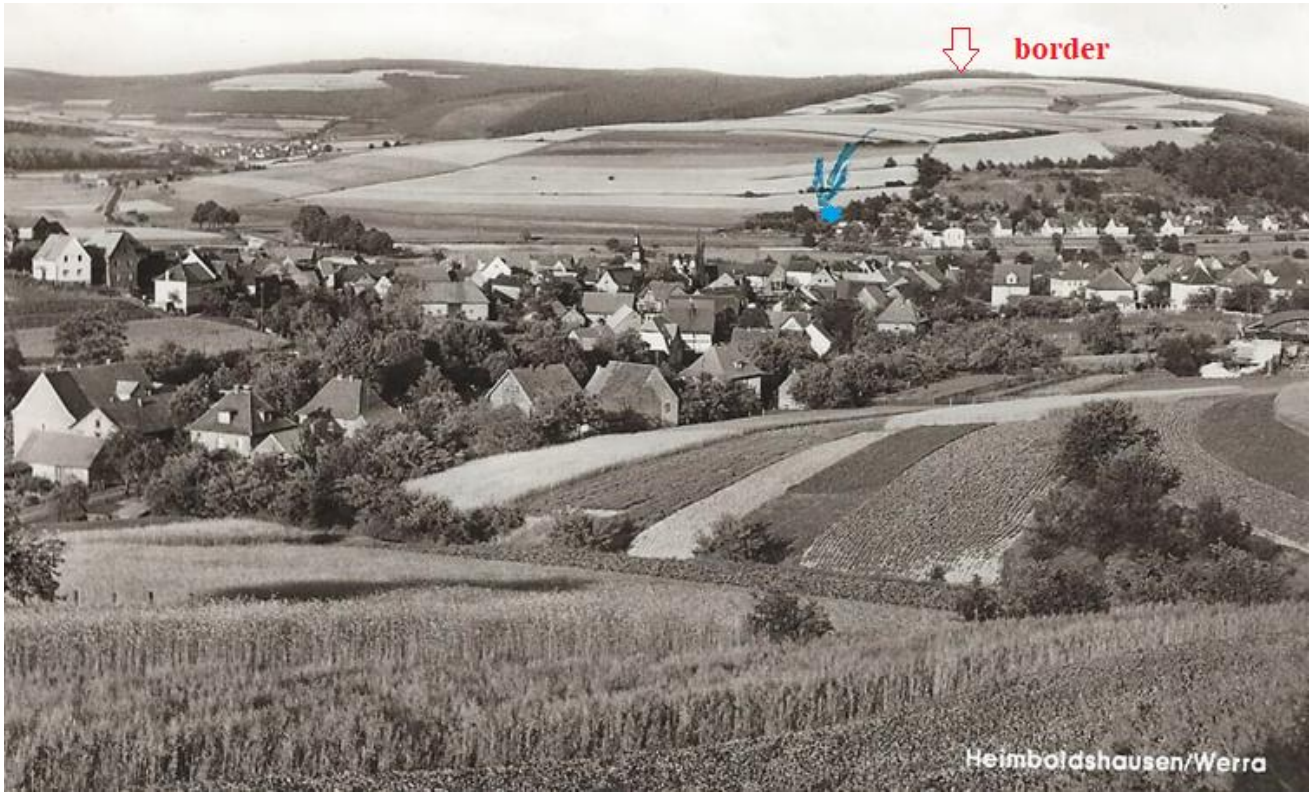

All buildings 'hand self-made' by the father with family support. A good mile from the border.

First: a wooden log cabin was built, in 1946

Living at home.

A source for own use

The 100 m long wooden fence asked for Ralf's care

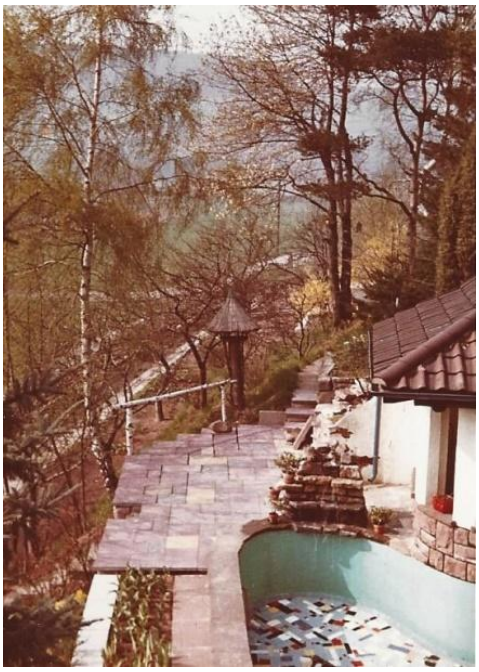

Family Life

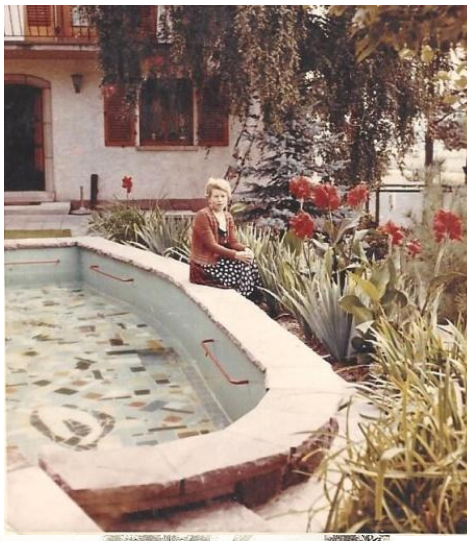

Working & Relaxing on the building site

With such good care, one had a good laugh

(left) Our master carpenter was the best butcher. His sausages were highly valued. Every year, the slaughter of a pig served to obtain an excellent food supply over the year.

chat with pastor

friends

Son & dad

Uncle and aunts

In the Grandparents general store at Heimboldshausen, where the author lived and collected experience as a young merchant until 1953.

From 1954 on:
The figure shows the later owner, my relatives Heinrich Koch and his wife Friedel, my 'second' mother.
About 1960.

With my Mother at her new home at Kassel

Visit of Sujeeth from Madras
at my mother's
new home at Kassel.

He learned German from cassettes!

My mother moved to Kassel
after my father had a fatal accident in the
garden in 1974

From time to time one guest in mother's home at Kassel was my friend Rolands Rikards, leader of the big Composites Institute at Riga and co-father of the Latvian constitution after the Soviets left Latvia.

Story, Rolands *told me:*

A special unit of the Soviet Interior Ministry (identified by their black caps, "Black Berets") stormed the Latvian Interior Ministry on Sunday evening, January 22, 1991, killing five people. After the ministry was evacuated, newly armed Latvians moved in as defenders. When the Black Berets ordered the Latvians to evacuate, they did not respond and did not fire a shot, so as not to give the Russians a pretext for storming the building. The changing tone of the voice from the Beret commander's megaphone indicated that the threat was slowly fading. If Rolands had been captured, he would certainly have been shot because he had intimate knowledge of the design of nuclear submarines.

Later, in 2004,
I experienced the grace of being present at my mother's passing away
and to be able to close her eyes.

My Living at the Inner-German Border

Grown up directly at the Hessian border to, where the spoil heaps (*200m above ground*) from potash extraction are no longer allowed to get higher than the surrounding mountains, 2024.

In this potash (salt) mine my father could finally again find work.
This 4 years after the WW-II end!

By cutting down and clearing strips of land up to 200 m wide, further measures were taken to build deeply staggered barrier systems, which made it impossible to overcome them and thus escape to the

west. Until the 1950s, a ‘small border traffic’, the occasional meeting through loopholes in the barbed wire entanglements, was still possible, but now the escape attempt could end fatally. The separation of people of the same history, language and thought was sealed.

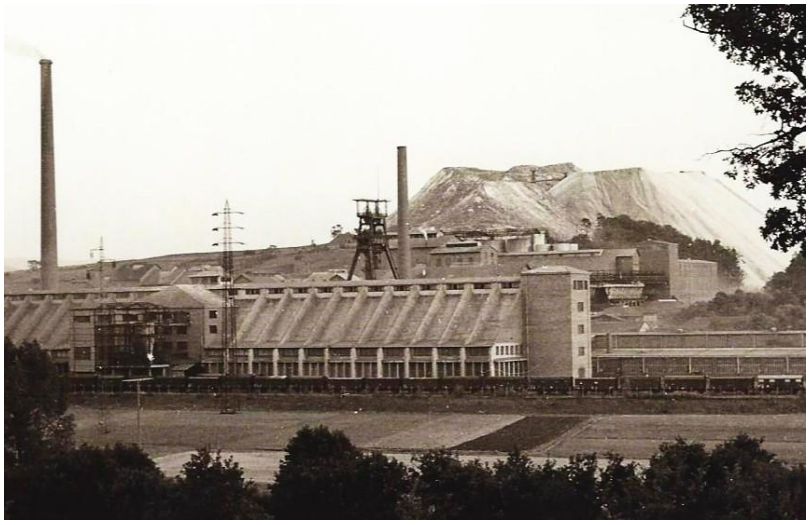

Salt Mine, 1967

Exclusion zone at the Philippsthal-Vacha zone border: The famous bridge

An exclusion zone was established on 26 and 27 May 1952. Its width was 5 km. This was the first tighter lockdown. You were no longer allowed to enter this restricted area of the GDR (DDR) unless you had a pass. The exclusion zone included a protective strip (500 m wide) and a control strip (10 m wide) directly at the border. On 4 June 1962, GDR work detachments began to build a three-metre-high wall from prefabricated elements on the banks of the Werra in Vacha, opposite of Philippsthal, where contact between acquaintances and relatives from Philippsthal and Vacha had previously been possible. (*I still used this to visit relatives. In 1950 I was also able to have an operation on my appendix in a clinic in Vacha*). This meant that the former Hoßfeld printing plant was divided into the FRG BDR) and the GDR. With effect from 1 January 1976, however, this well-known "house on the border" is no longer divided. The Hoßfeld family regains the right to unrestricted use of the walled-off eastern part of the printing house, which had previously been on the territory of the GDR, and the inner-German border is laid around the outside of the house in an imaginary line.
This meant further, that Philippsthal was deprived of an attraction popular with border visitors, all acquaintances living further away were brought there.

This was the point where I crossed the border last time from DDR to BRD , 1951,
at the printing office Hoßfeld

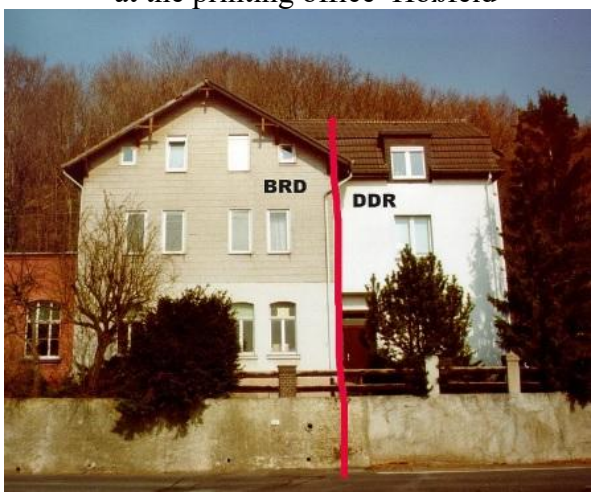

The famous old bridge
with DDR watchtower

In order to be allowed to print the Vachaer Zeitung, i.e. a Thuringian newspaper, this Hessian printing company had to have a wall on the Thuringian side when it was built. On New Year's Eve 1952, the eastern annex was walled up as a precaution

Thanks to the eightieth anniversary celebration of our common uncle, we two cousins were able to see each other again in 1988 after 1957.

The question of us eastern cousins, meeting after 30 years again, was not

How long the separation will last ?

We were only very thankful!
We could not imagine at that time that reunification would come a year later.

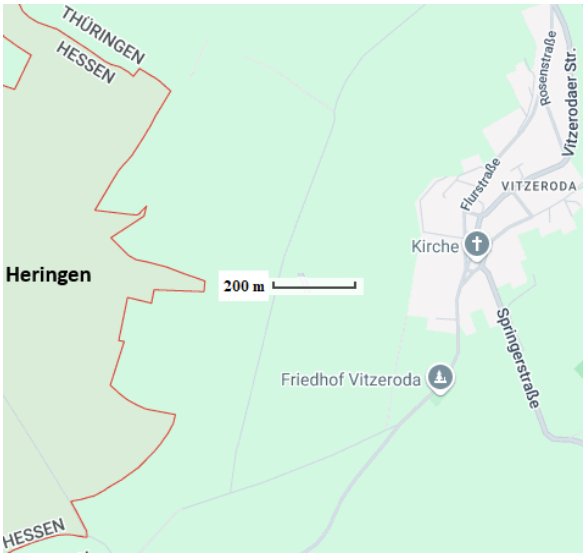

The ‘Sperrgebiet’, an area that is not accessible to the civilian population at all or temporarily!!!

As a result of the division of Germany, Vitzeroda was located in the border area and was declared a restricted area. A barracks of the border troops were built on the outskirts of the village, and access to the village was monitored. The small settlement of Gasteroda, located in the immediate vicinity of the border, was gradually abandoned, and in the autumn of 1989 only one farmstead was still inhabited.

View from the western side Philippsthal to the eastern side , the city Vacha at the beginning of the Rhön mountains. In the back there you can see the scarce basalt mountain Oechsen.

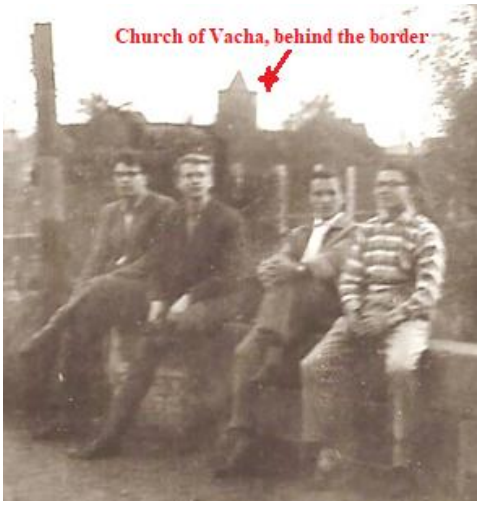

my western cousins at the border at the western side

and
vice versa
a recent view
from the eastern side ,
Vacha

Anyone who grew up directly on a border and had to suffer the increasing isolation between relatives and friends can certainly understand that I was very interested in the Korean border which might show differences (similar unfortunately in 2008) regarding this also a nation-separating border alike Corea.

North Corea

Similar exclusion zone (2006)
like with us at home

Looking at the
South-Corean Building
and
neutral demarcation place
from the north

Amber Room (Bernsteinzimmer): ‘Story’??

Transport of the real Amber Room from the Merkers Salt Mine by the US Armed Forces!?

In 1716, King Frederick William I, who was not very interested in art, exchanged the Amber Room with Russian Tsar Peter I for tall soldiers. During World War II, the Amber Room was captured by the Wehrmacht in Saint Petersburg in 1941 and subsequently installed in the Königsberg Castle Amber Room. During the advance of the Red Army, it was removed in 1944 and has been lost ever since. However, I found a handwritten message about the transport from the hidden safe place in the potash mine Merkers, Thuringia, per train etc in direction USA

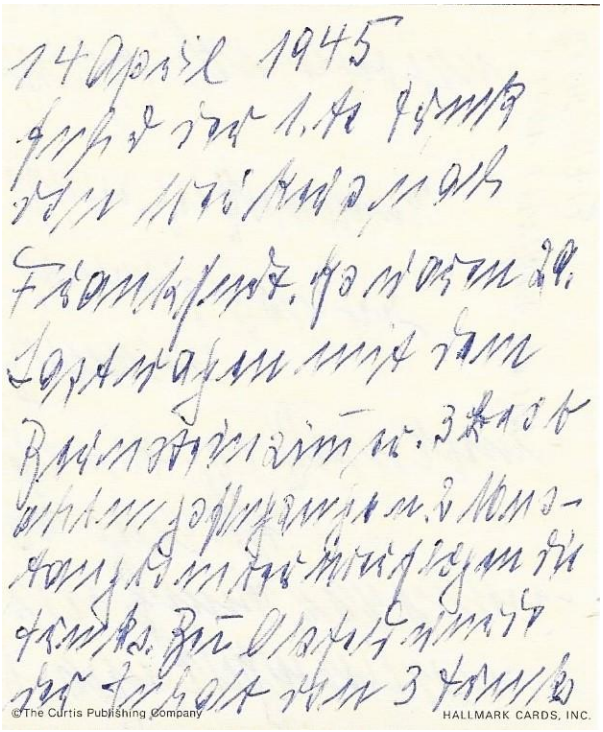

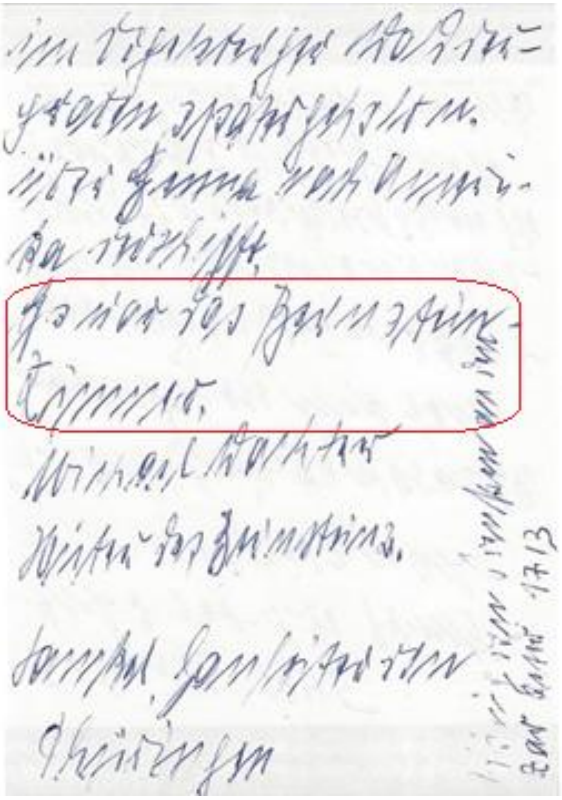

Photos of the confirmands 1954, 2004, 2024

Walter, Ralf, Kurt

Currency Reforms and “Berlin oblation" stamps

Währungsreformen

1923/ 1924

1948

1990

1923 / 1924

The changeover from the "Mark" (M) to the "Rentenmark" (RM) in November 1923 with a rate of 1,000,000,000,000 M : 1 RM ended the German inflation from 1914 to 1923, which was caused by the financing of the First World War by selling war bonds to the state's own population, the reparation payments after the First World War and the extremely high state expenditure caused by the occupation of the Ruhr.

1948

The RM largely lost its functions as a means of payment and store of value in favor of food stamps, barter, and substitute currencies. The currency reform of 1948 came into force on 20 June 1948 in the Trizone, Germany's three western occupation zones. From 21 June 1948, the Deutsche Mark was the sole legal tender there. Savings become almost worthless, but the shelves fill up with goods overnight. Americans are pushing ahead with currency reform against the will of the Russians.

My personal memory:

Changing RM into Deutschmark (DM): *I received 3000 RM from my Grandpa and proudly brought him back 30 DM with which one could buy something for.*

1990

Children under the age of 14 can exchange up to 2,000 GDR marks at a ratio of 1:1, 15 to 59-year-olds up to 4,000 GDR marks, and those older can exchange 6,000 GDR marks. Amounts above this will be converted at a ratio of 2:1.

‘Notopfer Berlin’ as solidarity surcharge.

People in Western Germany were naturally not pleased with the "Berlin oblation" stamps of 2 Pfennig for western Berlin.

Private donations from the U.S. people financed packages labeled "CARE" to alleviate suffering and hunger in the years after World War II. The abbreviation CARE stands for the aid organization "Cooperative of American Remittances to Europe", founded in 1945

Technical University of Hannover and Institute of Civil Mechanics

Costs of study, 5 years: 10000 DM, half of which was earned by myself.

Student flat: Unheated, water froze in washing bowl (c*entral heating I already enjoyed at home*).

Technische Hochschule Hannover

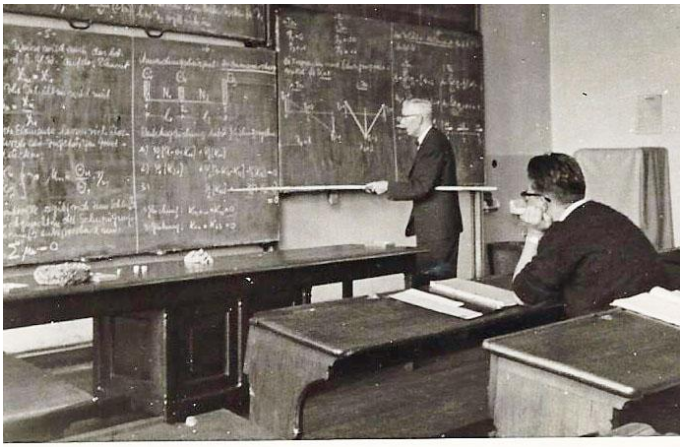

Supporting Prof. Eugen Doeinck by preparing his lecture tables. He had to stand in for his successor Hans Kauderer, *who died suddenly*, for a while.

Traditional get-together with the new 'boss' at the civil mechanics chair, Theodor Lehmann

The traditional summer trip of the chair members: Schäfer, Hartung, Lohmann, de Boer, Schroeder

(1962) Christmas table round with emeritus Doeinck

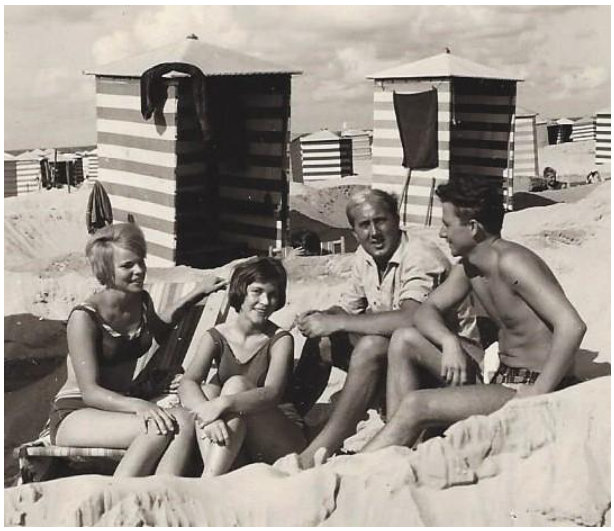

Final measurement exercise: Not without danger, because a young bull was 'guarding' a survey point in one area

The ‘inner circle’ of the 120 students (1 girl only!) of civil engineering at TU Hannover

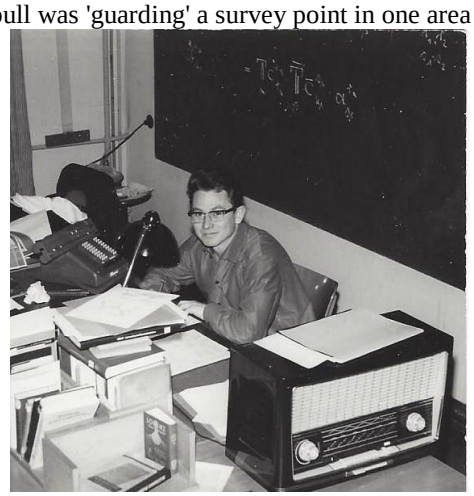

Tensor analysis. On the way to becoming an engineer. This is how we worked at the mechanics chair (1962), and this was also the case on Sundays: In the unheated cold student apartment the water in the washbowl froze.

Frederick-Heinz Schroeder:
February 11, 1968
“*What is this on your head* ??”

The job title ‘engineer’ supposedly appears for the first time in 'Le Roman de Rou' by Robert Wace (*about 1150, citing H. Lange, Technik in Bayern 5/2004).*

Following Google the term engineering is derived from the Latin ingenium, meaning “cleverness” and ingeniare, meaning “to devise”. Engineering has existed since ancient times, when humans devised inventions such as the wedge, lever, wheel and pulley. The term engineering is derived from the word engineer, which itself dates back to 1390 when an engine’er (one who operates an engine) referred to “a constructor of military engines.”

Later, as the design of civilian structures, such as bridges and buildings, the term ***civil engineering*** emerged to distinguish between military engineers and those specialized in the construction of civil projects

Meeting of former colleagues

Hartung, de Boer, Bothe, Seitz,Schäfer, Wetzell, Spierig, Köper

‘Radiant strength’ of all employees of the Chair of Construction Mechanics in Hannover (*interims time: Kauderer-Lehmann*) on the island of Juist.. Interimsboss: F.H. Schoeder (left), Assistants: de Boer, Lohmann, Seitz, Schäfer, supported by the 3 youngsters Hartung, Cuntze, Köper in the foreground.
This obvious excellent teamwork has made it possible to fill the interregnum until the new chairholder Th. Lehmann took over and thereby to maintain the mechanics standard for the students

Numerical Analysis and Finite Element Analysis

Tools for practicing engineering in 1960-1968

- ✓ Diploma work:
  Application of an Arithmetic Stick (slide rule: for multiplication, division), the short one and for more precise calculations the 25 cm long one (about 1% error). The slide stick allows you to extract square and cube roots, exponentiation and operations with trigonometric functions of given angles
- ✓ Dissertation:
  I could not finish my dissertation in 1967 because o and 0 where not clearly marked in the coding which cost two months filled with despair.
- ✓ FEA-Practice:
  Later in the sixties, Finite Element Analysis came up, however, there was no commercial tool available. The author had to beg for the building blocks of his intended program (in experience for the program below at the DLR) at his old university in Hannover. To punch cards was a must.
  Waiting for the result: One week !! Now on my PC about one second CPU.

(from WIKIPEDIA, I’m a member) Konrad Ernst Otto Zuse (born 1910 in Berlin, † 1995 in Hünfeld) was a German civil engineer, inventor and entrepreneur (Zuse KG, in my hometown Bad Hersfeld. My girlfriend at that time worked there around 1960). With his development of the Z3 in 1941 Zuse built the first functional, fully automatic, program-controlled and freely programmable computer working in binary floating-point calculation and thus the first functional computer in the world.

A lifelong close friend of Konrad Zuse and my father-friend once told me Zuse's retrospective:

"Looking back on my career, I can only hope that in the future there will be room not only for the specialist in his field, but also for the universally gifted. I believe that versatility in particular is the prescriptive for ideas that are out of the ordinary. Such an idea, an 'infidelity' of technology, if you will, was ultimately the computer”.

Progress being in my hand

in the Mechanics-institute at Uni Hannover:

The Friden Wurzelautomat model SRW was the only mechanical calculating machine that was able to pull square roots completely automatically. In addition to the four basic arithmetic operations, the SRW root machine is also capable of drawing precise square roots from up to ten-digit numbers.

The square root is pulled on this machine after the radicande has been adjusted by pressing one of the small key buttons in front of the full keyboard.

Vierspezies-Staffelwalzenmaschine mit Wurzelautomatik, © Arithmeum

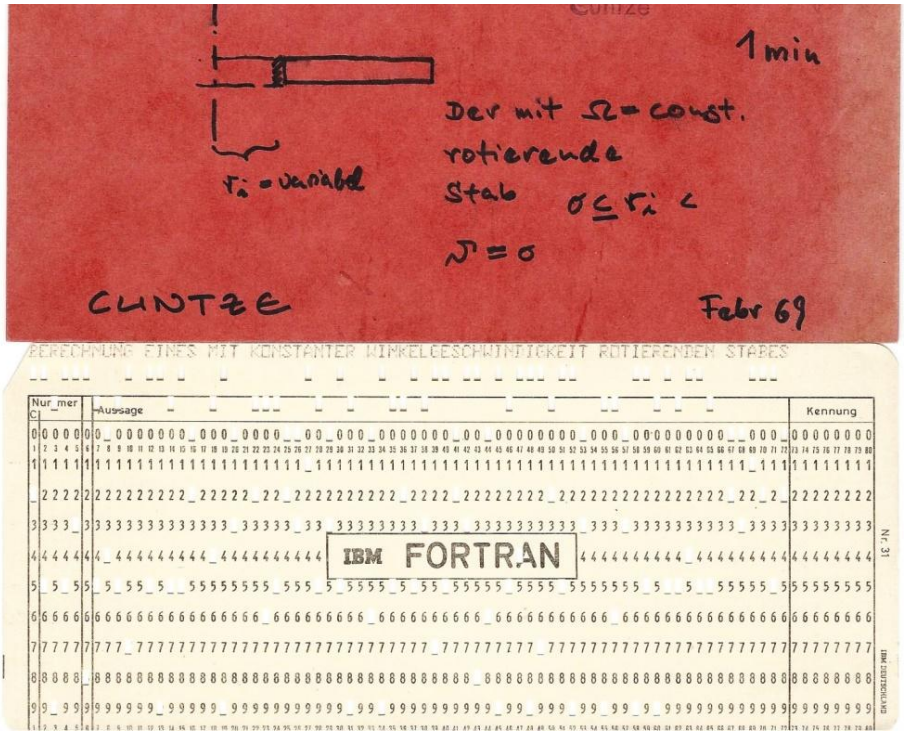

Bronstein-Semendjajev about
"**Calculation accuracy and presentation"**:

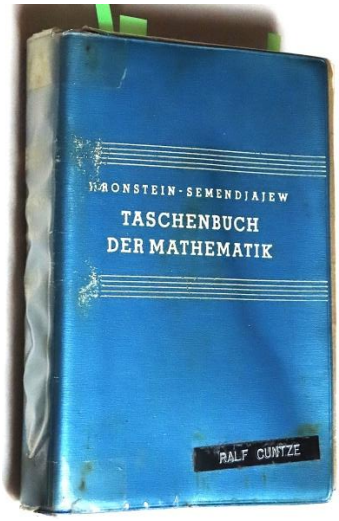

„*When calculating, it is always important to consider the accuracy that you either have to achieve or can achieve. It is quite inadmissible to calculate with great accuracy if the nature of the task either does not allow it or does not require it. If an approximate value contains superfluous decimal numbers, it must be rounded. In some cases, more realistic but more complicated models can be replaced by simpler ones that give a result with an acceptable error*."

(Written by about 1960 in their famous booklet)

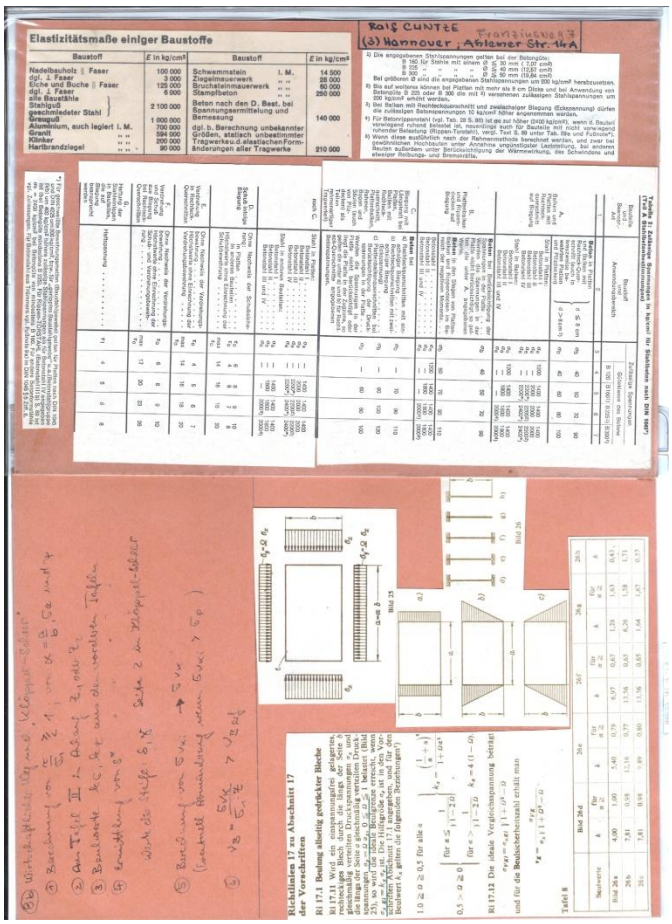

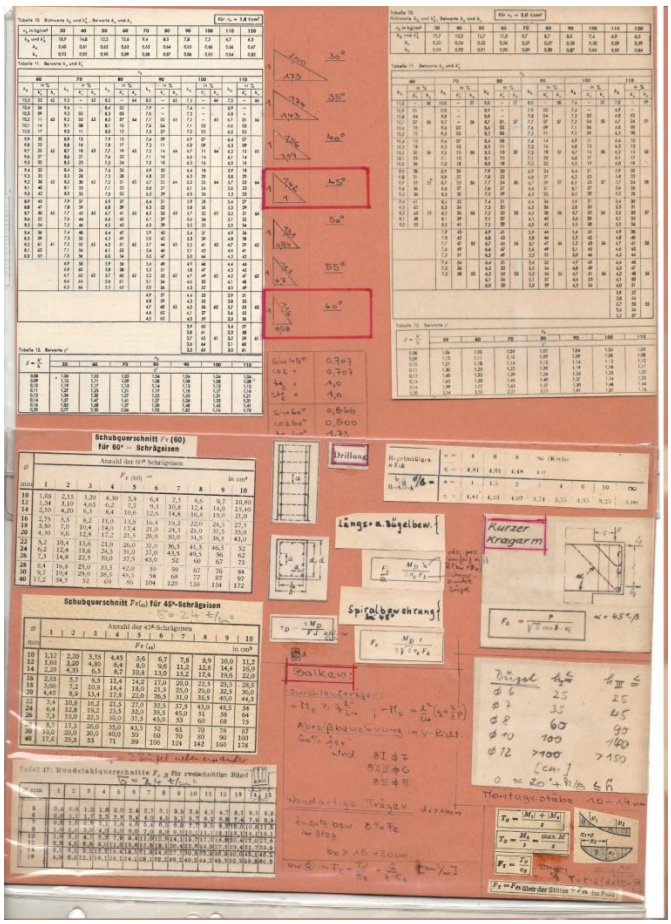

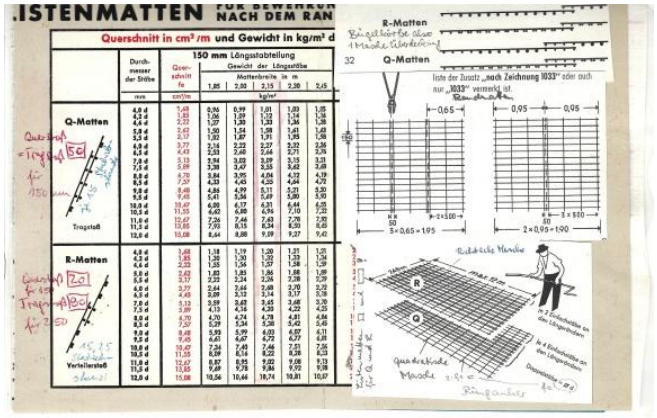

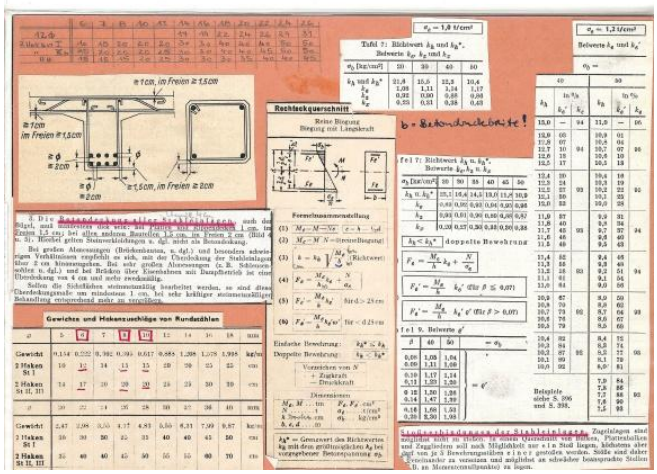

This was my/our way **How to dimension** ?
by generating above 'Dimensioning booklets',
thus becoming very fast when dimensioning.
This was very helpful for my concrete construction diploma exam and helped to compensate for the blackout I had during the oral exam on the topic of bridges. Just one second of looking at my paper would have helped.

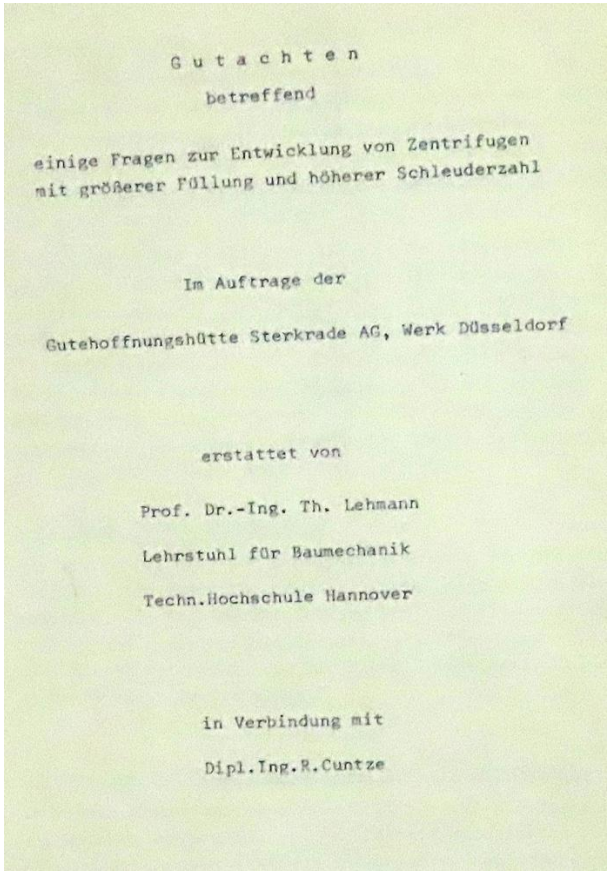

G u t a c h t e n

betreffend

einige Fragen zur Entwicklung von Zentrifugen
mit größerer Füllung und höherer Schleuderzahl

Im Auftrage der

Gutehoffnungshütte Sterkrade AG, Werk Düsseldorf

erstattet von

Prof. Dr.-Ing. Th. Lehmann

Lehrstuhl für Baumechanik

Techn.Hochschule Hannover

in Verbindung mit

Dipl.Ing.R.Cuntze

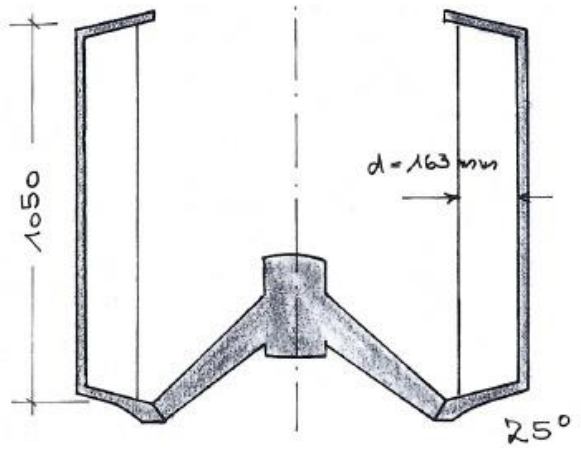

Development goal was a sugar molasses centrifuge for an increased capacity of 1000 kg.
Quasi-static calculation. Loading: Centrifugal forces. Stresses from starting and braking, as well as vibrations, are not taken into account, nor are imbalances.
Rotational symmetric model
The solution of the statically indeterminate system was carried out manually (*see page before*), using residual stress states with the statically indeterminate Xi, which were determined via the strain compatibilities at the joints

My first contact to centrifuges.
Expert Report of the university chair

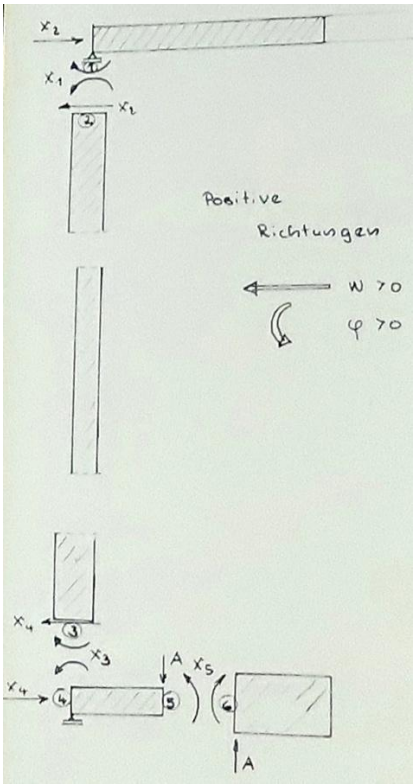

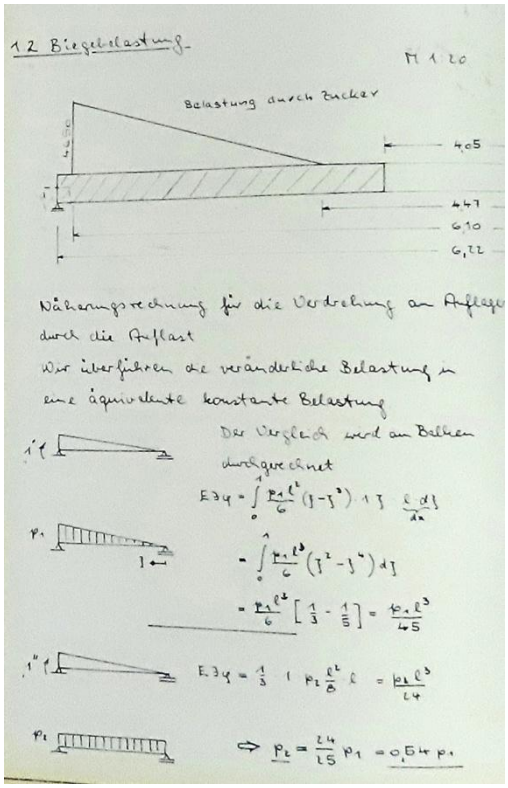

Building an own Home at Markt Indersdorf (*30 km north of Munich*)

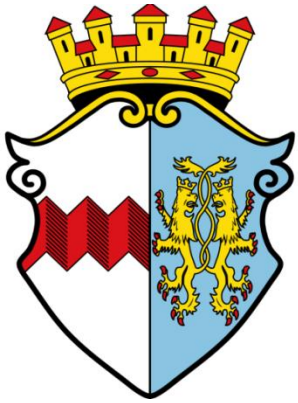

Village Indersdorf
founded in 972.
Districts Glonn and
Langenpettenbach
founded in 774.
Beer brewery since
1300.
Inhabitants: 10.600

Folk festival at Markt Indersdorf

not so far from the Alps

Break on the construction site
(*with me and a bottle of bear*)

Beginning to enjog the new garden.
No yet surrounding houses

In Indersdorf:
very large parades take place at carnival

from the street

from behind

with mountain hikers, bowling friends and Jutta

bees approaching our nut beam

Saying Good-bye to the old Year

Very seldom: high snow in the garden

babbling fountain.

Barbecue with Maria →

3 wood anamones: yellow, white, purple and red winter alpine lillys
(right): Who will win?
Summer alpine lily or the fern?

Former working place under the roof

Mausi: Checking my work
and my healthy food, the apple

Habitat of the Trolle

Habilitation (1978) and Honorary Professorship (1998)

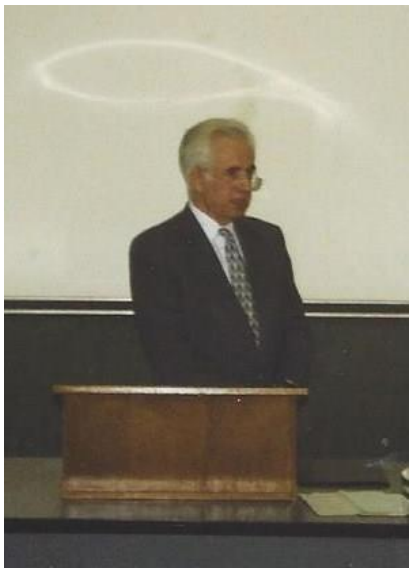

Dietmar Könke, vice president: presentation of the future honorary professor and the certificate

Honorary Professor Presentation

Gudlath, Zippe, Heimeshoff, Grundmann, Fahlbusch + friends behind

Working in Civil Engineer Applications

My work in the Aerospace domain is compiled in [CUN 22].

Application-oriented engineer with a scientific touch for material modelling and with the hope to be some bridge-builder between mechanical and civil engineering (*construction****).***

Working as a bricklayer:
(right, example) Wall of a so-called facing masonry. With piecework bricklaying, you were allowed to go home faster. Weekly working hours were 45 hours, overtime was gladly done because of the money, and it was also concreted until Saturday evening. There was no thought of 'work-life balance'. At the weekend, you received the so-called pay packet from the foreman. In this were billing, notes and remaining coins.

Structural engineering, armoring plans, pile foundation

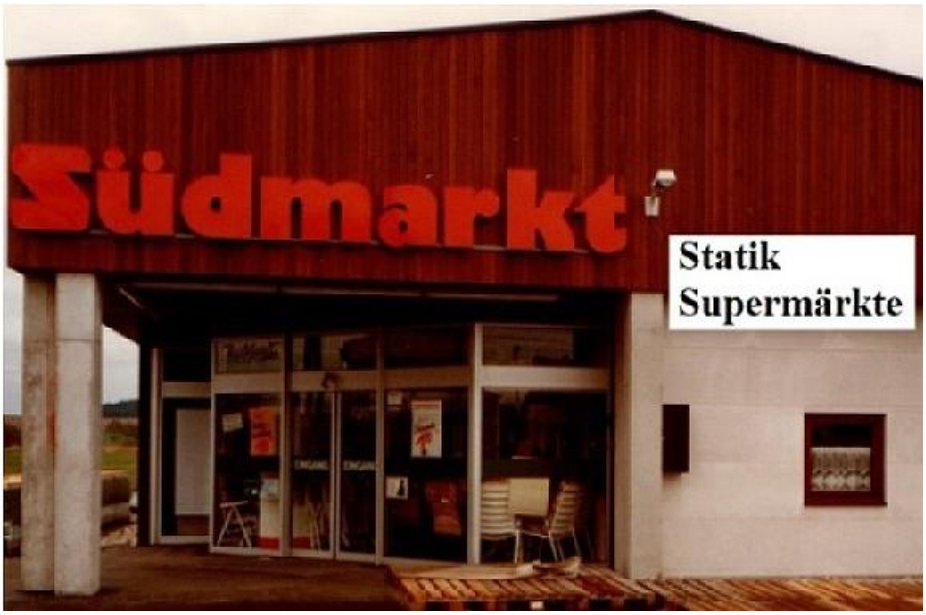
Südmarkt
Statik
Supermärkte

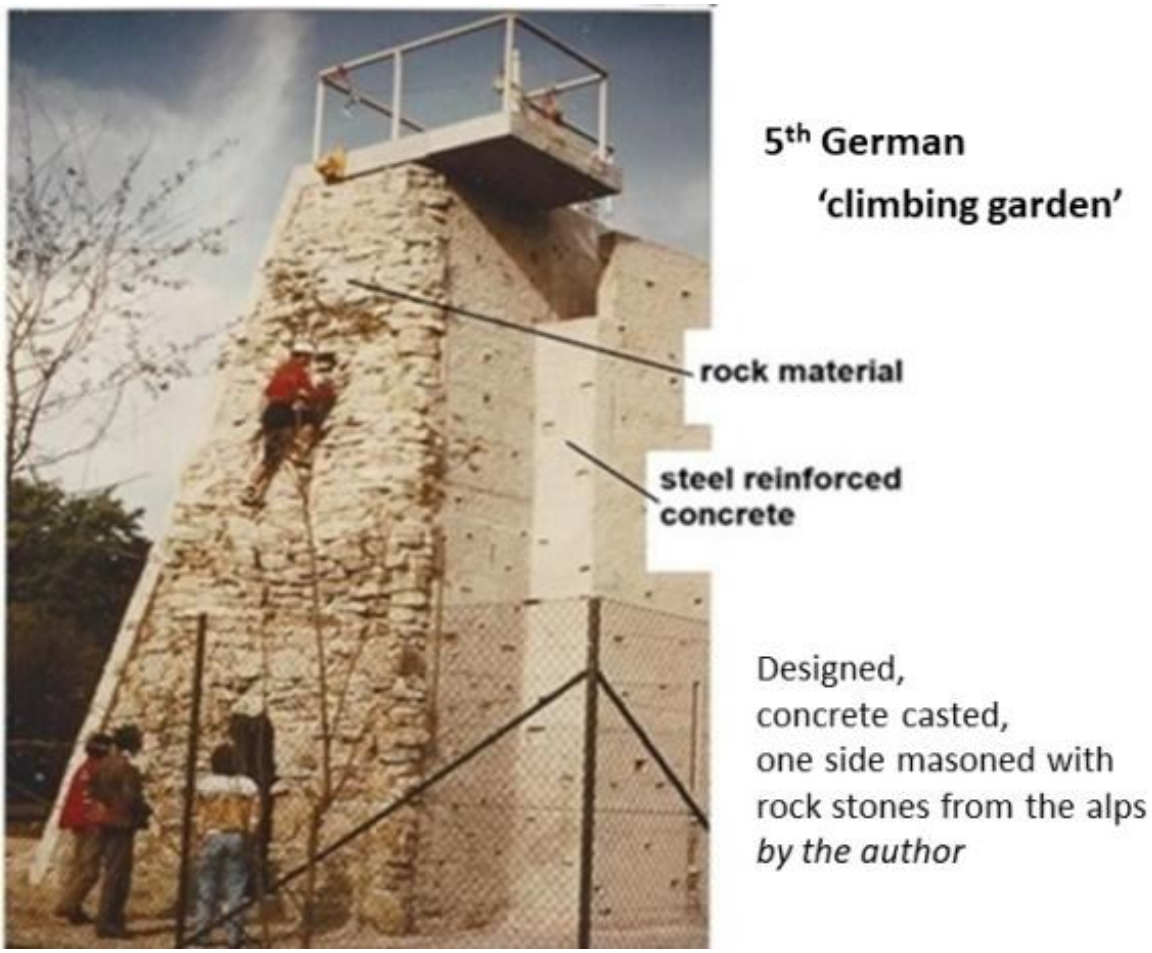
5th German
'climbing garden'
rock material
steel reinforced
concrete
Designed,
concrete casted,
one side masoned with
rock stones from the alps
by the author

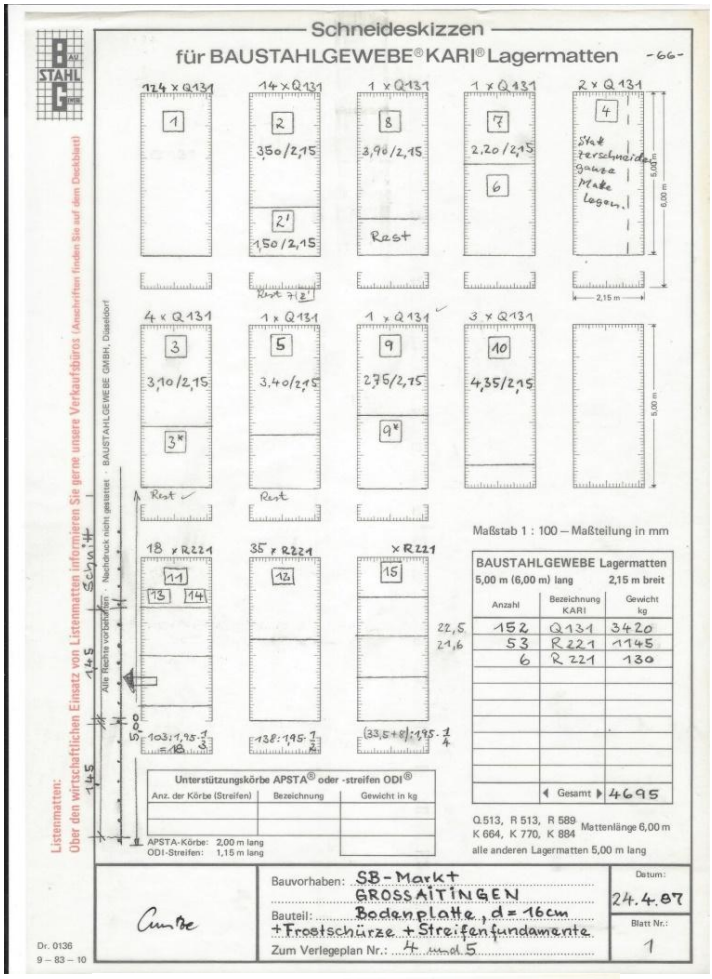

Schneideskizzen
für BAUSTAHLGEWEBE® KARI® Lagermatten -66-

Maßstab 1 : 100 – Maßteilung in mm

BAUSTAHLGEWEBE Lagermatten
5,00 m (6,00 m) lang 2,15 m breit

Anzahl	Bezeichnung KARI	Gewicht kg
152	Q 131	3420
53	R 221	1145
6	R 221	130
	Gesamt	4695

Unterstützungskörbe APSTA® oder -streifen ODI®

Anz. der Körbe (Streifen)	Bezeichnung	Gewicht in kg

APSTA-Körbe: 2,00 m lang
ODI-Streifen: 1,15 m lang

Q 513, R 513, R 589, K 664, K 770, K 884 Mattenlänge 6,00 m
alle anderen Lagermatten 5,00 m lang

Listenmatten: Über den wirtschaftlichen Einsatz von Listenmatten informieren Sie gerne unsere Verkaufsbüros (Anschriften finden Sie auf dem Deckblatt)

Alle Rechte vorbehalten – Nachdruck nicht gestattet – BAUSTAHLGEWEBE GMBH, Düsseldorf

Bauvorhaben: SB-Markt GROSSAITINGEN
Bauteil: Bodenplatte, d = 16cm +Frostschürze +Streifenfundamente
Zum Verlegeplan Nr.: 4 und 5
Datum: 24.4.87
Blatt Nr.: 1

Dr. 0136 9 – 83 – 10

Stb.- Bodenplatte — Pos. 35 — 58

$l_1 = l_2 = \infty$

$M_{max} = 20 \cdot 0{,}25 \cdot 0{,}75 = 3{,}75$ kNm/m

$k_m = 13 / \sqrt{3{,}75} = 6{,}7$

$A_s = 3{,}75 \cdot 3{,}8 / 13 = 1{,}1$ cm²/m

gewählt:

Q 131, unten

Betonierfugen:

Schachbrettartig betonieren. An den Rändern direkt aufbetonieren. Bewehrung durchführen.

Nachweis des Extruderschaums:

$F_{Rad} \approx 10 \cdot 14 = 140$ cm² (Lastverteilung)

$F_{Beton} = (10 + 2 \cdot 16)(14 + 2 \cdot 16) = 1920$ cm²

$P_{max} = 10$ kN

$\sigma = \frac{10}{1920} \approx 5$ N/cm² ≤ 30 N/cm²

Druckfestigkeit ausreichend.

Pos. 36 Ringbalken

Anordnung, wo die Wände nicht durch eine Deckenscheibe oder andere aussteifende Konstruktion gehalten sind.

gewählt (konstruktiv):

Betonformstein U-förmig für Innenwände

4 ∑ ϕ 10, Längs
∑ ϕ 6, a = 25

Auflager: Verankerung mit Aufhängedraht

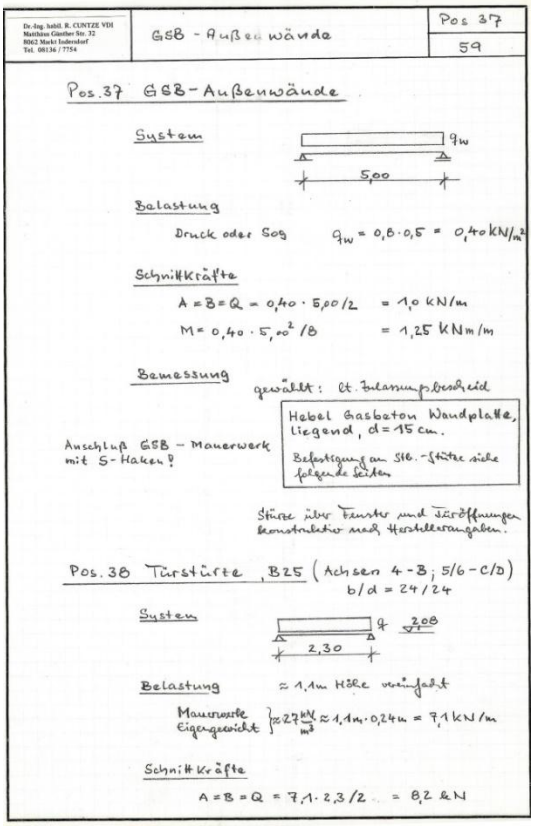

GSB - Außenwände — Pos 37 — 59

Pos. 37 GSB-Außenwände

System

Belastung

Druck oder Sog $q_w = 0{,}8 \cdot 0{,}5 = 0{,}40$ kN/m²

Schnittkräfte

$A = B = Q = 0{,}40 \cdot 5{,}00/2 = 1{,}0$ kN/m

$M = 0{,}40 \cdot 5{,}00^2/8 = 1{,}25$ kNm/m

Bemessung

gewählt: lt. Zulassungsbereich

Hebel Gasbeton Wandplatte, liegend, d = 15 cm.

Befestigung an Stb.-Stütze siehe folgende Seiten

Anschluß GSB – Mauerwerk mit S-Haken!

Stütze über Fenster und Türöffnungen konstruktiv nach Herstellerangaben.

Pos. 38 Türstütze, B25 (Achsen 4-B; 5/6-C/D)
b/d = 24/24

System

Belastung ≈ 1,1m Höhe vorhanden

Mauerwerke Eigengewicht $\approx 27 \frac{kN}{m^3} \approx 1.1m \cdot 0{,}24m = 7{,}1$ kN/m

Schnittkräfte

$A = B = Q = 7{,}1 \cdot 2{,}3/2 = 8{,}2$ kN

Stb-Stütze u. Köcherfundam. — Pos 32 — 57

Pos. 32 Stb-Stütze und Köcherfundam.

Analog (29)

Pos 33 Frostschürze, b = 30cm, B 15

gewählt (konstruktiv):

R 221 Mattenkorb
III ϕ 12 Längs

In der Aufkantung:
III ϕ 8, a = 20 Steckbügel
III ϕ 12, Längs

Pos. 34 Streifenfundamente, b = 50 cm, B 15

gewählt (konstruktiv):

R 221 Mattenkorb
III ϕ 12 Längs

Pos. 35 Stb.-Bodenplatte, d = 16 cm, B 15

Die Platte soll von 20 kN - Gabelstaplern befahren werden.
Unter der Bodenplatte ist eine Dämmschicht aus Extruderschaum angeordnet (zul p = 300 kN/m²).

Nach WÖLFER:

$E_S \approx 6000 \frac{M_P}{m^2}$; $\chi \approx 0{,}65$

$c = E_S/\chi = 6000/0{,}65 = 9230$ MP/m²

$L = \sqrt[4]{\frac{4 \cdot 2600000 \cdot 015^3}{12 \cdot 9230 \cdot 100}} = 0{,}75$ m

Dimensioning

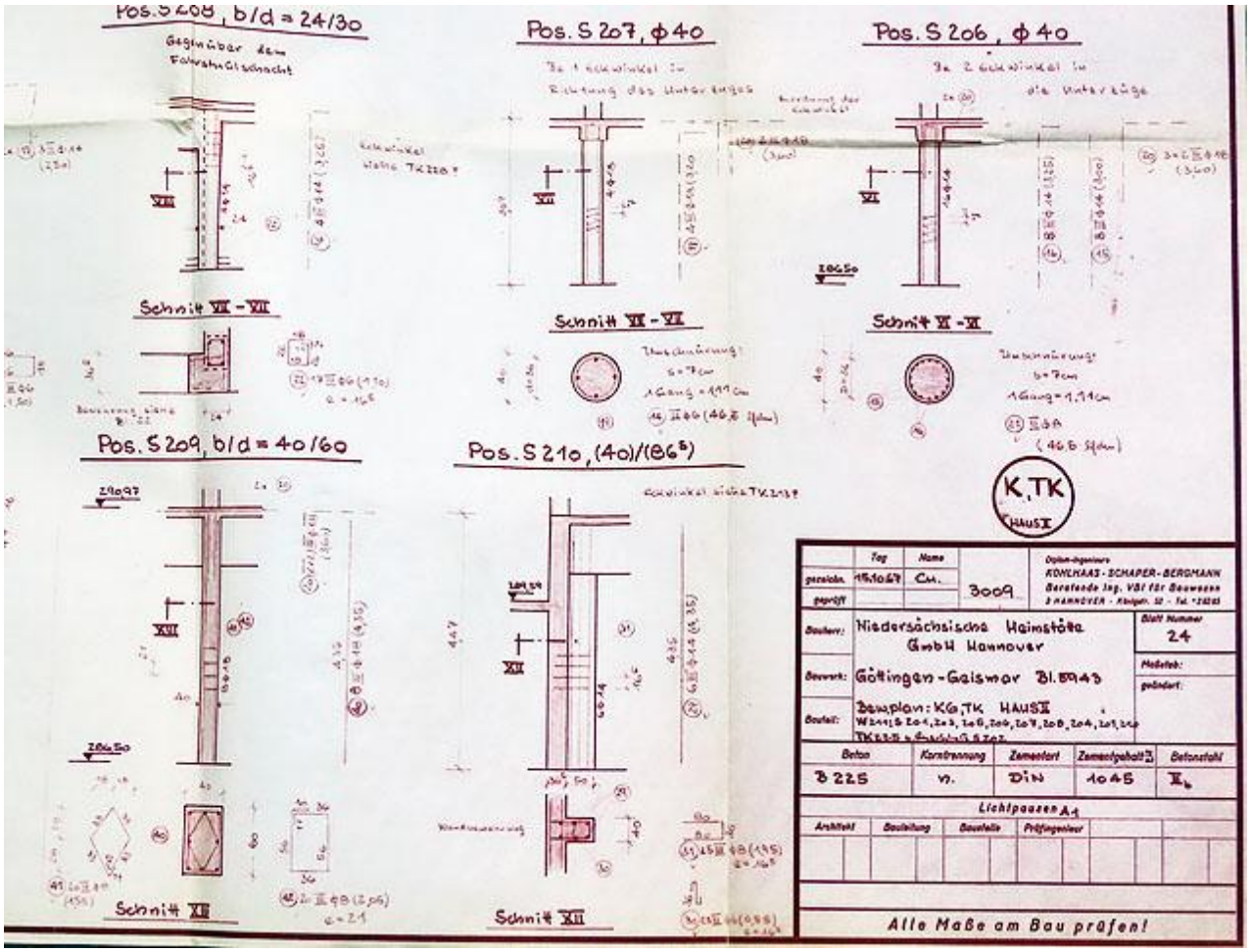

DGLR 1968-1970, German Society for Aeronautics & Astronautics

From DFL , DVL to DGLR
Christmas Festivity 1986
with Wolf Elber
(*Father of the crack closure concept in Fracture Mechanics,*
later director of a NASA institute investigating the
Challenger Columbia Booster tragedy reasons).
The sealing ring material became brittle in the cold January temperatures and failed!

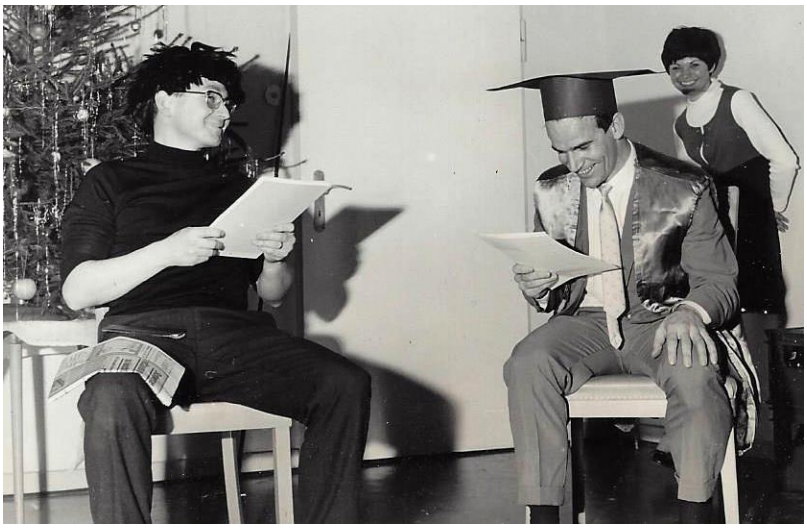

Invitation of Wolf regarding our Ariane Booster connection in 1986.

FE-programming: *Development of a Finite Element calculation program for the calculation of a rotationally symmetrical (more was not possible) centrifugal compressor wheel. However, at that time, the needed program modules for this had to be requested from friends at his former University at Hannover.*

Later at DLR: Participation in the farewell of the grand old lady of stability theory

(left) Prof. Kurt Klöppel (*Germany's steel bridge construction 'pope'*), honouring
(right) his former co-worker Prof. Maria Eßlinger when retiring after a structural stability-dedicated life.
(*Passing*: my friend Dr.-Ing. Bodo Geier)
(Klöppel, Geier, Lacher, Cuntze, Sorry, Eßlinger)

MAN-Neue Technologie (New Technology**)**

Founded in 1969 as an independent research and development division of MAN AG.
Objectives at that time: Development of new products and techniques, engage intensively in basic research, applying novel materials, open up new markets for the young division.

Rätz, Weppelink, Cuntze, Zippe Denk
The production of gas ultracentrifuges for UF6 enrichment was was completed at the end of the 80s, (right). One reason was that the failure rate was fantastically small

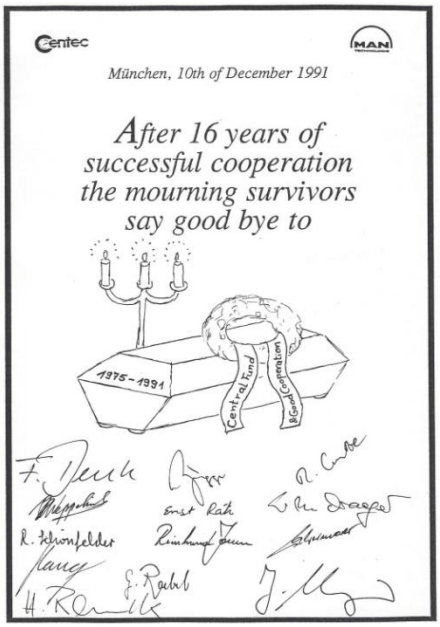

Continuing education at MAN

Finite Element Analysis Meeting at MAN Neue Technologie with the heads Dr. F. Laußermair (*he was responsible for my leaving the DVL*) and H. Rauck, *below*

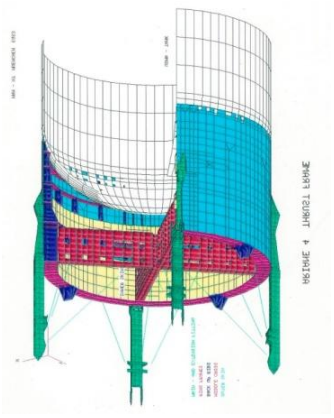

TEILNEHMERVERZEICHNIS ZUR FEM-TAGUNG AM 28./29. FEBRUAR 1980

Gutehoffnungshütte Sterkrade AG
Postfach 11 02 40
D-4200 Oberhausen 11
Tel. 0208/692-1

Hr. Enders
Hr. Kibelka
Hr. Krämer
Hr. Schmidt
Hr. Schwendler

M.A.N.
Katzwanger Str. 101
Postfach 44 01 00
D-8500 Nürnberg 44
Tel. 0911/18-1

Hr. Broscio
Hr. Bürkel
Hr. Fiedler
Hr. Gelnar
Hr. Hammen
Hr. Hartl
Hr. Kaposvari
Hr. Dr. Mohacsi
Hr. Pittr
Hr. Scholz
Hr. Siegl
Hr. Sima
Hr. Sustaric
Hr. Svarovsky
Hr. Vallon
Hr. Dr. Wagenknecht

ALCAN-Aluminiumwerk Nürnberg GmbH
Nopitschstraße 67
D-8500 Nürnberg

Hr. Deuber
Hr. Rösch

M.A.N.
D-6095 Ginsheim-Gustavsburg
Tel. 06134/55-1

Hr. Gabel
Hr. Dr. Kärcher
Hr. Purucker
Hr. Dr. Strigl

M.A.N.
Stadtbachstraße 1
Postfach 10 00 80
D-8900 Augsburg 1
Tel. 0821/322-1

Hr. Fröhlich
Hr. Schuster
Hr. Seidemann

M.A.N.-Wolffkran GmbH
Postfach 3720
D-7100 Heilbronn (Neckar
Tel. 07131/73081-5

Hr. Kloos
Hr. Tietz

MTU
Postfach 289
D-7990 Friedrichshafen
Tel. 07541/207-1

Hr. Kubisch
Hr. Richter

MTU
Dachauer Straße 665
Postfach 50 06 40
D-8000 München 50
Tel. 089/1489-1

Hr. Dr. Agatonovic
Hr. Dr. Belohradsky
Fr. Dr. Groß
Hr. Kerl
Hr. Knodl
Hr. Dr. Neumayer
Hr. Ölmez
Hr. Paul
Hr. Pester
Hr. Seyfried

M.A.N.
Dachauer Str. 667
Postfach 50 06 20
D-8000 München 50
Tel. 089/1480-1

Hr. Hartmann
Hr. Wobbe

M.A.N.-Neue Technologie
Dachauer Str. 667
Postfach
D-8000 München 50
Tel. 089/1480-1

Hr. Dr. Cuntze
Hr. Isleif
Hr. Dr. Kehl
Hr. Kohl
Hr. Kröger
Hr. Scharringhausen
Hr. Dr. Schmatz
Hr. Wein
Hr. Zaun

CONTROL DATA GmbH
Stresemannallee 30
D-6000 Frankfurt/Main

Hr. Lorenz

Technische Universität
Lehrstuhl für Baumechanik
Callinstraße 15
D-3000 Hannover

Hr. Prof. Dr. Stein

Universität Bochum
Inst. für Konstr. Ingenieurbau
Universitätsstraße 150
D-4300 Bochum

Hr. Prof. Dr. Wunderlich

In deep discussion with Dr. Gernot Zippe about (*I guess*) UF6-uranium enrichment centrifuge questions

Leaving for work: daily 6:19 o'clock

Keen soccer and mountain hiking team

Celebrating festivities together was an important fact

Two pictures of the team over the time

Ralf Cuntze, Raimund Schönfelder, Stan Smith
180 years celebration = 3 x 60 (*see drawings*)

The two Oldies after retirement.

Raimund suffered from a lung disease. He was therefore very pleased that he was only sick for 1 day in his 32 years at MAN. He always loved going to work!

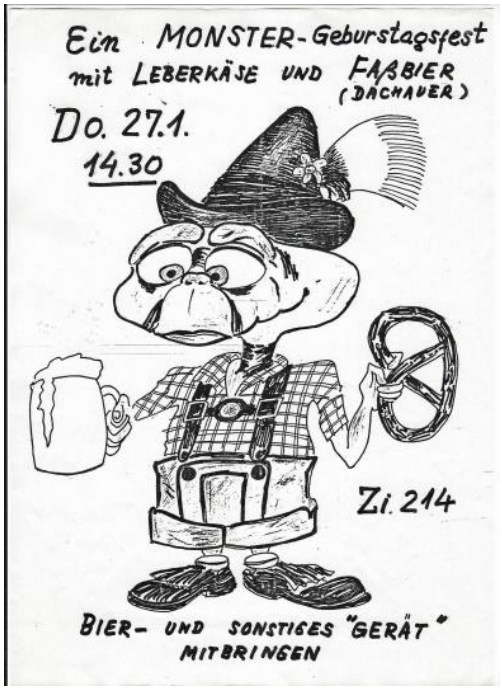

Tragen Sie ein Lächeln
in Ihrem Gesicht, dann
kann bei unserer runden
Geburtstagsfeier gar nichts
mehr schief gehen.

Wir lächeln trotz der 180 Jahre:

Ralf Cuntze
Stan. Smith
Reimund Schönfelder

3 mal 60 Jahre und kein bißchen weise !

Anläßlich unseres ersten Schrittes in das **Greisenalter** laden wir Sie hiermit als Zeuge dieses umwerfenden Ereignisses zu einem **Imbiß** mit gesundheitlich gerade noch vertretbaren **Betäubungs-getränken** ein.

Ansprechpartner:

Ralf Cuntze
Stanley Smith
Reimund Schönfelder

Telefonische Rückantwort bitte bis zum
2. 9. 99, Fr. Schwarz, RA
Tel.: **K 1867** bzw. **08131/891867**

Datum: 16.09.1999
Uhrzeit: **15^{30}**

Ort: **Karlsfeld, Liebigstr. 5a**
in: **Saal 3 und 4**

Probably my last participation with our 'Mountaineering team'. Alois took finally part

A good Place for a short report on Dr. Zippe (a GUZ- story):

Starting in 1946, while a Russian prisoner of war, Dr. Gernot Zippe, together with Russian and other scientists such as Prof. Steenbeck, developed the gas ultracentrifuge (GUZ) for the Russians. The researchers initially worked at an institute on the Black Sea, then in Leningrad from 1952 onwards. The system they developed was intended to be used for the isotope separation of Uranium-235 and Uranium-238. "*Give us an enrichment level of 15% U235, and we'll be satisfied"* the Russians said. The research group achieved an enrichment level of 30% and was allowed to return home in 1956. According to Zippe, the centrifuges they developed were then used on a large scale by the Soviet Union to produce atomic bombs (> 80%). Here, at Urenco, MAN centrifuges - developed with Zippe's assistance - delivered approximately 4% enrichment for the nuclear power plants. Method: Cascade plants, which achieve in a serial way the desired enrichment. Natural uranium is not harmful as long as natural concentrations are not exceeded. MAN- Technologie (New Technology at that time) cooperated with Dr. Zippe, father of the German GUZ, who told me, that he had transported natural uranium in his suit pocket for a meeting with a high soviet politician.

Uranium enrichment Centrifuges

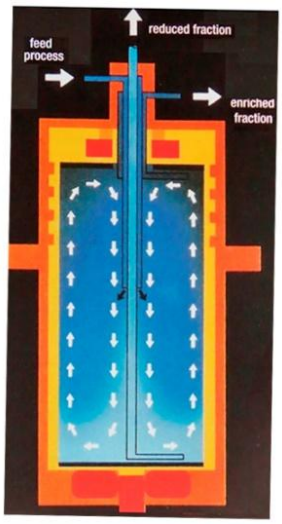

Production system

Tube:, sinle centrifuge
Block-concept
URENCO: Development of separation performance over the course of centrifuge development through longer overall centrifuges.
URENCO system with individual, single centrifuges

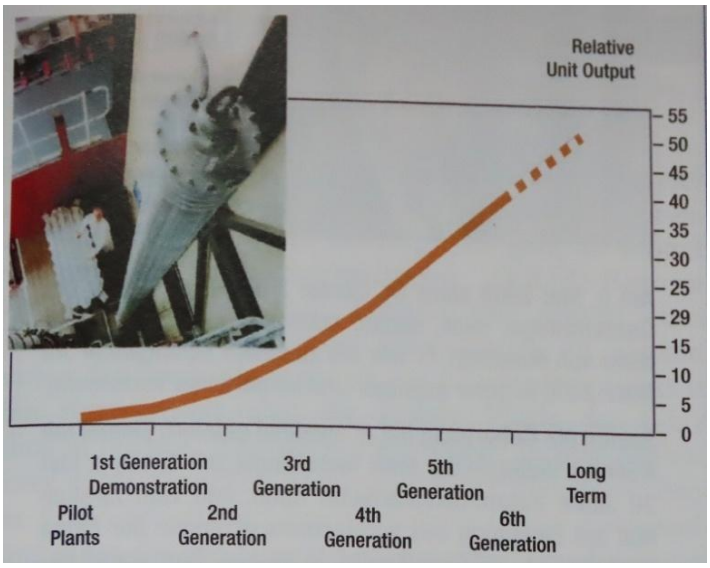

Bellow: necessary tool to combine several single centrifuges in order to obtain a longer separation length

Some MAN Project Activities

Book of remembrance

and

Software formerly applied

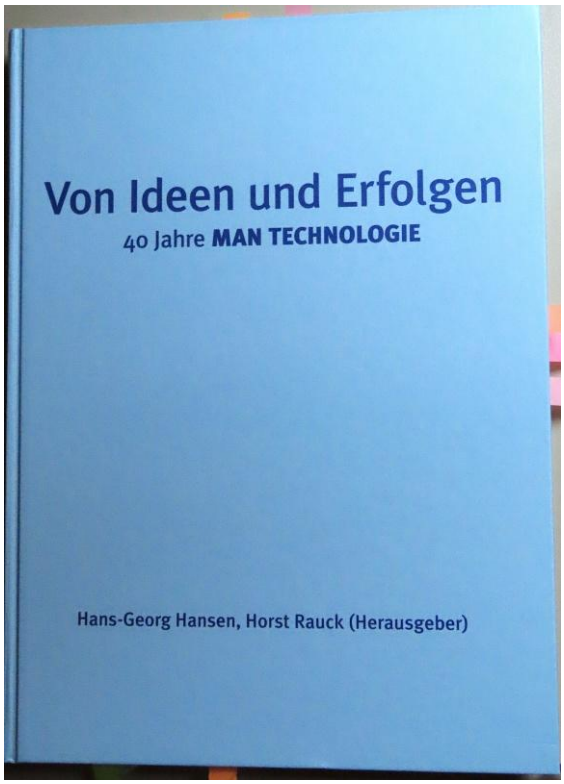

Book on MAN-Technologie history:

'Of ideas and successes'
461 pages, Paartal-Verlag

(The author could not contribute
due to his contract work for ESA)

Used Software Codes

Static, Dynamic and Thermal Structural Analysis Codes

* FEM: NASTRAN, MARC, NONSAP, SAPIV
* Finite differences: BOSOR, ROTOPT
* Pre- & postprocessor: PATRAN/II
  with links to NASTRAN, MARC and NONSAP
. Thermal analysis, heat radiation, heat convection: MARC
. Composite laminates computation: MSV 2
. Viscoelastic, -plastic behaviour: MARC
. Fracture Mechanics: MARC
. Component Life, Crack Propagation: ESA-CRACK, NASGROW
. Special programs for fibre wound vessels,
  bolt connection, ...
. Structure reliability analysis: FORM, SORM
  with links to MSV 2 → FRP Rel
. Structure optimization: SAPOP
. Test data evaluation and monitoring: BASMAN
  and rain flow counting code. Statistic codes, ...
  EV CREEP (θ- projection concept) for fatigue loading
. Computer graphics package: DISSPLA
. Material databank composites
. Geometrical nonlinear beam analysis: PROFI + GROBI
  for wind energy converter (GROWIAN, WKA 60, ...) statics

HARDWARE

Link-up MT Computer VAX 8550
4 TEKTRONIX 4115 Colour Graphics Display Terminal
1 Evans & Sutherland PS390 Colour Graphics Display Terminal
2 TEKTRONIX 4692 Colour Graphics Copier (Inkjet), DIN A 4
Personal Computers. Workstation DEC 2000

Software and Herdware used in the eighties

Toulouse,
sitting in the big conference room.
The clock counts.
98, 99, 100 , 99, 98.
SILENCE
We could directly interprete the backcounting !?

Was this failure perhaps due to the fact that the launch program
of Ariane 4 (100 s) < Ariane 5 (120 s)
was used??
That would be bad, because then the *existing* standards would not have been met.

The slip of paper below was the start of my work at MAN-Neue Technologie in 1970 regarding the development of the **Ariane launcher family**:
"Make a design proposal for an offer, please " (Thrust structure).

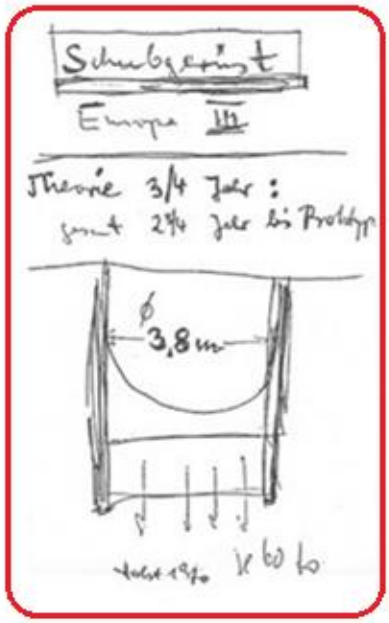

Offer **(**center slip**)** ***for Europe III as the Forerunner of Ariane I and following Family***
(nearly all structural parts during the Ariane launcher family Development had to be designed)

The name ARIANE: Officially, the goddess Ariadne is said to have lent her name. Wasn't it also decisive that a Dornier circle of friends discussed whether the name Ariane of a little girl would not be ideal for both sides? (The father of this girl told me this several years later at a dinner of the Chaine-de-Rotisseur)

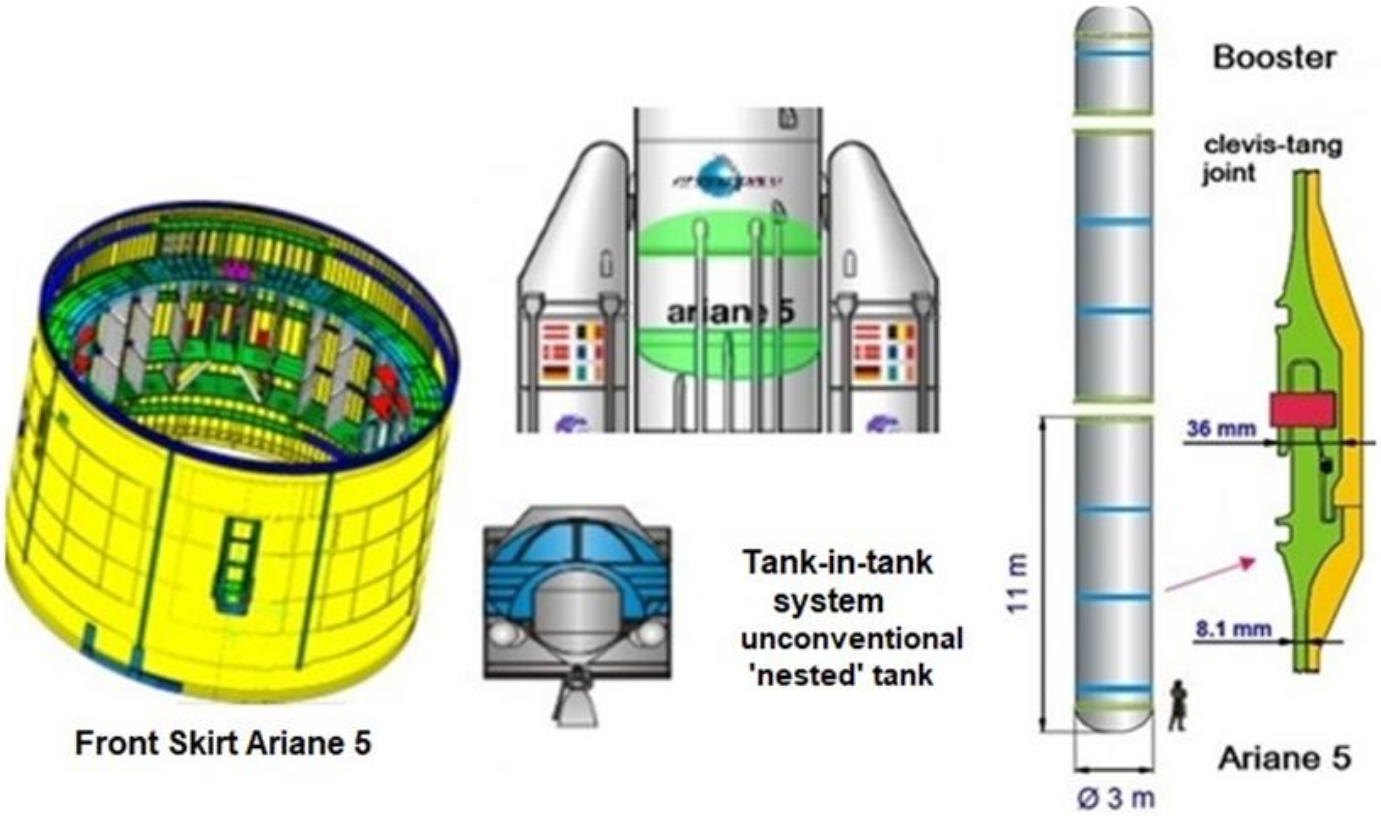

Ariane Launcher 1-5

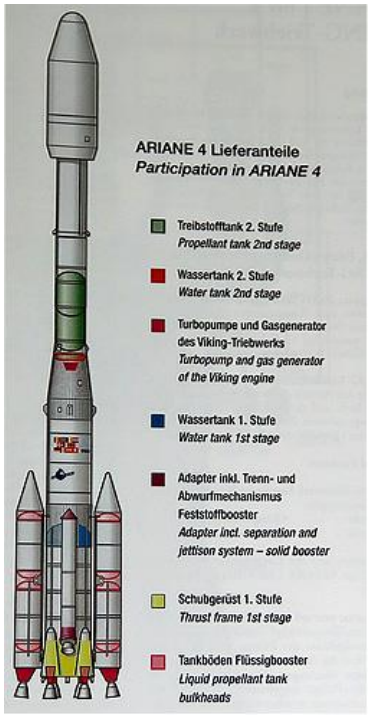

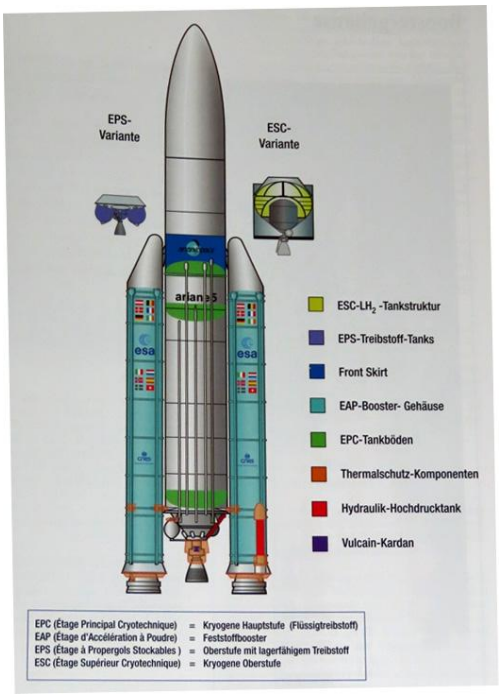

Notes on Tank-in-Tank system and Clevis-Tang Joint

The tank-in-tank construction system was absolutely new. My friend Huba Öry, ERNO, meant: "*We will have to solve a very challenging task*!" The reason was probably the low gate height in Kourou, right? Later, the gate was enlarged.

Clevis-Tang Joint: (Hardware was a Good bye present of my colleagues)

The Challenger tragedy came into play during the development of the Clevis-Tang booster connection. This gave me the opportunity to ask my former DVL colleague Wolf Elber, now head of a NASA institute and one responsible for the Challenger investigation, for his assessment.
Our design causes the joint to close when pressure is applied under a hazard condition in contrast to the Columbia design, sealing O.K..

Application of Software: the challenging Ariane 5, Booster Joint

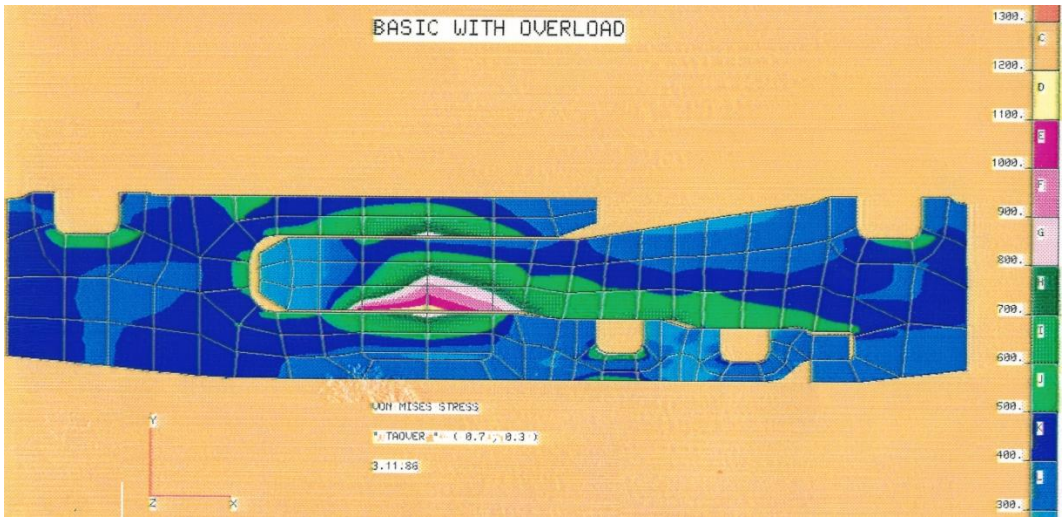

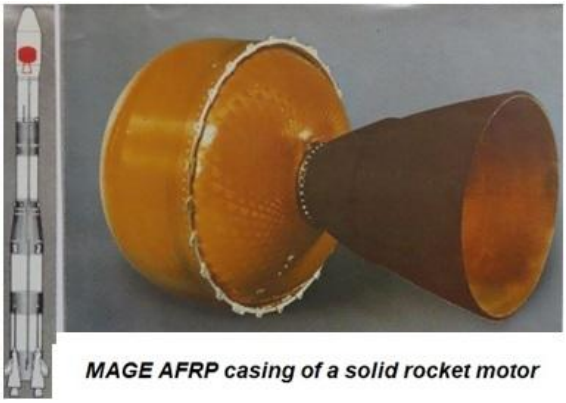

MAGE AFRP casing of a solid rocket motor

Airbus A330/340 drinking water tanks. High Pressure Vessels. Apogee Kevlar Motor Case

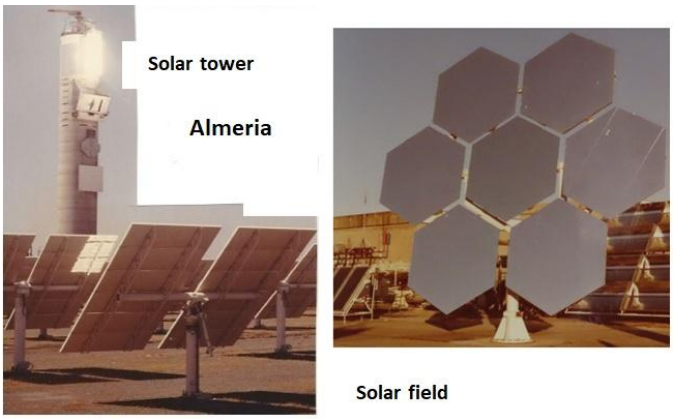

Solar Farm Plant with tower

Wind Energy Rotor GROWIAN, 1980, 51 m blade, GFRP shell with wind speed measurement facility

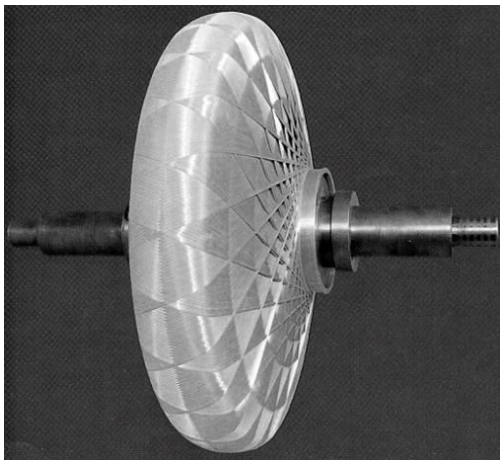

Process. Composite brake energy storage flywheel for a bus.

(right) Small wind energy rotors 1980

ŇIESŸTŎ design, Š. Guisard,

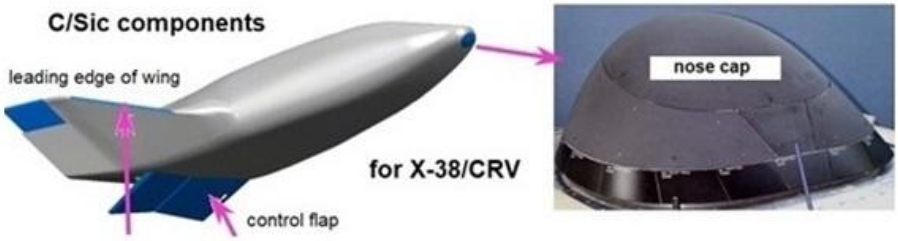

SOFIA telesope, ISS-linked structures

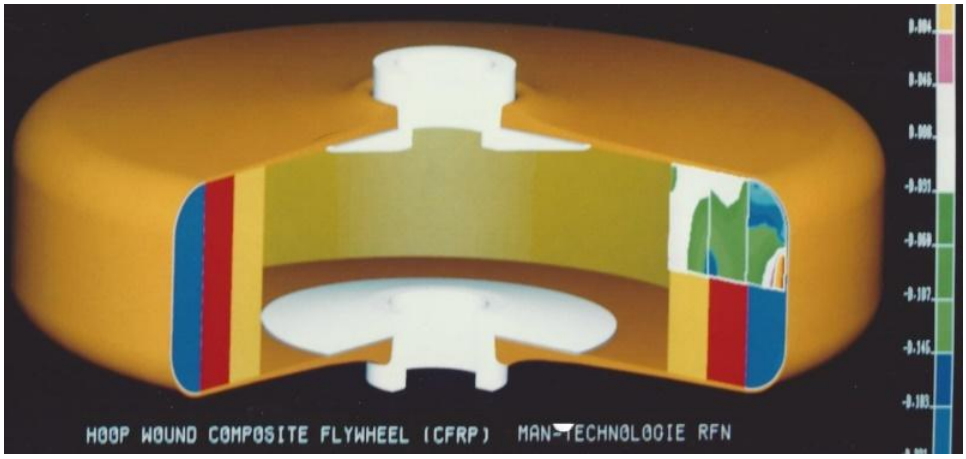

FEA of a no-delamination energy storing fly wheel, according to be able to design with the right stiffness course due to available different stiff fibers (Glass, T300, T700 : internal less stiff).

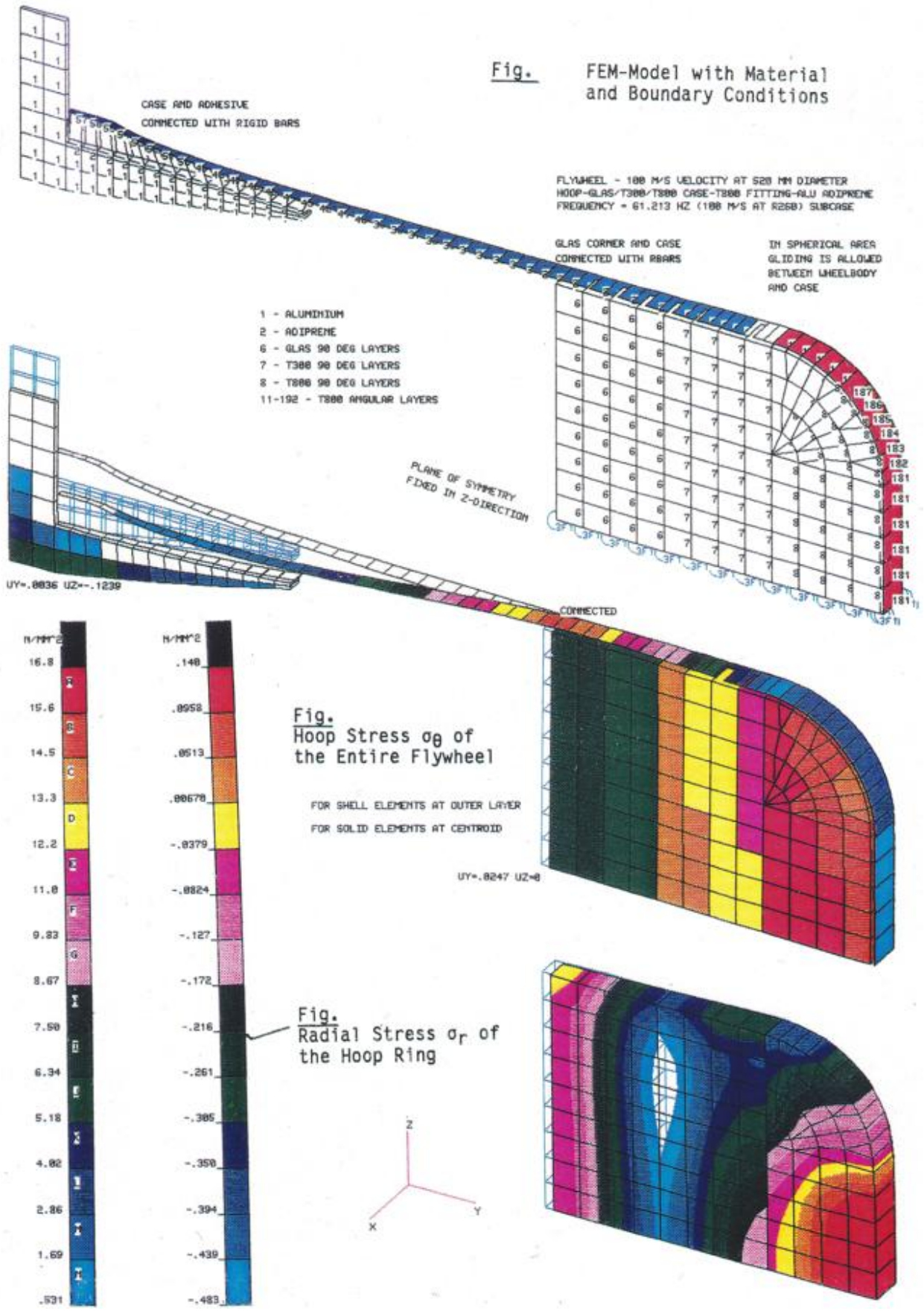

Fly-wheel design after having composites with different Young's moduli (1988)

Structure Analyses

Our working disciplines/experiences
☐ Statics, strength and stability
☐ Fiber composite and ceramic structures
☐ High-temperature metallic structures
☐ Stationary and non-stationary temperature fields
☐ Fatigue behavior
☐ Fracture mechanics (linear and non-linear)
☐ Structural dynamics and load analysis
☐ Applied statistics and structural reliability analysis
☐ Plasticity and creep behavior (material models)

Numerical methods
☐ FEM programs MSC/NASTRAN, MARC, SAP IV, NONSAP
☐ Finite difference programs BOSOR 4, BOSOR 5, and others
☐ Pre- and postprocessor program PATRAN G, also with link to MARC

Technical equipment
☐ VAX 11/780
☐ 2 high-performance color computer display terminals (Tektronix 4115 B)
☐ 1 color hard copy printer (Tektronix 4691)

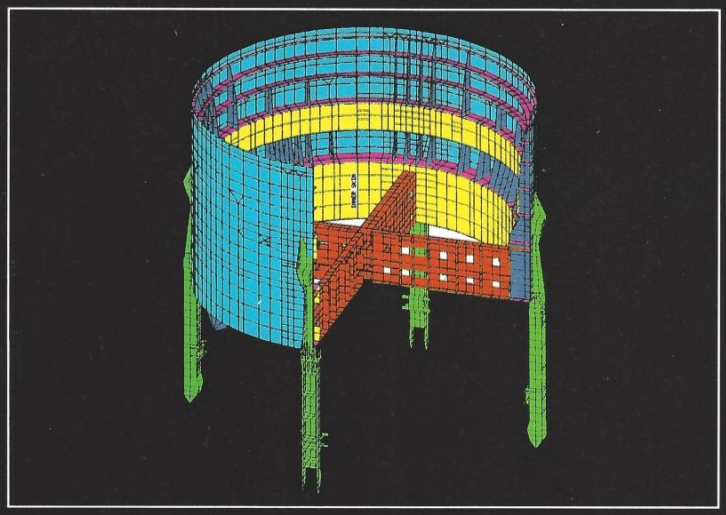

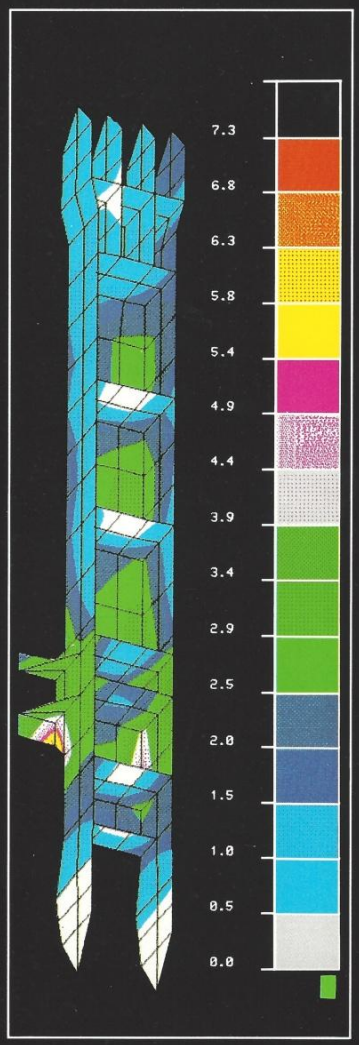

14

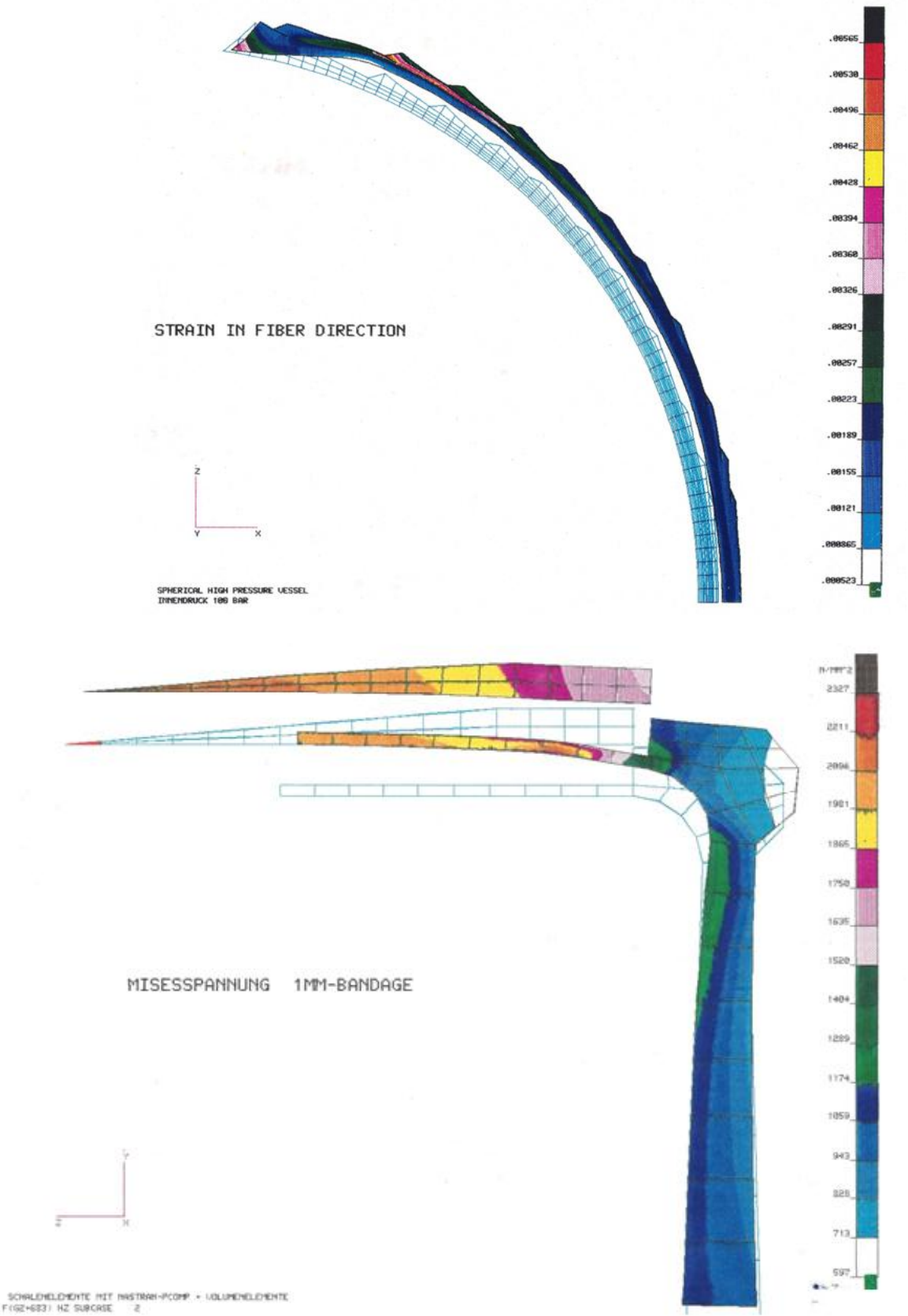

Two FEA's: Filament wound pressure vessel, (below) bottom of a centrifuge

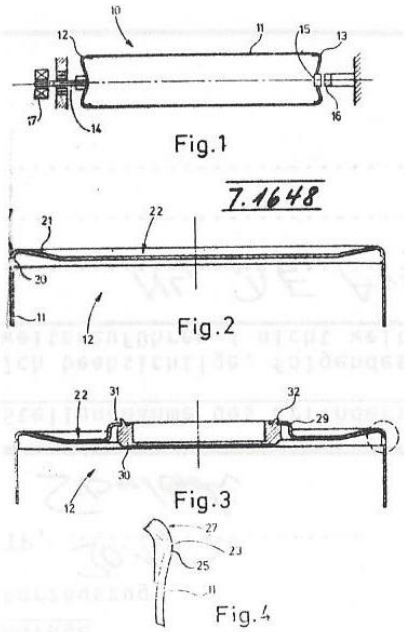

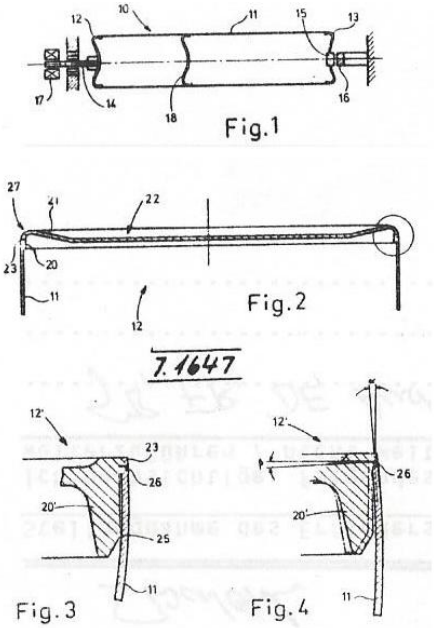

Anspruch 1

Schleudertrommel für hohe Drehgeschwir digkeiten mit einer dünnwandigen Trom- melwand und mindestens einem mit der Trommelwand verbundenen Deckel, dadurc gekennzeichnet, daß der Deckel (12,13) in seinem Grundaufbau eine aus hoch- festem Blech oder Band leicht kegel- förmig geneigte Scheibe ist, deren Aus senkontur für den Anschluß zur Trommel wand (11) einen Ringansatz (20) und deren Innenbereich (22) für die Aufnah oder Verbindung von Antriebs_ bzw. Lagerelementen annähernd kegelförmig oder topfförmig umgeformt ist.

2 - 10

Anspruch 1

Schleudertrommel mit mindestens einer mit der Trommelwand verbundenen ro- tationssymmetrischen Scheibe, dadurch gekennzeichnet, daß die Scheibe (12, 13) am Außenumfang ein im wesentlichen zylindrisches Teil (20) aufweist, das gegenüber dem Innendurchmesser der Trommelwand mit Übermaß ausgelegt ist und entlang einer Ringfläche mit der Innenseite der Trommelwand (11) ver- bunden ist, derart, daß die Scheibe be Betrieb der Trommel aufgrund von Zen- trifugalkräften eine Stülpbewegung ausübt, die Biegemomente der Trommel an der Fügestelle im wesentlichen auf- hebt.

2 - 11

Patentbeteiligung P 27 09 410.6-23 "Thin-walled centrifuge cylinder (Schleudertrommel)"

CFRP skis about 1980

The GROWIAN blade

Einladung

Mo., 4. Dezember 1978, 11.30 Uhr
Hochschule für Technik, Bremen
Langemarckstr. 116
AB-Trakt, Hörsaal 713

gez. Dr. Fette

Auslegung einer großen Windenergieanlage (GROWIAN)

Vortrag von Dr.-Ing. habil. Ralf Cuntze
M.A.N - München
Bereich Neue Technologie

Es wird in einem 1 1/2-stündigen Vortrag die Auslegung einer großen Windenergieanlage vorgestellt. Der Vortrag untergliedert sich wie folgt:

1. Allgemeines zu Windenergieanlagen
2. System des GROWIAN, Kinematik
3. Statische und dynamische Belastungen, Lastfälle
4. Auslegung von Mast, Abspannung und Gründung
   - 4.1 Auswahlkriterien
   - 4.2 Schwingungsberechnung
   - 4.3 Aerodynamische Anregungsmöglichkeiten
5. Maschinenhaus und Rotor-Nabe
6. Auslegung Rotorblatt
   - 6.1 Kräfte am Blatt
   - 6.2 Flügelanzahl
   - 6.3 Werkstoffauswahl und Vordimensionierung
   - 6.4 Bemerkungen zur Schwingungsberechnung
   - 6.5 Schwingfestigkeitsauslegung
7. Schwingungen des Gesamtsystems

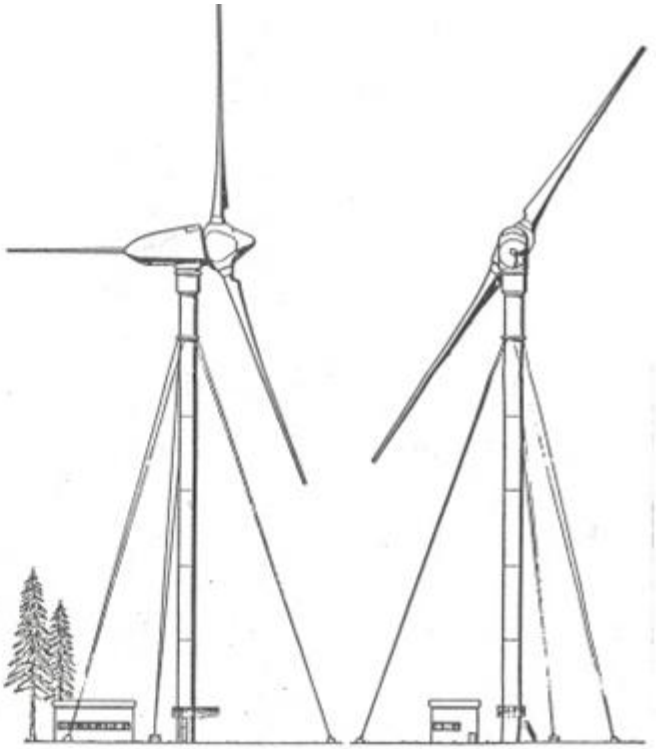

Große Windenergieanlage GROWIAN
3MW

International Progress-Meeting on

Wind Energy R & D Programs in Denmark, in the Federal Republic of Germany, in Sweden and in the USA.

- Exchange of Experiences -

Place: Munich, M.A.N.-Neue Technologie
Dachauerstraße 667

Date: October 15 - 16, 1980

Meeting Room: House VS, Großer Sitzungssaal

Time: 9.00 a.m.

Lecture Language: German and English

Discussion Language: German and English (if necessary)

Organisation: Dr. R. Windheim (PLE, KFA)
Dr. R. Cuntze (EGS, M.A.N.)

Lecture proposals are to be delivered to Dr. Cuntze (MAN) before July 31, 1980. They should include a short description of the lecture content.

Please ask for Overhead - and/or Dia-Projector.

The lecture will be published in the same way as the Seminar on Structural Dynamics in 1978. Please take: letter gothic/micronorm 5 mm/0,5.

Goal of the meeting

To show what is happening now,
what problems are dealt with,
what is the current stage of programs.

To offer an exchange of specialist experiences.

Presentations

The meeting is devided into 5 parts as may be seen in the list on the next page. This list contains the KFA-proposals for the German contributions. The exact lecture titles have to be chosen by each lecturer hinself.

0. IEA Works
   Overlook at the current stage and future programs.

IV. LS WECS and Storage

1. Integration of wind power into national electricity supply systems, taking particular account of storage systems.
   University of Regensburg.
   ET 4085A. 1 à 25 min.

PS.: To IEA-Members mentioned in the "Teilnehmerkreis" are offered 5 lectures.

A discussion time of different length is foreseen after each lecture.

Attendance list (Teilnehmerliste)

1. Vortragende aus Deutschland

2. Vortragende Gäste des IEA-Abkommens (zur Großtechnischen Nutzung der Windenergie:
   Dr. Spera, NASA
   Mr. Johannson, DEFK, Denmark
   Mr. Petersen, Copenhagen
   Hr. Hugossen, NE, Schweden

3. Gäste der Unterauftragnehmer von GROWIAN 1:
   DFVLR
   Siemens
   Leonhardt & Andrä (Hr. Dr. Kovacs)

4. Sonstige Zuhörer:
   Etwa 6 Interessenten deutscher Universitäten.
   Etwa 7 Interessenten der M.A.N.
   Etwa 8 Interessenten der deutschen beteiligten Firmen.

   Summe = 55 - 60 Teilnehmer

Anlage
Call for papers - formula.

Application of the government-desired CFRP was not possible.
SN-fatigue curves were not yet available.
However thes should be available for the chosen classical Railway Steel St 52.3.

Also here no *SN-Curves for fatigue design were generated.*
Due to good personal connections, freshly generated curves for the Deutsche Bundesbahn thankfully could be obtained from the LBF institute at Darmstadt !)

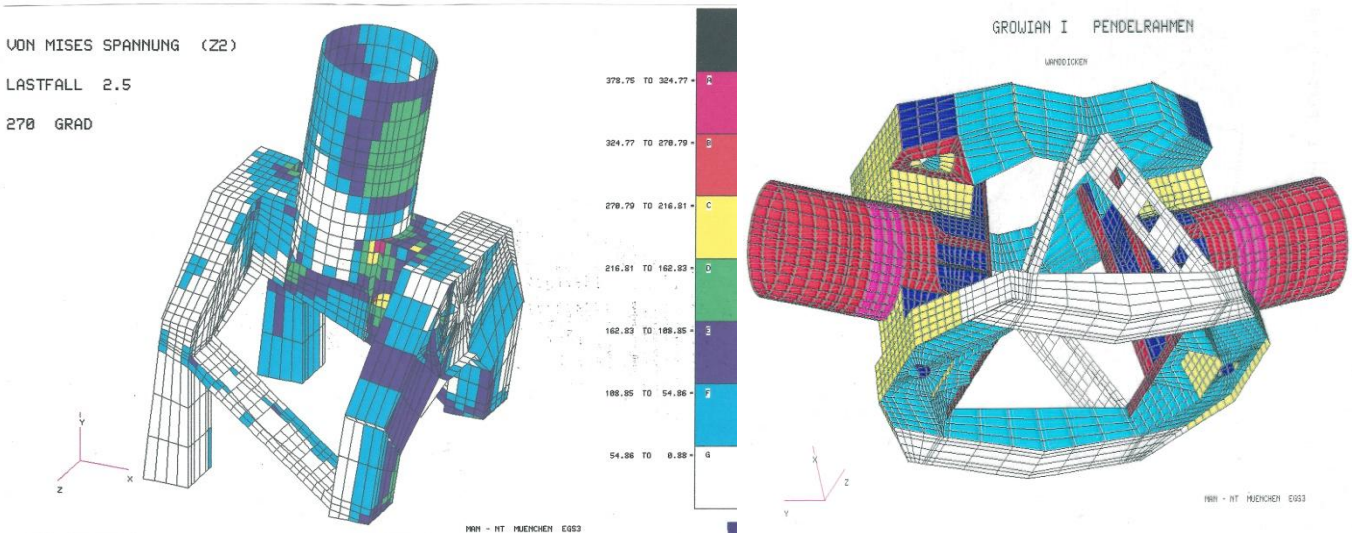

FE modellization of the hub

Josef Wein
and
'his' Evans & Sutherland PS 300

	Best.Menge	Bestelltext/Materialnummer	Gesamt Einzelpreis
A		**LEASING**	
B	2	**WB-TWO250SLD4 Indigo2 Solid IMPACT graphics, 250 MHz**	
C		**2MB cache, 128 MB Memory, 4GB System Disk, 20" Monitor**	**97888,-**
D	2	**CR-T5-NOPEN Upgrade to R10000 CPU from Indigo2**	
E		**IMPACT R4400 System**	**39976,-**
F	2	**CR-T5-NOPEN 250MHz R4400 Module, IMPACT 10000**	**-14896,-**
G	2	**CR-CPU-UPGRD Credit for Return of R4XXX based CPU**	**-4408,-**
H	2	**Vollwartung in der Gewährleistung für Indigo2**	**3000,-**
I			
J		**Gesamt: 121.560,- DM**	
K		**(Anlage: Vorabangebot von Silicon Graphics vom 04.03.96)**	
L			
M			
N			
O			
P			
Q		6.3.96	

Hardware and cost

Faserverbundwerkstoffe im Maschinenbau

MAN TECHNOLOGIE

Joints are the

essential structural parts

which make
optimum lightweight design
real

Technical data	
Volume	8200 l
Operating pressure	3 bar
Bursting pressure	6.8 bar
Wall thickness of cylindrical section	3 mm
Min. wall thickness of composite structure	1 mm
Weight	310 kg

Structural tank of ARIANE 4 for 6200 liter water in order to recool the hot gases that drive the turbopumps of th VIKING emngine

Architecture of a ceramic heat shield

C-SiC panel produced via the liquid polymer infiltration (LPI) process, as element of a capsule heat shield

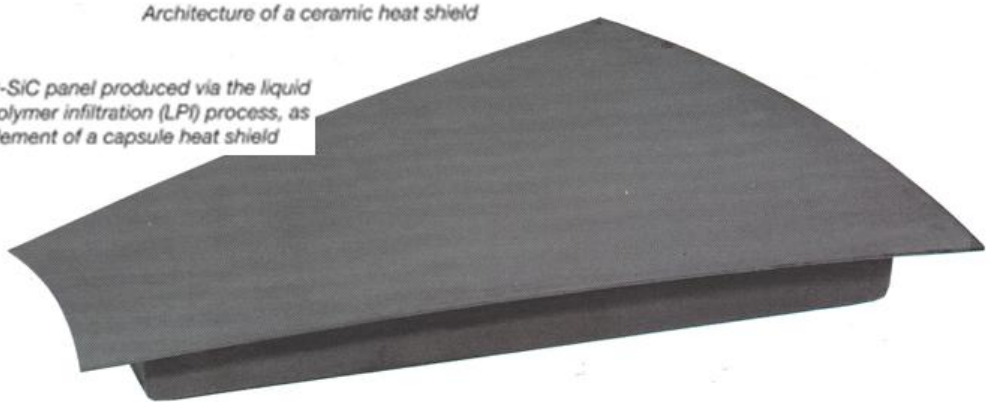

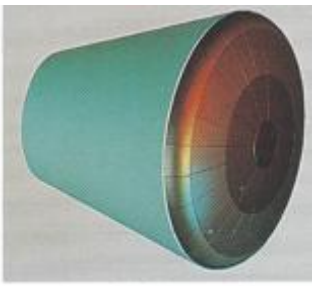

Computer model of a capsule heat shield made of C-SiC panels.

C-SiC panel, part of a re-entry heat shield

CFRP Booster section
Developed since 2001

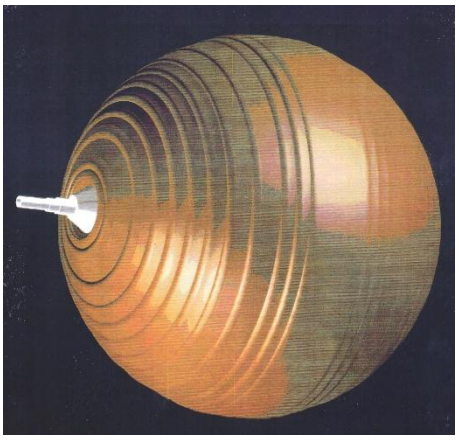

Sphere tanks since 1988.
Meteosat high pressure vessel, 8.2 kg. 1995

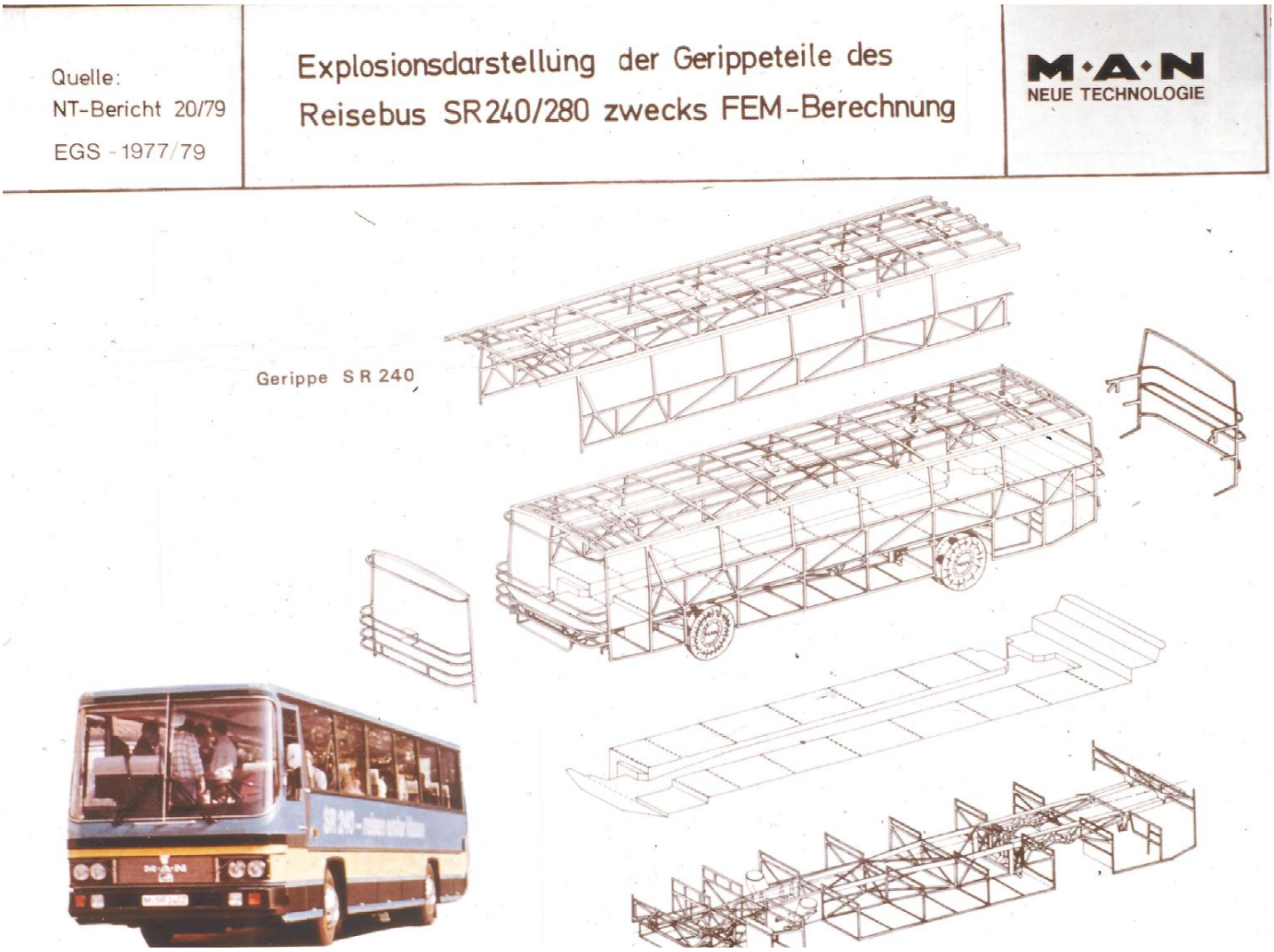

Statical FE- computation for an MAN bus

Delivery of struvtural parts

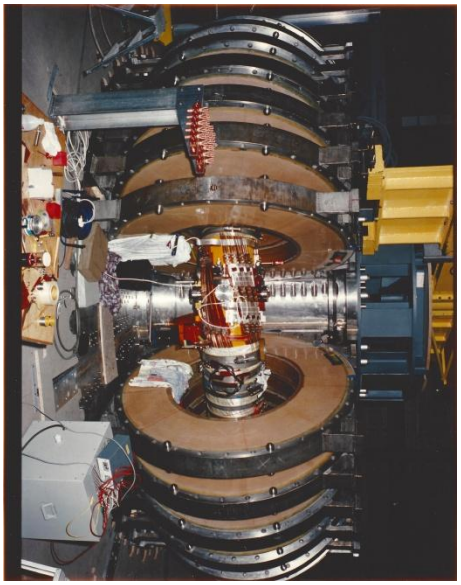

Wndelstein VII in Garching, 1975
Structural parts

Fusion reactors

The main fuels used in nuclear fusion are deuterium and tritium, both heavy isotopes of hydrogen. Deuterium constitutes a tiny fraction of natural hydrogen, only 0,0153%, and can be extracted inexpensively from seawater. Tritium can be made from lithium, which is also abundant in nature.

The amount of deuterium present in one litre of water can in theory produce as much energy as the combustion of 300 litres of oil. This means that there is enough deuterium in the oceans to meet human energy needs

In nuclear fusion 2 atoms join together to form one. In a fusion reactore hydrogen atoms come together to form helium atoms, neutrons and much energy One of the big challenges holding fusion energy back has been the ability to contain high-energy particles inside fusion reactors light atomic nuclei are compressed under intense pressure and heat to form heavier ones and release energy in the process Magnetic fields enclose the plasma so that the wall of the reactor does not melt This only works because the outermost centimetres in the magnetically formed plasma edge are extremely well insulated
150x 106 °C

Nuclear fusion, on the other hand, is based on the opposite principle. In fusion reactors, light atomic nuclei are compressed under intense pressure and heat to form heavier ones and release energy in the process. The process must be optimized to generate more energy than it consumes.

In the eighties:
MAN-T performed a Research project to establish a
Technical process for the Production of Wooden Pellets.

Biomechanical studies on bone transplantation, 1986

Medical University of Munich (Dr. med. habil. Wolfgang Stock) with
(MAN technology (Dr.-Ing. habil. Ralf Cuntze)

Project part MAN:
Development of bone load-bearing capacity by performing Modelling and CT-measurements.

The still proven concept and excellent results of Dr. Stock halved the time to use a maximum damaged leg again, after about one year, and therefore to get to work much faster
► *reduction of medical + social costs.*

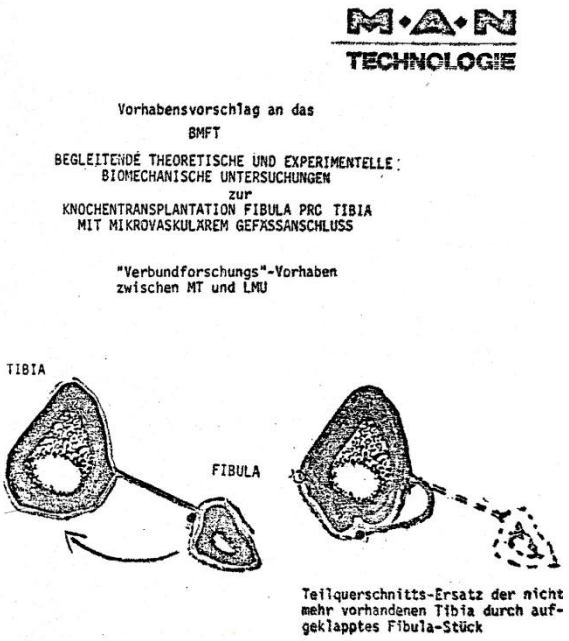

Presentation of this research idea
in a big meeting of project proposers to the DLR Project Management by Stock and me
under the Chair of an institute director of the medical university Hamburg-Binnenalster:
After Wolfgang's longer excellent presentation
I got 5 minutes for my part.
After about 2 minutes the chair tapped his watch at the other end of the very long table to say that he wants me (the only engineer in the group) to stop.
This was my most degrading experience in a meeting.

At lunch all were interested in Wolfgang's proposal. After his/our presentation there was silence.
Nothing happens.
After two years, colleagues had copied the concept and obtained the desired funding.
This was a pity for us/me because just MAN had still invested about DM 100,000 in my department.

Prosthesis

*1976 Prosthesis consisting of a CFRP stem, head, and socket. Artificial and thus foreign body parts – such as a hip joint endoprosthesis – must be compatible with the body's own tissue. Furthermore, the components must withstand the stresses of walking for as many years as possible. Otherwise, the replacement part must be replaced with a new one. The design requirements for a hip joint endoprosthesis are therefore: *Body tissue compatibility, *High surface pressure and low wear for the socket, *High bending strength of the stem, *Enabling cementless implantation. Re-growing bone material can bond, *Enabling patient-specific installation geometry.*
Stem: High-strength carbon fiber with epoxy matrix (CFRP).
Socket: Molded compound of short carbon fibers + epoxy matrix.
Ball: Ceramic ball.
Stem manufacturing: Core made of short fiber molded compound, pressed to final dimensions and cured. Angular layers on the surface wound onto a cured core using a knitting machine.
Test: Bending test of the stem. The stem clamping corresponds to the connection with the femur.
Human implantation and use: Implantation in some patients proved the implant to be a successful new alternative. However, its serial use was handicapped for various reasons, primarily because a competitor failed due to poor dimensioning,

Splar Tower and Solar Field at Almeria, Spain

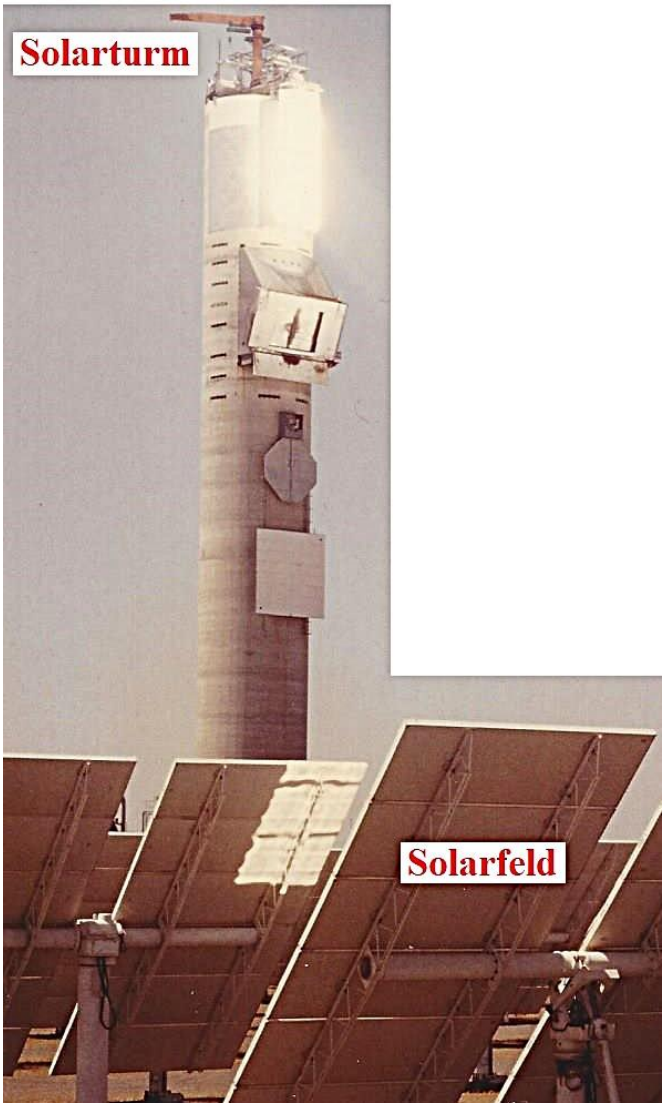

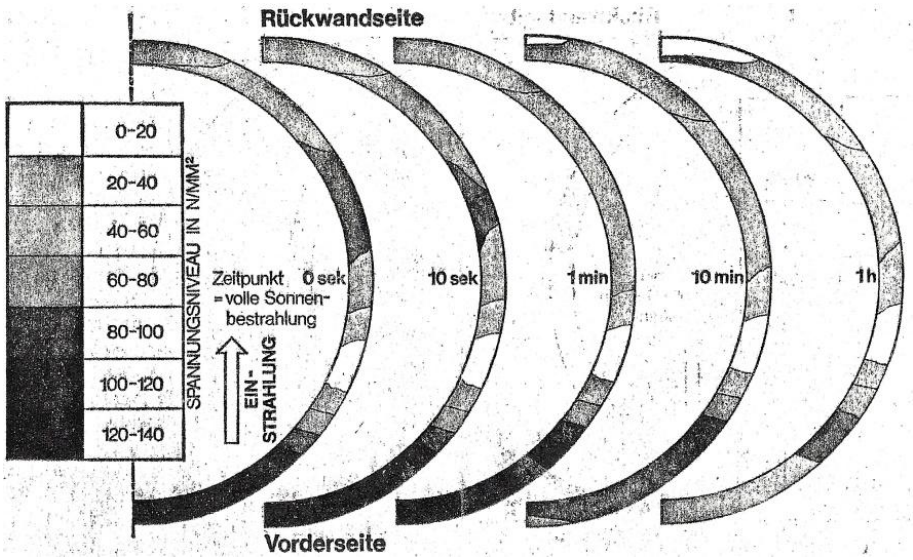

Heat Exchanger Almeria, Solar Tower

M·A·N Neue Technologie | ARBEITSAUFTRAG EGS - INTERN | Auftrags-Nr. B 099078

Beginn des Arbeitsauftrages	Ende des Arbeitsauftrages	Laufzeit des übergeordneten Projektauftrages
Datum: 12.7.	Datum:	von: bis:
Auftraggebende Stelle Abt.: Tel.: Name: Cuntze	Ausführende Stelle Abt.: Tel.: Name: Zielke	Personaleinsatz (Std.): Sachkosten (DM):
Dringlichkeit		

Werkstoff (T300) (M40) in N, mm — $\varphi = 64\,\%$

90°-Schicht: $E_{11} = 147200$; $E_{\perp} = 10500$; $G_{\#} = 5800$; $\nu = 0{,}27$; $\sigma_{11B} = 2540$; $\sigma_{\perp B} = 58$; $\tau_{\perp\#B} = 141$; $\tau_{\#B} = 93$

α-Schicht: $E_{11} = 256000$; $E_{\perp} = 9000$; $G_{\#} = 5500$; $\nu = 0{,}22$; $\sigma_{11B} = 1300$; $\sigma_{\perp B} = 33$; $\tau_{\perp\#B} = 141$; $\tau_{\#B} = 76$

Randbedingungen Zeichnungs-Nr.

$u_{max} = 0{,}8 \cdot u_{krit.\,gl.}$ $R = const = 78$ mm $t_v = 0{,}595$ mm

$= u_{max} = f(zul\ \sigma_{11}) = 800$ m/s. (1733 Hz)

Gute später $\alpha \geq 25°$ 28°, g,e

Titel: Ermittlung der Abhängigkeit der Trennleistung $\bar{T}$ von Dickenverhältnis t_α / t_{90} und verschiedenen Werkstoffpaarungen

Auszuführende Arbeiten:

0. Anpassung des vorhand. Rotordatensatzes (C6,5) an gewünschten Rotor. In Abstimmung mit H. Einmann. Festlegung der "Nicht-Trennlänge" für $L_{eff} = L_D - L_{NT}$ Berechnung. TC11 (neue Bezeichnung)

0,1 H. Sh. Prüfung Bezug MSV2 77 — 26mm Rotoptspannungen

1. Durchführung von ROTOPT-Rechnungen für folgende Werkstoffpaarungen und Parametervariationen unter näherungsweiser Berücksichtigung des Werkstoff-nichtlinearitätseinflusses bzgl. Spannungen und krit. Drehzahl γ

Axiall. $E_{11\alpha}$ / Umfangsl. $E_{11_{90}}$	256000	288000	320000
147200	① Beginn	②	③
179200	/	④	/

$E_{F_{90}} = 230000; 280000$ N/mm²

$E_{F_{25}} = 400000; 450000; 500000$ N/mm²

L_D = Abstand der Deckel-aufnahmen

4. Berechnung der bezogenen Trennleistung $\bar{T} = u^2 \cdot L_{eff}$ und zeichnerische Darstellung

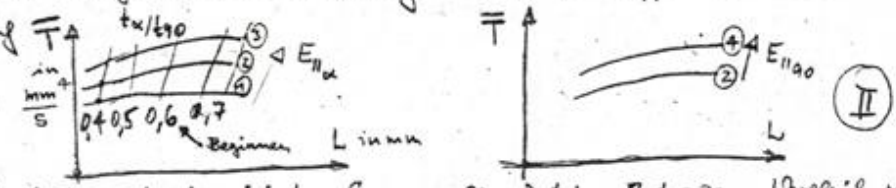

unter Berücksichtigung der korrigierten Spannungen, jetzigen Rotor zum Vergleich rechnen und eintragen (Abspräche mit Cu).

3. Tabellarische Darstellung der Maximalwerte von σ_{11K}, $\sigma_{\perp K}$, $\tau_{\#K}$ über Rotor Genaueres noch absprechen. (Da Rotopt nur orthotrop mit MSVZ zu berechnen!)

5. Auswahl der trennleistungsgünstigsten Rotore nach Festigkeits-kriterien inkl. Zwischenfaserbruchkriterium. 2. Feststellung des Werkstoffnichtlinearitätseinflusses mit ROTOPT + MSV2.

Rechengang bei den Parametervariationsläufen:

1) V_{SPEED} = 800 m/s vorgeben ; Safety = 0,80

2) L = variabel (KACND = 1 ...) ; Fall 4.1b)

Vorher neue BRK-Formel durch Wein/Hartinghausen einbauen.

Für Auftraggebende Stelle verantwortl. Name: Einmann Datum:	Bestätigungszeit Tage	Für Ausführende Stelle verantwortl. Name: Datum:	Erledigungsvermerk

Bei Unklarheiten Originale mit Cu

AV 190116 £65001

"Strukturnotiz": Formulation of a departmental work

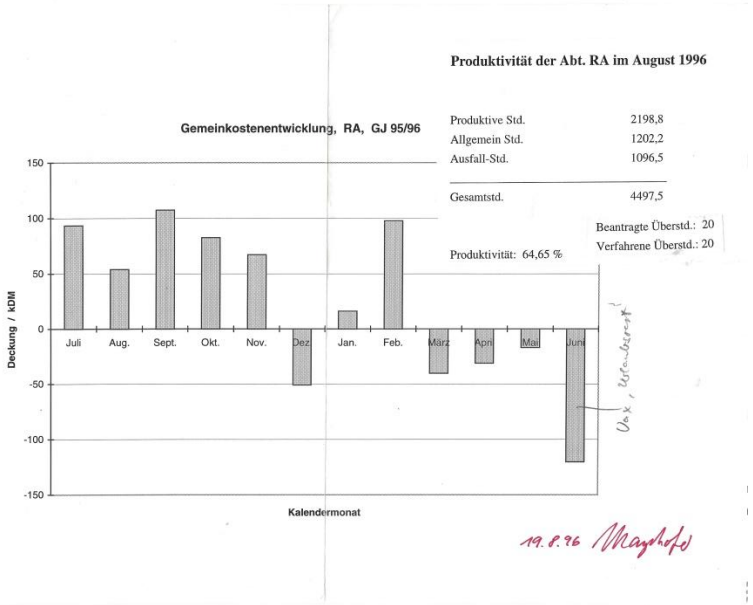

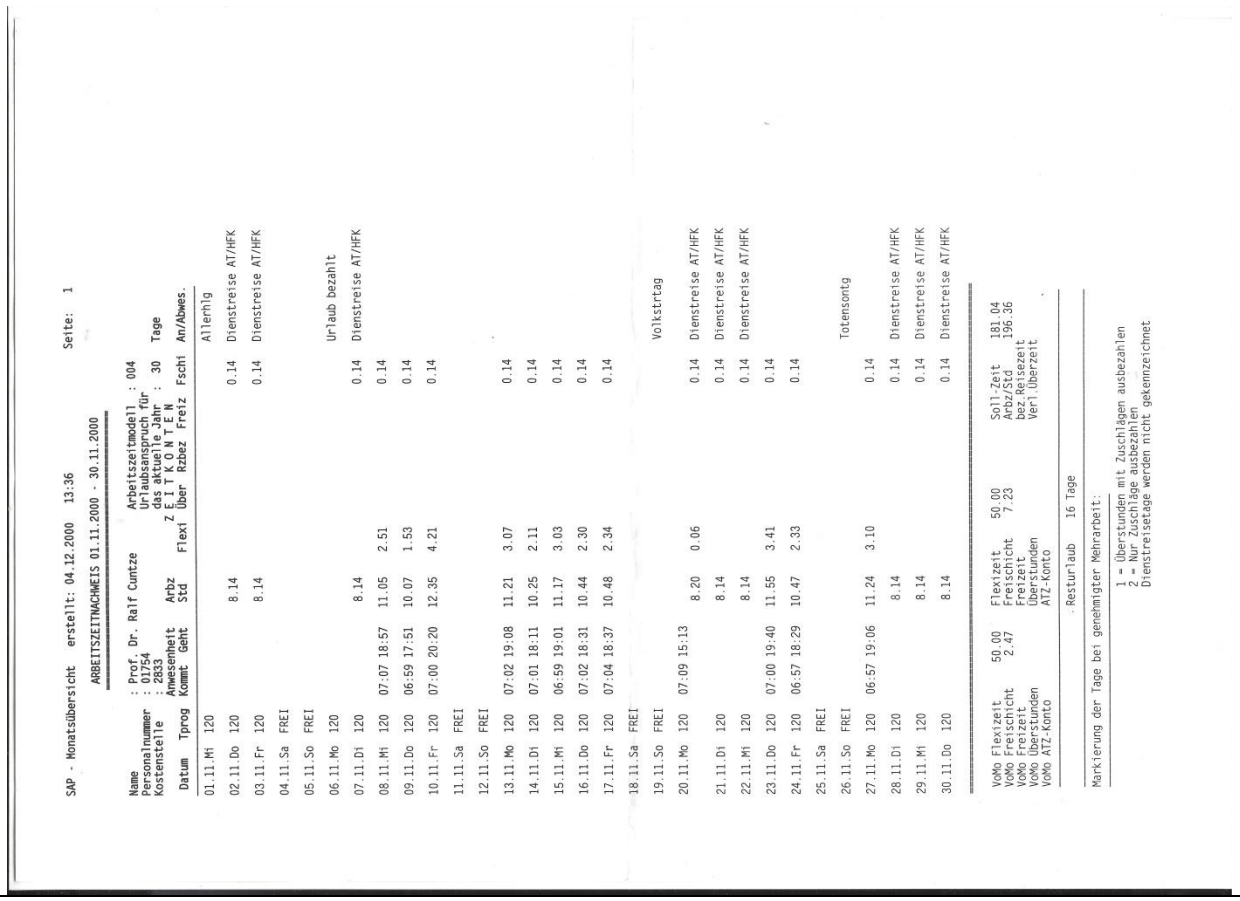

SAP - Monatsübersicht erstellt: 04.12.2000 13:36 Seite: 1

ARBEITSZEITNACHWEIS 01.11.2000 - 30.11.2000

Name : Prof. Dr. Ralf Cuntze Arbeitszeitmodell : 004
Personalnummer : 01754 Urlaubsanspruch für
Kostenstelle : 2833 das aktuelle Jahr : 30 Tage
Anwesenheit Arbz Z E I T K O N T E N
Datum Tprog Kommt Geht Std Flexi Über Rzbez Freiz Fschi An/Abwes.

Datum	Tprog	Kommt	Geht	Arbz Std	Flexi Über	Rzbez	Freiz	Fschi	An/Abwes.
01.11.Mi	120								Allerhlg
02.11.Do	120			8.14				0.14	Dienstreise AT/HFK
03.11.Fr	120			8.14				0.14	Dienstreise AT/HFK
04.11.Sa	FREI								
05.11.So	FREI								
06.11.Mo	120								Urlaub bezahlt
07.11.Di	120			8.14				0.14	Dienstreise AT/HFK
08.11.Mi	120	07:07	18:57	11.05	2.51			0.14	
09.11.Do	120	06:59	17:51	10.07	1.53			0.14	
10.11.Fr	120	07:00	20:20	12.35	4.21			0.14	
11.11.Sa	FREI								
12.11.So	FREI								
13.11.Mo	120	07:02	19:08	11.21	3.07			0.14	
14.11.Di	120	07:01	18:11	10.25	2.11			0.14	
15.11.Mi	120	06:59	19:01	11.17	3.03			0.14	
16.11.Do	120	07:02	18:31	10.44	2.30			0.14	
17.11.Fr	120	07:04	18:37	10.48	2.34			0.14	
18.11.Sa	FREI								
19.11.So	FREI								Volkstrag
20.11.Mo	120	07:09	15:13	8.20	0.06			0.14	Dienstreise AT/HFK
21.11.Di	120			8.14				0.14	Dienstreise AT/HFK
22.11.Mi	120			8.14				0.14	Dienstreise AT/HFK
23.11.Do	120	07:00	19:40	11.55	3.41			0.14	
24.11.Fr	120	06:57	18:29	10.47	2.33			0.14	
25.11.Sa	FREI								
26.11.So	FREI								Totensontg
27.11.Mo	120	06:57	19:06	11.24	3.10			0.14	
28.11.Di	120			8.14				0.14	Dienstreise AT/HFK
29.11.Mi	120			8.14				0.14	Dienstreise AT/HFK
30.11.Do	120			8.14				0.14	Dienstreise AT/HFK

VoMo Flexizeit 50.00 Flexizeit 50.00 Soll-Zeit 181.04
VoMo Freischicht 2.47 Freischicht 7.23 Arbeitszeit 196.36
VoMo Freizeit Freizeit bez Reisezeit
VoMo Überstunden Überstunden Verl.Überzeit
VoMo ATZ-Konto ATZ-Konto

Resturlaub 16 Tage

Markierung der Tage bei genehmigter Mehrarbeit:
1 = Überstunden mit Zuschlägen ausbezahlen
2 = Nur Zuschläge ausbezahlen
Dienstreisetage werden nicht gekennzeichnet

Stringent continuous check of productivity at MAN

►***Constant Life Challenge:*** *Having too many non-financed co-workers or too few to tackle financed tasks.*

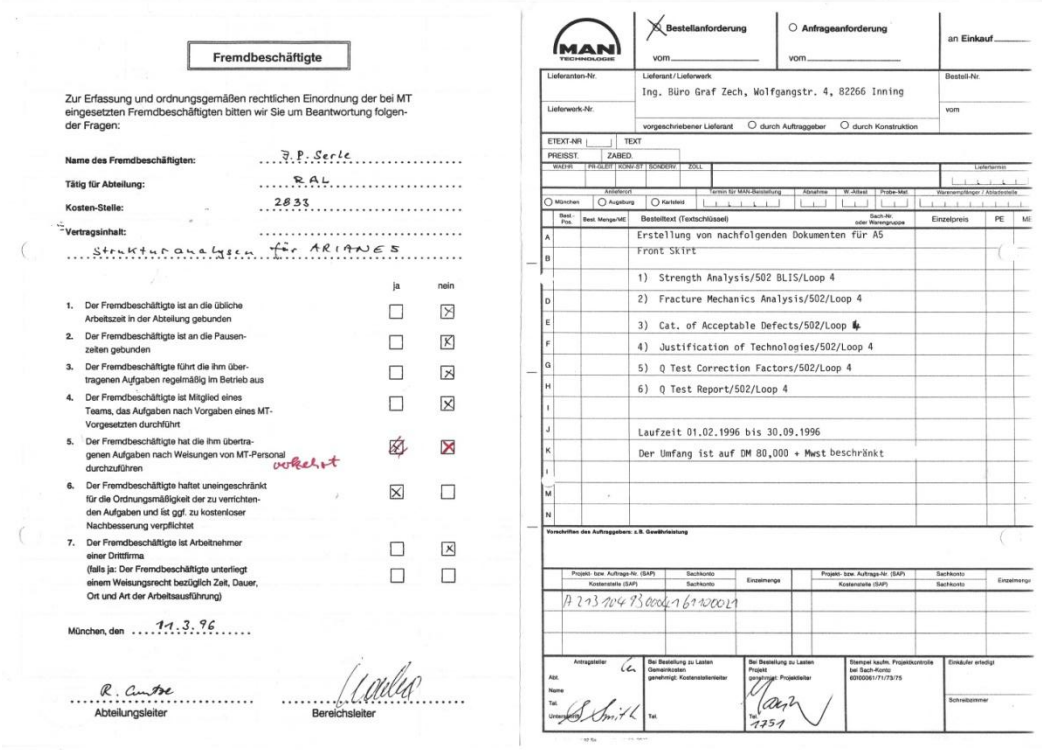

Fremdbeschäftigte

Zur Erfassung und ordnungsgemäßen rechtlichen Einordnung der bei MT eingesetzten Fremdbeschäftigten bitten wir Sie um Beantwortung folgender Fragen:

Name des Fremdbeschäftigten: J.P. Serle
Tätig für Abteilung: RAL
Kosten-Stelle: 2833
Vertragsinhalt: Strukturanalysen für ARIANE 5

		ja	nein
1.	Der Fremdbeschäftigte ist an die übliche Arbeitszeit in der Abteilung gebunden	☐	☒
2.	Der Fremdbeschäftigte ist an die Pausenzeiten gebunden	☐	☒
3.	Der Fremdbeschäftigte führt die ihm übertragenen Aufgaben regelmäßig im Betrieb aus	☐	☒
4.	Der Fremdbeschäftigte ist Mitglied eines Teams, das Aufgaben nach Vorgaben eines MT-Vorgesetzten durchführt	☐	☒
5.	Der Fremdbeschäftigte hat die ihm übertragenen Aufgaben nach Weisungen von MT-Personal durchzuführen (widerruft)	☒	☒
6.	Der Fremdbeschäftigte haftet uneingeschränkt für die Ordnungsmäßigkeit der zu verrichtenden Aufgaben und ist ggf. zu kostenloser Nachbesserung verpflichtet	☒	☐
7.	Der Fremdbeschäftigte ist Arbeitnehmer einer Drittfirma (falls ja: Der Fremdbeschäftigte unterliegt einem Weisungsrecht bezüglich Zeit, Dauer, Ort und Art der Arbeitsausführung)	☐	☒
		☐	☐

München, den 11.3.96

R. Cuntze — Abteilungsleiter
Bereichsleiter

MAN TECHNOLOGIE

☒ Bestellanforderung vom ____ ○ Anfrageanforderung vom ____ an Einkauf ____

Lieferanten-Nr. / Lieferant / Lieferwerk: Ing. Büro Graf Zech, Wolfgangstr. 4, 82266 Inning
Bestell-Nr. / vom
Lieferwerk-Nr.
vorgeschriebener Lieferant ○ durch Auftraggeber ○ durch Konstruktion

ETEXT-NR | TEXT
PREISST. | ZABED.
WÄHR | PR-GLIEF | KONF-BT | SONDERV | ZOLL | Lieferfrist

Anlieferort: ○ München ○ Augsburg ○ Karlsfeld | Termin für MAN-Bestellung | Abnahme | W.-Attest | Probe-Mat | Warenempfänger / Abladestelle

Best.-Pos.	Best. Menge/ME	Bestelltext (Textschlüssel)	Sach-Nr. oder Warengruppe	Einzelpreis	PE
A		Erstellung von nachfolgenden Dokumenten für A5 Front Skirt			
B		1) Strength Analysis/502 BLIS/Loop 4			
D		2) Fracture Mechanics Analysis/502/Loop 4			
E		3) Cat. of Acceptable Defects/502/Loop 4			
F		4) Justification of Technologies/502/Loop 4			
G		5) Q Test Correction Factors/502/Loop 4			
H		6) Q Test Report/502/Loop 4			
I					
J		Laufzeit 01.02.1996 bis 30.09.1996			
K		Der Umfang ist auf DM 80,000 + Mwst beschränkt			
L					
M					
N					

Vorschriften des Auftraggebers: z.B. Gewährleistung

Projekt- bzw. Auftrags-Nr. (SAP) / Kostenstelle (SAP)	Sachkonto / Sachkonto	Einzelmenge	Projekt- bzw. Auftrags-Nr. (SAP) / Kostenstelle (SAP)	Sachkonto / Sachkonto	Einzelmenge
A 293 204 93 0004 1 6 1 2 0 0 2 9					

Antragsteller: Abt. Name Tel. Unterschrift | Bei Bestellung zu Lasten Gemeinkosten genehmigt: Kostenstellenleiter Tel. | Bei Bestellung zu Lasten Projekt genehmigt: Projektleiter Tel. 7751 | Stempel kaufm. Projektkontrolle bei Sach-Konto 6010/0061/71/75/75 | Einkäufer erledigt Schreibzimmer

Special problems when employing Freelancers

Urlaubsantrag / Gleitzeitantrag

MAN TECHNOLOGIE | MAN Systemelektronik | MAN Dezentrale Energiesysteme

1754 | Dr. Ralf Cuntze | 2833 | RA
Pers.-Nr. | Name | Kostenstelle | Abtlg.

Urlaubsguthaben in Arbeitstagen:
Stand 01.01.1998
Resturlaub Vorjahr : 11,00
Urlaubsanspruch lfd.: 30,00
Insgesamt : 41,00

Bearbeitungsweg → Sekretariat/Vorgesetzter → Gleitzeitbeauftragte zum Verbleib

Abwesenheitsart	von	bis	Anzahl Tage	Rest-Tage	Datum	Unterschrift Mitarbeiter	Unterschrift Vorgesetzter
TU	16.2.98	22.2.98	40	32	14.1.98		
TU	6.7.98	28.7.98	15	17	19.7.98		
	20.2. abgelehnt						
	15.5.98		1	16	11.7.98		
	7+8.7.	Gleitzeit	18		1. GL-Antrag		
	6/8/10.7	Gleitzeit	27		3. GL-Antrag		

00 = ABBAU GLEITZEIT TAG/STD.; 0910 = FREIZEITAUSGLEICH FÜR MEHRARBEIT TAG/STD.

PERS.-NR. NAME: Cuntze

Abwesenheitsart	von Tag (Uhrzeit)	bis Tag (Uhrzeit)	Anzahl Tage	Datum	Unterschrift Mitarbeiter	Unterschrift Vorgesetzter
GC	26.5.	27.5. (Überstg. 8.5. genehmigt, 8h-Tag)	2	27.5.97	Cuntze	
GL	14.7.97	18.7.97 (KORRIGIERT conforma)	5	11.7.97	Cuntze	

Hinweis zur Beachtung: Gem. § 7 Abs. 3 Satz 1 BUrlG muß der Urlaub im laufenden Kalenderjahr gewährt und genommen werden. Der Jahresurlaub ist deswegen im Grundsatz bis zum 31. 12. des laufenden Kalenderjahres abzuwickeln.

0100 = Urlaub, 0900 = Gleitzeitabbau, 0910 = Freizeitabbau

Form ...

Blatt 2

Urlaubsantrag / Gleitzeitantrag

MAN TECHNOLOGIE | MAN Systemelektronik | MAN Dezentrale Energiesysteme

1754 | Dr. Ralf Cuntze | 2833 | RA
Pers.-Nr. | Name | Kostenstelle | Abtlg.

Urlaubsguthaben in Arbeitstagen:
Stand 01.01.1998
Resturlaub Vorjahr :
Urlaubsanspruch lfd.:
Insgesamt :

Bearbeitungsweg → Sekretariat/Vorgesetzter → Gleitzeitbeauftragte zum Verbleib

Abwesenheitsart	von	bis	Anzahl Tage	Rest-Tage	Datum	Unterschrift Mitarbeiter	Unterschrift Vorgesetzter
0300	22.4.98	24.4.98	5		15.4.98	Cuntze	
	(Reise Hamburg MCM'98, Vortrag)						
	19.6.98		1		27.5.98	Cuntze	
	(Vortrag auf dem Breslauer Luftfahrtsymposium 98)						
	7.7.98	8.7.98	2		23.5.98		
	(Vortrag und Chairmanship auf der ICAF 15)						
	6.9.-9.9.		5		28.7.98		
	(Vortrag auf der Konferenz für die Sowjetunion)						

Hinweis zur Beachtung: Gem. § 7 Abs. 3 Satz 1 BUrlG muß der Urlaub im laufenden Kalenderjahr gewährt und genommen werden. Der Jahresurlaub ist deswegen im Grundsatz bis zum 31. 12. des laufenden Kalenderjahres abzuwickeln.

0100 = Urlaub, 0900 = Gleitzeitabbau, 0910 = Freizeitabbau

Form ...

Overtime-Balancing *of my time outside of MAN for conference memberships and presentations*

Pflichtvorlesung Konstruktiver Ing.bau
an der Hochschule der Bundeswehr, München.

1980-1983

EINFÖHRUNG
IN DIE
BRUCHMECHANIK

GLIEDERUNG

EINFÜHRUNG

1. DEFINITION
2. KONTINUUMSMECHANISCHE GRUNDLAGEN
3. KLASSISCHE BRUCHMECHANIK IDEAL SPRÖDER KÖRPER
4. LINEAR ELASTISCHE BRUCHMECHANIK (LEBM)
5. FLIESSBRUCHMECHANIK
6. STABILES RISSWACHSTUM
7. EXPERIMENTELLE METHODEN
8. VERSCHIEDENES

1. DEFINITIONEN UND ZIELE DER BRUCHMECHANIK

1.1 WAS IST EIN BRUCH?
1.2 BRUCHTYPEN
1.3 EINTEILUNG DER BRÜCHE NACH AUSSEHEN DER BRUCHFLÄCHEN
1.4 ZUR RIßENTSTEHUNG UND -AUSBREITUNG
1.5 TECHNISCHE BRUCHMECHANIK

2. KONTINUUMSMECHANISCHE GRUNDLAGE

2.1 EINIGE ELASTIZITÄTSTHEORETISCHE BEGRIFFE
2.2 LÖSUNGSMETHODEN DES LINEAREN ELASTIZITÄTSPROBLEMS
2.3 ELLIPTISCH GELOCHTE, UNENDLICH AUSGEDEHNTE SCHEIBE UNTER ZUG
  2.3.1 EXAKTE LÖSUNG DES SPANNUNGSFELDES MIT HILFE DER KOMPLEXEN SPANNUNGSFUNKTIONEN
  2.3.2 SPANNUNGSERHÖHUNGEN AM LOCH UNTER EIN- UND ZWEIACHSIGER ZUGBELASTUNG
2.4 EINZELRIß IN EINER UNENDLICH AUSGEDEHNTEN SCHEIBE (GRIFFITH-RIß) UNTER ZUGBELASTUNG
  2.4.1 SPANNUNGSFELD IN DER UMGEBUNG DES EINZELRISSES
  2.4.2 VERSCHIEBUNG DER RIßRÄNDER UNTER EIN- U. ZWEIACHSIGER ZUGBELASTUNG
2.5 NÄHERUNGSWEISE LÖSUNG DES VOLLSTÄNDIGEN ELASTIZITÄTSPROBLEMS AN EINEM GRIFFITH-RIß
  2.5.1 HERLEITUNG DES SPANNUNGSFELDES UNTER EINACHSIGER ZUGBELASTUNG IN Y-RICHTUNG
  2.5.2 SPANNUNGS- UND VERSCHIEBUNGSFELD IN UNMITTELBARER UMGEBUNG DER SPITZE EINES GRIFFITH-RISSES ($r \ll a$)
2.6 EINFÜHRUNG DER SPANNUNGSINTENSITÄTSFAKTOREN FÜR DIE 3 GRUNDLEGENDEN RIßÖFFNUNGSARTEN
2.7 ZUSAMMENHANG SPANNUNGSINTENSITÄTSFAKTOREN K_i - SPANNUNGSKONZENTRATIONSFAKTOREN (KERBFAKTOREN) α_k

3. KLASSISCHE BRUCHMECHANIK IDEAL SPRÖDER KÖRPER

3.1 THEORIE VON GRIFFITH
3.2 OBERFLÄCHENENERGIE UND THEORETISCHE FESTIGKEIT FESTER KÖRPER
3.3 ELASTISCHE ENERGIE EINER SCHEIBE MIT RIß (GRIFFITH-RIß)
3.4 ANWENDUNG DES BRUCHKRITERIUMS VON GRIFFITH AUF EINE SCHEIBE MIT GRIFFITH-RIß UNTER EINACHSIGEM ZUG.
3.5 EXPERIMENTELLE BESTÄTIGUNG (GLASSCHEIBE)

4. LINEAR ELASTISCHE BRUCHMECHANIK (LEBM)

4.1 ÖRTLICHE BRUCHBEDINGUNG AN DER RIßSPITZE
4.2 RIßAUSBREITUNGSKRAFT (ENERGIEFREISETZUNGSRATE)
4.3 BRUCHKRITERIUM DER LEBM
4.4 EINFLUßGRÖßEN AUF DIE KRITISCHE SPANNUNGSINTENSITÄT (BRUCHZÄHIGKEIT)
4.5 BERÜCKSICHTIGUNG DER PLASTISCHEN ZONE
4.6 AUFGABEN DER LEBM

5. FLIESSBRUCHMECHANIK

5.1 GÜLTIGKEITSGRENZEN DER LEBM
5.2 DAS J-INTEGRAL
5.3 DAS COD-KONZEPT

6.1 ALLGEMEINES

6.2 SCHWINGBEANSPRUCHUNG (ERMÜDUNGSRISSAUSBREITUNG)
  6.2.1 RISSFORTSCHRITTSBEZIEHUNGEN
  6.2.2 EINFLUSSGRÖSSEN

6.3 MONOTON ANSTEIGENDE BEANSPRUCHUNG

6.4 ZEITABHÄNGIGE VORGÄNGE
  6.4.1 KORROSION
  6.4.2 KRIECHEN

6.5 ÜBERLAGERUNG VON MECHANISCHER ERMÜDUNGSRISSAUSBREITUNG UND ZEITABHÄNGIGEN VORGÄNGEN
  6.5.1 SCHWINGUNGSKORROSION
  6.5.2 ERMÜDUNGSRISSAUSBREITUNG MIT ÜBERLAGERTER SPANNUNGSRISSKORROSION
  6.5.3 KRIECHEN

7. EXPERIMENTELLE METHODEN

7.1 PRÜFMETHODEN UND PROBENFORMEN
7.2 ERMITTLUNG DER BRUCHMECHANIKKENNWERTE
7.2.1 K_{IC}-WERT
7.2.2 "R-KURVE"
7.2.3 KRITISCHES COD (δ)
7.2.4 KRITISCHES J-INTEGRAL
7.2.5 KORREKTURFUNKTION
7.2.6 RISSFORTSCHRITTSGESCHWINDIGKEIT
7.3 BESTIMMUNG DER ÄQUIVALENTEN FEHLERGRÖSSE
7.4 ÜBERTRAGBARKEIT DER PROBENERGEBNISSE AUF DAS BAUTEIL

Lecture on Fracture Mechanics at the German 'University of the Bundeswehr', München

M·A·N
NEUE TECHNOLOGIE

Protokoll der 1. Sitzung des FKV-Diskussionskreises am 6.12.83 bei der Fa. MAN-Neue Technologie, München

1. Anwesende Diskussionskreis-Mitglieder

Herren Prof. Ahrendts
Dr. Bansemir
Bessler
Buchs
Dr. Cuntze
Prof. Einsfeld
Dr. Geier
Prof. Giencke
Lutz
Prof. Moser
Prof. Puck
Dr. Rother
Dr. D. Schütz
Dr. Schulte
Dr. Stellbrink
Dr. Wurtinger

Die Anwesenden danken Herrn Krawinkel für die Einladung und das Nikolausgeschenk des VDI.

2. Kurzvorträge

Die Vorträge wurden bis auf den Beitrag Lutz/Moser "Sicherheitskonzept" gehalten. Der aus Zeitgründen entfallende Beitrag liegt als Anlage dem Protokoll bei.

3. Vorstellungen zum Thema Diskussionskreis

Die Nützlichkeit eines derartigen Diskussionspodiums wurde allgemein betont.

Als zeitlichen Abstand zwischen Zusammenkünften könnte ein Jahr vorgesehen werden.

Table of contents of my main scientific works

1 **Creation of the 'Failure Mode Concept'** (FMC, 1995) 84

2 ***Interaction of Stresses*** **by the application of Strength Failure Criteria** 87

3 **Material Symmetry and 'Generic' Number** *(material inherent?)* 88

4 **Direct use of a Friction Value μ in the SFCs of Isotropic and UD materials** 89

5 **Material stressing effort *Eff*** 91

6 **So-called 'Global' SFCs and (failure mode-linked) 'Modal' SFCs, Mode-interaction** 92

7 **Collection of Derived SFCs, Interaction of Failure Modes and a Multi-fold Mode** 94

8 **Cracking at statically-loaded Notches using FM and Finite Fracture Mechanics (FFM)** 100

9 **'Curiosities' in Material Mechanics 'Normal Yielding' and 'Compressive Fracture Toughness'** 128

10 **Automated Generation of Constant Fatigue Life curves considering Mean Stress Effect** 132

11 **Evidencing 120°-symmetrical Failure Bodies of Brittle and Ductile Isotropic Materials** 139

12 **Completion of the Strength Mechanics Building** 145

13 **Safety Concept in Structural Engineering Disciplines** 146

14 **Nonlinear Stress-Strain relationships, Beltrami Theory with Change of Poisson's Ratio ν** 154

15 **A measurable parameters'-based 'Extended-Mises' Model instead of a 'Gurson' Model?** 165

16 **Note on Continuum (micro-)Damage Mechanics (CDM)** 180

17 **Multi-scale Structural modelling with the concern Material Modelling and some Analysis** 188

18 **Some Lessons Learned from Testing and from Evaluation of Test Results** 194

19 **2D-Laminate Design: Determination of Tsai's 'Omni principal FPF strain failure envelopes** 202

20 **Note on Criticality of Fiber Micro-Fragments and Dusts of CFR-P**lastic/**CFR-C**oncrete 209

21 **A novel Determination of the Residual Strength *R*res, non-cracked, Fatigue Phase 2** 215

22 **Full UD-Mohr Envelope $\tau_{nt}(\sigma_n)$, Derivation of $\Theta_{fp}(\sigma_n)$ and of Cohesive shear Strength** 220

23 **Replacing fictitious UD Model Parameters $a_{\perp\perp}, a_{\perp\shortparallel}$ by measurable Friction Values μ** 227

24 **Fracture Envelopes and Bodies of Grey Cast Iron, Glass C90, Normal Concrete, UHPC, Foam** 231

25 **Improved Mohr-Coulomb Curve and Cohesive shear Strength R^{τ} of Isotropic materials** 248

26 **Mapping 3D Test Results of Concrete and Rocks obtained on the Meridians TM and CM** 263

27 **UD-Strength Failure criteria: Which one should I take?** 277

28 **Technical Terms, Laminate Description, Material Stressing Effort *Eff*** 287

29 **Miscelleaneous** 294

30 **Glossary Book, Contributions to Handbooks, Guidelines, Courses, etc** 299

31 **References, Cuntze since 2000 and Acknowledgement** 336

32 Affiliations, professionally and privately 370

33 Documenting Hobbies: Globetrotter, Hiking, Photography, Sparrows & Alpine-cyclamen 'Breeding' 415

Of course, the text content in the scientific chapters would have deserved a revision and harmonization, but the author hopes to become 86 this year.

Foreword

This work is also widely *AI*-based,
but here with the meaning
***based on* hopefully some**
***A*stonishing *I*deas.**

Generative Deep Learning was always necessary.

Findings of the author during his long-lasting Private Research Activities

Novel simulation-driven product development shifts the role of physical testing to virtual testing, to simulation, respectively. This requires High Fidelity and therefore the use of reliable material models. *Simulation means: Imitation of the operation of a real-world process and model adaption due to test information by performing many analyses.*

Basic desire of the macro-scopically working structural engineer is a material model linked to an ideally homogeneous material which might be isotropic or anisotropic. Connecting desire is: Be provided with a clear Strength Mechanics Building in order to get a cost-saving basis due to only analyze and test what is really physically necessary.

For the 3D-Demonstration of Strength are required - *nowadays practically a must regarding the usual 3D FEA stress output* – validated 3D Strength Failure Criteria (SFC) rendered by 3D failure bodies to firstly perform Design Dimensioning and to finally achieve Design Verification. All this is targeted in the following elaboration.

Pre-information on the basic focus here, UD material:

* The following figure displays some of the different strengthening fibers applied in construction, and a comparison of a standard Carbon Fiber with a human hair.

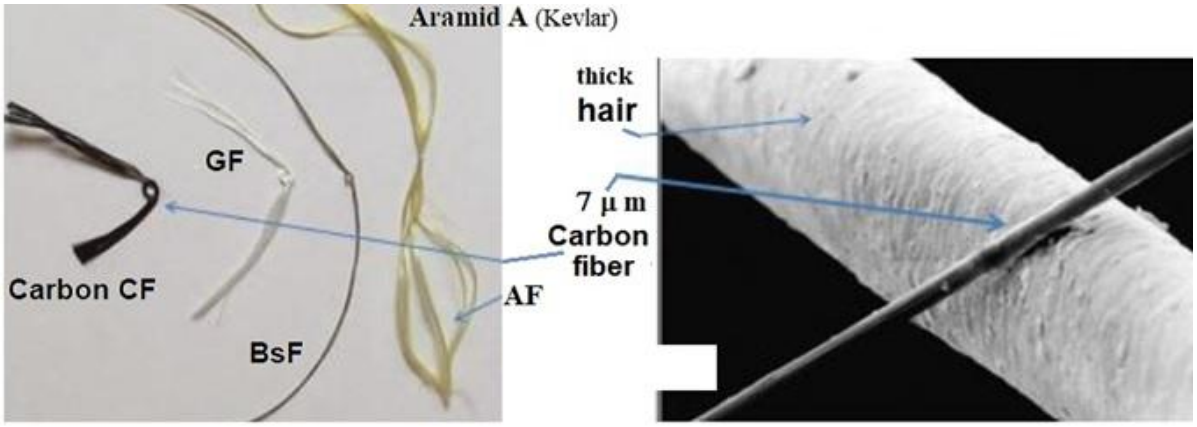

Glass GF (AR glass= alcali-resistant in concrete) **Basalt BsF** (alcali-resistant in concrete by ZrO_2)

* And the next figure shall provide for the applied stringent failure mode thinking the observed 5 failure modes faced with Uni-directional fiber-reinforced materials.

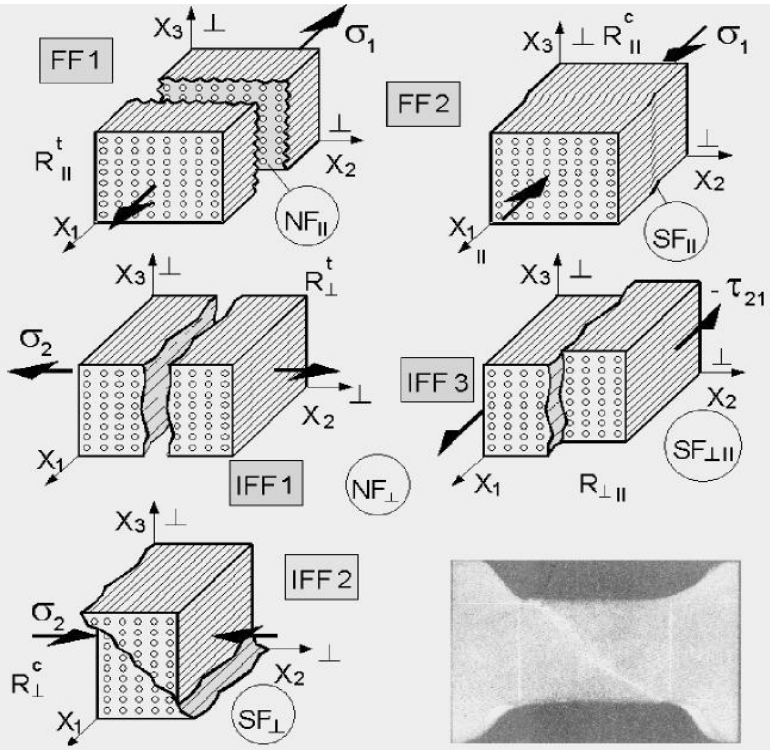

In the above context:

Two basic features are faced by the structure-designing engineers, three types of surfaces

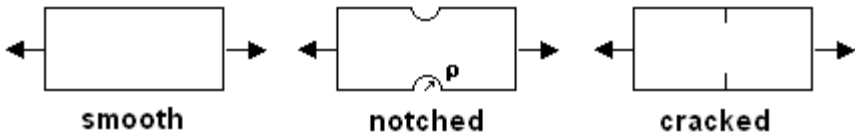

and the behavior of the material, whether it is brittle (about $R^c > \approx 3 \cdot R^t$) or ductile.

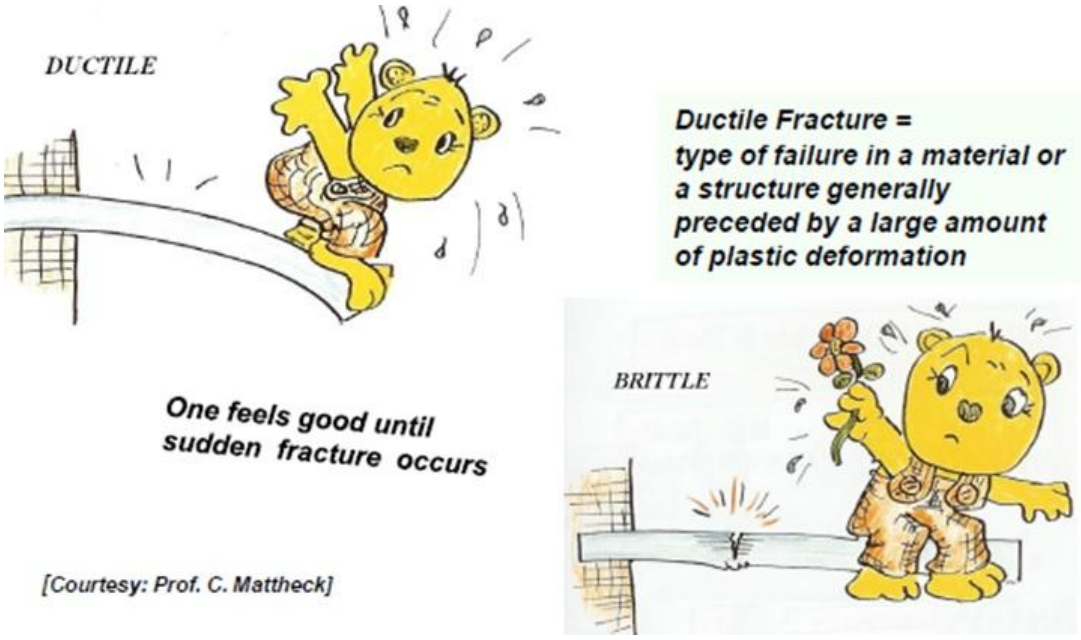

► Basic focus here: ***Smooth type structural parts***.

1 Creation of the 'Failure Mode Concept' (FMC, 1995)

***Aim**: Creation of a Static & Cyclic Strength Mechanics Building as basis for all material and of practical, physically-based SFCs.*

Being since 1970 in the industrial composite business the author tried to firstly sort out in regular discussions with Alfred Puck applicable SFCs for UD materials. Puck developed in 1990 his Hashin-based Action-plane Inter-Failure-Failure SFC which was included in 2006 into the VDI 2014 guideline, sheet 3 (editor *R. Cuntze*).
Working with practically all material types the author was encouraged to find a Concept for all the material families isotropic, UD and further orthotropic ones including dense with porous materials.

The finally developed so-called Failure-Mode-Concept (FMC) incorporates a rigorous thinking in failure modes and can be briefly described by the FMC features, derived about 1995, which were the basis for the development of Cuntze's macro-mechanical SFCs:

- Each failure mode represents 1 independent failure mechanism and thereby represents 1 piece of the complete failure surface.
- A failure mechanism at the lower micro-scopic mode level shall be considered in the applied desired macro-scopic SFC
- Each failure mechanism or mode is governed by 1 basic strength R, only (witnessed!)
- Each failure mode can be represented by 1 SFC.

This further includes:

* Failure mode-wise mapping,
* Stress invariant's-based formulation,
* Equivalent stress generation,
* Each neat failure mode is governed by just one strength R^{mode}, witnessed for ductile and brittle materials, and
* All SFC model parameters are measurable entities! Each SFC represents a failure surface, therefore for the originator the FMC will be the foundation upon which he physically based SFCs generated.

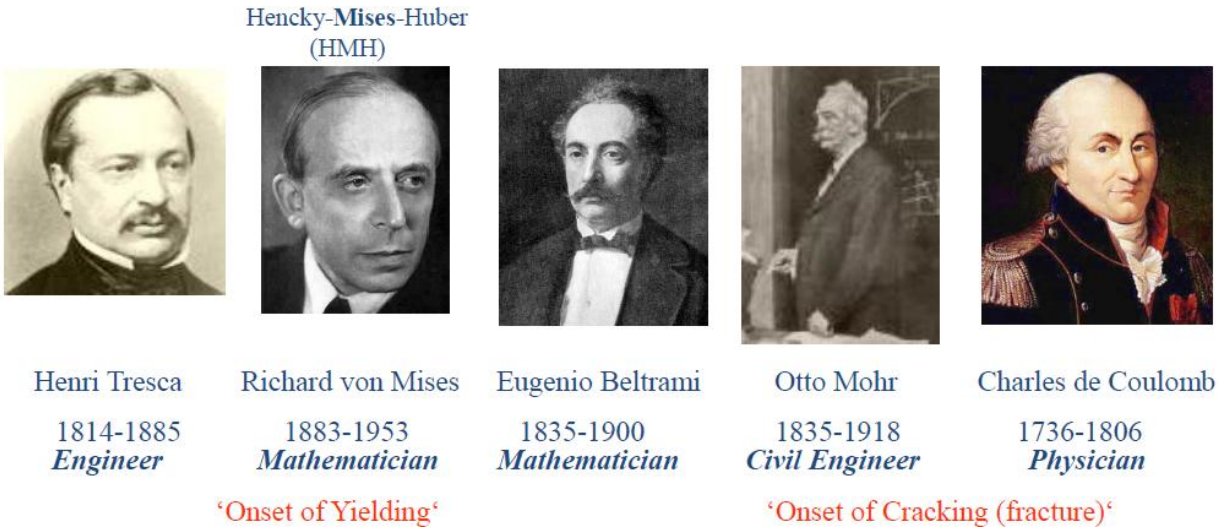

Fig.1-1: Some pioneers which set up strength failure hypotheses (ductile, brittle)

In the case of brittle materials the failure surface is the surface of a fracture failure body. Such a surface is determined by the peaks or ends of all failure stress vectors. The surface is mathematically defined by a Failure function *F,* which becomes 1 at 'Onset-of-Failure'. $F = 1$ is the formulation of the SFC (*mathematically, we write a condition*). Fig.1-1 above presents the pioneers in the isotropic SFC field.

The author's idea was to create physically-based SFCs and to note his Lessons Learned *LL* during the elaboration. The FMC was originally derived for UD materials because there was the big demand at that time. The employed stress invariants shall be presented via isotropic knowledge:

Beltrami, Schleicher et al. assumed at initiation of yield that the strain energy (denoted by *W*) in a solid cubic element of a material will consist of two portions:

$$W = \int\{\sigma\}\{\varepsilon\}\,d\{\varepsilon\} = W_{Vol} + W_{shape} \quad \text{with} \quad \{\sigma\}=(\sigma_1,\sigma_2,\sigma_3,\tau_{23},\tau_{13},\tau_{12})^T .$$

Including Hooke's law in the case of a ***transversely-isotropic*** (UD solid) the expression will take the form, using s_{ik} := compliance coefficients, E:=elasticity modulus, ν:=Poisson's ratio,

$$W = [s_{11}\cdot\sigma_1^2 + s_{22}\cdot\sigma_2^2 + s_{33}\cdot\sigma_3^2 + s_{44}\cdot\tau_{23}^2 + s_{55}\cdot(\tau_{12}^2 + \tau_{13}^2)] / 2 + s_{12}\cdot(\sigma_1\sigma_2 + \sigma_1\sigma_3) + s_{23}\cdot\sigma_2$$

$$\sigma_3 = \underbrace{\frac{I_1^2}{2\cdot E_{\parallel}}}_{\text{volume}} + \underbrace{\frac{I_2^2\cdot(1-\nu_{\perp\perp})}{4\cdot E_{\perp}}}_{\text{volume}} - \underbrace{\frac{\nu_{\perp\parallel}\cdot I_1\cdot I_2}{E_{\parallel}}}_{\text{volume}} + \underbrace{\frac{I_3}{2\cdot G_{\parallel\perp}}}_{\text{shape}} + \underbrace{\frac{I_4\cdot(1+\nu_{\perp\perp})}{4\cdot E_{\perp}}}_{\text{shape}} .$$

with the invariants $I_1 = \sigma_1,\ I_2 = \sigma_2 + \sigma_3$; $I_3 = \tau_{31}^2 + \tau_{21}^2$; $I_4 = (\sigma_2-\sigma_3)^2 + 4\tau_{23}^2$;

$I_5 = (\sigma_2 - \sigma_3)(\tau_{31}^2 - \tau_{21}^2) - 4\tau_{23}\tau_{31}\tau_{21}$.

In the ***isotropic*** case analogously follows, however simpler,

$$W = \underbrace{\left[\frac{1-2\nu}{3} I_1^{iso\,2}\right]}_{\text{volume}} + \underbrace{\frac{2+2\nu}{3} 3J_2^{iso}}_{\text{shape}} \Big] / 2E$$

with $I_1^{iso} = \underline{f(\sigma)} = \sigma_I + \sigma_{II} + \sigma_{III}$, $6\cdot J_2^{iso} = \underline{f(\tau)} = (\sigma_I - \sigma_{II})^2 + (\sigma_{II} - \sigma_{III})^2 + (\sigma_{III} - \sigma_I)^2$,

It is known, both portions in the bracket above are used to formulate a failure function

$$F = \underbrace{c_1\cdot\frac{(1-2\nu)\cdot I_1^{iso\,2}}{3\bar{R}^2}}_{\text{volume}} + \underbrace{c_2\cdot\frac{(2+2\nu)\cdot 3J_2^{iso}}{3\bar{R}^2}}_{\text{shape}} .$$

Cited, for us, for me especially :

: ***"All things are difficult before they are easy".*** Tomas Fuller (1608-1661)

Fig. 1-2 below displays for the 2 material families a physically-based choice of invariants:

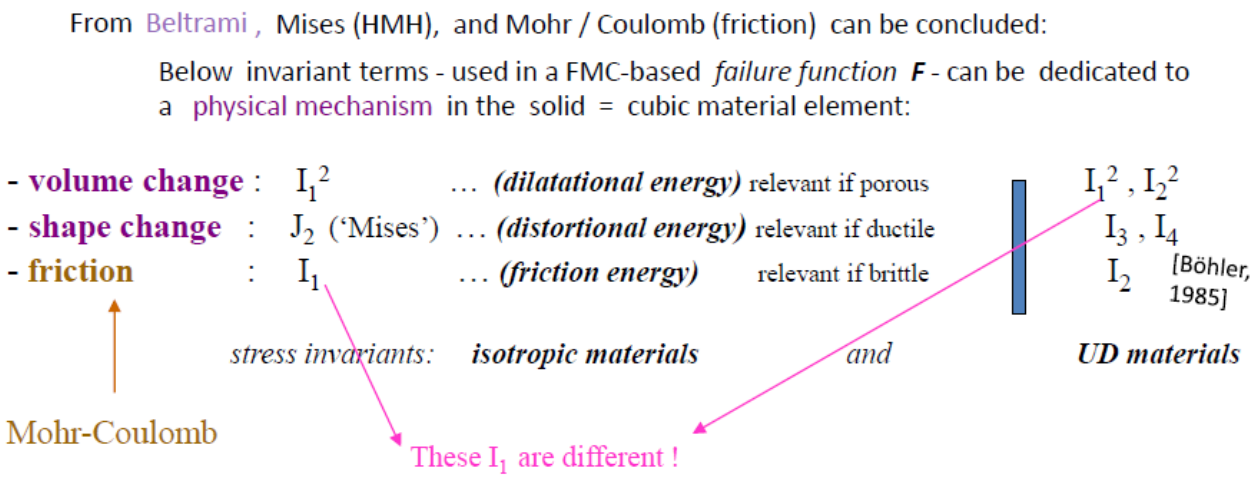

Fig.1-2: Reasons for choosing invariants when creating FMC-based SFCs

Exemplarily, the isotropic SFC model, spanning up the fracture body in the compression domain, shall be used for demonstration. The complete SFC reads:

$$\text{Shear Fracture SF, } I_1 < 0: \quad F^{SF} = F^{\tau} = c_1 \cdot \frac{6 \cdot J_2}{2 \cdot \bar{R}^{c2}} \cdot \Theta^{\tau} + c_2 \cdot \frac{I_1}{\bar{R}^{c}} + c_3 \cdot \left(\frac{I_1}{\bar{R}^{c}} \right)^2 .$$

Herein, the first part of the SFC represents the shape change, the second the friction effect, the third the volume change and the non-circularity parameter Θ^{τ} describing the inherent, nevertheless often not known 120°-symmetry of the failure bodies of isotropic brittle and ductile material, too (see a later chapter).

Above invariants can be formulated in 3D structural component stresses, in principal stresses and in Mohr stresses, which will become essential when deriving a stress state-caused fracture angle and the so-called cohesive strength.

Note, please: Strength notations

R means strength (resistance) in general and further Strength Design Allowable used for Design Verification. $\bar{R}$ means average strength used for modelling, mapping of the course of test data.

***LL**: Similarly behaving materials possess the same shape of a fracture body, when using the same SFC!*

Dr. Reinhart (Uni Bw): zur FMC.-Idee am 16.8.1995:
„Besser als andere Kriterien, man muss den Invariantenweg nur richtig gehen".

Someone said:

"Research =Transformation of Money to Knowledge and Innovation =Transformation of Knowledge to Money".

This is hopefully valid for non-finded research, too!

2 *Interaction of Stresses* by the application of Strength Failure Criteria

***Aim**: Provision of a failure mode-based stress-interaction ('Modal') and not a mathematical global one.*

The derivation of the FMC-based SFCs builds up on the hypotheses of Beltrami, Hencky-Mises-Huber (HMH) and Mohr-Coulomb. Therefore the depicted SFC approaches consider, that the solid material element may experience, generated from different energy portions, a shape change (HMH), a volume change and friction. FMC-based SFCs will be given for a large variety of isotropic brittle structural materials such as porous Concrete Stone, Normal Concrete, UHPC sandstone, monolithic ceramics and for the transversely-isotropic fiber-reinforced polymers Lamina (ply, lamella) and finally orthotropic fabrics inclusively fabric ceramics, see [*CUN22, Cun23a,24b*].

Since two decades the author believes in a macroscopically-phenomenological 'complete classification' system, where all strength failure types are included, see the figure below. In his assumed system several relationships may be recognized: (1) Shear stress yielding SY, followed by Shear fracture SF considering 'dense' materials. For porous materials under compression, the SF for dense materials is replaced by Crushing Fracture CrF. (2) In order to complete a mechanical system beside SY also NY should exist. This could be demonstrated by PMMA (plexiglass) with its chain-based texture showing NY due to crazing failure under tension and SY in the compression domain, [see *subsection 9.1 or CUN22,§4.1*]. The right side of the scheme outlines that a full similarity of the 'simpler' isotropic materials with the transversely-isotropic UD materials exists.

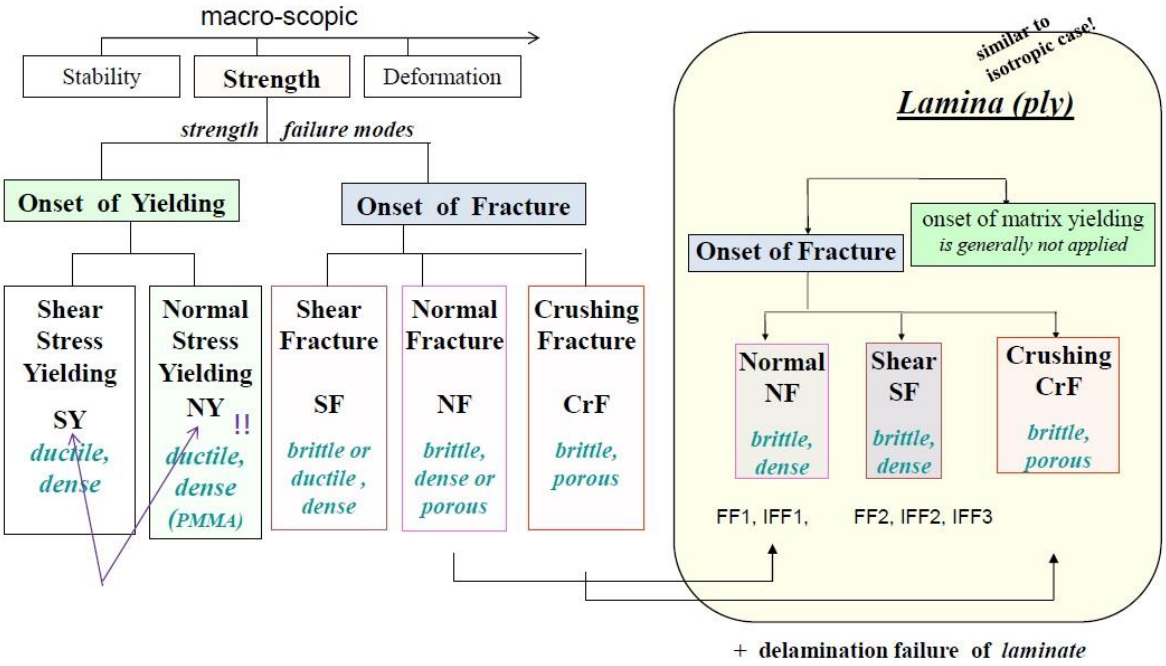

Fig.2-1.: Scheme of macro-scopic strength failure types and modes of isotropic materials and transversely-isotropic UD-materials (Cuntze1998)

LL:

** Failure behavior of Fiber-Reinforced materials is similar to isotropic ones*

** Principally, instead of stress-based SFC, strain-based SFC might be applied if the full stress-strain history is accurately considered. However, just limit strain conditions are used in pre-dimensioning (§22), because the certification process is stress-based.*

"The strain is not a quantity describing the material behavior" . Gottstein, RWTH-Aachen;

In application to the interaction equation *"The whole is more than the sum of its single parts".* Aristoteles

3 Material Symmetry and 'Generic' Number *(material inherent?)*

***Aim**: Consideration of the available material knowledge.*

During the derivation of the FMC a closer look at material symmetry facts was taken whereby the question arose: "Does a material symmetry–linked Generic Number exist with a number 2 for isotropic and 5 for UD materials?

Under the design-simplifying presumption "Homogeneity is a permitted assessment for the material concerned" and regarding the respective material tensors, it follows from material symmetry that the number of strengths equals the number of elasticity properties!

Fracture morphology gives further evidence: Each strength property corresponds to a distinct strength failure mode and to a distinct strength failure type, to Normal Fracture (NF) or to Shear Fracture (SF). This seems to mean, that a characteristic number of quantities is fixed: 2 for isotropic material and 5 for the transversely-isotropic UD lamina (≡ lamellas in civil engineering). Hence, the applicability of material sym*metry involves that in general just a minimum number of properties needs to be measured* (benefits:& test cost + time) which is helpful when setting up strength test programs. ⇒ Witnessed material symmetry knowledge seems to tell: "There might exist a 'generic' (*term was chosen by the author*) material inherent number for":

Isotropic Material: of **2**

- 2 e*lastic 'constants', 2 strengths, 2 strength failure modes fracture + Yielding* (NF with SF) and 2 fracture mechanics modes (defined as modes, where the crack plane does not turn)
- *1 physical parameter (such as the coefficient of thermal expansion CTE, the coefficient of moisture expansion CME, and the friction value μ, etc.)*

Transversely-Isotropic Material: of **5** for these basically brittle materials

- 5 e*lastic 'constants', 5 strengths, 5 strength failure modes fracture* (NFs with SFs)
- *2 physical parameters (CTE, CME, $\mu_{\perp\perp}$, $\mu_{\perp\parallel}$ etc.).*

Orthotropic Material: of **9** (6).

This looks to be proven by the investigation of Normal Yielding NY of plexiglass and (*theoretically*) by a compressive fracture toughness K_{IIcr}^{c} for a brittle material with an ideally homogeneous state at the crack tip [see *section 9 or CUN22§4*].

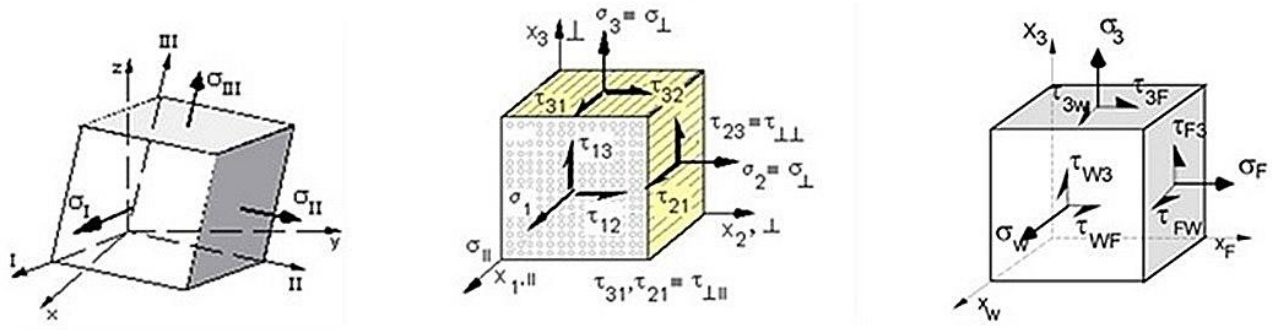

Fig.3-1: Presentation of the stresses faced with the envisaged three material families

***LL**: A 'generic' number seems to be inherent for the different material families, as the author found.*

4 Direct use of a Friction Value μ in the SFCs of Isotropic and UD materials

***Aim**: Direct use of the measurable μ instead of applying a μ-hiding friction model parameter.*

Mohr-Coulomb acts. Therefore, in the case of compressed brittle materials the effect of friction is to capture, which usually is performed by 'fictitious' friction-linked model parameters. Such a model parameter for friction, here the a or the b in the SFC, can be replaced by the measured μ.

In order to achieve this, the very challenging task to transform an SFC in structural stresses into a SFC in Mohr stresses had to be successfully to be performed [*§23* here, *Cun23c, Annex2*]. Ultimately, an engineer prefers the application of a measurable and physically understandable value μ, especially, because it does not scatter that much which is essential in design.

For isotropic materials this direct use is depicted in *Table 4-1*.

Table 4-1, Isotropic materials: Simple 2D formulation

Assumption: Fracture failure body is rotationally symmetric like Mises yield failure body.

$$I_1 = (\sigma_I + \sigma_{II} + 0) \;=\; f(\sigma)\;, \quad 6J_2 = (\sigma_I - \sigma_{II})^2 + (\sigma_{II} - 0)^2 + (0 - \sigma_I)^2 \;=\; f(\tau)$$

* Normal Fracture NF, $I_1 > 0$ $\quad\leftrightarrow\quad$ * Shear Fracture SF, $I_1 < 0$

The Strength Failure Criteria (SFC), mode interaction exponent $m = 2.7$, $\mu = 0.2$, read:

$$Eff^{NF} = \frac{\sqrt{4J_2 - I_1^2/3} + I_1}{2 \cdot R^t} = \frac{\sigma_{eq}^{NF}}{\bar{R}^t} \leftrightarrow Eff^{SF} = \frac{c_2^{SF} \cdot I_1 + \sqrt{(c_2^{SF} \cdot I_1)^2 + 12 \cdot c_1^{SF} \cdot 3J_2}}{2 \cdot R^c} = \frac{\sigma_{eq}^{SF}}{\bar{R}^c}.$$

$$c_1^{SF} = 1 + c_2^{SF},\; c_2^{SF} = (1 + 3 \cdot \mu)/(1 - 3 \cdot \mu) \;\text{ from }\; \mu \;=\; cos\;(2 \cdot \theta_{fp}^c\,° \cdot \pi / 180\;).$$

Mode interaction equation and the always required Reserve Factor RF are determined from:

$$Eff \;= [(Eff^{NF})^m + (Eff^{SF})^m]^{m^{-1}} \;\rightarrow f_{RF} = 1/Eff\,.$$

For UD material, the process is executed within the full SFC set in the *Table 4-2*:

Table 4-2, UD materials: 3D SFC formulations for FF1, FF2, and IFF1, IFF2, IFF3

FF1: $Eff^{\|\sigma} = \sigma_1^{\square} / \bar{R}_{\|}^t = \sigma_{eq}^{\|\sigma} / \bar{R}_{\|}^t$ with $\sigma_1^{\square} \cong \varepsilon_1^t \cdot E_{\|}$ (matrix neglected)

FF2: $Eff^{\|\tau} = -\sigma_1^{\square} / \bar{R}_{\|}^c = +\sigma_{eq}^{\|\tau} / \bar{R}_{\|}^c$ with $\sigma_1^{\square} \cong \varepsilon_1^c \cdot E_{\|}$

IFF1: $Eff^{\perp\sigma} = [(\sigma_2 + \sigma_3) + \sqrt{\sigma_2^2 - 2\sigma_2 \cdot \sigma_3 + \sigma_3^2 + 4\tau_{23}^2}\,]/2\bar{R}_{\perp}^t = \sigma_{eq}^{\perp\sigma} / \bar{R}_{\perp}^t$

IFF2: $Eff^{\perp\tau} = [a_{\perp\perp} \cdot (\sigma_2 + \sigma_3) + b_{\perp\perp}\sqrt{\sigma_2^2 - 2\sigma_2\sigma_3 + \sigma_3^2 + 4\tau_{23}^2}\,] / \bar{R}_{\perp}^c = \sigma_{eq}^{\perp\tau} / \bar{R}_{\perp}^c$

IFF3: $Eff^{\perp\|} = \{[b_{\perp\|} \cdot I_{23\text{–}5} + (\sqrt{b_{\perp\|}^2 \cdot I_{23\text{–}5}^2 + 4 \cdot \bar{R}_{\perp\|}^2 \cdot (\tau_{31}^2 + \tau_{21}^2)^2}\,]/(2 \cdot \bar{R}_{\perp\|}^3)\}^{0.5} = \sigma_{eq}^{\perp\square} / \bar{R}_{\perp\square}$

$$\left\{\sigma_{eq}^{\text{mode}}\right\} = \left(\sigma_{eq}^{\|\sigma},\; \sigma_{eq}^{\|\tau},\; \sigma_{eq}^{\perp\sigma},\; \sigma_{eq}^{\perp\tau},\; \sigma_{eq}^{\|\perp}\right)^T, \quad I_{23\text{–}5} = 2\sigma_2 \cdot \tau_{21}^2 + 2\sigma_3 \cdot \tau_{31}^2 + 4\tau_{23}\tau_{31}\tau_{21}$$

Inserting the compressive strength point $(0,\; -\bar{R}_{\perp}^c) \rightarrow a_{\perp\perp} \cong \mu_{\perp\perp} / (1 - \mu_{\perp\perp})$, $b_{\perp\perp} = a_{\perp\perp} + 1$

from a measured fracture angle $\rightarrow$ $\mu_{\perp\perp} = \cos\,(2 \cdot \theta_{fp}^c\,° \cdot \pi / 180\;)$, for $50° \rightarrow \mu = 0.174$.

$b_{\perp\|} = 2 \cdot \mu_{\perp\|}$. Typical friction value ranges: $0 < \mu_{\perp\|} < 0.25$, $0 < \mu_{\perp\perp} < 0.2$.

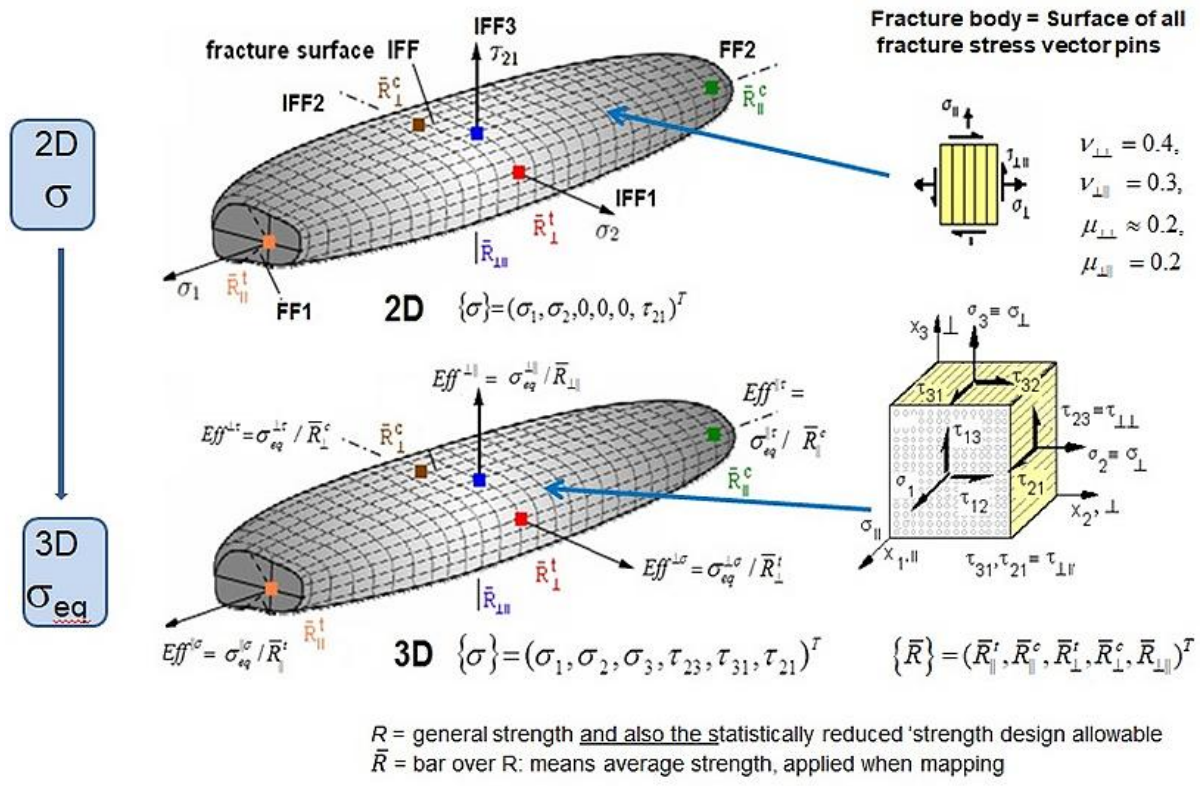

Fig.4-2: From a 2D failure body to a 3D failure body by replacing stresses by equivalent stresses

The upper figure displays the UD failure body as the visualization of the associated SFC set. The lower figure documents that if moving from the ply *stresses* to the mode-linked *equivalent ply stresses* one keeps the same UD failure body, usable now as 3D failure body!

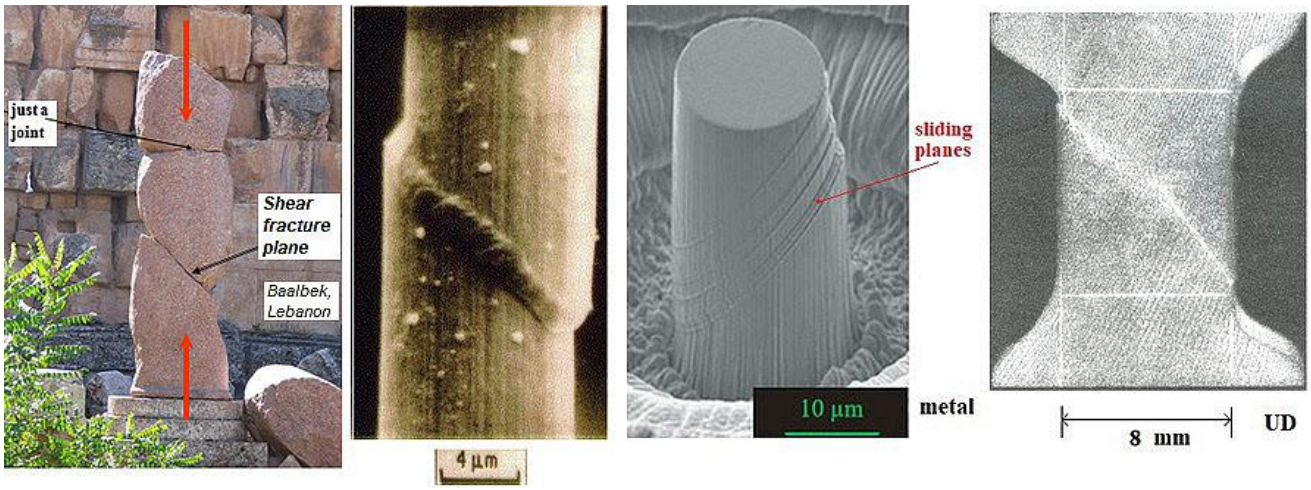

Fig.4-3,Friction driven shear fracture planes at extreme length scales.anes : Facture angles of the brittle materials Rock material, Carbon fiber [K. Schulte, TU Hamburg-Harburg], Ductile metal compression cut from a single crystal (deformed pillar after compression testing. Monnet, G. & Pouchon, M. A. (2013), Determination of the so-called critical resolved shear stress and the friction stress in austenitic stainless steels by compression of pillars extracted from single grains', Mater. Letters 98, 128-130) and laterally compressed UD-CFRP

LL:

** Often, SFCs employ just strengths and no friction value. This is physically not accurate and the undesired consequence in Design Verification is: The Reserve Factor may be not on the safe side..*

** In contrast to the 'doing': Friction must and can now be directly considered by the measured μ*

** Friction occurs similarly over the scales.*

5 Material stressing effort *Eff*

***Aim**: Generation of a physical basis for the interaction of failure modes and for an excellent understanding of a failure body (Eff = 100% , being the failure surface) with multi-axial strength (capacity) values.*

If several failure modes are activated by the stress state then the application of the so-called *material stressing effort Eff* is very helpful (*in German termed Werkstoffanstrengung). The artificial name had to be created in the World Wide Failure Exercise (WWFE) on UD-SFCs, together with its UK-organizers, because an equivalent term to the excellent German term is not known in English*.

The full *Eff* consists of all mode portions Eff^{mode}. It works analogous to 'Mises'

$$Eff^{\text{yield mode}} = \sigma_{eq}^{\text{Mises}} / R_{0.2} \;\rightarrow\; Eff^{\text{fracture mode}} = \sigma_{eq}^{\text{fracture mode}} / R \;.$$

The contribution of each single Eff^{mode} informs the designing engineer about the importance of the single portions in the SFC and thereby about the critical failure driving mode and thereby outlining the design-driving mode.

Whereas the structural engineer is more familiar with the equivalent stress the material engineer prefers above 'material stressing effort' *Eff*. The terms are linked by $\sigma_{\text{eq}}^{\text{mode}} = Eff^{\text{mode}} \cdot R^{\text{mode}}$.

The use of *Eff* supports 'Understanding the multi-axial strength capacity of materials' (s. *Fig.13-4)*: For instance, 3D-compression stress states have a higher bearing capacity, but the value of *Eff* nevertheless stays at 100%. Consequently, this has nothing to do with an increase of a (*uniaxial*) technical strength *R* which is a fixed result of a Standard!

The following fracture test result of a brittle concrete impressively shows how a slight hydrostatic pressure of 6 MPa increases the strength capacity in the longitudinal axis from 160 MPa up to 230 MPa - 6 MPa = 224 MPa. Thereby, the benefit of 3D-SFCs–application could be proven as the fracture stress states below depict both the Effs are 100% :

$$\sigma_{\text{fr}} = (\sigma_I\,,\ \sigma_{II}\,,\ \sigma_{III}\,)_{\text{fr}}^{\text{T}} = (-160,\ 0,\ 0)^{\text{T}}\ \text{MPa} \Leftrightarrow (-224-6,\ -6,\ -6)^{\text{T}}\ \text{MPa}\,.$$

Because both the *Eff*s are 100% for $(-160,\ 0,\ 0)^T$ and for $(-224-6,\ -6,\ -6)^T$ [*Cun22, §5.5*] ! This can be transferred to the quasi-isotropic plane of the transversely-isotropic UD-materials, $\sigma_2 - \sigma_3$, see [*Cun23c*], and to the orthotropic CMC fabric, when beside shear τ_{WF} the compressive stress σ_W^c acts together with σ_F^c and both activate friction on the sides [*Cun24b*].

LL:
The physically clear-based quantity Eff gives an impressive interpretation of what 100% strength capacity in 1D- 2D- and 3D stress states physically really means.

6 So-called 'Global' SFCs and (failure mode-linked) 'Modal' SFCs, Mode-interaction

***Aim**: Shortly explaining the difference of 'Global' and 'Modal' SFCs.*

There are a lot of possibilities to generate SFCs. *Fig.6-1* presents a survey:

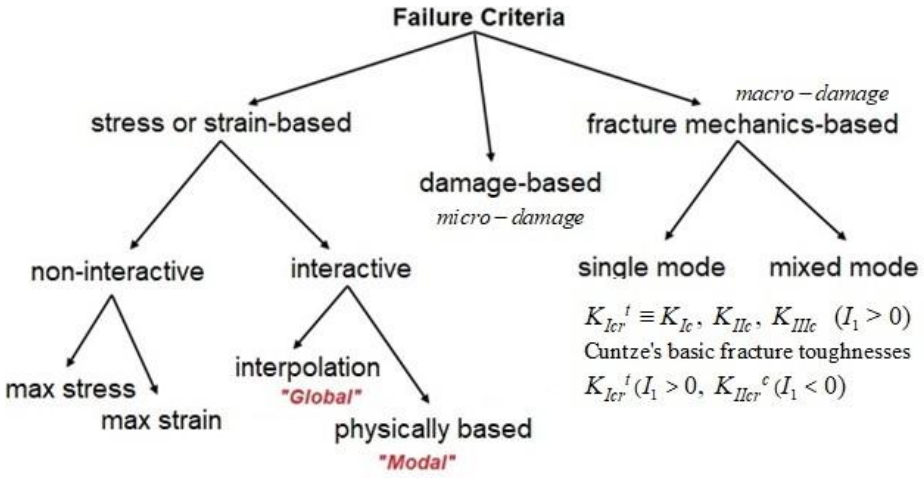

Fig.6-1: Possibilities to generate SFCs when following Klaus Rohwer [Rohwer K.: *Predicting Fiber Composite Damage and Failure*. Journal of Composite Materials, published online 26 Sept. 2014 (online version of this article can be found at: http://jcm.sagepub.com/content/early/2014/09/26/0021998314553885]

Present so-called interacting SFCs are a sub-part, which can be basically separated into two groups, 'global' and 'modal' ones. The HMH yield failure condition is a modal SFC that captures just one failure mode. The author choose the term global as a "play on words" to modal and to being self-explaining. Global SFCs describe the full failure surface by one single mathematical equation. This means that for instance a change of the UD *tensile* strength $\bar{R}_{\perp}^{t}$ affects the failure curve in the *compression* domain, where no physical impact can be. Global SFCs couple physically different failure modes whereas modal SFCs describe each single failure mode and therefore will better map the course of test data and not lead to a wrong Reserve Factor in any mode domain:

1 Global SFC $\quad F(\{\sigma\},\{R\}) = 1 \quad$ *mathematically 'married' modes*

Set of Modal SFCs $\quad F(\{\sigma\},\{R^{\text{mode}}\}) = 1 \quad$ *single mode formulations.*

In the case of modal SFCs (*such as the FMC-based ones*) also equivalent stresses can be computed, like 'isotropic Mises', $\left\{\sigma_{\text{eq}}^{\text{mode}}\right\} = \left(\sigma_{eq}^{\parallel\sigma},\ \sigma_{eq}^{\parallel\tau},\ \sigma_{eq}^{\perp\sigma},\ \sigma_{eq}^{\perp\tau},\ \sigma_{eq}^{\parallel\perp}\right)^{T}$.

and this is advantageous for design decisions. Within a 'global' SFC formulation all modes are mathematically married. This has a very bad impact: Each change, coming from a new test information for any pure mode, has an effect on all other independent failure modes and might include some redesign, see the full change of the ZTL-curve in *Fig.6-2*. Such a bad impact is never faced using a 'modal' formulation, like the FMC one.

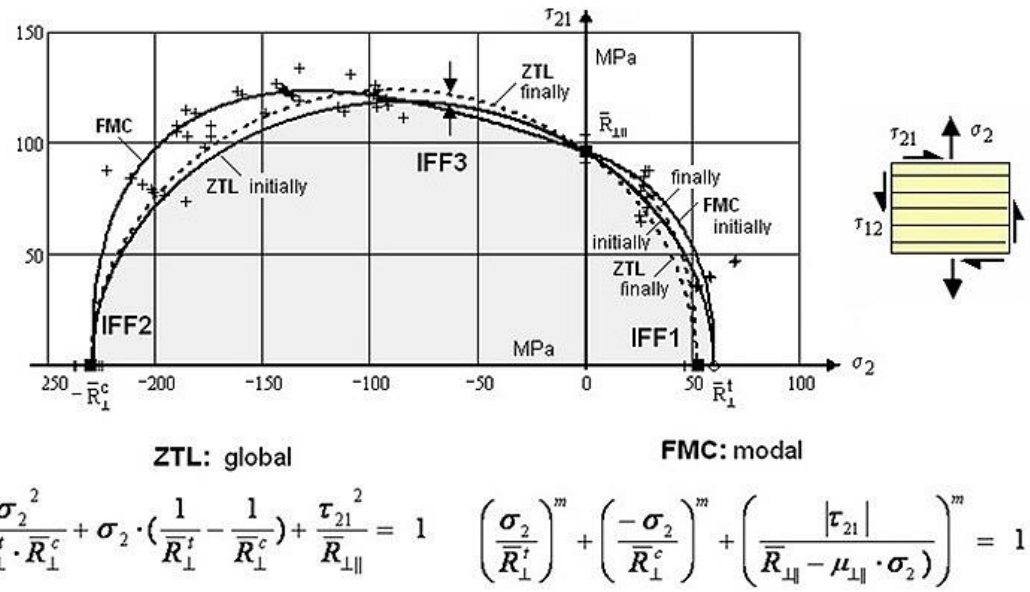

$$\frac{\sigma_2^2}{\bar{R}_\perp^t \cdot \bar{R}_\perp^c} + \sigma_2 \cdot \left(\frac{1}{\bar{R}_\perp^t} - \frac{1}{\bar{R}_\perp^c}\right) + \frac{\tau_{21}^2}{\bar{R}_{\perp\parallel}} = 1 \qquad \left(\frac{\sigma_2}{\bar{R}_\perp^t}\right)^m + \left(\frac{-\sigma_2}{\bar{R}_\perp^c}\right)^m + \left(\frac{|\tau_{21}|}{\bar{R}_{\perp\parallel} - \mu_{\perp\parallel} \cdot \sigma_2}\right)^m = 1$$

Fig.6-2: Modelling example, impact of a novel test information in the mode IFF1 considering a global (ZTL-SFC, still used in the HSB) and a modal SFC,

Considering the shortcomings of 'global' UD SFCs, my research friend John Hart-Smith cited two decades ago:

"It is scientifically incorrect to employ polynomial interaction failure models **(**the 'global' ones**),**
if the mechanism of failure changes"!

Of course, a modal FMC-approach requires an interaction in all the mode transition zones. This is performed by a probabilistic approach, using a 'series failure system' in the transition zone of the adjacent modes NF with SF, reading

$$Eff = \sqrt[m]{(Eff^{\text{mode } 1})^m + (Eff^{\text{mode } 2})^m + ...} = 1 = 100\% \qquad for \quad \text{Onset-of-Failure}$$

applying a 'mode interaction exponent' *m,* also termed rounding-off exponent, the size of which is high in case of low scatter and vice versa. The value of *m* is obtained by curve fitting of test data in the transition zone of the interacting modes. Experience delivered that *2.5 < m < 2.9*.

With the FMC-based SFCs for the three 'material families' available multi-axial fracture test data were mapped by the author to validate the SFCs being the mathematical descriptions of the envisaged fracture failure models. For a large variety of materials the associated fracture bodies were displayed in later chapters with distinct cross–sections of them, for instance for the isotropic applications: Principal stress plane, octahedral stress plane and tensile and meridian planes. Various links or interrelationships between the materials could be outlined.

LL:

* *So-called 'Global' SFCs couple physically different failure modes whereas the Modal SFCs describe each single failure mode and therefore will better map the course of test data and not lead to a wrong Reserve Factor*
* *Here, global and modal have a similar level of abstraction, as in the case of stability the terms 'global' and 'local' have*
* *Similarities between the materials could be found*
* *The surface of the failure body reads: F = 1 for a 'global' SFC-formulation and Eff = 1 = 100% for a 'modal' formulation.*

7 Collection of Derived SFCs, Interaction of Failure Modes and a Multi-fold Mode

7.1 Presentation of the derived Failure Mode Concept-based Strength Failure Criteria

Aim: *Provision of SFCs which were derived on the same concept basis.*

For the mentioned three material families the associate SFCs are tabled on the following pages:

I a ***: 3D-isotropic SFCs of dense Isotropic Materials*** *for* ***NF*** *and* ***SF****, 120°-rotational symmetry*

2 modes → 2 SFCs, is in line with 'generic' number according to the FMC.

Normal Fracture NF for $I_1 > 0$ ↔ Shear Fracture SF for $I_1 < 0$

$$F_\sigma^t = F^{NF} = c^{NF} \cdot \Theta^{NF} \cdot \frac{\sqrt{4J_2 \cdot \Theta^{NF} - I_1^2/3} + I_1}{2 \cdot \bar{R}^t} = 1 \quad \leftrightarrow \quad F_\tau^c = F^{SF} = c_{1\Theta}^{SF} \cdot \frac{6J_2 \cdot \Theta^{SF}}{2\bar{R}^{c2}} + c_{2\Theta}^{SF} \cdot \frac{I_1}{\bar{R}^c} = 1$$

$$Eff^{NF} = c^{NF} \cdot \frac{\sqrt{4J_2 \cdot \Theta^{NF} - I_1^2/3} + I_1}{2 \cdot \bar{R}^t} = \frac{\sigma_{eq}^{NF}}{\bar{R}^t} \leftrightarrow Eff^{SF} = \frac{c_{2\Theta}^{SF} \cdot I_1 + \sqrt{(c_{2\Theta}^{SF} \cdot I_1)^2 + c_{1\Theta}^{SF} \cdot 12J_2 \cdot \Theta^{SF}}}{2 \cdot \bar{R}^c} = \frac{\sigma_{eq}^{SF}}{\bar{R}^c}.$$

If a failure body is rotationally symmetric, then Θ = 1 like for the neutral or shear meridian.

A two-fold acting mode makes the rotationally symmetric fracture body 120°-symmetric and is modelled by $\Theta(J_3)$ using the invariant J_3 and Θ as non-circularity function with d as non-circularity parameter

$$\Theta^{NF} = \sqrt[3]{1 + d^{NF} \cdot \sin(3\vartheta)} = \sqrt[3]{1 + d^{NF} \cdot 1.5 \cdot \sqrt{3} \cdot J_3 \cdot J_2^{-1.5}}, \; \Theta^{SF} = \sqrt[3]{1 + d^{SF} \cdot 1.5 \cdot \sqrt{3} \cdot J_3 \cdot J_2^{-1.5}}$$

Lode angle ϑ, here set as $\sin(3 \cdot \vartheta)$ with 'neutral' shear meridian angle set $\vartheta = 0°$;

Tensile Meridian angle 30° $\rightarrow \Theta^{NF} = \sqrt[3]{1 + d^{SF} \cdot (+1)}$; Compr. Merid. angle -30° $\rightarrow \Theta^{SF} = \sqrt[3]{1 + d^{SF} \cdot (-1)}$.

Equation of the fracture failure body: $Eff = [(Eff^{NF})^m + (Eff^{SF})^m]^{m^{-1}} = 1 = 100\%$ total effort

$$Eff = \sqrt[m]{\left(c^{NF} \cdot \frac{\sqrt{4J_2 \cdot \Theta^{NF} - I_1^2/3} + I_1}{2 \cdot \bar{R}^t}\right)^m + \left(\frac{c_{2\Theta}^{SF} \cdot I_1 + \sqrt{(c_{2\Theta}^{SF} \cdot I_1)^2 + c_{1\Theta}^{SF} \cdot 12J_2 \cdot \Theta^{SF}}}{2 \cdot \bar{R}^c}\right)^m} = 1.$$

Curve parameter relationships obtained by inserting the compressive strength point (0, $-\bar{R}^c$, 0):

* Rotationally symmetric: $c_1^{SF} = 1 + c_2^{SF}$, $d^{SF} = 0$, friction parameters are equal $c_2^{SF} \equiv c_{2\Theta}^{SF}$

$c_2^{SF} = c_{2\Theta}^{SF} \approx (1 + 3 \cdot \mu)/(1 - 3 \cdot \mu)$ from $\mu = \cos(2 \cdot \theta_{fp}^c \,° \cdot \pi / 180)$ and for 50° → $\mu = 0.174$.

* 120°-rotationally symmetric: $c_{1\Theta}^{SF} = 1 + c_2^{SF} \cdot \sqrt[3]{1 + d^{SF} \cdot (-1)}$ with

c^{NF}, Θ^{NF} from the two points $(\bar{R}^t, 0, 0)$ and $(\bar{R}^{tt}, \bar{R}^{tt}, 0)$ or by a minimum error fit, if data,

c^{SF}, Θ^{SF} from the two points $(-\bar{R}^c, 0, 0)$ and $(-\bar{R}^{cc}, -\bar{R}^{cc}, 0)$ or by minimum error fit.

A paraboloid serves as closing cap $\frac{I_1}{\sqrt{3} \cdot \bar{R}^t} = s^{cap} \cdot \left(\frac{\sqrt{2J_2 \cdot \Theta^{NF}}}{\bar{R}^t}\right)^2 + \frac{\max I_1}{\sqrt{3} \cdot \bar{R}^t}$.

$$I_1 = (\sigma_I + \sigma_{II} + \sigma_{III}) = f(\sigma), \quad 6J_2 = (\sigma_I - \sigma_{II})^2 + (\sigma_{II} - \sigma_{III})^2 + (\sigma_{III} - \sigma_I)^2 = f(\tau)$$

$$27J_3 = (2\sigma_I - \sigma_{II} - \sigma_{III}) \cdot (2\sigma_{II} - \sigma_I - \sigma_{III}) \cdot (2\sigma_{III} - \sigma_I - \sigma_{II}).$$

I b : *3D-isotropic SFCs of dense Isotropic Materials* for *NF* and *SF*, 120°-rotational symmetry

Table I b collects all information necessary to design dimension a porous isotropic material like a foam or a concrete stone. These materials experience *120°-rotational symmetry*.

'Porous' isotropic material: SFC formulations for NF and CrF, 120°-rotational symmetry

Normal Fracture NF for $I_1 > 0$ $\leftrightarrow$ Crushing Fracture CrF for $I_1 < 0$

$$F^{NF} = c^{NF} \cdot \Theta^{NF} \cdot \frac{\sqrt{4J_2 \cdot \Theta^{NF} - I_1^2/3} + I_1}{2 \cdot \bar{R}^t} = 1 \leftrightarrow F^{CrF} = c^{CrF} \cdot \Theta^{CrF} \cdot \frac{\sqrt{4J_2 \cdot \Theta^{CrF} - I_1^2/3} + I_1}{2 \cdot \bar{R}^c} 1$$

$$Eff^{NF} = c^{NF} \cdot \frac{\sqrt{4J_2 \cdot \Theta^{NF} - I_1^2/3} + I_1}{2 \cdot \bar{R}^t} = \frac{\sigma_{eq}^{NF}}{\bar{R}^t} \leftrightarrow Eff^{CrF} = c^{CrF} \cdot \frac{\sqrt{4J_2 \cdot \Theta^{CrF} - I_1^2/3} + I_1}{2 \cdot \bar{R}^c} = \frac{\sigma_{eq}^{CrF}}{\bar{R}^c}.$$

If a failure body is rotationally symmetric, then $\Theta = 1$ like for the neutral or shear meridian, respectively .
A 2-fold acting mode makes the rotationally symmetric fracture body 120°-symmetric and is modelled by using the invariant J_3 and Θ as non-circularity function with d as non-circularity parameter

$$\Theta^{NF} = \sqrt[3]{1 + d^{NF} \cdot \sin(3\vartheta)} = \sqrt[3]{1 + d^{NF} \cdot 1.5 \cdot \sqrt{3} \cdot J_3 \cdot J_2^{-1.5}} \quad \leftrightarrow \quad \Theta^{CrF} = \sqrt[3]{1 + d^{CrF} \cdot 1.5 \cdot \sqrt{3} \cdot J_3 \cdot J_2^{-1.5}}$$

Lode angle ϑ , here set as $\sin(3 \cdot \vartheta)$ with 'neutral' (shear meridian) angle $\vartheta = 0°$ ($\rightarrow \Theta = 1$) ;
tensile meridian angle 30° $\rightarrow \Theta^{NF} = \sqrt[3]{1 + d^{NF} \cdot (+1)}$; compr. mer. angle -30° $\rightarrow \Theta^{CrF} = \sqrt[3]{1 + d^{CrF} \cdot (-1)}$.

Mode interaction $\rightarrow$ Equation of the fracture body: $Eff = [(Eff^{NF})^m + (Eff^{SF})^m]^{m^{-1}} = 1 = 100\%$

$$Eff = \sqrt[m]{(c^{NF} \cdot \frac{\sqrt{4J_2 \cdot \Theta^{NF} - I_1^2/3} + I_1}{2 \cdot \bar{R}^t})^m + (c^{CrF} \cdot \frac{\sqrt{4J_2 \cdot \Theta^{CrF} - I_1^2/3} + I_1}{2 \cdot \bar{R}^c})^m} = 1.$$

Curve parameter relationships obtained by inserting the compressive strength point (0, -$\bar{R}^c$, 0):

* Rotationally symmetric $\Theta = 1$: $d^{SF} = 0$, $c_{1\Theta}^{SF} = 1 + c_2^{SF}$

* 120°-rotat. symmetric $\Theta \neq 1$: $c_{1\Theta}^{SF} = 1 + c_2^{SF} \cdot \sqrt[3]{1 + d^{SF} \cdot (-1)}$, with

  c^{NF} , Θ^{NF} from the two points $(\bar{R}^t, 0, 0)$ and $(\bar{R}^{tt}, \bar{R}^{tt}, 0)$ or by minimum error fit, if data available,

  c^{CrF} , Θ^{CrF} from the two points $(-\bar{R}^c, 0, 0)$ and (-$\bar{R}^{cc}$,-$\bar{R}^{cc}$, 0) or by minimum error fit.

The failure surface is closed at both the ends: A paraboloid serves as closing cap and bottom

$$\frac{I_1}{\sqrt{3} \cdot \bar{R}^t} = s^{cap} \cdot (\frac{\sqrt{2J_2 \cdot \Theta^{NF}}}{\bar{R}^t})^2 + \frac{\max I_1}{\sqrt{3} \cdot \bar{R}^t} \quad , \quad \frac{I_1}{\sqrt{3} \cdot \bar{R}^t} = s^{bot} \cdot (\frac{\sqrt{2J_2 \cdot \Theta^{CrF}}}{\bar{R}^t})^2 + \frac{\min I_1}{\sqrt{3} \cdot \bar{R}^t}$$

Slope parameters s are determined connecting the respective hydrostatic strength point with the associated point on the tensile and compressive meridian, $\max I_1$ must be assessed whereas $\min I_1$ can be measured. $\bar{R}^t$ is normalization strength.

II a *: **3D-SFCs of (quasi-)Brittle Dense UD Materials***

5 modes → 5 SFCs, is in line with 'generic' number according to the FMC. IFF1 generates a straight line in the stress plane!

FF1: $Eff^{\|\sigma} = \sigma_1^{\sqcup} / \bar{R}_{\|}^{t} = \sigma_{eq}^{\|\sigma} / \bar{R}_{\|}^{t}$ with $\sigma_1^{\sqcup} \cong \varepsilon_1^{t} \cdot E_{\|}$ (matrix neglected)

FF2: $Eff^{\|\tau} = -\sigma_1^{\square} / \bar{R}_{\|}^{c} = +\sigma_{eq}^{\|\tau} / \bar{R}_{\|}^{c}$ with $\sigma_1^{\square} \cong \varepsilon_1^{c} \cdot E_{\|}$

IFF1: $Eff^{\perp\sigma} = [(\sigma_2 + \sigma_3) + \sqrt{\sigma_2^{\,2} - 2\sigma_2 \cdot \sigma_3 + \sigma_3^{\,2} + 4\tau_{23}^{\,2}}] / 2\bar{R}_{\perp}^{t} = \sigma_{eq}^{\perp\sigma} / \bar{R}_{\perp}^{t}$

IFF2: $Eff^{\perp\tau} = [a_{\perp\perp} \cdot (\sigma_2 + \sigma_3) + b_{\perp\perp} \sqrt{\sigma_2^{\,2} - 2\sigma_2\sigma_3 + \sigma_3^{\,2} + 4\tau_{23}^{\,2}}] / \bar{R}_{\perp}^{c} = \sigma_{eq}^{\perp\tau} / \bar{R}_{\perp}^{c}$

IFF3: $Eff^{\perp\|} = \{[b_{\perp\|} \cdot I_{23-5} + (\sqrt{b_{\perp\|}^{\,2} \cdot I_{23-5}^{\,2} + 4 \cdot \bar{R}_{\perp\|}^{\,2} \cdot (\tau_{31}^2 + \tau_{21}^2)^2}] / (2 \cdot \bar{R}_{\perp\|}^{\,3})\}^{0.5} = \sigma_{eq}^{\perp\|} / \bar{R}_{\perp\|}$

$$\left\{\sigma_{eq}^{\text{mode}}\right\} = \left(\sigma_{eq}^{\|\sigma},\ \sigma_{eq}^{\|\tau},\ \sigma_{eq}^{\perp\sigma},\ \sigma_{eq}^{\perp\tau},\ \sigma_{eq}^{\|\perp}\right)^T, \quad I_{23-5} = 2\sigma_2 \cdot \tau_{21}^2 + 2\sigma_3 \cdot \tau_{31}^2 + 4\tau_{23}\tau_{31}\tau_{21}$$

Inserting the compressive strength point $(0,\ -\bar{R}_{\perp}^{c}) \rightarrow a_{\perp\perp} \cong \mu_{\perp\perp} / (1 - \mu_{\perp\perp})$, $b_{\perp\perp} = a_{\perp\perp} + 1$

from a measured fracture angle → $\mu_{\perp\perp} = \cos(2 \cdot \theta_{fp}^{c}\,° \cdot \pi / 180)$, for 50° → $\mu = 0.174$.

$b_{\perp\|} \cong 2 \cdot \mu_{\perp\|}$. Typical friction value ranges: $0 < \mu_{\perp\|} < 0.25$, $0 < \mu_{\perp\perp} < 0.2$.

Interaction Equation:

$$Eff^{m} = [(\sigma_{eq}^{\|\sigma} / \bar{R}_{\|}^{t})^m + (\sigma_{eq}^{\|\tau} / \bar{R}_{\|}^{c})^m + (\sigma_{eq}^{\perp\sigma} / \bar{R}_{\perp}^{t})^m + (\sigma_{eq}^{\perp\tau} / \bar{R}_{\perp}^{c})^m + (\sigma_{eq}^{\perp\|} / \bar{R}_{\perp\|})^m]$$

or $Eff = \sqrt[m]{(Eff^{\text{mode }1})^m + (Eff^{\text{mode }2})^m + \ldots} = 1 = 100\%$ *for* Onset-of-Failure .

As abbreviation, $I_2 \cdot I_3 - I_5 = I_{23-5}$ is used. In the equations above, $\bar{R}$ denotes an average = typical strength value that should be used for the stress-strain curves in stress and deformation analysis. In the design verification the statistically reduced strength values are applied. The superscripts ^{t}, ^{c} stand for tensile, compressive. The superscripts $^{\sigma}$ and $^{\tau}$ mark the type of fracture failure whether it is caused by a tensile stress (Normal Fracture, NF, 'cleavage') or a shear stress (Shear Fracture, SF), e.g. due to a compressive normal stress $\sigma_{\|}^{c}$ or a transverse normal stress $\sigma_{\perp}^{c}$.

Failure activated in two directions is considered by adding a multi-fold failure term, proposed in [*Awa78*] for isotropic materials. It can be applied to brittle UD material in the transversal (quasi-isotropic) plane as well.

For the 2D-case, a simplified friction modelling (IFF3) is possible:

$$Eff^{m} = [(Eff^{\|\sigma})^m + (Eff^{\|\tau})^m + (Eff^{\perp\sigma})^m + (Eff^{\perp\tau})^m + (Eff^{\perp\|})^m]$$

with the mode portions inserted, 2D,

$$Eff = [(\frac{(\sigma_1 + |\sigma_1|)}{2 \cdot \bar{R}_{\|}^{t}})^m + (\frac{(-\sigma_1 + |\sigma_1|)}{2 \cdot \bar{R}_{\|}^{c}})^m + (\frac{\sigma_2 + |\sigma_2|}{2 \cdot \bar{R}_{\perp}^{t}})^m + (\frac{-\sigma_2 + |\sigma_2|}{2 \cdot \bar{R}_{\perp}^{c}})^m + (\frac{|\tau_{21}|}{\bar{R}_{\perp\|} + 0.5 \cdot \mu_{\perp\|} \cdot (-\sigma_2 + |\sigma_2|)})^m]^{1/m}.$$

II b*: 3D-SFCs of (quasi-)Brittle Porous UD Materials*

This practically meets just IFF2. The table below shows the difference.

* IFF2 Failure Function for the dense UD material (for comparison)

$F^{SF} = [a_{\perp\perp} \cdot I_2 + b_{\perp\perp} \cdot \sqrt{I_4}] \; / \bar{R}_{\perp}^{c} = 1$ with $a_{\perp\perp} = b_{\perp\perp} - 1$ after inserting $\bar{R}_{\perp}{}^{c}$

$= [a_{\perp\perp} \cdot (\sigma_2 + \sigma_3) + b_{\perp\perp} \cdot \sqrt{(\sigma_2 - \sigma_3)^2 + 4\tau_{23}{}^2}] \; / \bar{R}_{\perp}^{c} = 1$

$= [a_{\perp\perp} \cdot (\sigma_2{}^{pr} + \sigma_3{}^{pr}) + b_{\perp\perp} \cdot \sqrt{(\sigma_2{}^{pr} - \sigma_3{}^{pr})^2 + 0^2}] \; / \bar{R}_{\perp}^{c} = 1$ ← 2 structural stresses

* IFF2 Failure Function for the porous UD material (index por, *author's simple approach*)

$F^{SF}_{porosity} = \sqrt{a_{\perp\perp por}{}^2 \cdot I_2{}^2 + b_{\perp\perp por}{}^2 \cdot I_4} - a_{\perp\perp por} \cdot I_2 \;] \; / 2\bar{R}_{\perp}^{c} = 1$.

The two curve parameters are determined - as before performed - from insertion of the compressive strength point and from the bi-axial fracture stress point.

Mind: In contrast to an isotropic dense material the fracture body of a compressed dense UD-material has a closed bottom fracture surface, because the filaments may break under the tensile stress caused by biaxial compression due to the Poisson effect, when $\varepsilon^{t}_{axial} = \varepsilon^{fr}_{\perp}$.

III*: 3D-SFCs of the Orthotropic Fabrics,* (see [*Cun24b*])

9 modes → 9 SFCs. This is in line with Cuntze's 'generic' number 9 according to the FMC.
In this context, my thanks to Roman (Prof. Dr. Keppeler, UniBw; formerly Siemens AG).

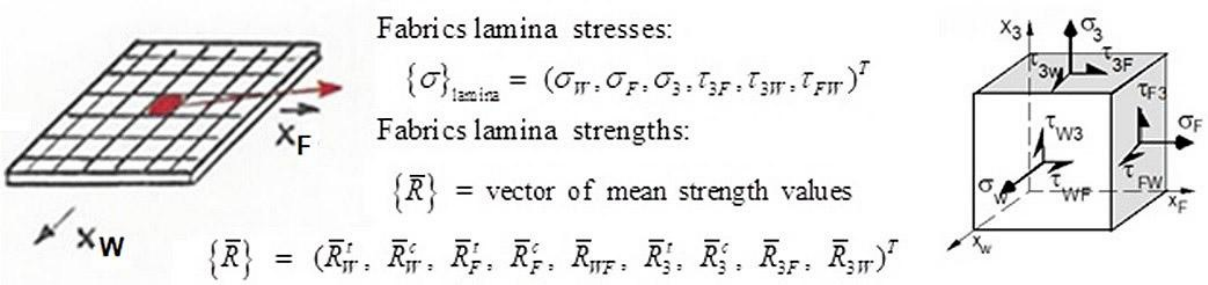

The following table includes the FMC-based SFCs for **porous orthotropic** (rhombic-anisotropic) **materials** composed for instance of 2D-woven fabrics**.** Three essential 2D-woven fabrics (Atlas or Satin) are depicted

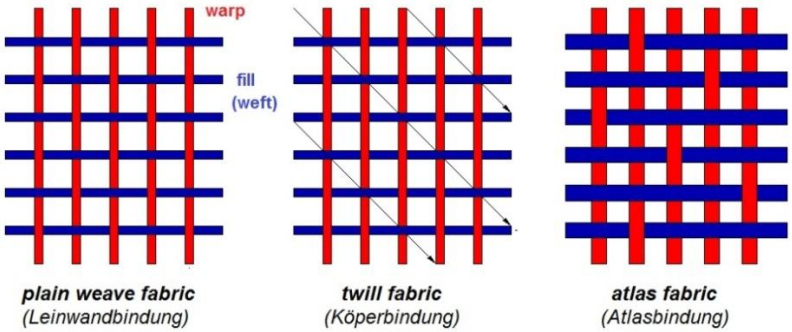

$$Eff = \left(\frac{\sigma_W + |\sigma_W|}{2 \cdot \bar{R}_W^t} \right)^m + \left(-\frac{\sigma_W + |\sigma_W|}{2 \cdot \bar{R}_W^c} \right)^m + \left(\frac{\sigma_F + |\sigma_F|}{2 \cdot \bar{R}_F^t} \right)^m + \left(\frac{-\sigma_F + |\sigma_F|}{2 \cdot \bar{R}_F^c} \right)^m + \left(\frac{|\tau_{WF}|}{\bar{R}_{WF} - \mu_{WF} \cdot (\sigma_W + \sigma_F)} \right)^m$$

$$+ \left(\frac{\sigma_3 + |\sigma_3|}{2 \cdot \bar{R}_3^t} \right)^m + \left(\frac{-\sigma_3 + |\sigma_3|}{2 \cdot \bar{R}_3^c} \right)^m + \left(\frac{|\tau_{3W}|}{\bar{R}_{3W} - \mu_{3W} \sigma_3^c} \right)^m + \left(\frac{|\tau_{3F}|}{\bar{R}_{3F} - \mu_{3F} \sigma_3^c} \right)^m = 1 = 100\% .$$

For a cross-ply fabric with Warp = Fill $\rightarrow$ $\bar{R}_W^t = \bar{R}_F^t$, $\bar{R}_W^c = \bar{R}_F^c$, the inter-laminar *Eff*s, suffix $_3$, vanish and just the in-plane (intra-laminar) *Eff*s remain.

The range of parameters is for the interaction-exponent $2.5 < m < 2.9$, and since the strong porosity-dependency is very different $\rightarrow$ recommendation: $\mu_{WF} < 0.2$, $\mu_3 < 0.2$.

If σ_F is also active, this double mode contributes via $\left(\frac{|\tau_{WF}|}{\bar{R}_{WF} - \mu_{WF} \cdot (\sigma_W^c + \sigma_F^c)} \right)^m$.

Modelling of laminates may be lamina-based (basic layers are UD layers), sub-laminate-based (semi-finished non-crimp orthotropic fabrics) or even laminate-based. Thereby, modelling complexity grows from UD, via non-crimp fabrics (NCF) through plain weave and finally to the spatial 3D-textile materials. Model parameters are just the measurable technical strengths *R* and the friction values μ, and on top the Weibull statistics-based interaction exponent *m*. The value of μ comes from mapping the compression stress-shear stress domain and of *m* by mapping the transition zone between the modes. A good guess is $m = 2.6$ for all mode transition domains and all material families. Model parameters are just the measurable technical strengths *R* and the friction values μ, and on top the Weibull statistics-based interaction exponent *m*. The value of μ comes from mapping the compression stress-shear stress domain and of *m* by mapping the transition zone between the modes. A good guess is $m = 2.6$ for all mode transition domains and all material families.

Of course, there are Validity Limits of UD SFC Applications:

“Models cannot map all test (average) data course domains equally well, because they are basic physics-modelling models.”

However, they are good enough to correctly re-design the hose blow!

Viewing the false angle:

I was sure that this hose had to be replaced!”

►One vital experience with boundary specifications (limits):

The 4 m long caiman mother Maria strictly observed the Limit "**No trespassing** (No pase!)".

Maria stopped at the tape, marked with "No pase"!

Her behavior was very good for the **personal** health of my friend Eddi

(*he unfortunately fell down 1.5 m in front of her snout while running away*).

We engineers should learn from this:

Engineers should always rationally observe the limits set by specifications etc.
*This is good for '**structural** health' or Structural Integrity, respectively.*
And: This fully meets application limits of the literature-offered SFCs.

►My present feeling considering the 3D-applications, especially of UD-materials:

(below left) Much is reached with plenty of effort!
(below right) However, much more effort is required for the 3D-Validation. Only when you get 'higher' the real '3D-peaks' do appear:

Linked to composites:
3D-applications are much more challenging, especially because data is missing.

8 Cracking at statically-loaded Notches using FM and Finite Fracture Mechanics (FFM)

Aim: *Giving the user some advices regarding the often used so-called 'Open Hole Panels'.*

Summary

Full Design Verification requires the verification of Strength and of Damage Tolerance in the case of potentially cracked (macro-damaged) statically-loaded structural components under sudden overloading. The Strength Analysis (SA) requires that the effective multi-axial stress state is not above the given Strength Design Allowable and the Damage Tolerance Analysis (DTA) the same for the so-called residual strength of the structural component containing a pre-crack.

Lying between Strength analysis and Fracture Mechanics (FM) analysis 'Onset-of-Cracking' (OoC) is experienced at stress concentration sites such as notches like open holes in a panel of a sufficiently brittle material. In this context, Leguillon's Hypothesis [1] says

"*A (*generating*) crack is (*becomes*) critical when and only when both the released energy and the local stress reach critical values along an assumed finite crack".*

This novel hypothesis, 'Neuber'-improving, shall be presented here. It captures the prediction of the instantaneous OoC. The name of the tool is Finite Fracture Mechanics (FFM), see *Fig.1*. It predicts for notched components that loading level where the Strength Failure Criterion (SFC) equals the FM criterion or it determines as a coupled (hybrid) stress-energy criterion the critical loading that causes the finite crack size Δa_c. Because FM is one part of the FFM as introduction and for better understanding at first the well-known FM analysis tool R-curve shall be presented.

smooth structure	**notched structure** "transition domain"		**cracked structure**
no steep stress decay SFC	stress concentration Neuber method (up to now) K_t	'onset-of cracking' *assumed crack, FFM* (novel replacement)	stress intensity *real pre-cracks, FM* K_{Ic} *'no hole' and 'with hole'*

Fig. 1: Stress situations in a structural component

Fig.2 visualizes the task to be solved. For practical application the concept of a linear-elastic stress intensity factor *K* may be sufficient and is usually applied. Coordinates used are depicted.

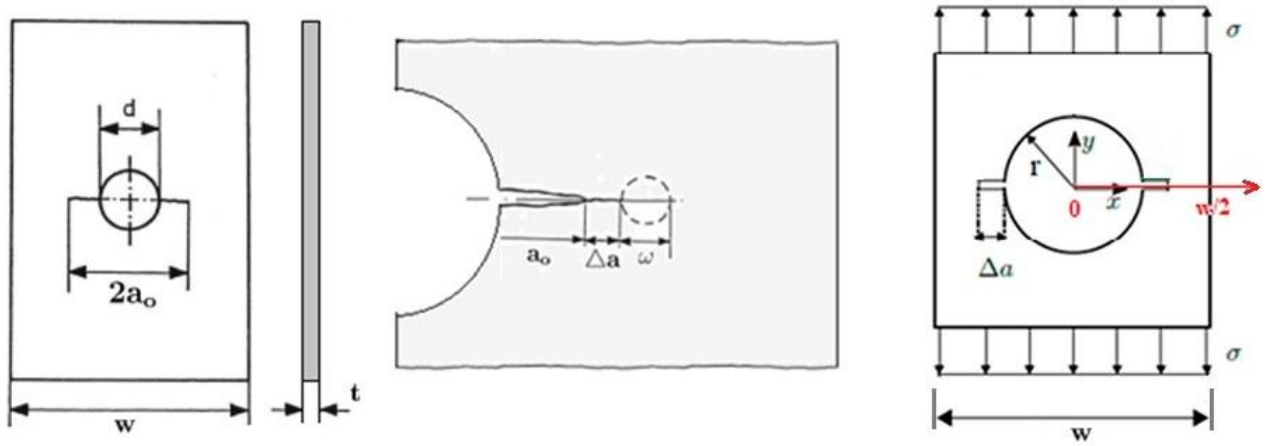

Fig.2: Plate strip with a central open hole and an existing through crack of the size $a = a_0 - r$.

(left) characterization of an open hole panel with existing crack , w= plate width, t = plate thickness, (center) crack growth details in the case of slight crack tip yielding ω of not fully brittle materials,
(right) σ = remote tensile stress, leading to cracking for $\sigma = \sigma_{fail}$, Δa = assumed FFM crack , d = 2r

Key Words: Residual strength, critical crack length, R-curve, Finite Fracture Mechanics, coupled criterion.

References

[1] Leguillon D: *Strength or toughness? A criterion for crack onset at a notch*. European Journal of Mechanics A, Solids 21(1), 61-72, 2002

[2] Weißgraeber P, Leguillon D and Becker W: *A review of Finite Fracture Mechanics: crack initiation at singular and non-singular stress raisers*. Archive of Applied Mechanics 86, 375-401, 2016

[3] HSB-draft, Nguyen-Hoang M and Becker W: *Finite Fracture Mechanics: A concept to assess structural integrity or failure in the case of stress concentrations*

[4] HSB 62232-02: *Evaluation of the residual strength and critical crack length using the R-Curve*, 1990

[5] HSB 62232-03: *Analytical model for the description of R-Curves*, 2006

[6] HSB 62232-05 *Application of R-curves*

[7] [Fla82] Flaggs D L and Kural M H*: Experimental Determination of the In Situ Transverse Lamina Strength in Graphite Epoxy Laminates*. J. Comp. Mat. Vol 16 (1982), S. 103-116

[8] HSB 34112-10: *Stress concentration and distribution in a finite pin-loaded plate under remote uniformly distributed tension*. Issue A, 2022

[9] Tada H, Paris P, and Irwin G: *The Stress Analysis of Cracks Handbook*. ASME Press, New York, 2000.

[10] HSB 63321-06: *Determination of the constants in the model describing the width dependency of the Feddersen-parameter*, 2009

[11] N.N.: *Standard Practice for R-Curve Determination*. ASTM E561-86, 1986

[12] Schwalbe K-H: *Bruchmechanik metallischer Werkstoffe*. Hanser-Verlag, München, 1980

[13] HSB 63203-03: *Experimental evaluation of fracture toughness of metallic materials.* 1993.

Luftfahrt-Technisches Handbuch (LTH): *HANDBUCH STRUKTUR BERECHNUNG* (HSB) *Fundamentals and Methods for Aeronautical Design and Analyses* issued by IASB (Industrie-Ausschuss für Struktur-Berechnung).

(As-member of the IASB this document is structured similar to a HSB design sheet)

1 General

There are three approaches available to perform Design Verification (DV) for occurring static stress situations: Strength Failure Criteria (SFC), Continuum (micro-)Damage Mechanics (CDM, *not yet DV-capable*) criteria and Fracture Mechanics (FM) criteria for cracked (macro-damaged) components. A novel approach is the hybrid tool Finite Fracture Mechanics (FFM) which captures the 'onset-of-cracking' (OoC) at stress concentration (SC) points and at higher stress singularities.

The FFM is a coupled (hybrid) criterion that fills a gap in FM by assuming an instantaneous formation of a crack of finite size [1, 2]. Intention is to initially show the classical application of FM, because FM provides one part tool of the FFM. *Fig.1* gave a survey on the situations faced.

Due to FFM, the Neuber method is now obsolete, but falls as a special case. What Neuber called "support length" is precisely the crack length supplied by the FFM, without the need for acceptance or experimental identification!

The provided analyses are restricted to the 2D-case, 3D-extension will be a future task.

A SFC is a necessary condition but might not be a sufficient condition for the prediction of 'Onset-of-cracking', seen here as onset of failure:

*This is known for the author for about 50 years from the so-called 'thin layer effect' of UD-layer-composed laminates: *Due to being strain-controlled, the material flaws in a thin lamina (*transversely-

isotropic material*) cannot grow freely up to micro-crack size in the thickness direction, because the neighboring laminas act as micro-crack-stoppers*. Considering fracture mechanics, the strain energy release rate, responsible for the development of damage energy in the 90° plies - from flaws into micro-cracks and larger -, increases with increasing ply thickness. Therefore, the actual absolute thickness of a lamina in a laminate is a driving parameter for initiation or onset of micro-cracks, i.e. [*Fla82*].
*Further and generally more known in metallic applications is the case of discontinuities of the here focused isotropic materials such as notch singularities with steep stress decays: only a *toughness + characteristic length-based energy balance condition* may form a sufficient set of two fracture conditions.

When applying SFCs usually ideal solids are considered which are assumed to be free of essential micro-crack-like flaws, whereas applying Fracture Mechanics the solid is considered to contain macro-cracks, respectively.

Since about 20 years Finite Fracture Mechanics (FFM) tries to fill a gap between the continuum mechanical strength analysis and the classical FM analysis. FFM is an approach to offer a criterion to predict the crack onset in brittle isotropic and UD materials.
This is a bridge that had to be built from the strength failure to the fracture mechanics failure ground. Attempts to link SFC-described 'onset of fracture' prediction methods and FM prediction methods for structural components have been performed. Best known is the still cited Hypothesis of Leguillon, where he assumes cracks of finite length Δa. Thus using FFM one obtains one more unknown but also a further equation to solve the equation system together with the SFC.
This coupled criterion does not refer to microscopic mechanisms to predict crack-*nucleation*!

Considering FFM it is referred to the literature [1, 2, 3].

Note on short Cracks according to citations in literature:

- In polycrystalline materials if $a <$ grain diameter / 5
- Size of the cyclic plastic zone at the crack tip
- Different crack closure due to the small crack and its flanks
- Notch surface quality.

2 List of Symbols

Symbol	Unit	Description
a	mm	crack length
a_0	mm	initial crack length (open hole panel: crack a + hole radius r)
a_c	mm	*critical* crack length
a_e	mm	*effective crack length* $a_e = a_p + \omega/2$
a_p	mm	*physical crack length* $a_p = a_0 + \Delta a$
c_{ij}		abbreviating functions and abbreviations
$f(a)$		correction function of the stress intensity factor (SIF)
f_d		correction function concerning the hole diameter d
f_w		correction function concerning the specimen width w
t; w	mm	panel specimen thickness; width of panel, test specimen
Δa	mm	stable increase of a due to static loading
Δa_e	mm	effective crack elongation (R-curve abscissa) $\Delta a_e = a - a_0$
A	mm	parameter of the R-curve model, cross-section
B	-	parameter of the R-curve model
E	MPa	Young's modulus (MPa = N/mm^2)
F	N	force
$\mathcal{G}_{Ic}$	MPa · m	Cracking resistance: potential strain energy release rate at failure. Under plane strain conditions (most critical case) $\mathcal{G}_{Ic} = K_{Ic}{}^2 \cdot (1-\nu^2) / E$, $\sqrt{\text{m}} = 31.6 \cdot \sqrt{\text{mm}}$
$K(\sigma,a)$	$\text{MPa} \cdot \sqrt{\text{m}}$	Cracking action: stress intensity factor, (SIF) $K = \sigma \cdot \sqrt{\pi \cdot a} \cdot f(a)$,
K_{as}	$\text{MPa} \cdot \sqrt{\text{m}}$	parameter of the R-Curve model (asymptotic value of R-curve)
K_b	$\text{MPa} \cdot \sqrt{\text{m}}$	parameter of the R-Curve model (value at beginning of R-curve)
K_{app}	$\text{MPa} \cdot \sqrt{\text{m}}$	apparent fracture toughness (general) = critical SIF (not the often used K_c)
K_p	$\text{MPa} \cdot \sqrt{\text{m}}$	physical value of the SIF K: $K_p = \sigma \cdot \sqrt{\pi \cdot a_p} \cdot \sqrt{\sec(\pi \cdot a_p / w)}$, sec =1/cos
K_e	$\text{MPa} \cdot \sqrt{\text{m}}$	Effective SIF: $K_e = \sigma \cdot \sqrt{\pi \cdot a_e} \cdot \sqrt{\sec(\pi \cdot a_e / w)}$, often termed K_R
K_{Ic}	$\text{MPa} \cdot \sqrt{\text{m}}$	Cracking resistance: critical SIF (fracture mechanics Mode I testing) at onset of unstable sharp crack propagation in the plane strain state = most brittle condition, otherwise called K_c; or = fracture toughness of uni-axially tensile-loaded, minimum ductile (*brittle*) material specimens = material resistance to crack propagation $K_{Ic} = \sigma \cdot \sqrt{\pi \cdot a_c} \cdot f(w,d) = \sigma_c \cdot \sqrt{\pi \cdot a} \cdot f$
K_R	$\text{MPa} \cdot \sqrt{\text{m}}$	Cracking resistance, R-curve ordinate
R-curve	$\text{MPa} \cdot \sqrt{\text{m}}$	material *Resistance* to fracture curve in case of slow, stable crack propagation from a sharp notch, accompanied by growth of the plastic zone at the crack-tip (*unfortunately also the letter R was taken*)
R; R_{p02}	MPa	failure stress ≡ strength (*Resistance to stress action*); tensile yield strength
W	N·mm	Energy = $\int_0^{\Delta\ell} F \cdot d(\Delta\ell) = \int_0^{\Delta\ell} \sigma \cdot A \cdot d(\varepsilon \cdot \ell) = A \cdot \ell \cdot \int_0^{e} \sigma \cdot d\varepsilon = A \cdot \ell \cdot \int_0^{\sigma} \frac{\sigma}{E} \cdot d\varepsilon = V \cdot \frac{\sigma^2}{2 \cdot E}$
ν	-	Poisson's ratio
ω	mm	full plastic zone at the crack-tip
σ	MPa	Action: remote (far field) uniform tensile stress
σ_c	MPa	critical value of σ = residual strength

(In structural mechanics x is usually the length coordinate, however in fracture mechanics the net section direction)

The following chapter represents an intended introduction for the focused Finite-Fracture-Mechanics.

3 Analysis using the Crack Growth Resistance curve = '*R*-curve'

3.1 General on Fracture Mechanics quantities and R-curve Concept

Aim: *Chapter is helpful for better grasping the novel FFM, because FM is one part of the FFM.*

Basic assumption: Use of largest crack size that can be expected, following the 'weakest link' failure model and regarding quality assurance measurement limits.

In the Damage Tolerance procedure of cracked (macro-damaged) structural components two basic questions are posed in analysis:

1. What is the static strength if a crack is present (residual strength problem)?
2. How is the propagation behavior of the present crack (large crack growth problem)?

In order to perform this for isotropic materials some different quantities are used to predict the stress state at the crack tip caused by a far-field stress or remote stress, respectively.

*The stress intensity factor (SIF) *K*, applied to homogeneous linear elastic materials. Its measured size depends on test specimen width w, the crack size *a*, the location of the present crack and the material. It can be written as $K = \sigma \cdot \sqrt{\pi \cdot a_0} \cdot f(a/w)$, where the SIF K_I of the fracture mechanics mode I is applied here, (*Fig. 4*).

*The strain energy release rate $\mathcal{G}$, defined as the instantaneous loss of total differential potential energy dΠ per unit crack growth area (crack length Δa · plate thickness *t*) of the fresh surface S, by $\mathcal{G} = -d\Pi / dS$. In the case of brittle materials for its 'basic' Fracture Mode-I a relationship exists $\mathcal{G}_I = K_I^2$ /E' with E'= E/(1-ν^2) for plane strain.

*The J-integral *J* , characterizing the singular stress field at the crack tip in nonlinear elastic-plastic materials where the size of the plastic zone is small compared to the crack length. It is one way of determining the strain energy release rate $\mathcal{G}$. For brittle materials *J* corresponds to $\mathcal{G}$.

Macrocrack extension occurs when the stress intensity factor (SIF) *K* attains a critical value. Thereby the *Action-linked* SIF is entirely dependent on the structure geometry and loading condition, whilst the *Resistance-linked R*-curve is basically a material property dependent on temperature, environment, and loading rate as well the geometric test specimen range, etc.

Crack-growth resistance curves, the so-called *R*-Curves, are used here to predict:

- the residual strength of the structure for a given crack position and crack length,
- the critical length of an initial crack under given loadings.

These curves are conveniently plotted with crack extension Δa instead of crack size *a*, because the shape of the R-curve does not vary with the crack size.

* For very brittle materials with its flat *R*-curves, there is no stable crack extension and the initial crack size a_0 is the same as the critical crack size a_c. Then a single value of toughness characterizes the material, the cracking resistance K_{Ic}.

* For ductile materials (*such as low strength steels*) with a rising *R*-curve there is no single value of toughness that characterizes the material. Reason is that the plastic zone ω at the crack tip increases with crack growth and length, hence the energy dissipated to overcome plastic deformation will increase. In materials with a rising *R*-curve, stable crack growth occurs and the critical crack size will be larger than the initial crack size.

For 'fatiguers', mind:

"These R-curves (italic R letter) shall not be mixed up with the 'R-curves' in fatigue R = minσ/maxσ".

Fracture mechanics regards small scale ductility (usually described by its diameter ω) at the crack tip and multi-axial stressing, *Fig 2*.

In the case of a mixed-mode loading and opening of a crack, the energy release rate consists of the three parts $\mathcal{G}_I$, $\mathcal{G}_{II}$, $\mathcal{G}_{III}$ that correspond to the respective three fracture modes. The fracture-effective formulation then is $\mathcal{G} = \mathcal{G}_I + \mathcal{G}_{II} + \mathcal{G}_{III}$.
Crack extension occurs when above strain energy release rate $\mathcal{G}$ attains a critical value $\mathcal{G}_c$. In the case of fracture it becomes $\mathcal{G} \geq \mathcal{G}c$. $\mathcal{G}$ is directly related to the stress intensity factor K. It is associated in two-dimensional fracture mechanics with the loading modes (Mode-I, Mode-II, or Mode-III) the so-called Mixed-Mode Problem, applicable to cracks under plane stress, plane strain and anti-plane shear, see *Fig.4*. For the Fracture Mode-I, the energy release rate $\mathcal{G}$ is related to the Mode-I stress SIF K_I for a linearly-elastic material.

The two questions at the beginning of this sub-chapter can be answered using the analytical methods of fracture mechanics. For practical application the concept of the linear-elastic K is usually applied:
"*A structural component will fail in the case of static loading if the stress intensity factor (SIF)* K *of a brittle material reaches its critical value at* $K = K_c$*, termed fracture toughness, which depends on the material behavior*".
The determination of the K_c -values requires in the so-called K-concept the fulfilment of a geometric bound in order to achieve the real minimum K_{Ic}-value by a test specimen thickness of

$$t \; > \; 2.5 \cdot (K_{Ic} \,/\, R_{p0.2})^2 \;\rightarrow\; \sigma_c = K_{Ic} \,/\, (\sqrt{\pi \cdot a_0} \cdot f(a_0)\,.$$

Instead of the "Plain Strain Fracture Toughness" K_{Ic} (which is a material property but subject to certain minimum geometric requirements), an "Apparent Fracture Toughness" is inevitably to apply, adapted to the current geometric conditions.

A plot of strain energy release rate $\mathcal{G}$ versus crack extension Δa for a particular loading situation is termed driving force curve $\mathcal{G}(\Delta a)$. The driving force for crack propagation can be quantified by above characterizing parameters K, $\mathcal{G}$, or J. A plot of R versus crack extension Δa is a resistance curve, as still cited termed R-curve $R(\Delta a)$.

3.2 Models for R-curve (resistance) and for Stress Intensity Factor (SIF)-curve

3.2.1 Resistance: R-curve, ordinate K_R (*using a test data mapping function*)

For well mapping the test data course of the R-curve J. Broede proposed the mapping function

$$K_e(a) = K_{as} - (K_{as} - K_b) \cdot \frac{1-B}{\exp\left(\dfrac{\Delta a_e}{A}\right) - B} \quad \text{with inverse} \quad \Delta a_e = A \cdot \ln\left(B + (1-B) \cdot \frac{K_{as} - K_b}{K_{as} - K_e}\right)$$

$$\Rightarrow \quad \text{new } a_0 = a_0 + \Delta a_e = a_0 - A \cdot \ln\left(B + (1-B) \cdot \frac{K_{as} - K_b}{K_{as} - K_e}\right)$$

in [2] including the effective quantities K_e and Δa_e. The plot $K_e(\Delta a_e)$ is termed effective R-curve. This mapping proposal addresses the usual structural materials which shall possess some ductility.

3.2.2 Action: *Stress Intensity Factor (SIF)-curve, K_{SIF}* (using a width correction function f_w)

With the so-called geometry correction functions *f - correcting the original infinite plate term* $\sqrt{\pi \cdot a}$ - concerning hole diameter (index d) and width (index w) of the centrally cracked panel ('plate strip') the SIF reads for the two cases:

Panel, version 'No hole' $_{nh}$ *:*

$K_{nh} = \sigma \cdot \sqrt{\pi \cdot a} \cdot f_w(a)$ with $f_w(a) = \sqrt{\sec \frac{\pi \cdot a}{w}}$ capturing the panel width

$$K_{nh}(a) = \sigma \cdot \sqrt{\pi \cdot a} \cdot \sqrt{\sec \frac{\pi \cdot a}{w}} \quad , \qquad (\sec = 1/\cos).$$

Panel, version 'With hole' $_{wh}$ *:* (Tada delivered in [9] a hole considering correction function *f(a))*:

$K = \sigma \cdot \sqrt{\pi \cdot a} \cdot f(a)$ with $f(a) = f_d(a) \cdot f_w(a)$ in the case of an open hole panel

$f_d(a) = \sqrt{1 - \frac{r}{a}} \cdot (1 + 0.358 \cdot \frac{r}{a} + 1.425 \cdot \left(\frac{r}{a}\right)^2 - 1.578 \cdot \left(\frac{r}{a}\right)^3 + 2.156 \cdot \left(\frac{r}{a}\right)^4)$, $f_w(a) = \sqrt{\sec(\frac{\pi \cdot r}{w}) \cdot \sec(\frac{\pi \cdot a}{w})}$.

$$K_{wh}(a) = \sigma \cdot \sqrt{\pi \cdot a} \cdot \sqrt{1 - \frac{r}{a}} \cdot (1 + 0.358 \cdot \frac{r}{a} + 1.425 \cdot \left(\frac{r}{a}\right)^2 - 1.578 \cdot \left(\frac{r}{a}\right)^3 + 2.156 \cdot \left(\frac{r}{a}\right)^4 \cdot \sqrt{\sec \frac{\pi \cdot r}{w} \cdot \sec \frac{\pi \cdot a}{w}}.$$

3.3 Conditions to Determine the Unknowns: critical quantities σ_c, a_{ce}

'*Crack growth will occur when dG/da > dR/da and G ≥ R*'.

This corresponds to '*The SIF driving force curve is tangent with the R-curve'* as depicted in *Fig.3*. It can be interpreted as the critical condition when the energy available in the component for crack growth exceeds the maximum amount that the material can dissipate.

For fully brittle materials the *R*-curve is a horizontal constant line, a tangent-condition is not of interest.

In order to solve this task the following conditions must be met:

3.3.1 $K_{SIF}(\sigma_c, a_{ce}) = K_e(a_{ce} - a_0)$ with $\Delta a_e = a - a_0$. This means, that:

firstly the coordinates of the touch point of SIF curve with R-curve are to determine.

$$K_e(a) = \sigma \cdot \sqrt{\pi \cdot a} \cdot f(a) = K_{as} - (K_{as} - K_b) \cdot \frac{1 - B}{\exp\left(\frac{\Delta a_e}{A}\right) - B} \quad \text{and}$$

3.3.2 $dK_{SIF}(\sigma_c, a_{ce})/da = dK_e(a_{ce} - a_0)/da$. This means, that:

secondly, the two slopes of both the curves must become the same at the touch point, task which requires a differentiation (*Mathcad 15 code* symbolic *application*), delivering

$$\frac{dK_e}{da} \Rightarrow \sigma \cdot \frac{d}{da}\left(\sqrt{\pi \cdot a} \cdot f(a)\right) = K_{as} + \frac{(B-1) \cdot (K_b - K_{as})}{B - \exp(\frac{\Delta a_e}{A})} \Leftarrow \frac{dK_R}{da} .$$

For the SIF-curve holds for the two versions, SIF_{nh} no hole and SIF_{wh} with hole:

$$\text{SIF 'no hole'}: \quad \frac{dK_{SIFnh}}{da} = \frac{d\left(\sigma\cdot\sqrt{\pi\cdot a}\cdot\sqrt{\cdot\sec\frac{\pi\cdot a}{w}}\right)}{da}$$

$$= \sigma\cdot\frac{\sqrt{\pi}/(2\sqrt{a}\cdot caw)+\pi^{1.5}\cdot\sqrt{a}\cdot saw/(w\cdot caw^2)}{2\cdot\sqrt{\sqrt{\pi\cdot a}/caw}},\ saw=\sin\left(\frac{\pi\cdot a}{w}\right), caw=\cos\left(\frac{\pi\cdot a}{w}\right).$$

SIF 'with hole' : (copied, Mathcad typing)

$$\frac{dK_{SIFwh}}{da} = \frac{d\left(\sigma\cdot\sqrt{\pi\cdot a}\cdot\sqrt{1-\frac{r}{a}}\cdot\left(1+0.358\cdot\frac{r}{a}+1.425\cdot\left(\frac{r}{a}\right)^2-1.578\cdot\left(\frac{r}{a}\right)^3+2.156\cdot\left(\frac{r}{a}\right)^4\right)\cdot\sqrt{\sec\frac{\pi\cdot r}{w}\cdot\sec\frac{\pi\cdot a}{w}}\right)}{da}$$

$$= \sigma\cdot\sqrt{\pi\cdot a}\cdot\left[c3\cdot\sqrt{1-\frac{r}{a}}\cdot(c1)+\frac{c3\cdot\sqrt{1-\frac{r}{a}}\cdot(c2)}{2\cdot a}+\frac{r\cdot c3\cdot(c2)}{2\cdot a^2\cdot\sqrt{1-\frac{r}{a}}}+\frac{\sin\left(\frac{\pi\cdot a}{w}\right)\cdot\sqrt{1-\frac{r}{a}}\cdot(c2)}{\sqrt{a}\cdot 2\cdot w\cdot\cos\left(\frac{\pi\cdot a}{w}\right)^2\cdot\cos\left(\frac{\pi\cdot r}{w}\right)\cdot c3}\right]$$

and the abbreviation functions

$$c1=\frac{4.734\cdot r^3}{a^4}-\frac{8.624\cdot r^4}{a^5}-\frac{0.358\cdot r}{a^2}-\frac{2.85\cdot r^2}{a^3},\quad c2=\frac{0.358\cdot r}{a}+\frac{2.156\cdot r^4}{a^4}+\frac{1.425\cdot r^2}{a^2}-\frac{1.578\cdot r^3}{a^3}+1,\quad c3=\sqrt{\frac{1}{\cos\left(\frac{\pi\cdot a}{w}\right)\cdot\cos\left(\frac{\pi\cdot r}{w}\right)}}$$

* In the HSB sheet 62232-3 *J. Broede* mapped the *R*-curve by an appropriate analytical model, model parameters were determined there and finally $\sigma_c = R_{res}$ was derived by iteratively increasing the crack size up to a_c. This provides the failure stress for the maximally sustainable loading of the pre-cracked component.

* In *Table 1*, bottom, Cuntze delivers a continuous implicit mathematical computation.

3.4 Solution of the equation set to predict the unknowns

The Mathcad computation delivers the searched quantities for the open hole panel. *Fig.3* provides the full data set. In the computation, the usually in $\text{MPa}\cdot\sqrt{\text{m}}$ given fracture toughness (= critical SIF) is taken, which however requires a final factorization of the obtained critical stress by $\sqrt{1000}$ to get into the MPa, mm system.

In *Fig.3,* for the envisaged panel, the *R*-curve is plotted together with two SIF-curves, one for an initially guessed reference stress of sigwh=15 (dashed) and one for the computed critical reference value sig_c =12.5 (**bold**).

*For the 'no hole-panel' the critical SIF reads $K_c = 180\ \text{MPa}\cdot\sqrt{\text{m}} = 180\cdot\sqrt{1000}\ \text{MPa}\sqrt{\text{mm}}$ and the results are: $a_{ce} = 55.4$ mm, $\sigma_c = 12.5\cdot\sqrt{1000} = 396$ MPa.

*For the 'hole panel', in order to check any influence of the hole the associated rising **SIF-curve** was plotted, too. The same tangent point is obtained for this SIF-curve.

The computation of the 'no hole-panel' delivers as critical stress = residual strength, the value σ_{res} = 396 MPa (Mathcad computation scheme in *Table 1*).

*Table 1: Determination of the touch point = instability tangent point (*w width effect, no hole*)*

Vorgabe sigw = 11 a = 33

$$sigw\cdot\sqrt{\pi\cdot a}\cdot\sqrt{Sek\left(\frac{\pi\cdot a}{w}\right)} = Kas - (Kas - Kb)\cdot\frac{1 - B}{\exp\left(\frac{a - a0}{A}\right) - B} \quad \textbf{(point)}$$

$$\frac{\pi\cdot sigw\cdot\left(\frac{\cos\left(\frac{\pi\cdot a}{w}\right) + \frac{\pi\cdot a}{w}\cdot\sin\left(\frac{\pi\cdot a}{w}\right)}{\cos\left(\frac{\pi\cdot a}{w}\right)^2}\right)}{2\cdot\sqrt{\frac{a\,\pi}{\cos\left(\frac{\pi\cdot a}{w}\right)}}} = \frac{e^{\frac{a-a0}{A}}\cdot(B - 1)\cdot(Kb - Kas)}{A\cdot\left[B - e^{\frac{1}{A}\cdot(a-a0)}\right]^2} \quad \textbf{(slope)}$$

Aa := Suchen(sigw, a) $Aa = \begin{pmatrix} 12.5 \\ 55.4 \end{pmatrix}$ sigw := Aa_0 sigw = 12.5 awc := Aa_1 awc = 55.4

$\sigma wc := sigw\cdot\frac{MPa\cdot\sqrt{m}}{\sqrt{mm}}$ $\sigma wc := sigw\cdot\sqrt{1000}$

KSIFwc0 := $sigwc\cdot\sqrt{\pi\cdot awc}\cdot\sqrt{Sek\left(\frac{\pi\cdot awc}{w}\right)}$ w = 300 KSIFwc0 = 180 σwc = 396

For information, however – no practical effect in *Fig.3* comparing the blue curve KSIFwh – the associated (point) condition with considering the hole is added below:

$$sig\cdot\sqrt{\pi\cdot a}\cdot\left(c3\cdot\sqrt{1 - \frac{r}{a}}\cdot c1 + \frac{\sqrt{\pi}\cdot sig\cdot c3\cdot\sqrt{1 - \frac{r}{a}}\cdot c2}{2\cdot\sqrt{a}} + \frac{\sqrt{\pi}\cdot sig\cdot r\,c3\cdot c2}{2\cdot a^{1.5}\cdot\sqrt{1 - \frac{r}{a}}} + \frac{\pi^{1.5}\cdot\sqrt{a}\cdot sig\cdot\sin\left(\frac{\pi\cdot a}{w}\right)\cdot\sqrt{1 - \frac{r}{a}}\cdot c2}{2\cdot w\cdot\cos\left(\frac{\pi\cdot a}{w}\right)^2\cdot\cos\left(\frac{\pi\cdot r}{w}\right)\cdot c3}\right)$$

with the to be inserted abbreviation functions c1, c2, c3

$$= Kas + \frac{(B - 1)\cdot(Kb - Kas)}{B - e^{\frac{1}{A}\cdot(a-a0)}}$$

The computation of the critical crack length a_c at the end of static loading is determined by the application of the formula below and there inserting K_{ec} (see application later). As K-values are usually given in $MPa\cdot\sqrt{m}$ this is intentionally widely followed here!

$$\text{new } a_0 = a_0 + \Delta a_{ec} = a_0 - A\cdot\ln\left(B + (1 - B)\cdot\frac{K_{as} - K_b}{K_{as} - K_{ec}}\right) .$$

Results:

The R-test curve (resistance, marked KR) captures all physical effects such as small scale yielding at the crack tip, marked by the letter ω! It is effective, therefore K_e. Therefore, in order to be compatible the SIF-curve (action, marked KSIF) has to incorporate this effect. It does not depend on a_0,w.

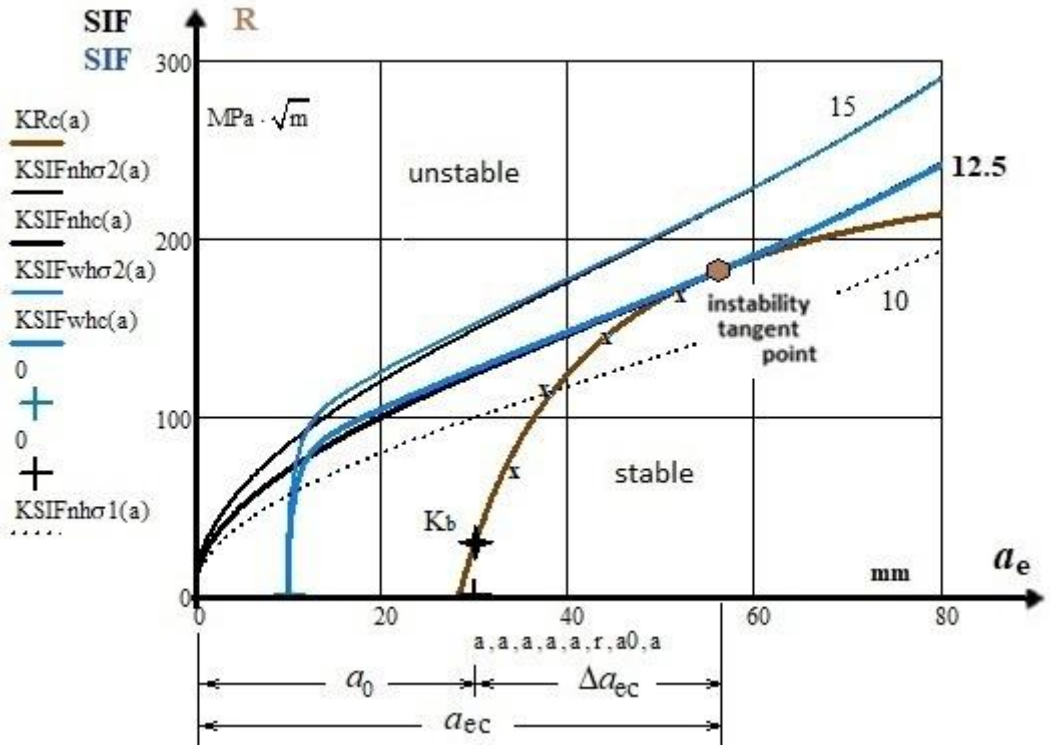

Fig.3: Wide panel example (HSB 62232-03) with w =300 mm, *t = 8*mm, a_0 *= 30* mm, *d =20* mm.
Aluminum Alloy 7475-T7351 in LT-direction: A =55.7 mm, *B = 0.75*, K_{as} *=246* $\text{MPa} \cdot \sqrt{\text{m}}$,
K_b *=29* $\text{MPa} \cdot \sqrt{\text{m}}$, R_{p02} *=425* MPa *(B-value for t = 6...38* mm) .
Instability point: K_e *= 180* $\text{MPa} \cdot \sqrt{\text{m}} = \text{MPa} \cdot \sqrt{\text{mm}} \cdot \sqrt{1000}$, a_{ce} *= 55.4* mm.
SIF-curve: reference stresses in MPa, to factor by $\sqrt{1000} = 31.6$: $\sigma_2 = 15 > \sigma_c = 12.5 > \sigma_1 = 10$, *Table* 1.
(For simplification the simple letter a was taken in the formulas instead of ae)

Notes:

*The R-curve does not run out from a_0. This is caused because just the test data domain has to be fitted best. In the HSB sheet the beginning is therefore not sketched. The model point Kb lies on the a_0-line.

*Very brittle materials possess a horizontal *R*-curve.

► The test-based *R*-curve is essential for FFM to determine in future a more correct fracture toughness value K_{app} instead of the previous K_{Ic} for the usually FFM-treated very brittle material.

4 Analysis using Finite Fracture Mechanics (FFM)

4.1 General

To prove Structural Integrity several design verifications (DVs) must be performed for components having the following features: Smooth, notched (stress concentrations) and cracked (stress singularities), see *Fig.4, left*. Thereby, static and cyclic loadings must be taken into account focusing uni-axial and multi-axial stress states.

FFM-focus here is static loading under uni-axial stresses, which means Mode I-linked.

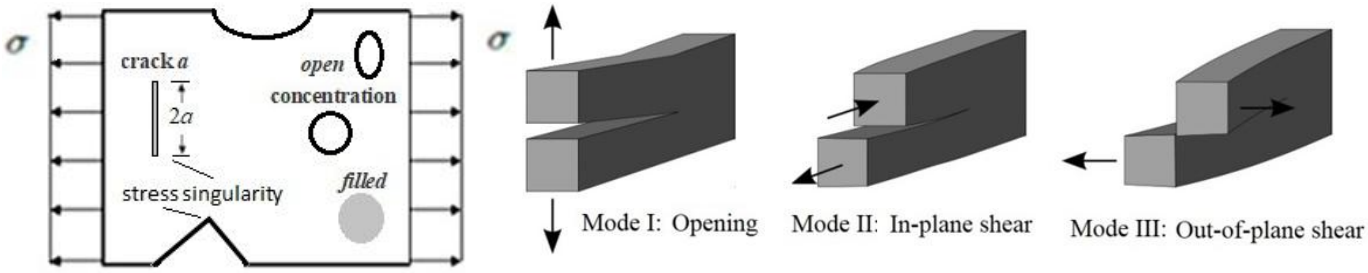

Fig. 4: (left) Stress concentrations and stress singularities under uni-axial stressing.
(right) The 3 FM-modes, crack length a

The following levels are relevant when generating stress-related DV tools:

1. Stresses: *Strength Failure Conditions (SFC), as local design verifications* to predict onset-of-cracking (*several strength fracture failure modes and one yield mode*, practically just one for tension loading,)
2. Stress concentration: *Application of (local) stress concentration factors* K_t to predict onset-of-cracking (fracture)
3. Stress intensity (singularity): (*non-local*) *Fracture mechanics methods using stress intensity factors* $K = \sigma \cdot \sqrt{\pi \cdot a}$ *(SIFs) and fracture toughness (*representing the resistance of brittle materials to the propagation of flaws under an activated stress, assuming: the longer the flaw, the lower the bearable fracture stress) *being a critical* K_c *which is needed for a crack to grow under monotonic loading. For the usually envisaged tension loading* (pressure-linked geo-mechanics is not the focus*) there are three fracture mechanics modes to consider as depicted in Fig.4 above.*

All design verifications are required <u>in parallel</u> in accordance with the applicable regulations.

Tackling above three structural cases, then it can be attributed:

1. Stresses: *In the strength* fracture *failure criterion (SFC) strength values R (isotropic:here* $R^t \equiv R_m$ *) are to insert, which capture any flaws and micro-cracks in the material data set of the test specimen. All effects are considered.*
2. Stress concentrations: *Experience tells that the application of a SFC with the application of a factor* K_t *is not sufficient. Here, a non-local DV method is required, which combines a strength fracture criterion and fracture mechanics criterion. This is the focus of FFM.*
3. Stress intensity: The necessary *('large') crack size value is identified by Quality Assurance or fixed as the minimum measurable crack size. The crack situation at hand is to model and toughness values* K_{Ic} *are to insert. A large crack analysis does not need a coupled DV in order to predict onset-of- further cracking, because the SFC is fulfilled.*

<u>Note</u>: There are stress-related and strain-related SFCs. Stress-related ones have the advantage, compared to strain-related ones that "*Residual stresses can be simply incorporated"*).

4.2 Introduction

Since about 20 years Finite Fracture Mechanics (FFM) intends to fill the gap between the continuum mechanical strength failure criteria (SFC) and the classical FM. FFM is an approach to offer a criterion

to predict 'Onset-of-Cracking' in brittle isotropic and UD materials. This is a bridge that had to be built from strength failure to fracture mechanics failure.
Attempts to link SFC-described 'Onset-of-Cracking (OoC, fracture)' prediction methods and FM prediction methods for structural components have been performed. Best known is the still cited Hypothesis of Leguillon "*A crack is critical when and only when both the released energy and the local stress reach critical values along an assumed finite crack*". Within the FFM, Leguillon assumes instantaneous cracks of finite length Δa. Thus, using FFM one obtains one more unknown but also one more equation to solve together with the SFC the equation system.

Of the basic two previous FFM concept variants, the integral concept used here has proven to be the best. In this case, the stress curve is averaged over the fictitious, critical crack length for the SFC, i.e. converted into a locally evenly distributed stress curve averaged over this length.
As long as this is done over a comparatively small area, this is fine, but if it is a very large crack depth, where the crack extends far into an area of the stress profile where the stress peak has already been significantly reduced, the stress value averaged in this way becomes quite small. The question then is whether this procedure can still lead to a valid SFC application. In the future therefore, it would make sense to limit the range over which the stress curve is averaged appropriately in such cases?

This coupled criterion does not refer to microscopic mechanisms to predict micro-crack nucleation.

Reasons to develop the FFM were some facts from studying 'Onset-of-Cracking':

- Isotropic material

The minor failure behavior of absolutely small holes compared to large holes, although the stress concentration factor K_t takes the same value, namely 3. With large holes, more material volume is highly stressed and thus physically-based the probability of failure due to more activated, material-inherent flaws is increased.

Further known is in the case of discontinuities such as notch singularities with steep stress decays: only a *toughness + characteristic length-based energy balance condition* may form a sufficient set of fracture conditions. Hence, a SFC is a necessary condition but might not be a sufficient condition for the prediction of 'Onset-of-Cracking'.

When applying SFCs usually ideal solids are viewed which are assumed to be free of essential micro-voids or microcrack-like flaws, whereas applying Fracture Mechanics tools the solid is considered to contain macro-cracks.

- Transversely-isotropic material

It is also known for a long time from the so-called 'Thin layer effect' of UD-layer-composed laminate that the SFC-application is not sufficient to understand failure: *Due to being strain-controlled, the material flaws in a thin lamina cannot grow freely up to micro-crack size in the thickness direction, because the neighboring laminas act as micro-crack-stoppers*. In other words: Thin plies, embedded in a laminate, fail at a higher loading level than thick ones.

Employing here fracture mechanics, the strain energy release rate, responsible for the development of damage energy in the 90° plies - *from flaws into micro-cracks and larger cracks* -, increases with increasing ply thickness. Therefore, the actual absolute thickness of a lamina in a laminate is a driving parameter for initiation of cracks, i.e. [*Fla82*].
For laminates - composed of different isotropic layers – such singularities occur, too and are effortfully treated!

4.3 FFM modelling, isotropic material focused here

The FFM concept is demonstrated here by the example "Uni-axially loaded symmetric open-hole plate strip". For this case, the coupled criterion can be simplified and can be analytically solved. Thereby no initial crack a_0 is to treat. Brittle fracture behavior is presumed.

The energy criterion postulates that the critical energy release rate $\mathcal{G}_{Ic} = K_{Ic}^{\ 2} \cdot (1 - \nu^2) / E$, being proportional to the square of the fracture toughness, is met and that the stress criterion = SFC postulates that the concentrated stress within the net-section area, *averaged along the crack length* Δa, reaches a material strength value. This averaging is an assumption, which should to be checked.

From the differential FM strain energy release rate $\mathcal{G} = -d\Pi / dS \rightarrow$ the FFM incremental one $-\Pi / S$.

Whereas the FM is more concerned about the full net section width, in the FFM the concern is basically just the net section length Δa, a portion of the width!

The coupled FFM criterion

Goal of the coupled FFM criterion is to derive two fracture conditions, a strength *R*-related one and a fracture mechanical one assuming a crack of the size Δa. Finally the two conditions are combined and deliver an equation for the unknown critical crack Δa_c being the crack level at which OoC would occur under a critical stress and fracture mechanical condition, simultaneously.

The establishment of the coupled model is to perform on basis of average properties in order to obtain the optimally achievable reliability of 50 %. This means model validation, whereas in the DV statistically based Design Allowables are to apply.

The two parts of the coupled criterion can be expressed by equalities from a Fracture Mechanics (FM) criterion and a Strength Failure Criterion (SFC):

$$\text{FM:}\quad \frac{1}{\Delta a}\cdot\int_{r}^{r+\Delta a} K_1^2(x)\cdot dx = K_{1c}^{\ 2} \qquad \text{and} \qquad \text{SFC:}\quad \frac{1}{\Delta a}\cdot\int_{r}^{r+\Delta a} \sigma(x, y=0)\cdot dx = R_m .$$

For a simpler comparison, for the SFC the square usually is taken, whereby – advantageously - the remote stress σ cancels out in the coupled equation. Fracture failure occurs if both these criteria are simultaneously fulfilled. This leads to the required equation for the determination of

the generated critical crack size Δa_c via

$$\frac{\frac{1}{\Delta a}\cdot\int_{r}^{r+\Delta a} K_I^2(x)\cdot dx}{\left(\frac{1}{\Delta a}\cdot\int_{r}^{r+\Delta a} \sigma_y(x)\cdot dx\right)^2} = \frac{K_{Ic}^{\ 2}}{R_m^{\ 2}} = c_{KR} \ , \quad \text{r = d/2}$$

which is to be integrated in the Δa-process zone.

Later, the author will use the upper, two single versions, because this better displays the parallel working of FM-condition together with the SF-condition.

As the two required resistance quantities are not fully clear and not given, it is sufficient for the following first numerical application of the FFM to apply the available values '*Plain Strain Fracture Toughness' K_{Ic}* (*the inherent lowest material property, subject to certain minimum geometric test specimens requirements to achieve a plain strain condition*), and tensile strength R_m. This will mean the application to a brittle metal. In general, the real critical fracture toughness should be termed '*Apparent Fracture Toughness' K_{app}* (to be understood as a component property, adapted to the current geometrical

conditions). For K_{app} seldom a value is available. Hence, K_{Ic} will be used for the FFM here, despite of the necessity to consider small scale yielding at the crack tip when using structural metal materials, like shown in the chapter R-curve.

Validation of the FFM model is effort-fully to be performed by running isotropic test series for different w/d-ratios of panels.

5 Design Verification of a 'Through center cracked Open hole Panel'

Presumptions and given data for geometry, loading from testing

Presumptions:

- Linear Structural Analysis permitted
- Not fully brittle materials which generate small scale yielding at the crack tip
- Worst case loading situation, no residual *stresses.*

Material resistance: Aluminum alloy 7475-T7351 in L(ength)-T(ransverse) direction,

example from [3]

- *R*-curve: A = 55.7 mm, B = 0.75, K_{as} = 246 MPa $\cdot\sqrt{\text{m}}$, K_b =29 MPa $\cdot\sqrt{\text{m}}$. R_m = 850 MPa
- Yield strength: R_{p02} = 425 MPa (B-value, for t = 6...38 mm), HSB 62232-03, concluding the 445 MPa, as used in HSB 62232-01, can be seen an average value.
- K_{Ic} = 48 MPa $\cdot\sqrt{\text{m}}$ = 1518 MPa $\cdot\sqrt{\text{mm}}$, $(K_{Ic} / R_m)^2$ = 3.23 mm.

Panel dimensions

- Width w =300 mm, thickness t = 8 mm, open hole radius d = 25 mm
- Initial crack size a_0 = 30 mm.

Loading Action with Design Factor of Safety (FoS)

- j =1, Design Limit Load representative
- Uni-axial stress state $\{\sigma\}_{design} = \{\sigma_L\} \cdot j$ with $\{\sigma\}_L = (\sigma_x, \sigma_y, \tau_{xy})^T \cdot j = (0,\ 250,\ 0)^T$ MPa.

5.1 Application of FM, R-curve, concerning 'Open hole panel fracture', pre-crack a_0

See *Fig.3* with the procedure attached. a_0 = 30 mm, d = 25 mm, w = 300 mm.

Design case: Remote loading stress σ_{design} = 250 MPa $\equiv \sigma_I$.

5.1.1 Determination of the residual strength [HSB 62232-03] with the R-curve

The computation in *Table 1* delivers the following values in the instability point (touch point)

FM-resistance: $K_{ec} = 180$ MPa $\cdot\sqrt{\text{m}} = 180 \cdot \sqrt{1000}$ MPa $\cdot\sqrt{\text{mm}}$, proof in *Fig.3*

and further residual strength σ_c = 396 MPa and critical crack length a_{ec} = 55 mm.

Above remote failure stress = structural residual strength of the panel (plate strip) reads

$$\sigma_{fail} = R_{res} = R_{struct} = \sigma_c .$$

For comparison, the following analyses deliver the satisfactory information:

* Stress concentration: $\sigma_{fail} = R_m / K_t(d=\infty) = 850/3 = 283$ MPa $> \sigma_I = 250$ MPa.

* Fracture Mechanics: for a Quality Assurance-defined crack size such as $a_{defined} = 33$ mm,

$$\sigma_{fail}(33) > \sigma_{fail}(55).$$

Results for $\sigma_{design} = 250$ MPa = *sig3:*

The crack grew under the design stress by $\Delta a_{design\ loading} = 3$ *mm.*

$\rightarrow$ *new* $a_0 = a_0 + \Delta a_{design\ loading} = 30 + 3 = 33$ *mm.*

► Computation of the *Reserve Factor* for Design Limit load level, Design Load case $j = 1$

Linear analysis is sufficient (presumption of FFM model at hand): then σ load.

$$RF = \frac{\text{Structural strength Design Allowable } R_{struct}}{\text{Stress } \sigma \text{ at } j \cdot \text{Design Limit Loading}} = \frac{R_{struct}}{\sigma_{design}} = \frac{396}{250} = 1.58 > 1.$$

According to the regulations, R_{struct} has to be a Design Allowable too, which is assumed here due to R_m being a strength Design Allowable and K_{Ic} being statistically–based, too.

Yielding Check in the net-section: as a limit-of-usage check. One obtains:

$$\sigma_{fail} = \sigma_{netyield} = R_{p02} \cdot \left(1 - \frac{2 \cdot a_{ec}}{w}\right) = 425 \cdot \left(1 - \frac{2 \cdot 55}{300}\right) = 267 \text{ MPa} \rightarrow RF = \frac{267}{250} = 1.14 > 1.$$

Result: Due to the requirement $\sigma_{netyield} < \sigma_c$ net section yielding limits the loading here.

5.1.2 Determination of the critical crack length, touch point, considering 'no hole, 'with hole'

In the effective curve (*index e is written*) defined by $K_{ec} = 180 \text{ MPa} \cdot \sqrt{\text{m}}$ the plastic zone ω and the hole diameter are included.

The computation of the critical data set had to be still performed for the establishment of *Fig.3*.

► Computation of the design stress-linked Touch Point + generated crack growth $\Delta a_{design\ loading}$

Employing both the SIF functions from *§ 3.3.1*

$$KSIF_{nh}(a) = \sigma \cdot \sqrt{\pi \cdot a} \cdot \sqrt{\sec\frac{\pi \cdot a}{w}}, \quad \text{and}$$

$$KSIF_{wh}(a) = \sigma \cdot \sqrt{\pi \cdot a} \cdot \sqrt{1 - \frac{r}{a}} \cdot \left(1 + 0.358 \cdot \frac{r}{a} + 1.425 \cdot \left(\frac{r}{a}\right)^2 - 1.578 \cdot \left(\frac{r}{a}\right)^3 + 2.156 \cdot \left(\frac{r}{a}\right)^4 \cdot \sqrt{\sec\frac{\pi \cdot r}{w} \cdot \sec\frac{\pi \cdot a}{w}}\right.$$

the Mathcad computation in Table 2 was executed. (See [3]).

Table 2 Derivation of a ductility-considering SIF K with improved associate crack a

Kec = 180 Kas = 246 Kb = 29 A = 34.682 B = 0.75 a0 = 30 w = 300 Rp02 = 425

Vorgabe a := 33

Crack, no hole

$$sig3\cdot\sqrt{\pi\cdot a}\cdot\sqrt{Sek\left(\frac{\pi\cdot a}{w}\right)} = Kas - (Kas - Kb)\cdot\frac{1 - B}{\exp\left(\frac{a - a0}{A}\right) - B}$$

Aa := Suchen(a) Aa = 32.734 a := Aa a = 32.7

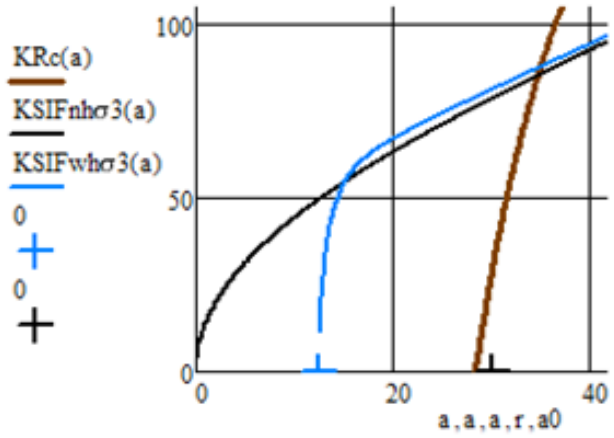

Additional information: Determination of the (physical) K_p from the effective values a_e

There are two methods to determine data of a R-curve The Potential method is used to determine physical data and the Compliance-Method (*applied here*) effective data for the given initial crack length a_0 and the loading stress σ [13, 12, 11].

If necessary, physical data can be derived from effective data by inserting

$$a_p = a_e - 0.5\cdot\omega,\quad \omega = \frac{1}{\pi}\cdot\left(\frac{K_p}{R_{p0.2}}\right)^2$$ into $$K_p = \sigma\cdot\sqrt{\pi\cdot a_p}\cdot\sqrt{\sec\left(\pi\cdot a_p / w\right)}$$ solving the generated implicit equation via

Vorgabe Kp := 180

$$Kp = \sigma\cdot\sqrt{\pi\cdot\left[ae - 0.5\left[\frac{1}{\pi}\cdot\left(\frac{Kp}{Rp02}\right)^2\right]\right]}\cdot\sqrt{\frac{1}{\cos\left[\pi\cdot\frac{ae - 0.5\left[\frac{1}{\pi}\cdot\left(\frac{Kp}{Rp02}\right)^2\right]}{w}\right]}}$$

D := Suchen(Kp)

.

Whether this might be important could be checked by inserting K_{pc} through K_{ec} calculating

$$\omega_{Kec} = \frac{1}{\pi}\cdot\left(\frac{K_{ec}}{R_{p0.2}}\right)^2.$$

In order to present a good feeling for the difference between K_p and K_e the respective values shall be computed in *Table 3* below for the critical case, indexed c :

Table 3:Difference of the critical values of physical K_p and effective K_e

$\sigma fail := 12.5 \quad \sigma := \sigma fail \cdot \sqrt{1000} \quad \sigma = 395 \quad Rp02 := 425 \quad w := 300 \quad a0 := 30 \quad Kec := 180 \cdot (\sqrt{1000})$

$aec := 55.4 \quad \Delta aec := aec - a0 \quad \Delta aec = 25.4 \ mm \quad Kec = 5692$

Vorgabe $\quad Kpc := 5555$

$$Kpc = \sigma \cdot \sqrt{\pi \cdot \left[aec - 0.5 \left[\frac{1}{\pi} \cdot \left(\frac{Kpc}{Rp02} \right)^2 \right] \right]} \cdot \sqrt{\frac{1}{\cos\left[\pi \cdot \frac{aec - 0.5 \left[\frac{1}{\pi} \cdot \left(\frac{Kpc}{Rp02} \right)^2 \right]}{w} \right]}}$$

$D := Suchen(Kpc) \quad D = 4479$

$$\omega ec := 0.5 \left[\frac{1}{\pi} \cdot \left(\frac{Kec}{Rp02} \right)^2 \right] \quad \omega pc := 0.5 \left[\frac{1}{\pi} \cdot \left(\frac{Kpc}{Rp02} \right)^2 \right] \quad apc := aec - 0.5 \cdot (\omega ec)$$

$\omega ec = 28.5 \quad \omega pc = 27.2 \ mm \quad apc = 41.1$

*5.2 **Application of FFM**, concerning 'Onset-of-Cracking' at a open hole edge, (no a_0)*

Determination of finite crack length *Δa* and failure stress of the panel: *Mathcad 15 application*

In this sub-chapter the 'classical' FFM-procedure with the square will be presented.

- The FM-linked failure portion: The equation reads:

$$\frac{1}{\Delta a} \cdot \int_r^{r+\Delta a} \left[K_I^2(x) \right] \cdot dx =$$

$$\frac{1}{\Delta a} \cdot \left[\int_r^{r+\Delta a} \left(\sigma \cdot \sqrt{\pi \cdot r} \cdot \sqrt{1 - \frac{r}{x}} \cdot \left(1 + 0.358 \cdot \frac{r}{x} + 1.425 \cdot \left(\frac{r}{x}\right)^2 - 1.578 \cdot \left(\frac{r}{x}\right)^3 + 2.156 \cdot \left(\frac{r}{x}\right)^4 \cdot \sqrt{\sec\frac{\pi \cdot r}{w} \cdot \sec\frac{\pi \cdot x}{w}} \right]^2 \cdot dx \right.$$

- The SFC-linked failure portion: For details see *Annex1*

For this portion a model for the stress distribution along the net section is to provide, namely,

$$\sigma_{netsec}(x) = \sigma \cdot c_{wd} \cdot [0.335 + 0.665 \cdot (1 + c_{11} \cdot \frac{x - r}{0.5 \cdot w - r})^{c_{12}} + c_{13} \cdot (\frac{x - r}{0.5 \cdot w - r})^4 \ , \ [8]$$

with the abbreviation functions $c_{wd} = 3.215 - (\frac{w}{d})^{-0.5} + 4.294 \cdot (\frac{w}{d})^{-1.5}$ and

$c_{11} = -3.765 + 2.148 \cdot (\frac{w}{d})^{0.879}$, $c_{12} = -2.552 - 42.894 \cdot (\frac{w}{d})^{-3.17}$, $c_{13} = -0.7497 \cdot (\frac{w}{d})^{-1.858}$.

The equilibrium equation of the SFC-portion reads

$$\frac{1}{\Delta a} \cdot \int_r^{r+\Delta a} \sigma(x, y = 0) \cdot dx = \frac{1}{\Delta a} \cdot \int_r^{r+\Delta a} \sigma_{netsec}(x) \cdot dx =$$

$$\frac{1}{\Delta a} \cdot \int_r^{r+\Delta a} \sigma \cdot c_{wd} \cdot [0.335 + 0.665 \cdot (1 + c_{11} \cdot \frac{x - r}{0.5 \cdot w - r})^{c_{12}} + c_{13} \cdot (\frac{x - r}{0.5 \cdot w - r})^4 \cdot dx$$

.

The implicit FFM-solution procedure of the Mathcad software in standard FFM-formulation is shown below in *Table 4* (Mathcad font):

Table 3:

Vorgabe

$\Delta a := 1 \qquad \sigma := 11$

$$\left[\frac{1}{\Delta a}\cdot\left[\int_{r}^{r+\Delta a}\left[\left[\sigma\cdot\sqrt{\pi\cdot x}\cdot\left[\sqrt{1-\frac{r}{x}}\cdot\left[1+0.358\cdot\frac{r}{x}+1.425\cdot\left(\frac{r}{x}\right)^{2}-1.578\cdot\left(\frac{r}{x}\right)^{3}+2.156\cdot\left(\frac{r}{x}\right)^{4}\right]\right]\cdot\sqrt{\mathrm{Sek}\left(\frac{\pi\cdot r}{w}\right)\cdot\mathrm{Sek}\left(\frac{\pi\cdot x}{w}\right)}\right]^{2}dx\right]\right] = \frac{KIc^{2}}{Rm}$$

$$\frac{1}{\Delta a}\cdot\left[\int_{r}^{r+\Delta a}\sigma\cdot crw\cdot\left[0.335+0.665\cdot\left(1+c11\cdot\frac{x-r}{0.5\cdot w-r}\right)^{c12}+c13\cdot\left(\frac{x-r}{0.5\cdot w-r}\right)^{4}\right]dx\right]$$

$$\frac{1}{\Delta a}\cdot\left[\int_{r}^{r+\Delta a}\sigma\cdot crw\cdot\left[0.335+0.665\cdot\left(1+c11\cdot\frac{x-r}{0.5\cdot w-r}\right)^{c12}+c13\cdot\left(\frac{x-r}{0.5\cdot w-r}\right)^{4}\right]dx\right] = Rm$$

$A := \mathrm{Suchen}(\Delta a,\sigma) \qquad A = \begin{pmatrix}1.77\\420.83\end{pmatrix} \qquad \Delta a := A_0 \qquad \Delta ac := \Delta a \qquad \sigma := A_1 \qquad \sigma fail := \sigma$

$\Delta ac = 1.77 \qquad \sigma fail = 421$

Results:

Within the FFM, two models from FM and from strength analysis are commonly employed to predict the failure event 'Onset-of-Cracking' at a non-cracked hole. In the case at hand, the instantaneously generated finite crack length reads $\Delta a_c = 1.77$ mm *and the associated remote average structural failure stress of the panel* σ_{struc} *reads* σ_{fail} *= 421 MPa.*

Fig.5 finally tries to illustrate the FFM hypothesis "*Both the conditions must be fulfilled*". It points out the failure-causing relationship and the dominated domains, where stress states may happen to be.

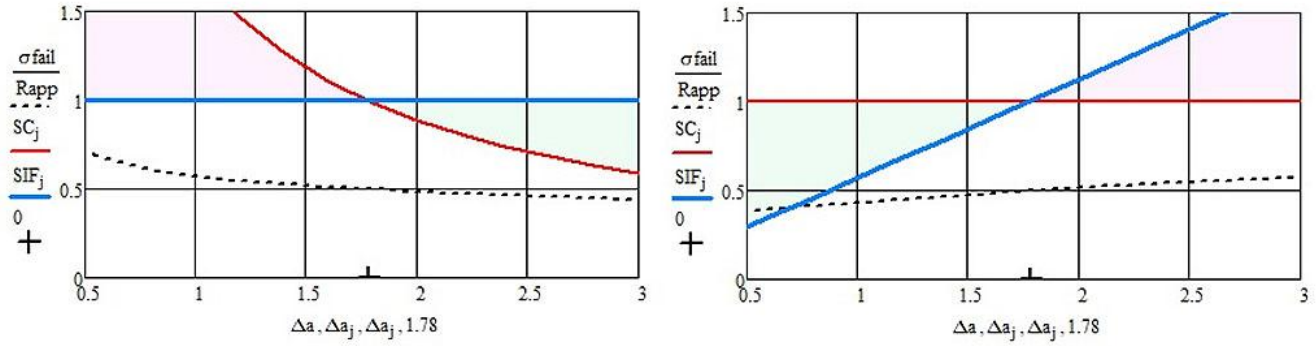

Fig. 5, w=36mm , a_0 *= 30 mm, d =6 mm:* $\Delta a_c = 1.77$ mm

(left) 'SIF' is assumed to be 100% with the question "When does the SC not show failure?
Vice versa: (right) SC assumed to be 100% with the question "When does the 'SIF' not show failure?

One basic interest is how a varying resistance ratio $c_{KR} = K_{Ic}^2/R_m^2$ affects critical **crack length** and **failure stress**. *Fig.6* shows the mapped numerical results for a number of ratios.

Result: With increasing resistance ratio both critical crack size and failure stress naturally grow.

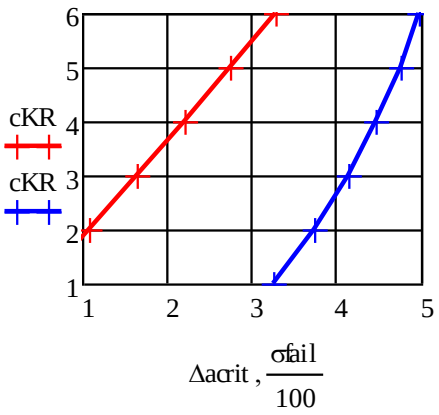

Fig.6, w=36mm , a_0 = 30 mm, d =6 mm:
Effect of varying resistance ratio c_{KR}, measured in mm, on Δa_c (left) and σ_{fail} (on the abscissa)

AA 7475-T7351:
$c_{KR0} = (K_{Ic} / R_m)^2 = 3.23$ mm, $\Delta a_c = 1.77$ mm

Of further interest might be how the FM-linked and the SC-linked portions change with the crack length. *Fig.7* depicts these courses after employing the two integrals, termed 'SIF' and SC, below.

$$\frac{\frac{1}{\Delta a}\cdot\int_r^a K_I^2(x)\cdot dx}{\left(\frac{1}{\Delta a}\cdot\int_r^a \sigma_y(x)\cdot dx\right)^2} = \frac{K_{Ic}^2}{(R_m)^2} = c_{KR} \quad \Rightarrow \quad \frac{\frac{1}{\Delta a}\cdot\int_r^a K_1^2(x)\cdot dx / K_{1c}^2}{\left(\frac{1}{\Delta a}\cdot\int_r^a \sigma_y(x)\cdot dx\right)^2 / R_m^2} = \frac{'SIF'}{SC} \quad \text{with}$$

$$SIF_i := \frac{\frac{1}{\Delta a_i}\cdot\int_r^{r+\Delta a_i}\left[\sigma\cdot\sqrt{\pi\cdot x}\cdot\left[\sqrt{1-\frac{r}{x}}\cdot\left[1+0.358\cdot\frac{r}{x}+1.425\cdot\left(\frac{r}{x}\right)^2-1.578\cdot\left(\frac{r}{x}\right)^3+2.156\cdot\left(\frac{r}{x}\right)^4\right]\right]\cdot\sqrt{Sek\left(\frac{\pi\cdot r}{w}\right)\cdot Sek\left(\frac{\pi\cdot x}{w}\right)}\right]^2 dx}{KIc^2}$$

$$SC_i := \frac{\frac{1}{(\Delta a_i)^2}\cdot\left[\int_r^{r+\Delta a_i}\sigma\cdot crw\cdot\left[0.335+0.665\cdot\left(1+c11\cdot\frac{x-r}{0.5\cdot w-r}\right)^{c12}+c13\cdot\left(\frac{x-r}{0.5\cdot w-r}\right)^4\right]dx\right]^2}{Rm^2}$$

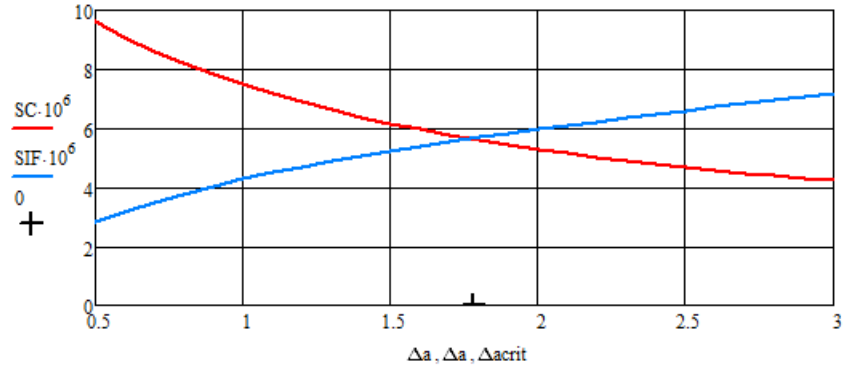

Fig.7, w =36mm, a_0 = 30 mm, d =6 mm: Course of growing FM-portion (SIF) and decaying Strength Mechanics portion (SC) over the finite crack size Δa

Result: The critical point at a_c = 1.78 mm is clearly marked at 'SIF' = SC.

After having depicted the influence of the resistance ratio $c_{KR} = K_{Ic}^2/R_m^2$ in *Fig.6* the effect of a fixed ratio 'panel width/hole diameter' w/d shall be displayed for two widths in *Fig.8* presenting how the remote failure stress σ_{fail} of the panel changes with Δa.

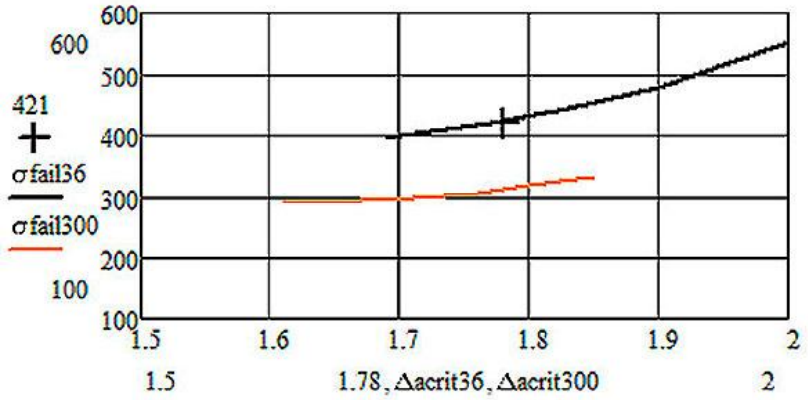

Fig.8, w=36mm, w = 300mm: Effect of different panel geometry, ratios w/d = 6.

Result:
For a given resistance ratio c_{KR}, for two panel widths, above stress failure curves are plotted as functions of the individually given critical crack size. The wider panel allows a lower stress only, because more volume is highly stressed.

► Computation of the *Reserve Factor* for Design Limit load level, j =1

Remote loading stress $\sigma = \sigma_I = 250$ MPa, $a_0 = 30$ mm, d =25 mm.

Linear analysis is sufficient (presumption of FFM model): then $\sigma \sim$ load

Assumed σ_{fail}, to be a Design Allowable, the Reserve Factor against 'Onset-of-Cracking' at the hole edge is

$$RF = \frac{\sigma_{struct}}{\sigma_{design}} = \frac{421\ \text{MPa}}{250\ \text{MPa}} = 1.7\ .$$

According to the regulations, a Design Allowable has to be applied, too, which is assumed here, because R_m is a Strength Design Allowable and K_{Ic} is assumed to be statistically based.

Yielding Check in the net-section:, as a limit-of-usage check. One obtains:

$$\sigma_{fail} = \sigma_{netyield} = R_{p02} \cdot \left(1 - \frac{2 \cdot a_{ce}}{w}\right) = 425 \cdot \left(1 - \frac{2 \cdot 55.4}{300}\right) = 268\ \text{MPa}\ .$$

$$RF = \frac{268}{250} = 1.14\ >\ 1.$$

Result: Due to the requirement $\sigma_{netyield} < \sigma_c$ net section yielding limits the loading here.

7 Application of the FFM to an HSB-example

Task: Mapping of the critical stress 'σ_c-curve' as function of the running crack size a.

The course of just 3 test points of a fixed open hole panel (from HSB 62232-01 on '*Width dependency of the Feddersen-parameter'*, [10], is to map. These fracture values are given for the original $a_0 = a + r$, also depicted in the plot.

Note, please, when assessing the test data set: The 3 test points with the different crack sizes are assumed average values. (1) In this context, in the HSB sheet the sample size number of tests belonging to one 'average' point was not given. (2) Further, an additional fitting process of the foreseen correction function was performed.

Fig.9, left, displays the geometry and the loading of the envisaged HSB-panel. The coordinate x has its origin in the hole center.
Fig.9 right, presents the course of the SIF K and of the net section stress along x together with the three average test points at the abscissa x with the coordinate points $r + a = a_0$.

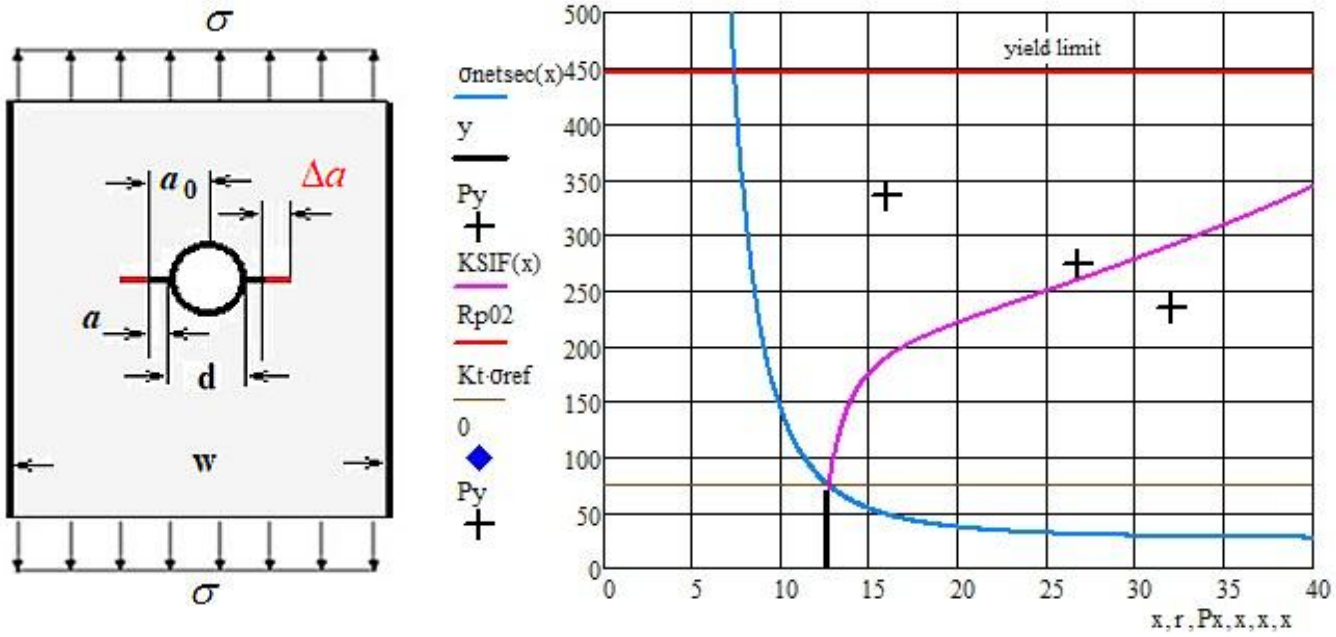

Fig.9: (left) Geometry of the fixed Open Hole Panel and its uniaxial loading.
(right) Test points with the courses of the 'SIF' and the net section stress in width x-direction
w =160 mm, t =2 mm, d =25 mm. *AA 7475-7761:* R_{p02}= *445 MPa,* $K_{c,\infty} = 2500\ \text{MPa} \cdot \sqrt{\text{m}}$ ·
Abscissa points in mm: x = r = 12.5; a_0 =16, 26.7, 32

Result:
Shifting the FFM failure stress point by Δa gives a point a little far from the derived FM-curve, This crack size Δa defines the a_0 *when analyzing future loading and crack growth.*

In *Fig.10* for the given hole, d = 2·r, the computed FFM-linked failure stress point σ_{fail} (bold) is depicted with the generated crack size Δa. The Mathcad computations are presented in *Table 3*, which presents a mixture of FFM and FM results. In order to map the FM-data course optimal two different K-values have been applied with a physically logic higher value for the higher a_0-values of $K_{upper} = 2700\ \text{MPa} \cdot \sqrt{\text{m}}$ than the mean value 2500.

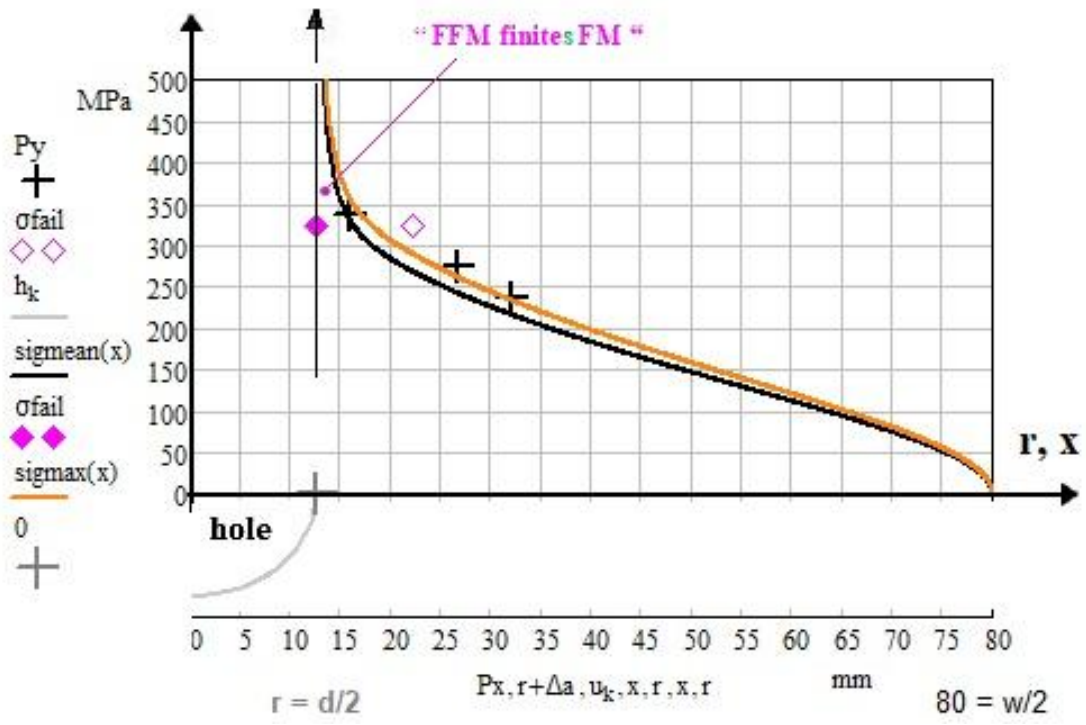

Fig.10, 80 mm= w/2, t =2 mm, r =25/2 = 12.5mm hole:

Depiction of the FFM-based failure stress at 'Onset-of-Cracking' for generating Δa = 9.6 mm and of the FM-based mapping of the course of the three test points with its associate initial different crack size a_0. For this mapping two different K-values are applied 2500 and 2700 (upper)

Result:

For the identical hole radius 12.5 mm the FFM-based failure stress (a_0 = 0) lies in the vicinity of the first FM-based failure stress (a = 16.0 - 12.5=3.5 mm) point +.

► ***In the frame of the scatter:***

the* FM-curve tendency of small initial cracks *a*→ 0 *matches well with the FFM!

The Mathcad computation is presented in *Table 4*.
The upper part depicts the classical FFM procedure and the center the Cuntze procedure with directly using the single equations.

Result: Both, the procedures end with the same numbers.

Also a FM-linked mapping of the three test point examples with its initial crack sizes a_0 was successfully performed, see the bottom of *Table 4*. Thereby the SIF *K* was varied, the above mentioned mean and the higher assumed value was applied.
This might be of interest for a rework of the 'Feddersen parameter sheet' HSB 63321-06.

Result:
Mapping was successful. The difference of the two K-values vanishes at both the ends.

Table 4, Mathcad computations:
*(up) Standard FFM procedure (*using the square*), however solved without necessary iterations, $a_0 = 0$*
(center) Cuntze's procedure: separate FFM- and SFC-equation, $a_0 = 0$
(down) FM-based mapping of the three test points with its individual initial cracks a_0

Vorgabe $\Delta a := 11$ $\boxed{\sigma := 111}$

$$\left[\frac{1}{\Delta a}\cdot\left[\int_{r}^{r+\Delta a}\left[\left[\sigma\cdot\sqrt{\pi\cdot x}\cdot\left[\sqrt{1-\frac{r}{x}}\cdot\left[1+0.358\cdot\frac{r}{x}+1.425\cdot\left(\frac{r}{x}\right)^2-1.578\cdot\left(\frac{r}{x}\right)^3+2.156\cdot\left(\frac{r}{x}\right)^4\right]\right]\cdot\sqrt{Sek\left(\frac{\pi\cdot r}{w}\right)\cdot Sek\left(\frac{\pi\cdot x}{w}\right)}\right]\right]^2 dx\right]\right] = \frac{Kc^2}{Rp02^2}$$

$$\left[\frac{1}{\Delta a}\cdot\int_{r}^{r+\Delta a}\sigma\cdot crw\cdot\left[0.335+0.665\cdot\left(1+c11\cdot\frac{x-r}{0.5\cdot w-r}\right)^{c12}+c13\cdot\left(\frac{x-r}{0.5\cdot w-r}\right)^4\right]dx\right]^2$$

$$\frac{1}{\Delta a}\cdot\left[\int_{r}^{r+\Delta a}\sigma\cdot crw\cdot\left[0.335+0.665\cdot\left(1+c11\cdot\frac{x-r}{0.5\cdot w-r}\right)^{c12}+c13\cdot\left(\frac{x-r}{0.5\cdot w-r}\right)^4\right]dx\right] = Rp02$$

$A := Suchen(\Delta a,\sigma)$ $A = \begin{pmatrix} 9.6 \\ 322.28 \end{pmatrix}$ $\Delta a := A_0$ $\sigma := A_1$ $\boxed{\Delta a = 9.6}$ $\boxed{\sigma = 322}$

Vorgabe $\Delta a := 11$ $\boxed{\sigma := 111}$

$$\left[\frac{1}{\Delta a}\cdot\left[\int_{r}^{r+\Delta a}\left[\left[\sigma\cdot\sqrt{\pi\cdot x}\cdot\left[\sqrt{1-\frac{r}{x}}\cdot\left[1+0.358\cdot\frac{r}{x}+1.425\cdot\left(\frac{r}{x}\right)^2-1.578\cdot\left(\frac{r}{x}\right)^3+2.156\cdot\left(\frac{r}{x}\right)^4\right]\right]\cdot\sqrt{Sek\left(\frac{\pi\cdot r}{w}\right)\cdot Sek\left(\frac{\pi\cdot x}{w}\right)}\right]\right]^2 dx\right]\right] = 1$$

$$Kc^2$$

$$\frac{\frac{1}{\Delta a}\cdot\int_{r}^{r+\Delta a}\sigma\cdot crw\cdot\left[0.335+0.665\cdot\left(1+c11\cdot\frac{x-r}{0.5\cdot w-r}\right)^{c12}+c13\cdot\left(\frac{x-r}{0.5\cdot w-r}\right)^4\right]dx}{Rp02} = 1$$

$A := Suchen(\Delta a,\sigma)$ $A = \begin{pmatrix} 9.6 \\ 322.3 \end{pmatrix}$ $\Delta a := A_0$ $\sigma := A_1$ $\boxed{\Delta a = 9.6}$ $\boxed{\sigma = 322}$

$$sigmean(x) := \frac{2500}{\left[\sqrt{\pi\cdot x}\cdot\left[\sqrt{1-\frac{r}{x}}\cdot\left[1+0.358\cdot\frac{r}{x}+1.425\cdot\left(\frac{r}{x}\right)^2-1.578\cdot\left(\frac{r}{x}\right)^3+2.156\cdot\left(\frac{r}{x}\right)^4\right]\right]\cdot\sqrt{Sek\left(\frac{\pi\cdot r}{w}\right)\cdot Sek\left(\frac{\pi\cdot x}{w}\right)}\right]}$$

Kc – Variants

$$sigmax(x) := \frac{2700}{\left[\sqrt{\pi\cdot x}\cdot\left[\sqrt{1-\frac{r}{x}}\cdot\left[1+0.358\cdot\frac{r}{x}+1.425\cdot\left(\frac{r}{x}\right)^2-1.578\cdot\left(\frac{r}{x}\right)^3+2.156\cdot\left(\frac{r}{x}\right)^4\right]\right]\cdot\sqrt{Sek\left(\frac{\pi\cdot r}{w}\right)\cdot Sek\left(\frac{\pi\cdot x}{w}\right)}\right]}$$

8 Conclusions, *concerning*

Strength criteria alone or energy-based fracture mechanical criteria alone cannot always lead to a reliable fracture failure prediction. Design Verification (DV) by using a coupled criterion will improve the situation and be an aid for understanding the stress state-depending Onset-of-Cracking. The so-called FFM concept should bring a solution to close the gap. It assumes the formation of cracks of finite size Δa at Onset-of-Cracking.

Fracture Mechanics

The crack-linked residual strength R_{res} is the gross-sectional tensile stress σ at failure of a structural component containing a crack. *(for fatiguers : R* of the last fatigue phase is to discriminate from R_{res} in the previous fatigue phase. Thereby, the crack length a_0 at the beginning of the static up-loading will increase to its critical value a_c in general).

A structural component will fail in the case of static loading if the SIF K of a brittle material reaches its critical value at $K = K_c$, termed fracture toughness, which depends on the material behavior. The determination of the K_c values requires in the so-called *K*-concept used above the fulfilment of a geometric bound in order to achieve a real minimum value by taking a minimum test specimen thickness of

$$t \; > \; 2.5 \cdot (K_{\mathrm{Ic}} / R^{t}_{0.2})^2 \;\; \rightarrow \;\; \sigma_c = K_{\mathrm{Ic}} / (\sqrt{\pi \cdot a_0} \cdot f(a_0)\,.$$

In the less brittle material case the limit reads $G = G_c$.

The influence of the geometry factor *f* decreases with the specimen thickness, resulting in fracture toughness independent of the specimen dimensions. For the same materials, the fracture toughness decreases with an increasing yield strength of 0.2 %.

Fig.11 shall illustrate how the failure stress is governed by the crack size. Plastic deformation plays a significant role.

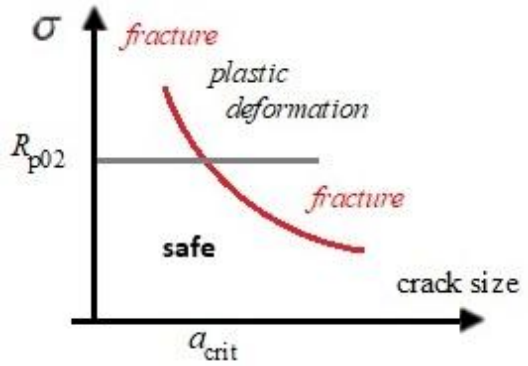

Fig.11: Illustration of the example with the concern plastic yielding

Strength

Dependent on the design requirements the average, the upper or a lower value of the property is used for the various physical properties.

In the case of the resistance property strength a statistically reduced value *R* is to apply and in order to achieve a reliable design a so-called Strength Design Allowable has to be applied. It is a value, beyond which at least 99% (“A”-value) or 90% (“B”-value) of the population of values is expected to fall, with a 95% confidence (*on test data achievement*) level, see MIL-HDBK 17.

In this context, note please: Measurement data sets are the result of a Test Agreement (norm or standard), that serve the desire to make a comparability of different test procedure results possible. The Test Agreement consists of test rig, test specification, test specimen, test procedure and the test data evaluation method. Therefore, one could only speak about '*exact test results and properties in the frame of the obtained test quality'*.

Test specimens shall be manufactured like the structure, 'as-built'.

Bearable load(ing)

The provision of bearable load(ing)s requires series tests of the distinctive structural component with statistical evaluation in order to determine a structural 'load-resistance design allowable'. This is valid for the FFM applications. See the 3 average open-hole dots in *Fig.10*.

Load-defined Reserve Factor *RF* and design Factor-of-Safety *FoS j*

* A *RF* is usually the result of worst case assumptions that does not take care of the joint actions of the stochastic design parameters and thereby cannot take care of their joint failure action and probability.
* The *RF* value does not outline a failure probability, and failure probability p_f does not dramatically increase if *RF* turns slightly below 1.
* A *FoS* is given and not to calculate such as a the Reserve Factor *RF* .

Application limits linked to FFM

In Design, as with each criterion, validity limits are faced, such as

- Application-extension of linear structural analysis and high brittleness
- Future task to capture small scale yielding at the crack tip which requires the provision of the associate statistically-based toughness K_c-values in order to master Design Verification
- The stress in the net-section of the panel should not exceed the tensile yield strength R_{p02}.
- 3D-application.

Many thanks to my friends, Prof. Dr.-Ing. habil. Wilfried Becker and Dr.-Ing. Jürgen Broede for the excellent exchange on this difficult novel topic FFM. " **FFM finites FM** "

Annexes

1. Course of net-section stress

In the context above and because it is necessary for understanding the FFM an illustration of the stress distribution along the net-section is to provide. In *Fig.12* the curves are depicted for the x- and an integration-simplifying normalized ξ-coordinate, proposed in HSB 34112-11. The relationship reads

$x = d/2$: $\quad \xi = \dfrac{2 \cdot x/d - 1}{w/d - 1} = \dfrac{x - r}{0.5 \cdot w - r} = 0$ (hole edge)

and $\quad x = a = d/2 + \Delta a$: $\quad \xi = \dfrac{2 \cdot x/d - 1}{w/d - 1} = \dfrac{2 \cdot \Delta a/d}{w/d - 1} = \Delta\alpha$, abbreviated .

In [10] was given $\quad \boxed{\sigma_y = \sigma_{netsec}(\xi) = \sigma \cdot K_{t,wd} \cdot [0.335 + 0.665 \cdot (1 + c_{11} \cdot \xi)^{c_{12}} + c_{13} \cdot \xi^4}$

with the geometry-dependent stress concentration factor K_t (w, d)

$$K_t(w,d) = 3.215 - \left(\frac{w}{d}\right)^{-0.5} + 4.294 \cdot \left(\frac{w}{d}\right)^{-1.5} \equiv \; c_{dw}$$

and the abbreviation functions

$$c_{11} = -3.765 + 2.148 \cdot (\frac{w}{d})^{0.879}, \quad c_{12} = -2.552 - 42.894 \cdot (\frac{w}{d})^{-3.17}, \quad c_{13} = -0.7497 \cdot (\frac{w}{d})^{-1.858}.$$

For the example w = 300 mm, d = 25 mm, c_{dw} = 3.03, c_{11} = 19.5, c_{12} = -2.56, c_{13} = -4.9· 10^{-3} follow

after normalization by $K_{t,\infty}$ $(w = \infty)$ =3, and setting a reference stress σ = 100 MPa the following plots:

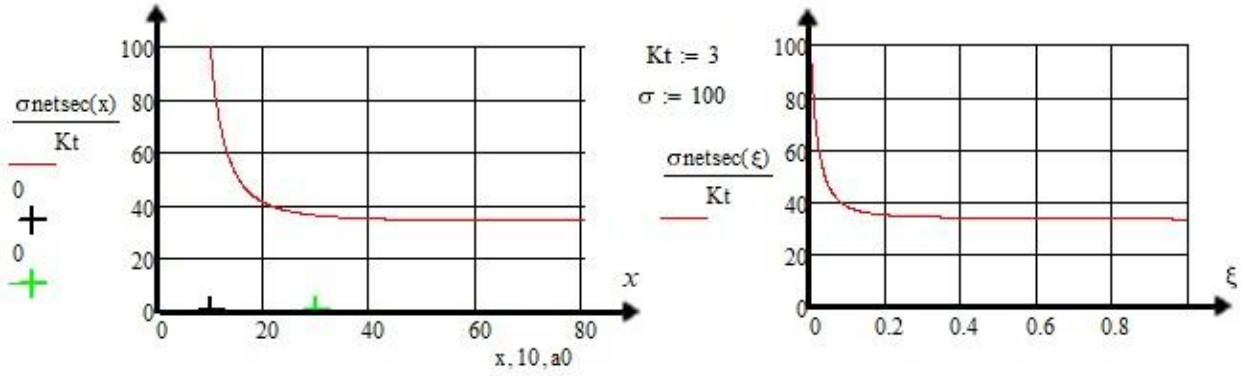

Fig.12: Contour of the stress along the net-section of the panel considering the coordinates x *and* ξ *.*

σ_{ref} = *100*MPa, r =*12.5* mm, *a0*= *30*mm, $K_{t,\infty}$ =3, *x width coordinate (ligament),* $\xi = (x - r) / (0.5 \cdot w - r)$,

Results:

With increasing distance to the hole edge the stresses are monotonically descending whereas the incremental energy release rate $\mathcal{G}$ is monotonically ascending (see *Fig.12).*

2. Integration of net-section stress

HSB 34112-11 computation, retraced:

Applying the afore mentioned coordinate transformation x → ξ enables the following symbolic integration

$$\frac{1}{\Delta a} \cdot \int_{r}^{r+\Delta a} \sigma_y \cdot dx = \frac{\sigma \cdot c_{wd}}{\Delta \alpha} \cdot \int_{0}^{\Delta \alpha} [0.335 + 0.665 \cdot (1 + c_{11} \cdot \xi)^{c_{12}} + c_{13} \cdot \xi^4] \cdot d\xi$$

$$= \frac{\sigma \cdot c_{wd}}{\Delta \alpha} \cdot \left[0.335 + c_{14} \cdot \frac{(1 + c_{11} \cdot \Delta \alpha)^{c15} - 1}{\Delta \alpha} + c_{16} \cdot \Delta \alpha^4 \right]$$

with $\quad c_{14} = \frac{0.665}{c_{11} \cdot (c_{12} + 1)}, \quad c_{15} = c_{12} + 1, \quad c_{16} = \frac{c_{13}}{3}.$

Variant Cuntze:

Despite of the more complicate integration limit $r + \Delta a$ instead of $\Delta \alpha$, the Mathcad solution process allows to stick to the x coordinate, avoiding a mixture of α with a within the solution process. Inserting into the equation above the relationship $\xi = (x - r) / (0.5 \cdot w - r)$ leads to

$$\frac{1}{\Delta a} \cdot \int_{r}^{r+\Delta a} \sigma_y \cdot dx = \frac{1}{\Delta a} \cdot \int_{r}^{r+\Delta a} \sigma \cdot c_{wd} \cdot [0.335 + 0.665 \cdot (1 + c_{11} \cdot \xi)^{c_{12}} + c_{13} \cdot \xi^4] \cdot dx$$

$$= \frac{1}{\Delta a} \cdot \int_{r}^{r+\Delta a} \sigma \cdot c_{wd} \cdot [0.335 + 0.665 \cdot (1 + c_{11} \cdot \frac{x - r}{0.5 \cdot w - r})^{c_{12}} + c_{13} \cdot \left(\frac{x - r}{0.5 \cdot w - r} \right)^4 \cdot dx.$$

Result:

The solution of the coupled equation delivers the remote failure stress with its associated crack length size Δa , see Table 3, too.

Of interest could be the effect of a varying panel width geometry. *Finally Fig.13 plots the influence of the resistance ratio* $c_{KR}= K_{app}^2/R_{app}^2$ *on the critical crack size* Δa_c *. The* c_{ik} *are the variables:*

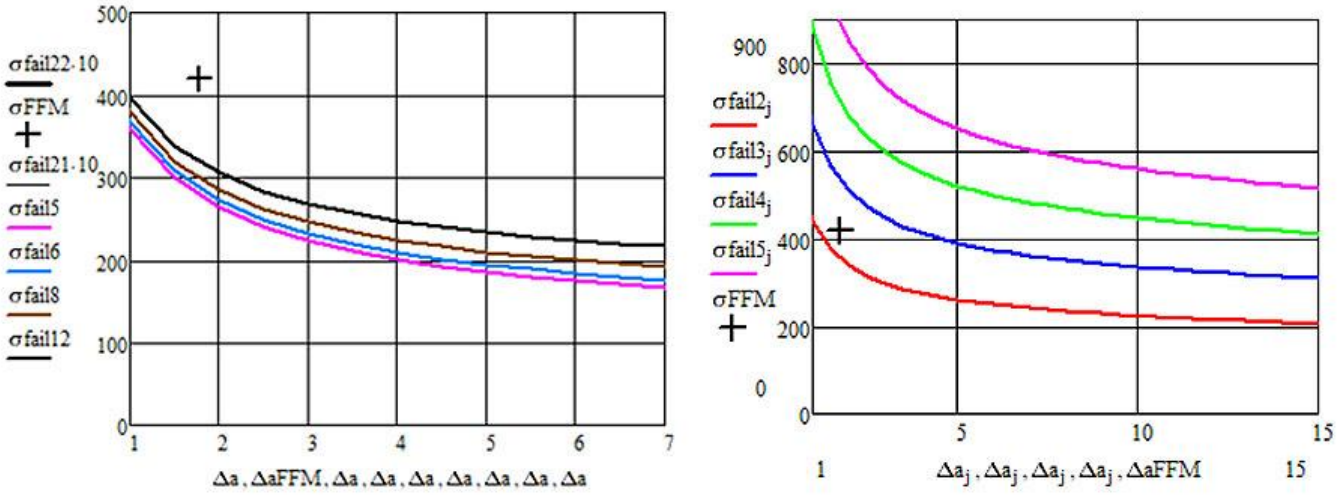

Fig.13 (l eft), general, w = 300mm: Effect of different panel geometry, ratios w/d=5, 6, 8, 12 as variables.
Fig.13 (right), general, w = 300mm: Effect of different resistance ratios KIc^2/Rm^2 *= 2, 3, 4, 5*

Lessons Learned on FFM and its two parts

FFM:

- *In the case of plain structural parts 'Onset-of-Cracking' in brittle and semi-brittle materials cannot be fully captured by the SFCs, because both a critical energy and a critical stress state must be fulfilled. Therefore, SFCs are 'just' necessary but not sufficient for the prediction of strength failure, onset of cracking. Also due to significant internal flaws an energy criterion is to apply*
- *The novel approach 'Finite Fracture Mechanics (FFM)' offers a 2D hybrid criterion to more realistically predict the stress-based 'Onset-of-Cracking' in brittle isotropic (the focus here) and UD materials.*
- *FFM enables to predict a hybrid (coupled) failure stress being assumed to be a resistance quantity on basis of the chosen statistically reduced resistances of the FFM-parts fracture mechanics (FM) and structural strength (SFC), the strength design allowables*
- *FFM is advantageous for the analysis of notched structural parts and captures applications usually treated by the well-known Neuber theory. The coupled FFM-criterion 'SFC-FM' can be used with some confidence to predict onset of cracking (failure) in brittle materials in design situations as never could be done before.*
- *Unfortunately there is still a lack of test data sets for the validation of FFM*
- *Multi-axial stress states are captured by the principal stress* σ_1
- *Using the chosen locally evenly distributed stress curve averaged over the finite length Δa is principally to check*
- *In the frame of the scatter the FM-curve tendency matches well with the FFM result. The FMC-application looks successful for the 'open hole panel' example, a realistic failure stress can be estimated, qualifying the Feddersen concept.* ***►FFM finites FM!***

FM (R-curve):

- *It is to regard, when considering the formulations to be applied: Short Cracks behave differently to Large Cracks*
- *It is unbelievable (see the treated HSB example Feddersen concept) that no test results can be found in literature concerning panels with different ratios 'width/hole radius'. Such tests should have been performed when investigating the Neuber theory (Where are these?)*
- *Notch surface quality and the metal homogeneity faced naturally have its impacts on the results.*
- *The R-curve does not depend on a_0 and w.*
- *The fracture stress is to base on* $a_e = a + \Delta a + \omega$ (ductile notch tip yielding).
- *Principal stress-linked procedure.*

SFCs Cuntze:

- *Full 3D- stress state-capable and of processing eqivalent stresses and principal stresses.*

9 'Curiosities' in Material Mechanics 'Normal Yielding' and 'Compressive Fracture Toughness'

***Aim**: Filling two rooms in the Material Mechanics Building by proving the assumed 'generic' number.*

Regarding a material 'generic' number of 2 to be valid for isotropic materials there are two 'empty rooms' in the author-assumed 'Mechanics Building' of Isotropic Materials to be filled by 'Normal Yielding (NY)' and by a counterpart of the tensile fracture toughness $K_{Icr}^{(t)}$ in the compressive domain.

9.1 Normal Yielding NY: [*CUN22, §4*]

Glassy, amorphous polymers like polystyrene (PS), polycarbonate (PC) and PolyMethylMethacrylate (PMMA = plexiglass) are often used structural materials. They experience two different yield failure types, namely crazing under tension (*Fig.9-1*) and under compression a

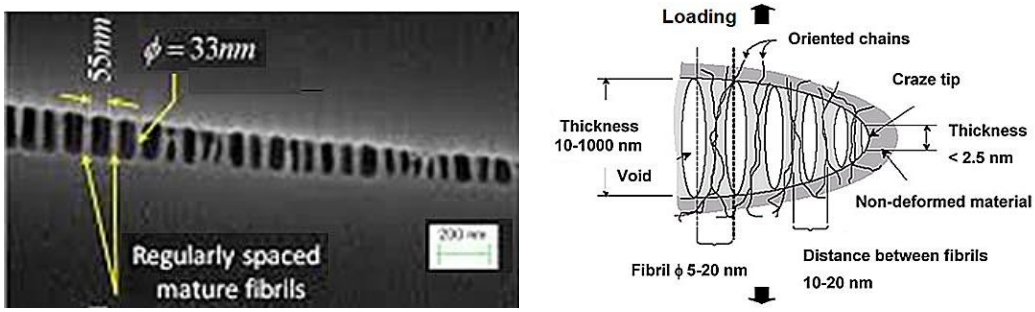

Fig. 9-1: PMMA, SEM image of a craze in Polystyrene Image (created by Y. Arunkumar)

shear stress yielding that is often termed by material specialist 'shear-banding'.

Crazing can be linked to Normal Yielding (NY) which precedes the crazing-following tensile fracture. Crazing occurs with an increase in volume through the formation of fibrils bridging built micro-cracks

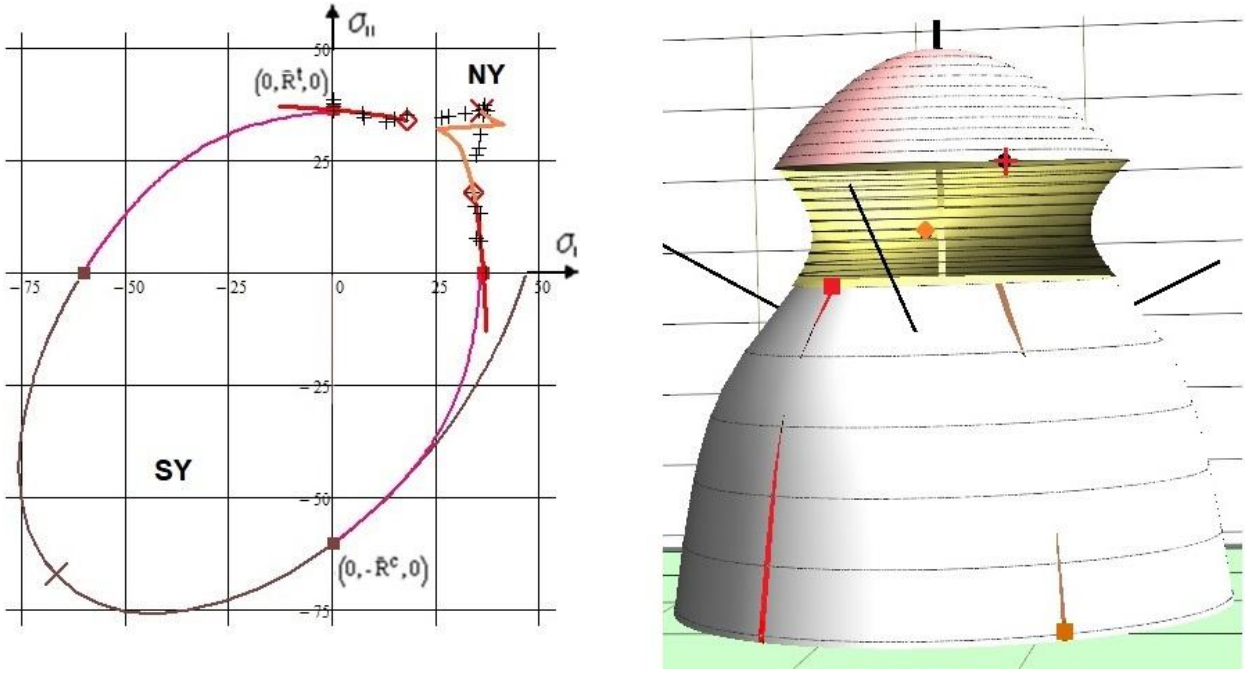

Fig. 9-2, PMMA: (left) Mapping of test data in tension and compression principal stress domain with and without interaction; (right) depiction of the fracture body shape with some representative points. For the validation of the FMC-based SFC for PMMA two data sets were available, one NY-2D-data set from Sternstein-Myers and a SY-3D-data set from Matsushige .

and shear banding keeps volume. Therefore, due to the FMC 'rules' the dilatational I_1^2 is to employ in the SFC-approach for tension $I_1 > 0$. Under compression, brittle amorphous polymers classically shear-band (SY) and experience friction. Therefore, I_1 must be employed in the approach for $I_1 < 0$ in order to consider material internal friction. 'Mises' means frictionless yielding and therefore it forms a cylinder.

For obtaining the complete yield failure body (*Fig.9-2*) its parts NY and SY are to interact in the transition zone. Doing this the used Mathcad 15 code had no problems to generate the **3D**-failure body, however the **2D**-cut visualization of the NY failure surface using Mathcad 15 code (*a 35 DIN A4-pages application*) was too challenging for the solver which had to face a concave 2D principal stress plane situation instead of the desired convex one.

LL: *The failure type crazing shows a 'curiosity' under tensile stress states: A non-convex shape exists for Onset-of-Crazing ($\bar{R}_{NY}^{t}$). This violates the 'convexity stability postulate' of Drucker, meaning "If the stress-strain curve has a negative slope then the material is not Drucker-stable". The inflection point of the hyperboloid results from the derivation dF/dI_1 of the NF criterion,*

$$F^{NF} = \frac{\sqrt{4J_2 - I_1^2/3} + I_1}{2 \cdot \bar{R}^t} = 1$$ *neglecting 120°-symmetry (results, see a later chapter.)*

9.2 Compressive (shear) Fracture Toughness $K_{IIcr}^{(c)}$, *[CUN22,§4.2]*

Some reasons caused the author to search a compressive fracture toughness:

- An early citation of A. Carpinteri, that approximately reads: "*With homogeneous isotropic brittle materials there are 2 real energy release rates $\mathcal{G}_{Icr}$, $\mathcal{G}_{IIcr}$, one in tension and one in compression*"
- The number of the (basic) fracture toughness quantities may be *theoretically at least* also 2, namely $K_{Icr}^{t} \equiv K_{Ic}$ together with K_{IIcr}^{c} (*Fig.9-3*) and
- The novel approach Finite Fracture Mechanics (FFM) that offers a hybrid criterion to more realistically predict the crack initiation in brittle isotropic and UD materials.

A stringent postulate for the author was crack path stability which can be explained "*Only an angle-stable, self-similar crack growth plane-associated critical Stress Intensity Factor (fracture toughness) is a 'basic' property*". This requires as presumption an *ideally* homogeneous isotropic material in front of the crack-tip. Therefore, the investigation is only for an ideal structural mechanics building of importance, because in practice, there are usually no ideal homogeneous conditions at the crack-tip.

Practically, facture mechanics is presently only tensile driven performed using $K_{Ic} = K_{Icr}^{t}$ as a clear critical fracture intensity, where the crack plane does not change (the index cr is necessarily to be taken in this document in order to separate tension ^{t} from compression ^{c}). Why shouldn't there not be a quantity K_{IIcr}^{c} that fits as an opposite complement to K_{Icr}^{t} and where, in an ideal case of no flaws in front of the crack tip, the crack plane grows further along the generated shear fracture angle under a compressive fracture load?

The Fracture Mechanics Mode I delivers a real, 'basic' fracture resistance property generated under a tensile stress. Both the Modes II K_{IIc}, and III K_{IIIc} do not show a stable crack plane situation but are nevertheless essential FM model parameters to capture 'mixed mode loading' for performing a multi-axial assessment of the far-field stress state. $\rightarrow \bar{R}^{t}$ and $\bar{K}_{I\,cr}^{t}$ correspond! They are 'just' very helpful model parameters driving the crack plane in direction of a finally KIc-driven failure.

With the Mode-II compressive fracture toughness K_{IIcr}^{c} it is like with strength. One says compressive failure, but actually shear (stress) failure is meant, compressive stress is 'only' the descriptive term. Therefore the shear index $_{II}$ is to apply with K_{IIcr}^{c} .

One has to keep in mind: In mechanical engineering the structural tasks are usually lie in the tension domain (*index ^{t} is skipped*), whereas oppositely in civil engineering the compression domain is faced (*index ^{c} is skipped*):

*Tension domain: One knows from K_{Icr}^{t} (tension), that – viewing the fracture angle - it corresponds to R^{t}.

*Compression domain: Above not generally known second basic SIF K_{IIcr}^{c} seems to exist under ideal conditions. It corresponds to shear fracture SF happening under compressive stress R^{c} and leading to the angle Θ_{fp}^{c}. The crack surfaces are closed for K_{IIcr}^{c}, friction sliding occurs.

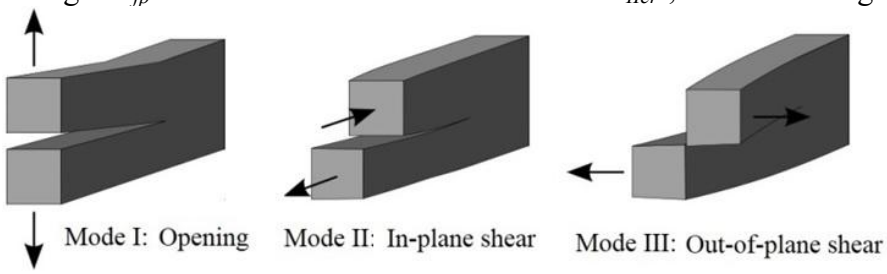

Fig.9-3: Classical Fracture Mechanics modes

Some proof of the author's postulate could be: There exists a minimum value of the compressive loading at a certain fracture angle. This means that the K_{IIcr}^{c} becomes a minimum, too. Liu et al performed in [*Liu14*] tests using a cement mortar material, (*Fig.9-4*). ► From his measured results, by now, it seems to - theoretically at least - that the 'generic' number 2 is met.

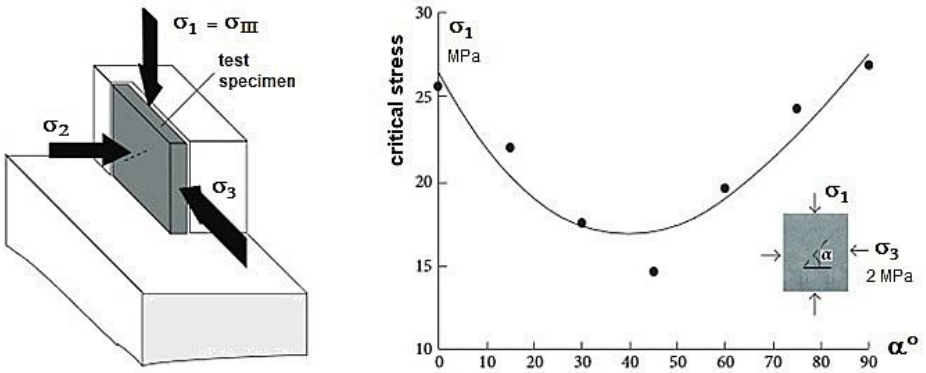

Fig.9-4: Scheme of the test set-up and of the test points obtained for cement mortar [Liu14], σ_1 represents the mathematical stress σ_{III} (largest compressive stress value).

[Liu J, Zhu Z and Wang B: *The fracture characteristic of three collinear cracks under true tri-axial compression*. The scientific World Journal, V 2014, article ID459025]

For the transversely-isotropic UD lamina materials it seems directly to match: ► 5 fracture toughness properties correspond to 5 strength properties, 'generic' number postulate is fulfilled.

LL:

**Fracture Mechanics seems to follow material symmetry 'rules' and seems to possess a 'generic' number, too.*

** Note on K_{IIcr}^{c} as a design entity: It is of theoretical, but not of practical value due to the usually faced not ideal homogeneous situation of 'isotropic materials' at crack tips.*

** The angle change of cracks under mixed-mode stress is a consequence of the singular stress field at the crack tip. Mode I drives the growth of the initial crack at the crack tip. The rotation of the propagating crack surface is caused by the non-singular stresses.*

10 Automated Generation of Constant Fatigue Life curves considering Mean Stress Effect

***Aim**: Automated derivation of the Constant Life Curve with discussion of the Mean Stress Correction.*

Generally, in Design Verification (DV) it is to demonstrate that "No relevant limit failure state is met considering all Dimensioning Load Cases (DLCs)". This involves cyclic DLCs, focusing lifetime with non-cracked and cracked structural parts (*the latter would require Damage Tolerance tools*).
Methods for the prediction of durability, regarding the lifespan of the structural material and thereby of the structural part, involves long time static loading which is linked to 'static fatigue' and in particular to 'cyclic fatigue'. Fatigue failure requires a procedure for the Fatigue Life Estimation necessary to meet above cyclic DV.

Domains of Fatigue Scenarios and Analyses are:

LCF: high stressing and straining
HCF: intermediate stressing 10.000 < n < 2.000.000 cycles (*rotor tubes, bridges, towers, off-shore structures, planes, etc*.)
VHCF: low stress and low strain amplitudes (*see SPP1466 Very High Cycle Fatigue > 10^7 cycles (in centrifuges, wind energy rotor blades, etc*.).

Principally, in order to avoid either to be too conservative or too un-conservative, a separation of the always needed 'analysis of the average structural behaviour' in Design Dimensioning (*using average properties and average stress-strain curves*) in order to obtain the best structural information (*= 50% expectation value*) is required from the mandatory single DV-analysis of the final design, where statistically minimum values for strength and minimum, or mean and maximum values for other task-demanded properties are applied as Design Values.

10.1 Fatigue Micro-Damage Drivers of Ductile and Brittle behaving Materials, see [*Cun23b*]

There are strain-life (*plastic deformation decisive, plastic strain-based $\varepsilon_{pl}(N)$*) and stress-life models (*SN*) used. For ductile materials, strain-life models are applied because a single yield mechanism dominates and the alternating stress amplitude counts. For brittle materials, the elastic strain amplitude becomes dominant and stress-life models are applied. With brittle materials inelastic micro-damage mechanisms drive fatigue failure and several fracture mechanisms may come to act. This asks for a modal approach that captures all failure modes which are now fracture modes.

Above two models can be depicted in a Goodman diagram and in a Haigh diagram. The Haigh diagram (σ_a, σ_m) will be applied here because the often used Goodman employs just one quantity σ_a or $\Delta\sigma = 2 \cdot \sigma_a$ or σ_{max} which is not sufficient. A Haigh Diagram represents all available SN curve information by its 'Constant Fatigue Life (CFL) curves, being the focus here and using the two quantities σ_a, R .

Basic differences between ductile and brittle materials are the following ones:

- Ductile Material Behavior, isotropic materials: mild steel
  1 *micro-damage* mechanism acts ≡ *"slip band shear yielding"* and drives micro-damage under tensile, compressive, shear and torsional cyclic stresses: *This single mechanism is primarily described by* 1 *SFC, yield failure condition (HMH, 'Mises')!*
- Brittle Material Behavior, isotropic materials: concrete, grey cast iron, etc.
  2 *micro-damage* driving mechanisms act ≡ 2 *fracture failure modes Normal Fracture failure*

(NF) and Shear Fracture failure (SF) under compression described by 2 fracture conditions, the 2 SFCs for NF and SF, where porosity is always to consider

- Brittle Material Behavior, transversely-isotropic UD-materials:
  5 *micro-damage* driving fracture failure mechanisms act ≡ 5 fracture failure modes *described by 5 SFCs or strength fracture failure conditions*.

A very essential topic is the so-called 'Mean stress sensitivity': Within [*Cun23b*] the author attempts to redirect the *'Thinking, resulting from ductile material behavior using 'Mean stress influence correction factors', which in reality means 'Walking on crutches',* into a direct *'Thinking* with *fracture modes facing a realistic brittle material behavior*'. Not fully ductile isotropic materials show an influence of the mean stress on the fatigue strength depending on the (static) strength ratio R^c/R^t and the material type. Mean stresses in the tensile range, $\sigma_m > 0$ MPa, lead to a lower permanently sustainable amplitude, whereas compressive mean stresses $\sigma_m < 0$ MPa increase the permanently sustainable amplitude or in other words.

LL:

** A tensile mean stress lowers the fatigue strength and a compressive mean stress increases the fatigue strength*

** If it is a pretty ductile material one has one mode 'yielding' and if the material is pretty brittle then many 'fracture modes' are to consider*

** Brittle materials like the transversely-isotropic UD material with its five fracture failure modes possess strong mean stress sensitivity, a brittle steel material just 2 modes*

** Whether a material has an endurance fatigue limit is usually open regarding the lack of VHCF tests. The strength at $2{\cdot}10^6$ cycles might be only termed apparent fatigue strength (*scheinbare Dauerfestigkeit*). However, e.g. CFRP could possess a high fatigue limit*

** Whether the material's micro-damage driver remains the same from LCF until VHCF is questionable and must be verified in each given design case (continuum micro-damage mechanics is asked here)*

** The 'ductile material behavior thinking' in 'Mean stress influence' is to redirect for brittle materials into 'thinking in fracture modes'.*

10.2 Mapping Challenge of the decisive Transition Zone in the Haigh diagram [Cun23b]

The course of the test data in the transition zone determines the grade of the mean stress sensitivity. In *Fig.10-1,* at first all essential quantities are illustrated. Further, two Constant Fatigue Life (**CFL**)-curves of a brittle material are displayed, for the envelopes N = 1 and N = 10^7. The pure mode domains are colored and the so-called transition zone is separated by R_{trans} into two influence parts. The course of the R-value in the Haigh diagram is represented by the bold dark blue lines. The CFL curve N = 1 is curved at top because 2 modes act in the case of brittle materials! This is in contrast to uniaxial static loading, depicted by the straight static envelopes, $N \neq N_f$: One micro-damage cycle results from the sum of 2 micro-damage portions, one comes from uploading and one from unloading! For fully ductile materials practically no transition zone between 2 modes exists, because just one single mode reigns, namely 'shear yielding'. Therefore, it is no mean stress effect to correct in this case!

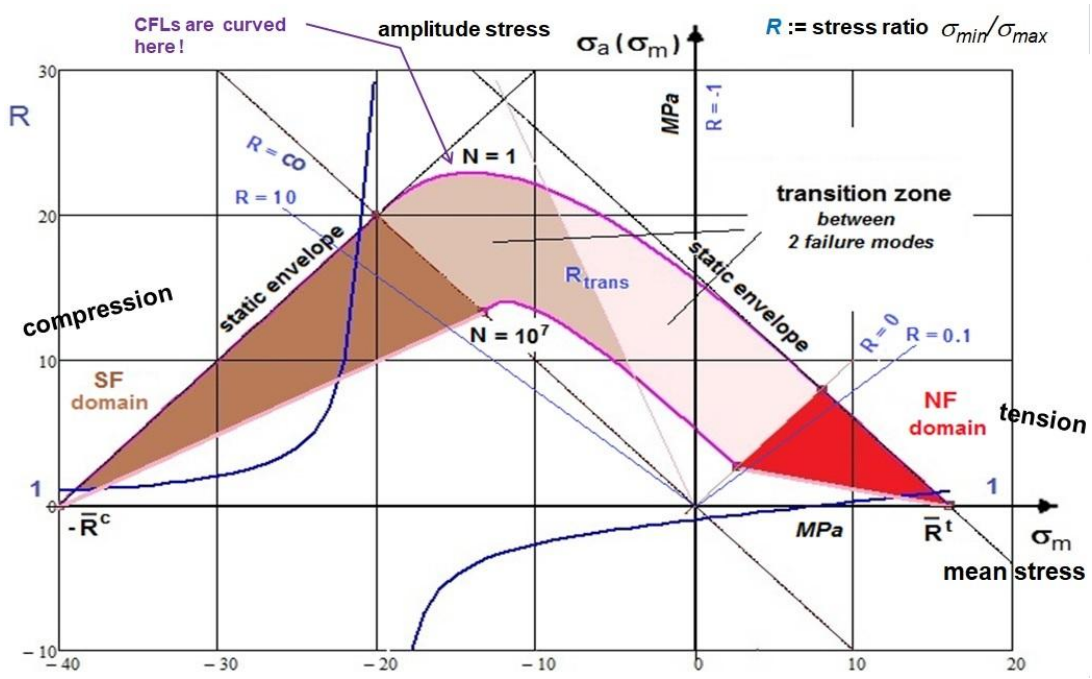

Fig.10-1, Haigh Diagrams: Scheme of pure mode domains, course of R *and transition zone parts .*
(a:= amplitude, m:= mean, N := number of fracture cycles, $\bar{R}$ *:= strength and* R := $\sigma_{min}/\sigma_{max}$

The quality of mapping the course of data in the transition zone is practically checked by "*How good is the more or less steep course along the stress ratio* R_{trans}*-line mapped*?" This is performed by following the physical reality, that the pure SF-domain is fully decoupled from the NF-domain, and employing oppositely running decay functions f_d, see *Fig. 10-2*.

$$Eff = [(Eff^{NF})^m + (Eff^{SF})^m]^{m^{-1}} = 100\% \quad \text{or}$$

$$\left(\frac{-(\sigma_{2m}-\sigma_{2a})+|\sigma_{2m}-\sigma_{2a}|)}{2\cdot\bar{R}_\perp^{\,c}\cdot f_d}\right)^m + \left(\frac{\sigma_{2m}+\sigma_{2a}+|\sigma_{2m}+\sigma_{2a}|)}{2\cdot\bar{R}_\perp^{\,t}\cdot f_d}\right)^m = 1$$

$\rightarrow$ $f_d^{IFF2} = 1/[1+\exp(\frac{c_1+\sigma_m}{c_2})]$ with c_1, c_2 fixed at $(-\bar{R}_\perp^c, 0.995)$, (-0.01,+0.01).

and analogously $f_d^{IFF1} = ...$.

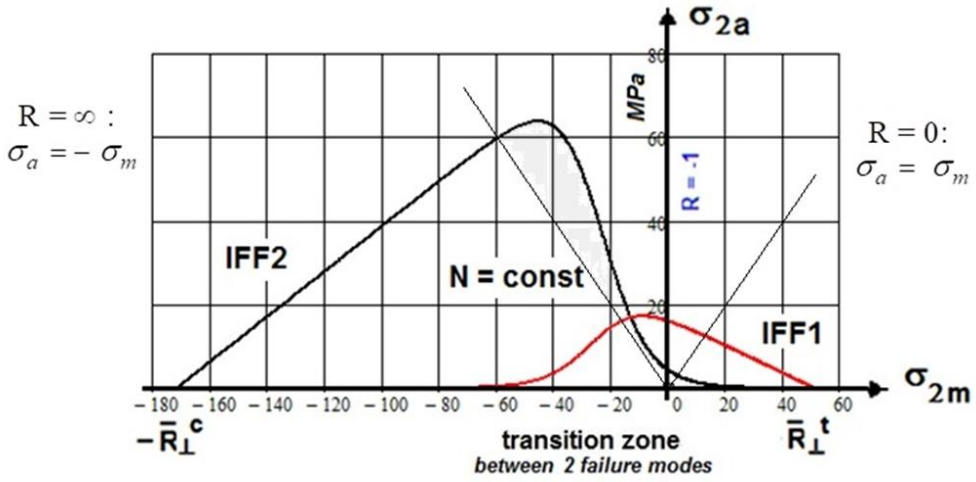

Fig.10-2, example UD material: Course of the decay functions in the transition zone $-\infty < R < 0$

Fig.10-2 illustrates the course of the mode decay functions f_d for the tension and the compression domain. The straight lines in the figure present the extreme SN curve beams, R = ∞ for the SF domain and R = 0 for the NF domain. In between, the envisaged slightly colored transition zone (- ∞ < R < 0) is located. Mean stress sensitivity of brittle materials is demonstrated very impressively if the so-called 'strength ratio' = compressive strength / tensile strength R^c/R^t is high. The two plots in *Fig.10-3 will* clearly document this.

LL:

* *A large strength ratio R^c/R^t stands for a large mean stress sensitivity*
* *A steep decay cannot be captured by a 'mean stress correction factor' as can be still performed with not fully ductile materials*

10.3 Estimation of the cyclic Micro-damage Portions of Brittle Materials

A very essential question in the estimation of the lifetime of brittle materials is a means to assess the micro-damage portions occurring under cycling. Here, for brittle behavior the response from practice is: It is permitted to apply validated static SFCs due to the experienced fact:

> *"If the failure mechanism of a mode cyclically remains the same as in the static case, then the fatigue micro-damage-driving failure parameters are the same and the applicability of static SFCs is allowed for quantifying micro-damage portions". This is supported because FMC-based static SFCs apply equivalent stresses of a mode SF or NF. See again Fig.10-2 above.*

10.4 Automatic Establishment of Constant Fatigue Life Curves (for details , see [Cun23b]

For a decade the author's intensive concern was to automatically generate Constant Fatigue Life curves on basis of just a few tested Master SN curves coupled to an appropriate physically based model. Such a model the author obtained when M. Kawai gave a presentation during the author's conference on composite fatigue in 2010 at CU Augsburg. Kawai's so-called '*Modified fatigue strength ratio'* Ψ - model was the fruitful tool found. Kawai's presented procedure was a novelty and is applicable to brittle materials such like UD plies (*depicted later in Fig.10-4*) and isotropic concrete material as well.

Fig.10-3 (left) displays the differently-colored failure mode domains FF1-FF2 in a UD FF Haigh diagram and (*right*) IFF1-IFF2 in a UD IFF Haigh diagram. The available test data set along R_{trans} in the transition zone is represented by the crosses.
The decay model quality in *Fig.10-3(right)* proves the efficiency of the decay functions in the transition zone. For proving this the author is very thankful because this was only possible because he got access to the test results of C. Hahne, AUDI.

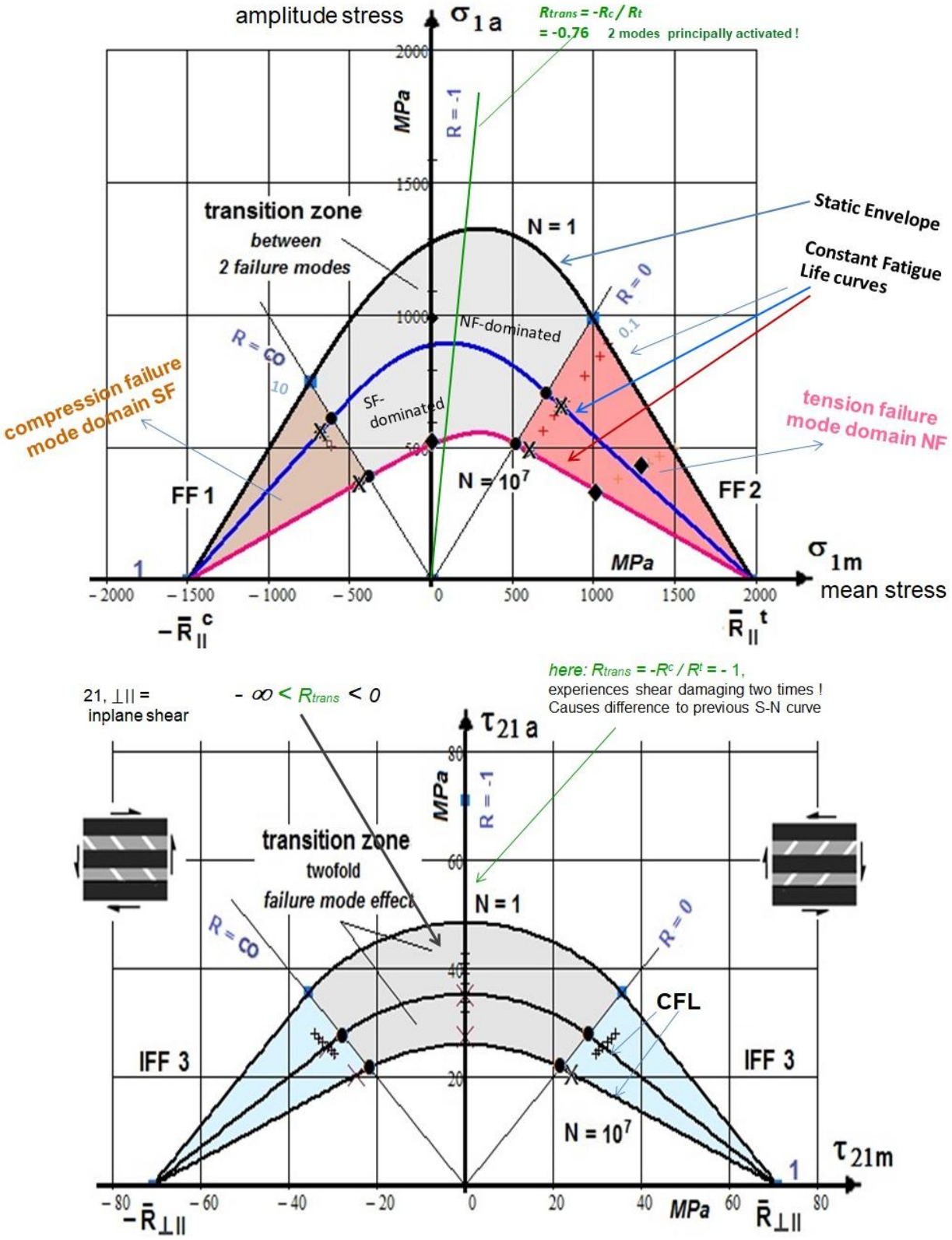

Fig.10-3, UD Haigh diagram: (up) FF with low strength ratio as with ductile materials. Rigorous Interpretation of the Haigh diagram for the UD-example FF1-FF2 displaying failure mode domains and transition zone [16], CFRP/EP, $\bar{R}^t_{||} = 1980,\ \bar{R}^c_{||} = 1500,\ \bar{R}^t_{\perp} = 51,\ \bar{R}^c_{\perp} = 172,\ \bar{R}_{\perp||} = 71$ [MPa].

(down) IFF with high strength ratio as with brittle materials Display of a two-fold mode effect (a:= amplitude, m:= mean, N := number of fracture cycles, $\bar{R}$ *:= strength and* R := $\sigma_{min}/\sigma_{max}$*). Test data CF/EP, courtesy Clemens Hahne, AUDI*

In *Fig.10-4* the course of the cyclic failure test data can be well mapped by the 4-paramater Weibull formula R = constant : $\sigma_{max}(R, N) = c_1 + (c_2 - c_1) / \exp(\log N / c_3)^{c4}$.

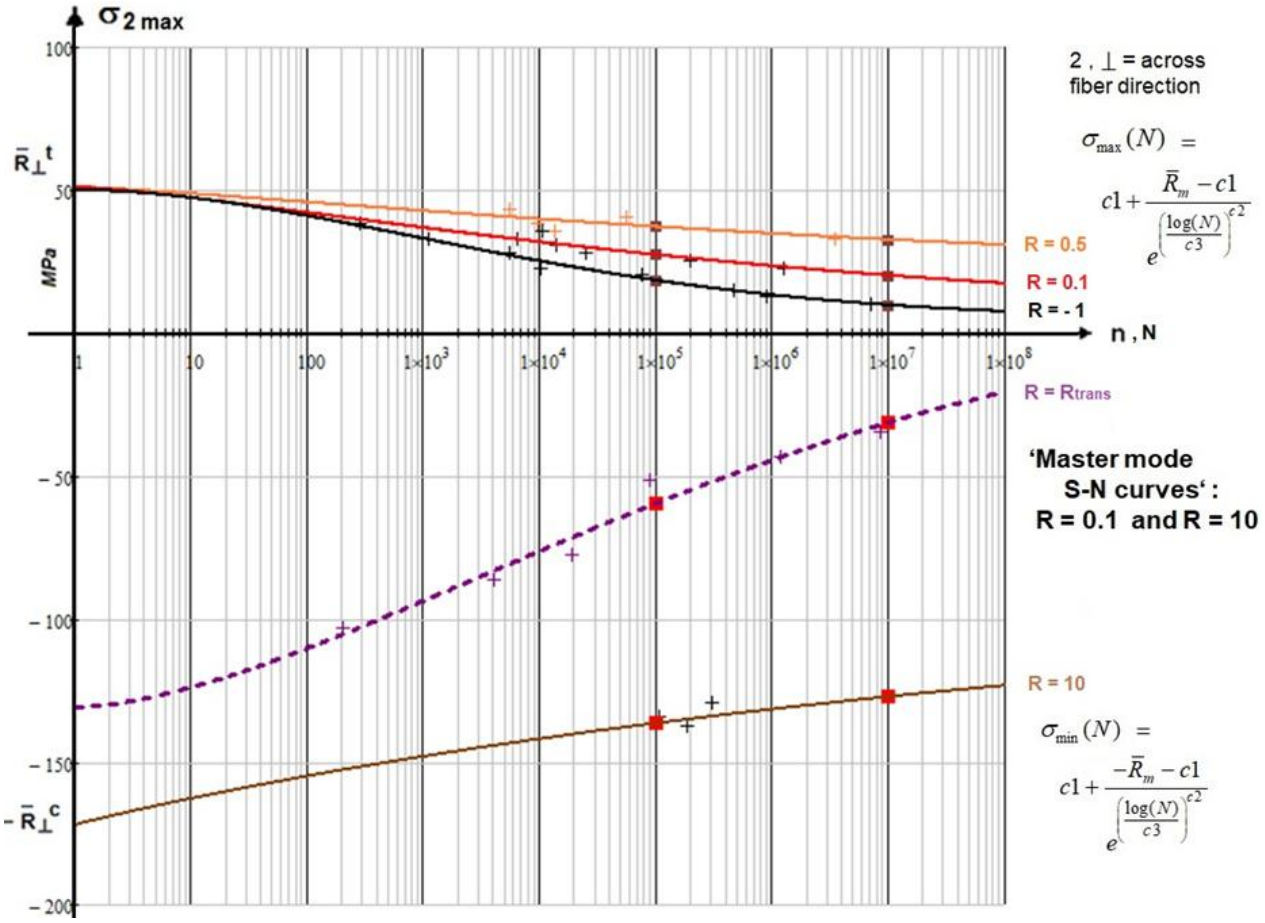

Fig.10-4: SN-curve, lin-log displayed IFF1-IFF2-linked SN curves [test data, courtesy C. Hahne, AUDI]
[Kawai M: A phenomenological model for off-axis fatigue behavior of uni-directional polymer matrix composites under different stress ratios. Composites Part A 35 (2004), 955-963]

10.5 Lifetime Estimation

The so-called Palmgren-Miner rule is applied for summing up the cyclic micro-damage portions. Statistical analyses in the German aeronautical handbook HSB have shown that the fatigue life estimation using the linear accumulation method of Palmgren-Miner tends to be too optimistic. However a satisfactory reason with correction could not yet found:

- One explanation is the 'Right use of the right SFC: Mises is not anymore fully applicable?'
- A more severe second explanation is the loss of the loading sequence, an effect which is different for ductile and brittle materials. This inaccuracy is practically considered in design by the application of the so-called Relative Miner with defining a $D_{feasible}$ and which must be < 100 %.

In the case of variable amplitude loading several SN curves are needed. An example for the computation of the lifetime estimation is displayed by *Fig.10-5*.

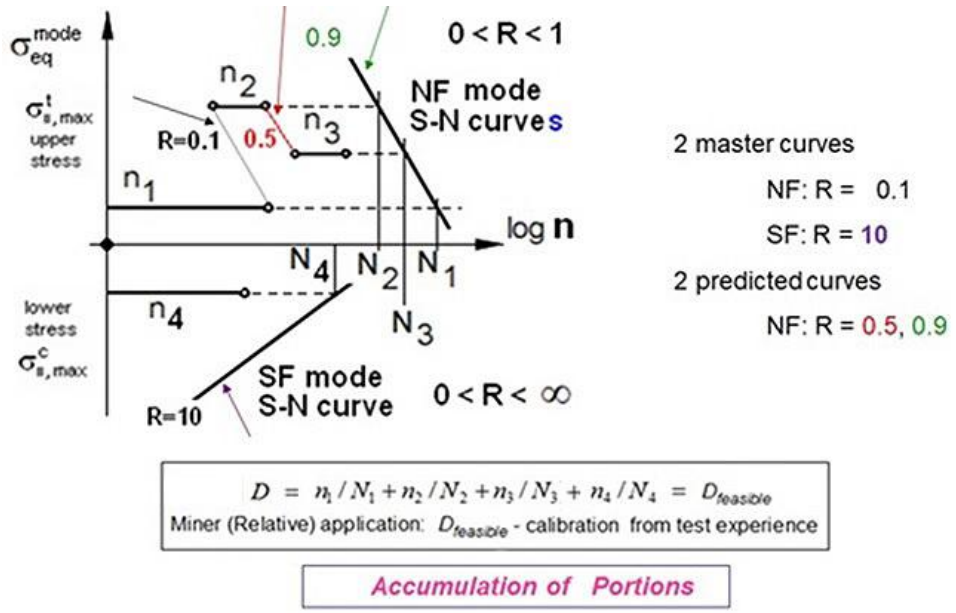

Fig.10-5: Lifetime Prediction (estimation) Method .Summing up of micro-damage portions by application of the Palmgren-Miner rule. Schematic application of a simple example, 4 blocks.
$D_{feasible}$ *from test experience*

LL:

* *A 'closed CFL-procedure' - as a coupled method - could be found to generate mandatory test data-based Constant Life Fatigue curves by using a Master SN curve plus the supporting model to determine other required SN-curves employing Kawai's Ψ-model*
* *The challenging decay along* $R_{trans} = -R^c / R^t$ *could be modelled (strength has a bias letter)*
* *Test data along* R_{trans} *are more helpful than for* $R = -1$*, which is standard with ductile behavior*
* *Right use of the right SFC. One cannot blame 'Mises' if yielding is not anymore decisive for the creation of the micro-damage portions*
* *The Palmgren-Miner rule cannot account for loading sequence effects, residual stresses, and for stresses below the fatigue limit (life → ∞ ?)*
* *Viewing brittle materials, all the SN curves have their physical origin in the strength points.*

► *The author would like to recommend: Redirect the traditional* 'Thinking, resulting from ductile material behavior regarding Mean stress correction' *into a* 'Thinking with fracture modes' *in the case of the usually not fully ductile structural materials.*

11 Evidencing 120°-symmetrical Failure Bodies of Brittle and Ductile Isotropic Materials

***Aim**: Structural Materials Building, Proof that 'All isotropic materials possess 120° rotational symmetry' with presentation of 3D-SFCs for isotropic, transversely isotropic UD-materials and orthotropic ones.*

11.1 General

From experiments is known, that brittle isotropic materials possess a so-called 120°-axially symmetric fracture failure body in the compressive domain. The question arises: Should ductile materials in the tensile domain not also possess a 120°-axially symmetric yield loci envelope instead of having just the rotationally symmetric 'Mises cylinder'?

According to the French saying " *Les extrêmes se touchent* " and based on his FMC-thinking the author assumed that there is a large similarity in the description of the behavior of very ductile and very brittle materials. Also with ductile materials a 120°-rotational symmetry should be found. In order to prove a general 120°-rotational symmetry, test results from bi-axially measuring test specimens are necessary, such as a cruciform or a cylinder.

Searched is the description of a complete failure body. This requires that the SFC captures both the positive and the negative I_1-domain. Further, the 120°- rotational symmetry should be mapped by the SFC approach (*traditional use of J_3*), too.

Thereby, brittle and ductile material behaviors are to discriminate:

Brittle: In order to show the difference of brittle to ductile materials *Fig. 11-1* outlines the brittle material with its features $\bar{R}^{tt} < \bar{R}^{t}$ and $\bar{R}^{cc} > \bar{R}^{c}$. (*Probably not considering the natural flaws in concrete, in [Lem08] was published $\bar{R}^{tt} > \bar{R}^{t}$ which is physically not explainable and might be the consequence of the difficult measurement*).

Ductile: Deformation measurements prove that for the same strain value of the growing yield surface it holds that equi-biaxial stress $\bar{\sigma}^{tt}(2D) > \bar{\sigma}^{t}(1D)$. This is similar to brittle concrete in the compressive domain where $\bar{R}^{cc} > \bar{R}^{c}$ and demonstrates the validity of the 120°-axial symmetry.

Note:

Brittle: bi-axial tension = weakest link failure behavior
*Brittle: bi-axial compression = redundant (*benign*) failure behavior*
*Ductile: bi-axial compression = redundant (*benign*) failure behavior.*

11.2 Brittle Isotropic Materials (Metals, Glass, Ceramics, Concrete, Soil, ..)

2 modes → 2 SFCs, which is in line with the 'generic' number 2 according to the FMC.

3D-SFCs of Isotropic Dense Materials

* Normal Fracture NF for $I_1 > 0$ ⇐ SFCs ⇒ Shear Fracture SF for $I_1 < 0$

$$F^{NF} = c_\Theta^{NF} \cdot \frac{\sqrt{4J_2 \cdot \Theta^{NF} - I_1^2/3} + I_1}{2 \cdot \bar{R}^t} = 1 \quad \leftrightarrow \quad F^{SF} = c_\Theta^{SF} \cdot \frac{\sqrt{4J_2 \cdot \Theta^{SF} - I_1^2/3} + I_1}{2 \cdot \bar{R}^c} = 1$$

after inserting $\sigma = R \cdot Eff$ and dissolving for Eff follows

$$Eff^{NF} = c_\Theta^{NF} \cdot \frac{\sqrt{4J_2 \cdot \Theta^{NF} - I_1^2/3} + I_1}{2 \cdot \bar{R}^t} = \frac{\sigma_{eq}^{NF}}{\bar{R}^t} \quad \leftrightarrow \quad Eff^{SF} = c_\Theta^{SF} \cdot \frac{\sqrt{4J_2 \cdot \Theta^{SF} - I_1^2/3} + I_1}{2 \cdot \bar{R}^c} = \frac{\sigma_{eq}^{SF}}{\bar{R}^c}.$$

The formulation of F^{NF} generates a straight line in the principal stress plane! It is hyperbolic in the spatial domain, where Haigh-Lode-Westergaard coordinates are used.

3D-SFCs of Isotropic Porous Materials with model parameter determination

* Normal Fracture NF for $I_1 > 0$ $\Leftarrow$ SFCs $\Rightarrow$ Crushing Fracture CrF for $I_1 < 0$

$$F^{NF} = c_\Theta^{NF} \cdot \frac{\sqrt{4J_2 \cdot \Theta^{NF} - I_1^2/3} + I_1}{2 \cdot \bar{R}^t} = 1 \quad \leftrightarrow \quad F^{CrF} = c_\Theta^{CrF} \cdot \frac{\sqrt{4J_2 \cdot \Theta^{CrF} - I_1^2/3} + I_1}{2 \cdot \bar{R}^c} = 1$$

after inserting $\sigma = R \cdot Eff$ and dissolving for Eff follows

$$Eff^{NF} = c_\Theta^{NF} \cdot \frac{\sqrt{4J_2 \cdot \Theta^{NF} - I_1^2/3} + I_1}{2 \cdot \bar{R}^t} = \frac{\sigma_{eq}^{NF}}{\bar{R}^t} \leftrightarrow Eff^{CrF} = c_\Theta^{CrF} \cdot \frac{\sqrt{4J_2 \cdot \Theta^{CrF} - I_1^2/3} + I_1}{2 \cdot \bar{R}^c} = \frac{\sigma_{eq}^{CrF}}{\bar{R}^c}.$$

with $I_1 = (\sigma_I + \sigma_{II} + \sigma_{III}) = f(\sigma)$, $6J_2 = (\sigma_I - \sigma_{II})^2 + (\sigma_{II} - \sigma_{III})^2 + (\sigma_{III} - \sigma_I)^2 = f(\tau)$

$$27J_3 = (2\sigma_I - \sigma_{II} - \sigma_{III}) \cdot (2\sigma_{II} - \sigma_I - \sigma_{III}) \cdot (2\sigma_{III} - \sigma_I - \sigma_{II}).$$

If a failure body is rotationally symmetric, then Θ = 1 like for the neutral or shear meridian, respectively .
A 2-fold acting mode makes the rotationally symmetric fracture body 120°-symmetric and is modelled by using the invariant J_3 and Θ as non-circularity function with d as non-circularity parameter

$$\Theta^{NF} = \sqrt[3]{1 + d^{NF} \cdot \sin(3\vartheta)} = \sqrt[3]{1 + d^{NF} \cdot 1.5 \cdot \sqrt{3} \cdot J_3 \cdot J_2^{-1.5}} \quad \leftrightarrow \quad \Theta^{CrF} = \sqrt[3]{1 + d^{CrF} \cdot 1.5 \cdot \sqrt{3} \cdot J_3 \cdot J_2^{-1.5}}$$

Lode angle ϑ, here set as $\sin(3 \cdot \vartheta)$ with 'neutral' (shear meridian) angle $\vartheta = 0°$ ($\rightarrow \Theta = 1, d = 0$);
tensile meridian angle 30° $\rightarrow \Theta^{NF} = \sqrt[3]{1 + d^{NF} \cdot (+1)}$; compr. mer. angle -30° $\rightarrow \Theta^{CrF} = \sqrt[3]{1 + d^{CrF} \cdot (-1)}$.

Mode interaction → Equation of the fracture body: $Eff = [(Eff^{NF})^m + (Eff^{CrF})^m]^{m^{-1}} = 1 = 100\%$

$$Eff = \sqrt[m]{\left(c_{1\Theta}^{NF} \cdot \frac{\sqrt{4J_2 \cdot \Theta^{NF} - I_1^2/3} + I_1}{2 \cdot \bar{R}^t}\right)^m + \left(c_\Theta^{CrF} \cdot \frac{\sqrt{4J_2 \cdot \Theta^{CrF} - I_1^2/3} + I_1}{2 \cdot \bar{R}^c}\right)^m} = 1.$$

* 120°-rotat. symmetric $\Theta \neq 1$:

$c_\Theta^{NF} \rightarrow c^{NF} = 1$ ($\Theta^{NF} = 1$ in practice chosen).

c_Θ^{NF}, d^{NF} from the 2 points $(\bar{R}^t, 0, 0) \rightarrow c_\Theta^{NF}$ and $(\bar{R}^{tt}, \bar{R}^{tt}, 0) \rightarrow d^{NF}$ or min.error fit of data course

c_Θ^{CrF}, d^{CrF} from the 2 points $(-\bar{R}^c, 0, 0) \rightarrow c_\Theta^{CrF}$ and $(-\bar{R}^{cc}, -\bar{R}^{cc}, 0) \rightarrow d^{CrF}$. See also §26.

The failure surface is closed at both the ends! A paraboloid serves as closing cap and bottom

$$\frac{I_1}{\sqrt{3} \cdot \bar{R}^t} = s^{cap} \cdot \left(\frac{\sqrt{2J_2 \cdot \Theta^{NF}}}{\bar{R}^t}\right)^2 + \frac{\max I_1}{\sqrt{3} \cdot \bar{R}^t} \quad , \quad \frac{I_1}{\sqrt{3} \cdot \bar{R}^t} = s^{bot} \cdot \left(\frac{\sqrt{2J_2 \cdot \Theta^{CrF}}}{\bar{R}^t}\right)^2 + \frac{\min I_1}{\sqrt{3} \cdot \bar{R}^t}$$

Slope parameters s are determined connecting the respective hydrostatic strength point with the associated point on the tensile and compressive meridian, $\max I_1$ must be assessed whereas $\min I_1$ can be measured. $\bar{R}^t$ works as normalization strength. [*CUN* 22, §5]).

[Lem08] Lemnitzer L, Eckfeld L, Lindorf A and Curbach M (IfM TU Dresden): *Bi-axial tensile strength of concrete – Answers from statistics*. In: Walraven, J. C.; Stoelhorst, D. (Hrsg.): Tailor made concrete structures. New solutions for our society. Amsterdam, The Netherlands: CRC Press / Balkema, 2008, S. 1101-1102

In order to illustrate the two SFCs with their common interaction zone a full view with the 3D-concrete Fracture Body is presented:

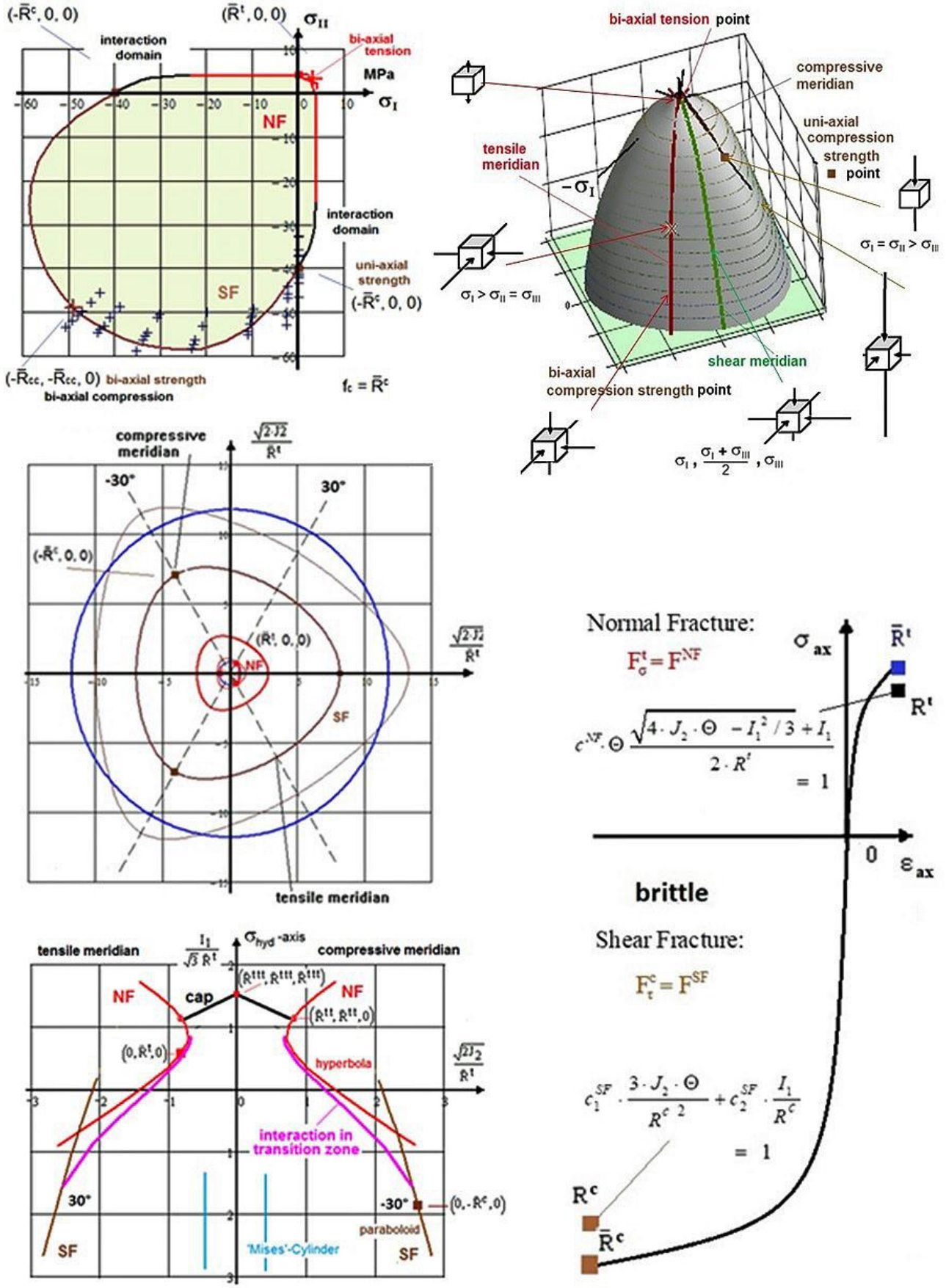

Fig.11-1: Visualization of the behavior of a brittle material (Normal Concrete) considering 1D stress-strain curve with 2D- and 3D-fracture failure curves and fracture body (surface). 120°-rotationally-symmetric

11.5 Ductile Materials, Metal

In *Fig.11-2(left)*, the failure body is presented with its meridians as axial lines. The center figure fully proves the general isotropic 120°-material rotational symmetry which is supported by the Mises **ellipse** being the *inclined cross-section of the Mises cylinder failure body* is added. The right octahedral figure shows the inner green curve with the Mises circle at the '**Onset**-of-yielding' and the outer one at tensile strength R^t.

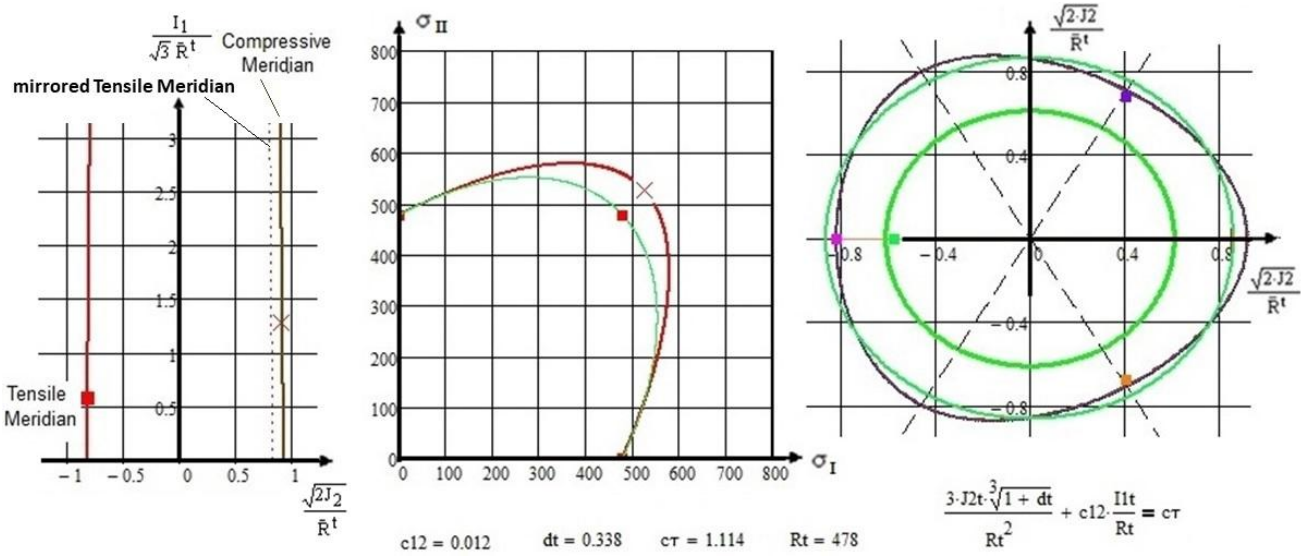

Fig.11-2, isotropic steel AA5182-0: Visualization of the behavior of a ductile material. (left) Yield body in Haigh-Lode-Westergaard coordinates; (center) 120°-symmetry, visualized in the principal stress plane; (right) 120°-symmetry, visualized in the octahedral stress plane

The 120°-rotational symmetry can be best displayed in the octahedral stress plane which is a 'horizontal' cross-section of the failure body at a distinct I_1, *Fig.11-2(right)*. The points and curves on the spatial body (*left figure*) are projected onto the octahedral plane (*right figure*). Since they depend on I_1, they have different cross-section heights I_1, such as the uniaxial tensile strength point which is located higher than the equi-biaxial strength point x.

In the center figure, Mises is the green curve; red square: the tensile strength point; cross: the equi-biaxial tensile strength point ductile (trueR^{tt}, trueR^{tt}, 0), i. e. the cross x. In the case of ductile metals it can be assumed $R^{tt} \cong 1.1 \cdot R^t$.

An elaboration of four materials with the Mathcad calculation program leads to the *Fig.11-3* below:

Fig.11-3(left) presents curves through the uniaxial tensile strength points and the equi-biaxial strength R^{tt}. The curves are inclined cross-sections of the failure body. *Fig.11-3(right)*, for completion, displays the Beltrami potential surface (egg shaped), the 'Mises' cylinder and the three principal axes.

The figure shows extreme curve examples at *true*R^t level in the positive principal stress range.

The red curve is occupied by the data of Kuwabara given below in the table, shown within *Fig.11-4*.

The metal test data AA 5182-0 are from *[Kuw98] T. Kuwabara et al: Journal of Materials Processing Technology 80–81 (1998) 517–523.*

Gotoh's biquadratic yield criterion (not given here) was used to map the test data of the cold-rolled low-carbon steel AA 5182-0 sheets.

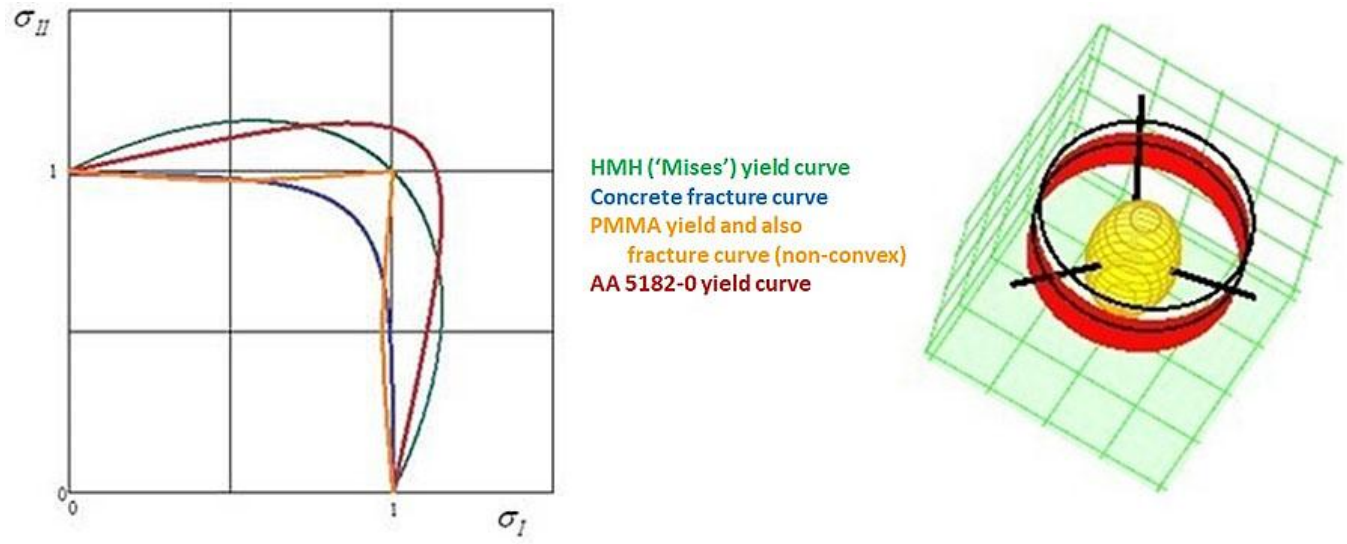

Fig.11-3: (left) Normalized principal stress plane failure curves of a set of fully different isotropic materials. (right) Failure body surface

Fig.11-4 depicts several failure cross-sections of an isotropic ductile steel demonstrating 120°-rotational symmetry like the brittle isotropic materials such as concrete in the compression domain and other ductile ones in the tensile domain.

For the generation of *Fig.11-4* biaxial tensile tests of cold-rolled low-carbon steel sheet were carried out using flat cruciform specimens with the biaxial loads maintained in fixed proportion. Contours of plastic work (of flow potential) were determined in stress space under the shown strain range.

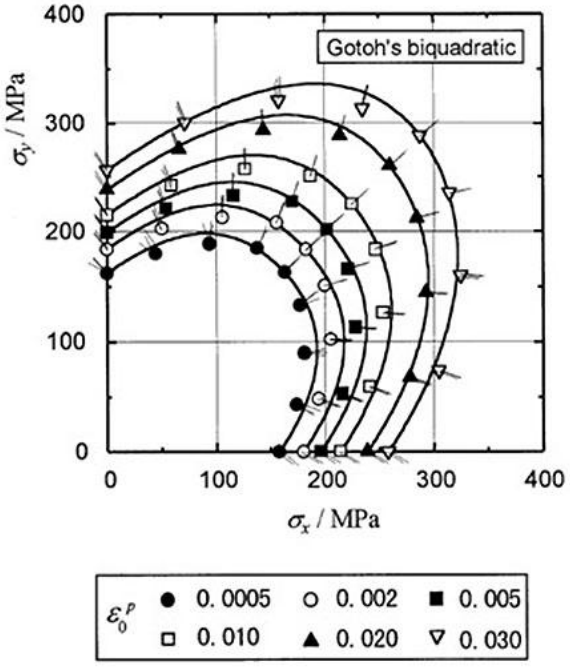

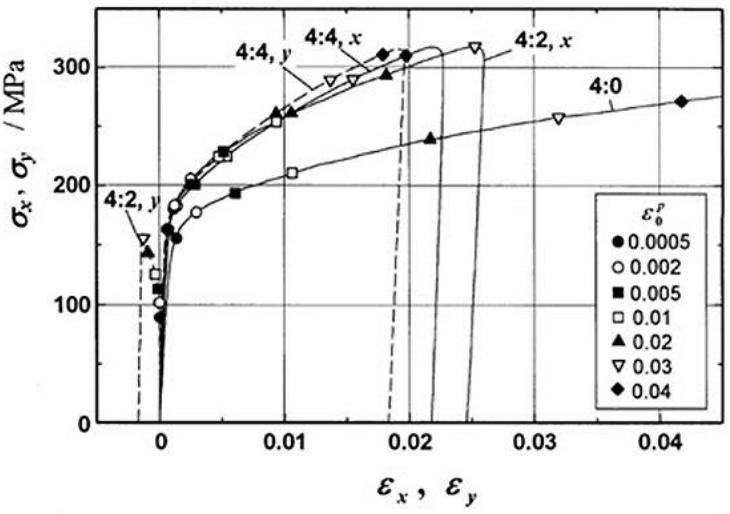

ε_0^p	0.0005	0.002	0.005	0.010	0.020	0.030	0.040
W (MPa)	0.07	0.33	0.89	1.92	4.19	6.68	9.33
σ_0 (MPa)	158	180	196	214	239	258	273
σ_{90} (MPa)	162	184	199	215	238	256	271
σ_{bi} (MPa)	163	184	202	225	260	288	310

Fig.11-4: (left) Test points as function of the experienced plastic straining ε_0^{pl}; mapping by using Gotoh's bi-quadratic criterion. (right) True stress–true strain curves for different biaxial loadings= different stress ratios. Measured values using r_0, r_{45}, r_{90}. T = 1mm, flat cruciform

LL:

** The author was able to map the course of all the corresponding courses of test data points with his isotropic SFC models.*

** Also for the ductile materials, the 120°-rotational symmetry was demonstrated, see further [CUN22, §5.8].*

** The 120°-rotational symmetry of isotropic materials is nothing else than a 'double mode effect, a two-fold danger'.*

** This effect is faced with all isotropic materials independent whether they are ductile or brittle.*

Reminder to illustrate elastic and plastic behavior:

* Elastic deformation of crystalline structures occurs on the atomic scale: The bonds of the atoms in the crystal lattice are stretched. When de-loading, the energy stored within these bonds can be reversed. The material behaves elastic.

* Plastic deformation or sliding occurs along gliding planes inter-crystalline or intra-crystalline and is permanent (plastic). No volumetric change is faced. 'Mises' applied.

In the context above *Fig.11.5* displays the strains when an axial stress comes out of the elastic state into the plastic state:

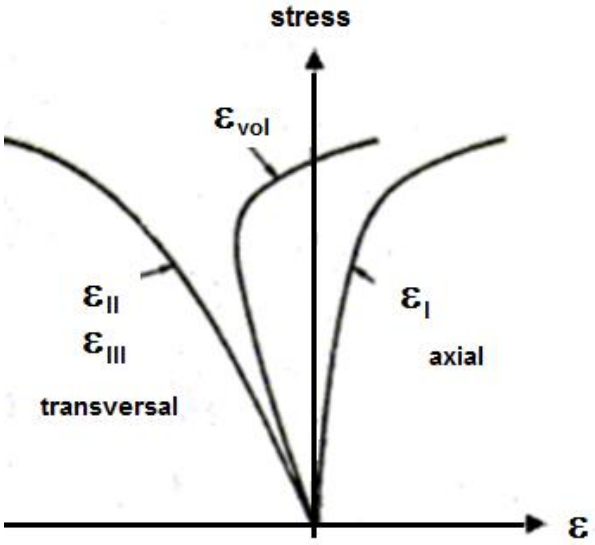

Fig.11.5:
Display of the volume change with increasing axial tensile stress

12 Completion of the Strength Mechanics Building

***Aim**: Completion of author's material-'generic' number- driven Strength Mechanics Building*

In the frame of his material symmetry-driven thoughts the author intended to test-proof some ideas that help to complete his envisaged Strength Mechanics Building by finding missing links and by providing engineering-practical strength criteria (SFCs), the parameters of which are directly measurable.

All this supports the assumption of a 'generic' number for a smeared-modelled material.

LL:

- ✓ *Beside the standard Shear (band) Yielding SY there also exists Normal Yielding NY analogous to the failure modes Shear Fracture SF and Normal Fracture NF* (author assumption proven)
- ✓ *120°-rotational symmetry is inherent to brittle and ductile isotropic materials* (author assumption proven)
- ✓ *Generic number 2, K_{Icr}^{t} with $K_{IIcr}^{c} : K_{IIcr}^{c}$ was theoretically proven for the non-real, ideal case of no flaws in front of crack tip*
- ✓ *Also in consequence of above building: Different but similar behaving materials can be basically treated with the same SFC. Examples are: Concrete ↔ foam, different fabrics*
- ✓ *The obtained Strength Mechanics Building matured, became clearer and more complete.*

Material Symmetry seems to tell:

"In the case of ideally homogeneous materials a generic number is inherent. This is valid for elastic entities, yield modes and fracture modes, for yield strengths R_{02} and fracture strengths R, fracture toughness entities K_{cr} and for the invariants used to generate strength criteria".

This **generic number** would be

2 for isotropic and 5 for transversely–isotropic materials.

One might think:

"Mother Nature gives Strength Mechanics a mathematical order!"

13 Safety Concept in Structural Engineering Disciplines

***Aim**: Providing basic knowledge for design, in order to pace the required finally necessary design verification of a component.*

Exemplarily, the *designer* of a structure (e.g. aerospace) has to demonstrate to the *operator* (airline) and the *regulator* (airworthiness authority) compliance with the design requirements concerning Structural Integrity of flight hardware components such as: Stiffness, strength, vibration, fracture behaviour as well as to material selection, manufacturing process, hardware tests, inspection methods, quality assurance and documentation. This procedure is principally valid for other disciplines like civil engineering, too.

Structural Integrity of Hardware shall be proved by analyses and verified by tests under mission environmental conditions considering the complete life history of each item.

13.1 General with Mentioning the Old safety Concept

A *Safety Concept* means to implement reliability into the structural component by 'capturing' the uncertainty of the design parameters! It can just provide an unknown safety distance between load ('stress' *S*) and load resistance ('strength' *R*). *FoS* capture uncertainties, small inaccuracies, and simplifications in analyses w.r.t. manufacturing process, tolerances, loadings, material properties (strength, elasticity etc.), structural analysis, geometry, strength failure conditions. *FoS* do not capture missing accuracies in modeling, analysis, test data generation and test data evaluation!

In the *deterministic concepts* or *formats*, respectively, the worst case scenario is usually applied for loadings considering temperature, moisture, undetected damage. Further, a load is to increase by a 'Design *FoS*' and the resistances are to decrease. For the decrease of the strength, statistical distributions are used. If the loading is also based on a statistical distribution, then one speaks about a *semi-probabilistic format*.

Design Development was the basic work of the author in industry. This is why at first the Flow Chart below shall remind of the structural analysis tasks. There are basically four blocks, where – after the material Model Validations - the fulfillment of the Design Requirements has to be demonstrated for obtaining Design Verification as precondition of the final Certification Procedure.

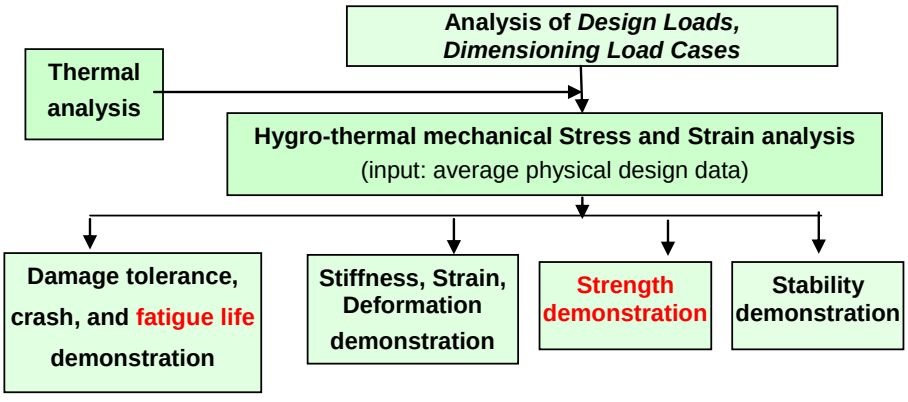

Fig13-1: Structural Design-Analysis Flow Chart

Essential question of engineers in mechanical and in civil engineering is:

"*How much could one further increase the loading. Which is the reserve*"?

Old Safety Concept of Allowable Stresses:

At least since 1926 the civil engineer M. Mayer questioned the old safety concept, which used allowable stresses, meaning: resistance was reduced by a design safety factor.
This gives no accurate results in the case of non-linear behavior. In construction this was replaced since some decades in DIN 1054 by the Partial Safety Factor concept, which applies design safety factors and combination factors for general service loads, live loads, snow, ice loads, and wind loads. Temperature effects are specified in DIN 1055-100.

Material resistance must be generally demonstrated by a positive Margin of Safety *MoS* or a Reserve Factor $RF = MoS - 1 > 1$ in order to achieve Structural Integrity for the envisaged Design Limit State! A *FoS* is given and not to calculate (***as it is too often to read even in FEA code manuals***) like the Margin of Safety *MoS* or the Reserve Factor $RF = MoS + 1$.

Fig.13-2 visualizes the stress-strength distribution which outlines that the crossing over will determine the probability of failure $p_{f.}$ Its value is the area of the p_f-distribution within the overlapping (gusset) of the stress and the strength distribution tails, see for details [CUN22, §16]

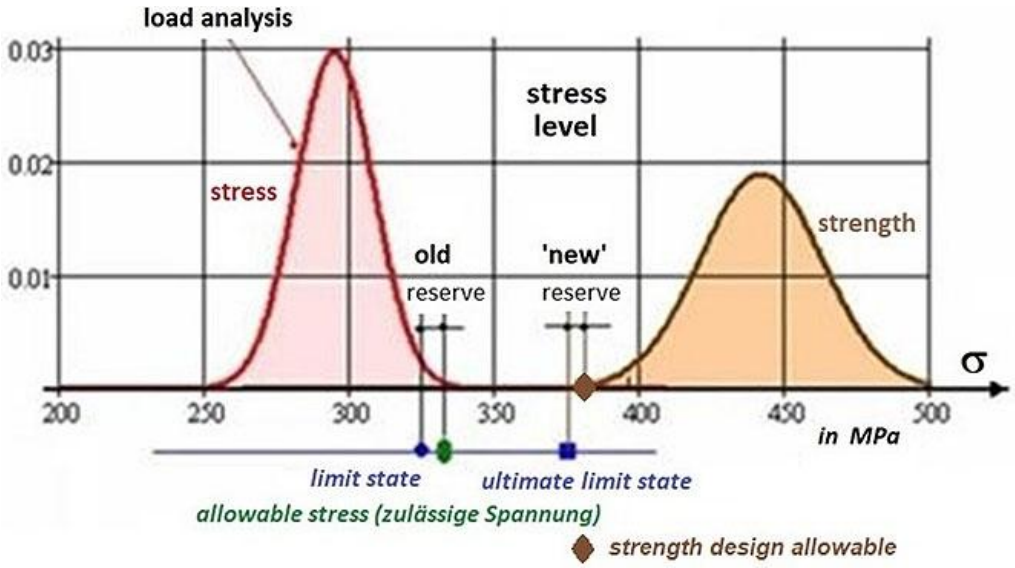

Fig.13-2: Visualization of the present ('new') and the old safety concept

LL:
The citation of the term 'allowable stress' is restricted to the former 'Concept of Allowable Stresses' and shall be not applied within present concepts anymore. Why? The usual application of the abbreviating term 'allowable' instead of 'strength design allowable' may not confuse, but 'allowable stress' is error-prone because the relation below is valid:

j · allowable stress = strength design allowable *!! (see again the figure above)* !

13.2 Global (lumped) Factor of Safety Concept ('deterministic format') on Loading

Concept, that deterministically accounts for design uncertainties in a lumped (global) manner by enlarging the 'design limit loads' through multiplication with a design Factor of Safety FoS j.

As still mentioned, FoS are applied to decrease the chance of failure by capturing the uncertainties of all the given variables outside the control of the designer. In the design process the scatter of individual values and parameters is usually treated by using fixed deterministic *FoS*, which act as load increasing multiplying factors *FoS* and should be called, more correctly, *Design FoS*.

Personal Experience:
A safety distance pays off ".

Comodo waran ≈ 80 kg

Presently, in mechanical engineering the loading is increased by one lumped (global) FoS *j*, and in civil engineering the procedure was improved by using several partial Design FoS γ for the uncertain stochastic design variables. These *FoS* are based on long term minimum risk experience with structural testing. Depending on the risk consequences different classes of *FoS* are applied, e.g. for manned space-crafts higher *FoS* are used than for unmanned space-crafts.

Present spacecraft safety concept is an *improved global deterministic format (intention: semi-probabilistic)* = 'Simplest' Partial Safety Factor concept: It discriminates load model uncertainties considering factors (K_{Model} , $\boldsymbol{K_{Project}}$) from design uncertainties which are considered by one global FoS *j* !

The to be applied values *j* for the *FoS* are risk or task driven. Facts to consider are:

- As mentioned exemplarily: Different application in cases of manned, un-manned spacecraft
- Design verification by 'Analysis only' (*by the way this is the usual case in construction*)
- Different risk acceptance attitude of the various industries.

  Example: $DUL = j_{ult} \cdot$ design limit load DLL

Mind: The virtual design value must be written DUL, because is the real test fracture load.

Different loading (action) FoS in aircraft and space engineering:

The first task in aerospace industry is load analysis. In any load analysis there are to establish all load events the structure is likely to experience in later application. This includes as well the estimation of loadings induced by the hygro-thermal, the mechanical *(static, cyclic and impact)* and the acoustical environment of the structure as further the corresponding lifetime requirements (*duration, number of cycles*), specified by an authority or a standard.

Then, the so-called Design Limit Load values are determined, usually derived from mission simulations utilizing the so-called mathematical models of the full structure (*dynamical analyses, at first on basis of the preliminary design*).

When preparing the HSB sheet [*Cun12*] the author sorted out, that there practically is no different risk view between air-craft and space-craft:

* Spacecraft: using a *d*ynamic *L*imit *L*oad model obtaining a basic load prediction d*LL* considering a load model uncertainty considering factor j_{LM} =1.2. This delivers a Design Limit Load DLL= 1.2 ·d*LL*, and from this follows DUL = d*LL*· j_{LM} ·j_{ult} , with 1.2 ·1.25 = **1.5** ! In spacecraft, the DLL level is applied in fatigue life demonstration.
* Aircraft: Definition of a so-called (design) Limit Load *LL* delivering DUL = *LL*·**1.5.**

***LL**:*

** Hence, the author could conclude after comparing the ESA/ESTEC aerospace Standards* (the author had to work on them)*, that the DUL-value is practically the same value in aircraft and in spacecraft !*

** Loads are most often the parameters of highest uncertainty. Therefore checking the loads pays off. Otherwise a bad design with a money grave may be faced.*

The resistance strength and the bearable loads (at joints etc ...):

Dependent on the design requirements the average, the upper or a lower value of the property is used for the various properties. In the case of strength a statistically reduced value *R*. To achieve a reliable design the so-called Design Allowable has to be applied. It is a value, beyond which at least 99% ("A"-value) or 90% ("B"-value) of the population of values is expected to fall, with a 95% confidence (*on test data achievement*) level, see MIL-HDBK 17. A "B"-value is permitted to use for multi-layered, redundant laminates.

Bearable loads require series tests of the distinctive structural component with statistical evaluation in order to determine the 'load-resistance design allowables'.

Measurement data sets are the result of a Test Agreement (norm or standard), that serve the desire to make a comparability of different test procedure results possible. The Test Agreement consists of test rig, test specification, test specimen and test data evaluation method and the Test Procedure. Therefore, one can only speak about *'exact test results in the frame of the obtained test quality'*. Hence, there are no exact property values.
Test specimens shall be manufactured like the structure ('as-built').

Considering property input: When applying test data from 'isolated lamina' test specimens (*like tensile coupons*) to an embedded lamina of a laminate one should consider that coupon test deliver tests results of 'weakest link' type. An embedded or even an only one-sided constrained lamina, however, possesses redundant behavior → "B"-values permitted.

Reserve Factor *RF* and Margin of Safety *MoS*: Formulas:

Linear analysis is sufficient (presumption): σ □ load $\Rightarrow RF \equiv f_{RF} = 1 / Eff$

Material Reserve Factor $$f_{RF,\,ult} = \frac{\text{Strength Design Allowable } R}{\text{Stress at } j_{ult} \cdot \text{Design Limit Load}} > 1,$$

Non-linear analysis required: σ not proportional to load

Reserve Factor (load-defined) $$RF_{ult} = \frac{\text{Predicted Failure Load at } Eff = 100\%}{j_{ult} \cdot \text{Design Limit Load}} > 1.$$

***LL**:*

** A FoS is given and not to calculate such as a Margin of Safety MoS or the Reserve Factor RF = MoS + 1.*

** A MoS is usually the result of worst case assumptions that does not take care of the joint actions of the stochastic design parameters and thereby cannot take care of their joint failure action and probability. This failure probability is a 'joint failure probability' because it considers the probability of joint acting*

** A material with a high coefficient of variation CoV disqualifies itself, when computing the statistically-based 'strength design allowable' value. Therefore, one must not penalize it further as performed in some standards in the past in the case of new materials.*

** Both, an increasing mean value and a decreasing standard deviation will lower* p_f

* *The MoS value does not outline a failure probability. Failure probability p_f does not dramatically increase if MoS turns slightly negative. Check as below, whether one may get more material and structural data to reduce scatter*
* *A local safety measure of MoS = -1 % is no problem in design development if a 'Think (about) Uncertainties' attitude is developed in order to recognize the main driving design parameters and to reduce the scatter (uncertainty) of them*
* *Nowadays often non-linear analyses are performed, delivering true quantities, however Design Verification is executed with engineering strength values R. Why do we not use in such a case the true tensile strength, however calculate f_{RF} with four numbers 'accuracy'?*
* *Fig.13-3 (left) visualizes strength distribution, Eff versus micro-damage growth and material reserve factor f_{RF}*
* *'True-in' requires 'True-out' and an assessment by* $true\bar{R}^t$. *Fig.13-3 (right) shows for an aluminum alloy a difference between the mean (material model) strength values* $eng\bar{R}^t \rightarrow true\bar{R}^t$ *of 8%.*

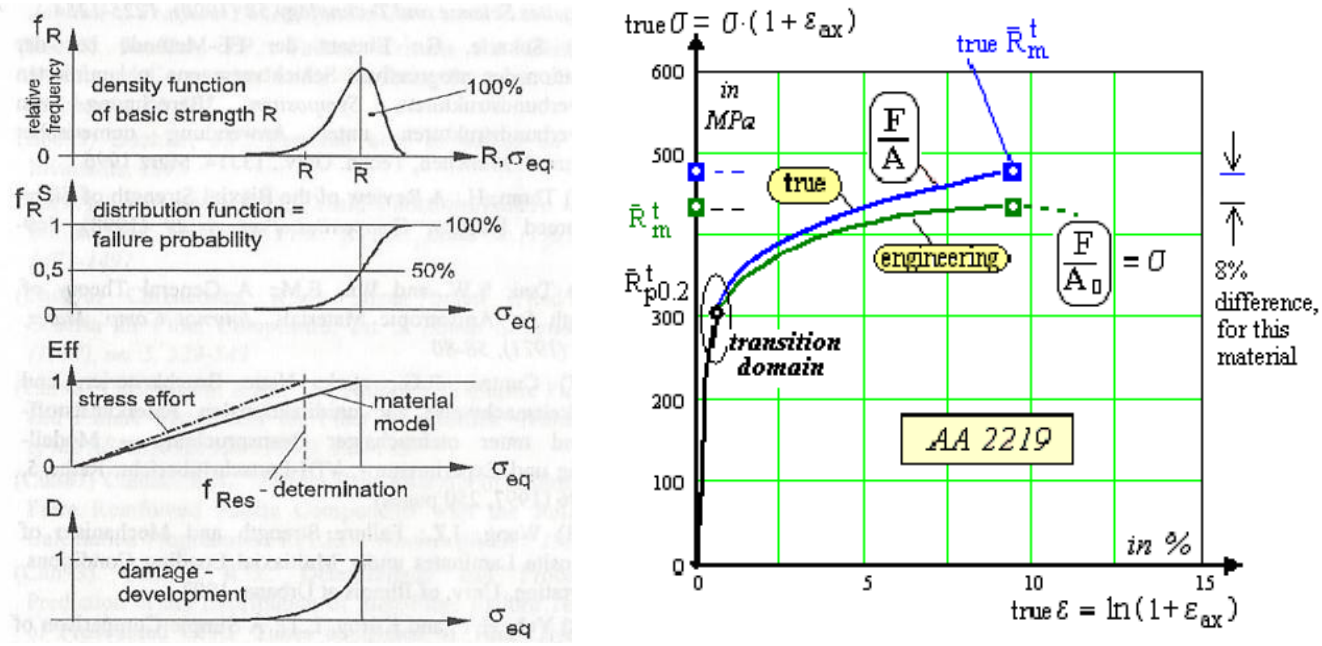

Fig.13-3: (left) Design quantities when approaching failure in Design Verification. (right) Difference engineering and true tensile strength of AA2219

Robust Design Requirements:

The goal of any design engineer should be to end up with a robust design. In order ta o achieve this, the main stochastic design parameters have to be used to outline the robustness of the design against the envisaged actual failure mode by firstly computing the sensitivity measures α and then investigating the reduction of the design's sensitivity to changes of *Xj while* keeping p_f at the prescribed level. This is important for the production tolerances. Probabilistic design may be used as an assessment of the deterministic design or is necessary as design method if a *reliability* target $\mathfrak{R}$ is assigned instead of a *FoS*. or its complement, the probability of failure p_f.

A structural reliability analysis in a Hot Spot reveals the influence of each stochastic design parameter on the distinct failure mode by means of the sensitivity measures. Robust designs (*robust to later*

changes of the design parameters) are required with identification of the most sensitive design parameters!

For better illustration of the Safety Concepts from *[CUN22, §12]* the *Fig.13-4* is included. It clearly depicts the definition of the failure probability in this two-parameter case.

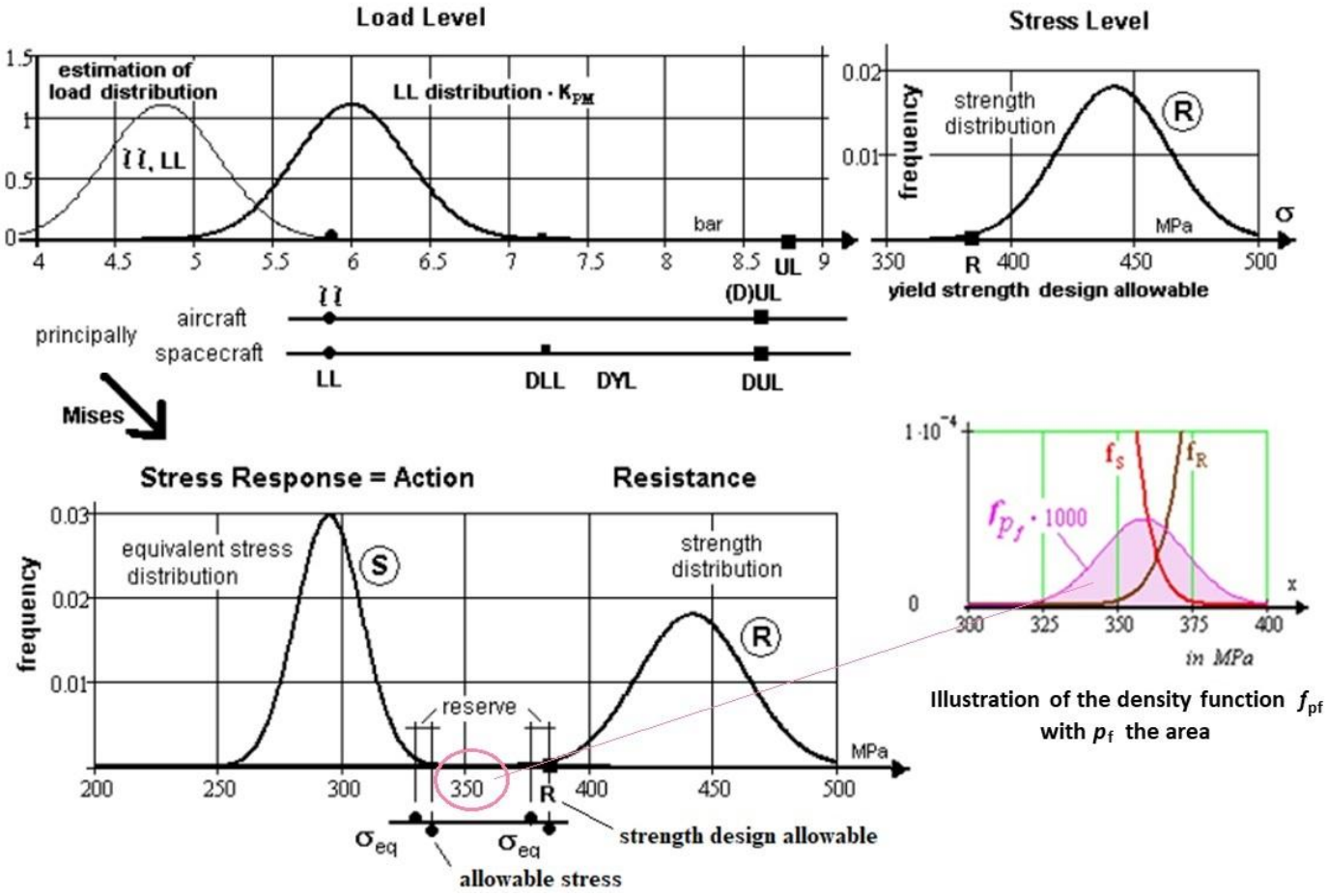

Fig.13-4: Visualization of the difference of the aerospace load terms used in the Strength Design Allowable Safety Concept and of the 'hopefully forgotten' Allowable Stress Safety Concept

Design advantages found with the Ariane Booster design, when using a probabilistic tool:

Two advantageous applications of the probabilistic tool shall be shortly demonstrated where probabilistic modelling and computation were successfully applied:

* A reduced production tolerance width leads to a reduced mass which sequentially reduced further fuel mass savings. Improved production reduced the wall thickness tolerance from 8.2 +- 0.20 mm to 8.2 +- 0.05 mm. Keeping the same given reliability value $\Re = 1 - p_f = 1 - 5 \cdot 10^{-6}$ the nominal wall thickness could be set → 8.1 +- 0.05 mm leading to mass and fuel savings.
  (*As early as 1985 for our pre-design of the Ariane 5 launcher so-called target survival probabilities* $\Re$ *were fixed for the several structural parts*!)

* Probabilistic modelling of the geometrical tolerances of bore hole, pin, position (pitch) and strength minimum restrains with minimum residual stresses could be achieved, for the pin connection an optimum number of pins of 130 pins for a simpler assembly process and for reduced mounting stresses.

Fig.13-5 presents a numerical example how exemplarily a UD reserve factor *RF* is to compute.

Asssumption: Linear analysis permitted, design FoS $j_{ult} = 1.25$

* Design loading (*action*): $\{\sigma\}_{design} = \{\sigma\} \cdot j_{ult}$

* 2D-stress state: $\{\sigma\}_{design} = (\sigma_1, \sigma_2, \sigma_3, \tau_{23}, \tau_{31}, \tau_{21})^T \cdot j_{ult} = (0,\ -76,\ 0,\ 0,\ 0,\ 52)^T$ MPa

* Residual stresses: 0 $\left(effect\ vanishes\ with\ increasing\ micro-cracking\right)$

* Strengths (*resistance*): $\{\bar{R}\} = (1378,\ 950,\ 40,\ 125,\ 97)^T$ MPa average from mesurement

statistically reduced $\{R\} = (R_{||}^t, R_{||}^c, R_{\perp}^t, R_{\perp}^c, R_{\perp||})^T = (1050,\ 725,\ 32,\ 112,\ 79)^T$ MPa

* Friction value(s): $\mu_{\perp||} = 0.3,\ (\mu_{\perp\perp} = 0.35)$, Mode interaction exponent: $m = 2.7$

$$\left\{Eff^{\text{mode}}\right\} = \left(Eff^{||\sigma},\ Eff^{||\tau},\ Eff^{\perp\sigma},\ Eff^{\perp\tau},\ Eff^{\perp\square}\right)^T = \left(0.88,\ 0,\ 0,\ 0.21,\ 0.20\right)^T$$

$$Eff^m = (Eff^{||\sigma})^m + (Eff^{||\tau})^m + (Eff^{\perp\sigma})^m + (Eff^{\perp\tau})^m + (Eff^{\perp||})^m = 100\%\ .$$

The results above deliver the following material reserve factor $f_{RF} = 1/Eff$

* $Eff^{\perp\sigma} = \dfrac{\sigma_2 + |\sigma_2|}{2 \cdot \bar{R}_{\perp}^t} = 0, \quad Eff^{\perp\tau} = \dfrac{-\sigma_2 + |\sigma_2|}{2 \cdot \bar{R}_{\perp}^c} = 0.60, \quad Eff^{\perp||} = \dfrac{|\tau_{21}|}{\bar{R}_{\perp||} - \mu_{\perp||} \cdot \sigma_2} = 0.55$

$$Eff = [(Eff^{\perp\sigma})^m + (Eff^{\perp\tau})^m + (Eff^{\perp||})^m]^{1/m} = 0.80.$$

$\Rightarrow \quad f_{RF} = 1/Eff = 1.25 \rightarrow RF = f_{RF}$ (if linearity permitted) $\rightarrow$ MoS $= RF - 1 = 0.25 > 0$!

Fig.13-5: Computation scheme of a UD Reserve Factor RF

LL:

- **Lightweightesign becomes easier by reducing uncertainties!**
- We should focus robust products and fabrication processes
- Robust Design: 1 / (uncertainty·complexity). Design optimization must consider the scatter of the stochastic design variables
- Uncertainty quantification opens the door for a successful lightweight dimensioning
- Loadings are most often the design variables of highest scatter or uncertainty
- The basis for determining reliability is the recording of uncertain parameters
- Uncertainty, citing *Freudenthal*: "The application of probabilistics makes me aware of my risk, since it provides numbers, whereas deterministics does not. You can buy certainty." However, concerning costs: How safe is safe enough?
- *Random variation (aleatory: dice rolling; physical in nature such as fluctuations in material properties, stress). *Uncertainties (epistemic: knowledge, inference from sample to population of a design parameter, weakness of used models)
- Design Limit Load (NASA: not just Limit Load !!)= Limit Load of load model ·uncertainty factor. DLL is a statistically evaluated value if a distribution is available or (b) value from an engineering judgement following a rationale
- Optimum fulfilling of product liability: Secured, validated design procedures + reproducible manufacturing processes

In a European Structural reliability working group we distinguished *Failure Rate* from *Failure State* people. Both work together in the reliability assessment of an overall system, as we had to do with the Ariane 5, below: **Reliability of an Ariane 5 sub-system**

As early as 1985 for the pre-design of the Ariane 5 launcher target survival probabilities $\Re = 1 - p_f$ were fixed for the several structural parts! The following *Fig.13-6* presents an example of the Ariane launcher for a distinct mixed scenario:

The full system is divided into subsystems and these in turn are divided into elements. The individual elements are then assigned a required probability of failure so that the full system can meet the target value of the survival reliability $\Re = 1 - p_f$ of the launcher subsystem.

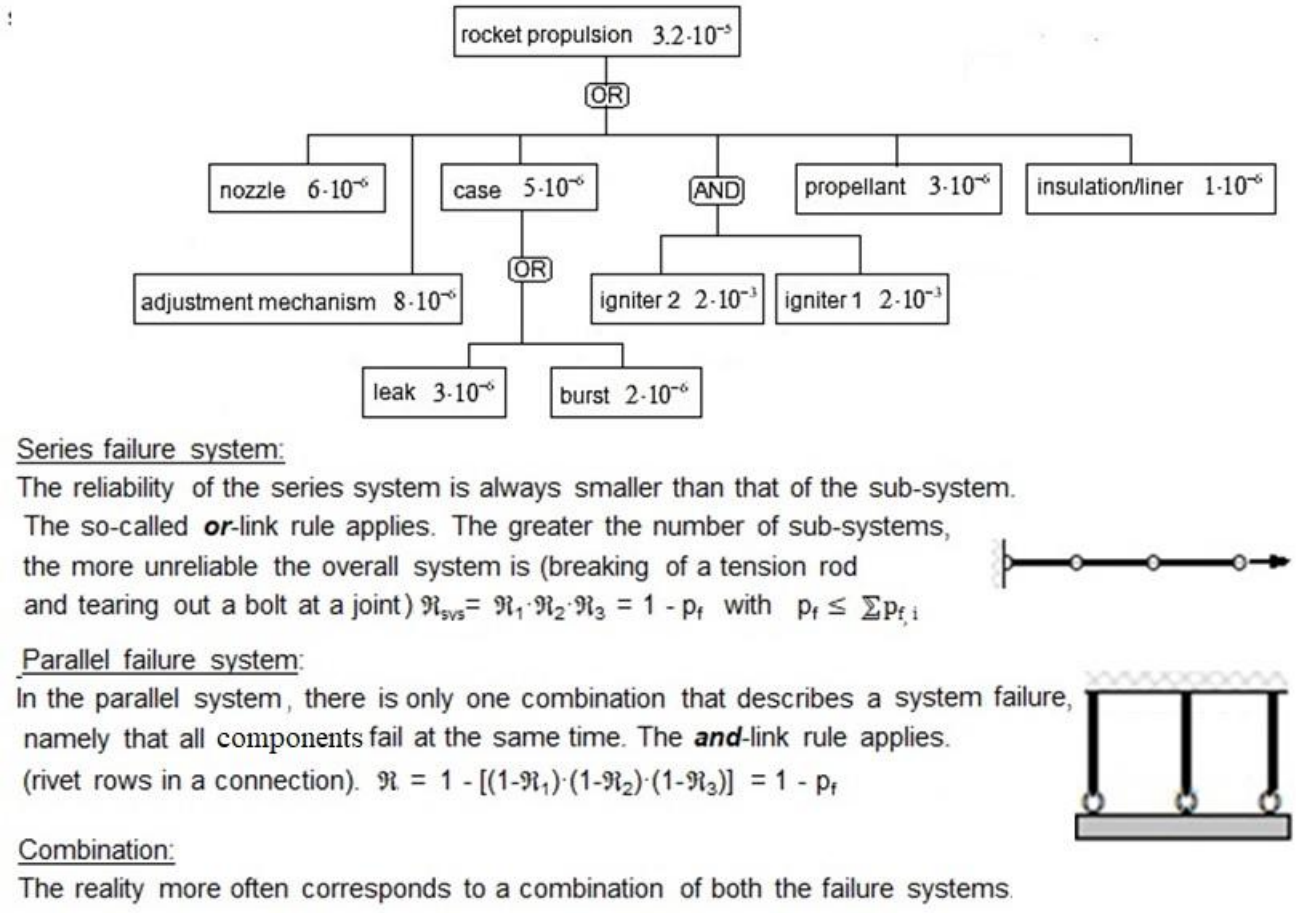

Fig.13-6: Procedure to estimate the reliability of a sub-system of the Ariane launcher

14 Nonlinear Stress-Strain relationships, Beltrami Theory with Change of Poisson's Ratio ν

Aim: *Provision of a Basis to generate an 'Extended Mises' model to later replace a multi-parameter 'Gurson model'*

14.0 General on Stress-Strain curves σ(ε), Strengths R and Poisson's Ratio ν

There are two different stress-strain curves existing: the *monotonic* and the *cyclic stress-strain curve*. The first curve is derived by the static tests, whereas the second one is generated by fatigue tests. Strain-controlled cyclic hysteresis loops (*Fig.14-1, left down*) are performed on different strain levels with several test specimens. Dependent on hardening and softening behavior of the actual material these two curves may discriminate significantly. Monotonic stress-strain curves have long been used to obtain design parameters for limitation of the stresses in engineering structures subjected to static loading. Similarly, cyclic stress-strain curves are useful for assessing the durability of structures subjected to repeated loading.

Further, in the case of monotonic σ-ε-curves there are very different, material-specific stress-strain curves in the elastic-plastic transition domain, see *Fig.14-1, left up* and *right*. Some show an 'Onset-of-yield' at an upper yield stress level $\bar{R}_e^{upper}$ and others at a lower yield strength $\bar{R}_e^{upper}$. In this case usually the lower yield point is taken as the yield strength of the metal.

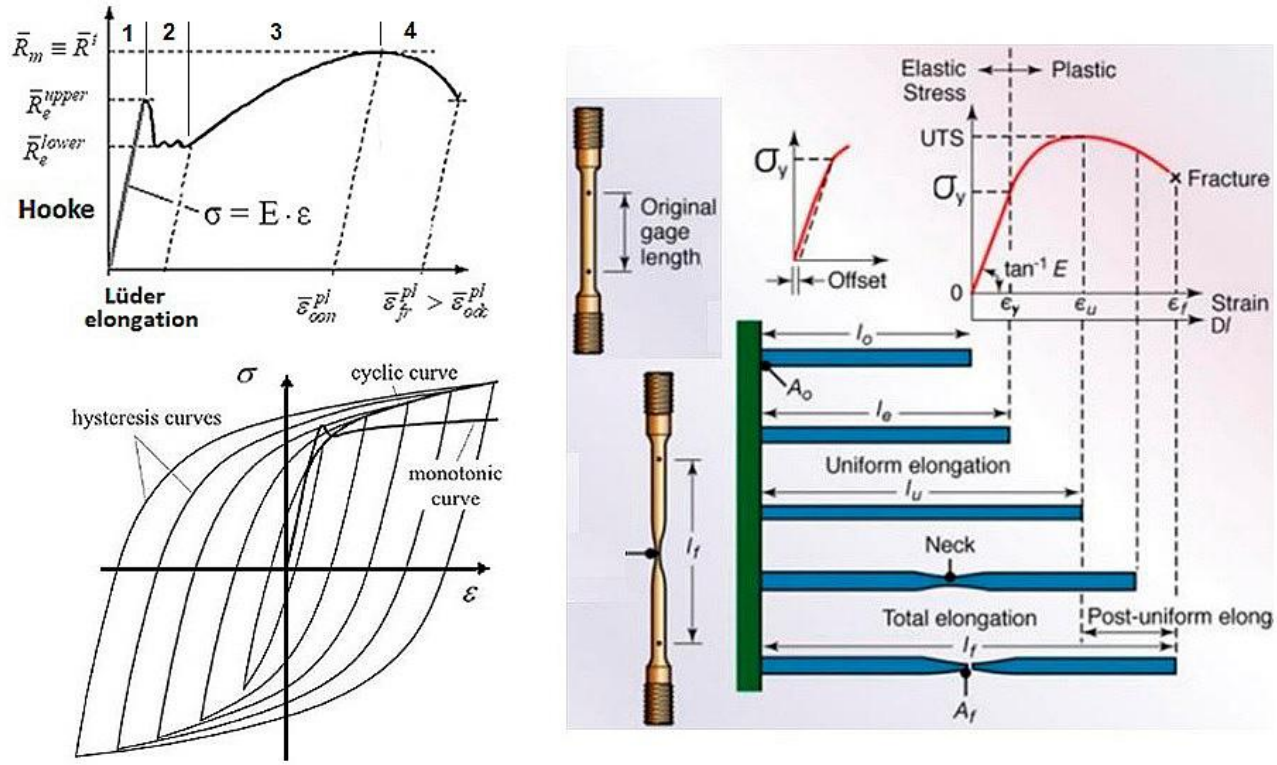

Fig.14-1, engineering quantities. modelling: (left,up) Discontinuous yielding, mean curve for mild steel showing the yield point phenomenon, termed Lüder's elongation effect. (left, down) Cyclic curves. (right) Tensile-test specimen with gage length, elongation before and after testing and finally after rupture (from Kalpakjian S and Schmid S: *Evaluation of the Possibility of Estimating Cyclic Stress-strain Para-meters and Curves from Monotonic Properties of Steels*. Manufacturing Engineering & Technology. 2013

For the 'left up'- metals in the paper of Hai Qiu and Tadanobu Inoue: *Evolution of Poisson's Ratio in the Tension Process of Low-Carbon Hot-Rolled Steel with Discontinuous Yielding. Metals* ***2023****, 13, 562.* https://doi.org/10.3390/met13030562 four different regimes are distinguished: Phase 1: Uniform elastic

elongation, Phase 2: Discontinuous yielding, Phase 3 beyond R_{02}: Uniform elongation in the hardening regime, Phase 4 beyond $\overline{R}^{t}$: Macroscopic plastic-strain localization experiencing radial deformation. Low-alloy iron usually has such an upper yield limit R_e^{upper} (R_{eH}, *Streckgrenze*). If it is stretched during the tensile test, a spontaneous yielding in the crystals-compound takes place under loading. This so-called Lüder's elongation effect of mild metals as a part of plastic stretching disappears until all crystals are finally commonly stretched. Austenitic steels do not have a pronounced yield strength. Essential for an accurate analysis is a stress-strain curve which is derived from a set of test curves, delivering distributions for the *design parameters* $R_{p0.2}$, R_m, ε_{on}^{pl} *and* ε_{fr}^{pl}.

The yield strength is a material property defined as the stress at which a material begins to deform plastically. If it is not well-defined (*remind Lüder*) on the stress-strain curve, it is difficult to determine a precise onset-of-yield point. In general, discriminating the proportional tensile limit R_{prop} and $R_{p0.2}$ ($\equiv R_{0.2}^{t}$), the offset yield point is taken as the stress at which 0.2% plastic deformation remains (*in English literature $R_{p0.2}$ is termed proof stress).* The mean stress at Onset-of-Yielding, denoted $\bar{R}_{0.2}$ will be applied for ductile modeling. The stress $\sigma(\varepsilon_{pl})$, considering only the plastic deformation or plastic flow of the material, is termed Flow stress σ_F.

By the way, the actual 'Onset-of-yielding at $R_{prop} \equiv \sigma_{prop}$ *can be determined by a temperature measurement. If a metallic material is subjected to tensile stress, it first cools down in the area of elastic elongation analogous to an ideal gas , thermo-elastic effect. With onset of plasticization heat is released, which leads to an increase in temperature. This temperature is measurable with glued thermocouples.*

In other words: The ***proportionality stress σ_{prop} can be allocated to that applied stress level, where the test specimen experiences a temperature increase due to internal dislocations.***

Regarding not only metals - for a conflict-free understanding – it will be denoted $R_{p0.2}$ ($\rightarrow R_{0.2}^{t}$) and $R_{c0.2}$ ($\rightarrow R_{0.2}^{c}$) in the body text from now on. At the maximum of the curve, characterized by the so-called '*End–of–uniform elongation'* = '*Onset-of-(ductile) necking'* in the ductile material case, the tensile strength R_m ($\rightarrow R^{t}$) is given. For very ductile materials is valid $R_{0.2}^{c} \cong R_{0.2}^{t}$.

Beyond the tensile strength R^{t} a multiaxial state of stress follows in the tensioned ductile behaving test specimen. Therefore, the index $_{ax}$ holds up to the 'End–of–uniform elongation' (Gleichmaßdehnung) at R^{t} (*index $_{pl}$ for plastic strain, $_{oon}$ for Onset-of-(ductile) necking, and $_{odc}$ for Onset-of-ductile cracking located before rupture = plastic collapse*).
In this respect, any formulations in this domain afford equivalent quantities in order to perform an accurate non-linear analysis with a correct $\sigma(\varepsilon)$-input.

14.2 Engineering and True Stress and Strain Quantities

The larger the strains the more the engineering quantities lose their applicability in structural dimensioning. Therefore, logarithmic (*usually termed true*) strains have to be used in an accurate dimensioning process. The derivation of these quantities is collected in *Table 14-1*.
Fig.14-2 contains a true and an engineering stress-strain curve. The figure presents a general view and uses classical Ramberg-Osgood mapping. Mapping of the course of stress-strain data in the non-linear domain is well performed by taking the usually applied Ramberg-Osgood equation for the true stress-true strain curve (*maps the true curve better than the engineering curve*)

$$\text{eng}\varepsilon = \varepsilon = \varepsilon^{el} + \varepsilon^{pl} = \frac{\sigma}{E_0} + 0.002 \cdot \left(\frac{\sigma}{\bar{R}_{0.2}} \right)^{\bar{n}}, \quad \text{true}\varepsilon = \frac{\text{true}\sigma}{E_0} + 0.002 \cdot \left(\frac{\text{true}\sigma}{\text{true}\bar{R}_{0.2}} \right)^{\text{true}\bar{n}}, \quad \bar{n} = \frac{\ln\left(A_{gl} / 0{,}2\% \right)}{\ln\left(\bar{R}^t / \bar{R}_{p0.2} \right)}.$$

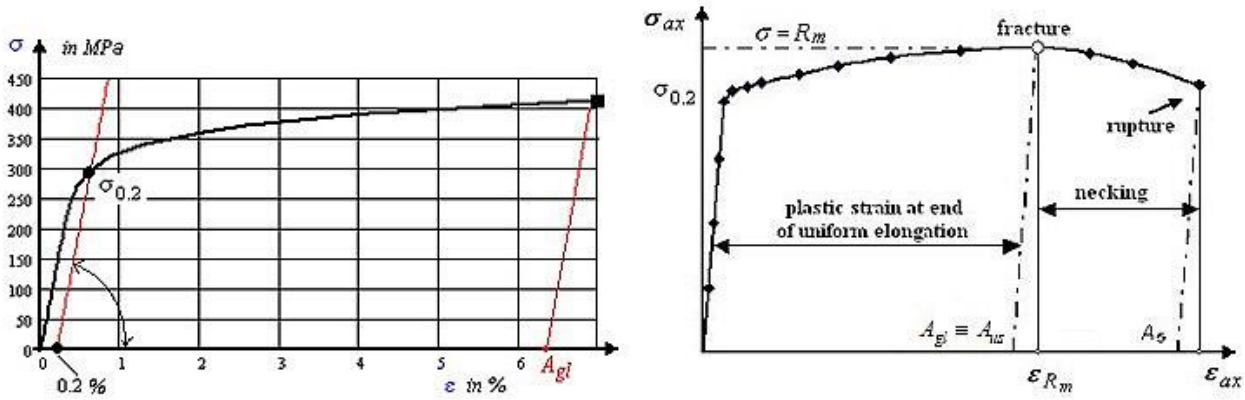

Fig.14-2: R-O mapping of a single engineering measurement test results, $A_{gl} = min\,\varepsilon_{oon}^{pl}$.

Typical (mean) engineering stress-strain curve of a distinct ductile metal material. End of uniform elongation (Gleichmassdehnung A_{gl} *)*

Table 14-1 presents the derivation of true stresses and true strains in the 'Mises'-validity domain.

In *Fig.13-4* the difference between the mean strength values $\text{eng}\bar{R}^t \rightarrow \text{true}\bar{R}^t$ was shown to be 8% for *AA2219!* *Fig.14-3(left)* depicts the linear elastic proportional domain and the hardening domain. *Fig.14-3(right)* presents stress-strain measurement with Ramberg-Osgood mapping. The course of the area reduction would show a slight kink beginning at 'Onset-of-ductile cracking $_{odc}$' (= o*nset-of-localized necking*) according to the deteriorating effect of the void coalescence.

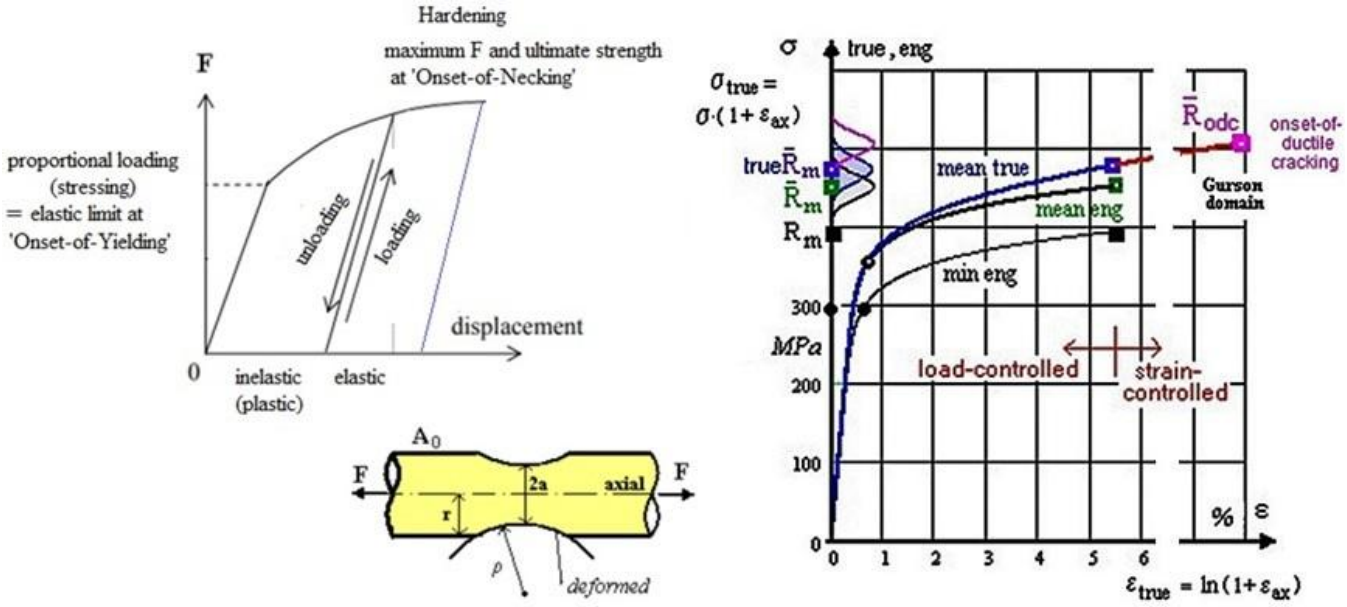

Fig. 14-3, modelling: (left) Display of proportional domain and hardening domain with the tensile rid test specimen. (right) Ramberg-Osgood-mapped true and engineering stress-strain curves of AA2219. F:= Force F_{ax}*,* A_0 *:= original cross-section, A:= actual cross section of the necked rod.* $\bar{R}^t = \max F / A_0$, $\varepsilon \le \bar{A}_{gl}$ *(permanent strain linked to load-controlled fracture at* $\bar{R}^t$*). Necking radius is* ρ*. A bar over* $\bar{R}$ *indicates a mean (average) value of a sufficiently large test data set, and no bar over R will generally mean strength and later indicate a 'strength design allowable'.*

Table 14-1: Derivation of true stresses and true strains in the 'Mises'-validity domain

True Strains (logarithmic strains):

The application of engineering strain cannot be correct for larger strains, since it is based on the original gage length ℓ_0, whereas the length is continuously growing. Ludwik [*Lud*09] therefore introduced the true strain (logarithmic strain), the increment of which for a given length is defined as $d(true\varepsilon) = d\ell / \ell$ and the total true strain, integrated from ℓ_0 to current length ℓ, is

$$true\varepsilon_{ax} = \int_{\ell_0}^{\ell} d\ell / \ell = ln(\ell / \ell_0) = ln(1 + eng\varepsilon_{ax}) .$$

Above equation delivers an accurate value up to 'onset-of-necking' or $\bar{R}^t$.

The replacement of the logarithmic function by a Taylor series

$$true\varepsilon_{ax} = eng\varepsilon_{ax} - eng\varepsilon_{ax}{}^2 / 2 + eng\varepsilon_{ax}{}^3 / 3 - .. +$$

clearly shows that identity is given for small strains, only. Applying the true strain has a physical and a numerical advantage: The incompressibility equation really becomes zero

$$\sum true\varepsilon_i = true\varepsilon_I + true\varepsilon_{II} + true\varepsilon_{III} = 0,$$

whereas in terms of engineering strains the correct equation from solid geometry reads

$$(1 + eng\varepsilon_I) \cdot (1 + eng\varepsilon_{II}) \cdot (1 + eng\varepsilon_{III}) - 1 = 0,$$

which reduces to 0 for negligible strains, only.

Once necking starts most of the deformation occurs in the smallest cross section. The longer the gage length used the smaller the percent elongation will be. Therefore, a better procedure is the measurement of the reduction of the cross-section. → Beyond $\bar{R}^t$, the true σ-ε curve can be more accurately obtained by measuring the radial strain

$$\text{eng}\varepsilon_{radial} = (r - r_0) / r_0 = r / r_0 - 1 \quad \text{and} \quad true\varepsilon_{radial} = -ln(1 + eng\varepsilon_{radial}) = -ln(r / r_0),$$

provided, the tensile test specimen has a circular cross-section, a rod. In this case $\varepsilon_{radial} = \varepsilon_{hoop}$

$$true\varepsilon_{ax} + true\varepsilon_{radial} + true\varepsilon_{hoop} = 0 \quad \text{and it holds} \quad true\varepsilon_{ax} = -2true\varepsilon_{radial} = 2\,ln(r / r_0),$$

which delivers an accurate value above 'onset-of-necking'. The equivalent strain in the center reads

$$true\varepsilon_{eq} = \frac{\sqrt{2}}{3} \cdot \sqrt{(true\ \varepsilon_{ax} - true\ \varepsilon_{hoop})^2 + 0 + (true\ \varepsilon_{hoop} - true\ \varepsilon_{ax})^2}$$

$$= \frac{\sqrt{2}}{3} \cdot \sqrt{2(2 - (-1))^2} \cdot true\varepsilon_{radial} = \frac{2}{3} \cdot \sqrt{3^2} \cdot true\varepsilon_{radial} = 2\,ln(r / r_0)$$

⇒ Transferring strain data: $true\varepsilon = ln(1 + eng\varepsilon)$, $eng\varepsilon = e^{true\ \varepsilon} - 1$.

True Stresses

Trueσ can be obtained from engσ, if the small changes in volume at the end of the transition domain are neglected. Then, incompressibility $\sum \varepsilon_i^{pl} = 0$ can be assumed and it follows:

$$\text{eng}\sigma = \text{F}/\text{A}_0, \quad \text{true}\sigma = \text{F/A} \quad \text{with } A \cdot \ell = A_0 \cdot \ell_0 \text{, F: = load } F_{ax}$$

wherein ℓ_0 : = original gage length, and A, ℓ current values of the necking cross-section.

Introducing the equation $\varepsilon_{ax} = (\ell - \ell_0) / \ell_0$ derived above, the true stress is linked by

$$true\sigma_{ax} = F / A = (F / A_0) \cdot (\ell / \ell_0) = eng\sigma \cdot (1 + eng\varepsilon_{ax}) = \sigma_{ax} \cdot (1 + \varepsilon_{ax}) \text{ usually written}$$

⇒ Transferring stress data: $true\sigma = eng\sigma \cdot (1 + eng\varepsilon)$ and $eng\sigma = true\sigma / exp(true\varepsilon)$.

Fig.14-4 (left) shows an experiment in the elastic-plastic transition region, carried out by O. Mahrenholtz /H. Ismar. The test was a flat compression test of a cube: One side constrained, one free, one compressed → Principal stress state ($\sigma_I = \sigma_{action}$, $\sigma_{II} = \sigma_{I\ (re\text{-}action)}$, $\sigma_{II} = 0$) → principal strain → ν . It turns out that R_{p01} is approximately ν = 0.4. The value at R_{p02} in H-L-W coordinates is 0.82 = $\sqrt{2/3} = \sqrt{2J_2} / R_{02}$, with $J_2 = 2R_{02} / 6$ (left, down). Poisson's ratio, determined by a coupon measurement, reads $\nu = -\varepsilon_{lat}/\varepsilon_{ax}$ or $\nu = -(\Delta d/d)/(\Delta \ell / \ell$.
Concerning sheet test specimens the measurement problem increases because localized necking will occur at 'onset-of-ductile cracking and this depends on the thickness of the test specimen.

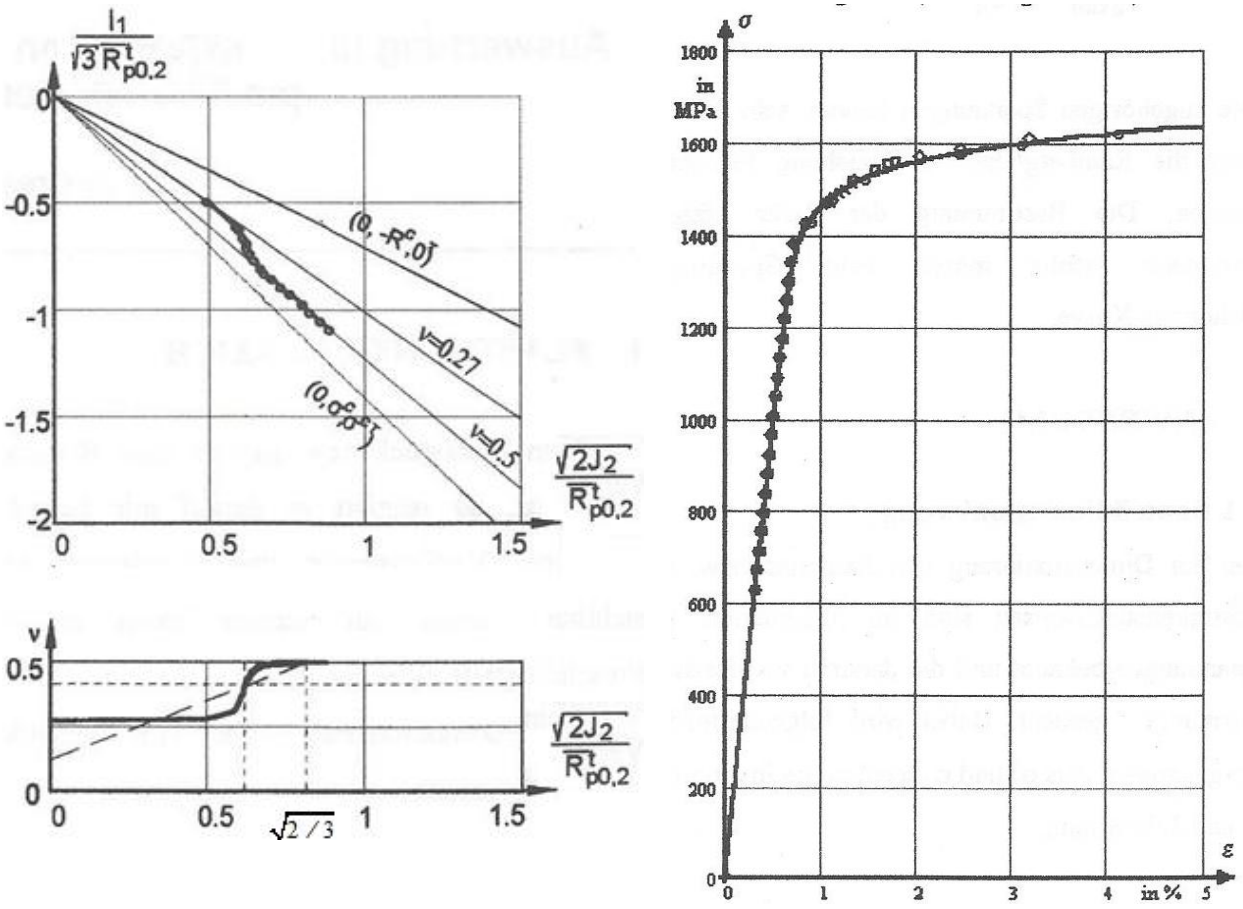

Fig. 14-4: (left) St37 Development of ν in Beltrami's elastic-plastic transition regime, a cube plane compression test. (right) D6AC, Ariane 5 Booster) Stress-strain measurement points with a Ramberg-Osgood engineering stress-strain data mapping curve under axial tension

14.4 Mapping of the measured stress-strain curve by the Ramberg-Osgood Model

In a contract of MAN-NT with the institute IWF at Freiburg all standard model-required properties have been determined. For completion, hopefully in a material-handbook given will be in addition the plastic strain A5 and also the final necking value Z, being usually minimum and not average values. $A_{fr} \equiv A_{rupture}$ comes from measurement of *A5* (*type:* $L_0 = 5 \bullet d_0$, *original length* L_0 *and initial diameter* d_0) as plastic or permanent change in length, measured on the load-controlled broken test specimen and Z the radial plastic necking A-reduction ratio value, in % (*Unfortunately, material mechanics also uses the letter A for this strain property).*

Table 14-2 lists analysis-relevant quantities (in MPa and %) to be applied in a Ramberg-Osgood curve modelling.

Table 14-2: AA2219 material properties and Ramberg-Osgood parameters. Isotropic materials, in MPa and %), *d= 4.0 mm . Regarding* $\bar{R}_{odc}$ *, see the following Sub-chapter 14-6.*

$\bar{R}_{p0.2}$	$\bar{R}_m$	A_{gl}	true$\bar{R}_m$	trueA_{gl}	$\bar{R}_{odc}$	$A_{fr} = A_{rupt}$	trueA_{fr}	Z	$\bar{n}$	true$\bar{n}$	$R_{p0.2}$	R_m	R_{odc}
352	*453*	*4.9*	*478*	*4.8*	*535*	*7.7*	*7.5*	*20*	*12.7*	*10.6*	*297*	*417*	*492*
MPa	MPa	%	MPa	%	MPa	%	%	%	-	-	MPa	MPa	MPa
average *(mean, typical, characteristic)* values for best mapping											Design Allowables		

$$\text{true}\varepsilon = \frac{\text{true}\sigma}{E_0} + 0.002\cdot\left(\frac{\text{true}\sigma}{\text{true}\bar{R}_{0.2}}\right)^{\text{true}\bar{n}} = true\varepsilon_{ax}^{el} + true\varepsilon_{ax}^{pl},$$

$$E_{sec}^{hard} = \frac{\sigma}{\varepsilon} = \frac{\sigma}{\frac{\sigma}{E_0} + 0.002\cdot\left(\frac{\sigma}{\bar{R}_{0.2}}\right)^{\bar{n}}} = \frac{E_0}{1 + 0.002\cdot\frac{E_0}{\bar{R}_{0.2}}\cdot\left(\frac{\sigma}{\bar{R}_{0.2}}\right)^{\bar{n}-1}},\quad E_{tan}^{hard} = \frac{d\sigma}{d\varepsilon} = \frac{E_0}{1 + 0.002\cdot\bar{n}\cdot\frac{E_0}{\bar{R}_{0.2}}\cdot\left(\frac{\sigma}{\bar{R}_{0.2}}\right)^{\bar{n}-1}}.$$

14.5 Poisson's ratio

If analytically necessary the value of Poisson's ratio ν, which increases when stresses narrow the plastic regime, can be determined for stability analyses as a function of the stress. The formula, which uses quantities of the R-O-mapped true stress-true strain curve, is derived in *Table 14-3.*

Table 14-3: Derivation of a formula for Poisson's ratio

$true\varepsilon = true\varepsilon^{el} + true\varepsilon^{pl}$ with $true\varepsilon_{ax} = true\varepsilon_{ax}^{el} + true\varepsilon_{ax}^{pl}$, $true\varepsilon_{lat} = true\varepsilon_{lat}^{el} + true\varepsilon_{lat}^{pl}$, $\nu_0 = \frac{-true\varepsilon_{lat}^{el}}{true\varepsilon_{ax}^{el}}$

from incompressibilityin the plastic range (≡ volume conservation law) $\frac{V}{V_0} = \frac{\ell}{\ell_0}\cdot\frac{A}{A_0} = 1$

follows $true\varepsilon_{ax}^{pl} + 2\cdot true\varepsilon_{lat}^{pl} = 0$ and $true\varepsilon_{lat}^{el} = -\nu_0\cdot true\varepsilon_{ax}^{el}$, which gives after insertion of above relations

$$true\nu = -\frac{true\varepsilon_{lat}}{true\varepsilon_{ax}} = -\frac{true\varepsilon_{lat}^{el} + true\varepsilon_{lat}^{pl}}{true\varepsilon_{ax}} = -\frac{true\varepsilon_{lat}^{el} - 0.5\cdot true\varepsilon_{ax}^{pl}}{true\varepsilon_{ax}} = -\frac{true\varepsilon_{ax}^{el}}{true\varepsilon_{ax}}\cdot\left(-\nu_0 - 0.5\cdot\frac{true\varepsilon_{ax}^{pl}}{true\varepsilon_{ax}^{el}}\right)$$

$$= -\frac{true\varepsilon_{lat}^{el} - 0.5\cdot true\varepsilon_{ax}^{pl}}{true\varepsilon_{ax}} = -\frac{-\nu_0\cdot true\varepsilon_{ax}^{el} - 0.5\cdot true\varepsilon_{ax}^{pl}}{true\varepsilon_{ax}} = -\frac{-\nu_0\cdot true\varepsilon_{ax}^{el} - 0.5\cdot\left(-true\varepsilon_{ax}^{el} + true\varepsilon_{ax}\right)}{true\varepsilon_{ax}}$$

$$= -\frac{-\nu_0\cdot true\varepsilon_{ax}^{el} - 0.5\cdot\left(-true\varepsilon_{ax}^{el} + true\varepsilon_{ax}\right)}{true\varepsilon_{ax}} = 0.5 + \frac{-\nu_0\cdot true\varepsilon_{ax}^{el} - 0.5\cdot\left(-true\varepsilon_{ax}^{el}\right)}{-true\varepsilon_{ax}}$$

$$= 0.5 - \frac{true\varepsilon_{ax}^{el}}{true\varepsilon_{ax}}\cdot\left(0.5 - \nu_0\right),\ \text{see. 14.5 .}$$

However, this formula does not fully lead to ν = 0.5 at R_{02} as can be seen in *Fig.14-5*. A better approximation $\nu = 0.5 - (E_{tan}^{hard}/E_0)\cdot(0.5 - \nu_0) \Rightarrow true\nu$ is usually applied in the elastic-plastic domain in stability analysis employing the tangent modulus function above in order to approximately consider the changing *ν* in analysis.

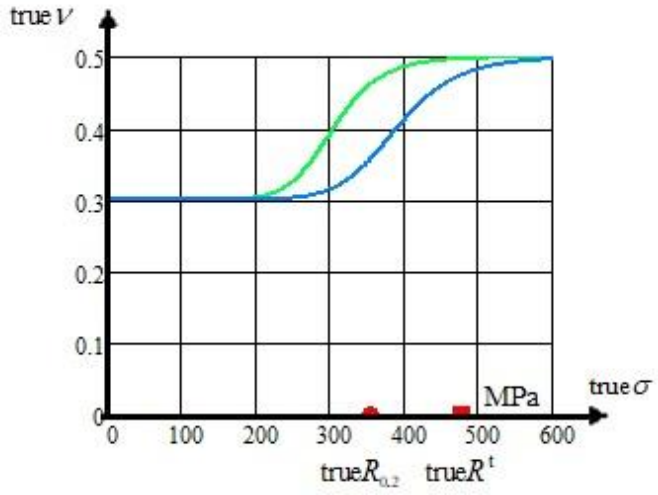

Fig.14-5: Course of Poisson's ratio in the elastic-plastic domain, determined with several formulas

***LL**:*

** The determination of the properties of a solid material requires a force-elongation curve which is then accurately to transfer into a stress-strain curve that is independent from the tested specimen type rod, sheet, coupon, cube.*

** Before any performance of a non-linear analysis is executed it is to check whether true or engineering curve quantities are to provide for numerical input. This then fixes the output*

** Beyond R^t necking occurs generating a hydrostatic stress σ_{hyd} in the tensile rod, which lowers the stress-strain curve (see Chapter 15) in the high plastic regime*

** Poisson's ratio can only approach the limiting points 0.5 > **ν** > (-1, principally.) So-called auxetic materials possess a negative ν. Being strained, the transverse strain in the material will also be positive*

** UD-materials have different ν-values in the directions of anisotropy*

** True strains can be added while engineering strains can not!*

In *Fig.14-6* the different growth of the engineering and the true stress-strain curve is displayed up to the tensile strength point at the 'End–of–uniform elongation'. Beyond R^t, in test data evaluation the axial stress has to be replaced by the equivalent stress because necking in the test specimen activates a hydrostatic residual stress state, dependent on the test specimen used.

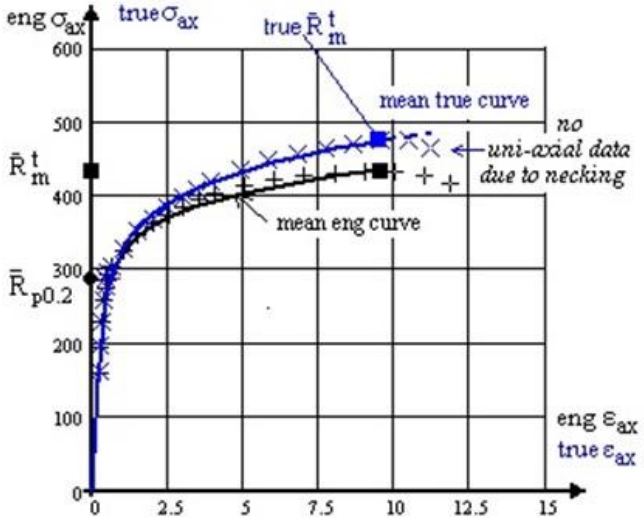

Fig.14-6, AA 2219:

Differences in R-O-mapping of engineering and true stress-strain curve, single measurement.

Bar over R indicates a mean value.

F/A_0 at 'End of uniform elongation' =

'Onset-of-(diffuse) Necking'

In *Fig.14-7* the full stress-strain curve is presented and associated significant points including strength design allowables points are depicted. Additionally for 'Onset-of-yielding' the Margin of Safety is rendered in order to visualize the size of the fulfillment of the 'Design Yield' Limit State.

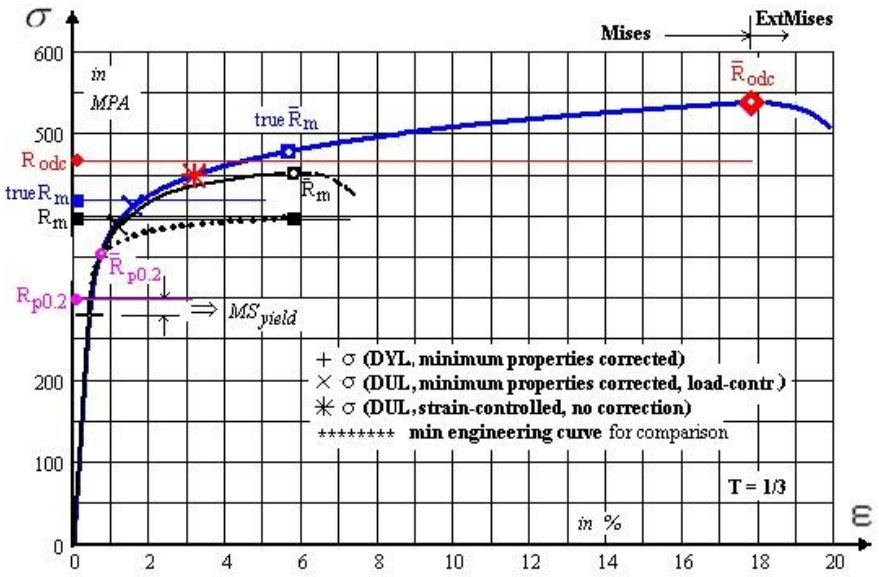

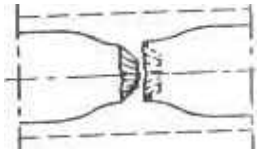

cup-cone picture
of the
failed rod

Fig. 14-7: Equivalent true stress-equivalent true strain curve. Proposed local strain-controlled extended stress-strain curve incl. mean fracture points and strength design allowables (no bar over)

The full curve ends with reaching the 'onset-of-ductile cracking' point at the associated strength R_{odc}.

LL:

** Opposite to some regulations it is to note "In general, it can be not correct to use a minimum engineering curve in order to obtain the desired realistic structural behavior because structures are usually statically indeterminate".*

** The elliptical shape of the 'Beltrami egg' and its surface potential description will be used in the 'Gurson domain' too, next chapter.*

14.6 Estimation of the Strength $\bar{R}_{odc}$

Beyond 'Onset-of-diffuse necking' the axial strain measurement becomes senseless, only representative is the rod radius-decrease measurement to investigate in this full plastic domain the influence of the hydrostatic stress. From the measured plastic cross-section reduction the plastic portion ε_{odc}^{pl} can be estimated and the 'plastic' curve point $\bar{R}_{odc}$ computed if the only counting associated plastic strain is known, fixed by the diameter reduction. Because the R/O-model excel- lently maps the true strength course of test data, its plastic part is employed to estimate a value for the *plastic point* $\bar{R}_{odc} \equiv$ 'Onset-of-ductile-cracking', which is of interest for plastic structural design.

This can be executed by using volume constancy applying the measured reduction of the initial radius $a = d/2$ of the tensile rod. With $Z(\bar{R}_{rup})$ taken as $Z(\bar{R}_{odc})$ the estimation of $\bar{R}_{odc}$ at trueε_{odc} from the Ramberg-Osgood curve is performed as shown in *Table 14-4*.

Ductile collapse or *rupture* $\bar{R}_{rupt}$, respectively, is of theoretical interest, only.

Table 14-4: Derivation of an estimate value for the Strength $\bar{R}_{odc}$

At $\bar{R}^t$ 'Onset-of- (diffuse) necking' $d_{oon} = 3.89$ mm, at 'Onset-of-ductile cracking' $d_{odc} = 3.78$ mm.

$$\varepsilon^{pl} = 0.002\left(\frac{\sigma}{\bar{R}_{0.2}}\right)^n \;,\quad \varepsilon_{rad}{}^{pl} = \ln(\frac{r}{a}) \;,\quad \frac{\Delta A}{A_0} = \frac{A_0 - A}{A_0} = 1 - \frac{A}{A_0} \;\rightarrow\; \frac{A_{rupt}}{A_0} = 1 - Z = \frac{r^2}{a^2}$$

$\varepsilon_{ax,\,00n}{}^{pl} = -2 \cdot \varepsilon_{rad}{}^{pl}$ at $\bar{R}^t$ and delivers $\text{true}\bar{n} = \dfrac{\ln\left(\varepsilon_{ax,\,00n}{}^{pl} / 0{,}2\%\right)^n}{\ln\left(\bar{R}^t / \bar{R}_{p0.2}\right)}$.

With known $\varepsilon_{rad}{}^{pl} = \ln(\frac{r}{a}) = \ln(\sqrt{1-Z}) = \ln(\sqrt{1-0.20}) = -11.2\ \%$ and $\varepsilon_{ax}{}^{pl} = -2 \cdot \varepsilon_{rad}{}^{pl}$

follow for the non-corrected odc-point $\rightarrow true\varepsilon_{ax}^{pl} = 0.002 \cdot \left(\dfrac{\bar{R}_{odc}}{\bar{R}_{0.2}}\right)^{\text{true}\bar{n}}$

$$\Rightarrow\ \bar{R}_{odc} \cong \bar{R}_{0.2} \cdot \sqrt[true\bar{n}]{\varepsilon_{ax}{}^{pl}} / 0.002 = 542 \text{ MPa} \quad \text{and}$$

$$\text{true}\varepsilon\text{odc} = true\varepsilon_{ax}^{el} + true\varepsilon_{ax}^{pl} = \frac{\bar{R}_{odc}}{E} + 0.002\left(\frac{\bar{R}_{odc}}{\bar{R}_{0.2}}\right)^{\text{true}\bar{n}} \;.$$

14.7 Beltrami's Potential Surfaces in the Elastic-plastic Regime and as Idea for the Porous Regime

From previous investigations the author knows, that any volume change, due to the FMC 'rules', is to describe by the term $I_1{}^2$. If a shape change occurs then the invariant J_2 is required.

Elastic-plastic transition regime:

Beltrami cites: "*The deformation of a material consists of two parts, a shape* and *a volume change*". Based on this, one can formulate for the elastic-plastic transition regime

$$\frac{(2+2\nu)\cdot 3J_2}{\bar{R}^2} \text{ and } \frac{(1-2\nu)\cdot I_1{}^2}{\bar{R}^2} \;\rightarrow\; \frac{3J_2}{\bar{R}^2} + \kappa \cdot \frac{I_1{}^2}{\bar{R}^2} = c^{\text{Bel}} \text{ with } \kappa = \frac{1-2\nu}{2+2\nu} \;.$$

Into this formulation a normalizing strength is inserted: $I_1 = \bar{R},\ J_2 = 2\bar{R}/6 \rightarrow c^{\text{Bel}} = 1+\kappa$ and

for the special yield potential surface (ν=0.5) yields $\dfrac{3J_2}{\bar{R}_{02}{}^2} + 0 \cdot \dfrac{I_1{}^2}{\bar{R}_{02}{}^2} = 1 + 0$ ('Mises' cylinder).

Beltrami bridges the elastic domain with the plastic domain ($3 \cdot J_2$ is Mises part). His formulation is not a failure function but a descriptive function to predict subsequent Beltrami surfaces $\nu(\bar{R})$, which are surfaces of equal potential. This means: A pair $(\nu, \bar{R})$ must be given for each desired ν-curve of the subsequent potential surfaces are obtained, *see Fig.14-8 left.* This part figure shows the change of the potential surface of the growing 'Yield' body with increasing ν in the elastic-plastic transition domain. The two center figures show the cross-section using the principal stresses and below the development of the yield body from the yellow egg ($\nu = \nu_0$) up to full yielding ($\nu = 0.5$) rendered by the 'Mises cylinder' → *Poisson's ratio ν drives the elliptic shaping!*

Plastic porosity affected regime: an anticipation, considering Chapter 15

Porosity causes a volume increase. This works oppositely as in the elastic-plastic transition regime, which can be described by Beltrami, too. Increasing porosity *f* means a decreasing Poisson's ratio *ν* and a more elliptic shape. In the outer figures of *Fig.14-7* both the regimes of the changing Poisson's ratio

are displayed. The right part figure, modelled by Beltrami, pre-informs (see *§15*) how the surface of the yield body changes its shape with decreasing *v* according to the increasing porosity *f*.

Fig.14-7(right) displays the development of the subsequent failure surfaces whereby an increasing true stress is considered. This is relevant for the critical material location. After achieving the tensile strength a small further radial increase of the surface is obvious together with the initiation of an increasing elliptic failure surface. With increasing degradation the subsequent surfaces become more and more elliptical. This is the opposite process regarding Beltrami in the elastic-plastic transition regime. A growing *f* means higher true stress but less cross-section or load-carrying material in the strain-controlled 'hot spot'.

The Beltrami formulation delivers an *Idea for the ductile porous regime* and is intended to replace the 'Gurson' formulation by Cuntze's so-called 'Extended Mises' one, reading

$$\frac{3J_2}{\bar{R}^t_{0.2}} + \frac{1-2\nu}{2+2\nu}\cdot\frac{I_1^{\,2}}{\bar{R}^t_{0.2}} = c^{\mathrm{Bel}} \quad \Rightarrow \quad \frac{3J_2}{\bar{R}^t_{0.2}} + c_{12}\cdot\frac{I_1^{\,2}}{\bar{R}^t_{0.2}} = c^{\mathrm{ExtMises}} \quad .$$

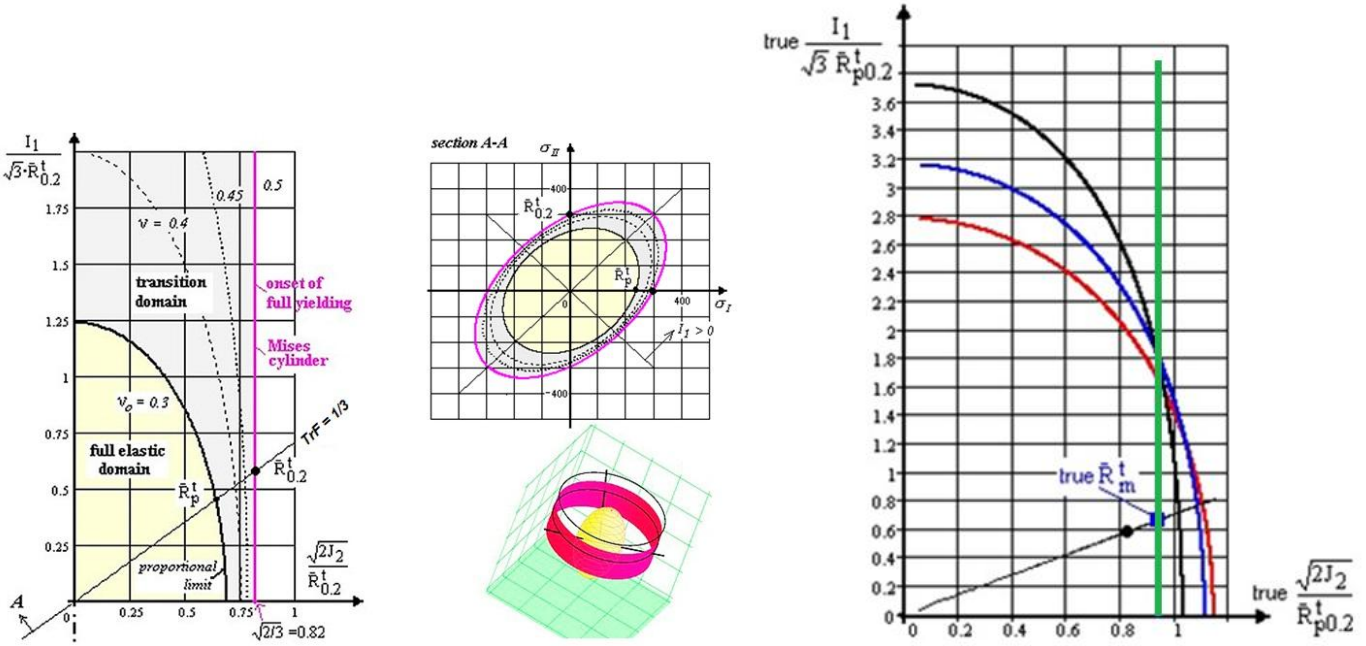

Fig.14-8: (left) Elastic-plastic transition domain, development of the Beltrami surfaces from egg shape (growing yield potential surface with ν_0 = 0.3 for metals (0 for foam = sphere) < ν < 0.5 ('Mises cylinder → J_2 = constant = incompressibility) depicted in Lode-Westergaard coordinates. (center) visualization of the Beltrami potential surfaces. (right) Change of potential surfaces in the porous domain computed with the Extended Mises formulation (see [CUN22, §17]), f = 0, 0.1, 0.2, 0.3

Also here, the yield strength can be used for normalization. The parameters c^{Bel}, c^{ExtMises} mark the size parameter of the changing potential surface (*see survey in* <u>*Table 15-4*</u>**).**

In order to understand the chosen Haigh-Lode-Westergaard coordinates <u>*Fig.14-9*</u> is provided below. The vector $\{\sigma_{\mathrm{prin}}\} = (\sigma_I, \sigma_{II}, \sigma_{III})^T$ is a vector-addition of the principal stresses. The cone angle between all principal axes and I_1 is 54.75°.

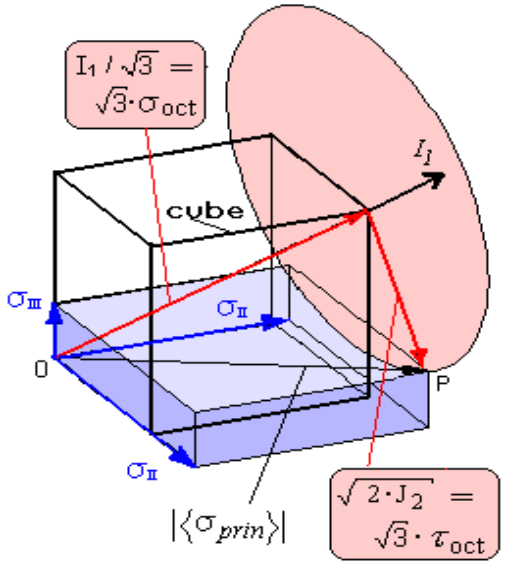

Fig.14-9:
Visualization of the used Haigh-Lode-Westergaard coordinates by the principal stresses acting at a material cube.

Octahedral stresses:

$$\sigma_{oct} = I_1 / 3 \quad \text{with } I_1 = \sigma_I + \sigma_{II} + \sigma_{III}$$

$$\sigma_{eq}^{Mises} = \sqrt{3 \cdot J_2} = f(\tau), \text{ with}$$

$$6 \cdot J_2 = (\sigma_I - \sigma_{II})^2 + (\sigma_{II} - \sigma_{III})^2 + (\sigma_{III} - \sigma_I)^2$$

$$\tau_{oct} = \sqrt{6J_2}/3 -$$

To make more familiar with potential surfaces ***Fig.14-10*** presents two potential surfaces dedicated to different *Effs*, for fracture *Eff* = 100% and for a loading that generates *Eff* = 50 %.

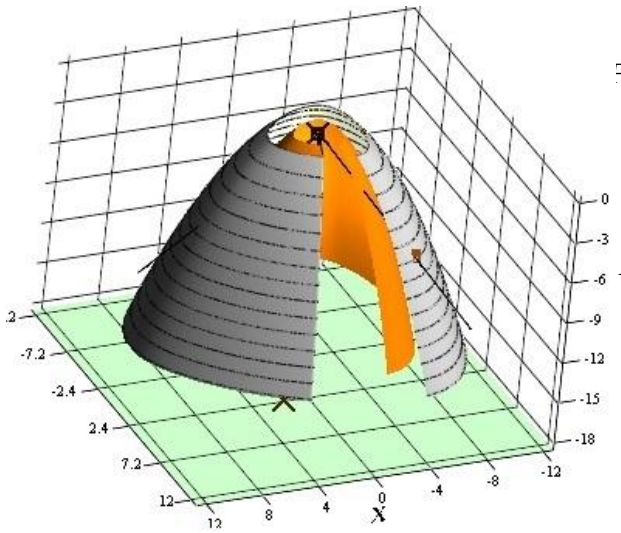

Fig.14-10: Two potential surfaces. Eff is the measure for the distinct potential surface with Eff=1=100% the fracture surface. The potential surfaces are Eff^{SF} *=50% and* Eff^{SF} *=100% = fracture.*

Indicated are the failure stress points

$\bar{R}^t = 4$ MPa, $\bar{R}^{tt} = 3$ MPa, $\bar{R}^c = 40$ MPa, $\bar{R}^{cc} = 49$ MPa

and the principle stress axes.

'Normal Concrete', 3D test data available

$$Eff^{SF} = c^{SF} \cdot \frac{\sqrt{4J_2 \cdot \Theta^{SF} - I_1^2 / 3} + I_1}{2 \cdot \bar{R}^c}$$

LL:

* *The shape of the potential surfaces in the plastic porosity regime changes oppositely to the shape in the elastic-plastic regime. Both the surface shapes one can dedicate to the change of the Poisson ratio v*
* *In structural analysis the stresses are most-often .determined in the elastic-plastic regime. This is performed very accurately, sometimes over-precise. However in this domain the Poisson's ratio changes significantly, which should be considered.*

15 A measurable parameters'-based 'Extended-Mises' Model instead of a 'Gurson' Model?

Aim: *De-complication of highly non-linear plastic analyses by generation of a simplified model to perform Design Verification in a Ductile Metal's high Porous Regime*

15.1 Introduction

There is stress- and strain-controlled behavior. Strain-controlled locations in a structure will not break, when the stress level reaches tensile strength R^t. A fuel-outlet hole in the upper tank of the Ariane 5 central stage was such a strain-controlled case at MAN, where the vicinity of the 'overstrained' critical material location takes over the reduced loading capability, no direct fracture is to face.

Such a (seldom) task caused MAN-Technologie to let perform an analysis together with IWM Freiburg applying a multi-parameter 'Gurson' yield model. Its model parameters cannot be measured directly, but are usually determined by a FE analysis which best models the deformation of the test specimen, a classical simulation process. An example for such a multi-parameter set, determined for the aluminum alloy AA2219 and by using the tensile rod test specimen, is given in the table below [*IWM Freiburg*]:

f_0	f_n	f_c	f_F	q_1	q_2	ε_n	s_n
0.00	0.05	0.04	0.15	1.5	1.0	0.20	0.01

.

The applied 'Gurson'-model (such a model is a model of the *Continuum (micro-)Damage Mechanics theory in the ductile materials regime)* of the IWM was a refined one. Refinement means that more parameters are to determine than for a simpler 'Gurson' model. Therefore, the optimal model parameter set *of a 'Gurson' model* depends on the mesh fineness and has to be inversely determined by an excellent simulation of the test specimen's behavior, see *Fig.15-1 left* for the tensioned rod

(Gurson A L: *Continuum Theory of Ductile Rupture by Void Nucleation and Growth. Part 1:Yield criteria and flow rules for porous ductile media*. J. Eng. Mater. Techn.99 (1977), 2-15)

Using 'Gurson' model results, the responsible design engineer must ask:

What about the scatter of the simulation-won parameters which are to insert in the analysis?

Without knowledge of the scatter there is not a generally accepted design verification possible. Might it be not better to apply a simpler model with 2 or 3 parameters at dispense of the little gain of the last load carrying portion after coalescence at 'onset-of-ductile cracking' marked by the corresponding strength value R_{odc}? This is the 'technically relevant point', where the coalescence of voids begins. Only a reduced procedure with directly measurable model parameters has the chance to capture the statistical Design Verification requirements.

In the context above the question comes up:

"*How much Gurson material modelling is necessary to achieve a reliable prediction of the local design-deciding ductile fracture level of the structure?"*

This failure mode 'ductile fracture' is defined here to be met at 'onset-of-ductile cracking' and it shall correspond to Design Ultimate Load. Such an application is a seldom case, where the deformation-controlled strength value $R_{odc} > R^t$ is used to *save the final design* not anymore possible via the load-controlled strength value R^t. A simpler model is required. Two challenging parts tasks are thereby faced:

(1) Creation of a model simpler than a multiple-parameter 'Gurson' model, and

(2) to capture the porosity *f* in the equivalent σ-ε-curve**,** to be provided, whereby *f* is an additional but measurable model parameter transferring the 'Mises' model to the 'Extended Mises' model. For its derivation, the various micromechanical mechanisms during ductile fracture are of basic interest:

* Void nucleation in the test rod at so-called second phase particles by debonding

* Void growth, controlled by stress Triaxiality Factor *TrF* and growing plastic strain ε_{eq}^{pl}, and

* Coalescence of voids by internal shear stress-driven rod necking with final ductile rupture.

For the evaluation of the usual rod test results, the widely used correction formula of P.W. Bridgman is employed. *Fig.15-1(left)* presents the dependency of the rod's diameter reduction on the load *F* and further shows simulation curve and test curve. The measurement of the diameter reduction is mandatory beyond the 'end of uniform elongation' at the tensile strength point $\bar{R}^t = max\,F\,/\,A$, depicting the 'onset-of-diffuse necking $_{oon}$ point and experiencing full plasticity. Beyond $\bar{R}^t$ only true values represent the reality.

Mind: $F(\Delta d)$ is not completely of the same shape like $true\sigma(true\varepsilon)$.

In the load-controlled regime axial strain measurements are performed whereas in the transversal, plastic strain-controlled necking regime diameter reduction measuremens are to execute. In the *Fig.15-1(right)* attention is drawn to the various stress-strain curves used and to the associated strengths. Displayed are the mean technical and mean true strengths together with the associated Design Allowables.

If materials do not fail when the tensile strength is reached, then this is accompanied by the fact (*Fig.15-1, left)* that max*F* does not essentially change over a certain range of the strain because hardening still works until a slight kink will occur due to void coalescence and destruction of piled–up dislocations. Degradation wins over hardening at the 'onset of ductile cracking' strength point R_{odc}. R_{odc} and marks the coalescence-linked kink and is defined here as the critical strength.

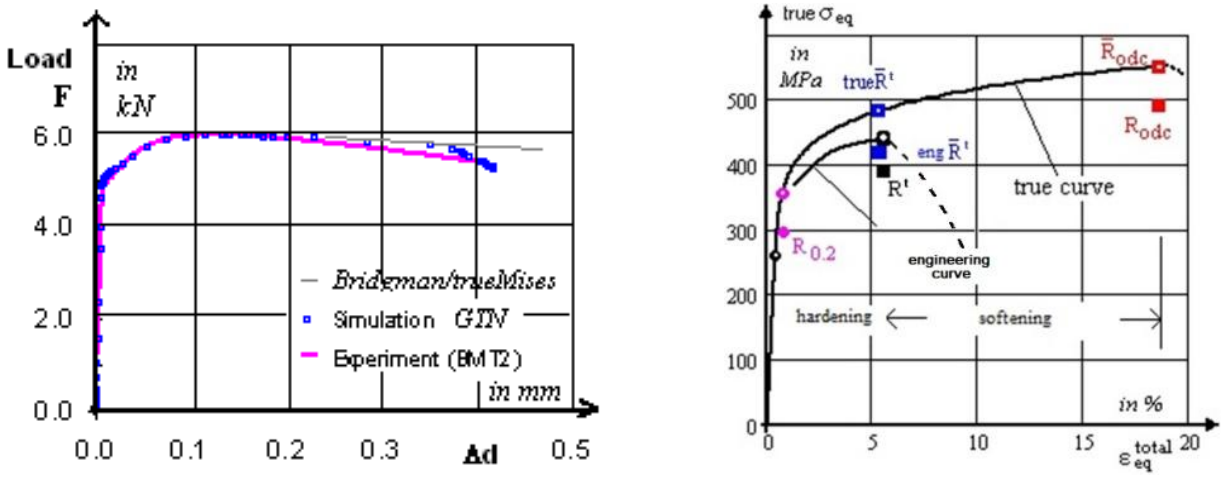

Fig.15-1: (left) Dependency of diameter reduction Δd on the applied load F. Comparison of global simulation and test results (IWM Freiburg, Dr. Sun). (right) Ramberg-Osgood-mapped true and engineering stress-strain curves of AA2219A bar over R indicates a mean value, no bar over R indicates a 'design allowable'

15.2 Bridgman-3D Correction of the true σ-ε-Curve, employing 'Mises'

Equivalent stress: $true\sigma_{ax} \rightarrow true\sigma_{eq}$

The validity of the uniaxial stress-strain curve measured in the smooth tensile rod test is terminated at the load-controlled strength point $max\sigma_{true} = \bar{R}^t = max\,F\,/\,A$, which corresponds to the maximum load *F* and to the actual minimum cross section of the neck. However, beyond $\bar{R}^t$ ('end-of-uniform-elongation') at the 'onset-of-diffuse necking $_{odn}$' point the 1D-stress situation in the tensile rod becomes a 3D one and an equivalent stress σ_{eq}^{Mises} has to be considered in order to capture spatial stress tasks.

Under tensioning, in the plastic regime the lateral contraction of the material at the center of the neck is impeded by neighboring material leading to a 3D-stress state. Hence, a simple extrapolation of the F/A (σ-ε)-curve beyond $\bar{R}^t$ cannot provide a physically accurate curve, because the necking-generated 3D-residual stress state σ_{hyd} is to consider in the evaluation of the tensile rod test results in order to obtain a real σ_{eq}. The three stresses within σ_{eq} reach their maximum values at the center of the rod's cross-section with an approximately equal value $\sigma_{radial} = \sigma_{hoop}$, except close to the surface, as depicted in *Fig.15-2(left)* below. The values of σ_{radial}, σ_{hoop} and of the created necking radius ρ raise with σ_{ax}. The former F/A-quantified capacity becomes continuously reduced with increasing necking. Hence, the true stress-strain F/A curve is to correct to obtain a realistic equivalent stress. In the center of the rod an increasing stress Triaxiality Factor *TrF* is faced.

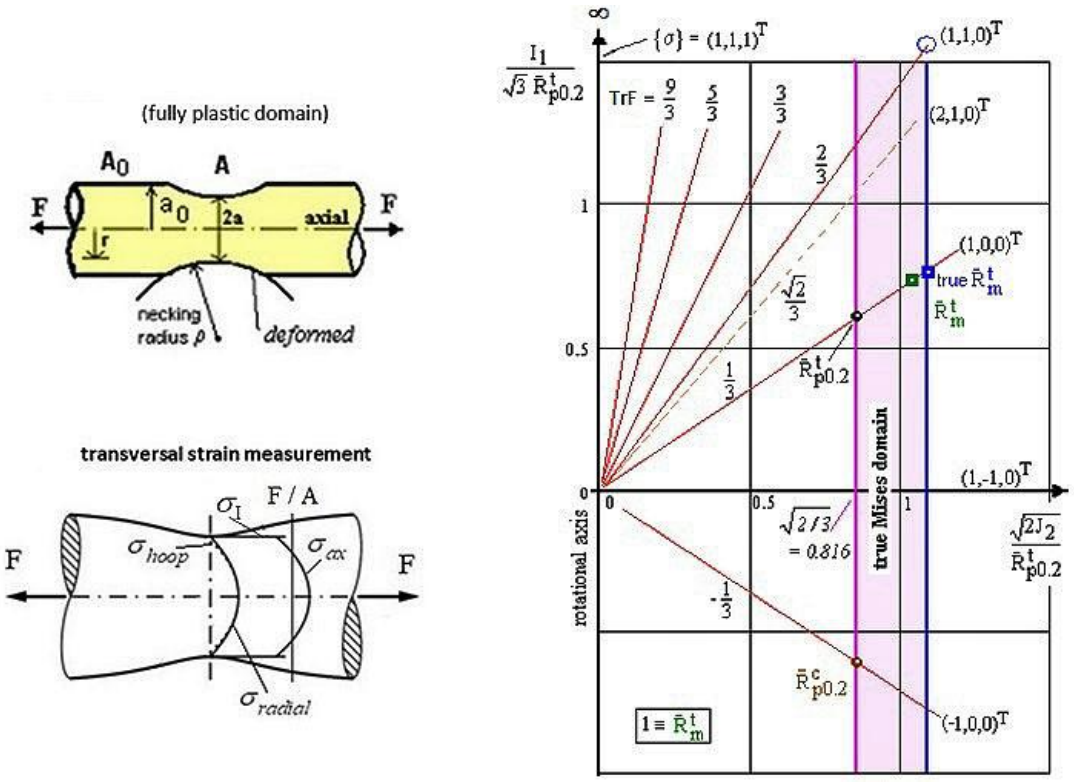

Fig.15-2: (left) Stresses and transversal (radial) strain measurement of the necked round tensile rod. F:=force, A:= minimum actual cross section of the neck. F:=Force F_{ax}, A_0 := original cross-section. $\bar{R}^t = \max F / A_0$, $\varepsilon \le \bar{A}_{gl}$ *(permanent strain linked to load-controlled fracture at* $\bar{R}^t$*). Necking radius is* ρ*. (right) Schematic visualization of the Triaxiality Factor TrF, responsible for failure in the rod center*

$$\{\sigma\} = \{\sigma_I, \sigma_{II}, \sigma_{III}\}^T,\ TrF\{\sigma_I, \sigma_{II} = \sigma_I, 0\}^T = 2/3.$$

Assuming a constant σ over the rod's cross-section, *Fig.15-2(right)* illustrates by a variety of *TrF*-beams that values higher than 2/3 (bi-axial stressing) are practically not possible. Assuming constancy is not anymore the case for a plastic rod neck, where the failure decisive location is the center of the cross-section with also there facing *maxTrF.* Notched test specimens are applied to capture higher multi-axial stress states, *TrF* = 1, values > 1/3.

Fig. 15-3 shows the void volume fraction in the necking region at failure. The highest values are reached in the center of the specimen (Element 20) as expected, *TrF* highest. From the central region micro-damage spreads out over the whole cross section.

Basic task now will be the necessary transfer from the uniaxial trueσ_{ax}(trueε_{ax}) → tri-axial trueσ_{eq} (trueε_{eq}) in the diffuse necking regime.

Bridgman provided a correction means how to adjust trueσ_{ax}, but had to make some essential assumptions:

(1) The cross section of the necked region remains angular *(like the 'Mises' cylinder, assuming a rotationally symmetric yield body*).

(2) The inner axial contour of the neck can be approximated by the arc of a circle with the radius ρ.

(3) 'Mises' can be applied (*effect of growing voids is therefore not considered*).

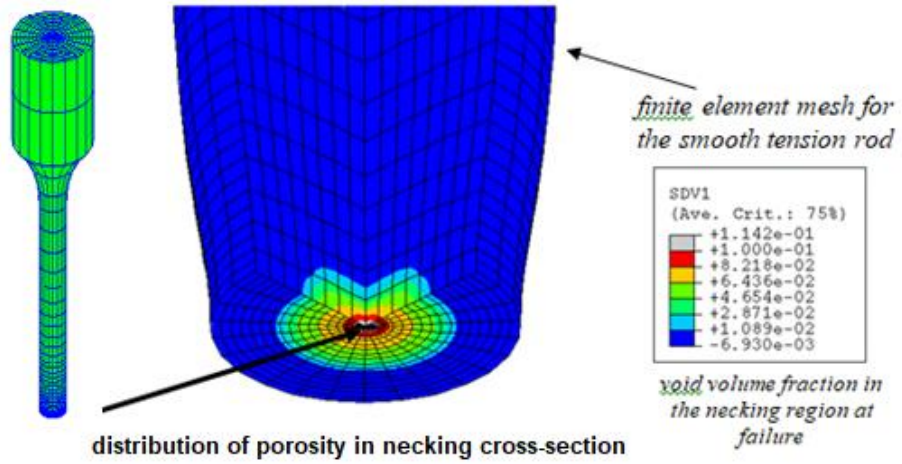

Fig.15.3: Tensile rod with porosity distribution in the 'Hot spot' center of the rod.). Finite element mesh of the rod. Void volume fraction f in the necking region at failure [Sun97, IWM 7] stresses in MPa, strains in %. Material *source, AA2219 variant, T2:* $\rho_{initial} = \infty$, *2 a = 4mm, Elasticity properties are E =70000MPa, ν = 0.3, t = 6 mm plate. Sample size n = 179, A5 = 7.4 %, Z = 20 %*

Due to the diffuse necking, an axial load increase-caused internal hydrostatic *tensile* stress state σ_{hyd} is generated, representing a deformation-dependent residual stress state. Its radial distribution can be Mises-based estimated - under the axial loading $\{\sigma\} = (\sigma_I, \sigma_{II}, \sigma_{III})^T = (F/A, 0, 0)^T$ - after Bridgman by $\sigma_{hyd}(r) \approx \sigma_I \cdot ln\left(1 + \frac{a^2 - r^2}{2 \cdot a \cdot \rho}\right)$ with $\sigma_I < \frac{F}{A} = \frac{F}{\pi \cdot a^2}$, *Fig.15-2*

with *F*:= load, *a*:= radius of actual cross section of neck, ρ := radius of neck curvature and F/A an integral quantity capturing the external loading *F* . The full set of relevant relations then reads:

$\sigma_{ax}^{t}(r) = \sigma_I + \sigma_{hyd}(r)$ and $\sigma_{radial}(r) \approx \sigma_{hoop}(r) = \sigma_{hyd}(r)$ and as equivalent stress follows

for a single stress $\rightarrow \sigma_{eq}^{Mises} = \sqrt{3 \cdot J_2} = \sqrt{\frac{1}{2}} \cdot \sqrt{\left[(\sigma_I)^2 + (0)^2 + (-\sigma_I)^2\right]} = \sigma_I$ and also

for a superimposed $\sigma_{hyd} \rightarrow \sigma_{eq}^{Mises} = \sqrt{3 \cdot J_2} = \sqrt{\frac{1}{2}} \cdot \sqrt{\left[(\sigma_I - \sigma_{hyd})^2 + (\sigma_{hyd} - \sigma_{hyd})^2 + (\sigma_{hyd} - \sigma_I)^2\right]} = \sigma_I$

$I_1 = max\,\sigma_{ax}^{t} + max\,\sigma_{radial} + max\,\sigma_{hoop} = \sqrt{3 \cdot J_2} + 3 \cdot \sigma_{hyd}$, $\sqrt{3 \cdot J_2} = \sigma_I$ ($\leftarrow$ no σ_{hyd} effect).

$TrF(r) = true\sigma_{mean} / true\sigma_{eq}^{Mises} = (I_1 / 3) / \sqrt{3J_2} = \left[\sqrt{2} / 3\right] \cdot (I_1 / \sqrt{3}) / \sqrt{2J_2} = \frac{1}{3} + \frac{\sigma_{hyd}}{\sigma_I}$.

Decisive for failure in the rod is the still mentioned Triaxiality Factor *TrF*, which increases with the true axial loading. Its maximum is in the center, the 'hot spot' at $r = 0$. In this micro-damage critical cup-cone center the 3D-state of stresses reads

$$max\sigma_{hyd}\ (r=0) = \sigma_I \cdot ln\ (1+\frac{a}{2\cdot\rho}),\quad max\sigma_{ax}^{t}(r=0) = \sigma_I + max\sigma_{hyd}$$

with the stress state in the rod's center $\{\sigma\} = (\sigma_I + max\sigma_{hyd}, \max\sigma_{hyd}, \max\sigma_{hyd})^T$.

In the necessary adjusting process of the F/A-curve in the diffuse necking regime (Phase 3) the first step is to integrate the axial stress, which varies over the radius. From load balance the following relations are yielded in *Table 15-1*.

The last unknown is the neck radius ρ. It could be computed during testing by measuring the shape change of the neck via a real-time Digital Image Correlation (DIC) 3D full-field measurement optical technique of the surface strains and an associated surface geometry model.

Table 15-1: Bridgman-Derivation of the cross-section quantities of the tensioned rod

$$\frac{F}{A} = 2\cdot\int_0^a \sigma_{ax}^{t}\cdot\pi\cdot r\cdot dr\ /\ (\pi\cdot a^2)$$

$$= 2\cdot\int_0^a (\sigma_I + \sigma_I(r))\cdot\pi\cdot r\cdot dr\ /\ (\pi\cdot a^2)$$

$$= 2\cdot\int_0^a (\sigma_I + \sigma_I\cdot\ln(1+\frac{a^2-r^2}{2\cdot a\cdot\rho}))\cdot\frac{\pi\cdot r\cdot dr}{\pi\cdot a^2}$$

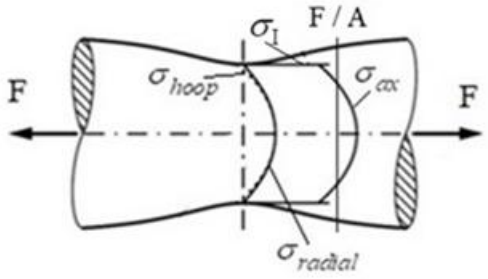

integrated follows $\frac{F}{A} = \sigma_I\cdot(1+\frac{2\rho}{a})\cdot\ln(1+\frac{a}{2\rho})$ with $\sigma_{eq}^{Mises} = \sqrt{3\cdot J_2} = \sigma_I$

$$\sigma_I = \sqrt{3\cdot J_2} = \sigma_{eq}^{MisBri} = \frac{F}{A}\ /\ (1+2\cdot\rho/a)\cdot\ln(1+a/2\cdot\rho),\quad \text{valid} > \bar{R}^t \text{ or } A < A_{oon},$$

an equation, in which the ratio a/ρ is not known.

If no test result is available, then Lorrek-Hill's approach for rupture is applied at $\bar{R}_{rodc}$:

$$\text{maximum}\ \frac{a}{\rho} = \sqrt{\ln(\frac{A_0}{A_{rupt}}) - \ln(\frac{A_0}{A_{oon}})}\quad ,\ \frac{A_{rupt}}{A_0} = 1 - Z \quad \text{with a}$$

given cross section reduction Z in % at maximum necking at $\bar{R}_{rupt}$

and A_{oon} the cross section at $\bar{R}^t \equiv \bar{R}_m^t$, being 'Onset-of-(diffuse) necking'.

$$\frac{a}{\rho} = c_1 + c_2 + \text{true}\varepsilon_{ax}R_{odc}^{\ 2} + c_3\cdot\text{true}\varepsilon_{ax}R_{odc}^{\ 3}.$$

Equivalent strain: $\text{true}\varepsilon_{ax} \rightarrow \text{true}\varepsilon_{eq}$

For the Mises equivalent strain is valid in the plastic domain (elastic part is negligible):

$$\varepsilon_{eq}^{Mises} = \frac{\sqrt{2}}{3}\cdot\sqrt{(\varepsilon_I-\varepsilon_{II})^2+(\varepsilon_{II}-\varepsilon_{III})^2+(\varepsilon_{III}-\varepsilon_I)^2} = \frac{\sqrt{2}}{3}\cdot\sqrt{(\varepsilon_I^{pl}-\varepsilon_{II}^{pl})^2+(\varepsilon_{II}^{pl}-\varepsilon_{III}^{pl})^2+(\varepsilon_{III}^{pl}-\varepsilon_I^{pl})^2}$$

considers plastic volume constancy (incompressibility) $\Sigma\varepsilon_i^{pl} = 0$ during plastic deformation it becomes

$$\varepsilon_I^{pl}/2 = -\varepsilon_{rad}^{pl} = -\varepsilon_{tan}^{pl} \text{ and } \varepsilon_{rad}^{pl} = ln(r/a) = \varepsilon_{tan}^{pl} \Rightarrow \varepsilon_I^{pl} = -2\cdot ln(r/a) \text{ and it reads}$$

$$\text{true}\varepsilon_{eq}^{Mises} = \frac{\sqrt{2}}{3}\cdot\sqrt{((\varepsilon_I^{pl}+\varepsilon_{rad}^{pl})-\varepsilon_{rad}^{pl})^2+0+(\varepsilon_{rad}^{pl}-(\varepsilon_I^{pl}+\varepsilon_{rad}^{pl}))^2} = \frac{\sqrt{2}}{3}\cdot\sqrt{2\varepsilon_I^{pl2}} = \frac{2}{3}\cdot\varepsilon_I^{pl}.$$

LL: ** Bridgman correction = approach, which considers the varying stress over the rod's cross-section regarding that the center is the critical line*

** Lorrek-Hill = approach, which formulates a final value for the change of the curvature radius under loading. The increasing curvature triggers the increasing hydrostatic stress and this is to map*

** Measured ratio F/A = stress capacity smeared over the cross-section = load ability-quantity, which represents an effective (smeared) value, which decays with increasing axial strain*

** $\sigma_1 \equiv \sqrt{3J_2}$ = constant basic stress quantity of the Bridgman approach, see Table 15-1*

** The applicability of axial measurement ends with 'End-of-uniform elongation' at $\bar{R}^t$*

** Bridgman model application is limited to about 30% cross-section reduction, due to not considering the coalescence of the voids*

** The Bridgman-correction is applied by using the 'Mises' yield function and not a 'Gurson'-type void growth-capturing (porosity f) yield function. This led the author 20 years ago to propose his so-called 'Extended Mises' yield condition at the end of a joint Research program MAN with IWF-Freiburg.*

Idea:

The replacement of a 'Mises'-based Bridgman correction by a porosity-considering one should lead to a more realistic stress-strain curve and should offer the advantage to escape in the analysis from the high number of non-measurable 'Gurson' model parameters except from *f*. In order to consider the void growth, the author proposes to replace the Bridgman-corrected Mises-model by the mentioned ***'Gurson' model-linked Extended Mises****-model*'.

15.3 Porosity-improved Bridgman 3D-Correction of true σ-ε-Curve employing 'Extended Mises'

Porosity means volume change due to void coalescence. Such a volume change can be transferred to a decaying Poisson's ratio as it is known from Beltrami. The author experienced, that the usual 'Gurson'-analyses base on a 'Mises'-linked equivalent stress-equivalent strain curve. This should be improved when considering the porosity *f*. The author's hypothesis from 2002 reads:

* Formulation of an egg-shaped yield model, termed Extended Mises, with
* Simplification to 1 measurable 'Gurson' parameter *f* , only
* Improvement of this simpler model idea by applying a porosity-capturing equivalent $\sigma - \varepsilon$ curve
* Taking a simple 'Gurson' yield model to obtain via a 'comparison of coefficients' a relation to the porosity *f* in the simple 'Gurson' -model from Gurson-Tvergaard-Needleman, index ^{GTN}
* Probable 120°-material symmetry in the high porosity regime is not documented and therefore not

considered. It can be captured by replacing $\frac{3J_2}{\bar{R}^2}$ through $\frac{3J_2}{\bar{R}^2}\cdot\Theta$ (see *Chapter 11*).

LL:
** The 'Mises' cylinder is a simplification* (remember: §11, 120°-symmetry, $\Theta = 1$)
** Increasing porosity also means decreasing Poisson's ratio ν and an increasing elliptic shape.*

From knowledge in *Chapter 13* is known: Values for the increasing porosity *f* are strain-controlled detectable. The effect of a probably initially not pore-free material is captured in the initial property values.

14.1 Measurement of rod failure stresses and estimation of the vertex of the failure body

Even for a porous plastic failure body its vertex should be known from theoretical reasons. A vertex represents the equi-triaxial tensile strength capacity of a load-controlled strength situation, remind *Fig.15-2*. Because the vertex stress state $\{\sigma\} = (\text{true}\bar{R}^{ttt}, \text{true}\bar{R}^{ttt}, \text{true}\bar{R}^{ttt})$ with $TrF = \infty$ practically cannot be measured as best substitute a 3D-stress state - closest possible to the vertex - must be employed. Realistic is a stress state $(\text{true}\sigma_{ax} + \sigma_{hyd}, \sigma_{hyd}, \sigma_{hyd})$ by investigating the center of an un-notched tension rod test specimen, being the 'hot spot' in this test specimen.
In such un-notched rods a neck radius builds up and increases with further increasing axial tensile stress. Due to the diameter reduction a hydrostatic stress state is generated and can be determined from the zero volume strain regime faced in the minimum neck cross-section. Hereby, difference due to rolling of the sheet material and how the test specimen is cut out are neglected and full isotropy assumed.
From the test rig loading comes the subsequently effective stress 'true σ_{ax}', whereas the remaining neck cross-section experiences in the center the multi-axial stress state $(\text{true}\sigma_{ax} + \sigma_{hyd}, \sigma_{hyd}, \sigma_{hyd})$, estimated by the Bridgman model. In order to better understand the stress situation in the rod center the effect of increasing σ_{hyd} is of interest, depicted below. It is to conclude from mechanics, that a hydrostatic stress does not change Mises's representative invariant J_2 for shape deformation of the solid. However, σ_{hyd} affects the tri-axiality value *TrF* which might be interpreted to cause some quasi-embrittlement of the material:

$$I_1 = (\sigma_I + \sigma_{II} + \sigma_{III}) = f(\sigma)\ ,\quad 6J_2 = (\sigma_I - \sigma_{II})^2 + (\sigma_{II} - \sigma_{III})^2 + (\sigma_{III} - \sigma_I)^2 = f(\tau)$$

$$(\text{true}\sigma_{ax} + \sigma_{hyd},\ \sigma_{hyd},\ \sigma_{hyd})\ ,\quad \sigma_{ax}^{t}(r) = \sigma_1 + \sigma_{hyd}\ (r)$$

$$\sigma_{eq}^{Mises} = \sqrt{3J_2} = \sqrt{3}\cdot\sqrt{(\sigma_1^{M.} - \sigma_{h.} - \sigma_{h.})^2 + 0 + (\sigma_{h.} - \sigma_1^{M.} - \sigma_{h.})^2} \quad\rightarrow\quad \sigma_{eq}^{Mises} = \sigma_1^{Mises}$$

$$TrF = \sigma_{mean} / \sigma_{eq}^{Mises} = (I_1 / 3) / \sqrt{3J_2} = \left[\sqrt{2} / 3\right]\cdot(I_1 / \sqrt{3}) / \sqrt{2J_2}$$

$$I_1 = (\text{true}\sigma_{ax} + 3\sigma_{hyd}) = f(\sigma)\ ,\quad 6J_2 = (\sigma_I - \sigma_{II})^2 + (0)^2 + (\sigma_{III} - \sigma_I)^2 = f(\tau)$$

uni-axial σ_{ax}, multi-axial $(\sigma_{ax} + \sigma_{hyd}, \sigma_{hyd}, \sigma_{hyd})$ in the rod's minimum neck section $\Rightarrow \sigma_{eq}^{Mises}$.

Again: The use of notched rods is principally also possible but considering that the original notch radius ρ increases. Thereby the critical rod surface stress concentration reduces a little and the originally surface-located critical material location moves to the center. *Fig.15-9(left)* shall display different stress

states and the associated points on the respective *TrF*-beams. In the subpicture down left the indicated 2D stress-states and up left further the 3D stress states all collected in the table right down.
Of interest for the designing engineer is that the spatially formulated SFC $F^{NF} = 1$ dents the failure body at the pressure vesessel situation $\{\sigma\} = (2,1,0) \rightarrow TrF = \sqrt{2}/3$, *Fig.15-2* and *15-9*. Remember: In the 2D principal stress plane F^{NF} is a straight line and in the 3D failure body a hyperbolic curve!
Fig.15-9 (right) shall make the non-linear development of *TrF* more clear and further make familiar with the design failure surfaces in the very ductile regime. The figure schematically shows that the strain-controlled failure surface is outside and thereby larger than the load-controlled one.

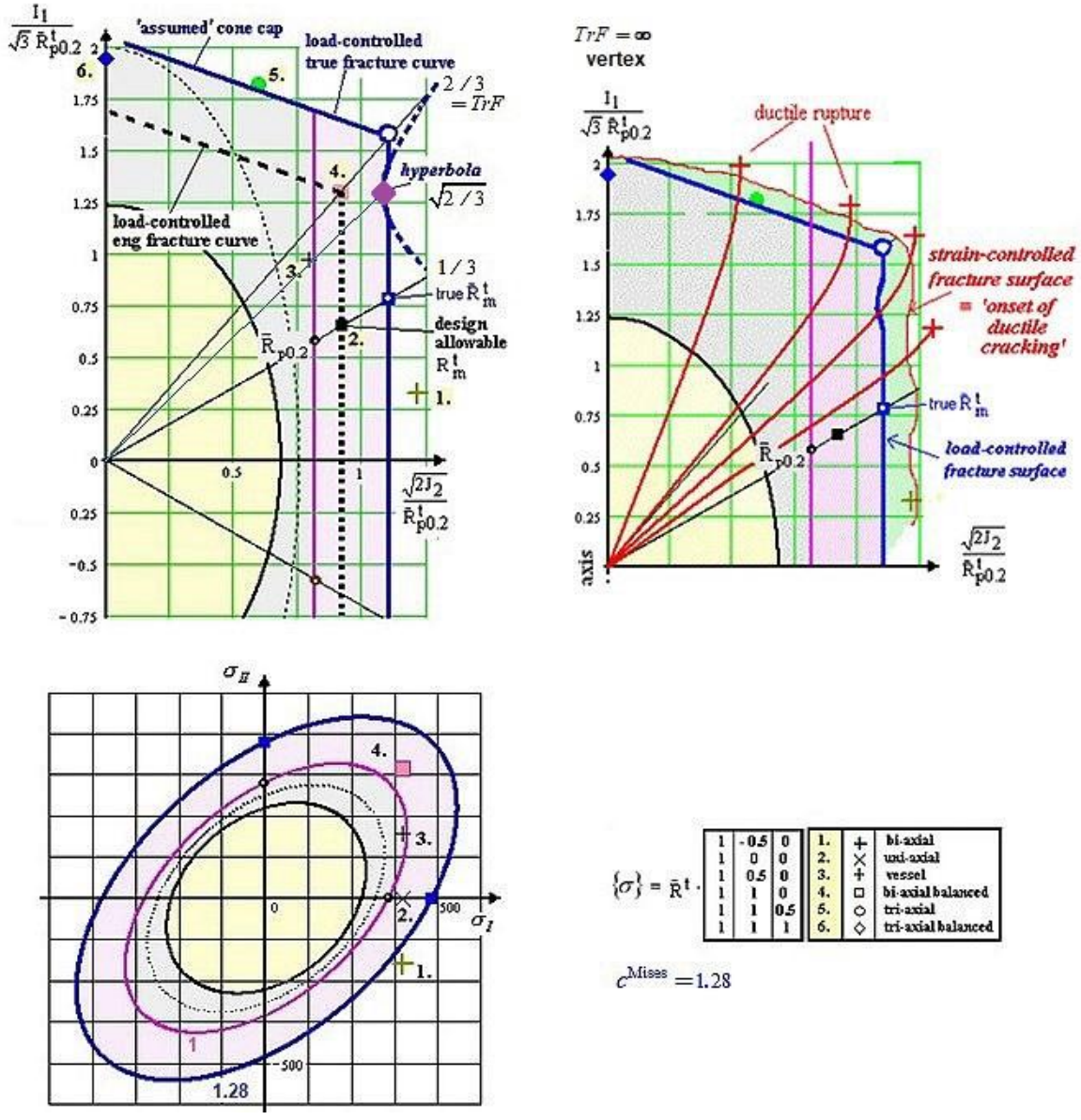

Fig. 15-9: Visualization of the effect of the TrF-beams and the related strengths, illustration of some stress state points and failure zones. 2D-potential surfaces on the inclined cross-section of the rot.-symmetric failure body

15.4 Proposal of the Two Parameter 'Extended Mises' Yield function in the porosity domain

Extended Mises yield potential function

Originally, Gurson proposed for a metal, containing well distributed voids, a yield condition-based solution for a single spherical void. The model was modified later by Tvergaard and Needleman,

including the porosity *f* and the increasing Flow stress σ_F of the 'matrix' material: The porous body, called bulk material (*smeared material*), consists of the matrix material and the voids or pores. The voids are nucleated in tension, only. The dense matrix phase follows the HMH ('Mises') model, and *f* represents the mean void volume fraction or porosity (*average value of a porous matrix*) as the so-called internal damage variable. For $f = 0$, fully dense material, the model reduces to that of von Mises, whereas a ultimate value f_{ult} implies that the material is ultimately voided that it has lost its stress carrying capacity due to local ductile rupture. Here, f_{ult} shall be replaced by the smaller $f_{odc} = f_{crit}$. Values for the increasing porosity *f* are strain-controlled detectable and therefore, the ratio is fixed. <u>*Table 15-2*</u> describes the procedure how a relationship

Table 15-2: 'Comparison of Coefficients' of the models 'Gurson' ↔ 'Extended Mises' with σ_F as increasing true Flow stress as running stress variable

$F^{GTN} = \frac{3J_2}{\sigma_F^2} + 2 \cdot f \cdot q_1 \cdot cosh(\frac{I_1 \cdot q_2}{2 \cdot \sigma_F}) + q_3 \cdot f^2 = 1$ ductile micro-damage failure function

simplified to $\frac{3J_2}{\sigma_F^2} + 2 \cdot f \cdot cosh(\frac{I_1 \cdot q_2}{2 \cdot \sigma_F}) + f^2 = 1$ appropriate for idea demonstration, $q_3 = q_3 = 1$

If the cosh-function is replaced by the first two terms of the associated Taylor row [*Cun*98,*Cun*01]

$cosh\, x = \pm (1 + x^2 / 2 + ...) \rightarrow \cosh(I_1 \cdot q_2 / 2 \cdot \sigma_F) = \pm (1 + (I_1^2 \cdot q_2^2 / 8 \cdot \sigma_F^2) + ..)$.

The negative sign is to chose because porosity reduces strength capacity

$$\frac{3J_2}{\sigma_F^2} - 2 \cdot f \cdot (1 + \frac{I_1^2 \cdot q_2^2}{8 \cdot \sigma_F^2}) + f^2 = 1 \quad \Rightarrow \frac{3J_2}{\sigma_F^2} - 1 \cdot f \cdot (\frac{I_1^2 \cdot q_2^2}{4 \cdot \sigma_F^2}) + 2f - f^2 = 1.$$

With $f^2 << f$ can be derived

$\frac{3J_2}{\sigma_F^2} - f \cdot \frac{q_2^2}{4} \cdot \frac{I_1^2}{\sigma_F^2} - 2f = 1$ with $q_2 = 1.5$ as guess for the plastic damage flow function

$\frac{3J_2}{\sigma_F^2} - f^* \cdot \frac{I_1^2}{\sigma_F^2} - 2f = 1$ with the elliptic shape parameter f^*

$$\kappa = \frac{1-2\nu}{2+2\nu} \equiv f \cdot \frac{q_2^2}{4} = f^* \quad \rightarrow \quad \nu = (4 - f^*) / (8 + 2f^*).$$

$\Rightarrow$ Failure state, normalized again with the shear strength, to insert is $\sigma = \bar{R}_{odc}$

$F = \frac{3J_2}{\bar{R}_{0.2}^2} + f_{ult}^* \cdot \frac{I_1^2}{\bar{R}_{0.2}^2} + 2 f_{ult} = 1 = Eff = 100\%$ material stressing effort,

$F = 100\%$ = potential surface, which may be a fracture surface or a yield surface.

From 'Comparison of Coefficients' finally is obtained

ExtendedMises $F = \frac{3J_2}{\bar{R}_{0.2}^2} + c_{12} \cdot \frac{I_1^2}{\bar{R}_{0.2}^2} = c^{ExtMis}$, generally

Analogous to 'Mises' $Eff^{Mises} = \sigma_{eq}^{Mises} / \bar{R}_{0.2} = \sqrt{3J_2} / \bar{R}_{0.2} \Rightarrow Eff^{ExtMises} = \sigma_{eq}^{ExtMises} / \bar{R}_{0.2}$

follows $\sigma_{eq}^{ExtMises} = \sqrt{\frac{3J_2 - f^* \cdot I_1^2}{1 + 2f}}$.

between the subsequent 'Gurson' type yield model and the 'Extended Mises' model was developed. A further equation is needed to determine the size parameter, such as with c^{Mises} of the 'Mises cylinder'.

Void Porosity-linked reduction of Poisson's ratio $0.5 > \nu$

Porosity means volume change due to void coalescence and volume change may be transferred to a decaying Poisson's ratio, remind Beltrami. From the ExtM-model can be geometrically deduced $f^* = f \cdot q_2^2$ and $\nu = (4 - f^*) / (8 + 2 \cdot f^*)$.

Fig. 15-10 points out how the Poisson ratio is linked to the true strains (left), schematically to the true equivalent stress (center), and to the porosity f^*.

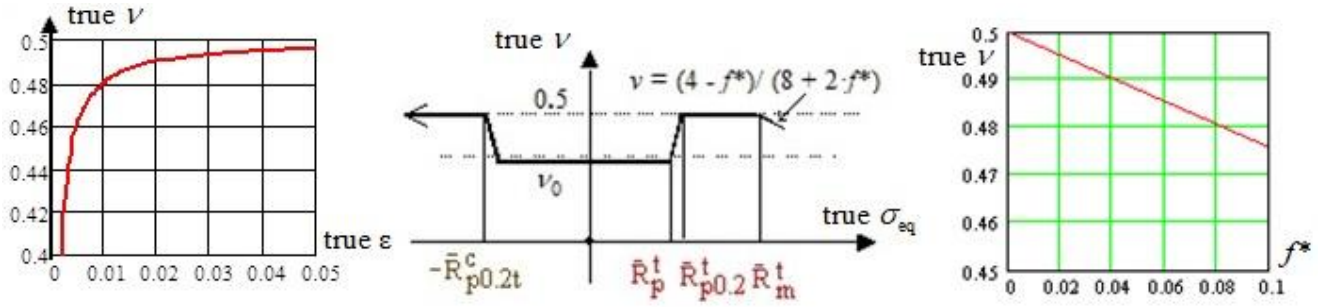

Fig. 15-10: Dependence of ν on the different parameters, the various regimes

Here, $f_{ult}\,(\bar{R}_{odc}) < f_{rup}$ is employed as that critical porosity which was dedicated by the author to 'Onset of ductile cracking', in order to 'remain on the safe side'. The evolution function of f is assumed to follow an exponential course with practically $f = 0$ at the tensile strength point up to the defined ultimate value f_{ult} located at $\bar{R}_{odc}$.

15.3 Visualization of a specific 'Gurson'-model versus 'Extended Mises'-model

Failure conditions enable the designer to assess multi-axial states of stress $\{\sigma\}$ by an equivalent stress σ_{eq} and to map multi-axial stress-strain behavior $\sigma_{eq}(\varepsilon_{eq})$ via a measured, smeared stress *F/A*.

For $f = 0$, fully dense material, the model reduces to that of HMH, whereas a maximum value f_{ult} implies that the material is ultimately voided that it loses its stress carrying capacity due to local ductile rupture.

The conventional visualization – as a parameter investigation - of the Gurson model is presented in *Fig.15-11 (left)* with f being the porosity parameter of the curves and q2 a Gurson parameter from the comparison. A growing f means higher true stress but less cross-section or load-carrying material in the strain-controlled 'hot spot'. This is displayed in the figure by the change of the cylinder shape versus an egg shape.

Another visualization, usually practiced in structural mechanics, is given by using the Lode-Haigh-Westergaard parameters. This leads to a change in the shape, *Fig.15-11 (center)*. For $f = 0$ the Mises cylinder is obtained.

Fig.15-11 (right) depicts the various strength values such as $true\bar{R}^t, \bar{R}_{odc}$ as increasing true strength points to be inserted into the Extended Mises function size parameter, finally visualized as flow potential surfaces for four strength-linked porosity levels.

The parameter comparison with 'Gurson' let to take a reduced value $q_2 = 1.13$, however, due to missing test data the author sticks to 1.5. In this context, the respective Extended Mises parameter c_{12} can be determined, decoupled from the 'Gurson' Comparison of Coefficients, if having a reliable test data set available

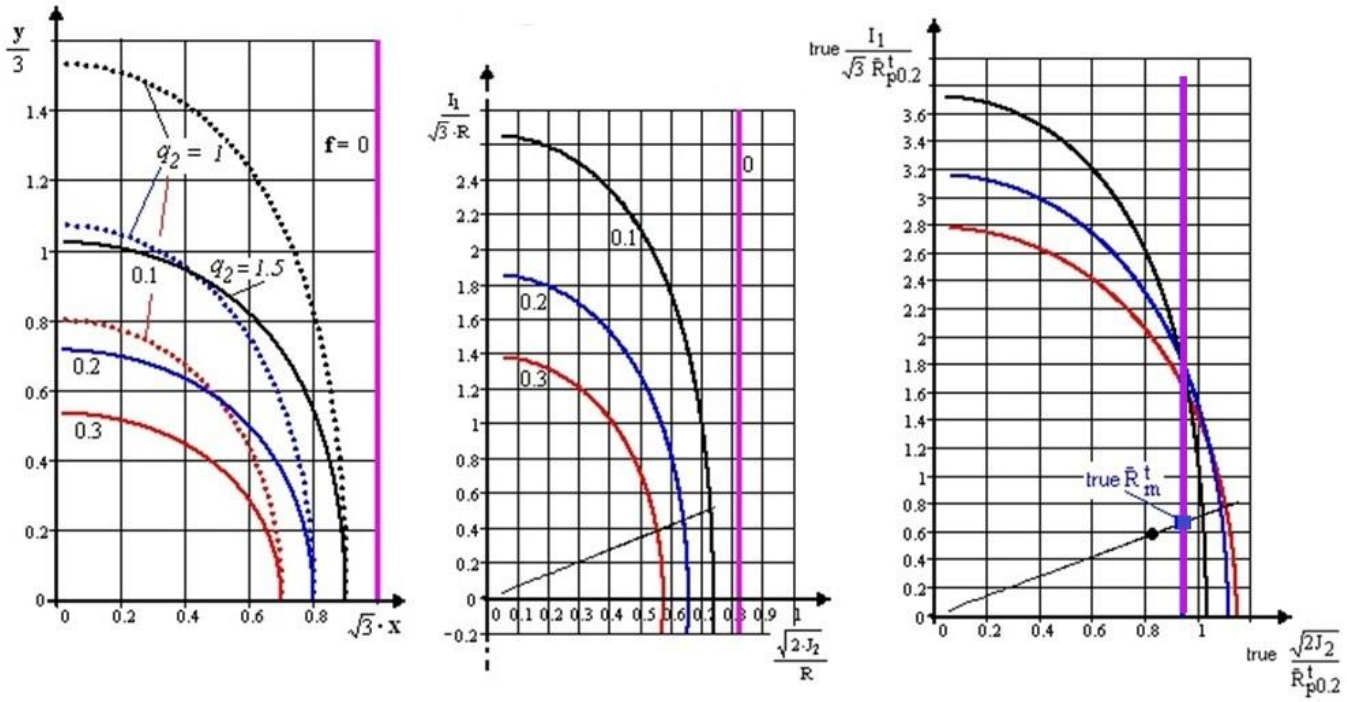

Fig. 15-11: Schematic comparison of the Gurson model (dots) and Extended Mises model Potential surfaces. (left) Display of curve parameter porosity f influence, using the 'Gurson' coordinates $x = (\sqrt{J_2}/\sigma_F)$, $y = (I_1/\sigma_F)$, $\sigma_F = \bar{R}^t_{p0.2}$; *(center) Display of the Gurson yield model in Lode-Haigh-Westergaard parameters* $\bar{R}^t_{p0.2}$ = *normalisation strength); (right) Ppotential surfaces of the ExtMises-model with four increasing true (graphs made about 2001) AA2219, (q2=1.5,* $q2_{ExrM}$*=1.13)* $true\bar{R}^t$, $\bar{R}_{odc}$.

Table 15-3: Replacement of the Mises-based Bridgman curve $\sigma_{eq}(\varepsilon_{eq})$ *by an ExtMises one*

Table 25 - 1: $\sigma^t_{ax}(r) = \sigma_I + \sigma_{hyd}(r)$ and from Bridgman $\sigma_{hyd} \approx \sigma_I \cdot \boldsymbol{ln}\left(1 + \frac{a^2 - r^2}{2 \cdot a\rho}\right)$

$\sigma^{MisBri}_{eq} = \sqrt{3 \cdot J_2} = \sigma_I = \frac{F}{A} / (1 + 2 \cdot \rho / a) \cdot \ln(1 + 0.5 \cdot a / \rho)$, valid > $\bar{R}^t$ < ?,

$I_1 = \sigma_I + 3\sigma_{hyd} = \sigma_I \cdot \left(1 + 3 \cdot \boldsymbol{ln}\left(1 + 0.5 \cdot a / \rho\right)\right)$ for the critical central 'fiber' at r = 0

considering Bridgman (above) and the notch-curvature change by Lorrek-Hill's approach,

giving a maximum value for the unknown → $\max \frac{a}{\rho} = \sqrt{\ln\left(\frac{1}{1 - Z}\right) - \ln\left(\frac{A_0}{A_{oon}}\right)}$,

inserting $\sqrt{3 \cdot J_2} = \sigma_I$ and $\frac{F}{A} = true\sigma_{ax}$ the equivalent stress reads:

$$\sigma^{ExtMises}_{eq} = \sqrt{\frac{3J_2 - f^* \cdot I_1^{\,2}}{1 + 2f}} = \sigma_I \sqrt{\frac{1 - f^* \cdot \left(1 + 3 \cdot \boldsymbol{ln}\left(1 + 0.5 \cdot a / \rho\right)\right)^2}{1 + 2f}}$$

valid $\bar{R}^t < \bar{R}_{odc}$, (shape parameter) $f \cdot \frac{q_2^2}{4} \equiv f^*$, set $q_2 \cong 1.5 \rightarrow 1.13$.

Porosity parameter f and curvature parameter a/ρ increase from about 0 to the maximum at $\bar{R}_{odc}$.

The author's full idea consisted of the two parts: Above ExtMises model plus porosity-improved Bridgman evaluation, which was depicted in *Table 15-3*. The table displays all relations in order to establish the 'searched' equivalent stress $\sigma^{ExtMises}_{eq}$.

Reminder: To capture '120°-rotational symmetry' would require to replace J_2 by $J_2 \cdot \Theta$.

15.3 Visualization of the Bridgman–corrected true curve with consideration of porosity

In order to obtain a realistic equivalent stress curve it is physically mandatory to consider the increase of porosity *f* and the increase of the notch curvature by applying $a\ /\ \rho$. The mapping of the changing notch curvature and the changing porosity is shown below:

Mapping of the changing notch curvature: Data and determination procedure by Mathcad

$$\frac{a}{\rho} = \sqrt{\ln\left(\frac{A_0}{A_{rupt}}\right) - \ln\left(\frac{A_0}{A_{oon}}\right)} = 1.096 \quad \text{from} \quad \frac{A_{rupt}}{A_0} = 1 - Z = 1 - 0.20 = 0.80,$$

$$\frac{A_0}{A_{rupt}} = \frac{1}{0.80} = 1.25, \quad \frac{A_0}{A_{oon}} = \left(\frac{4.0}{3.89}\right)^2 = 1.057 \rightarrow \max\frac{a}{\rho} = 0.409 \ \text{at} \ R_{rup}.$$

Applying Lorrek-Hill's value Bridgman's approach delivers $\max\left(1+\frac{2\rho}{a}\right)\cdot\ln\left(1+\frac{a}{2\rho}\right) = 1.096.$

Then, for the previously proposed formulation the curve parameters can be computed:

$$\text{stressing} \qquad \frac{a}{\rho} = a\rho = c_1 + c_2 + \text{true}\varepsilon_{ax}R_{odc}{}^2 + c_3 \cdot \text{true}\varepsilon_{ax}R_{odc}{}^3.$$

$a\rho = 1.096$ $\text{true}\varepsilon\text{axR02} = 0.0071$ $\text{true}\varepsilon\text{axRt} = 0.055$ $\text{true}\varepsilon\text{axRodc} = 0.231$

Vorgabe $c1 := 1$ $c2 := 100$ $c3 := 1$

$1 = c1 + c2 \cdot \text{true}\varepsilon\text{axR02}^2 + c3 \cdot \text{true}\varepsilon\text{axR02}^3$

$1.00005 = c1 + c2 \cdot \text{true}\varepsilon\text{axRt}^2 + c3 \cdot \text{true}\varepsilon\text{axRt}^3$

$a\rho = c1 + c2 \cdot \text{true}\varepsilon\text{axRodc}^2 + c3 \cdot \text{true}\varepsilon\text{axRodc}^3$

$A\rho := \text{Suchen}(c1, c2, c3)$

$$A\rho = \begin{pmatrix} 1 \\ -0.548 \\ 10.148 \end{pmatrix}$$

$c1 := A\rho_0$ $c1 = 1$ $c2 := A\rho_1$ $c2 = -0.5476$ $c3 := A\rho_2$ $c3 = 10.1478$

$A\rho_j := c1 + c2 \cdot \left(\text{true}\varepsilon\text{ax}_j\right)^2 + c3 \cdot \left(\text{true}\varepsilon\text{ax}_j\right)^3$

Mapping of the changing porosity *f*: Data set used and determination by Mathcad

The set points of the curve are the porosity values at the tensile strength point R^t and at R_{odc}.

Vorgabe $e1 := 0$ $e2 := 1$

$$0.0002 = \left(e1 \cdot \exp\left(\frac{\text{true}\varepsilon\text{axRt}}{\text{true}\varepsilon\text{axRodc}} - 1\right)\right)^{e2} \qquad fodc = (e1 \cdot \exp(1-1))^{e2}$$

$Af := \text{Suchen}(e1, e2)$

$$Af = \begin{pmatrix} 0.6292 \\ 6.9469 \end{pmatrix}$$

$e1 := Af_0$ $e1 = 0.6292$ $e2 := Af_1$ $e2 = 6.947$

$$fexp_j := \left(e1 \cdot \exp\left(\frac{\text{true}\varepsilon\text{ax}_j}{\text{true}\varepsilon\text{axRodc}} - 1\right)\right)^{e2}$$

Fig.15-12 displays the author's design verification idea, about 2000. The influence of the practically starts at R_{odc}.

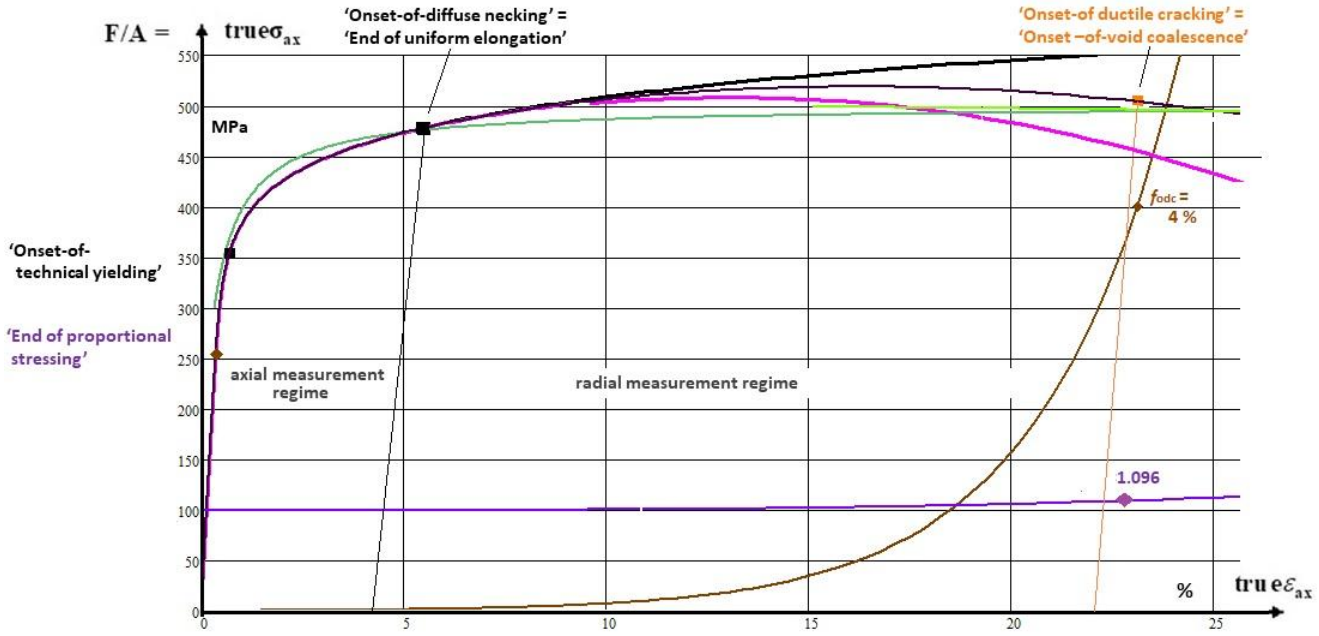

Fig. 15-12, AA2219, base material T2, 6 mm thick: Visualization of the equivalent stress curve $\sigma_{eq}^{ExtMises}$ *; Ramberg-Osgood-mapped measured cross-section smeared axial stress F/A; Increase of plastic porosity f with* f_{odc} *= 4% at* R_{odc} *; Increase of the notch curvature* a / ρ *with* $a / \rho = 0.409$ *at* R_{ult} (replacing the higher R_{odc}); *Increase of ν in the elastic-plastic transition domain approaching 0.5 and barely visible the decrease in the porous domain*

15.4 Specific Potential Surfaces being Strength Failure Criteria

Brittle 'porous' materials may still fracture in the elastic-plastic transition domain. For this fact, Ismar and Mahrenholtz [*Ism82*] developed a Beltrami-based SFC model describing the failure behavior of a material between the proportional limit and the 'onset of yielding'. In *Table 15-4* the SFC-formulations in all regimes shall be comparatively displayed. This includes potential surface descriptions and associate strength failure criteria SFCs.

LL:

- ✓ *Whereas with the elasticity formulation of Beltrami the Poisson ratio ν is growing this is opposite with the formulation of a porosity-linked plastic model due to the increasing porosity*
- ✓ *The hypotheses of Beltrami, Mises, Gurson describe an increase or decrease of surfaces of constant potential. The shape of the surface theoretically begins with* $\nu = 0$ *(sphere, found with foams) growing up from* $0 < \nu$ *to* $\nu = 0.5$ *via the growing Mises cylinder keeping* $\nu = 0.5$ *and ending with an ellipsoid, which shrinks into a spherical direction represented by 0.5 > ν.*
- ✓ *For two domain limits a clear value for the varying Poisson ratio is given:*

$$\text{proportional limit } \sigma \le \bar{R}^t_{prop} \Rightarrow \nu = \nu_0 \quad \text{and} \quad \text{yield limit } \sigma = \bar{R}^t_{p0.2} \Rightarrow \nu = 0.5$$

- ✓ *Designing requires to use limit state formulations, termed failure criteria (SFCs). These are fracture failure criteria for brittle materials namely for 'Onset-of-fracture' and yield failure criteria for ductile materials. In practice, for ductile materials these failures are 'Onset-of-yielding' and - for the author - 'Onset-of-void coagulation = Onset of ductile Cracking ' in the case where strain-softening applies*
- ✓ *A Strength Failure Criterion represents a defined Design Limit State and is therefore a special*
- ✓ *critical Potential Surface F.*

** *The novel Extended Mises model just requires the determination of one more parameter, the porosity value f . All model parameters are measurable quantities.*

** *With the novel porosity-capturing σ-ε curve, being a ductile porosity-improved Bridgman correction, a simplified plastic analysis procedure could be achieved.*

** *For engineering reasons* $true\bar{R}^t \Rightarrow \bar{R}_{odc}$ *will represent the load carrying capacity to be considered.*

Table 15-4, Isotropic materials: Determination of model parameters, single mode view.

* Modelling Functions F describing a subsequent potential surface

elastic-plastic	plastic	plastic porous
Beltrami	Hencky-'Mises'-Huber	'Gurson' type

$$\bar{R}^t_{prop} < \sigma_{\mathrm{Bel}} < \bar{R}^t_{0.2} \quad \leftrightarrow \quad \bar{R}^t_{0.2} < \sigma_{\mathrm{Mis}} < \bar{R}^t_{m} \quad \leftrightarrow \quad \bar{R}^t_{m} < \sigma_{eq} < \bar{R}^t_{\mathrm{odc}}$$

stress - controlled *strain – controlled*

σ : = running variable of the subsequent potential surfaces

$$\bar{R}^{t\,2}_{prop} / \bar{R}^{t\,2}_{0.2} < c^{\mathrm{Bel}} < 1 \quad \leftrightarrow \quad 1 < c^{\mathrm{Mis}} < \bar{R}^{t\,2}_{m} / \bar{R}^{t\,2}_{0.2}$$

ellipsoid → cylinder → ellipsoid

$$I_1 = (\sigma_I + \sigma_{II} + \sigma_{III}) = \mathrm{f}(\sigma), \quad 6J_2 = (\sigma_I - \sigma_{II})^2 + (\sigma_{II} - \sigma_{III})^2 + (\sigma_{III} - \sigma_I)^2 = \mathrm{f}(\tau)$$

$$\frac{3J_2}{\bar{R}^{t\,2}_{0.2}} + \kappa \cdot \frac{I_1^{\,2}}{\bar{R}^{t\,2}_{0.2}} = c^{\mathrm{Bel}} \leftrightarrow \quad F^{Mis} = \frac{3J_2}{\bar{R}^{t\,2}_{0.2}} = c^{\mathrm{Mis}}, \; \kappa = \frac{1-2\nu}{2+2\nu}$$

Insertion of a (measurable) normalizing strength, yield strength point with $\nu = 0.5 \rightarrow \kappa = 0$

$$\mathrm{F}^{Bel} = \frac{3\bar{R}^{t\,2}_{02} / 3}{\bar{R}^{t\,2}_{02}} + \kappa \cdot \frac{\bar{R}^{t\,2}_{02}}{\bar{R}^{t\,2}_{02}} = c^{\mathrm{Bel}} * \rightarrow c^{\mathrm{Bel}} = 1 + \kappa = 1, \text{ and } \kappa \text{ an elliptic shape parameter}$$

* Strength FailureCriteria (SFC), $\bar{R} \rightarrow R$, (with $\Theta = 1$ for full rotational symmetry)

R : = strength design allowable, marking a special potential surface ≡ design limit state

elastic, very brittle	ductile	very ductile

$$Eff = \frac{\sigma_1}{\bar{R}^t_{\mathrm{m}}} = 1 \; * \quad \leftrightarrow \quad Eff = \frac{3J_2}{\bar{R}^{t\,2}_{m}} = 1 \quad \leftrightarrow \quad Eff = \frac{3J_2}{\bar{R}^{\,2}_{\mathrm{odc}}} + c_{12} \cdot \frac{I_1^{\,2}}{\bar{R}^{\,2}_{\mathrm{odc}}} - 2\, f_{odc} = 100\%.$$

For similarity reasons: for the 2 modes Normal Fracture NF , Shear Fracture SF (brittle)

and after inserting $\sigma = R \cdot Eff$ and dissolving for Eff follows

$$\mathrm{I}_1 > 0 : F^{NF} = 0.5 \cdot \frac{\sqrt{4J_2 - I_1^{\,2} / 3} + I_1}{2 \cdot \bar{R}^t} = 1 \; ; \; Eff^{NF} = 0.5 \cdot \frac{\sqrt{4J_2 - I_1^{\,2} / 3} + I_1}{2 \cdot \bar{R}^t}$$

$$\mathrm{I}_1 < 0 : F^{SF} = c_1^{SF} \cdot \frac{3J_2}{\bar{R}^{c\,2}} + c_2^{SF} \cdot \frac{I_1}{\bar{R}^c} = 1; \; Eff^{SF} = \frac{c_2^{SF} \cdot I_1 + \sqrt{(c_2^{SF} \cdot I_1)^2 + 12 \cdot c_1^{SF} \cdot 3J_2}}{2 \cdot \bar{R}^c} = \frac{\sigma^{SF}_{eq}}{\bar{R}^c}$$

$c_1^{SF} = 1 + c_2^{SF}$ with direct consideration of the Poisson ratio $c_2^{SF} = (1 + 3 \cdot \mu) / (1 - 3 \cdot \mu)$

Last unknown to be searched is the elliptic shape linked parameters such as c_1^{SF} by insertation of a bi-axially compressive failure stress or a fracture angle $\mu = \cos(2 \cdot \theta^c_{fp}\,° \cdot \pi / 180)$.

Note on Non-linear stress–strain analysis:

Usually Co-axiality, Prandtl-Reuss equations and an Associated Flow Rule is employed in order to predict strain rate $\dot{\varepsilon}_{ij}$ and the Lagrange multiplication (*proportionality*) factor $\dot{\lambda}$.

Research proposal experience in the context above:

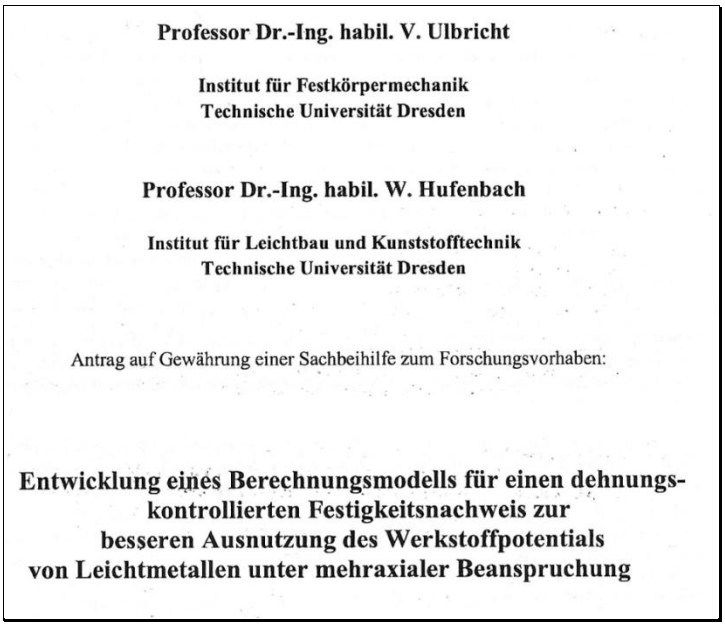

Professor Dr.-Ing. habil. V. Ulbricht

Institut für Festkörpermechanik
Technische Universität Dresden

Professor Dr.-Ing. habil. W. Hufenbach

Institut für Leichtbau und Kunststofftechnik
Technische Universität Dresden

Antrag auf Gewährung einer Sachbeihilfe zum Forschungsvorhaben:

Entwicklung eines Berechnungsmodells für einen dehnungs-kontrollierten Festigkeitsnachweis zur besseren Ausnutzung des Werkstoffpotentials von Leichtmetallen unter mehraxialer Beanspruchung

"Development of a calculation model 'Strain-controlled strength design verification' for a better utilization of the material potential of light metals under multiaxial loading".

(MAN-driven idea for a DFG project to create a verification procedure for critical boreholes of the Ariane 5 upper stage tanks concerning the design of rocket tanks, submitted by my friends Volker and Werner)

In the case of strength verification of components made of ductile metals, design verification must be provided both with regard to 'Onset-of-yielding' and with regard to the ductile fracture (rupture) behaviour. For the latter process, a distinction must be made between the load-controlled fall and the strain-controlled case. In the case of ductile material behavior 'Onset-of-yielding' is usually decisive for the dimensioning, but in many applications fracture design verification is also required. Essential for the detection of fracture are the true stresses and distortions which can be determined for the component to be detected by means of nonlinear numerical calculation methods.

For the evaluation of these true stresses, however, the corresponding true strengths may not be used in the currently valid verification procedure, even in the load-controlled case. In the strain-controlled case, there is still no accepted verification philosophy in the current regulations. These deficits are mainly due to the insufficient knowledge of the material-mechanical behavior in the range of high strains and the lack of suitable calculation models.

In the area of high tensile strains, the reduction in cross-section is determined by a uniform proportion and a constriction proportion from 'Onset-of-yielding' the beginning of the constriction of the test specimen.

While the stress-strain curve his is generally known at the beginning of necking, its further course can only be estimated, e.g. with the help of Bridgman's formula. Since the stress state in the test specimen becomes multiaxial above the constriction, a comparative stress-strain curve must be used for a realistic evaluation of the test results in order to be able to take into account the multiaxial stress state in the critical cross-section of the test body. See chapter 15 text before.

Previous simulation work shows that the curve can be suitably extended beyond the tensile strength value R_m, and that it falls off at the end due to pore growth with pores-agglomeration.

The computational approach to the problem has so far used a so-called 'Gurson model', which contains parameters that can be determined in simulation-manner and cannot be determined individually by test. In addition to the diameter parameter of the Mises model cylinder, now only one other measurable, porosity-related parameter will be determined in the project (see chapter). By the way 'Onset-of-yielding' of metals can be determined on the basis of the Jule-Thomson effect by temperature measurement for uniaxial and multiaxial states.

This research proposal was considered unworthy of funding by three DFG reviewers. The corresponding sparse response indicated that the proposal was not understood. I was ashamed of my DFG fellow reviewers and the poor DFG because I always gave a justification in my proposal reviews.

(*As a result, I ended my work as a sad permanent industry reviewer for the DFG).*

16 Note on Continuum (micro-)Damage Mechanics (CDM)

***Aim**: Primarily checking CDM application whether it is mature for a reliable Static Design Verification.*

CDM is applied for ductile and brittle materials. The loading may be static and cyclic, with the latter requiring fatigue investigation. Regarding stress-strain curves, CDM principally captures the load-controlled hardening part and the deformation-controlled softening part. Softening part examples are the still mentioned embedded UD layer (*Fig.16-1*) and the ductile metal tensile rod described in the last Chapter by a porosity–capturing 'Gurson' model. Results of isotropic analyses, employing the softening curve branch, can be used to better design notches, openings in pressure vessels (fuel tank task in Ariane 5 upper stage) etc.

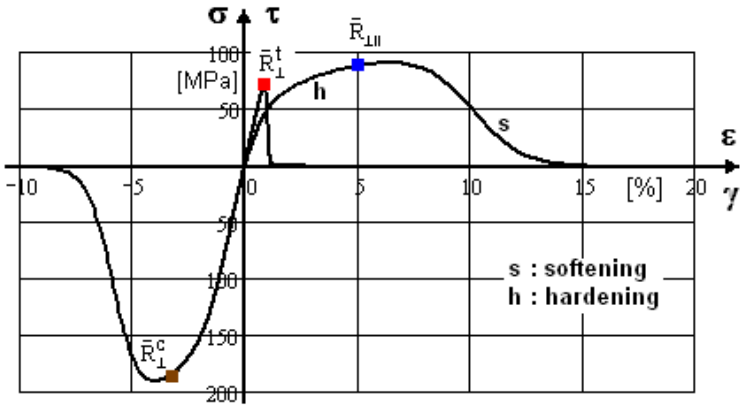

Fig.16-1, example UD ply: Full stress-strain curve with load-controlled hardening and deformation-controlled softening of the layer (ply) embedded in a laminate

CDM is pretty linked to multi-scale modelling, which will be looked at in the next Chapter.
All materials are generally composites. Applying CDM one goes down to the constituents of a composite to metallic grains or to fiber and matrix for instance. Moving down on the scales it is helpful to use the physical formulations gained on the macro-scale such as Mises yielding with ductile metals in the tension and compression loading domain and Mohr-coulomb friction behavior of brittle materials in the compression domain. Shear stress loading is composed of a tensile stress with a compressive stress. This activates two failure modes, which leads to normal fracture in the case of brittle materials. These physical effects stay valid at the lower scale and are to consider *adjusted*.

***LL**:*

It is always to check, whether a Mises yield criterion can be applied to quantify micro-damage portions or a fracture criterion in the case of very brittle behavior, i.e. Fiber Reinforced Plastics (FRP) experiencing matrix yielding:

16.1 Static Behavior

Micro-damage formulations:

CDM is basically used to capture the evolution of the micro-damage state from micro-damage $D = 0$ up to 'Onset-of-Failure' at *maxD*, which is for brittle materials at the end of hardening or at achieving the strength *R*.

In CDM, the formulation of the describing constitutive equation is based on one of the following two approaches (*Here the stress-strain curve is meant*):

(1) The strain equivalence principle approach or on
(2) The stress equivalence principle approach.

From engineering side, the latter is preferred because 3D stress states and residual stresses have to be considered in design dimensioning.

The constitutive relationships are formulated in the effective undamaged configuration $\sigma_{eff} = \sigma / (1-D)$ with a stress-strain relation linked by the stiffness elasticity matrix [C], which reduces due to growing micro-damage. *Fig.16-2* exemplarily depicts the relationship for a 2D-loaded transversely-isotropic UD material. By inversion of the effective compliance matrix S_{eff} the decaying stiffness matrix C_{eff} is obtained.

$$\{\sigma\} = [C] \cdot \{\varepsilon\} \rightarrow \{\varepsilon\} = [S] \cdot \{\sigma\} \quad \text{as practical test-data evaluation formulation}$$

$$S_{\text{eff}} = \begin{bmatrix} \frac{1}{E_1 \cdot (1-D_{11})} & \frac{-\nu_{21}}{E_1} & 0 \\ \frac{-\nu_{12}}{E_2} & \frac{1}{E_2 \cdot (1-D_{22})} & 0 \\ (\text{symm}) & 0 & \frac{1}{G_{12} \cdot (1-D_{66})} \end{bmatrix} \quad \text{with } D = \begin{bmatrix} D_{11} & D_{21} & 0 \\ D_{21} & D_{22} & 0 \\ (\text{symm}) & 0 & D_{66} \end{bmatrix}$$

usually not considering the off-diagonal D_{21}.

Fig.16-2, 2D-example UD material: Compliance matrix [S] and micro-damage matrix [D].

The D_{ij} represent the accumulation of the micro-damage process portions and are theoretically terminated by max$D$ at the tensile strength point in the case of brittle materials and at the rupture point for very ductile isotropic materials. These portions may occur during a monotonically increasing static loading. For brittle materials micro-damage starts at the 'elastic end' being a level where *Eff* has still reached a value, see *Fig.16-3*. Unfortunately, max$D$ in static CDM cannot become 100% due to its usual modelling basis! The center figure outlines how a stress-man views the 'onset

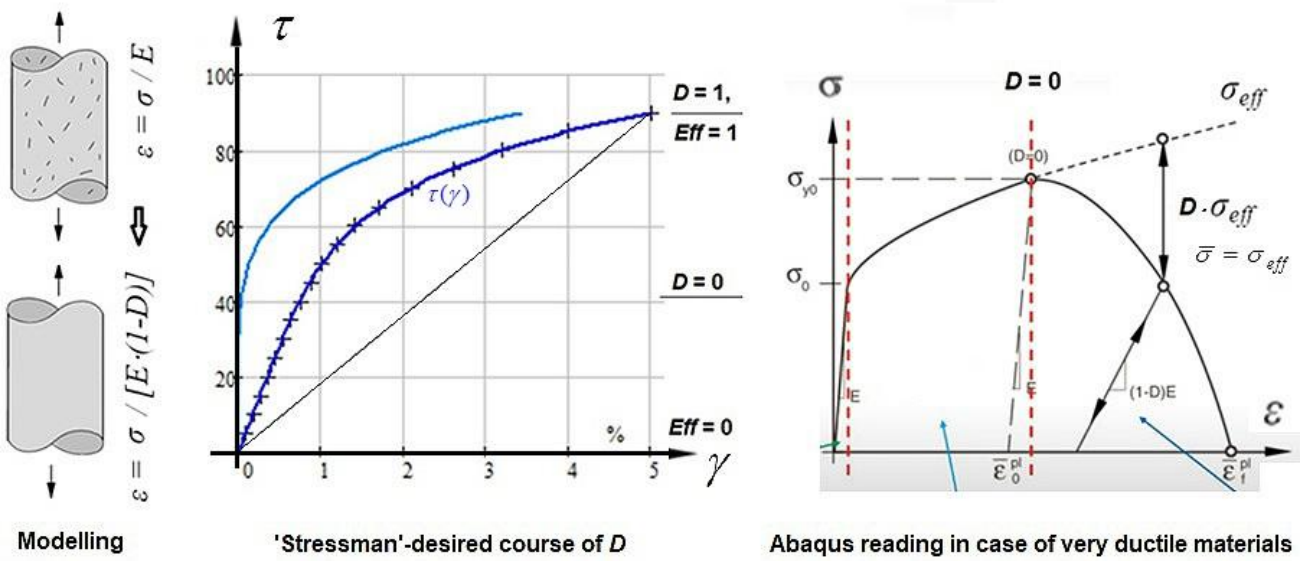

Fig.16-3: The various 'Onset- of- Failure' envelopes: (left) Smearing of the micro-damaged material, (center) shear of a slightly brittle material, (right) Ductile material (Ansys FEA code)

of micro-damage' of a slightly brittle material. In the elastic domain < $R_{prop} \equiv R_{e(lastic)}$ there is no D-contribution. The blue 'flow curve' then will contribute.
The right figure (from Abaqus) surprisingly outlines that there micro-damage first begins with void nucleation and coagulation which rises the Question:

Does really not any micro-damage happens below R^t ??

Micro-Damage-free (*in German schädigungsfrei, nicht schadensfrei*) and crack (= macro-damage, *in German Schaden*)-free does not mean free of flaws.

***LL**:*
** CDM is generally always good for understanding static & cyclic material behavior*
** Confusing is faced regarding 'onset of counting micro-damage'portions in static case: once < R^t but also > R^t*

Material behavior-determined slip and failure angles:

The number of slip systems in ductile metals is usually high, and those that are active possess an orientation near to the planes with maximum shear stress. Under uniaxial loading the planes of micro-cracks are always inclined approximately 45° to the direction of the applied tensile stress, see (*Fig.16-4*). In single crystals, the lattice structure is spatially oriented in such a way that a sliding plane is obtained at an angle of 45°. In poly-crystalline metals with randomly distributed lattice sub-structures this will change a little.

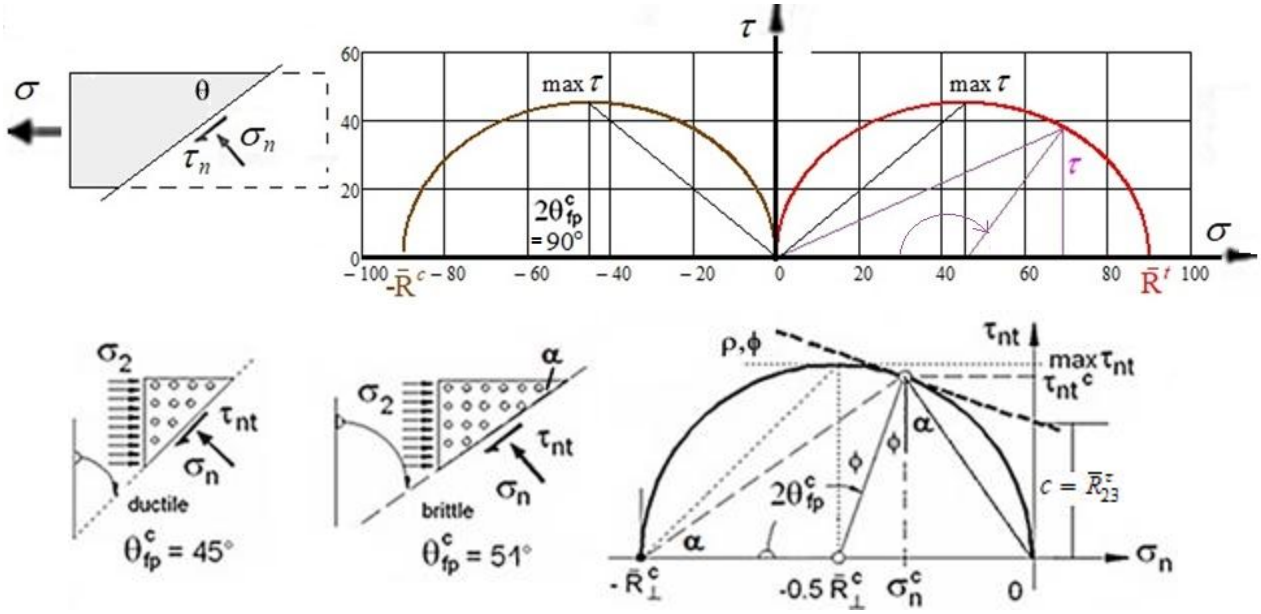

Fig. 16-4, very ductile metal material: (up) Mohr stresses and failure angles. (below) Mohr stress circle for a compressive and a tensile uniaxial external stress of a semi-brittle material

$\tau_n = \sigma \cdot \cos(\alpha) \cdot \sin(\alpha)$ with α the angle to σ direction, $2 \cdot \max \tau = \sigma$ for $\alpha = 45°$

Known from brittle material behavior under compression is: *The failure angle depends on the friction value μ*. After the formula, derived in [§22 later, *Cun23c*], the computation of the failure angle with the Mohr-Coulomb model delivers exemplarily for a material friction value μ = 0 (= *fully ductile)* the

expected value of 45° and for a friction value μ = 0.2 the angle 51°, see <u>*Fig.16-5*</u>. The author presents in this figure that the angle changes from the 51° at the compression strength point $\bar{R}_{\perp}^{c}$ up to 90° at the tensile strength point $\bar{R}_{\perp}^{t}$.

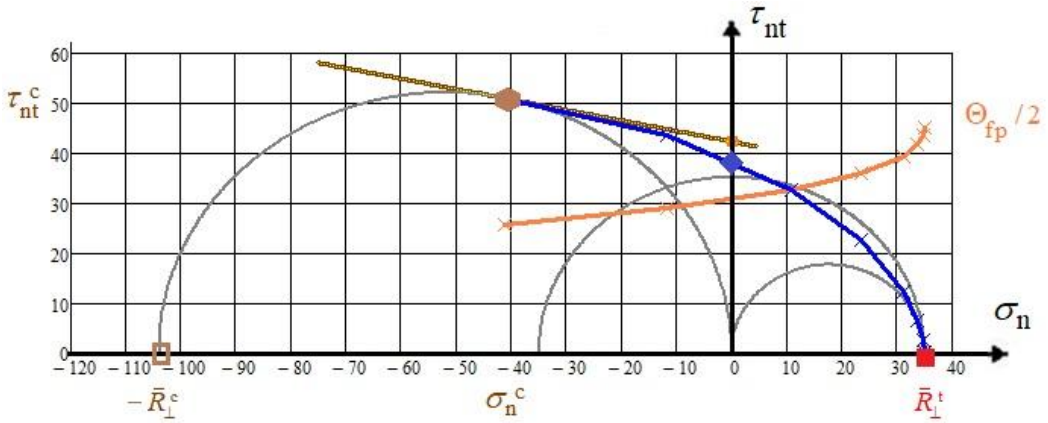

Fig.16-5, brittle UD-material: Joint display of the UD failure curve in Mohr stresses, indicating a fracture angle increase Θfp° when approaching $\bar{R}_{\perp}^{t}$ *. Shear fracture plane angle in the touch point 51° and linear Mohr-as well as a more realistic curved Mohr-Coulomb friction curve. Touch point is defined by* $(\sigma_n^c, \tau_{nt}^c)$*, linked to* $\bar{R}_{\perp}^{c}$*. (see §22)*

16.2 Cyclic Behavior of Ductile Metals applying Micro-scale Material Modelling

Once micro-cracks have nucleated due to strain accumulation from cyclic slipping, they grow in the early stage typically in the order of the material's grain size (text from M. Mlikota - S. Schmauder: *Thanks to Siegfried*). In the course of further cyclic loading, micro-cracks, formed along these slip bands, will grow and link together. In metals and alloys they grow predominantly along the crystallographic planes because they are highly affected by microstructural barriers such as grain boundaries or other micro-structural features. The coalescence of trans-granular micro-cracks, namely, if two micro-cracks meet each other at the same grain boundary, is performed in the numerical simulation of the crack initiation after Tanaka-Mura. It occurs if the average stress in between their tips surpasses the elastic limit *Re* of the material's new micro-crack, created on this grain boundary line, uniting the two trans-granular micro-cracks into a single one (*example pure iron Re = 260 MPa).*

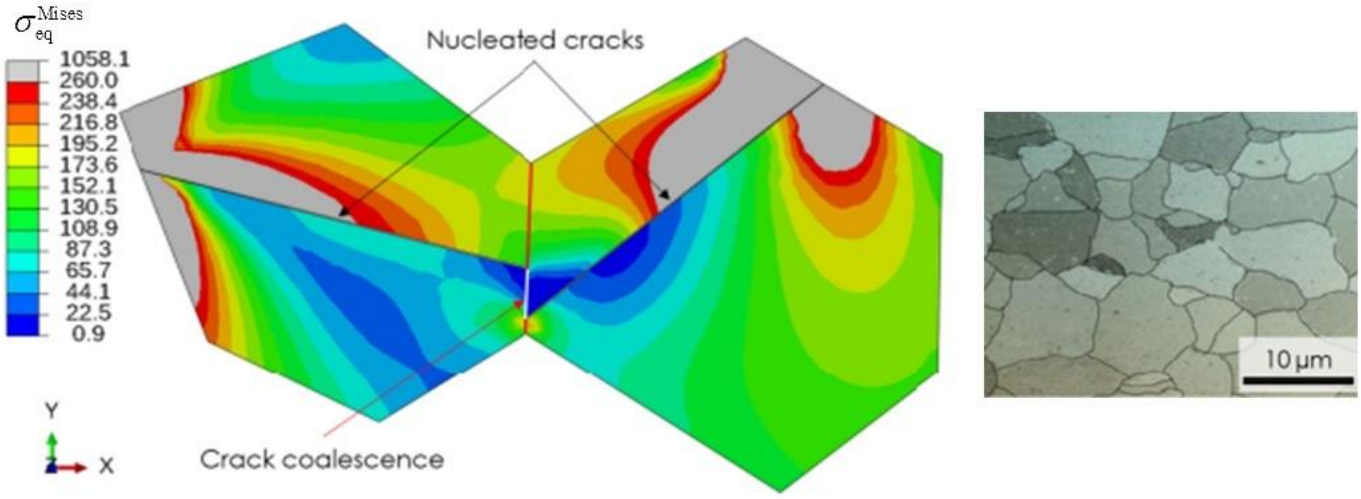

Fig.16-6: Simulation of AA micro-crack coalescence (Lorenzino, P., Navarro, A. & Krupp, U. (2013), 'Naked eye observations of microstructurally short fatigue cracks', Int. J. of Fatigue 56(0), 8-16.

Already nucleated crack segments tend to extend along the whole grain, causing local stress relaxation as well as concentrations at their tips and by that amplifying the likelihood for new crack formation in the vicinity. In the course, micro-cracks form along the slip bands, grow and join.

The change of the crack plane from the crystallographic plane to a non-crystallographic plane perpendicular to the external stress axis is called the transition from Stage I (*crystallographic growth*) to Stage II (*non-crystallographic growth*) or transition from the micro-crack initiation to a micro-crack growth stage resulting in a short crack, as depicted in *Fig.16-6*.

However, the dominant short crack does not always continue propagating. Namely, in the case of a lower stress level, the short crack may stop growing. Such a situation is typically known as run-out, which indicates that at very low stress levels an infinite life may be obtained. Run-out below the endurance limit means crack-retardation, *Fig.16-7*. In the long-crack regime the fatigue crack growth rate da/dn can be characterized by the stress intensity factor range ΔK as a dominant driving parameter.

The CDM-driven Region I in the figure below is here of interest, but should be illustrated as part of the full crack failure picture: A typical fatigue crack growth rate curve da/dn (ΔK) for the long crack is illustrated in *Fig.16-7*, too. If in a double logarithmic scale the long crack propagation rate follows a straight line in Region II, in sufficient distance from the threshold ΔK_{th}, then the long crack growth rate domain can be well described for most engineering alloys by the so-called Paris law:

$$\text{Paris:} \quad da/dn = C_{Paris} \cdot \Delta K^{n_{Paris}} \quad , \quad \text{Forman:} \quad da/dn = \frac{C_{Forman} \cdot \Delta K^{n_{Forman}}}{(1\text{-}R) \cdot K_{Forman} - \Delta K} \quad [HSB\ 63205\text{-}01]$$

In the figure and in the formulas above *da/dn* is the crack growth increment per cycle, $\Delta K = maxK - minK$ is the range of stress intensity factor, and *C* (intercept with the y-axis) and n_{Forman} (slope) are material curve parameters that are deduced by fitting the course of experimental data. *KIc* is the so-called fracture toughness.

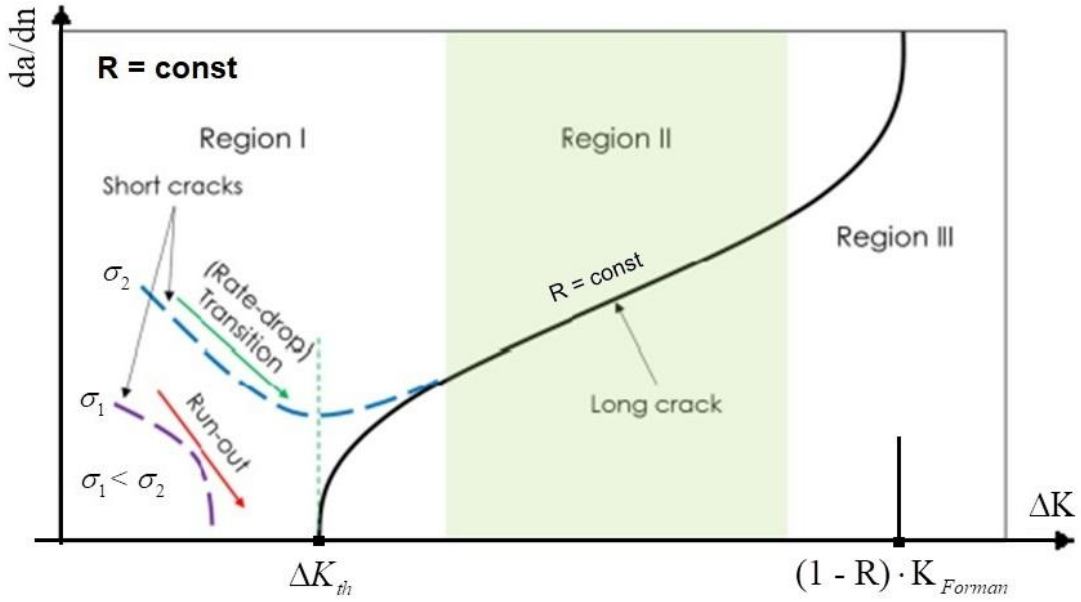

Fig.16-7: Fatigue growth rates of micro-cracks (short) and long cracks in dependence of Δ stress intensity factor. Schematic representation of the loading level- dependent transition from region I into region II.

n = number of cycles, a is crack size-

(Newman, J.; Phillips, E. & Swain, M. (1999), 'Fatigue-life prediction methodology using small-crack theory', Int. Journal of Fatigue 21(2), 109-119)

***LL**:*

** There is a hope, that in future for metals a basis will provided, that the estimation of an endurance limit will be possible.*

** A grain is usually polycrystalline with crystal planes in various spatial orientations. Hence, a metallic 'composite' material can be only termed homogeneous and isotropic if these orientations are randomly distributed in order to become quasi-homogeneous. By the way, this is the same for an isotropic short fiber-reinforced polymeric material, otherwise the so-called orientation tensor has to take care of the non-isotropy.*

16.3 Note on Application of Continuum (micro)-Damage Mechanics (CDM) in Static Strength

Note on Stress effort *Eff* versus micro-damage development *D*:

For the designer of interest is how the material's stiffness decreases with increasing stress effort or load, respectively. Design allowable *R* and average strength $\overline{R}$ lead to different stress efforts in *design verification* and in *modelling of material damaging* (50% value = highest expectance probability), see *Fig.16-8.* The enlarging effect of the design FoS *j* on the value of *Eff*, when reaching failure, is considered in the design verification curve (*dashed line*) depicted below. The more reserve is, indicated by a positive Margin of Safety *MoS*, the lower *Eff* is. This has an effect on the actual strain in the non-linear analysis case. It becomes smaller and the strain is less plastic, which is of interest for the validity limit of an elastic analysis.

In the case of 3D modal SFCs (*for comparison*) the common micro-damage-caused degradation is considered by an interaction equation that reflects the micro-damage influence of all acting stress states and associated modes. The single mode efforts are interact via the experience-based interaction exponent *m* being about *m* = 2.6.

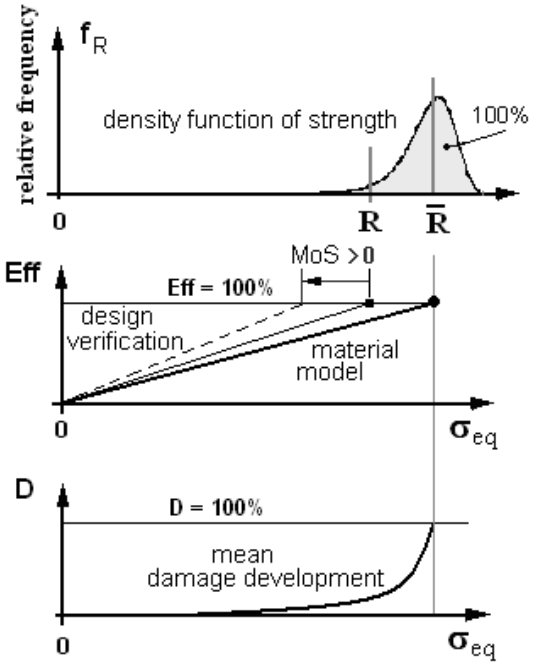

Fig.16-8:

Visualization of the development of stress effort, strength value, equivalent strength, and
Micro-damage understanding of a 'stressman'.

MoS = RF - 1

'Stressman's' Assessment of CDM applications:

During his engineering life CDM was often propagated to make in future a Design Verification

possible. In literature, i.e. [*Jai20*], Continuum (micro-)Damage Mechanics (CDM) models are also used to determine a *RF*. However, this intention faces some obstacles.

Analogous to the standard procedure then statistically-based micro-damage model parameters would be required and a total maximum value *D* is to define according to $D < D_{admissible} < 100\%$ at failure and this must be statistically based. Defining such a *D*–value is a challenge for the application of (micro-)Damage Models in the Design Verification (DV) for serial production certification. This challenge is novel and higher than providing the classical strength design allowables *R,* necessary for computing *Eff*.

Further, in known standard procedures *Eff* runs $0 < Eff < 100\%$, whereas *D* begins at a distinct *Eff*-value but should principally also end at 100%, see [*CUN22, §15.3*]. Here, a very essential question comes up: "*How does the designer assess a stress level that is below the 'onset-of-micro-damage'?"* In this context another question arises: "*How are to consider low stresses in Low Cycle Fatigue*?"
The provision of a CDM-failure body would be mandatory for obtaining DV. Hence, up to now CDM seems not to meet the authority-demanded DV-requirements regarding the statistically reduced design strength *R* and regarding the relationship $\sigma \sim R \cdot Eff$, which is valid in the linear elastic and in the non-linear regime.

***LL**:*
** Stiffness decay CDM model parameters are difficult to apply*
** The 'stress-man' will not understand that at maximum load, which is at the strength point, the sum of micro-damage does not approach 100%.*
** The author could not sort out a consistent procedure that might be used in design verification. A clear derivation of the maximum micro-damage values seems to be missing.*
** How is the interaction of the damage portions in 3D-CDM solved?*
** Stiffness decay CDM model parameters are difficult to apply*
** Looking at 'well analyzing', which requires well-mapping of the stress-strain behavior in the hardening domain, one should always remember the scatter of the measured curves.*

Engineer's question, regarding the body text above**:**

"Is it possible in future to provide the engineer the necessary design verification data when using micro-damage quantities D_i?"

Fig.16.-9 left shows the scatter and distributions of some strain curves depicting strength and strain quantities.
Fig.16.-9 right up demonstrates that a compression test can, due to barreling, can just give a value for the yield strength $R^c_{0.2}$. This requires the determination of the increased hoop diameter, when aiming at realistic R_{02}- and *E*-values for tensile and compression. The figure also informs that for a static test specimen of a product the directions are marked by the subscripts L, LT and ST and that these are used for the description of sheet-type test specimens. These specimens are machined in the rolling direction (letter L), transversal direction (T) and thickness direction (S). In the case of thick structural parts smooth tension bar test specimens are cut out, in the case of thin plates flat test specimens are investigated, which better represent 2D-structural shapes.
This is similarly performed for the radial and axial direction of a cylindrical test specimen.

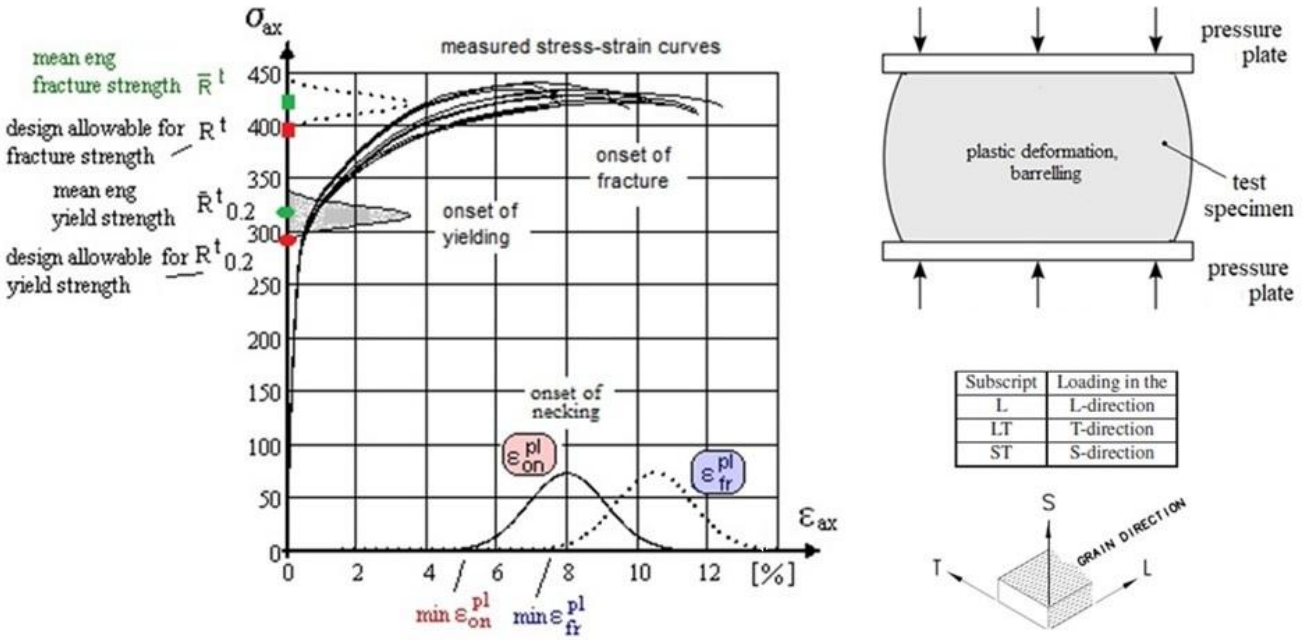

Fig.16-9: AA2219 engineering quantities and curves, deformation of a compressed ductile test specimen. (right down) Marking of sheet-type test specimens

Eventually *Fig.16.10* shall show the shape of the tensile rod test specimen and a picture of the porous fracture surface of the ductile material used

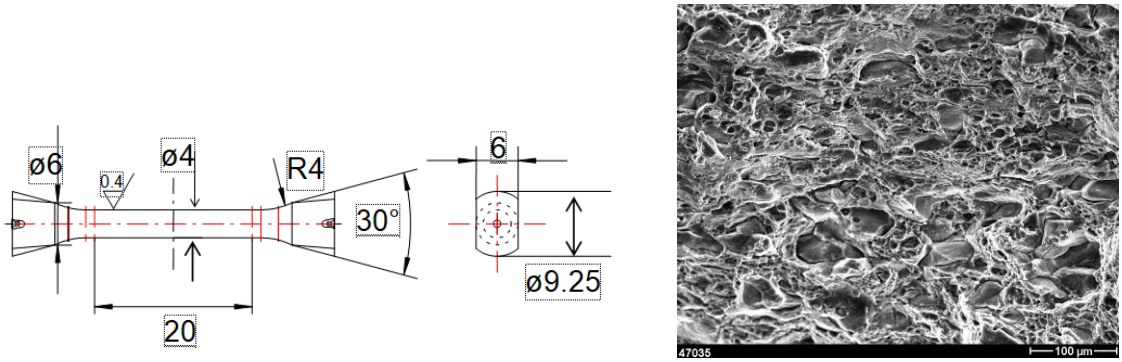

Fig.16-10: (left) Geometry of the tensile rod; (right) Voids on the fracture surface [IWM]

LL:

** Before executing any analysis with a distinct code the designer has to check whether the actual stress-strain curve fits to the shape of the implemented curve*

** For the best possible estimation of the component behavior, the average stress-strain curve $\overline{\sigma\varepsilon}$ must be taken*

** The average stress-strain curve $\overline{\sigma\varepsilon}$ does not inescapably run through the means of yield $(\bar{\sigma}-\bar{\varepsilon})_{yield}$ and of fracture $(\bar{\sigma}-\bar{\varepsilon})_{fr.}$*

17 Multi-scale Structural modelling with the concern Material Modelling and some Analysis

Aim: *Making aware of limits when applying validated macro-scale formulations at lower scales.*

17.1 Structural Analyses over the Scales

Structural modelling with associate analyses is performed at many scales, see *Fig.17-1*, from the macro-scale up to the Burj Khalifa building size.
Thereby, the challenging task is the input of the right material properties: Which values are to insert when analyzing at the lower scale? What about the stress-strain curve, and which for instance for the anisotropic UD material remains always bound to the macro-scale?

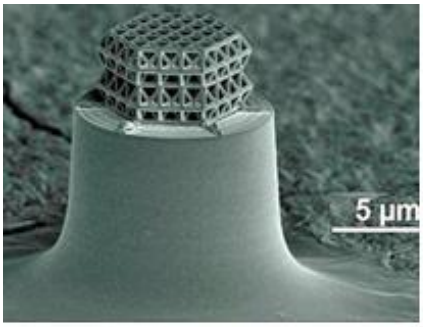

Fig.17-1: *Size variety of structures.*

(left) Truss structure, created by J. Bauer and O. Kraft with laser lithography.

Glass-like carbon nano-framework R^c = 3000 MPa. Advanced Materials, Progress Report, 'Nanolattices: An Emerging Class of Mechanical Metamaterials'. JensBauer, Lucas R. Meza, Tobias A. Schaedler, Ruth Schwaiger, Xiaoyu Zheng, Lorenzo Valdevit. 2017,Wiley Online Library

Burj Khalifa, 828 m

All this requires investigating the applicability of the usual macro-scale formulations especially concerning static strength, fatigue and fracture mechanics. For the assessment of a stress state, when viewing Design Verification (DV), it is to know the 'Onset-of-micro-damage' and the later following 'Onset-of-micro-cracking'.

Multi-scale modelling is executed for static and cyclic problems. In the cyclic case, there are three key 'points' that separate the regions in *Fig.17-2*:

- Ultimate strength $R_m^{\,t}$: Stress level required to fail with one cycle, n = 1
- Onset of Yield, R_e: Stress value at onset of plastic behavior with being $R_e < R_{0.2}$
- Endurance limit $S_{e(ndurance)}$: Stress corresponding to the horizontal asymptote of the SN-curve.

The course of the cyclic failure test data, termed SN-curve, is again mapped by the 4-parameter Weibull formula $\mathrm{R = constant:}\quad \sigma_{max}(\mathrm{R}, N) = c_1 + (c_2 - c_1) / \exp(\log N / c_3)^{c4}$.

As the average SN-curve cannot be applied in fatigue life DV, a statistically reduced curve is to determine as design curve. This design curve defines a full D_{design} = 100% -SN-curve from the tensile strength as original point and ends in the running-out defining an endurance limit stress.

17.2 Macroscopic SN-curve with Relation Material Stressing Effort Eff ↔ Micro-damage D

There are practically two possibilities to present SN curves:

(1) Ductile: Applying the stress amplitude $\sigma_a(R,N)$, also termed alternating stress

(2) Brittle: Applying the upper stress $\sigma_{max}(R,N)$

The maximum stress is physically simpler to understand by the 'stress-man' than the

amplitude, according to smooth transfer from the static to the cyclic behavior, Fig.17-2. Namely, a decaying SN curve is interpretable like a decaying 'static' strength after a micro-damage process with *n* cycles.

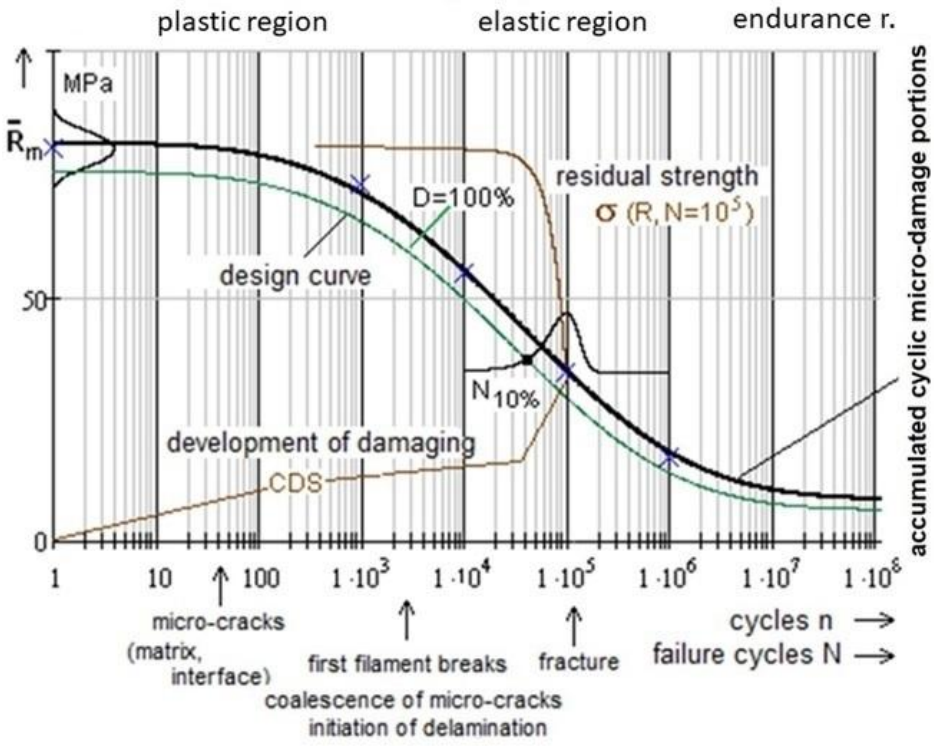

Fig.17-2, Design Verification: Fatigue average curve and ***design curve*** **R = 0.1.** *D = D_{design} for a survival probability P with a confidence level C. CDS is 'characteristic damage state' of a lamina*

[Hiatt, J. (2016), 'What is a SN-Curve?', Technical report, Siemens PLM Community). $N_f = N_{initial} + N_{crackgrowth.}$ Run-out below the endurance limit means crack-retardation]

Thereby, the static material stressing effort *Eff* (Werkstoffanstrengung, $N_f = 1$) is replaced by the accumulated cyclic micro-damage sum *D(N).* Applied here is the classical 4-parameter Weibull curve with one parameter still fixed as strength point origin, because for brittle materials the strength value $\bar{R}^t = \sigma_{max}$ (n = N = 1) is preferably used as origin in the tension domain and anchor point of the SN curve and in the compression domain - $\bar{R}^c = \sigma_{min}$ (n = N = 1).

In detail, Fig.17-3 visualizes the transfer from the static load-driven increase of the material stressing effort (n = N = 1) *Eff* = 100% (expectance value 50%) at the strength point to the cycle-driven micro-damage sum $D_{mapping}$ = 100% (expectance value 50%) of the SN curve. The evolution of *Eff* is not linked to the accumulation of the micro-damage. At onset-of-micro-cracking *Eff* is still > 0.

$$\text{If static failure} \rightarrow \max\sigma = \bar{R}_{static} \text{ at } Eff = 1 \text{ and if cyclic failure } \max\sigma = \bar{R}_{cyclic}, \text{ at } D = 1.$$

LL:

** It is always necessary to check whether the material at the lower level behaves in such a way that physically-based macro-mechanical formulations can be used*

** The material data input should satisfy physical model demands, which includes measurable parameters*

** DV demands for a statistically reduced SN-curve.*

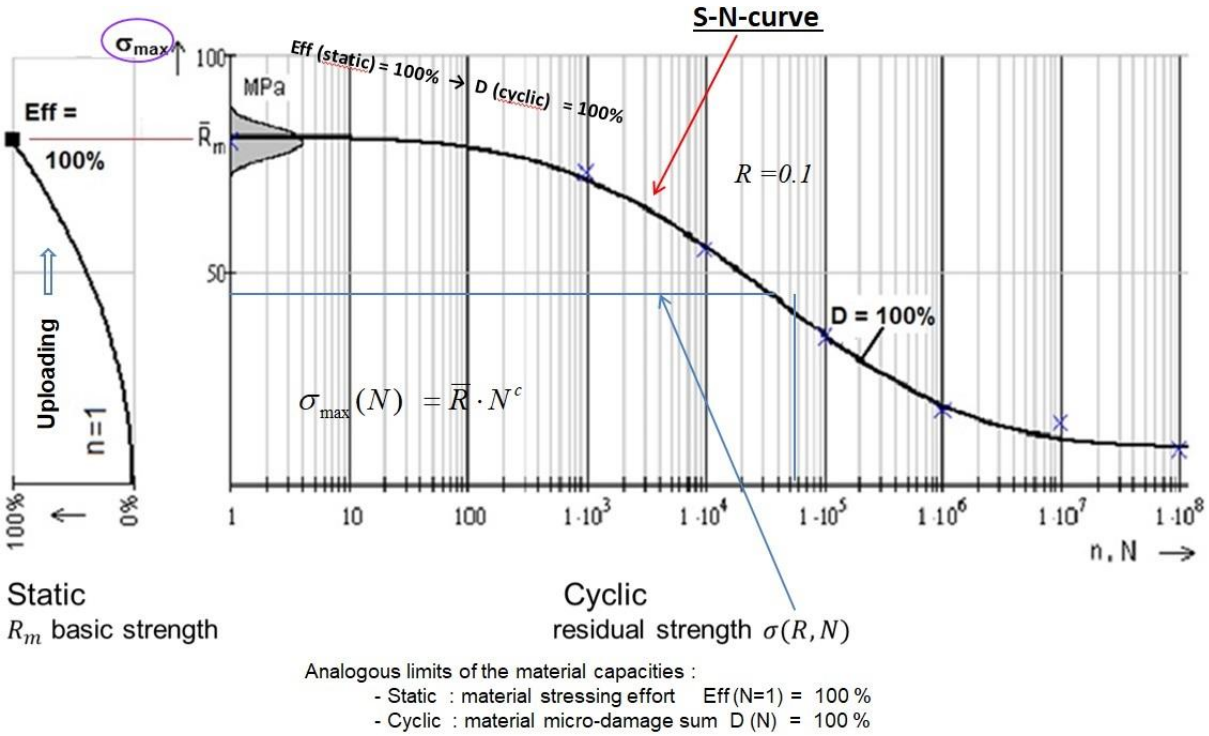

Fig.17-3, Mapping: Eff versus D. Mapping deals with averages ≡ 50% expectance value

17.3 Multi-scale Material Modelling regarding Infinite Life (endurance limit) of Metals

Infinite life or, in other words, the endurance limit is an ever-lasting topic of highest interest in structural design and concerns all materials.
Nowadays, valuable investigations on the micro-mechanics level seem to bring a significant progress for isotropic metals by using Continuum Damage Mechanics (CDM).

Mlikota and Schmauder found that the so-called 'Critical Resolved Shear Stress' CRSS is the relevant fatigue-responsible quantity, (*Fig.17-4*), regarding the behavior of ductile metals in the micro-scale regime. Multi-scale Material modelling (MMM), based on enough computer power will probably allow in future 'Computational material mechanics' from < micro-scale models (*Molecular Dynamics-treated and test results-supported from statically and cyclically loaded 10 µm thick pillars for instance*) via micro-scale to bridge with the necessary properties (*hopefully statistically based)* to the classical macro-scale models in structural design.

Multiscale materials modelling could grow and become a significant tool for understanding complex material micro-damage processes for many homogeneous isotropic materials, a benefit for macroscale investigations.

The conclusions of Mlikota are:

- The CRSS is the resistance for the dislocations to move through the crystal. It is governed by the present strengthening mechanisms in the crystal. The CRSS is - according to critical stress strength - a micro-shear strength.
- The fatigue crack growth modeling procedure in the High Cycle Fatigue regime should include the following steps: Micro-crack nucleation within a grain → Coalescence of already existing flaws and/or arrest at grain boundaries → Short crack or Stage I growth → Transition from Stage I to Long crack or Stage II growth

- The discovered relation between endurance limit and the CRSS allows the virtual selection of those types of materials, which are more fatigue resistant! The physically-based MMM approach represents a breakthrough in the field of fatigue research
- The higher the CRSS magnitude of the metal of interest, the higher the loading stress level σ will be necessary to accomplish the transition from infinite to finite life
- The multiscale fatigue simulation approach is capable of properly taking into account the mean stress $\sigma_m = max\,\sigma \cdot (1+R) / 2$ with the stress ratio R = minσ/maxσ and capturing the stress concentration factor K_t, which are influencing factors when designing structural components.
- Experimental tests demonstrate, that there is a drop in resistance to fatigue fracture with the increase of the grain size.

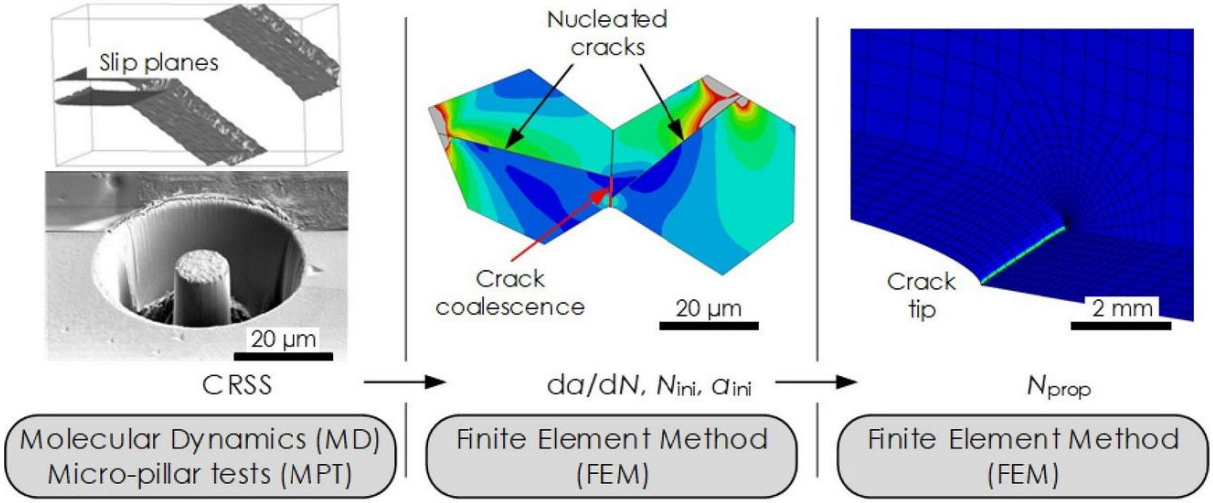

Fig.17-4: Full modelling approach. CRSS critical resolved shear stress, da/dn crack growth rate, N_{in} number of stress cycles until short-crack initiation, a_{ini} initiation short-crack length, N_{pro} number of stress cycles until short-crack propagation.

[Mlikota M. & Schmauder S. (2018), 'On the critical resolved shear stress and its importance in the fatigue performance of steels and other metals with different crystallographic structures', Metals 8(11), 883]

LL:

** There is a hope for some ductile materials in future to estimate the endurance limits of various metallic materials in the Ultra HCF regime just by knowing their CRSS values !*
Available CDM models seem to be neither to be clear-defined nor classified to be used for Design Verification (DV). A DV-procedure is searched

** A grain is usually polycrystalline with crystal planes in various spatial orientations. Hence, a metallic material can be only termed homogeneous and isotropic if these orientations are randomly distributed in order to become quasi-homogeneous. (*By the way, this is the same for an isotropic short fiber-reinforced polymeric material. Otherwise, the so-called orientation tensor has to take care of the non-isotropy*).*

** For the analysis the Mises SFC was employed in order to localize the peaks of shear banding (yielding) of the investigated steel material*

$$\sigma_{eq}^{Mises} = \sqrt{3 \cdot J_2} \quad \text{with} \quad 6J_2 = (\sigma_I - \sigma_{II})^2 + (\sigma_{II} - \sigma_{III})^2 + (\sigma_{III} - \sigma_I)^2 = f(\tau), \quad \tau_{oct} = \sqrt{J_2 / 3}$$

** Clearly to be defined is the quantification of the D-portions for ductile and brittle behavior with a maximum value of total D = 100%:*
- static case: the achieved micro-damage value at a distinct (equivalent) stress level
- cyclic case: the cycle-associated micro-damage portions with its derivation formula.

17.4 'Meso' –Modelling of the Example UD material

Fig.17-5 exemplarily gives a look at the present multi-scale modelling performed with Fiber-Reinforced-Polymers (FRP). Two scales are linked together, the micro-scale with the macro-scale by a meso-model. What is meso? Meso is no scale, per definitionem!

* Micro-scale > μ *m*, macro-scale > *mm*.
* The author experienced (1999) in a BMFT R&D discussion round on three MaTech Competence centers of institutes working from the polymer-scale to the structural macro-scale - after one day - that the term meso-scale is used in polymer mechanics by the research colleagues at the nano-level. This level is one thousand times smaller than the solid mechanics people apply meso.
* A further classification is available for porous materials, according to pore size: 'microporous' pores < 2 nm, 'mesoporous' pores between 2 nm and 50 nm, 'macro-porous' pores > 50 nm. [*International Union of Pure and Applied Chemistry*].

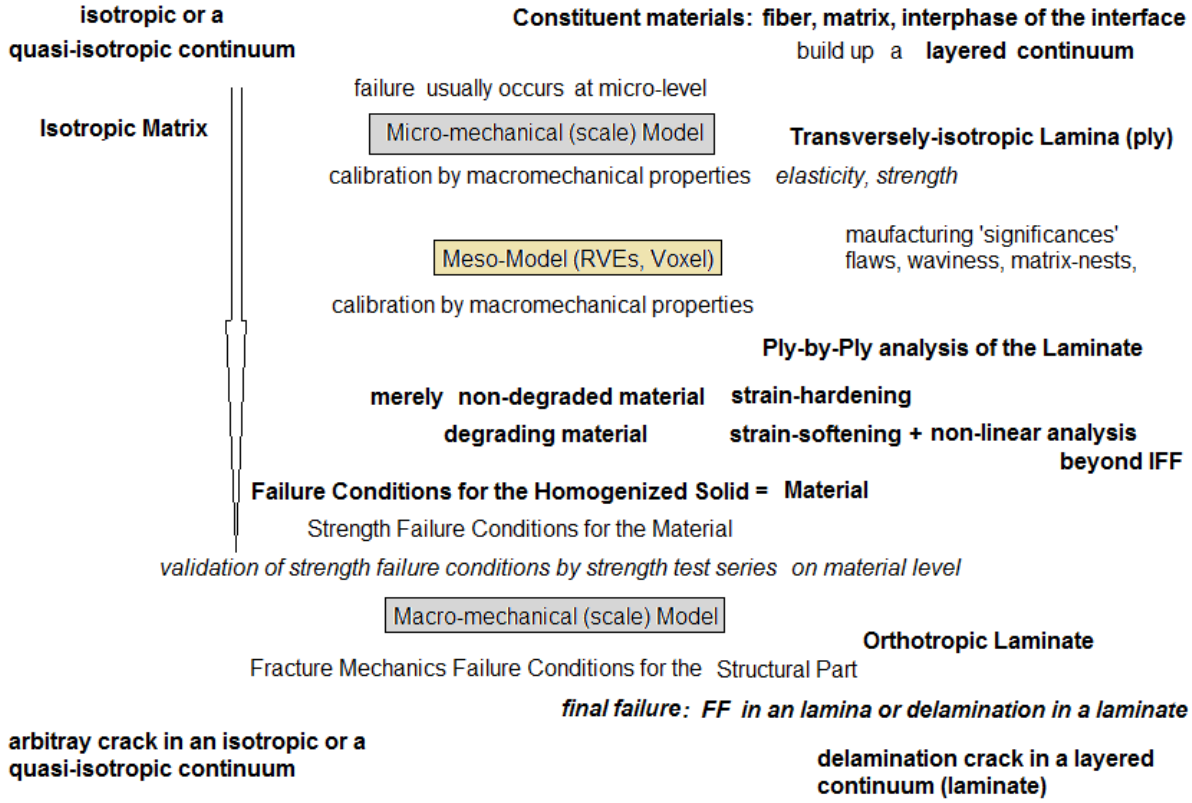

Fig.17-5:Multi-scale modelling, example FRP, brittle. 2 scales. RVE: Representative Volume Element, Voxel: volumetric pixel

LL:

The term meso is a task-linked chosen size level. Apply the term meso-model, not meso-scale, and define it.

In structural engineering meso is used at about 0.1 mm.

17.5 Note on Micro-mechanical Formulas (mixture rules) for Example UD lamina (ply)

***Aim**: Guideline how to use micro-mechanical models and properties with giving some warning.*

Mixture rules are employed in many technical disciplines (polymer and mineral composites like concrete). Exemplarily, here at the so-called micro-mechanical formulas of UD-materials will be looked at, only.

Creep investigations and pressure-related effects on the matrix and in consequence on the UD material of composite materials i.e. usually require a micro-mechanical input.

Examples of the author, a centrifuge and a WWFE Test Case: The non-creeping constituent fiber is to separate from the creeping/relaxing constituent matrix. In order to capture these features the use of 'micro-mechanical mixture rules' in structural engineering is common practice. It requires properties of the constituents and the so-called mixture rule, how these constituent properties are linked, to be able to predict properties of the envisaged ('smeared') material on the macro-scale.
Not all micro-mechanical properties applied can be measured. A solution will be obtained by setting up mixture rules and calibrate them via macro-mechanical test results on the lamina macro-level. This makes an inverse parameter-identification necessary.

Hence, the application of a micro-mechanical formula underlies the constraint that the given micro-mechanical properties can be only used together with the formulas they are based on. Otherwise the results might be pretty wrong. For example within the WWFE, Test Case 1, the organizer QinetiQ just provided micro-mechanical material properties but not the associated micro-mechanical formula. Therefore, the author had to apply micro-mechanical UD formulas from [VDI 2014, sheet 3] and found a discrepancy of a factor 2 for the data to be predicted! This is not acceptable for the WWFE-task model validation.

LL: Micro-mechanical properties can be used only together with the formulas they have been generated with ! ⇐ Significant *Warning due to painful time-wasting experience in the WWFEs !!*

18 Some Lessons Learned from Testing and from Evaluation of Test Results

***Aim**: Forwarding Lessons Learned.*

In structural design one basically faces 3 types of testing**:**

- Structural Testing (destructive, non-destructive)
- Materials Testing (destructive, non-destructive) and
- Non-Destructive Testing of structure and material (NDT, NDI, NDE).
  Other tasks here are: Failure detection, localization, size + shape, Failure assessment (risk-based).

All structural tests to be performed aim to uncover a deficiency: Workmanship, design mistake, oversight of a failure mode, tightness, shock resistance etc.

Fig.18-1 presents the test strategy of the MIL handbook 17, a forerunner guideline for the development of composite structures which are more challenging than developing isotropic structures.

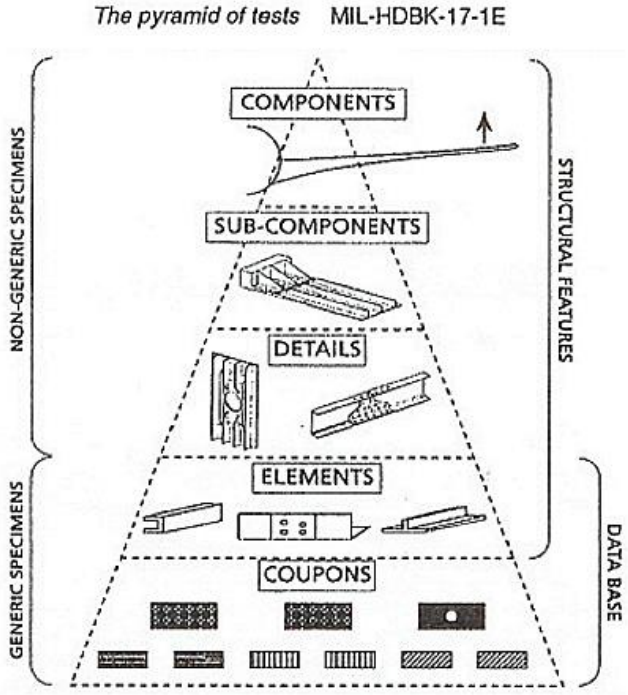

Fig18-1: Test strategy of MIL-HDBK 17 (original edition about 1970). MIL-HDBK-17/1F (VOL. 1 OF 5), DEPARTMENT OF DEFENSE HANDBOOK: COMPOSITE MATERIALS HANDBOOK - POLYMER MATRIX COMPOSITES GUIDELINES FOR CHARACTERIZATION

In this Chapter some personal experience is presented, beginning with structural testing.

***18.1 Structural Testing** primarily based on the Ariane launcher development*

At first, a Test Agreement is to provide. It consists of test rig, test specification, test specimen and test data evaluation method and the Test Procedure. Therefore, one can only speak about 'exact' test results in the frame of the obtained test quality.

Fig.18-2 presents the so-called sub-structuring (*affecting shares between the participating Ariane partners)* an example for violating mechanics: MAN was not permitted to include the neighboring structural part despite of the fact that it was also a MAN contract part. We could not implement the FE model of this neighboring part in order to optimally represent the real boundary stiffness conditions in the model of the 'studied structural part' but had to implement the given boundary

conditions of the contract. This caused a wrong behavior of the 'studied structure' and was a real mess regarding the evaluation of the test results and comparison with analysis results. The first test article has been allegedly strengthened, which was senseless.

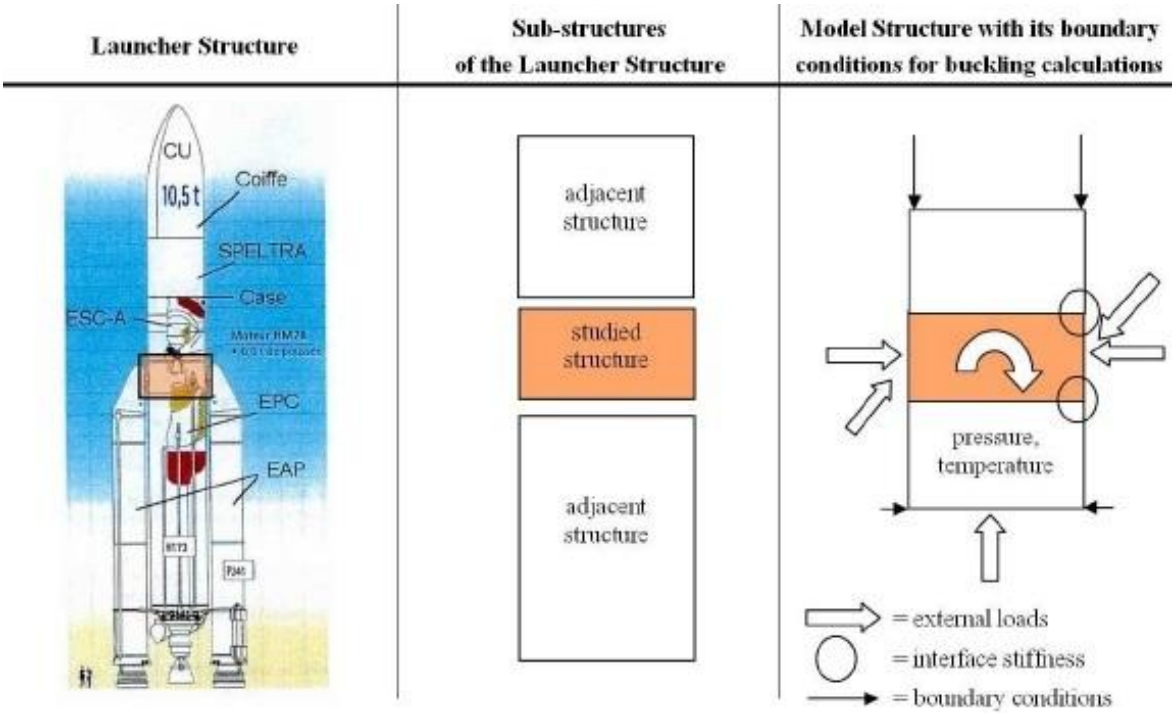

Fig.18-2: Sub-structuring of the Ariane 5 launcher, Front Skirt test

LL

** Test article analysis is mandatory to interpret the test results and simulation-based improve the design. Only well-understood experiments can verify the design assumptions made!*

** Splitting of a large structure (Ariane experience) is dangerous: The first buckling mode can appear on an adjacent structure and not on the studied one*

** Mandatory for a realistic qualification of a sub-structure is a realistic set of cross-section loadings and pressure loading with an accurate structural designing of the interface stiffness of the adjacent structural parts. If the interface is too stiff in the test assembly this will attract loading and lead to a non- realistic failure site (experience from Ariane 5 tests). The total system determines the behavior*

** Not all critical locations of a structural component can be tested, because an 'over-testing' of some parts may happen to be. 'Verification By-Analysis-Only' is to be considered if the structure is too big or if the test model shall e.g. be applied later as flight model*

** Put strain gauges there where a clear stress situation is in order to avoid useless discussions about the interpretation. Check locally by strain measurements and then rely globally on FEA-test result comparison*

** Specific design requirements drive testing*

** Requiring different so-called system margins MoS_{sys}* (suffered nonsense in a Ariane Technical Specification) *for the various structural parts, then not all critical locations can be tested without overloading other integrated parts. Components of such a structural assembly cannot be verified by a qualification test, because system margins cannot be used locally like a 'fitting factor'. They should have been considered directly in the Ariane 5 as a usual design FoS, applying $j_{sys} = (MoS_{sys} +1)\cdot j$. Otherwise, the design process is obscured and is prevented from applying the most economic measure in order to take risk out of the structure*

** Requirement to put a design FoS j on a design temperature violates physics and structure behavior*

** So-called test correction factors are applied to adjust the design verifications by accurately evaluated structural test results linked to the test article analysis results.*

This is a good place to remind that Sub-structuring is risky, if the boundary stiffness between the structural partners is not provided by the structural architect.
My personal experience is my inhouse response to Mr. Feustel's mail, below:

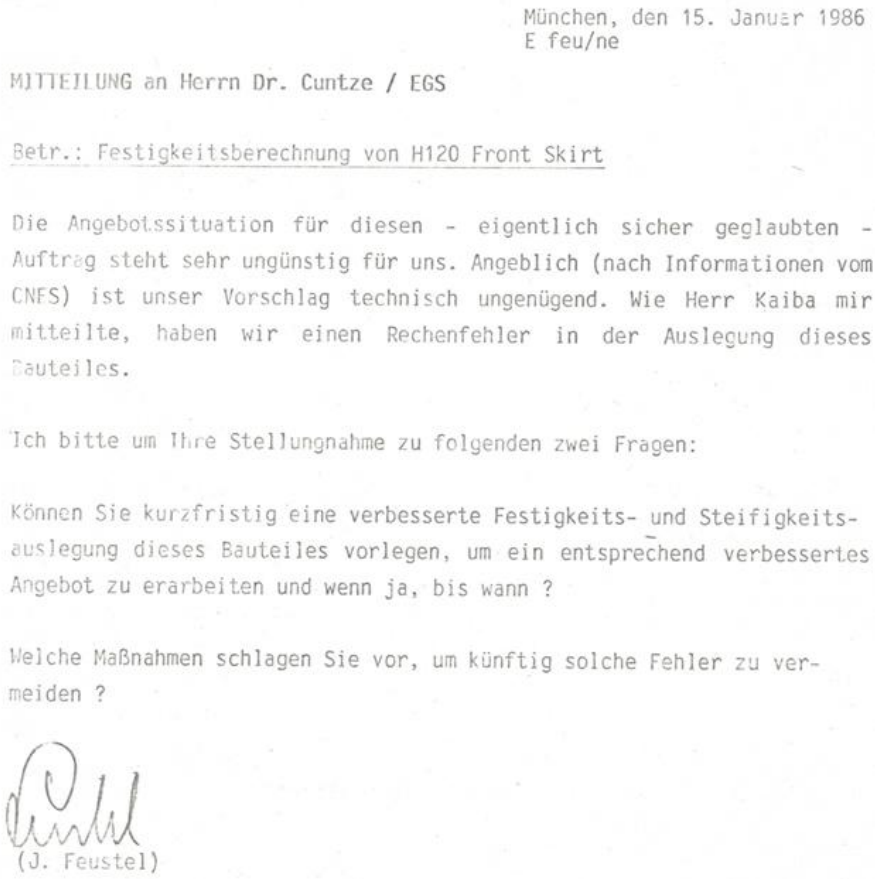

München, den 15. Januar 1986
E feu/ne

MITTEILUNG an Herrn Dr. Cuntze / EGS

Betr.: Festigkeitsberechnung von H120 Front Skirt

Die Angebotssituation für diesen - eigentlich sicher geglaubten - Auftrag steht sehr ungünstig für uns. Angeblich (nach Informationen vom CNES) ist unser Vorschlag technisch ungenügend. Wie Herr Kaiba mir mitteilte, haben wir einen Rechenfehler in der Auslegung dieses Bauteiles.

Ich bitte um Ihre Stellungnahme zu folgenden zwei Fragen:

Können Sie kurzfristig eine verbesserte Festigkeits- und Steifigkeits-auslegung dieses Bauteiles vorlegen, um ein entsprechend verbessertes Angebot zu erarbeiten und wenn ja, bis wann ?

Welche Maßnahmen schlagen Sie vor, um künftig solche Fehler zu vermeiden ?

(J. Feustel)

Yes, we had a calculation error that we should have discovered through a load-balance check, not executed unfortunarely. All performed checks failed to identify the error because the substructure specifications were too rigid, and design changes didn't provide a solution. In other words: the calculations led to the requirements being met within the stiffness specifications.
Substructuring is particularly problematic in statically indeterminate systems regarding loading, different boundary-linked frequencies. The total system determines the behavior. We could solve the problem!

*18.2 **Material Testing** primarily based on the World-Wide-Failure-Exercises-I and -II*

The author succeeded with test-validation of 3D-strength criteria models for isotropic concrete, transversely-isotropic UD-material, orthotropic ceramic (fabrics) with visualization of the derived 3D failure surfaces if reliable test data sets were given.

This was only partly given in the *the World-Wide-Failure-Exercises-I, concerning2D-mapping, and –II, concerning 3D-mapping of UD materials.*The author's WWFE-I and -II contributions had to be based on an intensive assessment of provided test results. In this sub-chapter the Lessons Learned during the examination of several WWFE-Test Cases (TC) will be collected.

Validation of the lamina-material SFCs models can be only achieved by 2D- together with 3D-lamina test results. Since SFC-model validation is focused just lamina-TCs are now investigated in detail. The normal user is just interested to well map his course of failure test data by a UD-SFC and not on the laminate analysis tools.

The laminate test cases serve for the verification of the laminate design. There the full WWFE failure theory is required. This makes a comparison between the contributions very challenging because different FE codes were applied by the contributing competing institutes. These better tools further had to be equally compared to the retired author's tools. He could just use his handmade non-linear CLT-code upgraded by experience and using his sensibleness for the problem and the delivered input.

***LL**, more general ones*

** Measurement data is the result of a Test Agreement (norm or standard), that serves the desire to make a comparability of different test procedure results possible. Hence, there are no exact property values. Material properties are the result of the material model applied inclusively mapping process.*

** Stresses, strength, strains, elasticity properties cannot be directly measured*

** Check of assumptions is necessary before designing (example: WWFE on UD-material). Pore-free material, specimen surfaces polished, well-sealed, fiber volume is constant, tube specimens show no warping and do not bulge, perfect bonding, no layer waviness, edge effects do not exist*

** Sometimes one must live with a substitute test situation in order to get some approximate properties (Example: UD-Tension/Compression-Torsion test device → Arcan test device)*

** Before thinking about test data evaluation the associated underlying micro-damage processes must be sorted out in order to get a better understanding of failure*

** Test specimens shall be manufactured like the structure ('as-built')*

** Comparisons between theoretical predictions and test data help to identify the major discrepancies, limitations, and areas which require further theoretical and experimental work. There is always a lot to be done and following Moslik Saadi: **"All is difficult prior to becoming simple**"! This begins with the provision of appropriate test specimens for the various material families being extreme ductile or brittle and ends with appropriate test procedures and an appropriate test data evaluation*

** Considering FE-results: We must more and more 3D-design! However the situation of properties, especially for composites is: „3D-property data test sets are seldom sufficiently available".*

* Achievement of a correlation test ⇔ analysis not just a comparison of numbers !

Of high interest for future scientists and engineers might be the following assessment results of the provided properties during the author's many WWFE-designated years. They are results which stem from a very careful and effortful test data evaluation lasting about *one man year*. Otherwise, a successful WWFE-contribution could not have been made possible.

Thereby, some essential WWFE TestCase-examples for lamina-input shortcomings were found:

* WWFE-I, TC1: the provided strengths have been changed from Part A to B and two test points are doubtful regarding own test results (*Reason is known: non-accurate raw test data evaluation of the test engineer at DLR Stuttgart. Organizers did not question the test data but required mapping of the false ones*!).

* WWFE-I TC2: the author informed the organizers that apples and oranges have been put here together in a diagram. One cannot fill into the same diagram 90°-wound tube test specimen data together with 0°-wound tube data. The 0°-stresses have to be transformed in the 2D-plane due to the fact that shearing under torsion loading turns the fiber direction (see *Fig.18-3*) and the lamina coordinate system CoS is not anymore identical with the structure coordinate system of the tube. In order to also use these test data the author exemplarily transformed magenta-colored two fracture test points by the occurring twisting angle γ using a non-linear CLT-analysis. Then he could achieve a good mapping showing, that the two transformed fracture points accurately lie in the lamina CoS on the 90°-tube curve.

* WWFE-II, TC3: the same mistake happened again! However, here the much more complicated 3D-stress situation was to face, so that the 3D-transformation of the 0°-data set could be simply performed.

* WWFE-II, TC2 an average stress-strain curve should have been provided because otherwise no realistic treatment is possible. Therefore the Part A results could be only inaccurate. From the Part B information the author could derive an average curve and then all 3 TC test data courses could be mapped and the mutual check points in the fully connected TC2-TC3-TC4 matched. Incomprehensively, there was no response of the organizers to the author's idea, which made 3 TCs to successful test cases.

* Viewing the final papers of the WWFE-organizers "*A comparison of the predictive capabilities of current failure theories for composite (UD-composed) laminates, judged against experimental evidence*" and "*Maturity of 3D failure criteria for fiber-reinforced composites, comparison between theories and experiments*", there is not any doubt to find - concerning the quality of the only available, provided test data sets -

One third of the provided TC test data was at least questionable
till not applicable for a reliable model validation !!!

Mind, please:

**** Test results can be far away from the reality like an inaccurate theoretical model.***
**** Theory creates a model of the reality, one experiment shows one realization of the reality.***

$\tau_{21}{}^{fr}(\sigma_2)$ basic cross-section of the fracture failure body: (right) WWFE-I, TC2, UD lamina, CFRP, T300/BSL914C Ep ; (left) Tube test specimen picture: [Courtesy IKV Aachen] The normal user is just interested to well map his course of failure test data by a SFC

(More WWFE etc test evaluations are found in [Cun13, 25])

MAN thread winding machine
(pin winding)
with CNC control and
heatable multi-thread guide.
Thread placement from 0° to 90° possible.
See Fig. 18-3

"Theory is the Quintessence of all Practical Experience" *(A. Föppl)*

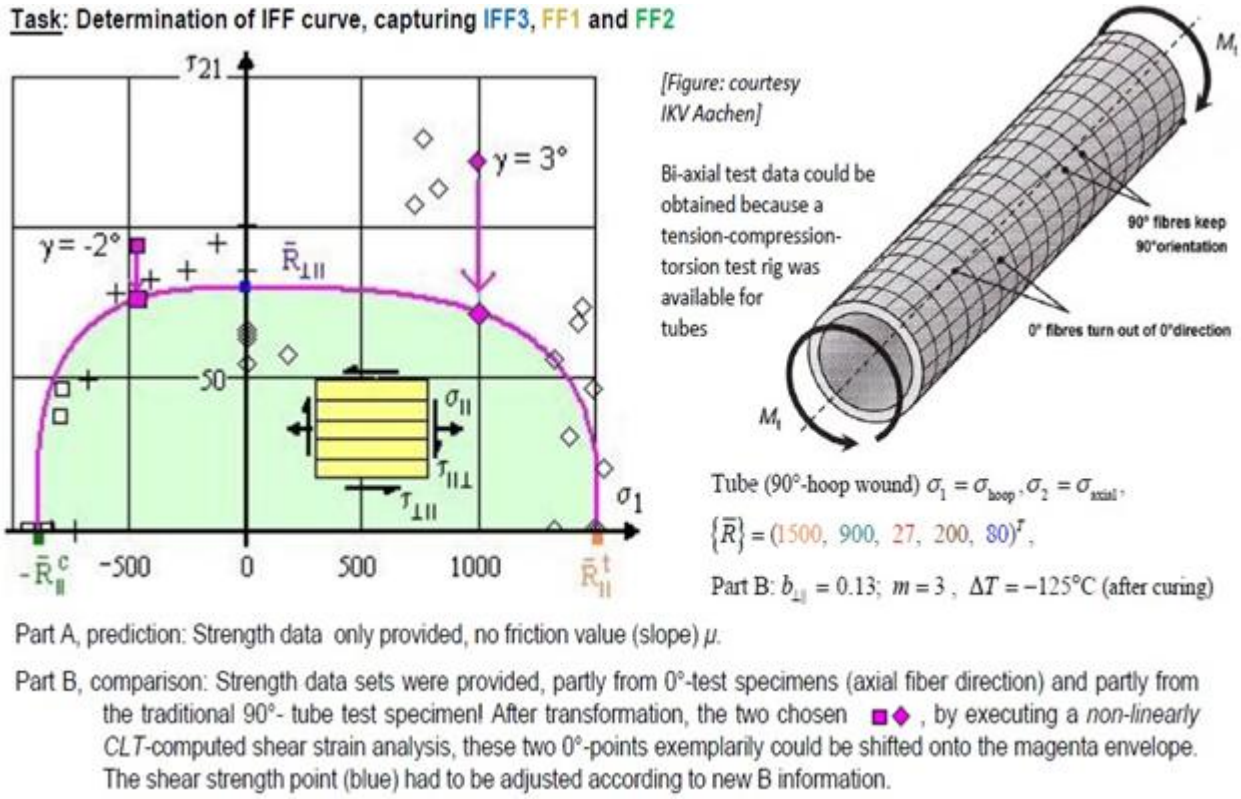

Fig.18-3: Example WWFE-I TC2, WWFE-II, TC3

Finally, *Fig. 18-4* presents details of the high-qualified tension-compression-torsion test rig.

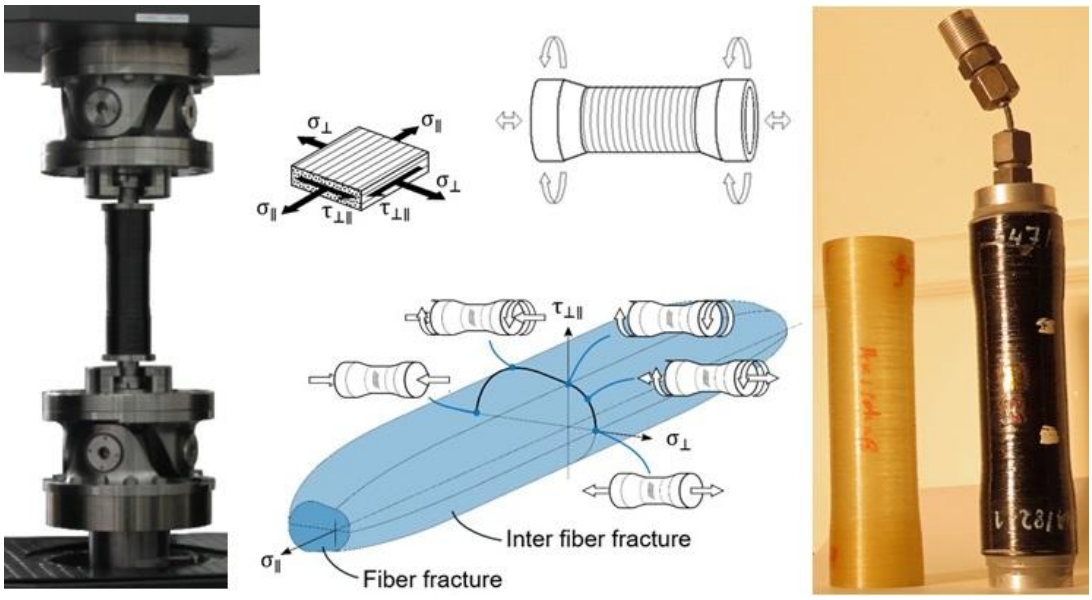

Fig.18.5: The tension-compression-torsion test: Test set-up of Leibniz-Institut für Verbundwerkstoffe GmbH Kaiserslautern and (right) GFRP and CFRP test specimens of MAN Technologie

*18.4 **Derivation of an accurate average strain-stress curve,** example UD*

The use of accurate stress-strain curves of materials builds the basis of structural fidelity.

These curves may show a vast scatter. Therefore, a practical method of handling, analyzing and averaging theses curves has to be found for the nonlinear, statistically scattering stress-strain behavior of materials. The measured stress-strain curves are approximated by a mapping function. That makes it possible to extract, store and update the complete nonlinear behavior of above metals or of composite materials in form of a distinct number of real parameters.

Three different evaluation methods are presented for the statistical analysis of a sample (bunch) of test curves. (The derivation is found in [*Evaluation of Stress-strain Test Results for effective use in Computational Analysis and Adequate Statistical Quantities curves*. Ralf Cuntze, M.A.N.-Advanced Technology Division München, and Gustav Löbel (Institute of Technical Mechanics, Erlangen. Germany). ICOSSAR 85 4th Int Conference on Structural Safety and Reliability, III-664→668]).

Test data recording: The material properties, usually extracted from recorded stress-strain curves are E_0, R and ε_{fr}. However, the amount of information contained in a nonlinear stress-strain curve is much larger. A complete storage of all curves is quite an effort. For numerical analyses, it would therefore be very advantageous to be able to work with only a few parameter values describing a substitute curve. So, for effective storing and processing of a large number of complete curves on a digital computer it is inevitable to substitute the test curves by analytical functions. In addition this leads to a representation, which is very suitable for computational analysis. The industry most often applies the well-known 3-parameter R-O function (*see Mil Hdbk 5, now MMPDS*), still used for aluminum before, that proved to be very suitable for composites (*the envisaged example*), too. The R-O function can be applied as mapping function (*Mind: In material data sheets like in the HSB R-O-parameters for strain-hardening are provided for metals*). For shear inter fiber failure IFF3 (torsion tests) it reads

$$\varepsilon_{hard} = \sigma / E_0^{\text{mode}} + 0.002\,(\sigma / \bar{R}_{0.2}^{\text{mode}})^n \rightarrow \text{example} \quad \gamma_{21} = \tau_{21} / G_{\|\perp} + 0.002 \cdot (\tau_{21} / \bar{R}_{0.2\,\perp\|})^n ,$$

and one can accept the excellent mapping quality of the R-O-function in the inelastic regime (hardening curve part. The four values E_0, R, ε_{fr} and n represent in compacted form the complete nonlinear behavior of the test specimen. The curve, or at least a good approximation, can easily be retrieved from them by the R-O formulas. By the way, the values E_0, R, ε_{fr} and R_{02} are also acceptance test values needed for quality assurance.

Statistical evaluation of a bundle of test curves: In *Fig.18-?* nine single stress-strain curves from identical tube torsional experiments made of the same CFRP-material are reproduced. For design analyses this vastly scattering bundle of curves has to be averaged. For the visualization: If we imagine all the curves being written by purling sand onto a surface, the result would be a hill shape, *Fig.18-? right*. The height of the sand hill at each point is a measure of the probability with which a single curve passes through exactly this place. And the ridge of the resulting hill defines a meaningful average curve $\bar{\varepsilon}\bar{\sigma}$ not to be mixed up with a mapping through the mean points, indicated by $\bar{\varepsilon}(\bar{\sigma})$ and described in Method I.

Method I: As a first naive trial it looks plausible simply to take the arithmetic averages of the curve parameters $\bar{E}_0$, $\bar{R}$, $\bar{\varepsilon}_{fr}$, $\bar{R}_{02}$ or $\bar{n}$, respectively. This method, described by $\bar{\varepsilon}(\bar{\sigma})$, fails due to the strong non-linearity.

Method II: not detailed here, because to being extremely complicate. *See ICOSSAR 85*.

Method III: To avoid the horrendous calculations necessary, within method II, a third procedure was developed with the following steps:

- harmonic averages for $\bar{E}_0$ from values $E_{0,i}$,
- harmonic averages for $\bar{R}_{02}$ from values $R_{02,i}$,
- arithmetic averages for R_i, $\varepsilon_{fr,i}$ with computing *n* using the averages above.

(*The harmonic average is a numerical average. It is calculated by dividing the number of observations by the reciprocal of each number in the series. Thus, the harmonic mean is the reciprocal of the arithmetic mean of the reciprocals. Steps to calculate the arithmetic average: Count the number of values in the set. Add all the values together. Divide the sum by the number of values in the set to obtain the arithmetic average.)*

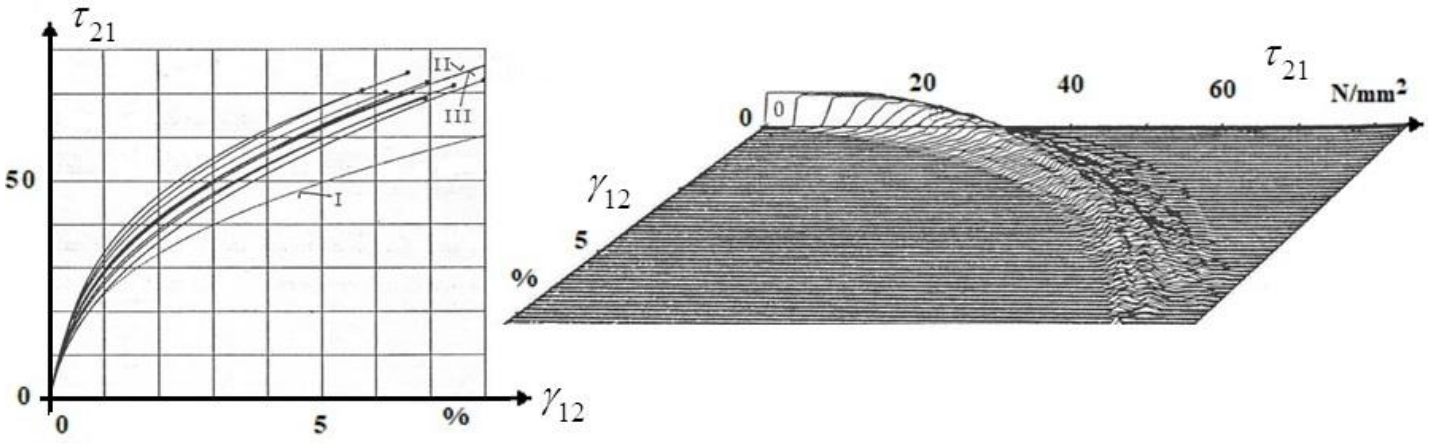

Fig.18-?: (left) R-O- 'reconstructed' curves from a torsion tube test specimen sample test. (right) Probability 'density hill' (fiber T300/ matrix EP)

Fig.18-? (left) shows the results graphically.

*As can be seen, Method I leads to a curve, which is not acceptable.

*The curve defined by the parameters according to Method II gives accurately what is wanted but this is not engineering-like.

*Method III renders the same, but with less effort and is therefore recommended for usual practice.

Is this really considered in design, In FEA codes like Always?

19 2D-Laminate Design: Determination of Tsai's 'Omni principal FPF strain failure envelopes

Aim: *Replacing the ply-by-ply proof of multiple-ply laminates by a much simpler method*

Steve Tsai's idea was to by-pass the effortful ply-by-ply analysis of multiple-ply laminates by using a so-called 'Omni-(principal FPF strain) failure envelope'. This envelope surrounds an intact Non-FirstPlyFailure (FPF) area whereby FPF includes Fiber Failure FF and Inter-Fiber-Failure (IFF).

Such an 'Omni failure envelope' is to determine for each composite material, applying a FPF-Strength Failure Criterion (SFC), and will capture all possible laminate stacks. Naturally, the used SFC significantly determines the shape of the envelope, see *Fig.19-1*.

Dimensioning is performed by showing that the design loading-caused principal strains are lying within the Non-FPF area. Thisidea can serve as a very practical Pre-design tool!

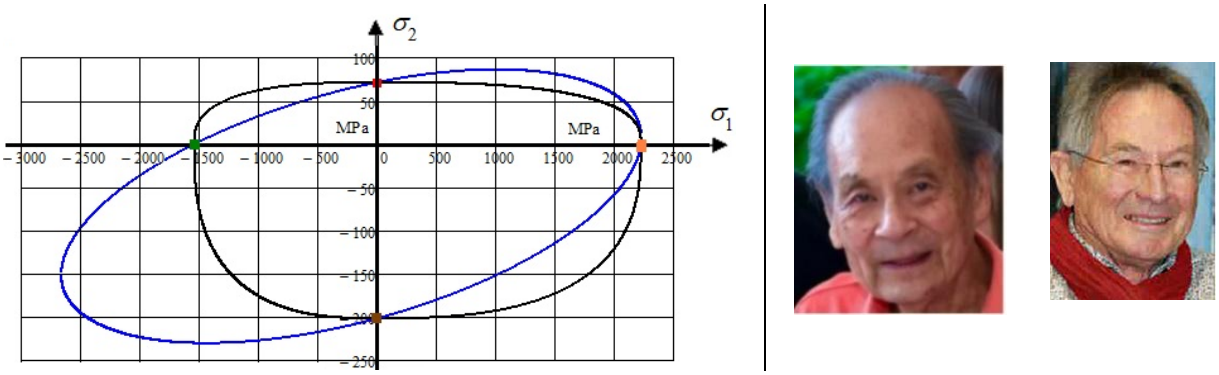

Fig.19-1: Cross-section $\sigma_2(\sigma_1)$ of the failure body, Tsai-Wu versus Cuntze

19.1 Tsai's indirect Determination of the 2D 'Omni envelope'

Fig.19-2 displays different 'butterflies' (*name, how the author Cuntze termed the bundle of* ***i*** *FPF-curves),* derived using the SFCs of Tsai-Wu and Cuntze). These numerical results of the FPF-linked

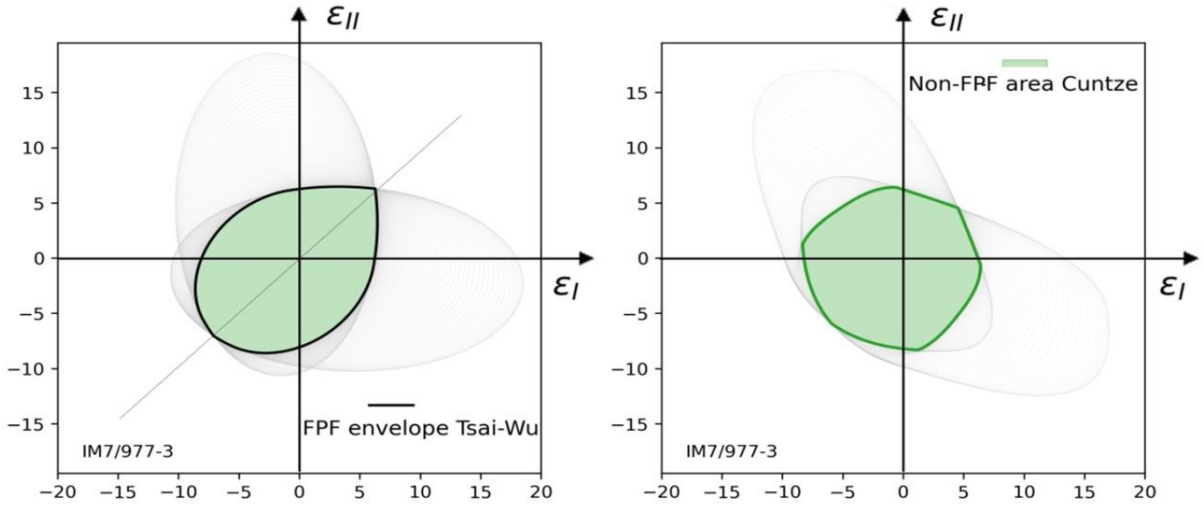

Fig.19-2, bundle of all FPF envelopes = 'butterflies veins': All ply FPF-envelopes enclosing a non-FPF failure area; 0°< α < 90° (91 ply angles). Principal strain in ‰, suffix FPF is skipped. CFRP IM7/977-3. In all pictures: (left) Tsai-Wu with $\mu_{\perp\square} = 0$, $F_{12} = -0.5$ and (right) Cuntze with $\mu_{\perp\square} = 0.2$, $m = 2.7$

principal strain curves clearly depict the significant effect of the chosen SFC, see above figure.
The different lateral properties determine the shape (wing edge) of the obtained symmetric 'butterfly' with its single, grey-marked principal strain curves provided by E. Kappel.

19.2 Cuntze's Determination of the 2D 'Omni Envelope'

The derivation of such an 'Omni failure envelope' is pretty effortful and no direct formulation could be found in the past. Recently, this bottleneck could be by-passed by an idea of the author, who examined various horizontal cross–sections τ_{21} = constant of the UD-FPF fracture body in *Fig.19-3* below. He found that τ_{21}=0 delivers the smallest Non-FPF area. ▶ Pre-Dimensioning can now be performed by showing that the design loading-caused principal strains are located within the Non-FPF area, a simpler pre-design of arbitrary laminates is possible.

.

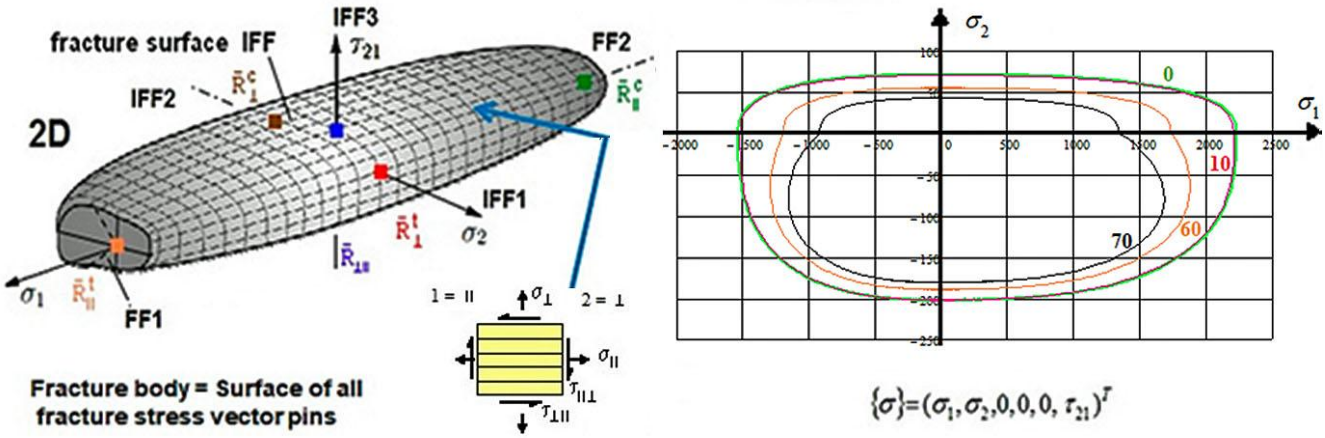

Fig.19-3: (left) 3D UD Failure body. (right) FPF-envelopes for 3 planes τ_{21}= const. CFRP IM7/977-3

Fig.19-4 (left) presents the resulting Omni principal strain FPF curves $\varepsilon_{II}(\varepsilon_I)$ with a not unambiguously solution $\varepsilon_{II}(\varepsilon_I)$ for each parameter level τ_{21} = const. → The failure curve $\sigma_2(\sigma_1, \tau_{21}=0)$ describes the 'Omni envelope'.

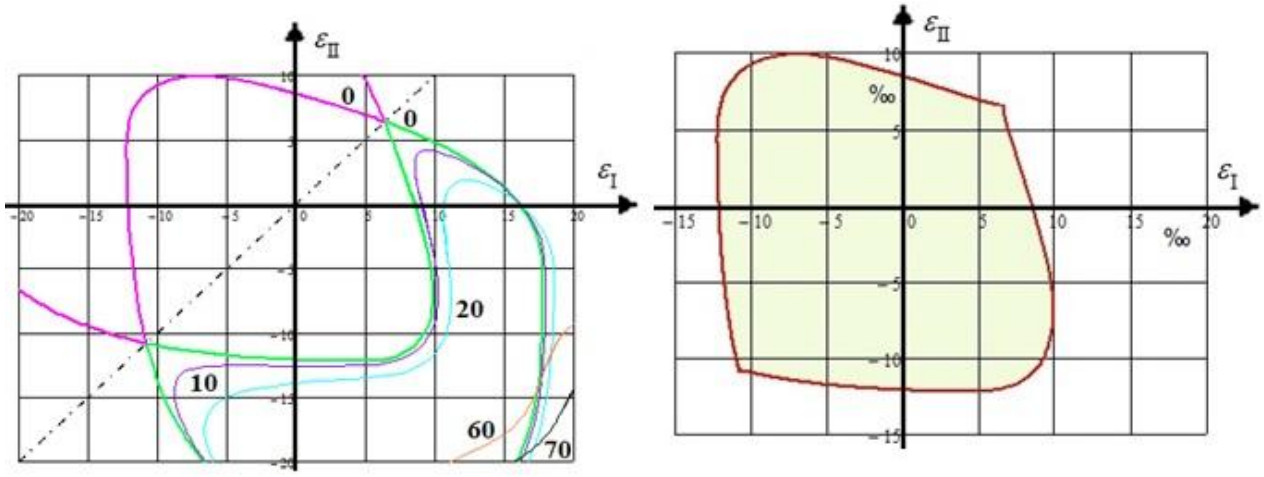

Fig.19-4: Mirrored envelope of the Non-FPF area (Cuntze procedure), CFRP IM7/977-3

Originally, the 'second' solution-linked additional outer curve parts were excluded in the graph and the right figure eventually shows the 'cleaned-up' envelope, representing the limit *Eff* = 100%, enveloping

the Non-FPF area. The cleaned-up graph is identical to the Non-FPF area obtained by the standard Tsai 'butterfly'-determination procedure.
Domains of the envelope could be dedicated to the locally faced failure mode types FF and IFF.

In a novel investigation, detailed in *Table 19-1*, Cuntze could give a complete look of the different envelopes in *Fig.19-4* (*left*). Depicted are the 'butterfly' wings (outside) and internally the green shadowed Non-FPF area. For optical comparison reasons E. Kappel 'traditionally' provided the 'butterfly' procedure plots for *Fig.19-4* (*right*) and *Fig.19-5*.

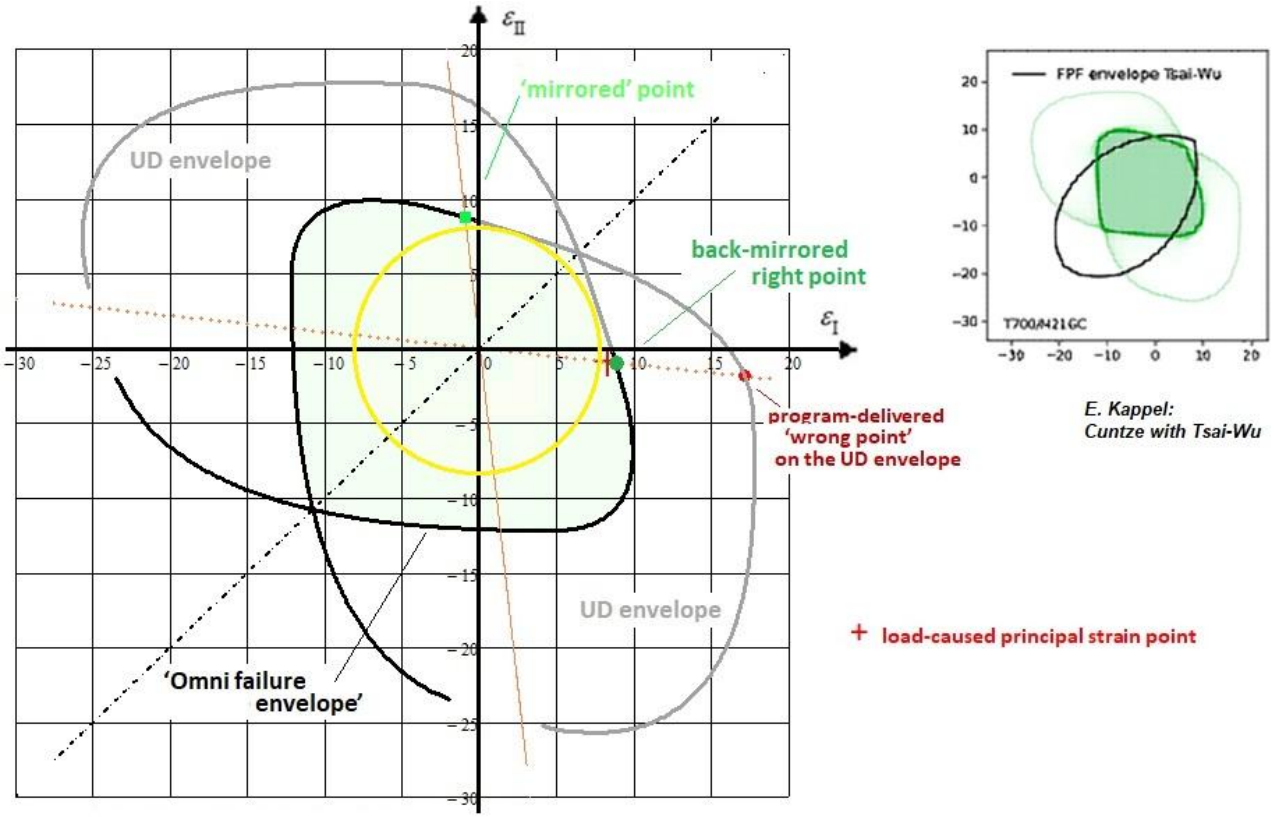

Fig.19-5: (left) Various envelopes of the Non-FPF area (Cuntze procedure following Principal Strain Procedure Cuntze in Table 19-1)..(right) 'Butterfly' and Non-FPF area applying the SFCs of Tsai-Wu and Cuntze

19.3 Pre-design Example using the 'Omni Non-FPF area' and Determination of Reserve Factor

Of highest interest is the reserve factor which must be smaller for a simplified design method than obtained by the classical 'Ply-by-ply procedure', thus remaining on the Safe Side. Laminate Design Verification is traditionally performed by above 'ply-by-ply' analysis, assessing the obtained ply (lamina) stresses $\{\sigma\}$ in the critical location of the most critical plies. Now, a simpler more global assessment is possible (*Table 19-2*) by using the in-plane principal strains of the laminate, strains

Table19-2: Procedure of checking a probably critical design stress state

A Non-FPF area within an 'Omni failure envelope' is given for the chosen laminate material
➢ FEA delivers the maximum state of the 3 strains of the laminate stack
➢ Transformation into the 2 principal strains as coordinates of the Non-FPF area
➢ Check, whether the strain point $(\varepsilon_I, \varepsilon_{II})$ lies within the envelope or Non-FPF area
➢ Determine material reserve factor f_{RF} = vector length ratio of *failure strain/design strain.*

which represent the loading. Such principal strains are a standard output of modern FE software. They are mathematical and not material symmetry-linked quantities.

Remember, please that the execution of the Design Check runs under the Presumption:
"*Linear Analysis, 'proportional stressing concept' $\sigma \sim \varepsilon$ is permitted*".

Table 19-1: Procedures, how to obtain the material reserve factor f_{RF}

SFC Cuntze: Failure Function $F\left(\{\sigma\},\{\bar{R}\},\mu \text{ directly}\right)=1$

$$Eff_{\text{FPF}} = [(Eff^{\|\sigma})^m + (Eff^{\|\tau})^m + (Eff^{\perp\sigma})^m + (Eff^{\perp\|})^m + (0)^m]^{m^{-1}} = 1, \quad m = 2.7$$

Input

$$\{\sigma\} = (\sigma_1,\sigma_2,\sigma_3,\tau_{23},\tau_{31},\tau_{21})^T \rightarrow (\sigma_1 = 900\ ,\sigma_2 = 20\ ,0,\ 0\ ,0\ ,\tau_{21} = 25)^{\text{T}}\text{MPa},$$

$$\{\bar{R}\} = (\bar{R}_{\|}^t,\bar{R}_{\|}^c,\bar{R}_{\perp}^t,\bar{R}_{\perp}^c,\bar{R}_{\perp\|})^{\text{T}} \rightarrow (2230,537,71,202,78)^{\text{T}}\ \text{MPa},\ \mu_{\perp\|} = 0.2.$$

$\{\sigma\}$-loading-caused ply strains and loading-reperesenting principal strains

$$\varepsilon_1 = s_{11}\cdot\sigma_1 + s_{21}\cdot\sigma_2,\ \varepsilon_2 = s_{21}\cdot\sigma_1 + s_{22}\cdot\sigma_2,\ \gamma_{21} = s_{66}\cdot\tau_{21}$$

$$\varepsilon_I = 0.5\cdot\left[(\varepsilon_1+\varepsilon_2) + \sqrt{(\varepsilon_1-\varepsilon_2)^2+\gamma_{21}^{\ 2}}\right],\ \varepsilon_I = 0.5\cdot\left[(\varepsilon_1+\varepsilon_2) - \sqrt{(\varepsilon_1-\varepsilon_2)^2+\gamma_{21}^{\ 2}}\right]$$

$$\varepsilon_I = 0.0083 \equiv \text{UD}\varepsilon\text{I},\ \varepsilon_{II} = f_\varepsilon\cdot\varepsilon_I = 0.0009,\ f_\varepsilon = \varepsilon_{II}/\varepsilon_I = -0.109.$$

*Stress Procedure Cuntze: Lamina task, solved by ply-by-ply failure analysis

$$Eff^m = [(Eff^{\|\sigma})^m + (Eff^{\|\tau})^m + (Eff^{\perp\sigma})^m + (Eff^{\perp\tau})^m + (Eff^{\perp\|})^m] \text{ with the mode portions inserted,}$$

$$Eff = \left[\left(\frac{(\sigma_1+|\sigma_1|)}{2\cdot\bar{R}_{\|}^t}\right)^m + \left(\frac{(-\sigma_1+|\sigma_1|)}{2\cdot\bar{R}_{\|}^c}\right)^m + \left(\frac{\sigma_2+|\sigma_2|}{2\cdot\bar{R}_{\perp}^t}\right)^m + \left(\frac{-\sigma_2+|\sigma_2|}{2\cdot\bar{R}_{\perp}^c}\right)^m + \left(\frac{|\tau_{21}|}{\bar{R}_{\perp\|}+0.5\cdot\mu_{\perp\|}\cdot(-\sigma_2+|\sigma_2|)}\right)^m\right]^{1/m}$$

$$\rightarrow Eff = 0.513 \Rightarrow \text{material reserve factor } f_{\text{RF}} = 1/Eff = 1.95.$$

*Principal Strain Procedure Cuntze: classical laminate task, solved by a laminate failure analysis; $\tau_{12} = 0$

Due to $\varepsilon_1 = \varepsilon_I$, $\varepsilon_2 = \varepsilon_{II}$ for the 2 failure determining stresses follows, $\gamma_{21} = 0$

$\sigma_1 = (s_{21}\cdot\varepsilon_2 - s_{22}\cdot\varepsilon_1)/(s_{21}^{\ 2} - s_{11}\cdot s_{22})$ and $\sigma_2 = (\varepsilon_2 - s_{21}\cdot\sigma_1)/s_{22}$ which is to insert into the FPF-criterion-based 'Omni principal strain failure envelope' formula

$$\left(\frac{(\sigma_1+|\sigma_1|)}{2\bar{R}_{\|}^t}\right)^m + \left(\frac{(-\sigma_1+|\sigma_1|)}{2\bar{R}_{\|}^c}\right)^m + \left(\frac{\sigma_2+|\sigma_2|}{2\bar{R}_{\perp}^t}\right)^m + \left(\frac{-\sigma_2+|\sigma_2|}{2\bar{R}_{\perp}^c}\right)^m + (0)^m = 1 = 100\%\ .$$

With the chosen SFC the $\rightarrow$ Non-FPF area $\varepsilon(\sigma_{FPF})$ is to derive .

On the strain beam $f_\varepsilon = \dfrac{\varepsilon_{II}}{\varepsilon_I} = \dfrac{\varepsilon_{II,\text{FPF}}}{\varepsilon_{I,\text{FPF}}}$ it will be finally obtained

$$f_{\text{RF}} = \sqrt{\left(\varepsilon_{I,\text{FPF}}^{\ 2} + \varepsilon_{II,\text{FPF}}^{\ 2}\right)} / \sqrt{\left(\varepsilon_I^{\ 2} + \varepsilon_{II}^{\ 2}\right)} = \varepsilon_{I,\text{FPF}}/\varepsilon_I = 1.06\ .$$

Cuntze's direct determination of the 'Omni failure envelope' enables to determine the reserve factor straightforward instead of using the *Non-FPF smaller* internal circle in *Fig.19-5,* how it was usually performed up to now, see [*Cun 24a, c*].
However, there was a solver computational problem:

Mathcad unfortunately delivers a principal failure strain value ε_{FPF} outside of the Non-FPF area as result of its solution process. The other solution seems to be received, if a shear strength is involved. This wrong point value can be localized on the UD 'butterfly wing' edge in *Fig 19-4* and this enabled to successfully use the symmetry of the envelope as it is executed in *Fig-19-5*.

Now, Design Verification can be performed as described below:

$$f\varepsilon = \frac{\varepsilon II}{\varepsilon I} \qquad f\varepsilon = -0.109 \qquad UD\varepsilon I = 0.0083$$

Vorgabe $\qquad \varepsilon IFPF := 0.01 \qquad \sigma 1 := 100 \qquad \sigma 2 := 10$

$$\boxed{\varepsilon IFPF = s11\cdot\sigma 1 + s21\cdot\sigma 2} \qquad \boxed{f\varepsilon\cdot\varepsilon IFPF = s21\cdot\sigma 1 + s22\cdot\sigma 2}$$

$$\left(\frac{\sigma 1 + |\sigma 1|}{2R1t}\right)^{mint} + \left(\frac{\sigma 2 + |\sigma 2|}{2R2t}\right)^{mint} + \left(\frac{-\sigma 1 + |\sigma 1|}{2R1c}\right)^{mint} + \left(\frac{-\sigma 2 + |\sigma 2|}{2R2c}\right)^{mint} = 1$$

$A\varepsilon := Suchen(\varepsilon IFPF, \sigma 1, \sigma 2) \qquad \varepsilon IFPF := A\varepsilon_0 \qquad \varepsilon IFPF = 0.01712$

$$f\varepsilon = -0.109 \qquad fRF\varepsilon := \frac{\varepsilon IFPF}{UD\varepsilon I} \qquad \boxed{fRF\varepsilon = 2.07}$$

This result of the Mathcad program leads to a value which belongs to another solution brunch (see the figure). Using the plot's symmetry the real value can be found after the replacement of fε by fεr = 1/ fε

$$f\varepsilon r := \frac{1}{f\varepsilon} \qquad f\varepsilon r = -9.214 \qquad fRF\varepsilon r := \frac{\varepsilon IIFPFr}{UD\varepsilon I} \qquad \boxed{fRF\varepsilon r = 1.06}$$

$$< \boxed{fRF\sigma = 1.95}$$

Fig.19-6 Successful computation of f_{RF} after utilizing the plot's symmetry (code Mathcad 15). $\varepsilon_I \equiv UD\varepsilon_I$

LL:

** The method is more or less a linear method.*

** The investigation of various cross–sections τ_{21}=constant, proved, that τ_{21}=0 delivers the smallest Non-FPF area, thus making a simpler pre-design of arbitrary laminates possible*

** Basic result:*

The principal strain approach delivers the required smaller reserve factor compared to the conventional ply-by-ply stress-based procedure. → *The approach is 'on the safe side' !*

(My successful idea was a welcomed Christmas gift for Steve, 2023).

Note, once again please:

Tsai's 'Omni principal strain envelope' principally surrounds a Non-FPF or even a Non-LPF area.

*FPF is required if the design requirement asks to fulfill a First-Ply-Failure in the critical locations of the plies of the laminate.

*LPF, if to apply, is required to fulfill a Last-Ply-Failure limit. However, this usually involves a non-linear analysis up to the ultimate failure load of the structural part.

In order to cope with the reserve factor definition these shall be sketched again below:

About 'linear' FPF, then a stress-defined $f_{RF} = \dfrac{\text{Strength Design Allowable } R}{\text{Stress at } j \cdot \text{Design Limit Load}} > 1$

For completion of §19,

a to be designed not unusual thick multi-ply laminate is displayed below:

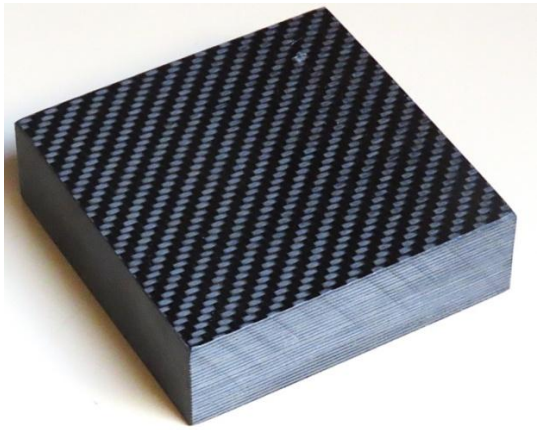

Many thanks to Steve for the remark below:

Von: Stephen W. Tsai [mailto:steve.tsai@mac.com]
Gesendet: Samstag, 17. Mai 2025 19:04
An: Ralf Cuntze
Cc: Chiara Bisagni; Dransfeld Clemens; Urs.Meier@empa.ch; Erik.Kappel@dlr.de; w.wagner@kit.edu; Michael Windisch; Meinhard Kuna; klaus.rohwer@dlr.de; permanni@ethz.ch; christian.huehne@dlr.de; joachim.hausmann@ivw.uni-kl.de; ingo.ehrlich@oth-regensburg.de; michael.magin@ivw.uni-kl.de; t.weber@fh-aachen.de; GABO05@libero.it
Betreff: Re: My private scientific papers: Excerpt from my overall CV

Dear Ralf,

I have never seen a master piece of work that you have shown to be possible. An incredible contribution treatise of the failure of composite materials.. You have set a standard that others have to learn to meet.

Congratulations for your achievement.

Steve

ICCM V, San Diego

San Diego 1985
Tuesday, July 30, PM
Mechanical Properties of Composites I
ROOM: Council/Chamber

Chairman: Dr. Steven Tsai, Chief, Mechanics & Surface Interactions Br., AFWAL, Wright-Patterson AFB, OH 45433
Vice Chairman: Dr. R. Cuntze, MAN - Nene Technologie, AbC, EGS, Dachaner Str. 667, Post fach 500620, D-8000 Munich 50, West Germany

40 years now

Below an associated Abstract for the annual

"Munich Symposium on Lightweight Design 2025"

Engineering Strength Assessment of UD-multiply-composed Elastic Laminates

Ralf Cuntze, Prof. Dr.-Ing. habil., supported by Erik Kappel, Dr.-Ing.***
* *Retired from industry, MAN-Technologie, Augsburg, Germany*, Ralf_Cuntze@t-online.de
** *Institute for Lightweight Systems (SY), German Aerospace Center (DLR), Braunschweig*

In practical multiply-laminate development there are to capture so-called 'Quad-stacked' laminates of the (0 / 45/90/-45)-family and Tsai's novel 'Double-Double-stacked' laminates of the $\{\varphi/-\psi/-\varphi/\psi\}$-family *(NCF, stitched layers product)*. Due to the fact, that these laminates are just in-plane loaded it is very helpful for a structural engineer to have 2D Design Sheets, at least for checking Finite-Element-Analysis results of arbitrarily-stacked multi-ply laminates. Since strength failure envelopes significantly depend on the applied Strength Failure Criterion (SFC) exemplarily two SFCs, those of Tsai-Wu and Cuntze are examined, which requires a challenging transformation of the Tsai-Wu SFC into the more often used notation of the *VDI 2014 guideline*.

An idea of Stephen Tsai is followed on 'Designing Laminates to First-Ply Failure (*FPF*)', which includes Fiber Failure (FF) and Inter-Fiber-Failure (IFF) and thereby marks the 'Onset-of-fracture'. When realizing this, failure stress-based 'Omni-(principal strain) failure envelopes' (*term from S.Tsai*) are to derive. These envelopes surround the intact 'Non-FPF area'. The process requires that combinations of each ply orientation angle with principal strain ratio (here 361, chosen 1°-increment) are to evaluate. Thereby the smallest reserve factor determines the FPF limit and thereby generates one point on the bias-symmetric envelope. Each computation represents a faint 'vein' in *Fig.1*, ($‰$). The principal strain approach delivers the required smaller *laminate* reserve factor compared to the conventional ply-by-ply stress-based procedure with its minimum *ply* reserve factor. The approach is 'on the safe side' if $f_{RF}^{lam} < \min f_{RF}^{ply}$!

The determined Non-FPF areas are further reduced to an internal circle in order to find a FPF-limit-defining envelope-function for the computation of the laminate reserve factor. The circle's radius depends on the principal strain magnitude $r = min\sqrt{\varepsilon_I^2 + \varepsilon_{II}^2}$. Cuntze sorted out a function for the envelope, because he found that $(\sigma_{\parallel} = \sigma_1, \sigma_{\perp} = \sigma_2, \tau_{\perp\parallel} = \tau_{21} = 0)$ defines it. This means that the full area can be exploited for f_{RF}^{lam}, not just the internal circle area, *Fig.2*.

A thereon based design sheet would enable to reduce the effort for Design Dimensioning.

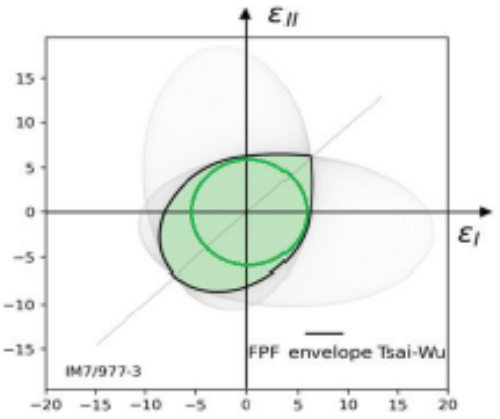

Fig.1:Faint 'Veins' of all computations for IM7/977-3 forming the merely visible veins of a butterfly's wing

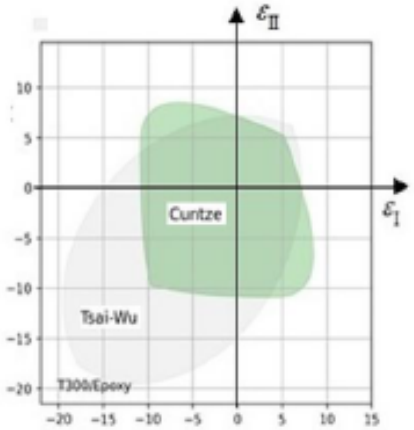

Fig.2: SFC-dependent Non-FPF areas for T300/Cytec (Tsai-Wu bottleneck in negative domain)

20 Note on Criticality of Fiber Micro-Fragments and Dusts of CFR-Plastic/CFR-Concrete

Matter of my heart:

Supporting the application of sustainable carbon concrete with low-risk PAN-CFs in Production and my special concern regarding Recycling.

Carbon Fibers (CFs) usually are produced using the precursors Polyacrylonitrile (PAN) and Pitch. Problem and question: Machined Pitch CFs generated many toxic split-up fiber fragments. What about the PAN-based CFs? They can be classified into the types: intermediate-modulus (IM), high-modulus (HM) and ultrahigh-modulus (UHM), whereby UHM-CFs seem to show some and the lower modulus Standard PAN no hazard. These facts ask for an investigation of the UHM-CF with the objective to finally sort out that the use of the less '*risky*' Standard PAN CF causes no threat.

Inhaled particles with its size, geometric shape and contaminants adhering to the surface are relevant for a health effect. Of course, targeted workplace prescriptions always have to counteract the occurrence of excessive stress on the lungs from inhaling too large amounts. Respirable bio-persistant particles accumulate in the alveoli of the lungs. These so-called 'WHO fibres' pierce the macrophages in the lungs and can migrate into the abdomen and pleural tissues and cause cancer.

CF application in Construction

As structural engineer, who has founded and led two working groups in the carbon concrete sector for 10 years: "*It is my deep wish to use more fatigue-resistant [VDI2014] PAN-CF in the construction industry in order to increase the life of bridges and to save concrete, a composite material, which has a negative CO_2 footprint due to the necessary clinker (cement constituent) production*."
The next figure displays a CFRP application by a fiber grid (*mat*) as a slack reinforcement (*no pretension*) of a bridge.

Fig.20-1: Bridge Wurschen, 2022: (left) Superstructure made exclusively of carbon concrete, shell construction. (right) Textile FRP mats in the super-structure) (Foto: Stefan Gröschel, IMB,TU Dresden)

Note: Full exploitation of the Carbon Fiber (CF) is only to achieve by pre-tensioning, which will advantageously compress the usual low tensile strength of the matrices concrete and plastic. Just pre-tensioning of plates is still series production.

Carbon Fiber Production

CF-properties strongly depend on the production process and above precursors which need different conditions but the essential processes are similar. A CF requires a heating and stretching treatment to get the high strength products. A thermoset treatment is first applied in the temperature range from 200 to 400 °C in air under stretching to get the stabilized fiber, followed by a carbonization process in the temperature range from 800 to 1500 °C in oxygen-free condition to remove impurities and to improve

the crystallinity of carbon. To further improve the performance of CFs, a graphitization process is required to graphitize carbonized fibers with temperature up to 3000 °C. During these processes, stretching is required to get preferred orientated carbon crystals, because the crystal alignment makes the fiber incredibly strong and stiff. The graphitization process leads to differences between PAN and Pitch and within the PAN-CFs. This will be later of interest.

The very expensive Pitch CF is mainly used in spacecraft and antennas. The market is dominated by the PAN-CF. With regard to possible toxic fragments, PAN-CF (Ø 7 µm, usually) is therefore of interest, especially the 'highly' graphitized UHM-PANCF such as Torayca's M60J, which comes next to the Pitch-CF considering the tensile modulus (stiffness). CF tensile modulus and fracture toughness naturally depend on the fabrication regarding precursor, on carbonization and graphitization. Furthermore, Pitch-CFs are more layer-like in their crystal structure in contrast to the more granular PAN-CF. This probably further explains the higher tensile modulus compared to the PAN-CF. Knowing the different crystal structure is therefore important for explaining the splintering process, originator of possible toxic fragments.

‘WHO-Fiber’ criticality

WHO criterion for respirable fibers: ‘WHO-Fiber‘ ≡ tiny fragment of a filament with a diameter Ø of less than 3 µm, a length L of greater than 5 µm and a length-to-diameter ratio of L/Ø > 3:1.

Naming Fiber: (1) Does not address a long CF, which of course never meets the WHO criterion. (2) Asbestos fiber, for example, is just a fiber-like looking particle, which may break into above tiny WHO-size fragments).

Too many dust-related particles, smaller than the WHO 'fiber' size, can also cause a hazard. A so-called Particulate Matter of the µm-size PM2.5 can penetrate into the alveoli and ultrafine particles with a diameter of less than 0.1 µm (*Corona virus size level*) can even penetrate into the lung tissue. Aerosol particles from the environment have diameters ranging from about 1 nanometer (nm) to several 100 micrometers (µm). Larger particles quickly sink to the ground, particles smaller than 10 µm can remain in the air for days.

The figure below summarizes the topics faced when considering the criticality.

The macrophage lifespan of a few weeks is one of the decisive factors for the success of disposal or 'cleaning'. ‘WHO-fiber’-pierced macrophages usually die.

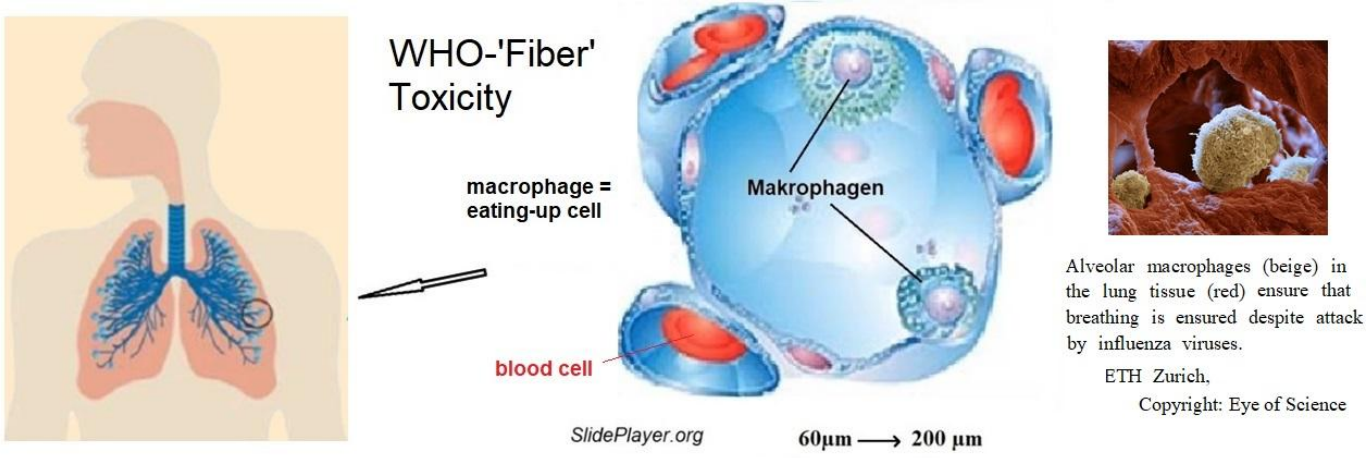

Fig.20-2: Effect of WHO-‘Fibers'

A distinction must be made between long fibers, micro-fragments of fibers such as the ‘WHO-fiber' size, as well as the micro-fragments of composite constituents, i.e. fiber-reinforced polymers FRP or fiber-reinforced concrete FRC. In addition to the fiber, the matrix with the interphase material in the fiber-matrix interface must be considered, too.

Criticality-relevant variables are geometry and bio-resistance:

Geometry: Critical are the already defined ‘WHO-'fiber', as well as dusts and fiber fragments with Ø < 3µm, which penetrate directly into the alveoli and the lung tissue. Since the ‘WHO-fiber’ size is smaller than the diameter of common CFs, the fiber fragment must experience a reduction of the diameter. This can happen by splintering or by burning. CF is not toxic per se!

Bio-persistance: High bio-persistance causes high toxicity, a low bio-solubility in living organisms already speaks as an indication of possible carcinogenicity. Fragments with short residence times that are quickly dissolved or removed are less risky.

Only if a sufficiently high amount of CF-‘WHO-'fibers' is produced and inhaled there is a potential for danger, whereby the following applies:

Risk = hazard potential (severity) probability of occurrence.

Hazard potential = exposure to CF-WHO (size) particles combined with toxicity.

The duration of the exposure in terms of quantity and the possible frequency of occurrence of the event per unit of time are therefore decisive.

Generation and Counting of WHO ’fibers’

A quantity for the risk assessment delivers the counting of the fragments which are generated in machining processes. Question: *Which machining processes seems to be the worst for the generation of ‘WHO-fiber' shaped CF particles, faced in production and recycling*?

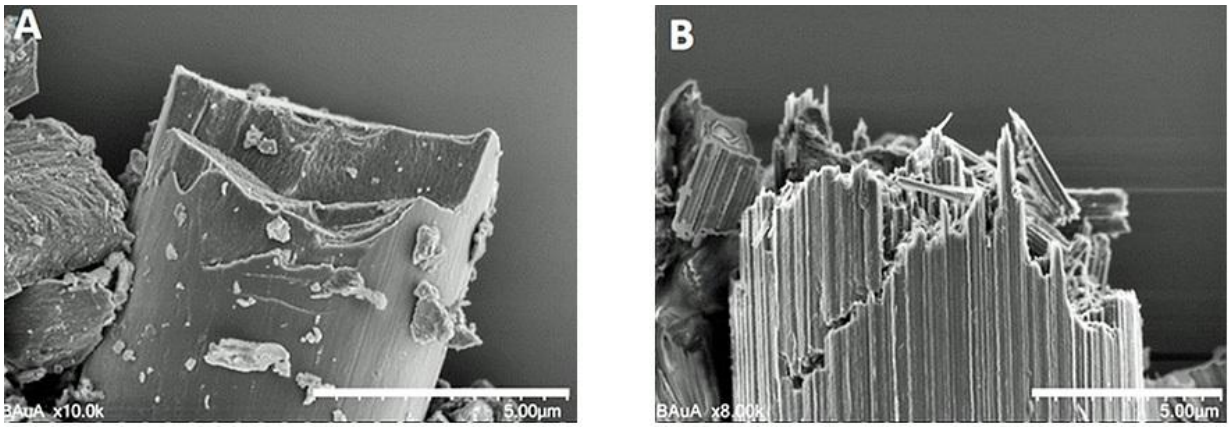

Fig. 20-3:(left) PAN-based, (right) Pitch-based. (Courtesy BAuA, Berlin)

Some answer is given in the BMBF research project *CarboBreak* (*headed by BAuA: the Federal Institute for Occupational Safety and Health conducts research for a safe, healthy and humane working environment*): Investigation of the release behaviour of respirable fragments made of pure fibres and fibre composites (*consisting of CF, sizing, matrix etc.*) under mechanical stress. Basically here, rovings were subjected to an extreme mechanical stress in a so-called ball vibrating mill (*an assumed 'worst case' machining process*), the resulting CF fragments were evaluated with regard to their morphology and then the WHO 'fibers' counted, namely the ‘WHO-Fiber’ quantity / unit volume. The CF portion is considered to be the critical part of the full composite. One significant finding was the different splintering process between PAN (left) and Pitch CF (right).

Fact & idea:

(1) Pitch fibers are obviously more dangerous because they do extremely splinter. Since the UHM-CF comes closest to the pitch fiber in terms of stiffness of all PAN-CFs, the PAN-UHM represents the more critical PAN CF in terms of risk of splintering.

(2) A CF-parameter is being sought that could be a parameter for explaining the fiber splintering hazard and finding a characteristic.

The sought-after, splinter hazard-descriptive parameter could be the fracture toughness. This property is likely to show some difference in relatively similarly stiff (Young's modulus) brittle materials. *The author lectured fracture mechanics, which he also had to apply at MAN*. His test proposal was a micro-fracture mechanics investigation of a laser-notched single fiber to determine the different brittleness based on the fracture toughness values of K_{Ic} to be measured. In fracture mechanics, fracture toughness describes the resistance of a material to unstable crack progression An ultra-high graphitized UHM PAN CF such as Torayca's M60J is to be basically investigated, because it is to place narrowest to the behavior of the critical Pitch-Fiber.

Asssumption: *Different fracture toughness values indicate different risk of splintering*.

*The proposed test specimens, together with the difficult notching of a single CF by a laser beam, have already been realized in Kaiserslautern by the institutes IVW with PZKL!

*The search for a fracture mechanics model that allows us to estimate the fracture toughness of a CF is essential for the qualitative differentiation of the envisaged fibers. A formula will provide a not realistic ‘exact’, but a quantified relationship which is fully sufficient.

The searched characteristic for the tensioned notched test specimen is the so-called critical stress intensity factor (SIF) K_{Icr} (= fracture toughness), at which unstable crack progression begins. Its formula reads $K_{Icr} = \sigma_{fracture} \cdot \sqrt{\pi \cdot a_{cr}} \cdot Y$, with the so-called geometry factor Y taking the fact into account that the SIF value is theoretically independent of the dimensions of the test specimen only for infinitely large plates. Therefore, the corresponding function Y must be sought for the intended test specimen 'Notched Single Fiber'. This was made possible by the author-available Manual "*NASGRO Reference Manual Version 9.01 Final; December 2018. Fracture Mechanics and Fatigue Crack Growth Analysis Software*".

The application of the full model requires several assumptions:

- CF is a very brittle material
- The crack instability, expressed by the formula, can be applied at the µm-level (micromechanics) for these brittle materials!
- The cross-section, cut by the laser beam, is just a circle section but can be transferred to the elliptical shape of a typical crack
- The 'model for a full cylinder' given as SC07 in the NASGRO document is applicable. Experience has shown that the impact is small, the model can be used also in the µm range
- The crack depth a is given by the laser notch depth.
- Diameter D = Ø = 0.007 mm, UHM 60J.
- The applied stress $\sigma_{fracture}$ at the fiber ends = breaking tensile force F / area A
- The cross-section cut by the laser beam can be transferred to the elliptical shape of a typical SC07 crack. The difference in surface area is neglected because it is the same for all tested fibers. In the SC07 associated Table C15: For R/t = 0, i.e. a solid cylinder with R = 0 (*t = wall thickness = R),* approximately to be expected a/t = 0.3, gives c/t = 0.35 and thus Y = 1.6.

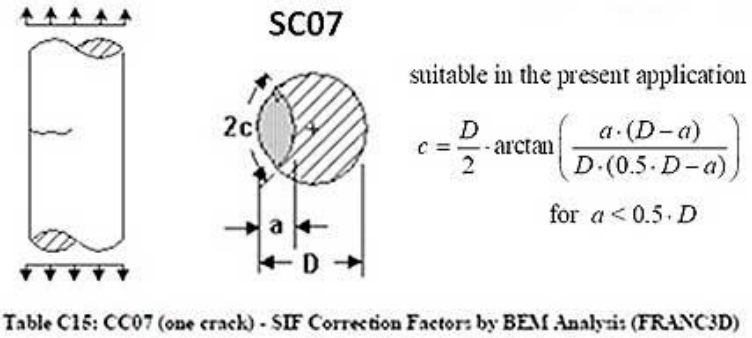

Fig. 20-4: Thumbnail crack in a solid cylinder. Surface crack case SC07
*Manual NASGRO Reference Manual Version 9.01 Final; December 2018***.**
Fracture Mechanics and Fatigue Crack Growth Analysis Software

The author's big **wish**, driven as a GROWIAN wind turbine co-responsible (*about 1980*), in view of future fear-spreading media about a wind turbine fractures with blades made of standard CFs, i.e. not UHM-CFs:

Submission of an 'official recommendation' by the BAuA, together with Composites United (CU), including adapted recycling safety requirements. on working with CFRP in general and specially on PAN-CF carbon reinforced concrete.

.

LL:

*** The test idea could be fully realized, which is a seldom experienced luck when testing.*
Unfortunately there is no deeper research ongoing, which would give the basis for the realization of the author's desire to open the CF-market in construction by providing an answer to the many sensitivities, published in media, concerning new carbon fiber-reinforced products.

Read in Sikkim, about 2011 !

Personal Note on Oil consumption in CF-production and Carbon Concrete Recycling (rCF)

Fig.20-5 shall give a survey about the portions of the structural materials in the market, dated 2016. It shows how insignificant the carbon fiber content presently is in relation to its origin oil and to the material competitor steel. A yearly CF output of 50000 t equals 4 min steel production (2018). The

yearly concrete production equals oil production. This is of basic interest and helpful for many discussions. CF is not yet a real market in construction, basically due to the present regulations of the authorities which does not permit a faster gain of knowledge which is always the result of widespread application, only.

Of course, if the concrete mass saving Carbon Concrete market will become significant (*presently about 100.000 t / year*), then the CF-production has to be multiplied.

In the context of this chapter's focus and considering recycling: (1)*Why is this marginal crude oil consumption very often considered to be very harmful to the environment. (2) Why must Carbon Concrete be recycled by separating the CF and thereby downgrading it to rCF! T*he author does not consider it reasonable for ecological and economic reasons to extract CF – as required by the current regulations – from shredded carbon concrete parts instead of bringing the recycled CF material parts together with the multifold concrete content into the superstructure of a bridge or street. For safety reasons one can provide measurements of the traffic-generated abraded dust if no further cover is foreseen and the official recommendation above is not yet available.
If basalt fibers BsF will reach a general approval from sustainability reasons they would be much better ecologically and economically due to the fact that enough base material is available. Added ZrO_2 is foreseen to provide alkali resistance. Unfortunately, the available reliable property knowledge is not made public. Of course, the production of carbon fibers still requires energy. However, this will also be the case if carbon fibers are produced from natural fibers in the future.

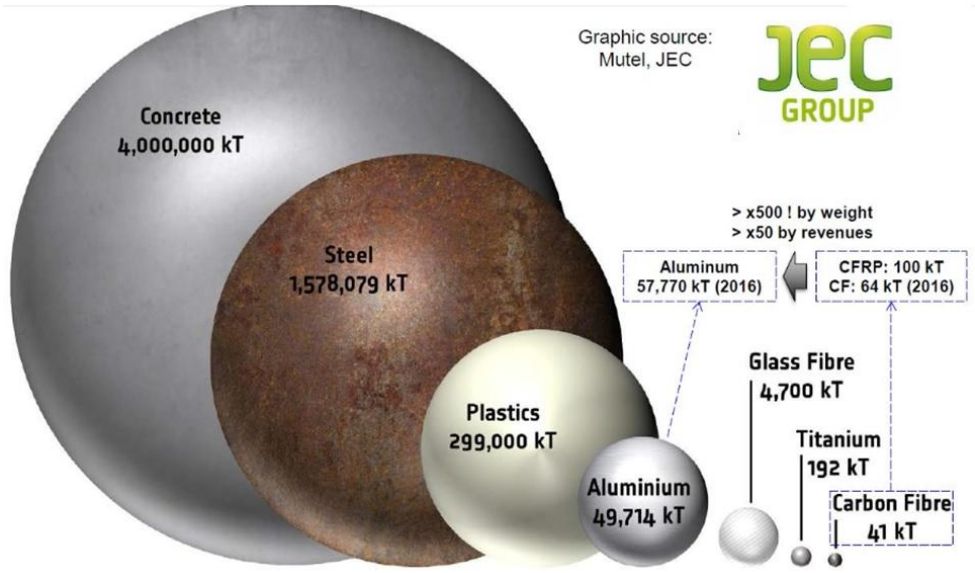

Fig.20-5: Weight ratios of structural materials, year 2016

Please keep in mind:
40000 tons carbon fibers would require just about 40 /4,000,000 = 0.001 % crude oil.

CF total / Steel = 1/10000.
In Germany it is CF total / concrete reinforcing steel ≈ 0.1%.
Concrete / crude oil = 1, GF / CF = 100.
Single car consumes about *1 t oil / year.*

rCF = Erhalt einer faserlängenverteilung, so dass ein Festigkeitsverlust gegenüber langen Fasern die Foge ist, also degradation eingetreten ist. Außerdem darf Dauer- und Dauerstandfestigkeitsverlust durch die notwendige Matrixüberleitung - infolge kurzer rCF - von Kräften nicht vergessen werden beim Design. rCF-Gewinnungskosten sind hoch durch hohen Energieverbrauch mit Sortierung und sind preislich relativ gleichwertig zu jungfräulichen CF.

21 A novel Determination of the Residual Strength *R*res, non-cracked, Fatigue Phase 2

Aim: *Derivation of a procedure to determine and rendering the design-significant residual strength value R*res

21.1 General for a Proof of Structural Integrity in Projects

Residual strength *Rres* is the fracture stress after pre-damage and re-loading. Not only in mechanical engineering design but also in civil engineering residual strength values are required such as in soil mechanics or for UD-hangers of a railway bridge at Stuttgart, below a hanger or for tension rods of cranes.

Fig.21-2 Stuttgart Stadtbahn bridge. World's first network arch railway bridge (127 m) that hangs entirely on tension elements made of carbon fiber-reinforced plastic (CFRP). The 72 hangers are produced by Carbo-Link AG

The value is of basic interest, because – due to authority demands - Design Ultimate Load is to sustain even after a distinct fatigue life. The residual strength task is one task to demonstrate structural integrity.

This subject is linked to cyclically micro-damaged structural components (*Phase 2 of fatigue life, strength tools applied*) and macro-damaged ones (*Phase 3 of fatigue life, fracture mechanics problem, damage tolerance mechanics tools applied*), as displayed in *Fig.21-2*. The cyclic loading may range from constant amplitude-loading up to spectrum-loading and has to capture proportional and non-proportional loading scenarios.

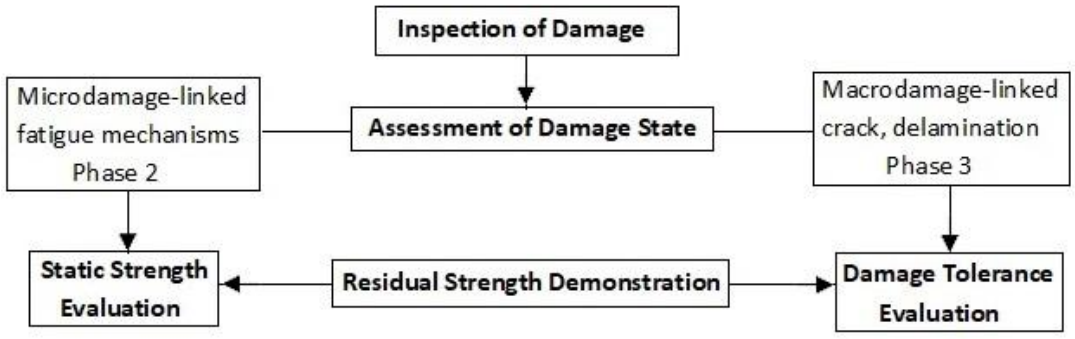

Fig.21-2: Ways of residual strength determination

This task especially comes up in cases such as: A multiple site damage phenomenon is faced with aerospace components such as fabrication-induced flaw clouds (fatigue strength problem, Ariane 5 Booster wall) or real short-crack 'clouds' from e.g. multiple rivet holes in stringer-stiffened panels of aging aircraft components (fracture mechanics problem). Here, the focus is on the Phase 2 residual strength *Rres*. Mind: R_{res} should not be confused with *residual stress* σ_{res}).

In some projects a number for the residual strength at a certain operation cycle value is required. This is well known from impact cases of laminated panels. There, a Compression-After-Impact (CAI) test is to execute after the impact event because the impact may result in a barely visible external damage and it may generate a dramatic reduction of compressive strength due to separation of layers resulting in a large bending stiffness loss. Regarding crack-linked fatigue life Phase 3 residual strength problems the reader is referred to fracture mechanics.
Residual strength tests are long-lasting and expensive. Therefore, procedures are searched that help to reduce the test effort if enough physical knowledge is available.

First step is to map the relevant SN-curve (Wöhlerkurve) by taking the widely used 4-parameter Weibull function

$$\text{stress ratio } R = \sigma_{min} / \sigma_{max} = \text{constant}: \quad \sigma_{max}(R,N) = c1 + (c2 - c1) / \exp(\log N / c3)^{c4}.$$

(stress ratio → straight letter R, strength→ bias letter *R*).

A SN-curve describes the relation between the cyclic loading and the number of cycles to failure *N*. On the horizontal axis in *Fig.21-3* the number of cycles to failure is given on logarithmic scale. On the vertical axis (*either linear or logarithmic*) the stress amplitude $\sigma_{amplitude}$ of the cycle is often given. In the case of brittle materials *sometimes the maximum stress* $\sigma_{max.}$. The provided mean SN-curves, R = constant, base on the fatigue test measurement types 'pearl-chain testing' or 'horizontal load level testing'. Fatigue curves are given for un-notched test specimens (K_t = 1) and for notched ones, the loading can be uniaxial or multi-axial. Considering residual strengths, measurements on the vertical axis at *n* = constant are required.

In design verification very often as fractile (quantile) numbers, representing the failure probability p_f, 5% or 10% are taken in order to capture some uncertainty compared to the average of 50%. For the loading side the design FoS *j,* in construction *γ,* capture the uncertainty of the loading. The residual strength design verification has to meet Design Ultimate Load. Following HSB 62200-01 the determination of the static residual strength for single load paths must be made with statistically significant A-values; for possible multiple load path structural parts B-values may be used.
Moving to the required statistical properties some notions are to depict. Capturing the uncertainty of the resistance quantities, the following is performed: Denoting P the survival probability and C the confidence level applied, when estimating a basic population value from test samples, partly enriched by some knowledge of the basic population. Regarding C a one-sided tolerance level it reads:

Static → Statistical reduction of average strength from (P= 50%, C= 50%) to e.g. (B-value: P = 90%, C = **95**%).
Cyclic→ Statistical reduction of average SN curve from (P=50%, C= 50%) to e.g. (P= 90%, C= **50**%).

All this is executed to keep a generally accepted survival reliability of about $\Re = 1 - p_f > 1 - 10^{-7}$.

21.2 Classical way to determine Rres

Determination via the interpretation "*The course of the residual strength is the difference of the static strength* and *the maximum strength* $\sigma_{max}(N)$ *of an SN curve* R", see Fig.21-3. This leads to the formulation $R_{res} = \sigma_{max}(N) + [R^t - \sigma_{max}(N)] \cdot \rho(n)$ with $\rho(n) = 1-(n/N)^p \equiv 1-D^p$,
where the exponent p describes the decay of the residual strength capacity and D the micro-damage quantity, (see Hahne C: *Zur Festigkeitsbewertung von Strukturbauteilen aus Kohlenstofffaser-Kunststoff-Verbunden unter PKW-Betriebslasten*. Shaker Verlag, Dissertation 2015, TU-Darmstadt).

Fig.21-3 depicts for R = 0.1 the mean (average) 50% SN-curve and the 90% SN-curve. The residual strength curve *Rres* is given for the point (10^5 cycles, σ = 34 MPa). The stress σ belongs to a so-called 'one stage test' or constant amplitude test. Regarding the residual strength value at the 90% SN-curve the question arises: "*Where does the necessary statistical basis for a reduced SN-curve come from, if not sufficient test series on vertical and horizontal levels were run*"?
Due to missing test data a test data-based work case cannot be presented. Therefore, the author tried to figure out a procedure which gives an understanding of the subject.

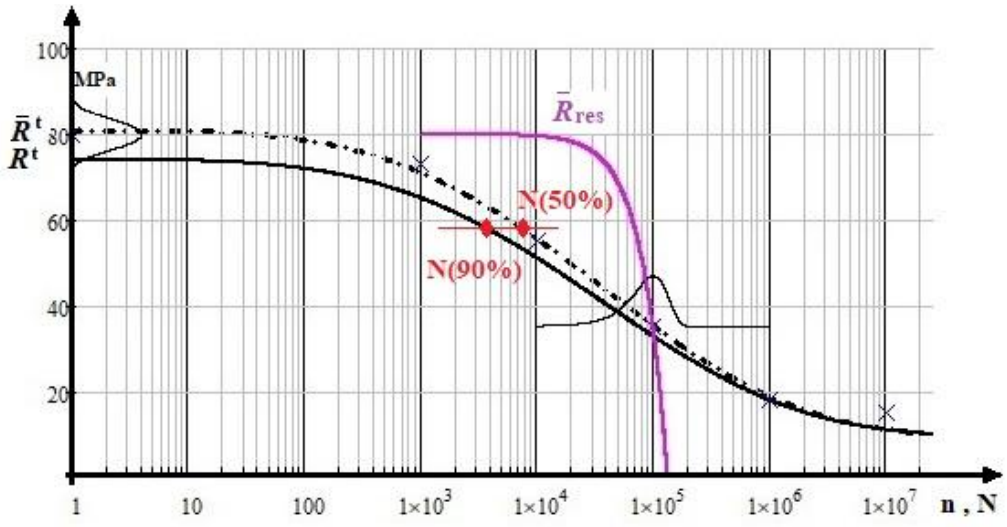

Fig.21-3, Schematic example, uniaxial loading: R= 0.1. $\bar{R}_{res}$ *is mean tensile residual strength*

21.3 Idea Cuntze, probabilistic way to determine a 90% value by using the convolution integral

A possibility to determine a 90%-value is given by the application of the so-called convolution integral, using density distributions of R_{res} and of N with just a little hope to find the distribution measured, Fig.21-3. The output of the mathematical expression convolution integral represents the probability of failure p_f. The numerical analysis is based here on the assumption: 'The density distributions on x- (f_N) and y-axis (f_{Res}) are approximately basic populations and of Normal Distribution-type' f_{ND} (for the density distributions also a logarithmic, a Weibull density function or a truncated function could be employed). The convolution integral, solved by Mathcad 15, reads

$$(1-p_f) = \Re = p_{ü} = \int_{-\infty}^{\infty} \left(\int_{Rres}^{\infty} f_{Res}(R) \cdot dR \cdot f_N(N)\, dN \right) = 90\% \text{ fractile} \quad \text{for ND density distributions}$$

Data base of the numerical

$$\text{with} \quad f_{ND}(x) = \frac{1}{\sigma \cdot \sqrt{2 \cdot \pi}} \cdot exp\ \left[-\frac{1}{2} \left(\frac{x-\mu}{\sigma} \right)^2 \right] \quad \text{for abscissa } N \text{ and ordinate } R^t .$$

probabilistic example (statistical: μ = mean, σ = standard deviation) is:

* Static strength distribution μ = 80 MPa, σ = 3.2 MPa
* R_{res} distribution in computation point, y-axis, μ = 43.5 MPa, σ = 2.9 MPa
* Cycle distribution in computation point, x-axis, μ = 3431 cycles, σ = 446 cycles and the Coordinates of the chosen computation point * (38 MPa, n = 2000 cycles in *Fig.21-4*).

(Note, please: The presented application outlines a limit of the Mathcad 15 code application. Mathcad has

(Note, please: The presented application outlines a limit of the Mathcad 15 code application. Mathcad has no computation problem with the computation of the required so-called convolution integral. However, when visualizing the probability hill in Fig.21-5, it was only partly able to manage the 'big data' problem and runs into endless loops. Therefore the author had to sort out a work case with reduced stress and cycle regimes. The original SN data set was for fiber fracture (FF) of CFRP considering the hanger. This reduction to a relatively simple numerical example does not matter because the procedure is of interest and will explain the posed task.)

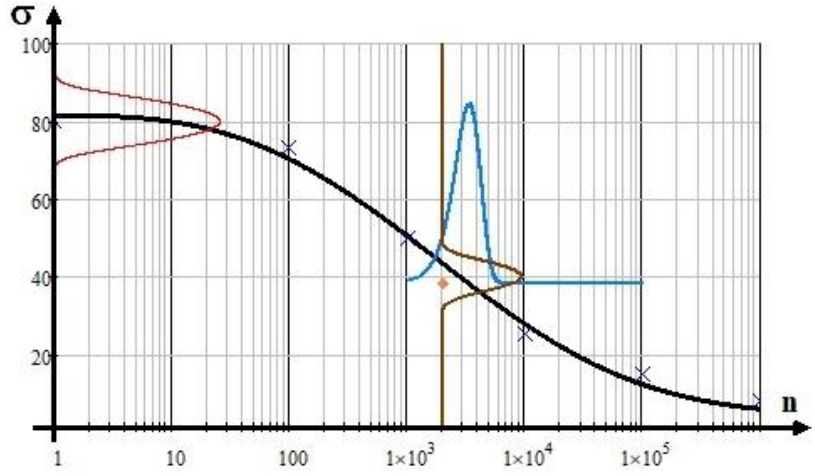

Fig.21-4, Simplified Mathcad calculable example: Assumed distributions of residual strength and cycles linked to R_{res} (38 MPa, 2000 cycles). SN-curve, R = 0.1: *c1= 20 MPa, c2= 80 MPa , c3= 3.77, c4= 2.92*

Fig.21-4 depicts the SN-curve, the chosen computation point, static strength distribution with an assumed residual strength distribution and cycle distribution, all through the computation point *. It is a semi-logarithmic graph. As it is a brittle example material, the use of σ_{max} (*involves R^t as origin*!) as ordinate is of advantage for the 'strength-oriented' design engineer compared to using a stress amplitude σ_a .

The probabilistic treatment delivers the 'joint' probability hill of both the distribution functions in *Fig.21-5*, (right). The hill's average center coordinates are 43.5 MPa, 3430 cycles. The figure further depicts the density distributions of the residual strength $R_{res}(\sigma)$ and of the fracture cycle N .

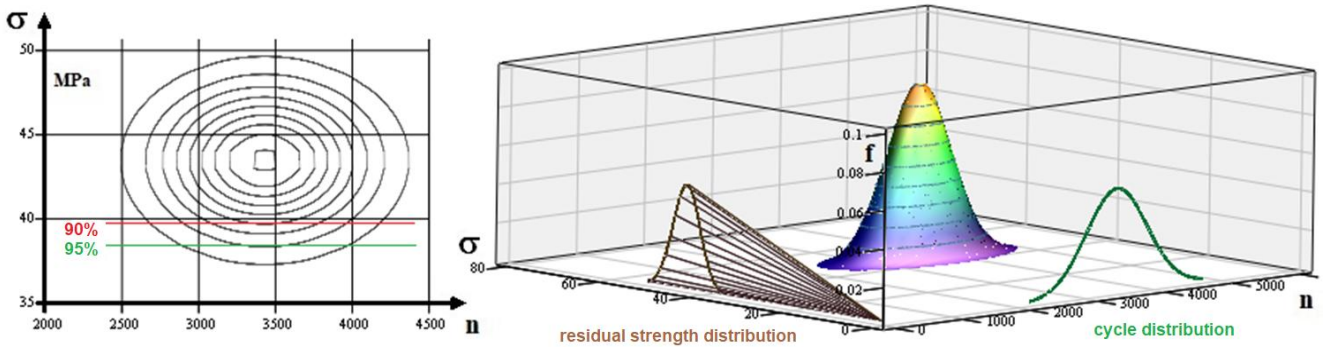

Fig.21-5: (right) Cyclic distributions and assumed residual strength distribution with survival probability hill applying the convolution integral. (left) Projection of lines of equal probability with two chosen residual strength cut-offs , M is the hill designation

In the right part figure, the residual strength distribution is not clearly visible due to additional Mathcad-drawn beams running out from the origin, which are to neglect. The task seems to be an overloading of the Mathcad code which could not anymore handle the numerically effortful task for too large cycle numbers. The left figure shows the projection of the probability hill with lines of equal probability belonging to the chosen computation point *. Below, the computation parameter input set is depicted.

Design Safety considering the scatter of the design parameters is tackled as follows:

The scatter of loading is considered in the residual strength design verification because DUL with its design safety factor j_{ult} has to be verified. The scatter of the residual strength R_{res} and of the fracture cycle N is captured by a joint probability calculation indicated below. This procedure is effortful, however of high fidelity if test data is available.

Under above assumptions an estimation of a required 90%-linked residual (tensile) strength value can be determined according to the formula below representing the probability hill volume truncated by R_{res}

$$\mu NR = 3431 \quad \sigma NR = 446 \quad \mu\sigma R = 43.5 \quad \sigma\sigma R = 2.9 \qquad n := 2000..6000 \quad \sigma := 0..80$$

$$x_n := dnorm(n, \mu NR, \sigma NR) \qquad y_\sigma := dnorm(\sigma, \mu\sigma R, \sigma\sigma R) \qquad F(x,y) := x \cdot y \qquad M_{n,\sigma} := F(x_n, y_\sigma) \cdot 750$$

$$p\ddot{u} := \int_{\sigma res}^{Rt+\sigma Rt} \int_{2500}^{5500} \frac{1}{\sigma\sigma R \cdot \sqrt{2\pi}} \cdot e^{\left[\frac{-1}{2} \cdot \left(\frac{y-\mu\sigma R}{\sigma\sigma R}\right)^2\right]} \cdot \left[\frac{1}{\sigma NR \cdot \sqrt{2\pi}} \cdot e^{\left[\frac{-1}{2} \cdot \left(\frac{x-\mu NR}{\sigma NR}\right)^2\right]}\right] dx\, dy$$

The computation delivers for the point ($\sigma_{res} \equiv R_{res}$ = 38.0 MPa, 2000 cycles) the value pü = P = 95% = ℜ.

Setting the value 39.5 MPa, the demanded survival probability pü = 90% = (1- p_f) is obtained for R_{res} .

LL:

- *The proposed procedure clearly shows how to statistically understand a residual strength value*
- *It could be proven that the proposed model leads to an acceptable value for the residual strength of fatigued, non-cracked structural parts.*

21.4 Residual Strength R_{res}, pre-cracked, Fatigue phase 3, Fracture Mechanics (for completion)

To estimate the residual strength of a pre-cracked structural part or the critical length of an initial macro-crack is essential regarding the questions:

(1) Is the crack-length at the end of static loading critical?

(2) Is the crack-length at the end of cyclic loading critical for further static loading, considering a SN-curve? Here, the certification of cracked components in aircraft structures requires a damage tolerance assessment.

22 Full UD-Mohr Envelope $\tau_{nt}(\sigma_n)$, Derivation of $\Theta_{fp}(\sigma_n)$ and of Cohesive shear Strength

Aim: *Unlocking the 'mystery' behind the shear quantities* R_{23}, R_{23}^{τ} and R_{23}^{A} *faced in UD analyses.*

22.1 Shear Strength Quantities in Analysis, Survey

Fig.22-1 collects all figures which are necessary to understand the difference of applied shear quantities (*upper part figure*): Shear fracture stress (Tsai-Wu, Hashin) and so-called cohesive strength R_{23}^{τ} (construction, rock mechanics) and the Action plane shear strength R_{23}^{A} (Puck).

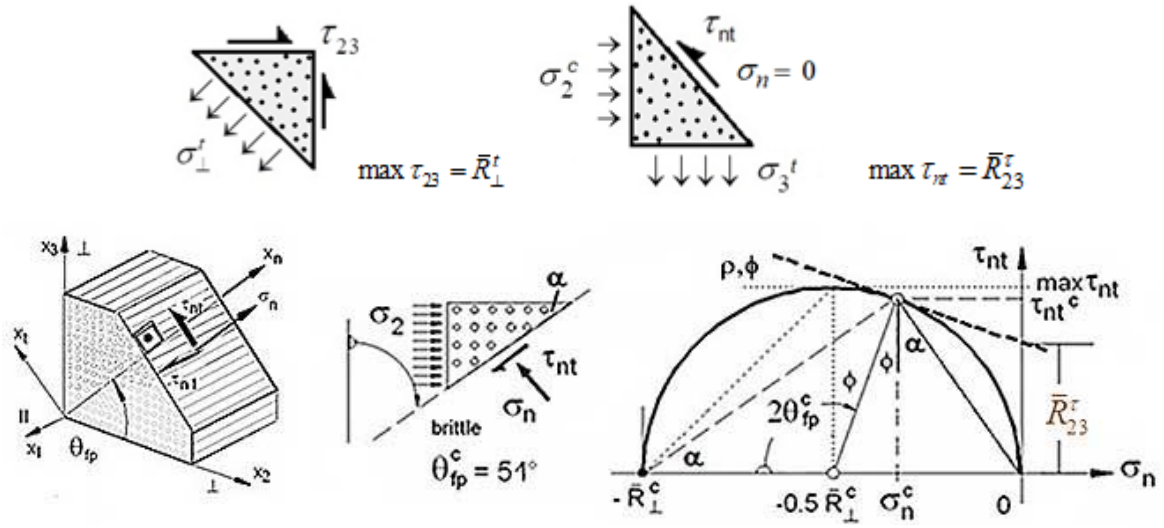

Fig. 22-1: Difference of transversal shear fracture stress and cohesive strength.

The brown curve in *Fig.22-1* is the Linear Mohr-Coulomb (M-C) curve. This approach is a simple IFF2-extrapolation from the compressive strength point, keeping the fracture angle measure $C = C_{fp}^{c}$ constant, when estimating the so-called cohesive strength by $R_{23}^{\tau} = \tau_{nt}{}^{c} + \mu \cdot \sigma_n{}^{c}$ at $\sigma_n = 0$. The letters $\rho = \phi$ address the so-called friction angle. The 3 sketches above the bottom figure demonstrate that the cohesive strength point $\bar{R}_{23}^{\tau}$ is located in the mode's transition zone and cannot be reliably estimated just by an IFF2-Extrapolation, employing just SF! The parallel acting normal fracture part NF, namely IFF1, was neglected. But IFF1 usually causes much more failure danger than the compression-linked shear mode IFF2 from the transition zone beginning on.

The analytical determination of the M-C failure curve and of a value for the cohesive strength depends on the quality of the used IFF2-model and the interaction of both in the transition zone.
Therefore, in order to accurately determine $\tau_{nt}(\sigma_n)$ both the modes are to include in the derivation process of a realistic M-C curve, the determination of the fracture angle $\Theta_{fp}°$ and of the cohesive strength $\bar{R}_{23}^{\tau}$ at $(\tau_{nt}^{fracture}, \sigma_n = 0)$. An improved treatment by a correction f_{corr} of the M-C curve has been effortful executed by the author in [*Cun23b*]. This became necessary because any SFC has to be as simple as possible. Of course, this means that all presently applied SFCs have a deficiency in the mode transition zones. The author has compensated for this with a correction. The bottom figure in *Fig.22-1* displays, how the fracture angle increases, when approaching $\bar{R}_{\perp}^{t}$. Thereby the **bold** curve represents the optimum corrected mapping of the M-C curve in the transition zone around $\sigma_n = 0$.
Now the steps of the tedious way to obtain *Fig.22-1* shall be presented.

22.2 Relations for a Transformation from a Test Fracture Curve $\sigma_3(\sigma_2)$ to Mohr's $\tau_{nt}(\sigma_n)$

The general stress state $\{\sigma\}$ in the material point of the lamina has to be transformed around the 1-axis to the arbitrary Mohr stress state $\{\sigma^{\theta}\} = [T_{\sigma}(\theta)]\cdot\{\sigma\}$, a fibre-parallel plane, by applying <u>*Fig.22-1*</u>, wherein *c*: = cos θ, *s* = sin θ and *n* is normal to the 'action plane' [*Cun22*]. Values of the parameters depend on the approach, whether it is a linear or a parabolic one.

$$\begin{matrix}\\ \rightarrow\\ \\ \rightarrow\\ \\ \rightarrow\end{matrix}\begin{bmatrix}\sigma_1\\ \sigma_n\\ \sigma_t\\ \tau_{nt}\\ \tau_{t1}\\ \tau_{n1}\end{bmatrix} = \left\{\sigma^{\theta}\right\} = \left[T_{\sigma}(\theta)\right]\{\sigma\} = \begin{bmatrix}1 & 0 & 0 & 0 & 0 & 0\\ 0 & c^2 & s^2 & 2sc & 0 & 0\\ 0 & s^2 & c^2 & -2sc & 0 & 0\\ 0 & -sc & +sc & c^2-s^2 & 0 & 0\\ 0 & 0 & 0 & 0 & c & -s\\ 0 & 0 & 0 & 0 & +s & c\end{bmatrix}\begin{bmatrix}\sigma_1\\ \sigma_2\\ \sigma_3\\ \tau_{23}\\ \tau_{31}\\ \tau_{21}\end{bmatrix}$$

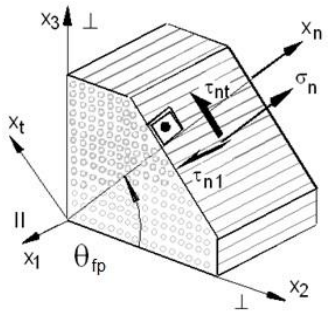

Fig. 22-2: Visualization of the transformation of lamina stresses into associated Mohr stresses. $\theta = \Theta_{fp}$ denotes the angle of the anti-clockwise transformation from the (1, 2, 3)-CoS to the (1, n, t)-CoS

According to

$$\sigma_n^A(\theta) = c^2\cdot\sigma_2 + s^2\cdot\sigma_3 + 2\cdot s\cdot c\cdot\tau_{23},\ \tau_{n1}^A(\theta) = c\cdot\tau_{21} + s\cdot\tau_{31},\ \tau_{nt}^A(\theta) = -s\cdot c\cdot(\sigma_2-\sigma_3) + (c^2-s^2)\cdot\tau_{23}$$

the transformed stresses $\sigma_n(\theta)$, $\sigma_t(\theta)$, $\tau_{nt}(\theta)$, which Puck termed 'Action Plane' Stresses, *Fig.22-1, <u>right,</u>* in the turned CoS depend on (σ_2, σ_3, τ_{23}) only, whereas τ_{t1}, τ_{n1} is linked to (τ_{31}, τ_{21}). They are acting in the potentially physical (fracture) failure 'plane' and are decisive for fracture. In case of normal stress-induced fracture (NF) σ_n will be responsible for fracture and in case of shear stress-induced fracture τ_{nt} will be the fracture dominating Mohr stress. The Mohr stress τ_{t1} has no impact but has to be considered in the derivations of the *Eff*-functions until it vanishes during the later transformation process.
Fracture plane will become that 'action plane' where the material stressing effort *Eff*($\sigma(\theta)$) will reach the value 1 = 100% at (maximum) failure loading and by that, where the theoretical material reserve factor f_{RF} will become a minimum.

*22.2 Accuracy Problem of the IFF2-model in the transition zone IFF2 (*SF*) - IFF1 (*NF*)*

In this subchapter the cohesion strength R_{23}^{τ}, activated by τ_{nt} in the quasi-isotropic plane of the UD material is envisaged. This quantity is located in the transition zone of the two modes IFF1 and IFF2. With isotropic materials the author learned that a transformation from UD lamina stresses into the desired Mohr stresses τ_{nt}, σ_n must be also possible. Thereby a closer look at R_{23}^{τ} and at the Mohr envelope $\tau_{nt}(\sigma_n)$ or M-C curve will be possible.

Here addressed is the <u>quasi-isotropic</u> UD plane (*works <u>similar</u> to isotropic concrete materials, using **available** multi-axially compression test-based data [Cun22]*). The compromise is on the 'safe Reserve Factor side'. This means: The engineering approach of above $Eff^{\perp\tau}$ (SF) is not problematic for Design Verification, because *Eff* = 1 delivers conservative *RF*-values in the transition zone, since the curve runs more internally due to the generally *minimum value choice* of the interaction exponent *m*.

Focus here is the derivation of $\tau_{nt}(\sigma_n)$, $\theta_{fp}(\sigma_n)$ and R_{23}^{τ} from a measured fracture curve $\sigma_3(\sigma_2)$ and its course in the 2nd quadrant of $\sigma_3(\sigma_2)$. In <u>*Table 22-1*</u> all relations necessary for the transformation are compiled and formulas for the searched entities τ_{nt}, σ_n, $\theta_{fp}°$ are presented. After transformation of the

UD lamina (layer) stresses σ_2, σ_3, τ_{23} in the quasi-isotropic plane into the principal stresses σ^{pr} (*index ^{pr} means principal*), the shear stress τ_{23} vanishes. Therefore, with no loss of generality σ^{pr} can be simpler written in the further text, back again as plain letter σ, but thinking they might be principal stresses acting in the quasi-isotropic plane. In the addressed quasi-isotropic plane this transformation of the lamina stresses into Mohr stresses practically works via addition theorems and using $C(\Theta_{fp}°) = cos\Theta^2 - sin\Theta^2$, which is termed here 'fracture angle measure'.

As the author still found with isotropic materials, the interaction considering magenta curve (thinly-marked) in *Fig.22-3* cannot accurately map the course of test data. The improved **bold-**marked curve is physically more accurate and this local mapping shortcoming is to model more detailed as follows. *Fig 22-1* shows that with the IFF2-function the shear effort $Eff^{\perp\tau}$ cannot become zero in the M-C domain at $\sigma_2 = 0$. This numerical behavior is a shortcoming in the transition zone of the 'simple' engineering FMC-based IFF2 approach. An accurate alteration of the fracture angle $\Theta_{fp}°$ and of the associated Mohr stresses τ_{nt}, σ_n is not to achieve with the mathematical course of the given 'engineering' IFF2 function. The mapping quality of the given IFF2 is not fully sufficient if the alteration of the fracture angle Θ_{fp} in the transition zone is to determine. This bi-axially stressed transition zone between the normal fracture mode domain NF and the shear fracture mode domain SF is ruled by interaction and therefore requires both the Eff-modes to be inserted into the interaction equation $Eff = 1$. Specific points of the investigated M-C domain are: $(\sigma_2 = -\bar{R}_\perp^{\,c}, 0) \rightarrow (\sigma_2, \sigma_3 = -\sigma_2) \rightarrow (0, \sigma_3 = \bar{R}_\perp^{\,t})$. In order to sort out a better mapping description it is essential to know how the pure mode efforts of the activated modes IFF1 and IFF2 change its influence along the σ_2-axis, which is depicted in *Fig.22-2*. $Eff^{\perp\tau}$ firstly becomes zero at the equi-biaxial tensile 'strength' point $(\bar{R}_\perp^{\,tt}, \bar{R}_\perp^{\,tt}) < \bar{R}_\perp^{\,t}$. This zero point lies physically 'too late' for a more accurate revised local mode description. An improvement is to achieve.

22.3 Improvement of the IFF2 Criterion in the Transition Zone

The required entities $\tau_{nt}, \sigma_n, \Theta_{fp}°$ and $\bar{R}_{23}^{\tau}$ only become accurate if a physically necessary correction of $Eff^{\perp\tau}$ is considered by using a correctively acting decay function f_{corr}. In order to implement f_{corr} one just has to replace $a_{\perp\perp}$ by $f_{corr} \cdot a_{\perp\perp}$ and $b_{\perp\perp}$ by $f_{corr} \cdot b_{\perp\perp}$. For a realistic transformation of the test curve, formulated in lamina stresses into a Mohr stress formulation, it is considered that $Eff^{\perp\tau}$ (SF) physically must become zero when reaching the pure NF domain at the point ($\sigma_3 = \bar{R}_\perp^{\,t}, \sigma_3 = 0$), see the course in *Fig.22-3*):

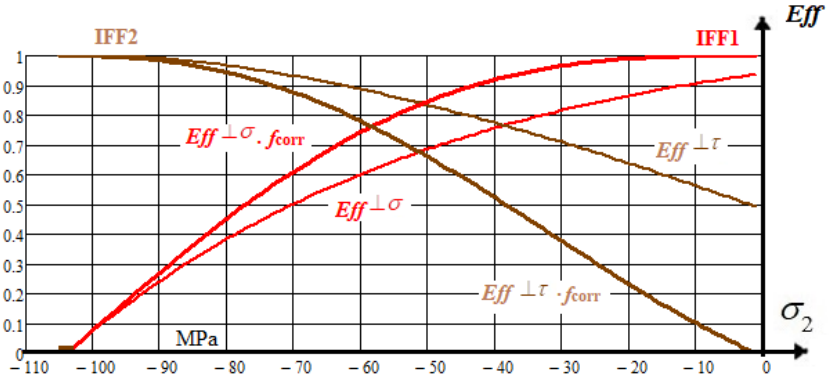

Fig.22.3: Course of the two efforts $Eff^{\perp\sigma}$, $Eff^{\perp\tau}$ composing the fracture stress curve Eff =1= 100%.

Table 22-1: IFF2-IFF1-interacted Derivation of $\tau_{nt}(\sigma_n), R_{23}^{\tau}, \theta_{fp}$ from a measured curve $\sigma_3^{fr}(\sigma_2)$

$SF: Eff^{\perp\tau} = [a_{\perp\perp}\cdot(I_2) + b_{\perp\perp}\cdot\sqrt{I_4}] / \bar{R}_{\perp}^{c} = 1$

$= [a_{\perp\perp}\cdot(\sigma_2^{pr}+\sigma_3^{pr}) + b_{\perp\perp}\cdot\sqrt{(\sigma_2^{pr}-\sigma_3^{pr})^2+0^2}] / \bar{R}_{\perp}^{c} = 1$ (lamina stresses)

$\equiv [a_{\perp\perp}\cdot(\sigma_n+\sigma_t) + b_{\perp\perp}\cdot\sqrt{(\sigma_n-\sigma_t)^2+4\tau_{nt}^2}] / \bar{R}_{\perp}^{c} = 1$ (in Mohr stresses)

$NF: Eff^{\perp\sigma} = (\sigma_2^{pr}+\sigma_3^{pr}) + \sqrt{(\sigma_2^{pr}-\sigma_3^{pr})^2+0^2}] / 2\cdot\bar{R}_{\perp}^{t} = 1$

$\equiv [(\sigma_n+\sigma_t) + \sqrt{(\sigma_n-\sigma_t)^2+4\tau_{nt}^2}] / 2\cdot\bar{R}_{\perp}^{t} = 1.$

Known: σ_2^{pr}, σ_3^{pr}. Searched is: σ_n, τ_{nt}, Θ_{fp} with $C = \cos(2\cdot\Theta_{fp}{}^{\circ}\cdot\pi/180°)$.

Use of addition theorems, $\sigma_{\lambda} = 0$. For lamina stresses ^{pr} now dropped for simplification

$$\sigma_n - \sigma_t = c^2\cdot(\sigma_2-\sigma_3) - s^2\cdot(\sigma_2-\sigma_3) = C\cdot(\sigma_2-\sigma_3), \quad S = \sqrt{1-C^2}$$

$$\sigma_t = \sigma_n - C\cdot(\sigma_2-\sigma_3),\ C = c^2-s^2 = 2c^2-1 = 1-2s^2,\ \sigma_n+\sigma_t = \sigma_2+\sigma_3,$$

$$\tau_{nt} = -0.5\cdot S\cdot(\sigma_2-\sigma_3) = -0.5\cdot\sqrt{1-C^2}\cdot(\sigma_2-\sigma_3),\ \sigma_n = (C+1)\cdot0.5\cdot\sigma_2 + (1-C)\cdot0.5\cdot\sigma_3.$$

Differentiation of structural stresses-linked Mohr stresses delivers (minus due to implicit derivation)

$$\frac{d\tau_{nt}}{d\sigma_n} = \frac{(s^2-c^2)\cdot(\sigma_2-\sigma_3)}{-2\cdot s\cdot c\cdot(\sigma_2-\sigma_3)} = \frac{C}{S},$$ valid *uni* - and *bi* - *axial* (like isotropic!).

Fracture (interaction) equation ≡ mathematical equation of the fracture body

$$Eff = [(Eff^{NF})^m + (Eff^{SF})^m]^{m^{-1}} \quad or \quad \text{computationally simpler}$$

$$(Eff^{NF})^m + (Eff^{SF})^m = 1 = 100\% \quad \text{total effort fracture curve}$$

From differentiation of the interaction equation (σ_t goes away)

$$\{[(\sigma_n+\sigma_n-C\cdot(\sigma_2-\sigma_3)) + \sqrt{(\sigma_n-\sigma_n-C\cdot(\sigma_2-\sigma_3))^2+4\tau_{nt}^2}] / 2\cdot\bar{R}_{\perp}^{t}\}^m +$$

$$+\{[a_{\perp\perp}\cdot(\sigma_n+\sigma_n-C\cdot(\sigma_2-\sigma_3)) +$$

$$+ b_{\perp\perp}\cdot\sqrt{(\sigma_n-\sigma_n-C\cdot(\sigma_2-\sigma_3))^2+4\tau_{nt}^2}] / \bar{R}_{\perp}^{c}\}^m = 1.$$

are obtained the two equations

$$d[(Eff^{NF})^m + (Eff^{SF})^m]/d\sigma_n =$$

$$m\cdot\{2\sigma_n - C\cdot(\sigma_2-\sigma_3) + \sqrt{(C\cdot(\sigma_2-\sigma_3))^2+4\tau_{nt}^2}]/2\bar{R}_{\perp}^{t}\}^{m-1}/\bar{R}_{\perp}^{t} +$$

$$+2a_{\perp\perp}\cdot\mathrm{m}\cdot\{a_{\perp\perp}(2\sigma_n - C\cdot(\sigma_2-\sigma_3)) + b_{\perp\perp}\sqrt{(C\cdot(\sigma_2-\sigma_3))^2+4\tau_{nt}^2}] / \bar{R}_{\perp}^{c}\}^{m-1}/\bar{R}_{\perp}^{c},$$

$$d[(Eff^{NF})^m + (Eff^{SF})^m]/d\tau_{nt} =$$

$$\frac{2m\cdot\tau_{nt}\cdot\{2\sigma_n - C\cdot(\sigma_2-\sigma_3) + \sqrt{(C\cdot(\sigma_2-\sigma_3))^2+4\tau_{nt}^2}]/2\bar{R}_{\perp}^{t}\}^{m-1}}{\bar{R}_{\perp}^{t}\cdot\sqrt{(C\cdot(\sigma_2-\sigma_3))^2+4\tau_{nt}^2}} +$$

$$+4b_{\perp\perp}\cdot\mathrm{m}\cdot\{a_{\perp\perp}(2\sigma_n - C\cdot(\sigma_2-\sigma_3)) + b_{\perp\perp}\sqrt{(C\cdot(\sigma_2-\sigma_3))^2+4\tau_{nt}^2}] / \bar{R}_{\perp}^{c}\}^{m-1}/\bar{R}_{\perp}^{c}.$$

Equating above two equations and replacing Mohr stresses by ply stresses

via $\sigma_n = (C+1)\cdot0.5\cdot\sigma_2 + (1-C)\cdot0.5\cdot\sigma_3,\ \tau_{nt} = -0.5\cdot\sqrt{1-C^2}\cdot(\sigma_2-\sigma_3)$

yields an implicitely to solve equation for the fracture angle measure C

$$\frac{C(\sigma_2,\sigma_3)}{\sqrt{1-C^2}} = -\left[\frac{A}{\bar{R}_{\perp}^{t}} + \frac{2\cdot a_{\perp\perp}\cdot B}{\bar{R}_{\perp}^{c}}\right] / \left[\frac{2\cdot A}{\bar{R}_{\perp}^{t}\sqrt{(\cdot\sigma_2-\sigma_3)^2}} + \frac{4\cdot b_{\perp\perp}\cdot\tau_{nt}(C)}{\bar{R}_{\perp}^{c}\sqrt{(\cdot\sigma_2-\sigma_3)^2}}\right] \text{ with}$$

$$A = \left[\frac{\sigma_2+\sigma_3+\sqrt{(\sigma_2-\sigma_3)^2}}{2\cdot\bar{R}_{\perp}^{t}}\right]^{m-1},\quad B = \left[\frac{a_{\perp\perp}\cdot(\sigma_2+\sigma_3)+b_{\perp\perp}\cdot\sqrt{(\sigma_2-\sigma_3)^2}}{\bar{R}_{\perp}^{c}}\right]^{m-1}$$

and finally via $C = \cos(2\cdot\theta_{fp}) \rightarrow \theta_{fp} = 0.5\cdot\arccos C,\ \theta_{fp}{}^{\circ} = \theta_{fp}\cdot 180°/\pi.$

By insertion of any stress state the associated 'running' C can be computed.

Cohesion strength $\bar{R}_{23}^{\tau}$ is determinable for $\tau_{nt}^{fail}(\sigma_n) = 0$

Similar to the isotropic case the bi-axial stress-ruled quasi-isotropic M-C curve, located in the quasi-isotropic plane, is oppositely dominated by two modes, IFF2 (SF) with IFF1 (NF). Therefore, attention was paid to the interaction of both these modes in the transition zone in order to finally obtain an 'accurate' fracture angle $\Theta_{fp}°$, being the pre-condition to determine the envisaged two Mohr stresses τ_{nt}, σ_n. the shear material stressing effort $Eff^{\tau} = Eff^{SF}$ must physically become zero at the tensile strength point (0, R^t). This specific shortcoming is brought about by a correction function that defines the decay of Eff^{τ} and is practically performed by setting $Eff^{\tau} = 0$ at $\sigma_{II} = 0$. As decay function the author often took (§10) an exponential one: $f_d = 1/(1+\exp(\frac{c_{1d}+\sigma_{II}}{c_{2d}})$, with c_{1d}, c_{2d} fixed at ($-\bar{R}^c$, 0.995) , (-0.01,+0.01).

Here it is sufficient to apply for the decay of $Eff^{\perp\tau}$: $f_{corr} = 1 + c_0 \cdot (\bar{R}_{\perp}^{c} + \sigma_2)^2$.

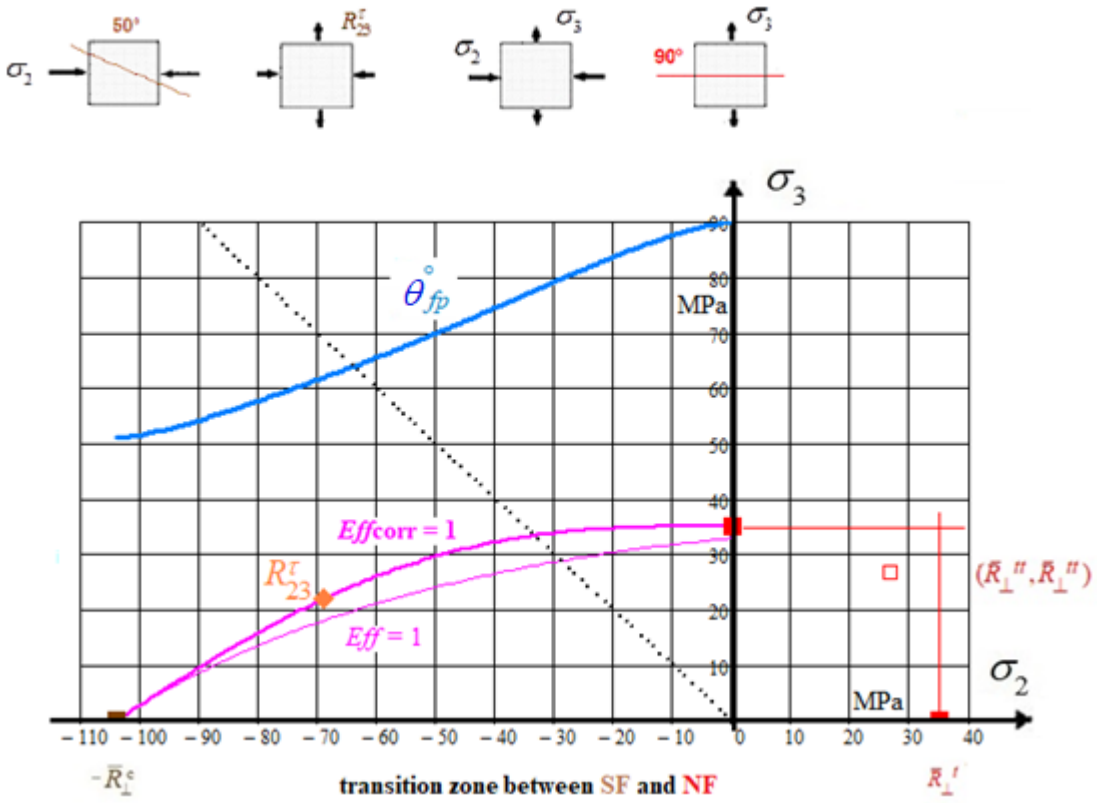

Fig. 22-4: Interaction curve $\sigma_3^{fracture}(\sigma_2)$ *with Eff = 1Failure stress curve* $\sigma_2(\sigma_3)$ *with alteration of fracture angle* $\theta_{fp}°$ *in the transition zone. (Numerical example stems from a measurement of the fracture plane angle* $\theta_{fp}°$ *in [VDI97, bi-axial failure stress* $\bar{R}_{\perp}^{tt}$*). Marked* R_{23}^{τ}*-point.*

- IFF2-IFF1- interacted fracture curve (*thin, original IFF2. With this 'simple' approach, the curve cannot run through* $\bar{R}_{\perp}^{t}$ = 35 MPa)
- IFF2-IFF1- interacted fracture curve *(bold, IFF2 decay function corrected, which better maps the course of measured fracture stress data)* and
- Course of the fracture plane angle $\theta_{fp}°$ (*bold, corrected*)

Data set:

$\bar{R}_{\perp}^{c} = 104 MPa,\ \bar{R}_{\perp}^{t} = 35$ MPa, $\Theta_{fp}° = 51°, C^{c} = -0.21 \leftrightarrow a_{\perp\perp} = 0.26,\ \mu_{\perp\perp} = 0.21.$

$f_{corr} = 1 + c_0 \cdot (\bar{R}_{\perp}^{c} + \sigma_2)^2$ with c_0 from inserting $(\sigma_2 = 0,\ \sigma_3 = \bar{R}_{\perp}^{t})$, $c_0 = 8.9 \cdot 10^{-5}$.

IFF1: $Eff^{\perp\sigma} = [(\sigma_2 + \sigma_3) + \sqrt{\sigma_2^{\,2} - 2\sigma_2 \cdot \sigma_3 + \sigma_3^{\,2}}] / 2\bar{R}_{\perp}^{t}$,

IFF2: $Eff^{\perp\tau} = [a_{\perp\perp} \cdot f_{corr} \cdot (\sigma_2 + \sigma_3) + b_{\perp\perp} \cdot f_{corr} \sqrt{\sigma_2^{\,2} - 2\sigma_2\sigma_3 + \sigma_3^{\,2}}] / \bar{R}_{\perp}^{c}$.

This correction changes the formula for the determination of the fracture angle measure *C* in *Table 22-1.*

Therewith, after effortful MathCad programming and implicit numerical computations the desired accurate bi-axial fracture stress M-C-curve τ_{nt} (σ_n) could be derived by the refined IFF2 model and by re-transformation also ply stresses could be obtained. The fracture angle becomes now the realistic value of 90° instead 71°.

$$\frac{C}{\sqrt{1-C^2}} = -m \cdot \left[\frac{A}{\bar{R}_{\perp}^{t}} + \frac{2 \cdot a_{\perp\perp} \cdot f_{corr} \cdot B}{\bar{R}_{\perp}^{c}}\right] / \left[\frac{2 \cdot A}{\bar{R}_{\perp}^{t}\sqrt{(\cdot\sigma_2 - \sigma_3)^2}} + \frac{4 \cdot b_{\perp\perp} \cdot f_{corr} \cdot B \cdot \tau_{nt}}{\bar{R}_{\perp}^{c}\sqrt{(\cdot\sigma_2 - \sigma_3)^2}}\right],$$

$$B_{corr} = \left[\frac{a_{\perp\perp} \cdot (\sigma_2 + \sigma_3) + b_{\perp\perp} \cdot \sqrt{(\sigma_2 - \sigma_3)^2}}{\bar{R}_{\perp}^{c}} \cdot f_{corr}\right]^{m-1} \quad \text{with} \quad f_{corr} = 1 + c_0 \cdot (\bar{R}_{\perp}^{c} + \sigma_2)^2 .$$

*22.4: **Determination of Cohesive** shear **Strength** R_{23}^{τ}*

The interaction curve can be dedicated to the basic Mohr-Coulomb curve which runs from the compression strength point till the tensile strength point $\sigma_3 = \bar{R}_{\perp}^{t}$. In order to find all relationships in one diagram the Mohr stresses are also inserted as functions of the lamina stresses σ_2 (σ_3) and not of σ_n alone, which is the usual diagram form. *Fig.22-4* includes the development of the fracture plane angle as function of the lamina stress σ_2. *Fig.22-1* still presented all MathCad-computed Mohr entities providing:

* Extrapolation from compressive strength point (IFF2-determined Mohr-Coulomb fracture curve)
  - A straight Linear Mohr-Coulomb curve, considering σ_2 (*linear Mohr*), *Cohesive Strength*
  - A straight Linear Mohr-Coulomb curve, considering σ_2 and σ_3; *Cohesive Strength* $\bar{R}_{23}^{\tau}$
* Full IFF2-IFF1-interacted Mohr-Coulomb fracture curve *(bold, decay function- corrected)*
* Course of the fracture plane angle $\theta_{fp}°/2$ (thin, not decay function corrected) and (bold).

The definition of the cohesive (shear) strength is $(\tau_{nt}^{fail} = \bar{R}_{23}^{\tau},\ \sigma_n = 0)$. Searching $\bar{R}_{23}^{\tau}$(C), the derived formulation permits to continuously MathCad-compute the alternating fracture plane measure C with the associate fracture angle $\theta_{fp}°$. The interpretation of the figures leads to the following conclusions:

- The general macro-mechanical IFF2 approach cannot offer a full accuracy of the realistically predicted Mohr-Coulomb curve. Just the *physically-based* decay function correction delivers the desired fidelity
- A SFC in lamina stresses can be transferred into a Mohr-Coulomb version
- The course of the fracture plane angle $\theta_{fp}°$ can be determined, too
- The idea of the FMC that IFF1 and IFF2 commonly add its *Eff* portions, which leads to the result that $\theta_{fp}°$ is in the sixty degrees ° at the cohesive strength point $\bar{R}_{23}^{\tau}$, with a degree value being the higher the higher the strength ratio $\bar{R}_{\perp}^{c} / \bar{R}_{\perp}^{t}$ is.

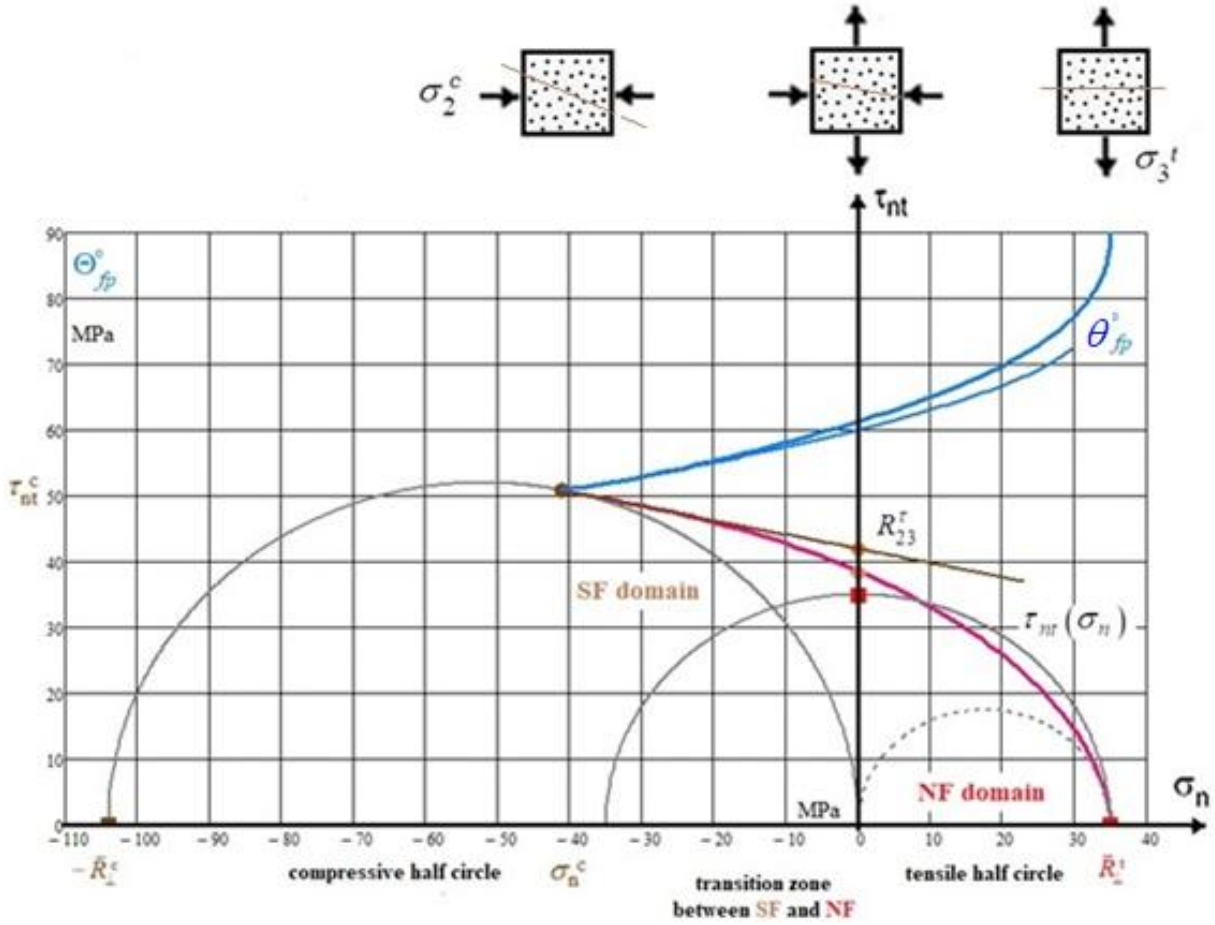

Fig. 22-1: Mohr-Coulomb curve characteristics, Mohr shear curves $\tau_{nt}(\sigma_n)$ with its special points and the 3 Mohr half-circles

LL:

- *Failure stress under pure shear* $\tau_{23}^{\text{fracture}} = max\,\tau_{23} \le R_\perp^t$ *, an in literature often applied approach-formalistically termed quantity*
- *Mohr-based approach linked so-called cohesive strength* $R_{23}^\tau = \tau_{nt}(\sigma_n = 0)$
- *Puck's Action plane shear resistance* R_{23}^A*: Puck formulated a full IFF-SFC and could model-associated dedicate his action plane resistance a relation with the inclination model parameters p and the other strengths reading* $\bar{R}_{23}^A = \left[\bar{R}_{\perp\parallel}\cdot\sqrt{1+2\cdot p_{\perp\parallel}^c\cdot\bar{R}_\perp^c/\bar{R}_{\perp\parallel}}-1\right]/2\cdot p_{\perp\parallel}^c$*. Above quantities are not measurable ones*
- *Generally, assuming a transverse shear failure stress , which would be a sixth strength, will contradict material symmetry demands, which seem to require for UD materials a 'generic' number of 5, meaning 5 measurable strengths and 5 elasticity properties*
- *The ability for mobilizing friction processes depends on active compression stresses that cause via the friction value μ the necessary shear stress.*

Analogous to the saying

" *If something becomes a fact it is no science anymore*",

Here, transferred to the input R_{23} in analysis:

"The cohesive shear strength $R_{23}{}^\tau$ ***should be no mystery anymore".***

23 Replacing fictitious UD Model Parameters $a_{\perp\perp}, a_{\perp\parallel}$ by measurable Friction Values μ

Aim: *Engineers prefer measurable friction values instead of fictitious friction parameters.*

23.1: Relation of Friction parameter $a_{\perp\perp}$ to Fracture angle $\theta_{fp}{}^{c}$ and Friction value $\mu_{\perp\perp}$

The measurement of a realistic fracture angle is practically not possible, just the determination of the friction curve parameter $a_{\perp\perp}(\mu_{\perp\perp})$ by mapping the course of test data points is a practical approach. Then, from the mapped test curve the relation of the curve parameter $a_{\perp\perp}$ to the friction value $\mu_{\perp\perp}$ and to the fracture angle $\theta_{fp}°$ can be derived according to the formulas in *Table 23-1*. This is to perform in the compressive strength point $\bar{R}_{\perp}{}^{c}$, see also the chapter before.

Basic assumption is the *brittle-fracture hypothesis* which goes back to O. Mohr's "*The strength of a material is determined by the Mohr stresses on the fracture plane".* This means for the Linear Mohr-Coulomb (M-C) formulation $\tau_{nt} = \bar{R}^{\tau}_{23} - \mu_{\perp\perp}\cdot\sigma_n$ including the friction value $\mu_{\perp\perp}$ being an intrinsic property of the UD material.

Table 23-1: Determination of the friction curve parameter $a_{\perp\perp}(\mu_{\perp\perp})$

IFF2: $F^{\tau}_{\perp} = [a_{\perp\perp}\cdot(\sigma_2+\sigma_3) + b_{\perp\perp}\cdot\sqrt{(\sigma_2-\sigma_3)^2+4\tau_{23}{}^2}\,] / \bar{R}^{c}_{\perp} = 1$, in Mohr stresses, after inserting $\bar{R}_{\perp}{}^{c}$

$= [a_{\perp\perp}\cdot(\sigma_n+\sigma_t) + b_{\perp\perp}\cdot\sqrt{(\sigma_n-\sigma_t)^2+4\tau_{nt}{}^2}\,] / \bar{R}^{c}_{\perp} = 1$ and $a_{\perp\perp} = b_{\perp\perp} - 1$ is friction parameter

$$\frac{dF}{d\sigma_n}\cdot\bar{R}^{c}_{\perp} = a_{\perp\perp} + b_{\perp\perp}\cdot(\sigma_n-\sigma_t)/\sqrt{(\sigma_n-\sigma_t)^2+4\tau_{nt}{}^2},\quad \frac{dF}{d\tau_{nt}}\cdot\bar{R}^{c}_{\perp} = 4\cdot b_{\perp\perp}\cdot\tau_{nt}/\sqrt{(\sigma_n-\sigma_t)^2+4\tau_{nt}{}^2}$$

$$\frac{d\tau_{nt}}{d\sigma_n} = -\frac{dF}{d\sigma_n}/\frac{dF}{d\tau_{nt}} = -[\frac{b_{\perp\perp}\cdot(\sigma_n-\sigma_t) + (b_{\perp\perp}-1)\cdot\sqrt{(\sigma_n-\sigma_t)^2+4\tau_{nt}{}^2}}{4\cdot b_{\perp\perp}\cdot\tau_{nt}}],$$ minus due to implicit derivation

Use of addition theorems ($\sigma_\lambda = 0$), gives the relationships $c = \cos(\theta_{fp}°\cdot\pi/180°)$

$$\sigma_n-\sigma_t = c^2\cdot(\sigma_2-\sigma_3) - s^2\cdot(\sigma_2-\sigma_3) = C\cdot(\sigma_2-\sigma_3),\quad S = \sqrt{1-C^2},\ C = \cos(2\cdot\theta_{fp}°\cdot\pi/180°)$$

$$\sigma_t = \sigma_n - C\cdot(\sigma_2-\sigma_3),\ C = c^2-s^2 = 2c^2-1 = 1-2s^2,\quad \sigma_n+\sigma_t = \sigma_2+\sigma_3 \quad \text{and}$$

$$\tau_{nt} = -0.5\cdot S\cdot(\sigma_2-\sigma_3) = -0.5\cdot\sqrt{1-C^2}\cdot(\sigma_2-\sigma_3),\ \sigma_n = (C+1)\cdot0.5\cdot\sigma_2 + (1-C)\cdot0.5\cdot\sigma_3.$$

Stress σ_t has no influence, as Mohr assumed! Failure responsible due to Mohr are just τ_{nt} with σ_n !

$$\frac{d\tau_{nt}}{d\sigma_n} = -\mu_{\perp\perp} = \frac{C}{S} = -[\frac{b_{\perp\perp}\cdot(\sigma_n-\sigma_t) + (b_{\perp\perp}-1)\cdot\sqrt{(\sigma_n-\sigma_t)^2+4\tau_{nt}{}^2}}{4\cdot b_{\perp\perp}\cdot\tau_{nt}}] =$$

$$= -[\frac{b_{\perp\perp}\cdot(C\cdot\sigma_2) + (b_{\perp\perp}-1)\cdot\sqrt{(C\cdot\sigma_2)^2+4\cdot(-0.5\cdot S\cdot\sigma_2)^2}}{4\cdot b_{\perp\perp}\cdot(-0.5\cdot S\cdot\sigma_2)}]$$

$$C = -[\frac{b_{\perp\perp}\cdot(C\cdot\sigma_2) + (b_{\perp\perp}-1)\cdot\sqrt{(C\cdot\sigma_2)^2+4\cdot(-0.5\cdot\sigma_2)^2\cdot(1-C^2)}}{4\cdot b_{\perp\perp}\cdot(-0.5\cdot\sigma_2)}]\ ;\ C\to C_{fp}{}^{c}$$ inserting strength $\bar{R}_{\perp}{}^{c}$

$$\to C_{fp}{}^{c} = -[\frac{b_{\perp\perp}\cdot C_{fp}{}^{c}\cdot(-\bar{R}_{\perp}{}^{c}) + (b_{\perp\perp}-1)\cdot\sqrt{C_{fp}{}^{c2}\cdot(-\bar{R}_{\perp}{}^{c})^2+4\cdot(-0.5\cdot(-\bar{R}_{\perp}{}^{c}))^2\cdot(1-C_{fp}{}^{c2})}}{4\cdot b_{\perp\perp}\cdot(-0.5\cdot(-\bar{R}_{\perp}{}^{c}))}]$$

Resolving: $b_{\perp\perp} = \frac{1}{C_{fp}{}^{c}+1} \cong \frac{1}{1-\mu_{\perp\perp}}$, $a_{\perp\perp} \cong \frac{\mu_{\perp\perp}}{1-\mu_{\perp\perp}}$, $\mu_{\perp\perp} = -\frac{C}{S} = -\frac{C_{fp}{}^{c}}{S_{fp}{}^{c}} \cong -C_{fp}{}^{c}$ (being a small value).

Assuming $\theta^{c}_{fp}° = 51°$: *Example* $C^{c}_{fp} = \cos(\frac{2\cdot\theta^{c}_{fp}°}{180°}\cdot\pi) = -0.21,\ \mu_{\perp\perp} = 0.21 \cong -C^{c}_{fp},\ a_{\perp\perp} = 0.26$.

If IFF occurs in a parallel-to-fiber plane of the UD lamina, the components of the failure stress vector are the normal Mohr stress σ_n and the two Mohr shear stresses σ_{nt} and σ_{n1}. The shear stress σ_{tl} and the normal stress σ_t will have no influence and this was proven in the derivation. Further, the Mohr stress σ_{n1} belongs to IFF3 and is not of interest, here.

The transformation of the IFF2 SFC in lamina stresses into Mohr stresses-based formulation works via above addition theorems.

During this transformation procedure there are a lot of Lessons to Learn**:**

- *The Linear Mohr-Coulomb model can be employed to obtain a sufficiently good relationship for the determination of the friction value μ in the compressive strength point* $\sigma_2 = -\bar{R}_{\perp}^{c}$.
- *Establishing the relationship* $a_{\perp\perp}(\mu_{\perp\perp})$ *it is assumed that the tangent of the FMC-curve has the same value as that of the straight Linear Mohr envelope curve* $\tau_{nt}(\sigma_n)$ *in the touch point of Mohr's circle, see Fig.23-1*
- σ_1 *is not relevant. The shear stress* τ_{23} *can be assumed zero because it would anyway vanish after a principal stress transformation. No reduction of generality is caused*
- *The stress* σ_t *has no influence! It is not representative such as Mohr supposes. Failure responsible are* τ_{nt} *and* σ_n *, only. But mind in the differentiation process: the Mohr stress* σ_t *cannot be simply set zero at the beginning of the derivations, it must be considered due to its relation to* σ_n *,*
- *Above derivation demonstrates that, if really desired, the fracture plane angle* $\theta_{fp}{}^{c}$ *of an UD-material could be also determined from an invariant-based SFC and not only from Mohr-based formulations*
- *Viewing Fig.23-1, it is obvious that the cohesive strength* $\bar{R}_{23}^{\tau}$ (Civil engineers take the letter c) *belongs to the transition zone of the normal fracture mode domain IFF1 and therefore not alone to the shear fracture mode domain IFF2. Hence, one cannot simply extrapolate from the compressive strength point.*
- *Reminder Mohr's Concept*:

$F^{\tau} = \tau_n / (R^{\tau} - \mu \cdot \sigma_n) = 1$, shear stress hypothesis. $F^{\sigma} = \sigma_n / R^{\sigma} = 1$, normal stress hypothesis

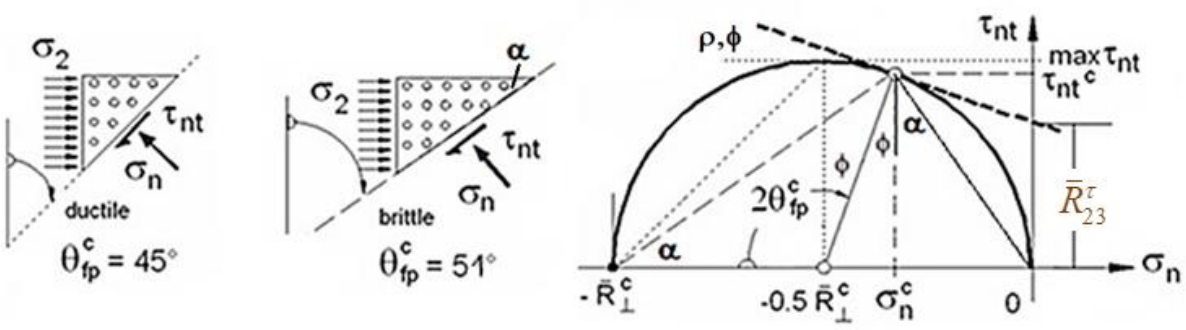

Fig.23-1, Shear stressing situation: Shear fracture plane angle in the touch point and 'linear' Mohr-Coulomb friction curve. The touch point is defined by $(\sigma_n^c, \tau_{nt}^c)$ *and linked to* $\bar{R}_{\perp}{}^{c}$. $90° = 2\theta_{fp}° - \phi°$

23.2: Relation of Friction parameter $a_{\perp\parallel}$ to *Friction value* $\mu_{\perp\parallel}$

The same procedure is analogously to perform for the mode IFF3, see *Table 23-2*.

Table 23-2: Relationships for the determination of friction curve parameter $a_{\perp\parallel}(\mu_{\perp\parallel})$

$F_{\perp\square} = \frac{I_3^2}{\bar{R}_{\perp\parallel}^{\,4}} + b_{\perp\parallel} \cdot \frac{I_2 \cdot I_3 - I_5}{\bar{R}_{\perp\parallel}^{\,3}} = 1$ with $I_{23-5} = 2\cdot\sigma_2\cdot\tau_{21}^2 + 2\cdot\sigma_3\cdot\tau_{31}^2 + 4\cdot\tau_{23}\tau_{31}\tau_{21}$ from

$I_2 = \sigma_2 + \sigma_3$, $I_3 = \tau_{21}^2 + \tau_{31}^2$, $I_5 = (\sigma_2 - \sigma_3)\cdot(\tau_{31}^2 - \tau_{21}^2) - 4\cdot\tau_{23}\cdot\tau_{31}\cdot\tau_{21}$.

The transfer to a Mohr-shaped SFC is directly possible, because the fracture plane is already known (parallel to the fibre direction) , via $(\tau_{n1},\ \sigma_n) \equiv (\tau_{21},\ \sigma_2)$, $|\tau_{21}| = \bar{R}_{\perp\parallel} - \mu_{\perp\parallel}\cdot\sigma_2$

* FMC: $\frac{\tau_{21}^4}{\bar{R}_{\perp\parallel}^{\,4}} + a_{\perp\parallel}\cdot\frac{2\cdot\sigma_2\cdot\tau_{21}^2}{\bar{R}_{\perp\parallel}^{\,3}} = \frac{\tau_{nt}^2}{\bar{R}_{\perp\parallel}^{\,4}} + a_{\perp\parallel}\cdot\frac{2\cdot\sigma_n\cdot\tau_{nt}^2}{\bar{R}_{\perp\parallel}^{\,3}} = 1 \rightarrow \sigma_n = \frac{\bar{R}_{\perp\parallel}^{\,3}\cdot(\tau_{21}^4/\bar{R}_{\perp\parallel}^{\,4} - 1)}{2\cdot\tau_{nt}^2\cdot a_{\perp\parallel}}$

$\frac{d\tau_{n1}}{d\sigma_n} \rightarrow$ simpler to perform is $\frac{d\sigma_n}{d\tau_{n1}} = \frac{2\cdot\tau_{21}}{\bar{R}_{\perp\parallel}\cdot a_{\perp\parallel}} - \frac{\bar{R}_{\perp\parallel}^{\,3}\cdot(\tau_{21}^4/\bar{R}_{\perp\parallel}^{\,4} - 1)}{\tau_{21}^3\cdot a_{\perp\parallel}}$

* Simple linear Mohr: $\tau_{n1} = \bar{R}_{\perp\parallel} - \mu_{\perp\parallel}\cdot\sigma_n \rightarrow \sigma_n = \frac{\bar{R}_{\perp\parallel} - \tau_{21}}{\mu_{\perp\parallel}}$ and $\frac{d\sigma_n}{d\tau_{nt}} = \frac{-1}{\mu_{\perp\parallel}}$.

In the strength point $\tau_{n1} = \bar{R}_{\perp\parallel}$ an equal slope exists, then equating delivers

$\frac{2\cdot\tau_{21}}{\bar{R}_{\perp\parallel}\cdot b_{\perp\parallel}} - \frac{\bar{R}_{\perp\parallel}^{\,3}\cdot(\tau_{21}^4/\bar{R}_{\perp\parallel}^{\,4} - 1)}{\tau_{21}^3\cdot a_{\perp\parallel}} = \frac{-1}{\mu_{\perp\parallel}} \rightarrow a_{\perp\parallel} = \frac{\mu_{\perp\parallel}\cdot(\bar{R}_{\perp\parallel}^{\,4} + \tau_{21}^4)}{\tau_{21}^3\cdot a_{\perp\parallel}} \Rightarrow a_{\perp\parallel} = 2\cdot\mu_{\perp\parallel}$,

being a good guess for $\mu_{\perp\parallel}$ and sufficient for application.

23.3: Evaluation of friction values $\mu_{\perp\perp}$, $\mu_{\perp\parallel}$ from test results

The determination of curve parameters *a(μ)* and thereby also of μ can be performed differently:

1. One strength value with one multi-axial failure stress point on the respective pure mode curves, usually applying a linear Mohr friction envelope (*sufficient*, *see Figs. 23-2 and -3 below, it requires some fitting to optimally map the course*)
2. A more sophisticated fitting optimization process of the test data course in the respective pure domain (*min error square*) in 'pure' failure mode domains
3. The so-called Tension/Compression-Torsion test machine delivered the test points in *Fig.23-2 left*. If such a test rig is not available, then, one point on the pure mode Iff2-curve plus one in the transition zone IFF2-IFF1, see *Fig.23-3,* become an approximation basis, see *Fig. 23-3 right*
4. For $\mu_{\perp\perp}$, in addition: Derivation from fracture angle measurements θ_{fp}^{c}°, see experience in the associate figure in [*VDI 97, p. 138*], facing a pretty high scatter.

The formulas for the friction values read:

- Linear Mohr envelope: $\mu_{\perp\square} \cong (\tau_{21}{}^{fr} - \bar{R}_{\perp\parallel}) / \sigma_2{}^{fr}$ from tension-compression/torsion test machine with tube test specimens, evaluating at least two curve points or if sufficient tests from curve fitting .
- From bi-axial compression test in order to compute the friction value from evaluating $\mu_{\perp\perp} = (\bar{R}_{\perp}^{c} + \sigma_3^{fr}) / \sigma_2^{fr}$. However, the danger to buckle is to face

- If the test machine only allows a $\mu_{\perp\perp}$-test in the transition zone of the modes, *Fig.23-3*, then, the estimation from strength point $(\sigma_3^{c\,fr}, \sigma_2^{t\,fr})$ demands for a qualified stress interaction-mapping SFC. For the evaluation the interaction equation has to be employed, shown by the following MathCad procedure below:

Mathcad implicite calculation: *Vorgabe* $\mu_{\perp\perp} := 0.1$ (estimation)

$$\left(\left[(\sigma_2+\sigma_3) + \sqrt{(\sigma_2-\sigma_3)^2+0}\,\right] / 2\bar{R}_{\perp}^{t}\right)^m + \left(\left[\left(\frac{\mu_{\perp\perp}}{1-\mu_{\perp\perp}}\right)\cdot(\sigma_2+\sigma_3) + \frac{1}{1-\mu_{\perp\perp}}\sqrt{(\sigma_2-\sigma_3)^2+4\tau_{23}^{\,2}}\,\right] / \bar{R}_{\perp}^{c}\right)^m = 1 = Eff = 100\% \;.$$

Search *Suchen* $(\mu_{\perp\perp})$.

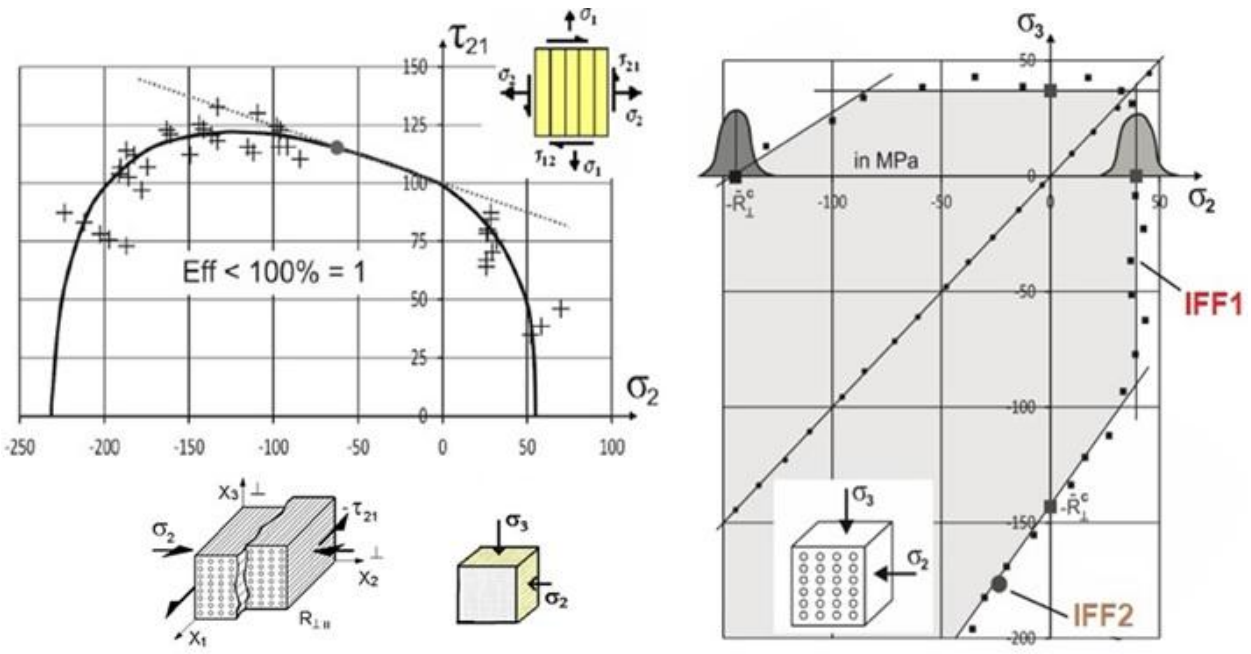

Fig.23-2: Determination of the friction values $\mu_{\perp\perp}$, $\mu_{\perp\square}$ (own results)

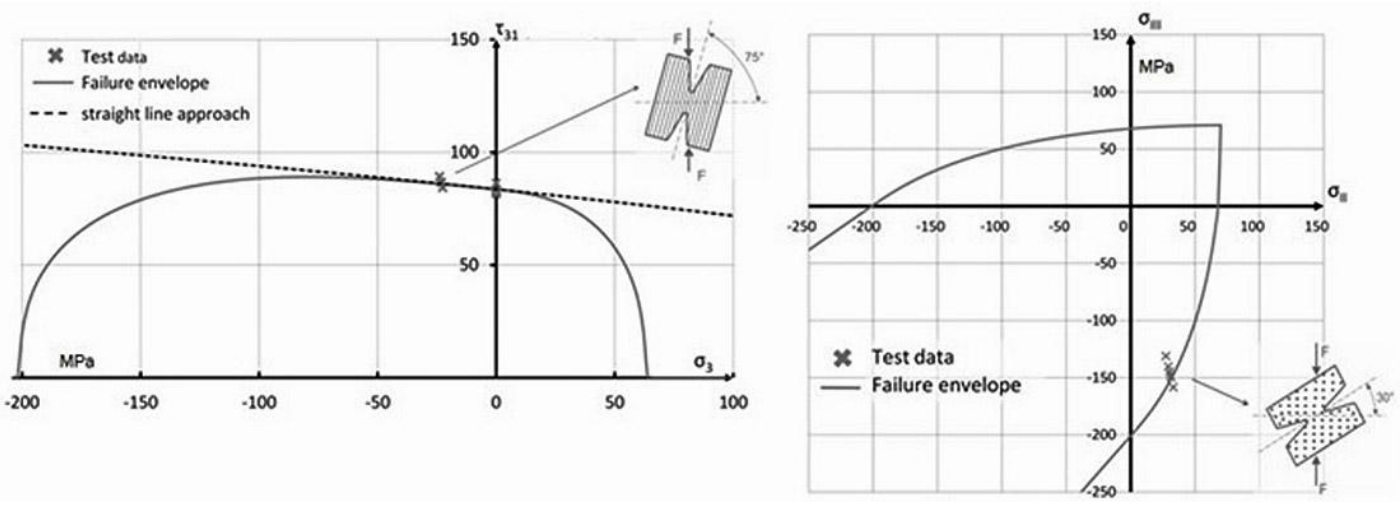

Fig.23-3: ARCAN tests performed on distinct stress paths. UD prepreg [*Pet15*]

LL:

- *A relationship of the measurable friction value and the fictitious friction parameter could be derived*
- *The application of the tension-compression-torsion test machine is recommended.*

24 Fracture Envelopes and Bodies of Grey Cast Iron, Glass C90, Normal Concrete, UHPC, Foam

Aim: *Making together with §26 'optically' familiar with multiaxial fracture stress states of isotropic materials.*

24.1 Introduction

Used Stresses and Invariants

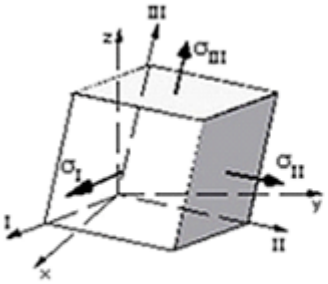

The stress states in the various COS can be transferred into each other

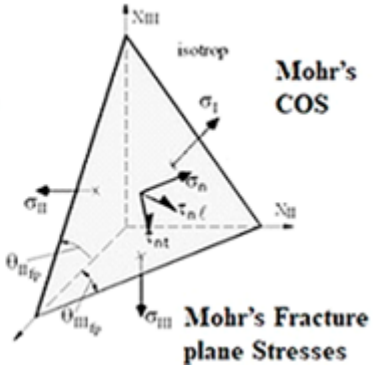

Mohr's COS

Principal Stresses Structural (component) Stresses Mohr's Fracture plane Stresses

$$\{\sigma_{\text{principal}}\}=(\sigma_I,\sigma_{II},\sigma_{III})^T,\quad \{\sigma_{\text{struct}}\}=(\sigma_x,\sigma_y,\sigma_z,\tau_{yz},\tau_{xz},\tau_{xy})^T,\quad \{\sigma_{\text{Mohr}}\}=(\sigma_\lambda,\sigma_n,\sigma_t,\tau_{nt},\tau_{\lambda t},\tau_{n\lambda})^T$$

In the transformation of structural stresses into Mohr stresses the advantage of invariants fully comes out: *They do not depend on the coordinate system, one can simply switch between the systems.*

Structural Stresses and Invariants, 3D and 2D:

$$I_1=(\sigma_I+\sigma_{II}+\sigma_{III})\ =\ f(\sigma),\quad 6J_2=(\sigma_I-\sigma_{II})^2+(\sigma_{II}-\sigma_{III})^2+(\sigma_{III}-\sigma_I)^2=\ f(\tau)\ \text{'Mises invariant'}$$

$$27J_3=\ (2\sigma_I-\sigma_{II}-\sigma_{III})\cdot(2\sigma_{II}-\sigma_I-\sigma_{III})\cdot(2\sigma_{III}-\sigma_I-\sigma_{II}),$$

$$3\cdot\sigma_{oct}=\sigma_I+\sigma_{II}+\sigma_{III}=\sigma_\ell+\sigma_n+\sigma_t\ ;\quad 9\cdot\tau_{oct}{}^2=6J_2=4\cdot(\tau_{III}{}^2+\tau_I{}^2+\tau_{II}{}^2),\quad \tau_{II}=\max\tau(\textit{mathem.})$$

$\sigma_I,\sigma_{II},\sigma_{III}$ are principal stresses, $\sigma_I>\sigma_{II}>\sigma_{III}$ are mathematical stresses (> *means more positive*).

Mohr Stresses and Invariants, 3D and 2D:

$$I_1=(\sigma_n+\sigma_t+\sigma_\lambda),\quad 6J_2=(\sigma_n-\sigma_t)^2+(\sigma_t-\sigma_\lambda)^2+(\sigma_\lambda-\sigma_n)^2+6\cdot\left(\tau_{nt}{}^2+\tau_{n\lambda}{}^2+\tau_{t\lambda}{}^2\right),\text{isotropic}\,\tau_{nt}\to\tau_n$$

Strength Failure Criteria (SFC), *Eff*-linked

At first the 'basic' formulations are displayed. Then, according to the 'proportional (stressing) concept' the relationships *Eff* (*F*) are performed. And finally, how the two shear mode parameters depend on another after having inserted R^c into F^τ. Some basic relationships are:

$$FNF=F\sigma=\frac{\sqrt{4\cdot J2-\frac{I1^2}{3}}+I1}{2\cdot Rt}=Eff\sigma=1$$

$$FSF=F\tau=c2\cdot\frac{I1}{Rc}+\frac{c1\cdot 6J2}{2\cdot Rc^2}=1$$

$$Eff\sigma=\frac{\sqrt{4\cdot J2-\frac{I1^2}{3}}+I1}{2\cdot Rt}$$

due to homogeneous F

$$c2\cdot\frac{I1}{Rc\cdot Eff\tau}+\frac{c1\cdot 6J2}{2\cdot Rc^2\cdot Eff\tau^2}=1$$

$$Eff\tau=\frac{\sqrt{I1^2\cdot c2^2+12\cdot J2\cdot c1}+I1\cdot c2}{2\cdot Rc}$$

Insertion of the compressive strength delivers a parameter -relation :

$$c2\cdot\frac{-Rc}{Rc}+\frac{c1\cdot 2\cdot Rc^2}{2\cdot Rc^2}=1\qquad c1=c2+1$$

Monotonic stressing of all stresses

Interaction requires to go from *F* to *Eff*, linked due to the 'proportional stressing concept'

for instance $$c_2^{SF}\cdot\frac{I_1/Eff}{\bar{R}^c}+c_1^{SF}\cdot\frac{6\cdot J_2/Eff^2}{2\cdot\bar{R}^{c2}}=1.$$

Table 24-1 summarizes the Eff^{mode} formulations for the usually as rotationally-symmetric *assumed* fracture failure body, and further the realistic isotropic 120°-rotational symmetry relations.

Fig.24-1: Procedure how to determine the Fracture Body

(1) Fracture failure body is rotationally symmetric (like the Mises yield body)

* Normal Fracture NF, $I_1 > 0$ ↔ * Shear Fracture SF, $I_1 < 0$

$$F^{NF} = F^{\sigma} = \frac{\sqrt{4J_2 - I_1^2/3} + I_1}{2 \cdot \bar{R}^t} \qquad F^{SF} = F^{\tau} = c_2^{SF} \cdot \frac{I_1}{\bar{R}^c} + c_1^{SF} \cdot \frac{6 \cdot J_2}{2 \cdot \bar{R}^{c2}}$$

with σ and τ as failure driving stresses. Resistances $\bar{R}$ are average values (We model !).

Strength Failure Criterion (SFC), mode interaction exponent m, friction μ

$$Eff^{NF} = \frac{\sqrt{4J_2 - I_1^2/3} + I_1}{2 \cdot R^t} = \frac{\sigma_{eq}^{NF}}{\bar{R}^t} \leftrightarrow Eff^{SF} = \frac{c_2^{SF} \cdot I_1 + \sqrt{(c_2^{SF} \cdot I_1)^2 + 12 \cdot c_1^{SF} \cdot 3J_2}}{2 \cdot R^c} = \frac{\sigma_{eq}^{SF}}{\bar{R}^c}.$$

with $c_1^{SF} = 1 + c_2^{SF}$, $c_2^{SF} = (1 + 3 \cdot \mu)/(1 - 3 \cdot \mu)$ from $\mu = -\cos(2 \cdot \theta_{fp}^c \cdot ° \cdot \pi / 180)$

or from fitting of the test data course.

(2) Fracture failure body is 120°-rotationally symmetric = Reality !

In a chapter before we had to learn: Each isotropic material is "120° – rot. symmetric",

which leads to the little more complicate *Effs* below

$$Eff_{\Theta}^{NF} = c^{NF} \cdot \frac{\sqrt{4J_2 \cdot \Theta^{NF} - I_1^2/3} + I_1}{2 \cdot R^t} \leftrightarrow Eff_{\Theta}^{SF} = \frac{c_2^{SF} \cdot I_1 + \sqrt{(c_2^{SF} \cdot I_1)^2 \cdot \Theta^{SF} + 12 \cdot c_{1\Theta}^{SF} \cdot 3J_2}}{2 \cdot R^c}$$

$c_{1\Theta}^{SF} \cdot \Theta^{SF} = 1 + c_2^{SF}$, and above friction parameter c_2^{SF} (later denoted c_2)

Modelling of the cap is performed by the function $y_{cap} = \frac{I_1}{\sqrt{3} \cdot \bar{R}^t} = s^{cap} \cdot (\frac{\sqrt{2J_2 \cdot \Theta^{NF}}}{\bar{R}^t})^2 + \frac{max\, I_1}{\sqrt{3} \cdot \bar{R}^t}$.

For $R^c >> R^t$ can be set : $\Theta^{NF} \rightarrow \Theta^{TM} = \sqrt[3]{1 + d^{NF} \cdot (+1)}$, $c^{NF} = \Theta^{NF} = 1$.

Θ as non-circularity function with d as non-circularity parameter, (d^{SF} later d^{τ})

$\Theta^{SF} = \sqrt[3]{1 + d^{SF} \cdot sin(3\vartheta)} = \sqrt[3]{1 + d^{SF} \cdot 1.5 \cdot \sqrt{3} \cdot J_3 \cdot J_2^{-1.5}}$, compr. angle -30° $\rightarrow \Theta^{SF} = \sqrt[3]{1 + d^{SF} \cdot (-1)}$.

3D-tests are performed by adding an axial load, generating a stress σ_{ax}, upon a hydrostatic loading $p_{hyd.}$ The associated 3D-concrete test data sets have been forwarded by Dr.-Ing. Silke Scheerer and Dr.-Ing. Kerstin Speck (*IfM, TU-Dresden, Prof. Dr. M. Curbach).* From their provided raw data sets as sub-sets the meridian data sets, the constant Lode angles for the envisaged meridians had to be extracted by the author. The usual tests are run along the tensile meridian (TM) and the compressive meridian (CM). This situation causes to apply the realistic isotropic 120°-rotationally-symmetric model in order to account for the Lode angle ϑ.

Determination of the model parameters in the mode domain of F^{τ} : The measurement of Θ_{fp} –based on the usually small-scale test level - is practically not possible. The determination of the curve parameters c_i by mapping the course of test data points is the better and practical procedure. Then, the relationship of the curve parameter c_2 to the friction value μ and to the fracture angle Θ_{fp} can be derived. These relations are obtained in the *touch point,* still pointed out in *Fig.22-1* for UD-materials.

Circularization of the fracture body

From mechanics is known that the fracture body possesses a circle-shape for I_1 =0 and from testing is known, that the body becomes circular with increasing negative I_1.

At least for the Ultra-High-Performance-Concrete (UHPC) this must be considered when mapping, because the SFC F^{τ} cannot capture this effect. In the next box are collected all relationships and further the determination of the two additional parameters $\alpha\tau$, $\beta\tau$:

Maximum $\Theta\tau cc$ in the bi-axial reference point (-Rcc, -Rcc.0) on the TM

$$\Theta\tau CM = \sqrt[3]{1 - d\tau ex} \qquad \Theta\tau TM = \sqrt[3]{1 + d\tau ex} \qquad x = \frac{\sqrt{2J2}}{Rc} \qquad I1 = \sqrt{3}\cdot Rc\cdot y$$

Model : $d\tau ex(y) = \alpha\cdot\beta\cdot(-y)^{\beta-1}\cdot\exp\left[-\alpha\cdot(-y)^{\beta}\right]\cdot d\tau cc$ Two unknowns require two equations

* Differentiation, in order to obtain a formula for the horizontal tangent in (-Rcc, -Rcc.0)

$$\frac{d}{dy}\left[\alpha\cdot\beta\cdot(-y)^{\beta-1}\cdot\exp\left[-\alpha\cdot(-y)^{\beta}\right]\cdot d\tau cc\right] \rightarrow \beta^2\cdot\alpha^2\cdot d\tau cc\cdot(-y)^{2\cdot\beta-2}\cdot e^{-\alpha\cdot(-y)^{\beta}} - \beta\cdot\alpha\cdot d\tau cc\cdot(-y)^{\beta-2}\cdot e^{-\alpha\cdot(-y)^{\beta}}\cdot(\beta-1)$$

$$\left[\alpha\cdot\beta\cdot\left(-\frac{I1cc}{\sqrt{3}\cdot Rt}\right)^{\beta-1}\cdot\frac{\beta-1}{\frac{I1cc}{\sqrt{3}\cdot Rt}}\cdot e^{(-\alpha)\cdot\left(-\frac{I1cc}{\sqrt{3}\cdot Rt}\right)^{\beta}} - \alpha^2\cdot\beta^2\cdot\left(-\frac{I1cc}{\sqrt{3}\cdot Rt}\right)^{\beta-1}\cdot\frac{\left(-\frac{I1cc}{\sqrt{3}\cdot Rt}\right)^{\beta}}{\frac{I1cc}{\sqrt{3}\cdot Rt}}\cdot e^{(-\alpha)\cdot\left(-\frac{I1cc}{\sqrt{3}\cdot Rt}\right)^{\beta}}\right]\cdot d\tau cc = 0$$

$d\tau cc$ vanishes

Dissolved for $\alpha\tau = \alpha$ (NF, $\alpha\sigma$ not of interest here)
delivers an equation for the first curve parameter

$$\alpha\tau = \frac{\beta\tau - 1}{\beta\tau\cdot\left(\frac{-1}{3}\cdot I1cc\cdot\frac{3^{0.5}}{Rz}\right)^{\beta\tau}}$$

* Second curve parameter is determined by assuming that the non-circularity reduction is 50% at 2 x I1cc

Vorgabe $\beta\tau := 1.5$ Material data insertion now !

$$0.5 = \frac{\frac{\beta\tau-1}{\beta\tau\cdot\left(\frac{-1}{3}\cdot I1cc\cdot\frac{3^{0.5}}{Rt}\right)^{\beta\tau}}\cdot\beta\tau\cdot\left(-\frac{I1cc\cdot 2}{\sqrt{3}\cdot Rt}\right)^{\beta\tau-1}\cdot\exp\left[-\frac{\beta\tau-1}{\beta\tau\cdot\left(\frac{-1}{3}\cdot I1cc\cdot\frac{3^{0.5}}{Rt}\right)^{\beta\tau}}\cdot\left(-\frac{I1cc\cdot 2}{\sqrt{3}\cdot Rt}\right)^{\beta\tau}\right]\cdot 1}{\frac{\beta\tau-1}{\beta\tau\cdot\left(\frac{-1}{3}\cdot I1cc\cdot\frac{3^{0.5}}{Rt}\right)^{\beta\tau}}\cdot\beta\tau\cdot\left(-\frac{I1cc}{\sqrt{3}\cdot Rt}\right)^{\beta\tau-1}\cdot\exp\left[-\frac{\beta\tau-1}{\beta\tau\cdot\left(\frac{-1}{3}\cdot I1cc\cdot\frac{3^{0.5}}{Rt}\right)^{\beta\tau}}\cdot\left(-\frac{I1cc}{\sqrt{3}\cdot Rt}\right)^{\beta\tau}\right]\cdot 1}$$

$A\tau := Suchen(\beta\tau)$ $\beta\tau := A\tau$ $\beta\tau =$ ▮ $\alpha\tau =$

$$\Theta\tau(y) = \sqrt[3]{1 + d\tau(y)\cdot\sin(3\theta)} \qquad \text{with} \qquad d\tau(y) = \alpha\tau\cdot\beta\tau\cdot(-y)^{\beta\tau-1}\cdot\exp\left[-\alpha\tau\cdot(-y)^{\beta\tau}\right]\cdot d\tau$$

$$\Theta\tau cc = \sqrt[3]{1 + \alpha\tau\cdot\beta\tau\cdot(-ycc)^{\beta\tau-1}\cdot\exp\left[-\alpha\tau\cdot(-ycc)^{\beta\tau}\right]\cdot d\tau\cdot(1)} \qquad \Theta\tau c = \sqrt[3]{1 + \alpha\tau\cdot\beta\tau\cdot(-yc)^{\beta\tau-1}\cdot\exp\left[-\alpha\tau\cdot(-yc)^{\beta\tau}\right]\cdot d\tau\cdot(-1)}$$

$$\Theta\tau TM_j = \sqrt[3]{1 + \alpha\tau\cdot\beta\tau\cdot\left(-y_j\right)^{\beta\tau-1}\cdot\exp\left[-\alpha\tau\cdot\left(-y_j\right)^{\beta\tau}\right]\cdot d\tau} \qquad \Theta\tau CM_j = \sqrt[3]{1 + \alpha\tau\cdot\beta\tau\cdot\left(-y_j\right)^{\beta\tau-1}\cdot\exp\left[-\alpha\tau\cdot\left(-y_j\right)^{\beta\tau}\right]\cdot d\tau\cdot(-1)}$$

Some 2D-test data are provided in literature for Grey Cast Iron and Glass C 90, the latter used as window pane of the ISS. For completion the author's accompanying evaluations shall be presented at the end of chapter 24.

(The generation of the following §24-figures has been performed about 2015/2016, whereas §25 is a present complement elaboration).

24.2 Visualization of 3D compression test data: Normal Concrete

In *Fig. 24-1, left*, the course of test data is mapped. As coordinates, the Lode-Haigh-Westergaard coordinates are used which equally count in all directions of the 3D stress space (*for understanding see Fig.14-9*). The tensile strength is used for normalization in the case of brittle materials.

The right part figure displays the fracture failure body, on which the 3 main meridians are depicted. For the tensile meridian a Lode angle $\vartheta = +30°$ is valid and for the compressive meridian $\vartheta = -30°$. The shear meridian was chosen by the author as neutral meridian with the Lode angle $\vartheta = 0$. For each mode, the SFC model parameters must be determined in each associated 'pure'failure mode domain. In this context physics of slightly porous isotropic materials is to remember: **bi-axial tension = weakest link failure behavior ($R^{tt}<R^{t}$, which partly seems to be not accepted in civil engineering) and * bi-axial compression = redundant (benign) failure behavior ($R^{cc}>R^{c}$).*

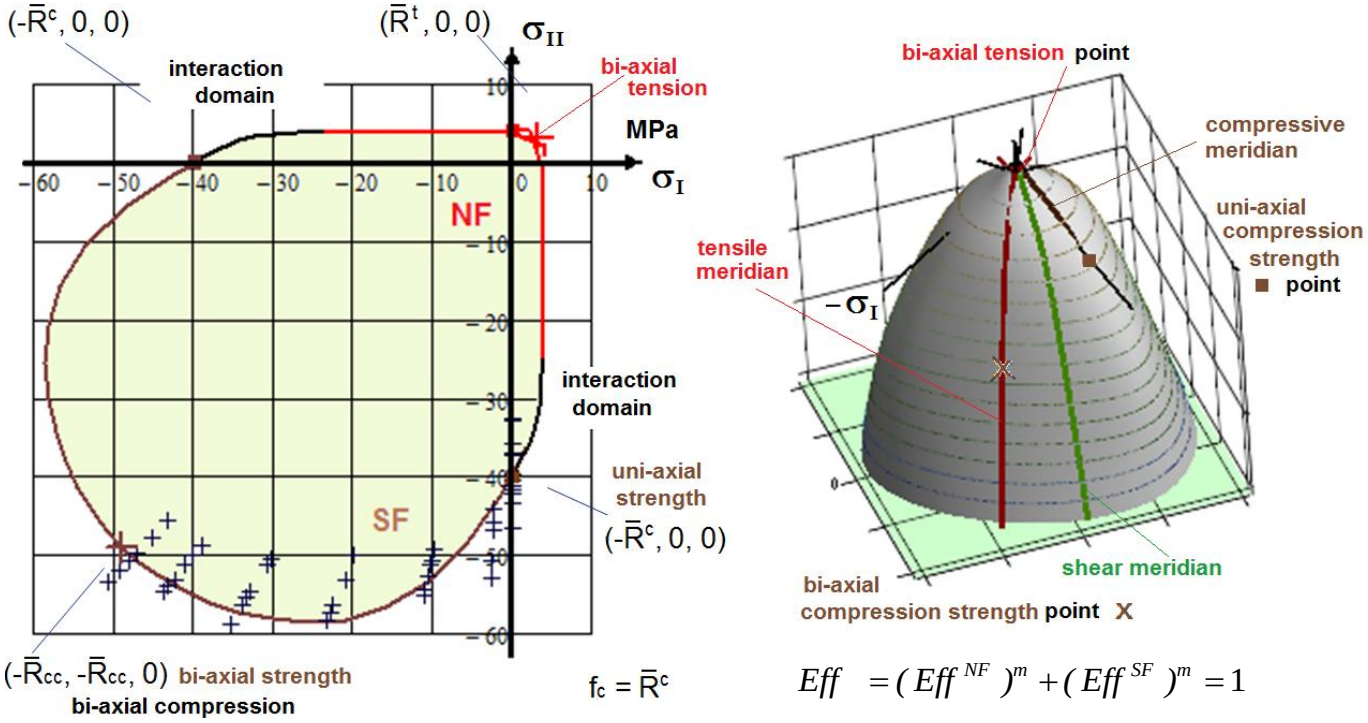

Fig.24-1, Normal Concrete: mapping of 2D-test data in the Principal Stress Plane as the bias cross-section of the fracture body. R= strength, t=tensile, c=compressive; bar over means average (mean) value. μ ≅ 0.2. (test data, courtesy: IfM Dresden)

Fig.24-2 through *24-4* present a hoop cross–section (*octahedral stress plane or so-called π-plane*), two axial cross-sections, the meridians of the failure body, and two views of the failure body.

The interaction to be performed has to capture both the modes. Hence for a common display, a normalization strength is to employ, generally the tensile strength.

Table 24-2, Normal Concrete: Data set

$$F^{NF} = F^{\sigma} = c^{NF} \cdot \frac{\sqrt{4J_2 - I_1^2/3} + I_1}{2 \cdot \bar{R}^t}\ ,\ F^{SF} = F^{\tau} = c_{1\Theta}^{SF} \cdot \frac{6J_2 \cdot \Theta^{SF}}{2 \cdot \bar{R}^{c2}} + c_2(\mu) \cdot \frac{I_1}{\bar{R}^c} = 1$$

Normalizing here with $\bar{R}^t$ and $\bar{R}^c$. Tension dent too small to be practically of interest $\rightarrow c^{NF} = 1$.

2 remaining unknowns require 2 fix stress fracture points on the surface of the fracture body:

$$\{\sigma_{fr}\}: \left(-\bar{R}^c, 0, 0\right)^T,\ \left(-\bar{R}^{cc}, -\bar{R}^{cc}\, 0,\ 0\right)^T,\ m = 2.9,$$

with the values in MPa = N/mm^2: $\bar{R}^t = 4$, $\bar{R}^c = 40$, $\bar{R}^{cc} = 49$, $\Theta_{fp}{}^{c} = 51° \rightarrow \mu = 0.21$,

$c_{1\Theta}^{SF} \cdot \Theta^{CM} = 1 + c_2$ with $c_2 = 4.3$ as friction parameter, $\vartheta = -30°$ for CM, +30° for TM

$c_{1\Theta}^{SF} = 6.8$, $d^{SF} = 0.51$, $\Theta^{SF} = \sqrt[3]{1 + d^{SF} \cdot \sin(3\vartheta)} \rightarrow \Theta^{TM} = 1.15$, $\Theta^{CM} = 0.79 \equiv \Theta^{\tau}$.

For the determination of the closing cap and the open bottom of the fracture body:

$\bar{R}^{ttt} = 3.6 \rightarrow$ closing cap point max $I_1 = 3 \cdot \bar{R}^{ttt}$, $\bar{R}^{ccc} = 1000$ MPa (set for computation).

With Awaji-Sato the non measurable $\bar{R}^{ttt}$ is estimated: $\bar{R}^{ttt} = \bar{R}^t / 3^{1/M}$, $M = \ln(2) / \ln(\bar{R}^t / \bar{R}^{tt})$.

$\bar{R}^{tt} = 0.9 \cdot \bar{R}^t$ (assumed), $s^{cap} = -0.57$. Further $\alpha_\tau = 0.0037$, $\beta_\tau = 1.92$.

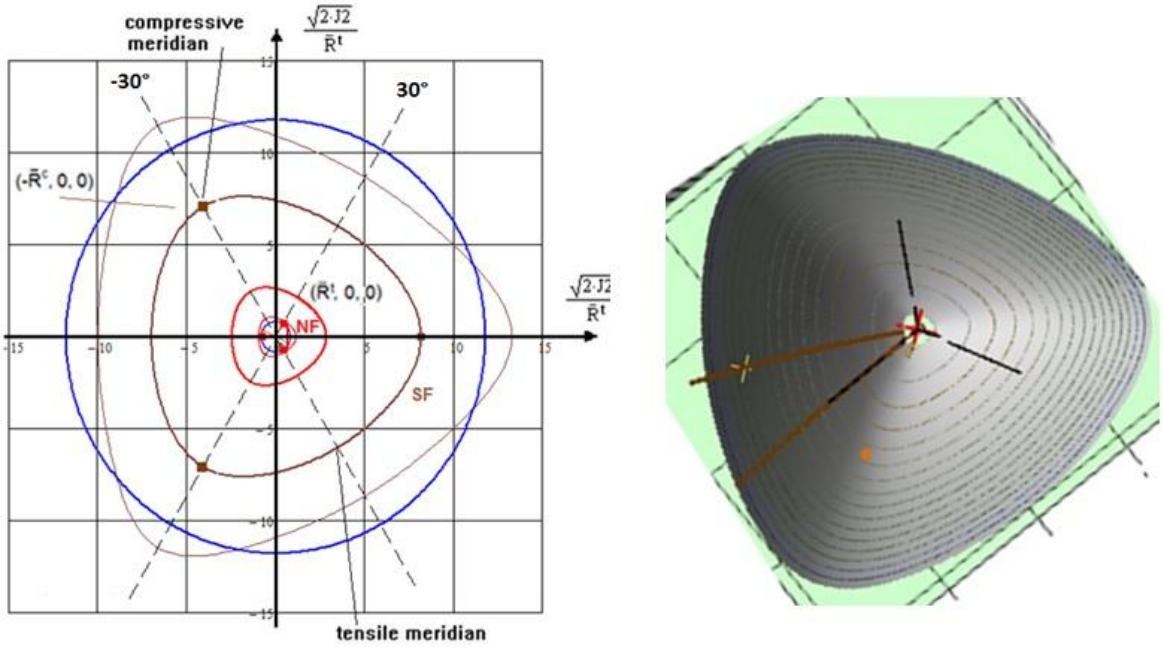

*Fig.24-2, Normal Concrete: Top view: Octahedral stress plane (π-plane) exhibiting the constant Eff- lines on the body (the **blue** line refers to $I_1 = 0$). Right: X R^{cc}, ● R^c.*

In *Fig.24-3* the modeling of cap, NF domain (marginal) and of the SF fracture domain is depicted. Modelling of a cap is shown in the sub-chapter foam.

Fig.24-4 shows the three basic meridians and two strength points, compressive strength (dot) and bi-axial compressive strength (cross).

Fig.24-5 informs about the test data scatter of the 3D fracture states experienced under hydrostatic pressure when running test on the tensile meridian and on the compressive meridian (-30°), selection of test data performed.

The Neutral Meridian represents the shear meridian.

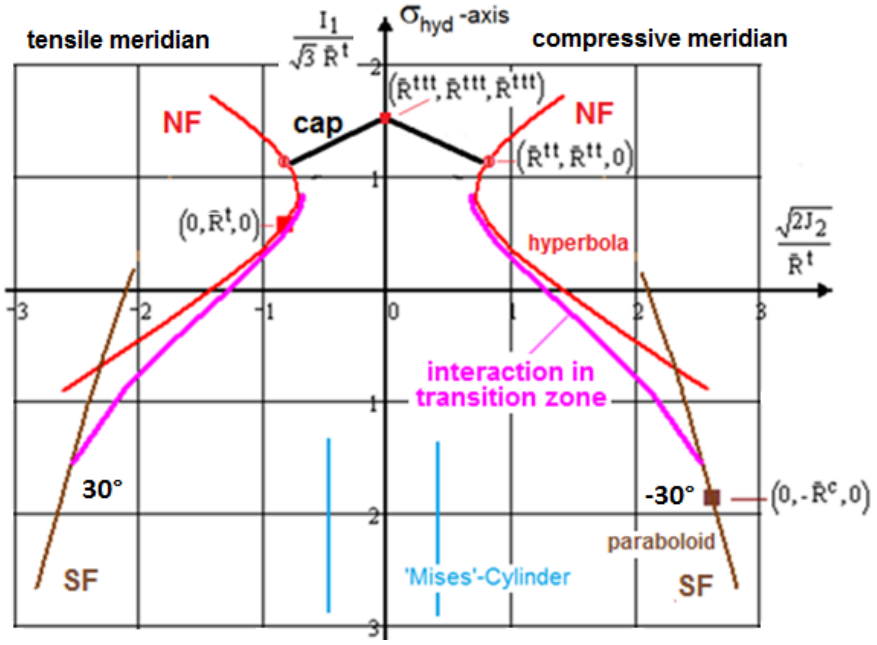

*Fig. 24-3, axial cut: Visualization of the courses of the 2 mode mapping functions for NF and SF along the meridian cross sections of the fracture body (180° cut of the 120°-body) and after **interaction***

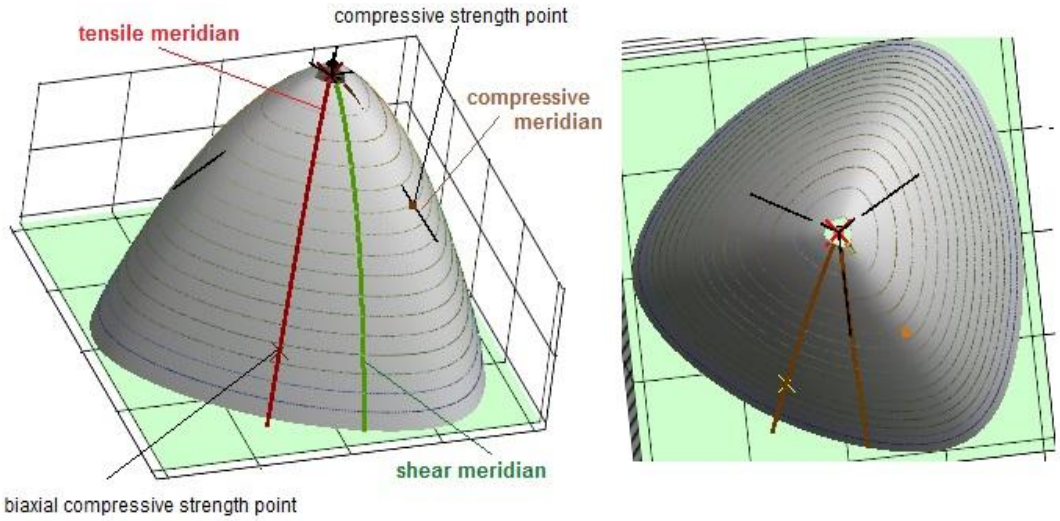

Fig.24-4: Two views of the 120°-rotationally-symmetric fracture body (hoop cross-section) of Normal Concrete with the basic three meridians and the strength points [Cun17]

In *Fig.24-6* the meridian failure curves are depicted and CM test points are inserted indicating where the determination of the Mohr quantities τ_n, σ_n, θ_{fp} has been performed. As coordinates, the Haigh-Lode-Westergaard coordinates are used which equally count in all directions of the space.

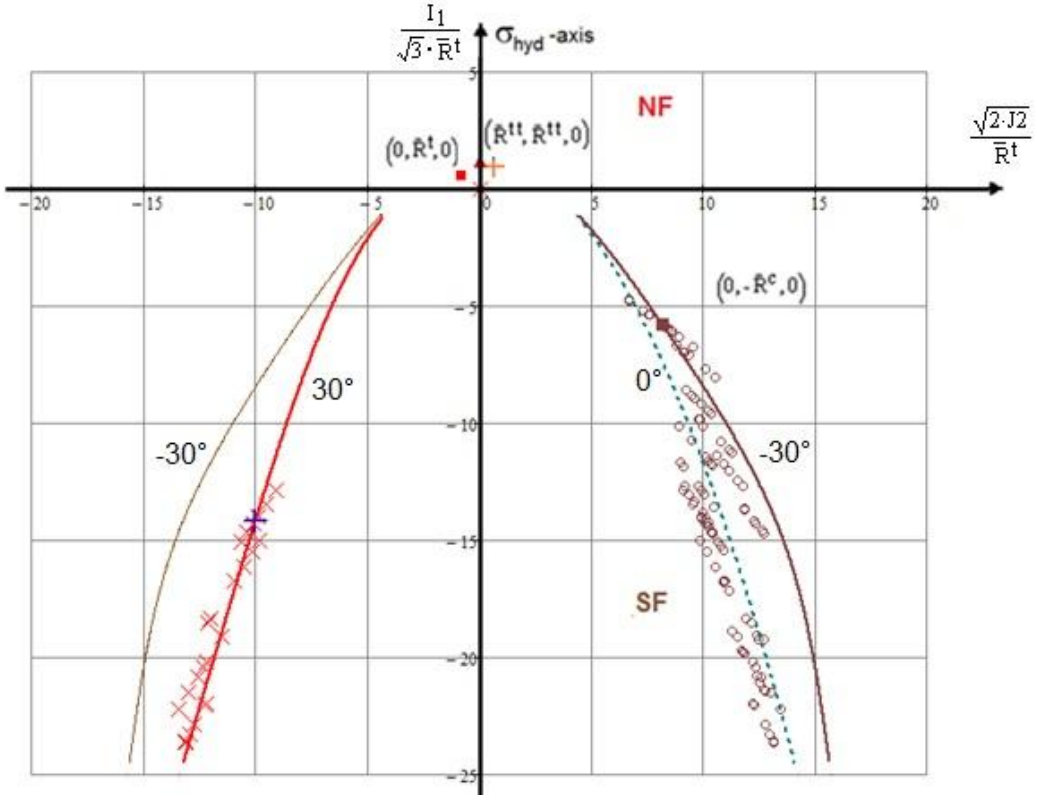

Fig.24-5: (left) Tensile meridian curve (TM) and associated test data (x, 30°), (right) compressive meridian (-30°) curve (CM) and test data on the respective hoop ring o (these circles o are located at different meridian angles ϑ), courtesy IfM Dresden

Extrapolated guess of the CM-curve on basis of mapped TM test data and vice versa:

Just replace the Lode angle part for 30°, sin (3ϑ) = 1, by that for -30°, sin (3ϑ) = -1.

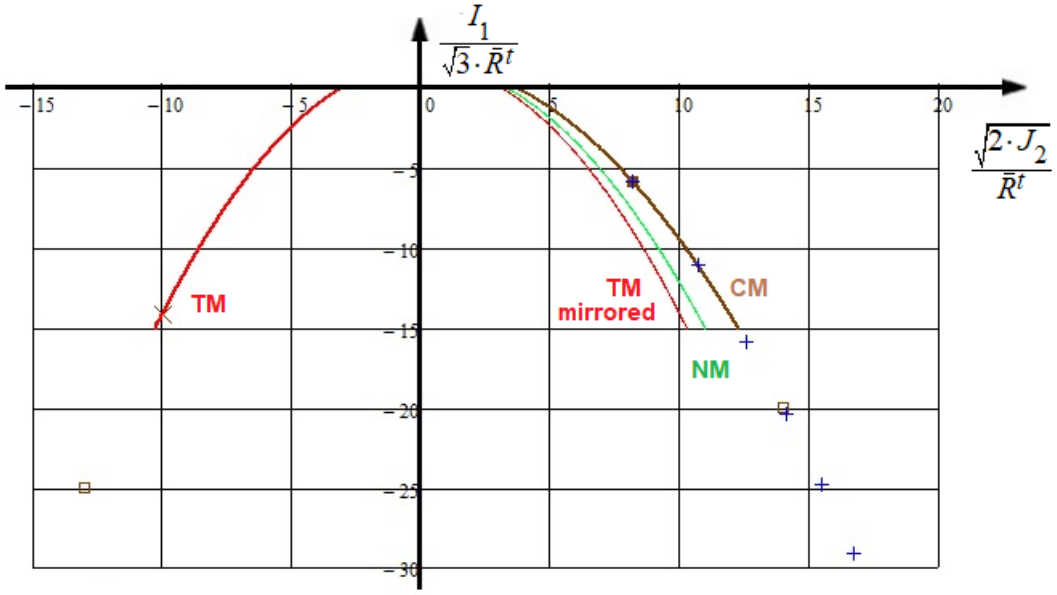

Fig.24-6: Display of all basic meridians of Normal Concrete. The + are the points where the evaluation of τ_{nt}, σ_n, θ_{fp} was performed. p = p_{hyd}. TM Tensile Meridian, CM Compressive Meridian, NM Normal Meridian.
(Mathcad unfortunately did not draw below y = -15, an often faced Mathcad problem)

The above depicted basic three meridians are: Tensile Meridian TM (ϑ = +30°) inside, Neutral Meridian NM (0°) and Compressive Meridian CM (ϑ = -30°), outside. Test points lie on the respective meridian, determined by ϑ, which means on different distances from the axis for a specific $x = I_1 / \sqrt{3 \cdot \bar{R}^t}$ value.

For Normal Concrete, *Fig.24-6* significantly supports the existence of the 120°-rotational symmetry of brittle isotropic materials.

24.3 Visualization of 3D compression test data: UltraHighPerformanceConcrete (UHPC)

Fig.24-7, left depicts the separated and later intensively investigated TM and CM test data points.

Fig.24-7, right presents all 3D test points located at different Lode angles.

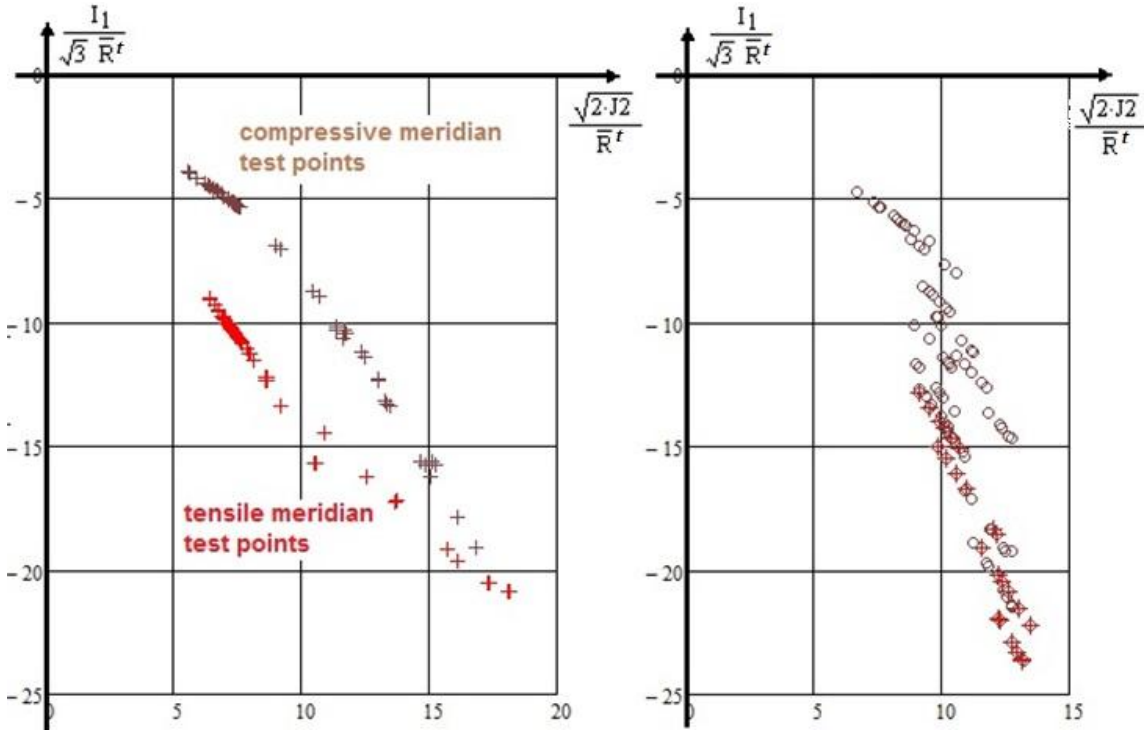

Fig.24-7 UHPC: Compressive and tensile meridian points
UHPC, separated test points: (left) tensile meridian + (ϑ = +30°) and compressive meridian + (ϑ = -30°) ; (right) all 3D test points are marked by **o** *(hoop ring, ($\vartheta \neq$,+, - 30°)), visualizing to be located at different meridians*

Fig.24-8 outlines modelling ideas for UHPC.

As could be still recognized for Normal Concrete, the failure body possesses inward dents for $I_1 > 0$ and outward dents for $I_1 < 0$ in contrast to porous concrete stone, where it is also inward, see *Fig.24-9.* Due to *Fig, 24-7*, the dents become smaller with increasing negative I_1. This is to consider by the envisaged correction function.

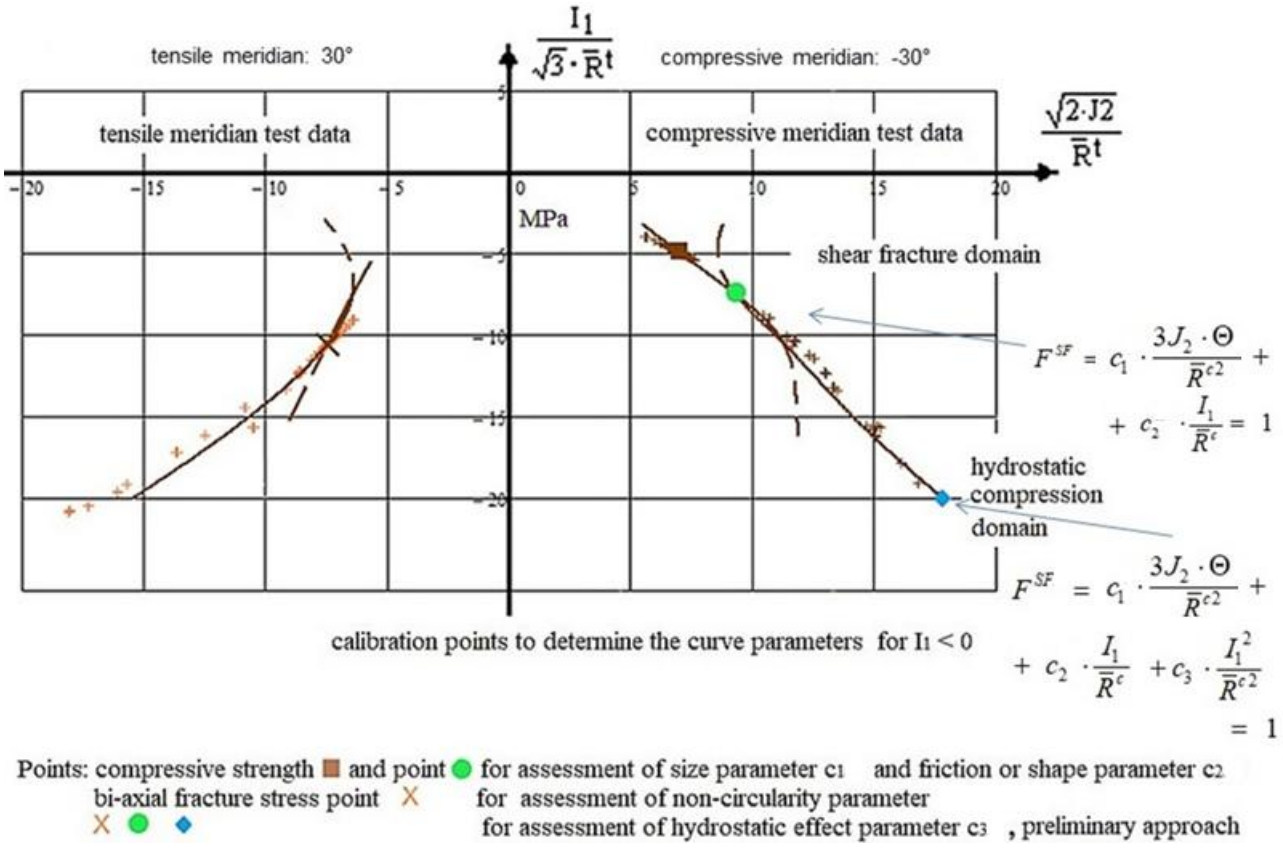

Fig.24-8 Ultra-High-Performance-Concrete (UHPC):
[Test data: Dr. Speck, IfM, TU-Dresden]. From this general data set as sub-sets the meridian data sets (constant Lode angles) have been extracted by the author

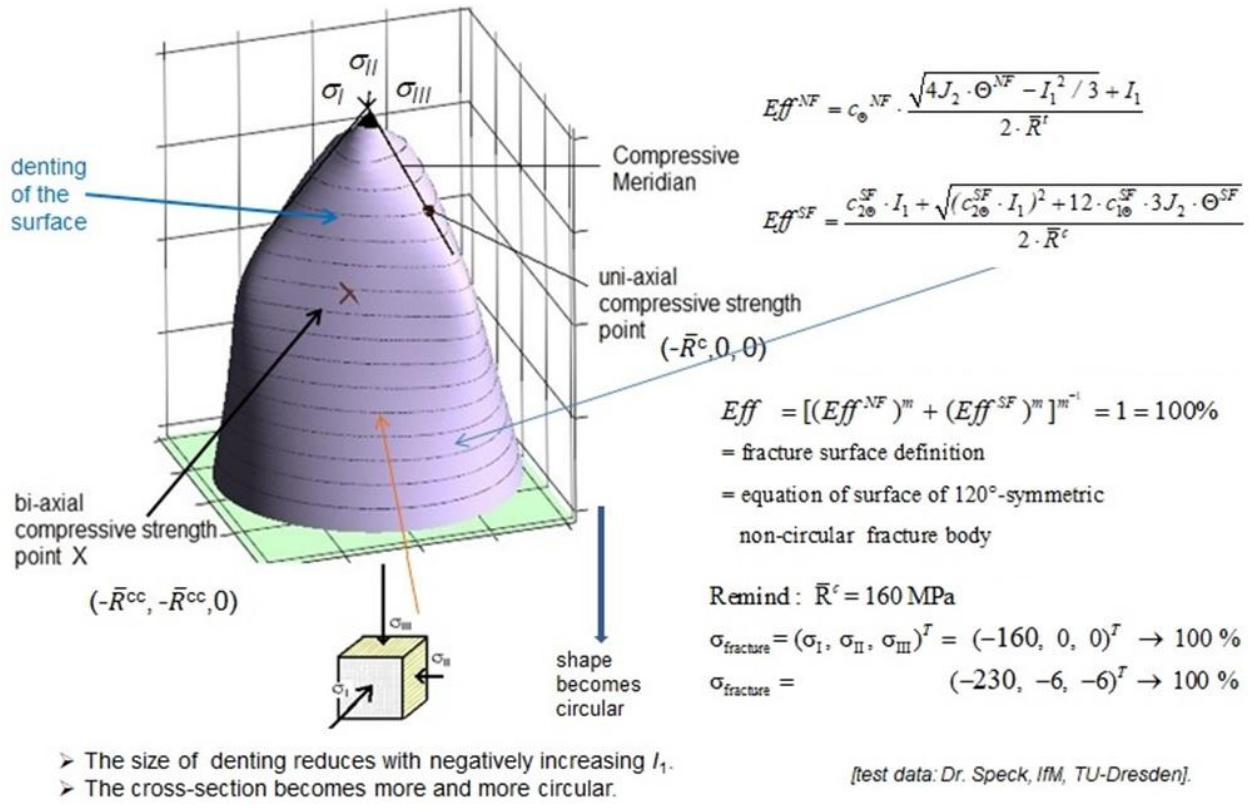

Fig.24-9, UHPC: Fracture body showing decay of denting with a negative I_1

Fig.24-10 shows a graph the bi-axial compressive strength over the uniaxial compressive strength. It turns out that with increasing uniaxial strength the bi-axial strength approximates the uniaxial strength. The author tries to explain this: The effect of redundancy under hydrostatic loading can be interpreted as an out-smoothing of stress concentrations. In the case of Normal Concrete this effect becomes more chances according to being more roughly grained than UHPC. This explains why the bi-axial strength capacity increase of a roughly grained Normal Concrete is higher than for UHPC.

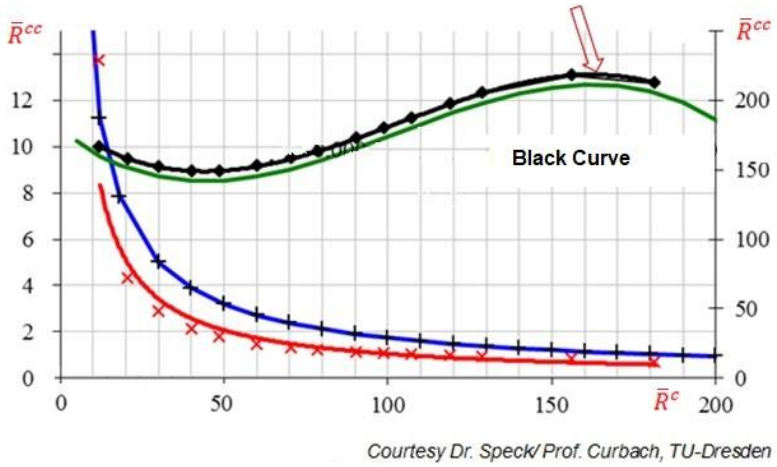

Fig.24-10: compressive strength capacity ratio of concrete $\bar{R}^{cc} / \bar{R}^{c}$ *(R = f),*

$\bar{R}^{cc} / \bar{R}^{c}$ (Normal Concrete) > $\bar{R}^{cc} / \bar{R}^{c}$ (UHPC)

In *Fig.24-11* are depicted the 2 mode domains and its transition zone obtained with the interaction formula. This task concentrated about performing an interaction in the principal plane $I_1 > -2R^{cc}$.

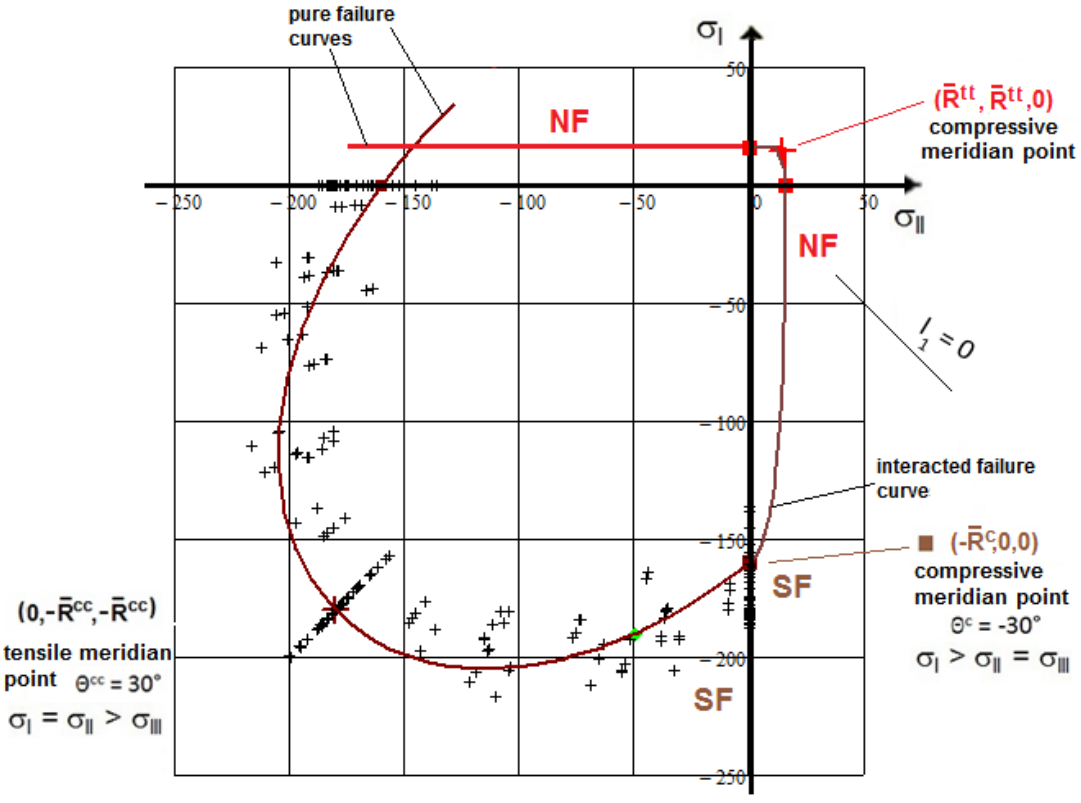

Fig.24-11, UHPC: Principal stress plane with measured test data and evaluated strength points

24.4 3D-Visualization of 2D compression test data: Porous Foam Rohacell 71 IG

With the Rohacell Hero (Evonik) a PMI (Poly-Methacryl-Imide) structural foam of an increased tensile fracture strain a light material is available which may replace the expensive honeycombs. Given is 'only' a 2D-Test Data Set and therefore just a realistic mapping in the Principal Stress Plane is possible data set used (*thanks to Dr. Kolupaev for the test data set*) reads:

$$\bar{R}^{t} = 1.8;\ \bar{R}^{tt} = 1.25;\ \bar{R}^{ttt} = 1.01;\ \bar{R}^{c} = 1.65;\ \bar{R}^{cc} = 1.4;\ \bar{R}^{ccc} = 1.53,\ \max I_1 = 3.03;$$
$$\min I_1 = -4.58,\ d^{NF} = -0.71;\ d^{CrF} = 0.21;\ c^{CrF} = 1.03, s^{cap} = -0.27;\ s^{bot} = 0.87,$$
$$\vartheta^{NF} = -0.57;\ \vartheta^{CrF} = 0.52;\ \Theta^{NF} = 1.2;\ \Theta^{CrF} = 1.07, m = 2.5.$$

The *Figs.* 24-12 and *24-13* show the application of the respective SFC for the given Rohacell.

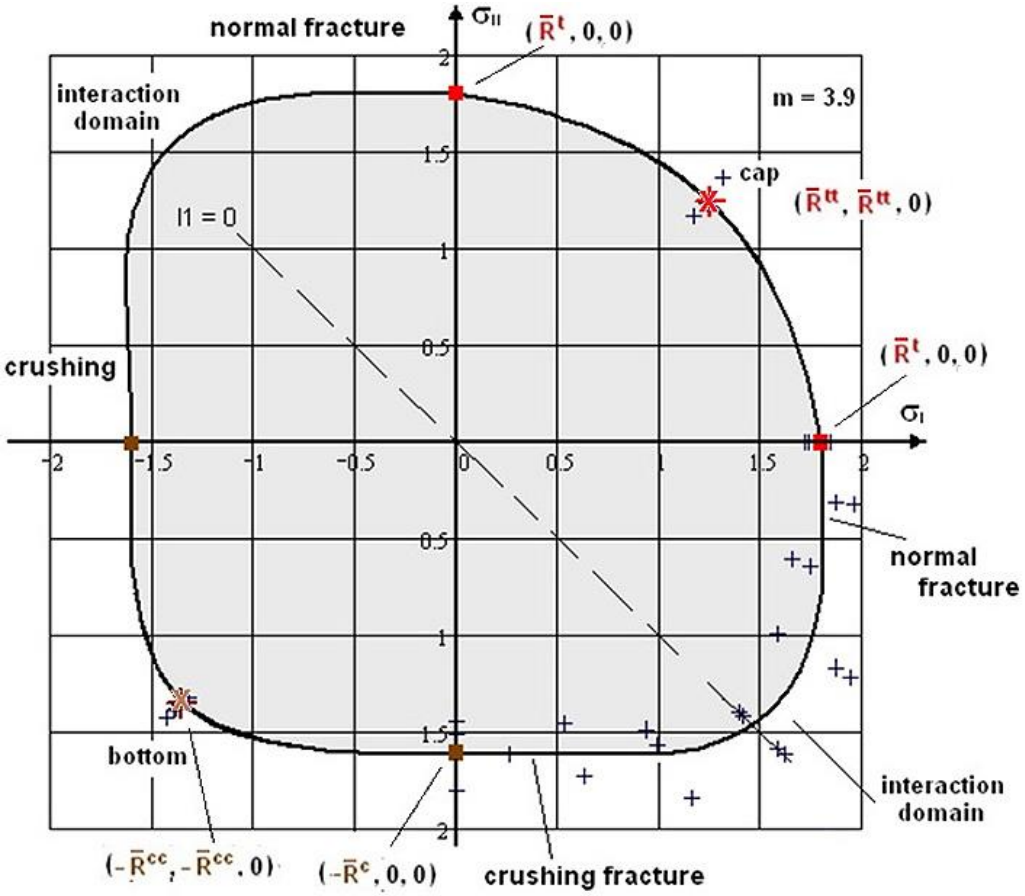

Fig.24-12, Foam Rohacell 71 IG: Mapping of 2D-test data in the Principal Stress Plane. MathCad plot [test data: courtesy V. Kolupaev, LBF Darmstadt]

The SFC-model for porous Foam Rohacell including the cap model is applicable for Concrete Stone material, too. On top a bottom is now to model.

Usually, for structural parts of high stiffness, honeycombs are used. With the new Rohacell Hero (Evonik) a PMI (Poly-Methacryl-Imide) structural foam of an increased tensile fracture strain is available which may replace the expensive honeycombs. In order to apply this material in structural parts Structural Integrity must be proven. This requires reliable multi-axial strength test data as well as reliable Strength Failure Conditions SFCs (criteria) for an optimal Design Development process. Given is 'only' a 2D-Test Data Set and therefore just a realistic mapping in the Principal Stress Plane is possible. To apply is the 2D subversion of the 3D SFC.

→ From this follows: Validation of the 3D SFC is ‘just’ 2D-based.

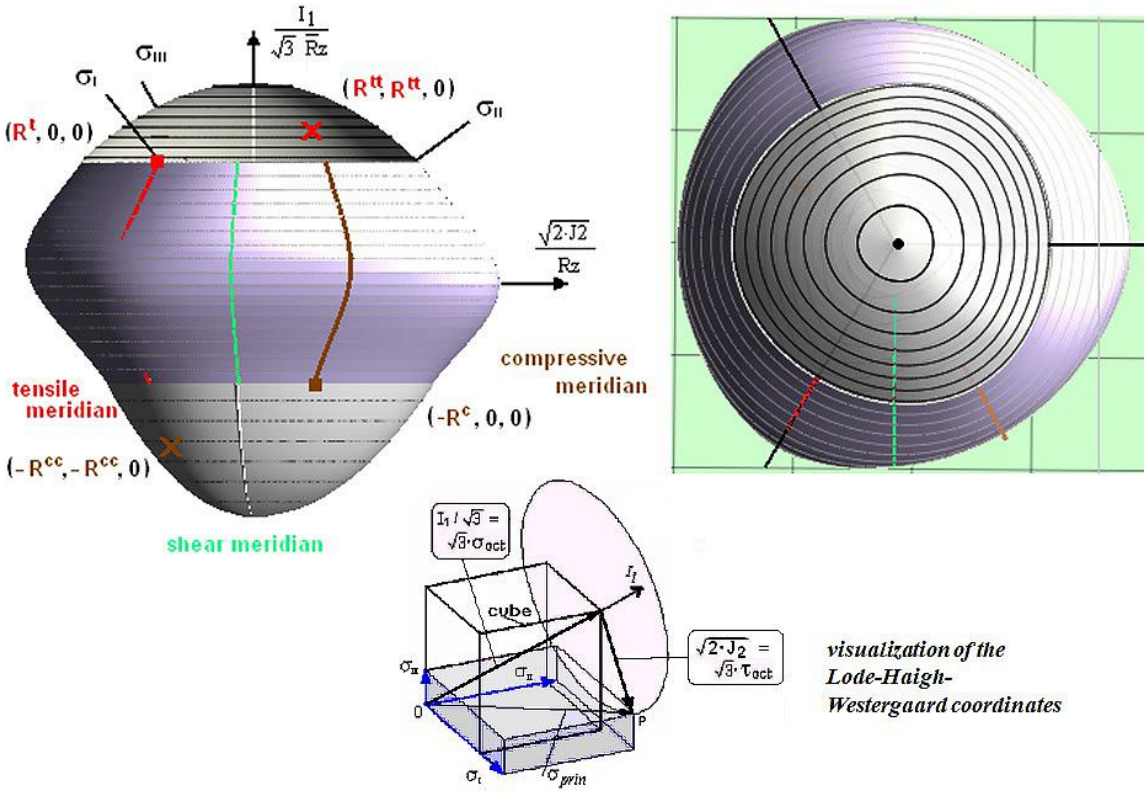

Fig.24-13, Rohacell 71 IG: Fracture body with its different meridians (left) and view from top (right).

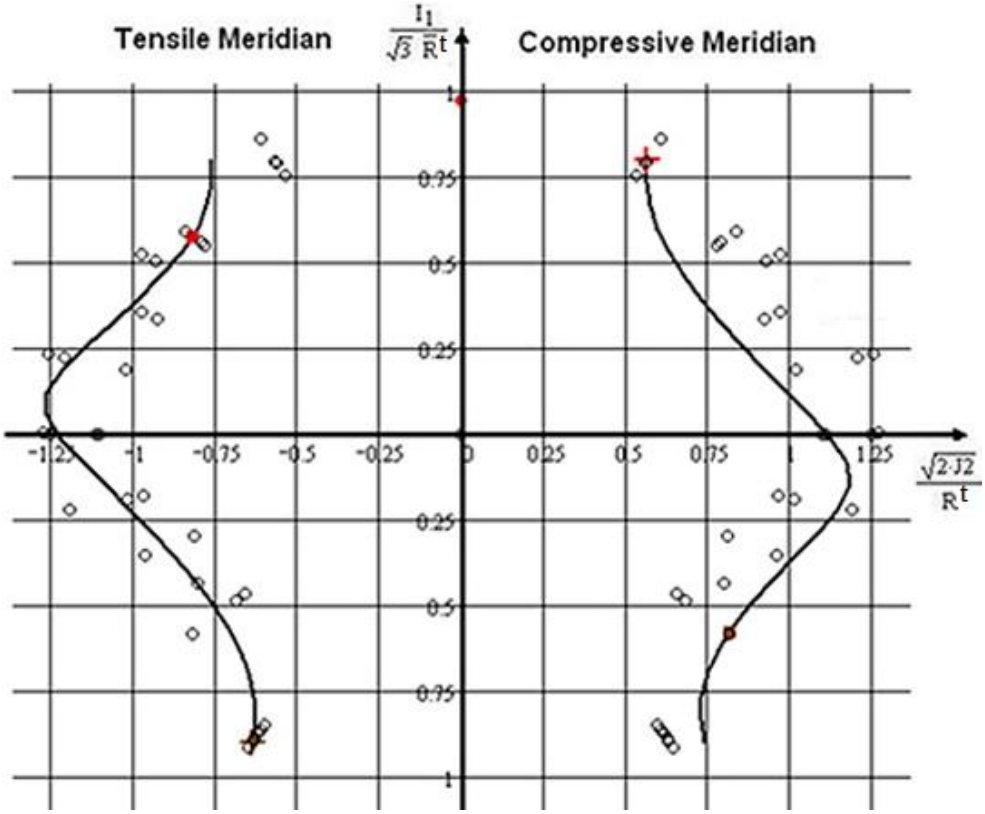

Fig24.14, Rohacell 71 IG: Meridional cross-section of the fracture body.

The test points in *Fig.24-14* are located at a distinct Lode angle of its associated ring o, 120°-symmetry. Cap and bottom are closed by a conical shape, a shape being on the conservative side, + bi-axial.

Table 24-3: Derivation of model parameters (θcr should read ϑ_{cr})

$Rc = 1.36 \quad Rcc = 1.35 \quad maxI1 = 3.03 \quad \frac{I1c}{\sqrt{3}\cdot Rt} = -0.57 \quad \frac{I1cc}{\sqrt{3}\cdot Rt} = -0.962 \quad \theta crc := -0.52 \quad \theta crcc := 0.52 \quad \theta\sigma ccc := 0$

$Rt = 1.62 \quad Rtt = 1.25 \quad minI1 = -3.67 \quad \frac{I1t}{\sqrt{3}\cdot Rt} = 0.642 \quad \frac{I1tt}{\sqrt{3}\cdot Rt} = 0.891 \quad \theta\sigma t := 0.52 \quad \theta\sigma tt := -0.52 \quad \theta\sigma ttt := 0$

$$x = \frac{\sqrt{2J2}}{Rt} \qquad ycap = \frac{maxI1}{\sqrt{3}\cdot Rt} + scap\cdot\left(\frac{\sqrt{2J2}}{Rt}\cdot\sqrt[3]{1 + d\sigma\cdot\sin(3\theta\sigma)}\right)^2 \qquad y = \frac{I1}{\sqrt{3}\cdot Rt}$$

Vorgabe $scap := 1 \quad d\sigma := -0.4$ **Cap: maxI1 > I1t**

$$\frac{I1t}{\sqrt{3}\cdot Rt} = \frac{maxI1}{\sqrt{3}\cdot Rt} + scap\cdot\left(\frac{\sqrt{2J2t}}{Rt}\cdot\sqrt[3]{1 + d\sigma\cdot\sin(3\theta\sigma t)}\right)^2 \qquad \frac{I1tt}{\sqrt{3}\cdot Rt} = \frac{maxI1}{\sqrt{3}\cdot Rt} + scap\cdot\left(\frac{\sqrt{2J2tt}}{Rt}\cdot\sqrt[3]{1 + d\sigma\cdot\sin(3\theta\sigma tt)}\right)^2$$

$Acap := Suchen(scap, d\sigma) \quad Acap = \begin{pmatrix} -0.506 \\ 0.168 \end{pmatrix} \quad scap := Acap_0 \quad d\sigma := Acap_1$ $scap = -0.51$ $d\sigma = 0.17$

$$F\sigma = c1\Theta\sigma\cdot\frac{\sqrt{4\cdot J2\cdot\Theta\sigma - \frac{1}{3}\cdot I1^2} + I1}{2Rt} = 1$$

Vorgabe $c1\Theta\sigma := 0.5$ **NF: I1t > I1**

$$c1\Theta\sigma\cdot\frac{\sqrt{4\cdot J2t\cdot\sqrt[3]{1 + d\sigma\cdot\sin(3\theta\sigma t)} - \frac{1}{3}\cdot I1t^2} + I1t}{2\cdot Rz} = 1$$

$A\sigma := Suchen(c1\Theta\sigma) \quad A\sigma = 0.885 \quad c1\Theta\sigma := A\sigma$ $c1\Theta\sigma = 0.88$

$$ybot = \frac{minI1}{\sqrt{3}\cdot Rt} + sbot\cdot\left(x\cdot\sqrt[3]{1 + dcr\cdot\sin(3\theta cr)}\right)^2$$

Vorgabe $sbot := 1 \quad dcr := -1$ **SF: 0 > I1c**

$$\frac{I1c}{\sqrt{3}\cdot Rt} = \frac{minI1}{\sqrt{3}\cdot Rt} + sbot\cdot\left(\frac{\sqrt{2J2c}}{Rt}\cdot\sqrt[3]{1 + dcr\cdot\sin(3\theta crc)}\right)^2 \qquad \frac{I1cc}{\sqrt{3}\cdot Rt} = \frac{minI1}{\sqrt{3}\cdot Rt} + sbot\cdot\left(\frac{\sqrt{2J2cc}}{Rz}\cdot\sqrt[3]{1 + dcr\cdot\sin(3\theta crcc)}\right)^2$$

$Abot := Suchen(sbot, dcr) \quad Abot = \begin{pmatrix} 0.977 \\ -0.558 \end{pmatrix} \quad sbot := Abot_0 \quad dcr := Abot_1$ $sbot = 0.98$ $dcr = -0.56$

$$Fcr = c1\Theta cr\cdot\frac{\sqrt{4\cdot J2\cdot\Theta cr - \frac{1}{3}\cdot I1^2} - I1}{2Rc} = 1$$

Vorgabe $c1\Theta cr := 1$

$$c1\Theta cr\cdot\frac{\sqrt{4\cdot J2c\cdot\sqrt[3]{1 + dcr\cdot\sin(3\theta crc)} - \frac{1}{3}\cdot I1c^2} - I1c}{2\cdot Rc} = 1$$

Bottom: I1c > minI1

$Acr := Suchen(c1\Theta cr) \quad Acr = 0.809 \quad c1\Theta c := Acr$ $c1\Theta c = 0.81$

Since there are no 3D test data and three-axis tensile fracture data are practically impossible to measure, the cap value can only be estimated probabilistically. According to Awaji-Sato [Awa73], a Weibull-based estimation of the 3-axis breaking stress value R^{ttt} results from measured values for R^{t} and R^{tt}. This type of estimation is adopted for the bottom. *For* R^{ccc}, a surcharge of 10% is applied because of the support effect.

Table 24-4: Estimation of hydrostatic points

$Rt = 1.8 \quad Rtt = 1.25 \quad Rc = 1.6 \quad Rcc = 1.35$

$Mt := \frac{\ln(2)}{\ln\left(\frac{Rt}{Rtt}\right)} \quad Rttt := \frac{Rt}{3^{\frac{1}{Mt}}} \quad Mc := \frac{\ln(2)}{\ln\left(\frac{Rc}{Rcc}\right)} \quad Rccc0 := \frac{Rc}{3^{\frac{1}{Mc}}} \quad Rccc = Rccc0 \cdot 1.1$

$maxI1 := 3 \cdot Rttt \quad maxI1 = 3.03 \quad \frac{maxI1}{\sqrt{3} \cdot Rt} = 0.97 \quad minI1 := -3 \cdot Rccc0 \quad minI1 = -3.67 \quad \frac{minI1}{\sqrt{3} \cdot Rt} = -1.18$

Table 24-5: Determination of the turning point of F_σ

$F\sigma = \frac{\sqrt{4 \cdot J2 - \frac{1}{3} \cdot I1^2} + I1}{2Rt} = 1$ Turning point of Fσ (index w)

$J2 = \frac{1}{3} \cdot I1^2 - I1 \cdot Rt + Rt^2$ derivation $\frac{d}{dI1}\left(\frac{1}{3} \cdot I1^2 - I1 \cdot Rt + Rt^2\right) \quad \frac{2}{3} \cdot I1W - Rt = 0 \quad I1W := 1.5 \cdot Rt$

$J2W = \frac{1}{3} \cdot (1.5Rt)^2 - 1.5Rt \cdot Rt + Rt^2 \quad J2W := .25 \cdot Rt^2 \quad minJ2 := 0.25 \cdot Rt^2$

$x1W := \frac{\sqrt{2J2W}}{Rt} \quad x1W = 0.707 \quad x2W := \frac{I1W}{\sqrt{3} \cdot Rt} \quad x2W = 0.866$

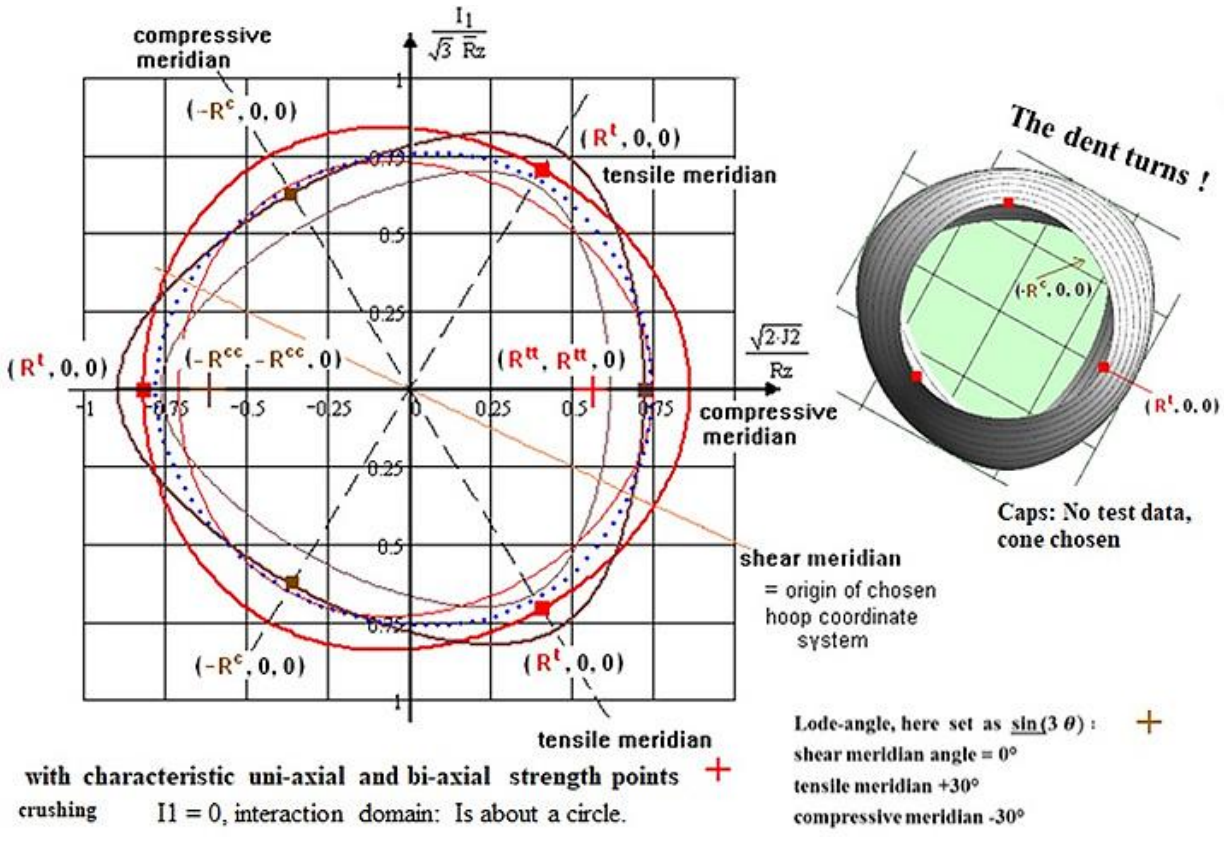

Fig.24-15: 2D Test Data and Mapping in the Orthogonal Stress Plane (brittle, porous)
Caps were taken away to better visualize that the dent turns for this material along the hydrostatic axis.

The following figure in *Table 24-5* proves that in the performed modelling no gap exists between Cap- and Fσ-domain at the axial coordinate x including the tensile strength point and between Fτ-domain and Bottom at the compressive point including coordinate x.

Cap and Bottom equations have to be resolved for xcap and xbot.

Table 24-5: Proof, that no gap exists between the differently modelled fracture body domains

$$\Theta\sigma_m = \sqrt[3]{1 + d\sigma \cdot \sin\left(3\,\delta_m\right)}$$

$$ycap = \frac{maxI1}{\sqrt{3}\cdot Rz} + scap\cdot\left(xcap\cdot\sqrt[3]{\sqrt{1 + d\sigma\cdot\sin\left(3\,\delta_m\right)}}\right)^2$$

$$x\sigma F_m = \frac{\sqrt{2\,\frac{I1t^2\cdot c1\Theta\sigma^2 - 3\cdot c1\Theta\sigma\cdot I1t\cdot Rt + 3\cdot Rt^2}{3\cdot\Theta\sigma_m\cdot c1\Theta\sigma^2}}}{Rt}$$

$$\Theta cr_m = \sqrt[3]{1 + dcr\cdot\sin\left(3\,\delta_m\right)}$$

$$xcrF_m = \frac{\sqrt{2\,\frac{I1c^2\cdot c1\Theta cr^2 + 3\cdot c1\Theta cr\cdot I1c\cdot Rc + 3\cdot Rc^2}{3\,\Theta cr_m\cdot c1\Theta cr^2}}}{Rt}$$

$$ybot = \frac{minI1}{\sqrt{3}\cdot Rt} + sbot\cdot\left(xbot\cdot\sqrt[3]{\sqrt{1 + dcr\cdot\sin\left(3\,\delta_m\right)}}\right)^2$$

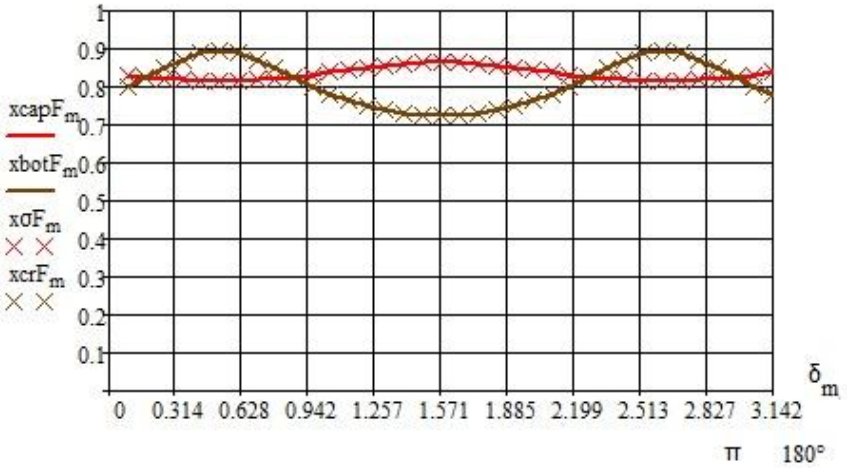

24. 5 Grey-cast Iron

Fig.24-16 presents an old evaluation (about 1995) of a data set for Grey-cast iron.
Of interest is the meridional cross section, which depicts a curvature change in the tensile domain, before the intended cut-off. Drucker 'Stability postulate' problem, like for PMMA in §9.

24. 6 Isotropic Glass C 90 (window pane of ISS, Mathcad 13, 2014)

A glass fiber SiO_2 (E, S, R, AR) is made by blending raw materials, melting them at 1720°C in a three-stage furnace, extruding the molten glass through a bushing in the bottom of the fore-hearth (Vorherd), cooling the filaments with water (*to prevent the crystallization to quartz and obtain a amorphous, randomly ordered atomic structure we know as glass*) and then applying a chemical sizing. The filaments then are gathered to rovings and wound on spools. Commercial glass fiber can be made from silica alone, other ingredients are added to reduce the working temperature and impart other properties that are useful in specific applications such as making alkali-resistant (by ZrO_2) for use in concrete. [*Source OCV*].

Fig.24-17 presents a 2D-SFC-visualization in the principal stress plane and a 3D-Visualization in the meridional cross-section.

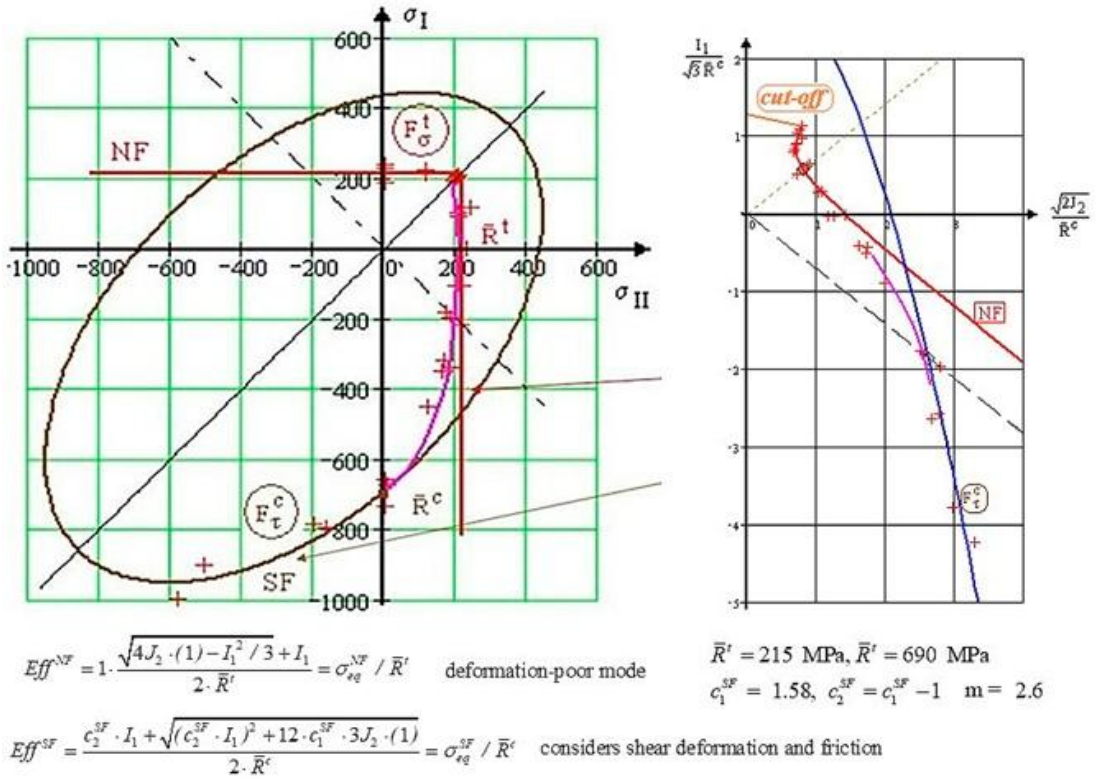

Fig.24-16: 2D-application to Grey-cast Iron [Coffin]. Principal stress plane and meridional cross section

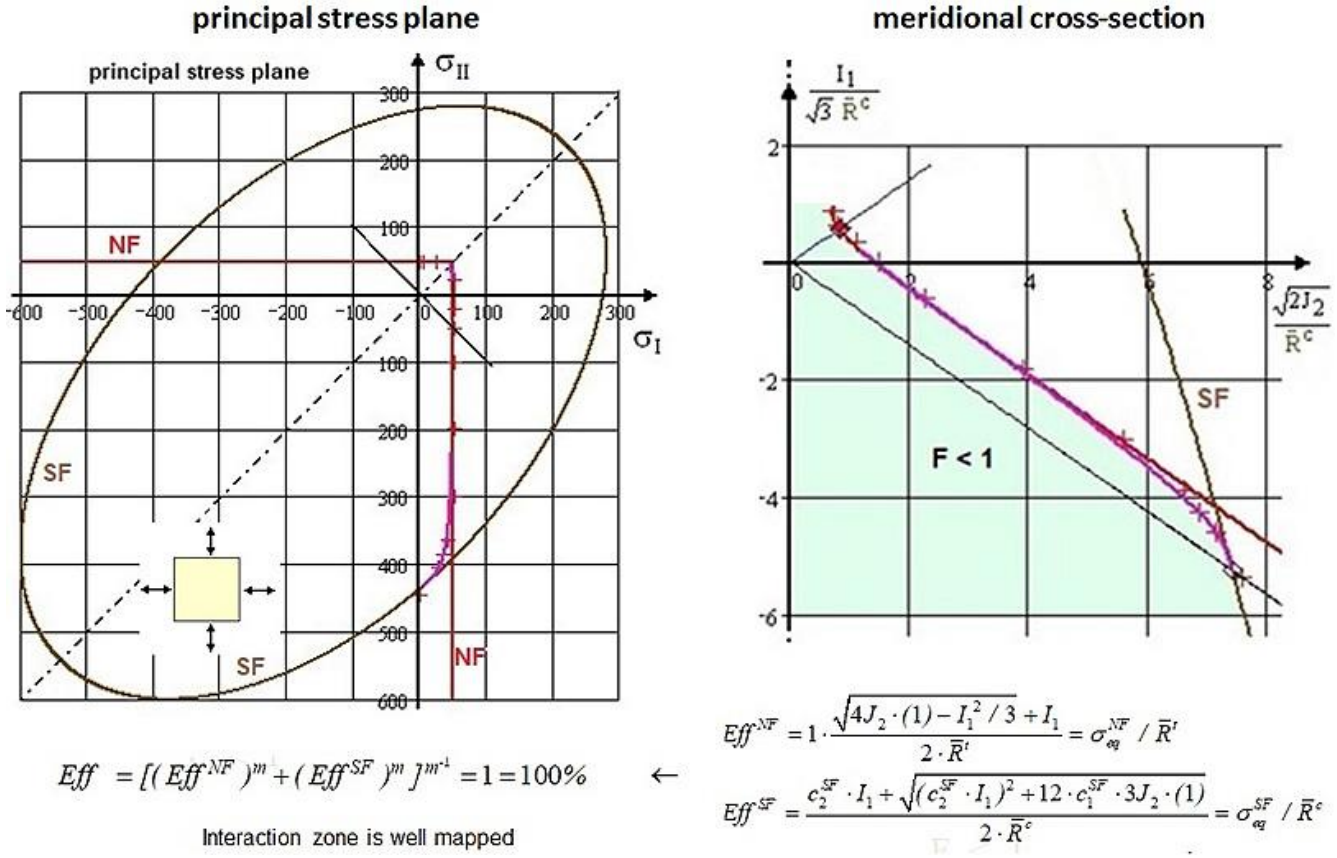

Fig.24-17, Glass C 90: [Kow83], 2D and 3D-visualizations

As still mentioned, $F = 1$ or $Eff = 100\%$ mathematically defines the surface of the fracture failure body. Such a body is rendered here using the Haigh-Lode-Westergaard coordinates with $I_1/\sqrt{3}$ as y-coordinate and $\sqrt{2 \cdot J_2}$ as x-coordinate. *Fig.5-4* depicts the stress states belonging to a tensile meridian and to a compressive meridian. These are those axial cross–sections of the failure body (right) along most of the compression tests are run.

Mechanical strength behavior shows up: Different structural materials

- can possess similar material behavior
- can belong to the same class of material symmetry.

Welcomed Consequence is:

The same strength failure function SFC can be used for different materials. The Foam SFC is exemplarily applicable to Concrete Stone offering the advantage:

→ For a concrete stone material more information is available for pre-dimensioning and modelling in the case of a newly applied material from available foam experiments as a still being tested similarly behaving material.

LL:

** 120°-rotational symmetry is inherent for isotropic materials*

** R^c lies on the CM, R^t on the TM and R^τ in the transition zone between the two modes F^σ and F^τ. This indicates, that an estimation of R^τ, obtained by just an extrapolation from R^c, will be questionable*

** The failure body possesses inward dents for $I_1 > 0$ and outward dents for $I_1 < 0$ in contrast to porous concrete stone, where it is also inward. These dents become smaller with increasing $|I_1|$.*

** There is a pretty large scatter of the compressive strength data in the 2D-figure*

** Mapping of the course of test data with the SFCs worked very well*

** Fracture body shows a decay of denting with increasing negative I_1*

** The higher the strength ratio $SR = R^c/R^t$ becomes, the more the Cohesive Strength value narrows R^t !*

** The strong influence of IFF1 is fully demonstrated.*

An extrapolation from the compression strength - just applying F^τ - cannot be accurate !

** A smaller μ value is more conservative.*

25 Improved Mohr-Coulomb Curve and Cohesive shear Strength R^{τ} of Isotropic materials

Aim: *Enabling a correct understanding of the cohesive strength value* $\bar{R}^{\tau}$ *as a bi-axial fracture quantity.*

25.1 General (work in 2025)

As the author had to design with all three basic material families isotropic, transversely-isotropic and orthotropic for him a conflict comes up, if the used index-letters are not material-dedicated, not self-explaining and not generally used in mechanics. This caused him as civil engineer to publish a Glossar.
In order to not disturb the co-working engineering family in construction the practiced fiber-reinforced polymer matrix-linked terminology (*world-wide applying the suffixes* $_{1,\,2}$) should be also used with fiber-reinforced mineral matrix-linked Carbon Concrete (*another field of the author*). Further, the following analogous letters will be intentionally proposed to use $c \rightarrow R^{\tau}$, $\sigma_1 \rightarrow \sigma_{II}$.
As some researchers in construction still began, when investigating Mohr-Coulomb friction, according to general mechanics they attribute usually positive marked compressive stresses a negative sign. Hence, the positive direction is to display rightward, *Fig. 25-1 (left)*. (Historically, civil engineers basically were more faced by compression and mechanical engineers by tension. This explains the different sign choice).

Fig.25-1 outlines at the left the Mohr entities and right the transformation matrix for transforming principal structural stresses into Mohr stresses.

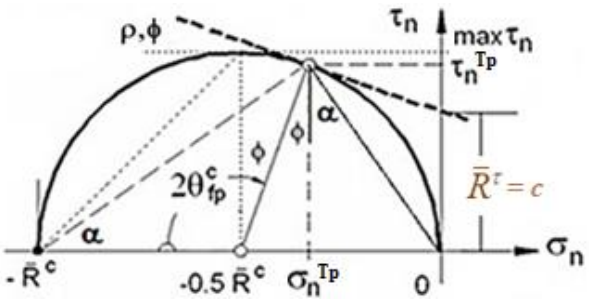

$$\begin{Bmatrix} \sigma_{\lambda} \\ \sigma_{n} \\ \sigma_{t} \\ \tau_{n} \\ \tau_{t\lambda} \\ \tau_{t\lambda} \end{Bmatrix} = \begin{bmatrix} 1 & 0 & 0 & 0 & 0 & 0 \\ 0 & c^2 & s^2 & 2sc & 0 & 0 \\ 0 & s^2 & c^2 & -2sc & 0 & 0 \\ 0 & -sc & sc & (c^2 - s^2) & 0 & 0 \\ 0 & 0 & 0 & 0 & c & -s \\ 0 & 0 & 0 & 0 & s & c \end{bmatrix} = \begin{Bmatrix} \sigma_{I} \\ \sigma_{II} \\ \sigma_{III} \\ 0 \\ 0 \\ 0 \end{Bmatrix}$$

With $\eta = \sigma_{II} - \sigma_{III}$ and σ_{λ}, $\tau_{t\lambda}$, $\tau_{n\lambda} = 0$, the used addition theorems read: $\tau_{nt} \equiv \tau_n$

$$\sigma_n - \sigma_t = c^2 \cdot \eta - s^2 \cdot \eta = C \cdot \eta \ , \quad S = \sqrt{1 - C^2}, \quad C = c^2 - s^2 = 2c^2 - 1 = 1 - 2s^2,$$

$$\sigma_n + \sigma_t = \sigma_{II} + \sigma_{III} = I_1, \quad \sigma_t = \sigma_n - C \cdot (\sigma_{II} - \sigma_{III}), \quad \eta = \sigma_{II} - \sigma_{III},$$

$$\tau_n = -s \cdot c \cdot \sigma_{II} + s \cdot c \cdot \sigma_{III} = -0.5 \cdot \sqrt{1 - C^2} \cdot (\sigma_{II} - \sigma_{III}) \quad \text{with} \quad c = \cos\theta, \quad s = \sin\theta,$$

$$\sigma_n = c^2 \cdot \sigma_{II} + s^2 \cdot \sigma_{III} = \frac{(C+1) \cdot \sigma_{II} + (1-C) \cdot \sigma_{III}}{2}. \qquad 2 \cdot \theta_{fp}\,^{\circ} = 90^{\circ} + \phi^{\circ}.$$

Fig. 25-1: Transformation of Principal Structural Stresses into Mohr Stresses and helpful Addition Theorems outlining the fracture plane angle measure C(θ_{fp}). (bar over due to model mapping)

Assumption of Otto Mohr:
Mohr's basic assumption was: *"The strength of a material is determined by the (Mohr) stresses on the fracture plane".* This means for the linear Mohr-Coulomb (M-C) formulation $\tau_n = \bar{R}^{\tau} - \mu \cdot \sigma_n$.
Herein, the value μ is the intrinsic friction value of the material and $\bar{R}^{\tau}$ the so-called cohesion strength. The other two shear stresses $\tau_{t\lambda}$, $\tau_{n\lambda}$ in *Fig.25-1* are zero. The normal stress σ_t must be accounted for in the transformation process but will finally have no influence, which has to be proven when following

Mohr and this must be proven. According to Mohr, the stresses σ_n and τ_n are the only fracture-responsible stresses, the normal stress σ_λ can be set zero.

On the history of the Mohr-Coulomb (M-C) curve = 'Mohr Envelope': Otto Mohr did not commit himself to the intersection of the envelope with the σ_n-axis. A. Leon was probably the first to use an envelope, taking a parabolic one.

A stress analysis with Mohr stresses is principally simpler than with structural stresses, however the fracture plane angle θ_{fp} must be known and this makes it difficult. Let's begin classically:

Linear M-C approach delivering a relationship C(μ) to friction value μ and Touch point coordinates

$$F_{\text{linM-C}} = \frac{\tau_n}{R^\tau - \mu\cdot\sigma_n} = 1. \qquad \text{Implicit differentiation (minus sign) of the SFC } F_{\text{linM-C}}$$

$$\frac{d\left(\frac{\tau_n}{R^\tau - \mu\cdot\sigma_n}\right)}{d\sigma_n} = \frac{\mu\cdot\tau_n}{\left(R^\tau - \mu\cdot\sigma_n\right)^2} \quad \text{and} \quad \frac{d\left(\frac{\tau_n}{R^\tau - \mu\cdot\sigma_n}\right)}{d\tau_n} = \frac{1}{R^\tau - \mu\cdot\sigma_n}$$

$$\text{finally gives a friction relation} \quad \frac{d\tau_n}{d\sigma_n} = -\frac{dF\tau/d\sigma_n}{dF\tau/d\tau_n} = -\frac{\frac{\mu\cdot\tau_n}{\left(R^\tau - \mu\cdot\sigma_n\right)^2}}{\frac{1}{R^\tau - \mu\cdot\sigma_n}} = \frac{-\mu\cdot\tau_n}{R^\tau - \mu\cdot\sigma_n} = -\mu\,.$$

The Touch point coordinates from a given fracture angle θ^c_{fp} or the related friction value μ: bar skipped

$$(\tau_n^{Tp},\sigma_n^{Tp}) \;\rightarrow\; (\tau_n = R^\tau, \sigma_n = 0) \quad \text{applying} \quad c = \cos\theta^c_{fp},\; s = \sin\theta^c_{fp},$$

$$\sigma_n^{Tp} = c^2\cdot\left(-R^c\right)\;,\; \tau_n^{Tp} = -s\cdot c\cdot\left(-R^c\right) \qquad \text{leading to} \qquad \tau_n = \tau_n^{Tp} + \mu\cdot\sigma_n^{Tp}.$$

Note on the Mohr-Coulomb (M-C) criterion (also see § 26.1):

In a paper, recently published in *Scientific Reports (2024) nature portfolio [Stress-dependent Mohr–Coulomb shear strength parameters for intact rock* [*Li24*], a critical assessment of the M-C criterion is performed. This report shall be not scientifically reworked here. However, my summarizing private elaboration at hand shall give some discussion points. It just tries to inform about my procedure to derive an accurate Mohr-Coulomb Envelope including Cohesive Strength.

Basis of my procedure is the knowledge, that the M-C Envelope, practically spanning from the Touch point $(\tau_n^{Tp},\sigma_n^{Tp}) \;\rightarrow\; (\tau_n = R^\tau, \sigma_n = 0)$, is affected (*Fig.25-1*) by the shear failure mode together with the tensile failure mode and thus belonging to a transition zone, as a mode interaction domain.

SFCs regarding the material-inherent 120°-rotational symmetry of the isotropic fracture body $\Theta^{SF} \equiv \Theta^\tau$

When using for the determination of the cohesive strength - for an extrapolation from the compressive strength point - just the SFC $F^{SF}\rightarrow F^\tau$, then the isotropic material-inherent 120°-rotational symmetry of the fracture body is to consider, as shown below, where both the SFCs $F^{NF}\rightarrow F^\sigma$ and F^τ are displayed in the next box together with the required invariants and non-circularity parameter Θ^τ.

The cohesive strength point lies in the interaction zone of the mode regimes, see *Fig.25-2*. Therefore, a generation of a realistic, decaying Mohr-Coulomb curve $\tau_n(\sigma_n)$ requires the determination of the slope *along* the realistic curved M-C curve up to $\sigma_n = 0$ at least, not a constant value $C = C^c$ in the compressive strength-linked Touch *point* only, being sufficient for the determination of the friction value

μ. This means, instead of the single F^{SF}-formulation the SF-NF-interaction managing *Eff*-formulation is to apply when moving from the structural stress formulation to a Mohr stress-based one.

To search is an equation for the unknown fracture angle measure $C(\theta_{fp})$, linked to the growing fracture angle θ_{fp}. This is performed by equating the slopes in the so-called Touch point:

$$F^{\sigma} = \frac{\sqrt{4J_2 - I_1^2/3} + I_1}{2 \cdot \bar{R}^t} \quad (\Theta^{NF}=1) \quad \text{and} \quad F^{\tau} = c_2^{SF} \cdot \frac{I_1}{\bar{R}^c} + c_1^{SF} \cdot \frac{6 \cdot J_2}{2 \cdot \bar{R}^{c2}} \cdot \Theta^{SF}$$

$$I_1 = (\sigma_I + \sigma_{II} + \sigma_{III}), \text{ considering Mohr-Coulomb skip } \sigma_I$$

$$6J_2 = (\sigma_I - \sigma_{II})^2 + (\sigma_{II} - \sigma_{III})^2 + (\sigma_{III} - \sigma_I)^2$$

$$\rightarrow 6J_2 = \sigma_{II}^2 + (\sigma_{II} - \sigma_{III})^2 + \sigma_{III}^2),$$

$$27J_3 = (2\sigma_I - \sigma_{II} - \sigma_{III}) \cdot (2\sigma_{II} - \sigma_I - \sigma_{III}) \cdot (2\sigma_{III} - \sigma_I - \sigma_{II})$$

$$\rightarrow 27J_3 = (-\sigma_{II} - \sigma_{III}) \cdot (2\sigma_{II} - \sigma_{III}) \cdot (2\sigma_{III} - \sigma_{II})$$

$$I_1 = (\sigma_n + \sigma_t + \sigma_\lambda), \quad \text{considering Mohr-Coulomb skip } \sigma_\lambda, \tau_{n\lambda}, \tau_{t\lambda}$$

$$I_2 = \sigma_n \cdot \sigma_t + \sigma_t \cdot \sigma_\lambda + \sigma_n \cdot \sigma_\lambda - \tau_{nt}^2 - \tau_{n\lambda}^2 - \tau_{t\lambda}^2 \quad \rightarrow \quad \sigma_n \cdot \sigma_t - \tau_n^2$$

$$I_3 = \sigma_n \cdot \sigma_t \cdot \sigma_\lambda - \sigma_n \cdot \tau_{t\lambda}^2 - \sigma_t \cdot \tau_{n\lambda}^2 - \sigma_\lambda \cdot \tau_{nt}^2 + 2 \cdot \tau_{nt} \cdot \tau_{n\lambda} \cdot \tau_{t\lambda} \quad \rightarrow \quad 0$$

$$6J_2 = (\sigma_n - \sigma_t)^2 + (\sigma_t - \sigma_\lambda)^2 + (\sigma_\lambda - \sigma_n)^2 + 6 \cdot (\tau_{nt}^2 + \tau_{n\lambda}^2 + \tau_{t\lambda}^2)$$

$$\rightarrow 6J_2 = (\sigma_n - \sigma_t)^2 + \sigma_t^2 + \sigma_n^2 + 6 \cdot \tau_{nt}^2$$

$$27J_3 = 2 \cdot I_1^3 - 9 \cdot I_1 \cdot I_2 + 27 \cdot I_3$$

$$\rightarrow 27J_3 = 2(\sigma_n + \sigma_t)^3 - 9 \cdot (\sigma_n + \sigma_t) \cdot (\sigma_n \cdot \sigma_t - \tau_n^2)$$

$$\Theta^{\tau} = \sqrt[3]{1 + d^{SF} \cdot \sin(3\vartheta)} = \sqrt[3]{1 + d^{SF} \cdot 1.5 \cdot \sqrt{3} \cdot J_3 \cdot J_2^{-1.5}}, \quad \sigma_t = \sigma_n - C \cdot (\sigma_{II} - \sigma_{III}).$$

A first slope equation $d\tau_n / d\sigma_n$ is given by the transformation of structural stresses into Mohr stresses.

The fracture angle differentiation of the Mohr stresses in the Touch point delivers:

$$\tau_n = -s \cdot c \cdot \sigma_{II} + s \cdot c \cdot \sigma_{III}, \quad \sigma_n = c^2 \cdot \sigma_{II} + s^2 \cdot \sigma_{III} \text{ with } c = \cos\theta, \quad s = \sin\theta,$$

$$\frac{d(-s \cdot c \cdot \sigma_{II} + s \cdot c \cdot \sigma_{III})}{d\theta} = (-c^2 + s^2) \cdot \sigma_{II} - (-c^2 + s^2) \cdot \sigma_{III} \quad \text{and}$$

$$\frac{d(c^2 \cdot \sigma_{II} + s^2 \cdot \sigma_{III})}{d\theta} = -2sc \cdot (\sigma_{II} - \sigma_{III})$$

$$\frac{d\tau_n}{d\sigma_n} = \frac{(-c^2 + s^2) \cdot \sigma_{II} - (-c^2 + s^2) \cdot \sigma_{III}}{-2sc \cdot (\sigma_{II} - \sigma_{III})} = \frac{c^2 - s^2}{2sc} = \frac{C}{S} \quad \Rightarrow \quad \frac{d\tau_n}{d\sigma_n} = \frac{C}{\sqrt{1 - C^2}},$$

$$\text{and } \operatorname{cotan}(2\theta_{fp}) = \frac{\cos(2 \cdot \theta_{fp})}{\sin(2 \cdot \theta_{fp})} = \frac{C}{S}, \; C^c = \cos(2 \cdot \theta_{fp}{}^\circ \cdot \frac{\pi}{180^\circ}) \; ; \; \tan(\rho) = -\operatorname{cotan}(2 \cdot \theta_{fp}{}^\circ \cdot \frac{\pi}{180^\circ}).$$

Secondly, one has to find a further tangent equation by the differentiation of F^{τ} or physically accurate F^{τ} with F^{σ}. *Table 25-1* depicts both the SFCs.

On the classical way 'Extrapolation from the compression strength point', represented by the touchpoint in the Mohr diagram, *Fig 25-1*, just the SFC F^{τ} is required.

Table 25-2 will later show the full procedure $C(\theta_{fp})$ of the different ways of an extrapolation.

Table 25-1: Formulation of Mohr stress-based Effs.

$$F^{NF} = F^{\sigma} = Eff^{NF} = c^{NF} \cdot \frac{\sqrt{4J_2 \cdot \Theta^{NF} - I_1^2/3} + I_1}{2 \cdot \bar{R}^t}, \quad \text{for Normal Concrete can be set} \quad c^{NF}, \Theta^{NF} = 1,$$

$$Eff^{NF} = 1 \cdot \frac{\sqrt{4 \cdot [(\sigma_n - \sigma_t)^2 + \sigma_t^2 + (-\sigma_n)^2 + 6 \cdot \tau_n^2] \cdot 1/6 - (\sigma_n + \sigma_t)/3} + (\sigma_n + \sigma_t)}{2 \cdot \bar{R}^t}.$$

Using the concept of 'proportional loading':

$$F^{SF} = F^{\tau} = c_2^{SF} \cdot \frac{I_1}{\bar{R}^c} + c_1^{SF} \cdot \frac{6 \cdot J_2}{2 \cdot \bar{R}^{c2}} \cdot \Theta^{SF} \quad \Rightarrow \quad c_2^{SF} \cdot \frac{I_1 / Eff}{\bar{R}^c} + c_1^{SF} \cdot \frac{6 \cdot J_2 / Eff^2}{2 \cdot \bar{R}^{c2}} \cdot \Theta^{SF}$$

$$Eff^{SF} = \frac{\sqrt{(c_2^{SF} \cdot I_1)^2 + 12 \cdot c_{1\Theta}^{SF} \cdot J_2 \cdot \Theta^{SF}}}{2 \cdot \bar{R}^c} + \frac{c_2 \cdot I_1}{2 \cdot \bar{R}^c} \quad \text{with} \quad \Theta^{SF} \to \Theta^{CM} = \sqrt[3]{1 + d^{SF} \cdot (-1)},$$

$$Eff^{SF} = \frac{\sqrt{c_2^{SF\,2} \cdot (\sigma_n + \sigma_t)^2 + c_{1\Theta}^{SF} \cdot \Theta^{SF} \cdot 2 \cdot [(\sigma_n - \sigma_t)^2 + \sigma_t^2 + (-\sigma_n)^2 + 6 \cdot \tau_n^2]}}{2\bar{R}^c} + c_2 \cdot \frac{\sigma_n + \sigma_t}{2\bar{R}^c}.$$

with $c_{1\Theta}^{SF} \cdot \Theta^{CM} = 1 + c_2$, $\Theta^{CM} = \Theta^{SF} = \sqrt[3]{1 + d^{SF} \cdot \sin(3\vartheta)} = \sqrt[3]{1 - d^{SF}}$ and

Θ non-circularity function, d non-circularity parameter, ϑ Lode angle.

Fig.25-2 displays the 2nd quadrant of the bi-axial failure curve in structural stresses. This fully represents the Mohr-Coulomb curve domain. The joint mode situation of the Mohr-Coulomb curve - capturing the transition zone between the pure mode domains NF and SF - requires the application of the interaction equation $Eff^m = (Eff^{NF})^m + (Eff^{SF})^m = 1$ (material stressing effort 100%) and it spans over the ordinate regime $0 < \sigma_{III} < \bar{R}^t$, the *transition zone* of the modes, and covers Lode angles $-30° < \vartheta < +30°$.

If the full M-C curve and the associated fracture angle are of interest up to $\sigma_{III} = R^t$, then both the modes are to employ with their *Effs*.

- Improved Mapping of Failure Stress data to obtain a more realistic $\theta_{fp}°(\vartheta)$, *Fig.25.2*

As still experienced with the UD-materials in a chapter before, also here it is to face that a SFC is 'just' a practical approach and therefore cannot sufficiently well map all domain parts in detail. Therefore, when searching a local fracture angle $\Theta_{fp}°$ in the transition zone a correction is to be material-dependently applied to numerically determine a better value for $\Theta_{fp}°$, if really desired.

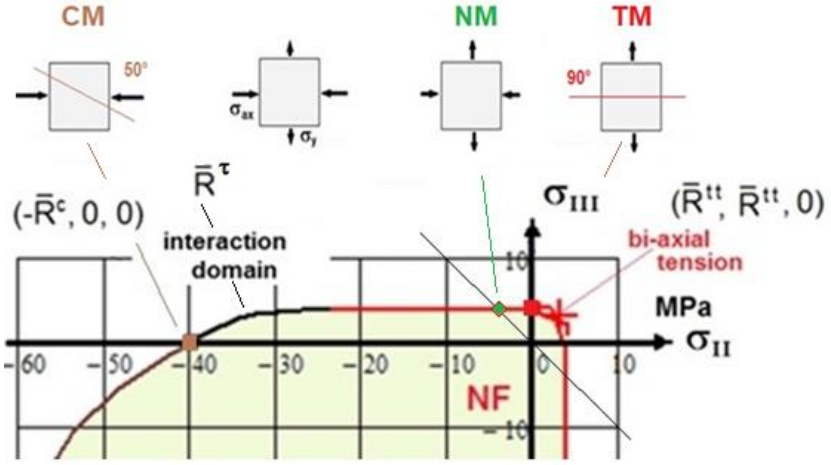

Fig.25-2: Second quadrant and associated stress states, transition zone between the 2 mode domains SF, NF. Tensile Meridian (TM), Compressive Meridian (CM)

According to the fact that the compression strength point is located on the compressive meridian and the tensile strength point on the tensile meridian the different Lode angle ϑ is to consider in order to achieve a locally necessary more accurate SFC-model. This requires to consider inherent '*120°-rotationally-symmetry'*.

The pure shear point in *Fig.25-3* is a point on the Neutral Meridian ($\delta = 0$, $\Theta = 1$, $I_1 = 0$) and also a characteristic point of the transition zone between the tensile domain and the compressive domain is when the first invariant becomes zero (*see the bias grey line in Fig.25-2*), meaning pure shear:

$$I_1 = \sigma_I + \sigma_{II} + \sigma_{III} = 0 \quad \rightarrow \quad \sigma_{II}{}^{c} = -\sigma_{III}{}^{t} \ .$$

A physical demands is given with θ_{fp} °= 90° at $\sigma_{III} = R^t$ (is σ_{III} coordinate) and $Eff^{\tau} = 0$ for $\sigma_{II} = 0$. The shear material stressing effort Eff^{τ} must physically become zero at the tensile strength point (0, R^t).

Fig.25-3 outlines the local shortcoming of the FMC-based choice of the SF-formula.

As simple correcting function f_σ , being just a crutch of-course,

$$f\sigma = 1 - \left(\frac{\sigma nTp + Rt - \sigma n0}{|\sigma nTp|}\right)^6 = 1 - \left[\frac{\sigma nTp + Rt - \frac{(Cc+1)\cdot\sigma II + (1-Cc)\cdot Rt}{2}}{|\sigma nTp|}\right]^6$$

was taken. This correction function is decisive in the low negative σ_{II} and σ_n-domain.

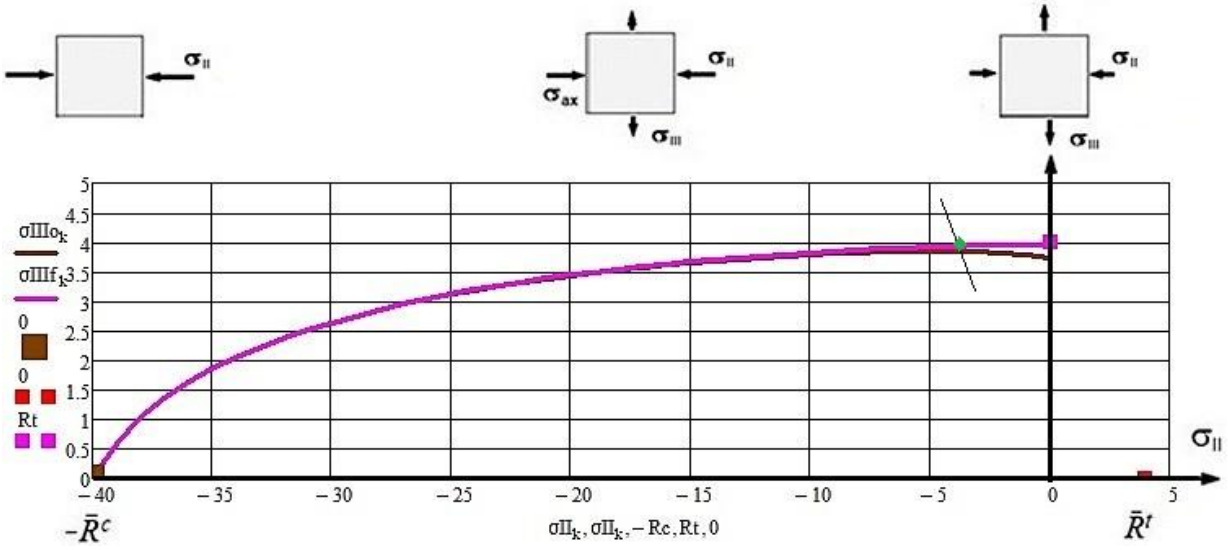

Fig.25-3, Θ-considered: Visualisation of the course of the original and the corrected $\sigma_{III}(\sigma_{II})$.

Note, please:
In any case, the given SFC F^{τ} calculates a conservative Reserve Factor, based on both the modes. The SFC is on the safe side and Design-Verification as well.

The next sub-chapters will outline:

- extrapolation approaches
- a trial on the physically accurate, much more complicated two modes approach and finally

- a guess of the cohesive strength R^{τ}.

At first the simplest way: There are three ways gone, each one an approximation.

25.2 R^c-extrapolation-based estimation of cohesive strength R^{τ}, M-C curve $\tau_n(\sigma_n)$ and angle $\theta_{fp}°$

1 Linear Mohr-Coulomb, C = C^c constant, $\theta_{fp}°$ =constant, classical path

$$F_{\text{linM-C}} = \frac{\tau_n}{R^{\tau} - \mu \cdot \sigma_n} = 1 \;\Rightarrow\; (\text{M-C curve})\;\; \tau_n = \tau_n^{Tp} - \mu \cdot \sigma_n \quad \text{and} \quad R^{\tau} = \tau_n^{Tp} + \mu \cdot \sigma_n^{Tp}$$

*This basic approach delivers the highest cohesion strength value and a straight M-C line.

2 Use of Shear Mode F^{τ} *only*, $\theta_{fp}°$ grows with *C*, $c_{1\Theta}^{SF} \rightarrow \; c_1 = c_2 + 1$, $C^c = \cos(2 \cdot \theta_{fp}^c° \cdot \frac{\pi}{180°})$

Two variants are possible to obtain an alternating fracture angle measure $C(\theta_{fp}°)$ and thereby R^{τ}.

If just performing an extrapolation from compression strength point no interaction of modes is needed: The simpler F^{τ} can be used instead of *Eff*$^{\tau}$. *Table 25-2* summarizes the relations for the derivation of

Table 25-2: Estimation of R^{τ}, $\tau_n(\sigma_n)$ and fracture plane angle $\theta_{fp}°$ considering the F^{τ} only

$$F^{\tau} = c_2 \cdot \frac{I_1}{\bar{R}^c} + c_1 \cdot \frac{6 \cdot J_2}{2 \cdot \bar{R}^{c2}} \cdot c_2 \cdot \frac{\sigma_n + \sigma_t}{\bar{R}^c} + c_1 \cdot \frac{(\sigma_n - \sigma_t)^2 + \sigma_t^{\,2} + \sigma_n^{\,2} + 6 \cdot \tau_n^{\,2}}{2 \cdot \bar{R}^{c2}} = 1$$

inserted $I_1 = \sigma_n + \sigma_t$, $6J_2 = (\sigma_n - \sigma_t)^2 + \sigma_t^{\,2} + \sigma_n^{\,2} + 6 \cdot \tau_n^{\,2}$ and resolved for

$$\tau_n = \sqrt{-\frac{c_2 \cdot Rc \cdot (\sigma_n + \sigma_t) - Rc^2 + c_1 \cdot (\sigma_n^{\,2} - \sigma_n \cdot \sigma_t + \sigma_t^{\,2})}{3 \cdot c_1}},$$

$$\frac{C}{\sqrt{1 - C^2}} = \frac{d\tau_n}{d\sigma_n} \quad \text{with} \quad \tau_n(\sigma_n) \quad \text{and/or} \quad \frac{C}{\sqrt{1 - C^2}} = \frac{d\tau_n}{d\sigma_n} = -\frac{dF\tau / d\sigma_n}{dF\tau / d\tau_n}$$

The latter will be taken: $\Theta^{\tau} = 1$

$$\frac{C}{\sqrt{1 - C^2}} = \frac{-c_2 \cdot \bar{R}^c + c_1 \cdot (\sigma_t - 2\sigma_n)}{6 \cdot \tau_n \cdot c_1} = \frac{-c_2 \cdot \bar{R}^c + c_1 \cdot (\sigma_t - 2\sigma_n)}{6 \cdot \tau_n \cdot c_1}$$

$$\sigma_n = (C+1) \cdot 0.5 \cdot \sigma_{II} + (1 - C) \cdot 0.5 \cdot \sigma_{III}, \;\; \tau_n = -0.5 \cdot \sqrt{1 - C^2} \cdot (\sigma_{II} - \sigma_{III}),$$

$$(\sigma_t - 2\sigma_n) = -0.5 \cdot [(\sigma_{II} + \sigma_{III}) + 3 \cdot C \cdot (\sigma_{II} - \sigma_{III})].$$

Guess $\bar{R}^{\tau} = \sqrt{\frac{-\bar{R}^{c2} + c_2 \cdot \bar{R}^c \cdot \sigma_{t0} + c_1 \cdot \sigma_{t0}^{\,2}}{3 \cdot c_1}}$ with $\sigma_{t0} = -C^c \cdot (-\bar{R}^c)$.

$\tau_{nt}(\sigma_n)$ and $\theta_{fp}°$ from σ_{II} (σ_{III}). It is to consider the change of the fracture plane angle $\theta_{fp}°$ with the Lode angle ϑ from $\theta_{fp}°$ at ϑ = -30° on up to a value < 90° (maximum at $\sigma_{III} = R^t$), which the model permits. The table shows the M-C formula $\tau_n(\sigma_n)$, the C-equation and the transformation of the Mohr stresses into principal structural stresses for determining C.

*This approach delivers an intermediate and lower value for the cohesive strength and the M-C curve.

3 Improved Estimation with F^{τ} and correction function f_{σ}

In the M-C-calculations the mode-linked Θ^{τ} and correction function f_{σ} ('crutch') principally should have been differentiated within the SFC F^{τ}. However, this makes no sense if F^{τ} is employed only. Therefore, in order to take their influence into account at all, the respective quantity is treated as being fixed, being a constant. Hence, this variant just applies the correction $\tau_n \cdot f_{\sigma}$.

*This approach delivers the lowest value for the cohesive strength but more accurate $\bar{R}^{\tau} > \bar{R}^{t}$.

25.3 Accurate Mode-interactive determination of R^{τ}, M-C curve, fracture angle $\theta_{fp}{}^{\circ} > \theta_{fpc}{}^{\circ}$

A physically accurate determination of above quantities may be possible by applying the jointly acting SFCs, F_{τ} with F_{σ}. *Table 25-3* collects all relevant relationships. It displays the final differentiation-

Table 25-3: Determination of R^{τ}, $\tau_n(\sigma_n)$, considering modes, Θ^{τ}

* Task: Known $\sigma_{II}, \sigma_{III}$; $\bar{R}^{t}$, $\bar{R}^{c}$; searched σ_n, τ_n, $\theta_{fp}{}^{\circ}(C)$, $C = \cos(2 \cdot \theta_{fp}{}^{\circ} \cdot \pi / 180^{\circ}))$

* Interaction equation, 2 modes are activated: $(Eff^{\sigma})^m + (Eff^{\tau})^m = 100\%$

$$Eff^{\sigma} = \frac{\sqrt{4 \cdot [(\sigma_n - \sigma_t)^2 + \sigma_t^2 + \sigma_n^2 + 6 \cdot \tau_n^2] / 6 - (\sigma_n + \sigma_t)^2 / 3} + (\sigma_n + \sigma_t)}{2 \cdot \bar{R}^{t}},$$

$$Eff^{\tau} = \frac{c_2 \cdot (\sigma_n + \sigma_t)}{2 \cdot \bar{R}^{c}} + \frac{\sqrt{(c_2 \cdot (\sigma_n + \sigma_t))^2 + 2 \cdot c_{1\Theta} \cdot \Theta^{\tau} [(\sigma_n - \sigma_t)^2 + \sigma_t^2 + \sigma_n^2 + 6 \cdot \tau_n^2]}}{2 \cdot \bar{R}^{c}}$$

* Solution of the task means: Equalizing the 2 slopes at each stress state $\sigma_{II}(\sigma_{III})$

- Slope 1: Differentiation of the structural stresses-linked Mohr stresses delivered before

$$\frac{d\tau_{nt}}{d\sigma_n} = \frac{(s^2 - c^2) \cdot \eta}{-2 \cdot s \cdot c \cdot \eta} = \frac{C}{S} = \frac{C}{\sqrt{1 - C^2}},$$ valid uni-axially and bi-axially, $\eta = \sigma_{II} - \sigma_{III}$

- Slope 2: Differentiation of the interaction equation, abbreviation $\eta_m = 2\sigma_n - C \cdot \eta$

$$Eff^{\sigma} = \left\{\sqrt{4 \cdot [(C \cdot \eta)^2 + (\sigma_n - C \cdot \eta)^2 + \sigma_n^2 + 6 \cdot \tau_n^2] / 6 - \eta_m^2 / 3} + \eta_m\right\} / 2 \cdot \bar{R}^{t}, \quad \Theta^{NF} = 1$$

$$Eff^{\tau} = \left\{c_{1\Theta} \cdot \eta_m + \sqrt{(c_2^2 \cdot \eta_m^2 + 2 \cdot c_{1\Theta} \cdot \Theta^{\tau} \cdot [(C \cdot \eta)^2 + (\sigma_n - C \cdot \eta)^2 + \sigma_n^2 + 6 \cdot \tau_n^2]}\right\} / 2 \cdot \bar{R}^{c}$$

$$\Theta^{\tau}(\vartheta) = \sqrt[3]{1 + d^{\tau} \cdot \sin(3\vartheta)} = \sqrt[3]{1 + d^{\tau} \cdot 1.5 \cdot \sqrt{3} \cdot J_3 \cdot J_2^{-1.5}}$$

$$Eff^{m} = (Eff^{\sigma})^m + (Eff^{\tau})^m \quad \text{with} \quad dEff / d\sigma_n \quad \text{and} \quad dEff / d\tau_n.$$

Equating the 2 equations, considering the implicit differentiation by a negative sign,

with $\frac{C}{\sqrt{1 - C^2}} = -\frac{dEff / d\sigma_n}{dEff / d\tau_{nt}}$, a huge formula for determining C is obtained.

This formula is to be re-transformed from Mohr stresses into structural stresses

$$\sigma_n = (C + 1) \cdot 0.5 \cdot \sigma_{II} + (1 - C) \cdot 0.5 \cdot \sigma_{III}, \quad \tau_n = -0.5 \cdot \sqrt{1 - C^2} \cdot (\sigma_{II} - \sigma_{III}).$$

The altering C depends on the bi-axial fracture stress states $\sigma_{III}{}^{fr}(\sigma_{II})$, achieved, when inserting σ_{II} into the failure criterion $Eff = 1$ along the span between Mohr's Touch point and Cohesive Strength point, providing. the fracture angle measure $C(\theta_{fp}{}^{\circ})$ and $R^{\tau}(C)$

$$C = C(\sigma_{II}, \sigma_{III}{}^{fr}) = \cos(2 \cdot \theta_{fp}), \quad \theta_{fp} = 0.5 \cdot \arccos C, \quad \theta_{fp}{}^{\circ} = \theta_{fp} \cdot 180^{\circ} / \pi.$$

equations and solution procedure. Naturally this huge 'improved' solution procedure is very challenging for a mathematical code concerning the necessary symbolic differentiation.

25.4 Application on Normal Concrete - computation data input

* Basic Data set

$\theta_{fp}^{c\,\circ} = 51°$ or friction value $\mu = 0.208.$, $C^c = \cos(2\cdot\theta_{fp}\,°\cdot\frac{\pi}{180°}) = -\mu$

$c_2 = (3\cdot C^c\text{-}1)/(3\cdot C^c+1) = (1+3\cdot\mu)/(1-3\cdot\mu) = 4.32.$

Inserting the compressive strength point into $F^\tau = c_2\cdot\frac{I_1}{\bar{R}^c} + c_{1\Theta}\cdot\frac{6\cdot J_2}{2\cdot\bar{R}^{c2}}\cdot\Theta^\tau = 1$

gives $c_2\cdot\frac{-\bar{R}^c}{\bar{R}^c} + c_{1\Theta}\cdot\frac{2\cdot\bar{R}^{c2}}{2\cdot\bar{R}^{c2}}\cdot\Theta^\tau \rightarrow c_{1\Theta} = \frac{c_2+1}{\Theta^\tau}$ (c_2 is not dependent on C).

* Determination of the missing parameters $c_{1\Theta}$, d^τ

In order to capture the 120°-symmetry requirement a 2-parameter approach is to employ. Its two missing model parameters are calculated in *Table.25-4*.

Table 25-4: Determination of SF-model parameters $c_{1\Theta}$, d_τ

$I1c := -Rc$ $J2c := \frac{Rc^2}{3}$ $I1cc := -2\cdot Rcc$ $J2cc := \frac{Rcc^2}{3}$

Vorgabe $c1\Theta := 2$ $d\tau := 0.6$ $c2 = 4.32$

$$\frac{\sqrt{I1c^2\cdot c2^2 + 12\cdot J2c\cdot c1\Theta\cdot\sqrt[3]{1-1\cdot d\tau}} + I1c\cdot c2}{2\cdot Rc} = 1$$ strength point on CM

$$\frac{\sqrt{I1cc^2\cdot c2^2 + 12\cdot J2cc\cdot c1\Theta\cdot\sqrt[3]{1+1\cdot d\tau}} + I1cc\cdot c2}{2\cdot Rc} = 1$$ bi-axial compressive failure stress point on TM

$A\tau := Suchen(c1\Theta, d\tau)$ $A\tau = \begin{pmatrix}6.727\\0.507\end{pmatrix}$ $c1\Theta := A\tau_0$ $c1\Theta = 6.7$ $d\tau := A\tau_1$ $d\tau = 0.51$

$\Theta^\tau = 1 : c_{1\Theta} \rightarrow c_1 = c_2+1 = 5.32$ and $\Theta^\tau \neq 1 : c_{1\Theta} = \frac{c_2+1}{0.79} = 6.73.$

$\Theta^t = \sqrt[3]{1+d_\tau}$ (tensile meridian TM) =1.15, $\vartheta = +30°$;

$\Theta^c = \sqrt[3]{1-d_\tau}$ (compressive meridian CM) = 0.79, $\vartheta = -30°$.

Touch point: $\tau_n^{Tp} = 19.6$ MPa, $\sigma_n^{Tp} = -15.8$ MPa.

Final task is equalizing the two slope angles along the full domain, generated by the joint action of the two modes and considering the correction function $f\sigma$. Focused are the uni-axial classical procedure and a realistic 'bi-directional mode' procedure.

25.5 Results: Extrapolation Solution Path Variants $\Theta_{fp}°(F^{\tau})$

Fig.25-4a ,b display several M-C failure curves and the course of the altering fracture plane angle $\Theta_{fp}°(F^{\tau})$. The angle changes from 51° up to 90°. Figure (*a*) presents the entities in Mohr stresses and (b) in structural stresses. This involves the classical Linear Mohr-Coulomb fracture curve an F^{τ}-based M-C curve $\tau_{nt}(\sigma_n)$ and an assumed, *fσ*-corrected one. The 3 Mohr half-circles are incorporated.

Fig.25-5 presents model-dependent cohesive strength values R^{τ}, the interaction-based $\tau_n(\sigma_n)$-curve, topped by the course of the increasing fracture angle, factored by 10. Datensatz Check + angle

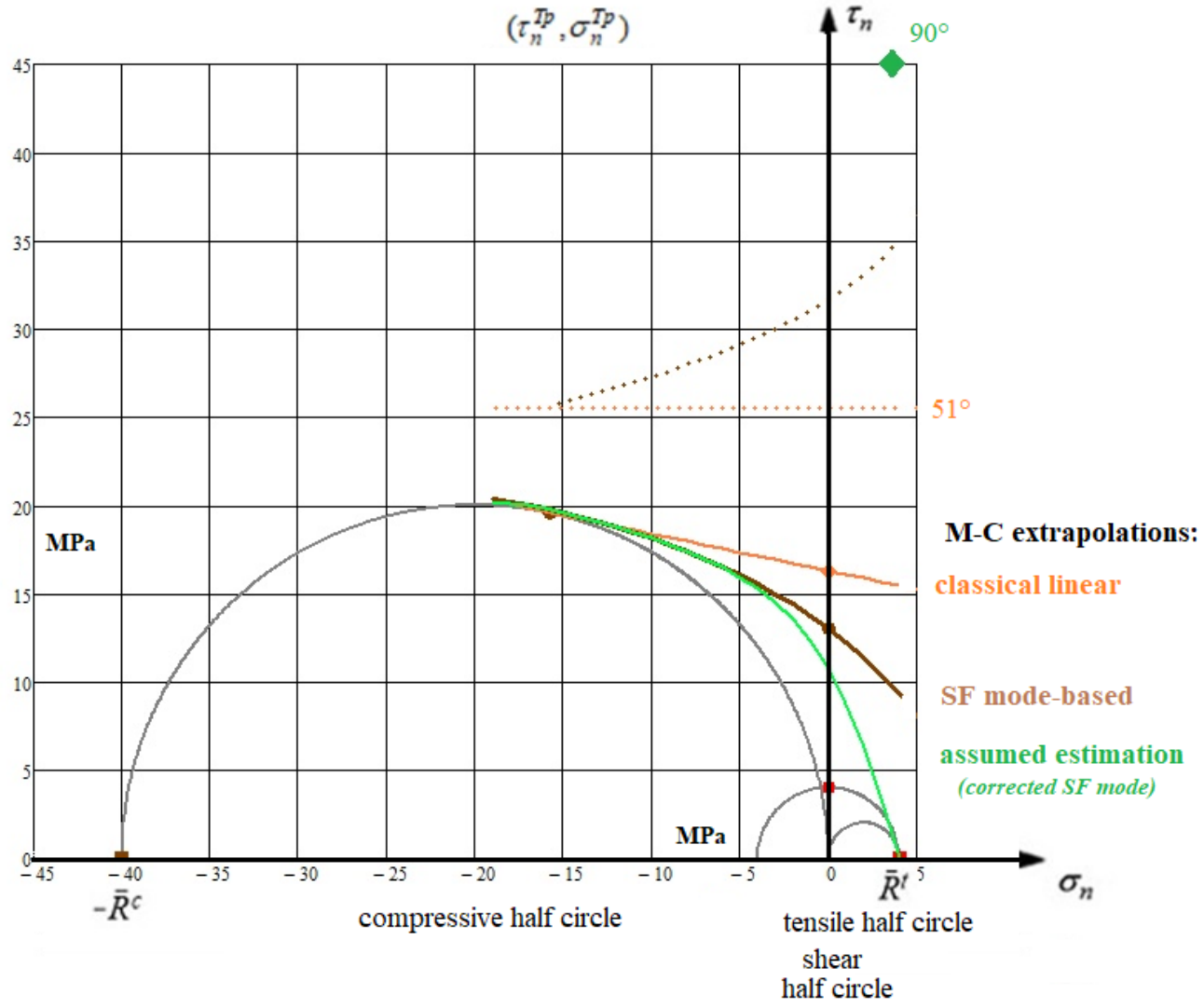

Fig.25-4a, Normal Concrete: $\bar{R}^{\tau}$, $\tau_n(\sigma_n)$.

Mohr-Coulomb extrapolations with fracture angle increase $\theta_{fp}°$, scaled by two.

First Lessons Learned from Fig.25-4a and viewing Fig.25-5:

**Classically, employing Fτ only, the angle θfp is linked to the slope of the plane M-C-curve.*

**Realistically, employing Fτ with Fσ, the angle θfp is linked to the slope of the fracture body surface. This makes the task still much more difficult.*

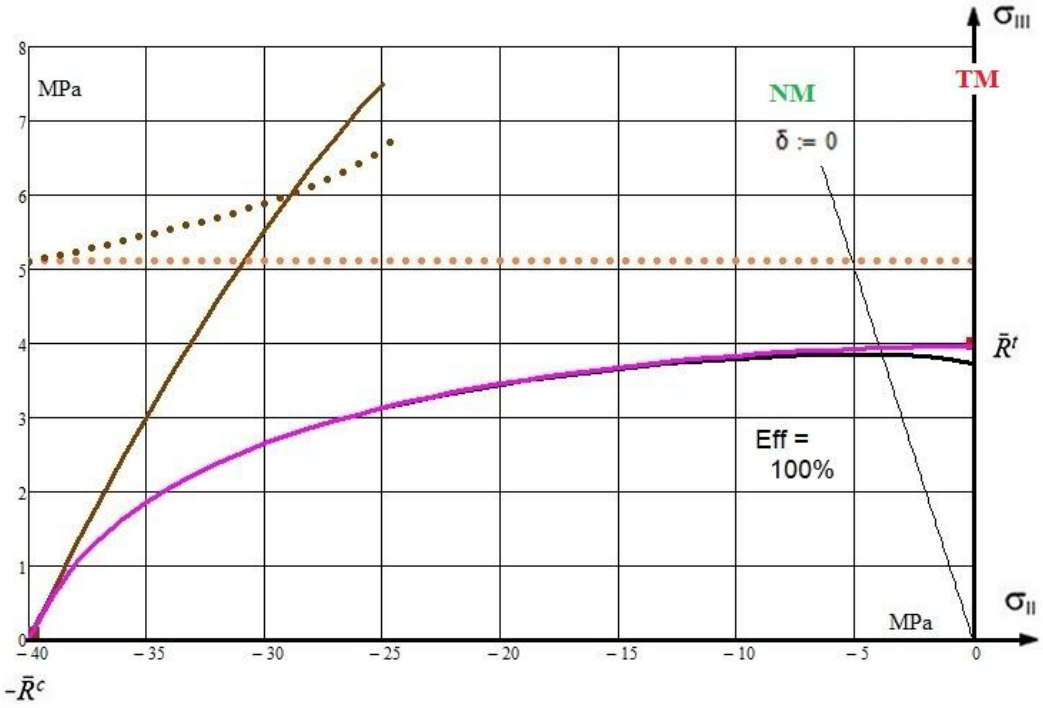

Fig.25-4b, Normal Concrete: $\bar{R}^{\tau}$, $\sigma_{III}(\sigma_{II})$

Joint display of the (fσ-corrected) failure curve in principal stresses, 120°-rotational-symmetric model.

Above figure leads to the result "*With decreasing* σ_{II} *an extrapolation of* $\theta_{fp}°(F^{\tau})$ *soon comes to its end. An estimation of values in the lower* σ_{II}*-domain is not possible. Both the modes have to be applied".*

In this context, *Fig.25-5* presents the span of the M-C curve on the 120°-rotationally-symmetric isotropic fracture body, outlining that it belongs to two modes the Shear Fracture mode (SF) F^{τ} and Normal Fracture mode (NF) F^{σ}. The envisaged accurate way consists of the following two paths.

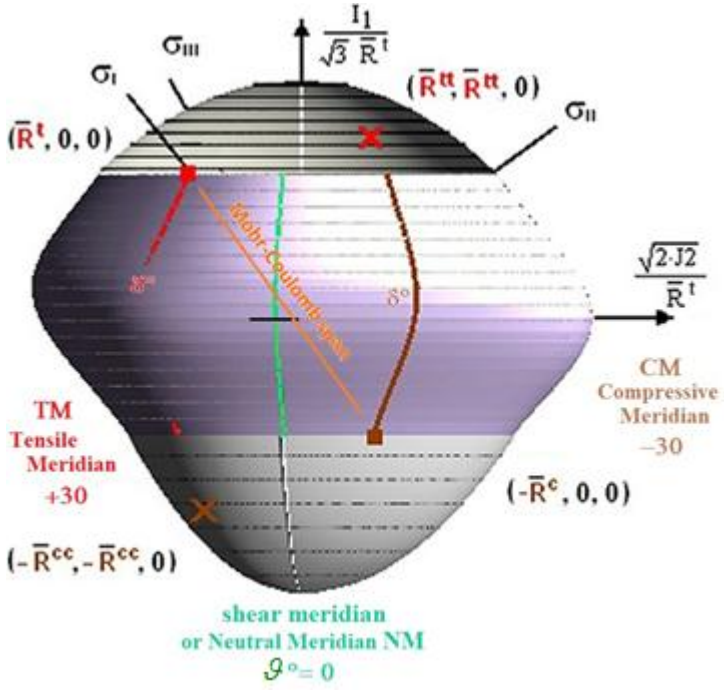

Fig.25-5, Normal Concrete: Visualization of all M-C-linked quantities

25.6 Results: Accurate Mode interaction Solution Path $\Theta_{fp}°(F^{\tau}, F^{\sigma})$.

25.6.1 Θ^{τ} **and** $f\sigma$ **simply applied as constants, not differentiated in** *Eff* **= 1**

Values for $\Theta_{fp}°(F^{\tau})$ are fictitious information values if just F^{τ} is applied, thereby the 120°-rotational symmetry of the fracture body not considering. This will be now executed beginning with a mathematically and mechanically simpler version by not considering Θ^{τ} and f_{σ} in the differentiation process. Its results are collected in *Table 26*.

The final formulation for C can be found after using the abbreviations below in the necessary re-transformation process of the Mohr stresses back to structural stresses. This is supported by using addition theorems and by inserting the well-known structural stress invariants I_1, J_2, J_3.

Re-transformation

$$2\sigma n = (C+1)\cdot\sigma II + (1-C)\cdot\sigma III \qquad \sigma t = \sigma n - C\cdot(\sigma II - \sigma III) \qquad 2\sigma n - \sigma t = 0.5\cdot(\sigma II + \sigma III) + 1.5\cdot C\cdot(\sigma II - \sigma III)$$

$$\sigma n = \frac{1}{2}\cdot[(C+1)\cdot\sigma II + (1-C)\cdot\sigma III] \qquad \sigma t = \frac{1}{2}\cdot[\sigma II\cdot(1-C) + \sigma III\cdot(1+C)] \qquad \tau n = -0.5\cdot\sqrt{1-C^2}\cdot(\sigma II - \sigma III)$$

$$a1 = \sigma II + \sigma III$$

$$a2 = \left[\frac{2\cdot\sigma t}{3} - 2\cdot\sigma n + \frac{4\cdot\sigma t}{3} = \frac{1}{3}\cdot(2\cdot\sigma t - 6\cdot\sigma n + 4\cdot\sigma t) = \frac{1}{3}\cdot(2\cdot\sigma t - 6\cdot\sigma n + 4\cdot\sigma t) = \frac{6}{3}\cdot(\sigma t - \sigma n) = -2C\cdot(\sigma II - \sigma III)\right]$$

$$a2 = -2C\cdot(\sigma II - \sigma III)$$

$$a3 = \left[\frac{2\cdot\sigma n^2}{3} - \frac{(\sigma t + \sigma n)^2}{3} + 4\cdot\tau n^2 + \frac{2\cdot\sigma t^2}{3} + \frac{2\cdot(\sigma n - \sigma t)^2}{3} = \frac{1}{3}\cdot\left[2\cdot\sigma n^2 - (\sigma t + \sigma n)^2 + 12\cdot\tau n^2 + 2\cdot\sigma t^2 + 2\cdot(\sigma n - \sigma t)^2\right]\right]$$

$$a3 = \frac{1}{3}\cdot\left[2\cdot\sigma n^2 - (\sigma t + \sigma n)^2 + 12\cdot\tau n^2 + 2\cdot\sigma t^2 + 2\cdot(\sigma n - \sigma t)^2\right] = \frac{1}{3}\cdot 3\cdot C^2\cdot(\sigma II - \sigma III)^2$$

$$a3 = C^2\cdot(\sigma II - \sigma III)^2$$

$$a4 = 12\cdot\tau n^2 + 2\cdot\sigma t^2 + 2\cdot\sigma n^2 + 2\cdot(\sigma n - \sigma t)^2 = 12\cdot\left[-0.5\cdot\sqrt{1-C^2}\cdot(\sigma II - \sigma III)\right]^2 + \left(3\cdot C^2\cdot\sigma II^2 - 6\cdot C^2\cdot\sigma II\cdot\sigma III + 3\cdot C^2\cdot\sigma III^2 + \sigma II^2 + 2\cdot\sigma II\cdot\sigma III + \sigma III^2\right)$$

$$= 12\cdot\left[-0.5\cdot\sqrt{1-C^2}\cdot(\sigma II - \sigma III)\right]^2 + \left(3\cdot C^2\cdot\sigma II^2 - 6\cdot C^2\cdot\sigma II\cdot\sigma III + 3\cdot C^2\cdot\sigma III^2 + \sigma II^2 + 2\cdot\sigma II\cdot\sigma III + \sigma III^2\right)$$

$$a4 = 12\cdot\left[-0.5\cdot\sqrt{1-C^2}\cdot(\sigma II - \sigma III)\right]^2 + \left[3\cdot C^2\cdot(\sigma II - \sigma III)^2 + a1^2\right]$$

$$a4 = 4\cdot\left(\sigma II^2 - \sigma II\cdot\sigma III + \sigma III^2\right)$$

$$a5 = [8\cdot\sigma n - 4\cdot\sigma t = 4\cdot(2\sigma n - \sigma t) = 4\cdot[0.5\cdot(\sigma II + \sigma III) + 1.5\cdot C\cdot(\sigma II - \sigma III)]]$$

$$a5 = 4\cdot[0.5\cdot(\sigma II + \sigma III) + 1.5\cdot C\cdot(\sigma II - \sigma III)]$$

Applying 'Mathcad 15 Symbolic Differentiation' on the interaction equation *Eff* = 1 results for $d(Eff)/d\sigma_n$ (*numerator of the formula for C*) and for $d(Eff)/d\tau_n$ (de-numerator) are obtained in Mohr stresses. Then, in order to achieve a practical equation for the final computation of *C*, an effortful manual evaluation by the determined re-transformation formulas above had to be performed.

However, this improved solution path, requiring the consideration of the 120°- rotational symmetry by capturing Θ^{τ} for the determination of cohesive strength R^{τ} and for the changing fracture angle θ_{fp} could not be gone to its end: The solver Mathcad found no solution. So the author had to 'suffer' that an elaborate, physically more accurate mathematical solution is not passable. The question came up, whether the fully accurate path below may change this unpleasant situation. Despite of the fact, that this path is even more risky, it is almost always worthwhile to present it viewing Lessons Learned (*LL*).

25.6.2 Physically and mathematically improved Θ^{τ} **and** $f\sigma$ **, now also differentiated**

Applying Mathcad Symbolic Differentiation on $d(Eff)/d\sigma_n$, the numerator in Mohr stresses, leads to the extremely long equation in *Table 27*. And, for the more complicated differentiation $d(Eff)/d\tau_n$, the

de-numerator, no applicable result was presented, only the citation "*The returned result is too large to* display". Trying to be physically and mathematically fully accurate this was a frustrating result.

However, due to the mountain experiences, one does not actually give up,
but only gives in to the unsolvable problem.

25.7 Results: Guessing a Cohesive Strength value R^{τ} considering *fσ*

After the failure to follow the above accurate path, the task remains to offer a practical estimate. Formulas, see Table 25-2. This approach consists of the following steps: $Eff^{m} = (Eff^{NF})^{m} + (Eff^{SF})^{m} = 1$

- Guess of a value for R^{τ}, employing *Fig.25-4a* and see *Table 25-6*
- Guess of a value for $\theta_{fp}°$, using the knowledge that it must lie much below the 90° but significantly higher than $\theta_{fpc}° = 51°$ → taking 71° = (51° + 90°) / 2 here
- Insertion into the relationships for the structural stresses
- Checking, whether the material stressing effort meets *Eff* =100%, considering *fσ*-correction.

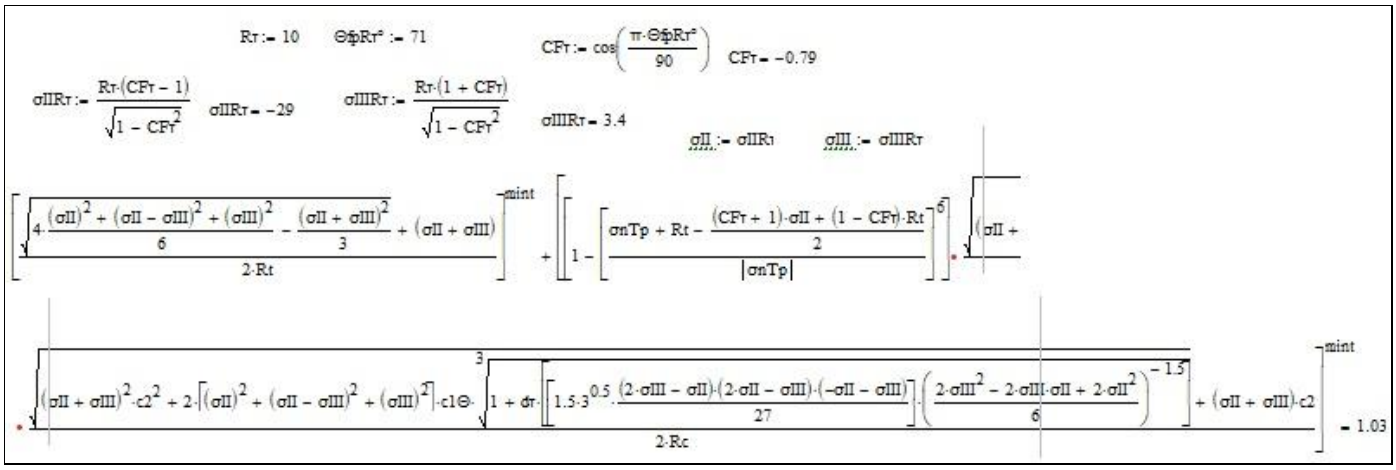

*The guess looks very satisfying. R^{τ} = 10 MPa is a good guess !

LL *from interpretation of the results including the Summary Table 25-6:*

- ✓ *The modes* F^{τ}, F^{σ} *and the interaction equation Eff - representing the surface of the fracture body in structural stresses - can be transferred into Mohr stresses and 'Addition Theorems-based' re-transformed in order to make a solution possible*
- ✓ *With the extrapolation approaches it was not possible to determine the full alteration of the nonlinear M-C curve (envelope), of the fracture plane angle* $\theta_{fp}°$ *and of* R^{τ}. *Just employing the SF mode* F^{τ} *cannot lead to a full course of the M-C curve and its quantities* $\theta_{fp}°$, R^{τ}
- ✓ *Due to the not locally full representing the course of the* $\sigma_{III}(\sigma_{II})$ *test data the mode* F^{τ} *is to correct by* $f\sigma$ *in order to simply obtain an approximation for a more realistic ('uni-axial') M-C curve*
- ✓ Θ^{τ} *must be considered, if the material is not ductile under compression. And ('bi-axially'), complete failure danger is the result of both the portions* Eff^{NF} *and* Eff^{SF}, *interaction is to consider*
- ✓ *For Normal Concrete it is the conclusion* that R^{τ} *is about 11 MPa and* $\theta_{fp}°$ *is approximately 70° at the cohesive strength point, compared to* $\theta_{fp}° = 51°$ *at the Touch point, representing* R^{c}.

✓ *Keep in mind: The presented results are averaged quantities and remind scatter!*

Applying - instead of the present Modal SFC - a so-called Global SFC, which globally maps by one single mathematical equation all test data with its two different modes, the same bottlenecks for the execution of this specific task would be found, too!

Note, please:

In the context of the chapters 24 and 25, before going into further investigations on isotropic concrete and later rock material, this is a good place to remind physics by stressing again the author's FMC-based failure mode thinking. This meets the action 'confining pressure' and the action 'bi-axial compressive stress':

Designing to hydraulic borehole fracturing 'Jaeger et al.' are still writing in 2007 (cited in [You15]) "Tensile strengths predicted by both the Coulomb criterion (onset-of cracking, solid mechanics) and the Griffith criterion (cracked, fracture mechanics) are much higher than the measured magnitudes of almost all rocks, although the two criteria have clear physical backgrounds".

This facts-neglecting citation is unbelievable for the author:

Each mode NF and SF is dominated by one technical strength R. And, it is also known that the cohesive (shear) strength is the result of two acting modes, namely SF with NF. Both these facts lead to the mechanics-based conclusion:

"*A Shear Failure-based criterion cannot give a prediction for a tensile strength* R^t".

Table 25-6: Summary of all cohesive strength–linked calculation results.
Lode angle ϑ, *fracture plane angle measure C, fracture plane angle* $\theta_{fp}°$, *normalizing strength* $\bar{R}^t$, *(right) Haigh-Lode-Westergaard coordinates of the fracture body* $\{\sigma\}$

	points	c_1, $c_{1\Theta}$	c_2	ϑ^o	C^t, C^c C^τ	$\theta_{fp}°$	Θ, Θ^τ	σ_{II}^τ, σ_{III}^τ	σn, τn	$\frac{I_1}{\sqrt{3}\cdot\bar{R}^t}$	$\frac{\sqrt{2\cdot J_2}}{\bar{R}^t}$
	$(\bar{R}^t, 0)$	-	-	+30	-1	90	1.15	-	-	0.6	0.8
linM-C	$\bar{R}^\tau$	5.32	4.32	-6.9	-0.21	51	1.06	-20.2 , 13.2	0, 16.3	-1.0	5.9
Fτ	$\bar{R}^\tau$	5.32	4.32	-11.6	-0.356	55	1.09	-18.7, 8.9	0, 12.9	-1.15	5.0
Fτ, fσ	$\bar{R}^\tau$	5.32	4.32	-11	-0.77	(70)	1.14	-30, 4	0, 11	-	-
I_1*=0*								-3.8, 3.8		0	1.34
Fτ + Fσ, Θ, *fσ*	$\bar{R}^\tau$	6.75	4.32	Accurate solution was mathematically not possible							
Fτ + Fσ, Θ, *fσ (guess)*	$\bar{R}^\tau$ =10	6.75	4.32		-0.79	71		-29, 3.4	0, 10	-2.3	5.3
	$(-\bar{R}^c, 0)$	5.32	4.32	-30	0.21	51	0.79	-40, 0	-15.8, 19.6	-5.8	8.2
ductile μ*=0*	$\bar{R}^t_{0.2}$	2	1	0	0	45	1	$\sigma_{II}^\tau = -\sigma_{III}^\tau$	horizontal M-C curve	Mises cylinder: I_1 varies, J_2 constant	

$$F\sigma = \frac{\sqrt{4 \cdot J2 - \frac{I1^2}{3}} + I1}{2 \cdot Rt} = Eff\sigma = 1 \; ; \quad Fr = c2 \cdot \frac{I1}{Rc} + \frac{c1\Theta \cdot \Theta r \cdot 6J2}{2 \cdot Rc^2} = 1 \; , \quad Eff r = \frac{\sqrt{I1^2 \cdot c2^2 + 12 \cdot J2 \cdot c1\Theta \cdot \Theta r} + I1 \cdot c1}{2 \cdot Rc}$$

extrapolation: $\frac{d}{d\sigma n} \tau n = \frac{C}{\sqrt{1 - C^2}} = -1 \cdot \frac{\frac{dFr}{\sigma n}}{\frac{dFr}{d\tau n}}$ accurate: $\frac{d}{d\sigma n} \tau n = \frac{C}{\sqrt{1 - C^2}} = -1 \cdot \frac{\frac{dEff r}{\sigma n}}{\frac{dEff r}{d\tau n}}$

$$Eff = \left[\frac{\sqrt{4 \cdot \frac{\sigma n^2 + (\sigma n - \sigma t)^2 + \sigma t^2 + 6 \cdot \tau n^2}{6} - \frac{(\sigma n + \sigma t)^2}{3}} + (\sigma n + \sigma t)}{2 \cdot Rt} \right]^{mint} + fr \cdot \left[\frac{\sqrt{(\sigma n + \sigma t)^2 \cdot c2^2 + 12 \cdot \frac{\sigma n^2 + (\sigma n - \sigma t)^2 + \sigma t^2 + 6 \cdot \tau n^2}{6} \cdot c1\Theta \cdot \Theta r} + (\sigma n + \sigma t) \cdot c2}{2 \cdot Rc} \right]^{mint}$$

General : $\tau n_j \square -0.5 \cdot \sqrt{1 - (C_j)^2} \cdot (\sigma II_j - \sigma III_j)$ $\sigma n_j \square \frac{(C_j + 1) \cdot \sigma II_j + (1 - C_j) \cdot \sigma III_j}{2}$

to insert $\Theta r = \sqrt[3]{1 + d r \cdot \sin(3\delta)} = \sqrt[3]{1 + dr \cdot 1.5 \cdot 3^{0.5} \cdot J3 \cdot J2^{-1.5}}$

with $3\delta = \left[1.5 \cdot 3^{0.5} \cdot \frac{2 \cdot (\sigma n + \sigma t)^3 - 9 \cdot (\sigma n + \sigma t) \cdot (\sigma n \cdot \sigma t - \tau n^2)}{27} \right] \cdot \left[\frac{\sigma n^2 + (\sigma n - \sigma t)^2 + \sigma t^2 + 6 \cdot \tau n^2}{6} \right]^{-1.5}$

$f\sigma$ is set constant for mathematical simplification $fr = 1 - \left(\frac{\sigma n Tp + Rt - \sigma n}{|\sigma n Tp|} \right)^6$ and

$$fr = 1 - \left[\frac{\sigma n Tp + Rt - \frac{(Cc + 1) \cdot \sigma II + (1 - Cc) \cdot Rt}{2}}{|\sigma n Tp|} \right]^6$$

Simplified Solution Procedure: Θ = 1, fσ = 1

Vorgabe $\sigma III := 2$ $\Theta := 1$ $fr := 1$

$$1 = \left[\frac{\sqrt{4 \cdot \frac{(\sigma II)^2 + (\sigma II - \sigma III)^2 + (\sigma III)^2}{6} - \frac{(\sigma II + \sigma III)^2}{3}} + (\sigma II + \sigma III)}{2 \cdot Rt} \right]^{mint} + fr \cdot \left[\frac{\sqrt{(\sigma II + \sigma III)^2 \cdot c2^2 + 2 \cdot \left[(\sigma II)^2 + (\sigma II - \sigma III)^2 + (\sigma III)^2 \right] \cdot c1\Theta \cdot \Theta} + (\sigma II + \sigma III) \cdot c2}{2 \cdot Rc} \right]^{mint}$$

$X(\sigma II) := Suchen(\sigma III)$ $j := 0,1 .. Rc$ $\sigma II_j := -Rc + j$ $\sigma III_j := V(\sigma II_j)$

accurate: $\frac{d}{d\sigma n} \tau n = \frac{C}{\sqrt{1 - C^2}} = -1 \cdot \frac{\frac{dEff r}{\sigma n}}{\frac{dEff r}{d\tau n}}$ to be re-transformed, using $\sigma n = \frac{1}{2} \cdot [(C + 1) \cdot \sigma II + (1 - C) \cdot \sigma III]$ $\tau n = -0.5 \cdot \sqrt{1 - C^2} \cdot (\sigma II - \sigma III)$

$\sigma t = \frac{1}{2} \cdot [\sigma II \cdot (1 - C) + \sigma III \cdot (1 + C)]$

Final solution equation for the fracture angle measure C: Θ = 1, fσ = 1

$a := \sigma II + \sigma III$ $b := 4 \cdot \left[(\sigma II)^2 - \sigma II \cdot \sigma III + (\sigma III)^2 \right]$

Vorgabe $C := -0.3$

$$-C = \left[\frac{mint \cdot \left[c2 + \frac{c2^2 \cdot (2a)}{2 \cdot \sqrt{c2^2 \cdot a^2 + c1\Theta \cdot \Theta \cdot \left[12 \cdot \left[-0.5 \cdot \sqrt{1 - C^2} \cdot (\sigma II - \sigma III) \right]^2 - a^2 + b^2 \right]}} \right] \cdot \left[\frac{c2 \cdot (a) + \sqrt{c2^2 \cdot a^2 + c1\Theta \cdot \Theta \cdot \left[12 \cdot \left[-0.5 \cdot \sqrt{1 - C^2} \cdot (\sigma II - \sigma III) \right]^2 - a^2 + b^2 \right]}}{2 \cdot Rc} \right]^{mint-1}}{2 \cdot Rc} - \frac{mint \cdot \left[\frac{2a}{3 \cdot \left[\frac{1}{\sqrt{3}} \cdot \sqrt{12 \cdot \left[-0.5 \cdot \sqrt{1 - C^2} \cdot (\sigma II - \sigma III) \right]^2 - a^2 + b^2} \right]} \right] - 1 \cdot \left[\frac{a + \frac{1}{\sqrt{3}} \cdot \sqrt{12 \cdot \left[-0.5 \cdot \sqrt{1 - C^2} \cdot (\sigma II - \sigma III) \right]^2 - a^2 + b^2}}{2 \cdot Rt} \right]^{mint-1}}{2 \cdot Rt} \right]$$

$$\frac{2 \cdot mint \left[-0.5 \cdot (\sigma II - \sigma III) \right] \cdot \left[\frac{a + \frac{1}{\sqrt{3}} \cdot \sqrt{12 \cdot \left[-0.5 \cdot \sqrt{1 - C^2} \cdot (\sigma II - \sigma III) \right]^2 - a^2 + b^2}}{2 \cdot Rt} \right]^{mint-1}}{Rt \cdot \left[\frac{1}{\sqrt{3}} \cdot \sqrt{12 \cdot \left[-0.5 \cdot \sqrt{1 - C^2} \cdot (\sigma II - \sigma III) \right]^2 - a^2 + b^2} \right]} + \frac{6 \cdot mint \left[-0.5 \cdot (\sigma II - \sigma III) \right] \cdot (c1\Theta \cdot \Theta) \cdot \left[\frac{c2 \cdot (a) + \sqrt{c2^2 \cdot a^2 + c1\Theta \cdot \Theta \cdot \left[12 \cdot \left[-0.5 \cdot \sqrt{1 - C^2} \cdot (\sigma II - \sigma III) \right]^2 - a^2 + b^2 \right]}}{2 \cdot Rc} \right]^{mint-1}}{Rc \cdot \sqrt{c2^2 \cdot a^2 + c1\Theta \cdot \Theta \cdot \left[12 \cdot \left[-0.5 \cdot \sqrt{1 - C^2} \cdot (\sigma II - \sigma III) \right]^2 - a^2 + b^2 \right]}}$$

$X(\sigma II, \sigma III) := Suchen(C)$ $C_j := V(\sigma II_j, \sigma III_j)$ $\Theta fp\Theta_j := 0.5 \cdot acos(C_j)$ $\Theta fp\Theta^\circ_j := \frac{180}{\pi} \cdot \Theta fp\Theta_j$

General : $\tau n_j \square -0.5 \cdot \sqrt{1 - (C_j)^2} \cdot (\sigma II_j - \sigma III_j)$ $\sigma n_j \square \frac{(C_j + 1) \cdot \sigma II_j + (1 - C_j) \cdot \sigma III_j}{2}$

***Table 26:* Θ° and *fσ* simply applied as constants, not differentiated**

final lines here added $Rt := 12.9$ $CFr = -0.356$

General : $\tau n_j \square -0.5 \cdot \sqrt{1 - (C_j)^2} \cdot (\sigma II_j - \sigma III_j)$ $\sigma n_j \square \frac{(C_j + 1) \cdot \sigma II_j + (1 - C_j) \cdot \sigma III_j}{2}$

For the cohesive strength point C becomes Cr: Numerical Example of 'just Fr' in Table 25-6

$\Theta fpRT^\circ := \frac{90 \cdot acos(Cr)}{\pi}$ $\Theta fpRT^\circ = 54.9$ $\sigma IIRr := \frac{Rr \cdot (Cr - 1)}{\sqrt{1 - Cr^2}}$ $\sigma IIIRr := \frac{Rr \cdot (1 + Cr)}{\sqrt{1 - Cr^2}}$ $\sigma IIRr = -18.7$ $\sigma IIIRr = 8.9$

$$\delta Fr := \frac{asin \left[1.5 \cdot 3^{0.5} \cdot \frac{(2 \cdot \sigma IIIRr - \sigma IIRr) \cdot (2 \cdot \sigma IIRr - \sigma IIIRr) \cdot (-\sigma IIRr - \sigma IIIRr)}{27} \right] \cdot \left[\frac{2 \cdot (\sigma IIIRr)^2 - 2 \cdot \sigma IIIRr \cdot \sigma IIRr + 2 \cdot (\sigma IIRr)^2}{6} \right]^{1.5}}{3}$$

$\delta Fr = -0.194$ $\delta Fr^\circ := \frac{180}{\pi} \cdot \delta Fr$ $\Theta rFr := \sqrt[3]{1 - dr \cdot \sin(3 \cdot \delta Fr)}$ $\delta Fr^\circ = -11.1$ $\Theta rFr = 1.09$

$I1Rr := \sigma IIRr + \sigma IIIRr$ $J2Rr := \frac{1}{6} \cdot \left[(\sigma IIRr)^2 + (\sigma IIRr - \sigma IIIRr)^2 + (\sigma IIIRr)^2 \right]$

$\frac{I1Rr}{\sqrt{3} \cdot Rt} = -1.15$ $\frac{\sqrt{2 \cdot J2Rr}}{Rt} = 4.98$

$\delta Fr^\circ = -11.62$

Table 27: Fully general Θ^{τ} and $f\sigma$ also differentiated

numerator could be symbolically derived de-numerator not

second term

26 Mapping 3D Test Results of Concrete and Rocks obtained on the Meridians TM and CM

Aim: *Provision of a test data evaluation formula for the test meridian, being a cross-section of a physically to be defined fracture body surface. Optimum mapping both in 2D- principal stress plane and in3D-stress space.*

A value for R^{τ} was the aim of § 25, here it is aimed at a good mapping in 2D-plane and 3D-space.

26.1 General

Sufficient strength of tunnels and dam slopes are vital Design Verification requirements in geo-engineering. In order to achieve this, the course of the measured fracture data on Tensile (TM) and Compressive Meridian (CM) is to map. For this design task several SFC approaches are applied:

" Classical, linear Mohr-Coulomb shear curve"

Shear stresses below the curve mean 'No fracture', or 'Stress states' below the τ^n- curve are not dangerous. In civil engineering this well-known simple SFC reads: $\tau^n(\sigma_I, \sigma_{III}) = \sigma \cdot tan\phi + c$.

→ values for cohesive shear strength c and friction angle $\phi(\mu)$ are required.
This is an extrapolation from the compressive strength point.

"Linear Mohr-Coulomb criterion in geo-mechanics"

In order to achieve Design Verification in several numerical Rock mechanics Codes the use of the widely applied 'Mohr-Coulomb (M-C) Criterion' is recommended in order to map the course on that meridian where the tests have been run, on TM or CM. The criterion below says that a stress below the M-C curve is conservative.

$\sigma_1 = \sigma_3 \cdot tan^2(\Phi) + 2 \cdot c \cdot tan(\Phi)$, applying $\Phi = \pi / 4 + \phi / 2$

where c = cohesive shear strength $\equiv R^{\tau}$, ϕ = internal friction angle, and

σ_1 = most negative principal stress $\rightarrow \sigma_{III}$, σ_3 = most positive principal stress $\rightarrow \sigma_I$,

which are transferred due to the mathematical principal stress convention $\sigma_I > \sigma_{II} > \sigma_{III}$.

The final formulation reads: $\sigma_{III} = \sigma_I \cdot tan^2(\Phi) + 2 \cdot c \cdot tan(\Phi)$.

However in application, a difficult to be answered question arises: Which parameters are to insert? This concerns the fracture angle ϕ and the cohesive strength R^{τ}.

→ values for cohesive shear strength c and friction angle are required.
This also is usually done as an extrapolation from the compressive strength point.

In *Fig.26-1* the derivation of the associated input data set is provided. Concerning R^{τ} it is referred to a previous chapter where the cohesive strength has been investigated.

"Cuntze's FMC-based SFCs regarding the common acting of SF and NF"

The SFC model, spanning up the isotropic fracture body, is shown in *Table 26-1*, too.

As still described before, the first part of the SFC in *Table 26-1* represents the shape change, the second the friction effect, the third the volume change and Θ^{τ} the 120°-symmetry of isotropic materials. Mapping the test data in the very high negative compression domain of UHPC could require a fifth part, which may be dedicated to a further effect: discontinuous densification including at first a failure body hoop reduction and later widening.

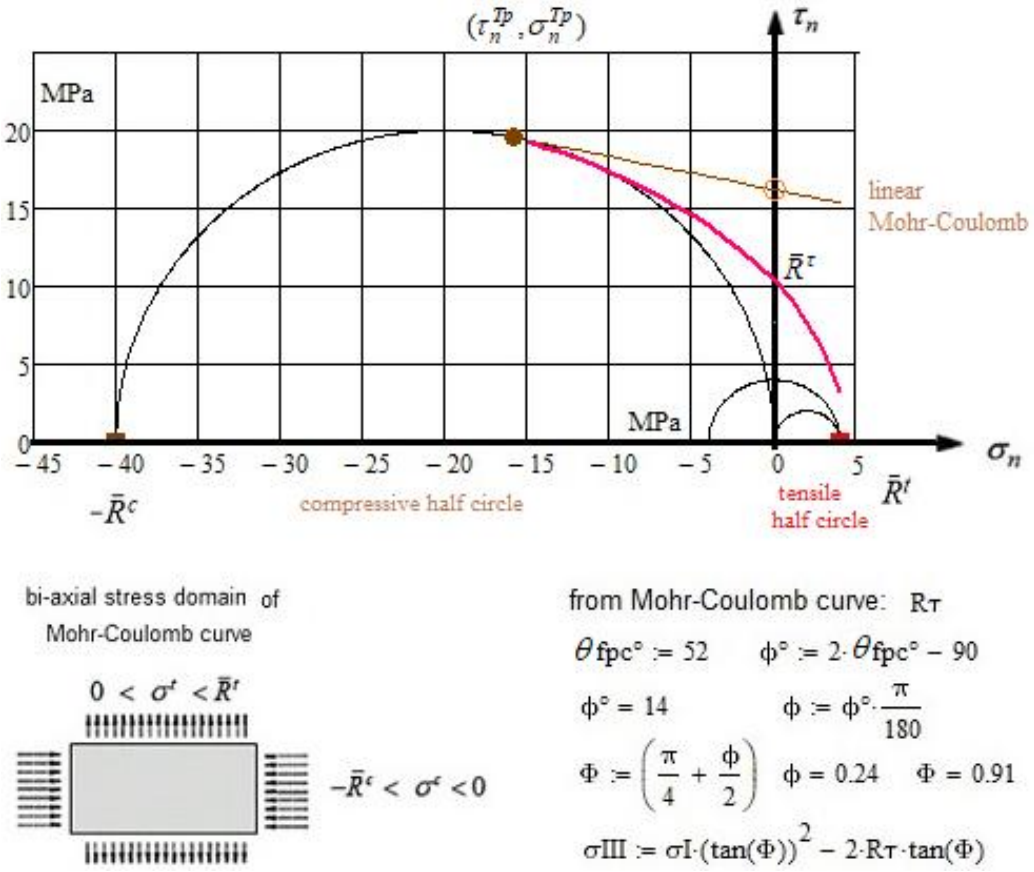

Fig.26-1, example Normal Concrete, 52°: Basics

The SFC contains five un-known parameters. For their determination, mathematically at minimum, five reliable test points on the surface of the fracture body are to provide by tests along the TM and CM. Better fitting procedures could be applied, of course.
Good Mapping requires to capture physics and to apply SFCs being as simple as possible.

Cuntze's approach includes a multifold mapping task, which can be a compromise, only:

(1) Mapping the 2D test data in the principal stress plane, considering here the friction effect.

(2) Mapping the 3D test data along tensile test meridian (TM) and compressive test meridian (CM) along these two axial (180°-opposite) cross-sections of the fracture body with
$(\sigma_I, \sigma_{II} = \sigma_{III}) \rightarrow \sigma_I(2\sigma_{III})$ and CM $(\sigma_I = \sigma_{II}, \sigma_{III}) \rightarrow 2\sigma_I(\sigma_{III})$.

All subfigures, principal stress plane and meridian cross-sections must be able to be derived from the well mapped fracture body and this with sufficient precision.

→ cohesive shear strength $c = R^\tau$ and friction angle ϕ are not required.
Points on the fracture body surface are used to fix the model parameters.

Reminder: All isotropic materials possess a more or less significant 120°-rotational symmetry of the fracture body most often depicted in Haigh-Lode-Westergaard coordinates, see *Fig.26-2*. Thereby, the well-known invariant J_3 is an excellent function to map this type of rotational symmetry (caused by $R^{cc} \neq R^c$ or $R^{tt} < R^t$) and to determine the Lode angle ϑ. Well-known is that the tests are run on the CM and on the TM, meaning that data sets are given for CM with $\vartheta = -30°$ and for TM with $\vartheta = 30°$.

For the chosen Model, depicted in *Table 26-1*, the tricky procedure how to obtain the required model parameters c_i is shown in *Table 26-2* by three steps. For the cohesive strength, required by the

extrapolation approaches, numerical values are determined in the third step. Different models deliver different values improved models deliver a lower value, because these consider both damaging modes SF and NF.

Table 26-1: UHPC-SFC model

shape change friction volume change

$$I_1<0:\ F^{SF}=F^{\tau}=\ c_1^{SF}\cdot\frac{6J_2\cdot\Theta^{SF}}{2\cdot\bar{R}^{c2}}\ +\ c_2^{SF}(\mu)\cdot\frac{I_1}{\bar{R}^c}\ +\ c_3\cdot\left(\frac{I_1}{\bar{R}^c}\right)^2\ +\ c_4\cdot\left(\frac{I_1}{\bar{R}^c}\right)^3\ =\ 1$$

'Mises Cylinder' formula

Above SFC is here normalized by the compressive strength $\bar{R}^c$. J_2 is the 'Mises' invariant.

$$I_1=(\sigma_I+\sigma_{II}+\sigma_{III})\ =f(\sigma)\ ,\quad 6J_2=(\sigma_I-\sigma_{II})^2+(\sigma_{II}-\sigma_{III})^2+(\sigma_{III}-\sigma_I)^2=\ f(\tau)$$

$$27J_3=\ (2\sigma_I-\sigma_{II}-\sigma_{III})\cdot(2\sigma_{II}-\sigma_I-\sigma_{III})\cdot(2\sigma_{III}-\sigma_I-\sigma_{II}),$$

$$3\cdot\sigma_{oct}=\sigma_I+\sigma_{II}+\sigma_{III}\ ;\ \ 9\cdot\tau_{oct}{}^2=6J_2=4\cdot(\tau_{III}{}^2+\tau_I{}^2+\tau_{II}{}^2),\ \tau_{II}=max\,\tau(mathem.)$$

$\sigma_I,\sigma_{II},\sigma_{III}$ are principal stresses, $\sigma_I>\sigma_{II}>\sigma_{III}$ are mathematical stresses (> more positive)

with $I_1=(\sigma_I+\sigma_{II}+\sigma_{III})$, $6\cdot J_2=(\sigma_I-\sigma_{II})^2+(\sigma_{II}-\sigma_{III})^2+(\sigma_{III}-\sigma_I)^2$

Consideration: 120°-rotational symmetry of isotropic materials: $d^{SF}\equiv d_\tau$ *later*

$$\Theta^{SF}(J_3,J_2)=\sqrt[3]{1+d^{SF}\cdot sin(3\vartheta)}=\sqrt[3]{1+d^{SF}\cdot 1.5\cdot\sqrt{3}\cdot J_3\cdot J_2{}^{-1.5}}$$

with the non-circularity function Θ^{SF} including d^{SF} as non-circularity parameter.

Compr. Meridian: $\Theta^{SF}=\sqrt[3]{1-d^{SF}}$, Tensile Meridian: $\Theta^{SF}=\sqrt[3]{1+d^{SF}}$, Neutral Meridian: $\Theta^{SF}=1$.

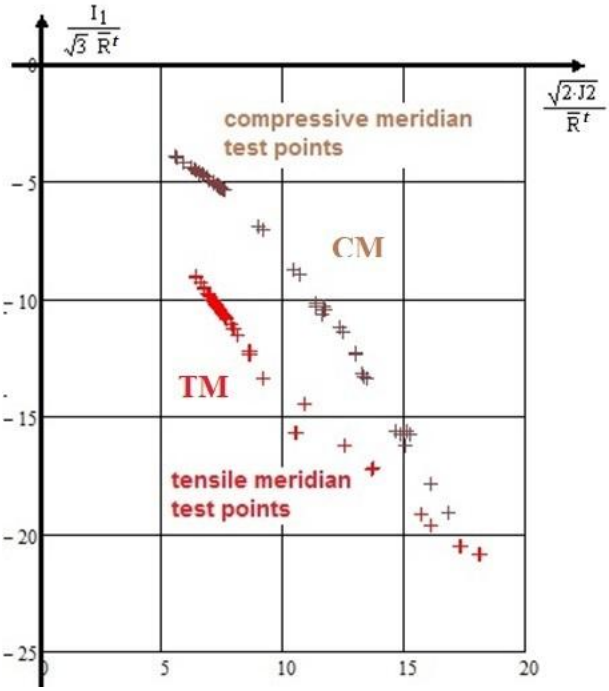

Fig.26-2, example UHPC:
Compressive + and
tensile meridian +test points.

Intentionally depicted on the positive abscissa to outlne the difference
stemming from the brittle isotropic material's inherent 120°-rotational symmetry of the fracture failure body

Table 26- 2, example Normal Concrete: Procedure to obtain the model parameters.

1 ***Relationship of friction parameter and value considering the simple Two Parameter Model***

$F^{\tau} = c_2 \cdot \frac{I_1}{\bar{R}^c} + c_{1\Theta} \cdot \frac{6 \cdot J_2 \cdot \Theta^{SF}}{2 \cdot \bar{R}^{c2}} = 1$ ← insertion of the compression point $c_2 \cdot \frac{-\bar{R}^c}{\bar{R}^c} + c_{1\Theta} \cdot \frac{6 \cdot \bar{R}^{c2} / 3 \cdot \Theta^{SF}}{2 \cdot \bar{R}^{c2}} = 1$

($c_{2\Theta} = c_2$, because the friction parameter does not depend on 120°-rotational symmetry)

$\Rightarrow c_{1\Theta} = \frac{1 + c_2}{\Theta^{CM}}$ with non-circularity function $\Theta^{CM} = \sqrt[3]{1 - d_\tau}$ (if rotationally-symmetric, $d^\tau = 0$, $\Theta^{SF} = 1$),

Estimation of c_2, by a guess of the friction value μ, from $c_2 = (1 + 3 \cdot \mu) / (1 - 3 \cdot \mu)$.

With a guess $\theta_{fp}^{c\,\circ} = 51°$ ≡ friction value $\mu = 0.208$ and $C^c = \cos(2 \cdot \theta_{fp}\,° \cdot \frac{\pi}{180°}) = -\mu$ follows

$c_2 = (3 \cdot C^c - 1) / (3 \cdot C^c + 1) = (1 + 3 \cdot \mu) / (1 - 3 \cdot \mu) = 4.32.$

2 ***Combined Determination of non-circularity parameter d^τ and $c_{1\Theta}$*** (Mathcad Coding)

If no test value is available, this would require an estimate for $\bar{R}^{cc} > \bar{R}^c$ (lies on the TM).

$I1c := -Rc \quad J2c := \frac{Rc^2}{3} \quad I1cc := -2 \cdot Rcc \quad J2cc := \frac{Rcc^2}{3}$

Vorgabe $\quad c1\Theta := 2 \quad d\tau := 0.6 \quad c2 = 4.32$

$$\frac{\sqrt{I1c^2 \cdot c2^2 + 12 \cdot J2c \cdot c1\Theta \cdot \sqrt[3]{1 - 1 \cdot d\tau}} + I1c \cdot c2}{2 \cdot Rc} = 1$$ strength point on CM

$$\frac{\sqrt{I1cc^2 \cdot c2^2 + 12 \cdot J2cc \cdot c1\Theta \cdot \sqrt[3]{1 + 1 \cdot d\tau}} + I1cc \cdot c2}{2 \cdot Rc} = 1$$ bi-axial compressive failure stress point on TM

$A\tau := Suchen(c1\Theta, d\tau) \quad A\tau = \begin{pmatrix} 6.727 \\ 0.507 \end{pmatrix} \quad c1\Theta := A\tau_0 \quad d\tau := A\tau_1$

$c1\Theta = 6.7 \quad d\tau = 0.51$

3 ***Estimation of the Touch point and Cohesive Strength*** for application of the Mohr-Coulomb Criterion

From §25:

Touch point: $\tau_n^{Tp} = 19.6$ MPa, $\sigma_n^{Tp} = -15.8$ MPa.

Cohesive strength: $\bar{R}^\tau = \sqrt{\frac{-\bar{R}^{c2} + c_2 \cdot \bar{R}^c \cdot \sigma_{t0} + c_1 \cdot \sigma_{t0}^2}{3 \cdot c_1}}$ with $\sigma_{t0} = -C^c \cdot (-\bar{R}^c) = 12.9$ MPa

26.2 Ultra-High-Performance-Concrete UHPC (relatively dense)

UHPC principally behaves similarly to Normal Concrete unless the normalized hydrostatic compression does not become larger than $I_1 / R^t \cdot \sqrt{3} \approx -10$ (> -300 MPa), see *Fig.26-2.*

Then however, in contrast to Normal Concrete with usually relatively low hydrostatic pressure loadings the UHPC experiences a hydrostatically activated effect, 'densification with volume shrinkage'. Therefore, the volume change must be considered by I_1^2. This explains why for the less 'dense' Normal

Concrete R^{cc}/R^{c} is higher than with UHPC according to the possible higher densification. Combined with this a 'healing' of the flaw effects is principally faced.

The fracture body of a theoretically dense concrete matrix possesses in the high hydrostatic compressive domain ($I_1 < 0$) an open fracture surface due to the densification. Practically however, the fracture body does only exist once according to the final spatial micro-crack state and cannot be loaded a second time after deloading.

Further, the bi-axial compressive strength R^{cc} ($\equiv f^{cc}$, internationally used letter in construction, stems from the German term Festigkeit) may be not only linked to SF but also to NF due to the Poisson's ratio activated tensile strain in the axial direction despite $\sigma_{ax} = 0$.

An SFC-model validation requires reliable test results. These have been provided as original data sets by the IMb Dresden (*many thanks to Prof. Curbach and his co-workers*). Hence, the author had to search out of the huge test data package which test points belong to TM and which to CM. Therefore, the full bunch of obtained 3D test data had to be processed. Such a separation bases on the use of the Lode angle (meridian angle) ϑ values: Which test point belongs more to the tensile meridian $\sin(3\vartheta) = 1$ or to the compressive meridian $\sin(3\vartheta) = -1$, see *Table 26-3* and *Fig.26-4*. For the shear meridian (neutral meridian NM) angle is valid $\sin(3\vartheta) = \vartheta = 0$.

Considering all physical aspects, cited before in *Table 26-1*, the basic F^{τ}-SFC reads (in MPa):

$$F^{\tau} = c_1 \cdot \frac{6J_2 \cdot \Theta^{SF}}{2 \cdot \bar{R}^{c2}} + c_2(\mu) \cdot \frac{I_1}{\bar{R}^{c}} + c_3 \cdot \left(\frac{I_1}{\bar{R}^{c}}\right)^2 + c_4 \cdot \left(\frac{I_1}{\bar{R}^{c}}\right)^3 = 1 \quad \text{with}$$

5 unknowns, which at least require 5 fix stress state failure points on the failure surface

$\{\sigma\} = (\ ,\ ,\ )^T : (-\bar{R}^{c},0,0),\ (-\bar{R}^{cc},-\bar{R}^{cc}0,0),\ (\sigma_I^{frict},\sigma_I^{frict},0),\ (\bar{R}^{c},0,0),\ (\bar{R}^{c},0,0).$

The values in MPa = N/mm² are: $\bar{R}^{c} = 175$, $\bar{R}^{cc} = 183$, $\sigma_{II}^{frict} = -195$, $\sigma_{II}^{frict} = -50$ (*Fig*.26 - 5),

Points: $\sigma_I^{TM} = -40$, $\sigma_{II}^{TM} = \sigma_{III}^{TM}$, $\sigma_{III}^{TM} = -375$; $\sigma_I^{CM} = -61$, $\sigma_{II}^{CM} = \sigma_I^{CM}$, $\sigma_{III}^{CM} = -420$.

As proven mode interaction coefficient is taken again $m = 2.7$.

Note, please: In order to meet the aim of optimum 2D-3D-mapping the parameter c_2 is also determined in the complete parameter computation process of Table 26-4 and not computed due to Table 26-2.

Table 26-3 presents the essential numbers of some measured failure stress states. The table indicates the Lode angle $\vartheta°$, too. On basis of redundancy effects it may be concluded that with increasing hydrostatic pressure both the meridians run into a common scatter band, ending with a circle shape of the hoop. Then, the effect of flaws generating micro-damaging in this heterogeneous material reduces. Thereby, the fracture failure body becomes more and more cylindrical.

Fig. 26-4 links multi-axial stress states to the Lode angles ϑ = -30° (CM) and +30° (TM). Only stress states on the two meridians can be really depicted in the cross-sections. All other test points lie on the fixed hoop radius on a Lode angle different to ϑ = +30° and -30°. These points are marked by o.

Table 26-3: Characteristic material data from evaluated UHPC fracture tests.

E = 20000 MPa, ν = 0.2, $\tau_{max} = \sigma_I - \sigma_{III}$

c1= , c2= , c3 = , c4= , d =

$\bar{R}^t = 16$ MPa, $\bar{R}^c = 160$ MPa, $\bar{R}^{tt} = 14$ MPa (assumed), $\bar{R}^{cc} = 175$ MPa

	Stress state *in MPa*	$I_1/\sqrt{3}$ $/R^t$	$\sqrt{2 \cdot J2}$ $/R^t$	τ_{max} *in MPa*	$(\sigma_{hyd}; \sigma_{ax})$ *in MPa*	$\vartheta°$	$\varepsilon_{ax\ el}$ *in 10^{-3}*	*remarks*
R^{tt}	(14, 14, 0)	1	0.7	-	-	-30	0.6	*two-fold NF*
R^c	(0 , 0, -160)	-5.8	8.2	80	(-0; -160)	-30	-8	Eff_{SF}
	(-6, -6,-230)	-8.7	11.4	111	(-6; -224)	-30	-11	
Compr	(-16,-16,-272)	-11.0	13.1	128	(-16; -256)	-30	-13	
essive	(-35,-35,-350)	-15.2	16.1	157	(-35; -315)	-30	-17	
	(-83,-83, -490)	-23.7	20.8	204	(-83; -407)	-30	-23	
comput.	(**-23,-23,-305**)	-12.6	14.4	141	(-23; -282)	-30	-15	
R^{cc}	(0,-175,-175)	-12.6	8.9	88	(0;-)	+30	3.5	*two-fold SF*
Tensile	(-2,-210,-210)	-15.2	10.6	104	(-2; -)	+30	4.1	
	(-24,-310,-310)	-23.2	14.6	143	(-24; -)	+30	5.0	
R^t	(-54,-388,-388)	-30	17	167	(-54; -)	+30	5.1	
	(16, 0, 0)	0.6	0.8	-	-	+30	0.8	Eff_{NF}
shear	(9, -9, 0)	0	0.8	9	-	0	0.5	$Eff_{NF} > Eff_{SF}$
change	(0,-52,-193)	-8.8	8.8	97	-	-15	-9.1	

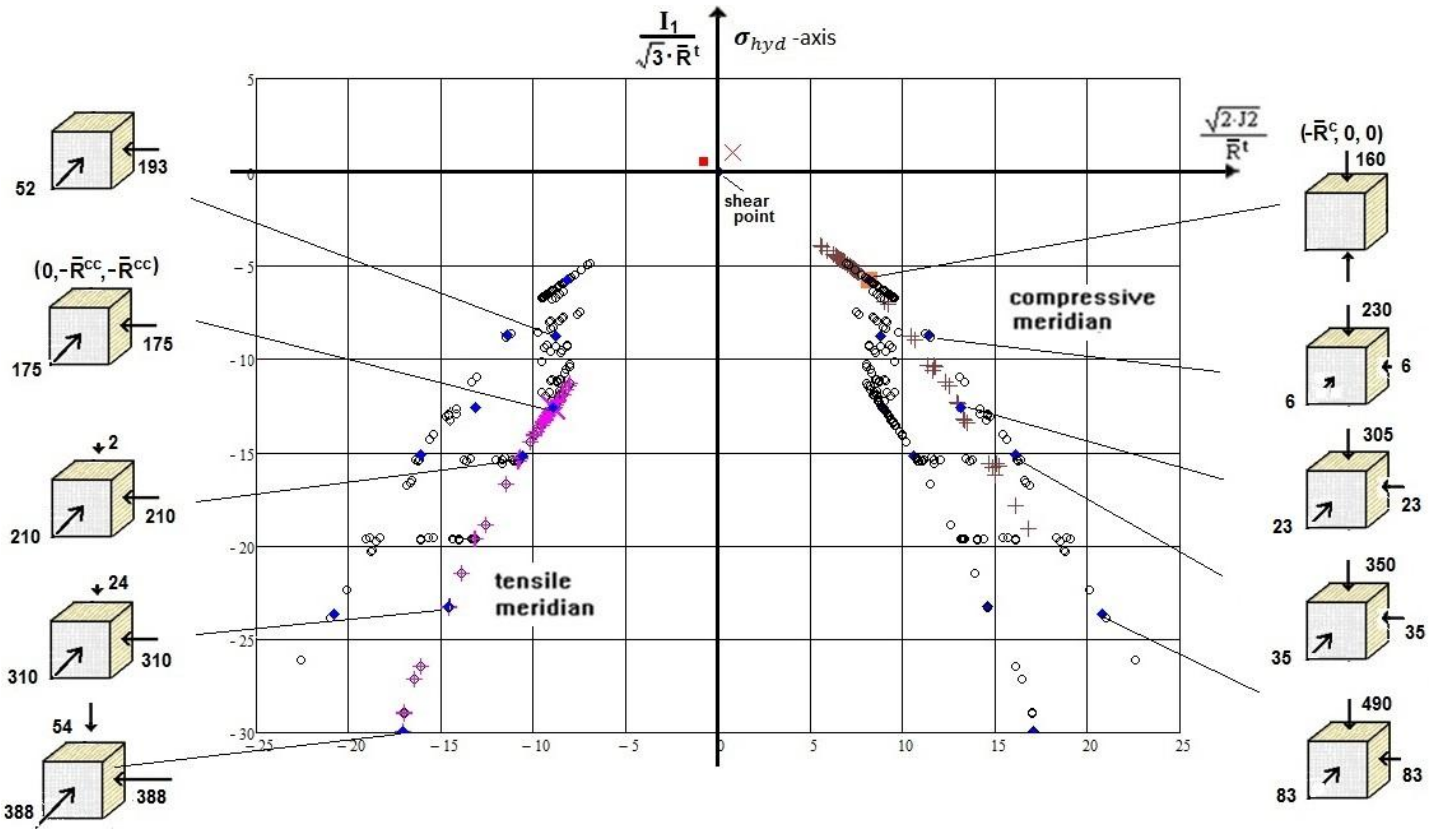

Fig.26-4, UHPC: Compressive and tensile meridian of the fracture body with associated stress states. (left) mirrored TM test points + with CM ones +; (right) all 3D test points are marked by **o** *(hoop ring), visualizing to be located at different meridians ϑ.*

Fig.26-5 displays the mapping quality in the principal stress plane. For comparison the elliptical curve, as the bias cross-section of a cylinder is included. The figure indicates that there is no Mises cylinder given, 120°- rotational symmetry acts.

Fig.26-6 (left) displays the mapping of the TM and the CM data course on the cross section of the fracture body in the traditional Haigh-Lode-Westergaard coordinates.
Fig.26-6 (right) depicts the mapping of the TM data set in a diagram using the 'rock mechanics coordinates' (σ_I, σ_{III}) for TM and $(2\sigma_I, \sigma_{III})$ for CM. How the effortful programming has been performed is compiled in *Table 26-4*. Unfortunately Mathcad did not compute the CM curve. The 'Mohr-Coulomb (M-C) Criterion', using the calculated UHPC-parameters, produces a straight line.
The author could not find any explanation for this unacceptable mapping.
According to the 180°-material symmetry the TM curve could be mirrored from the CM curve by switching from ϑ^{CM} to ϑ^{TM}.

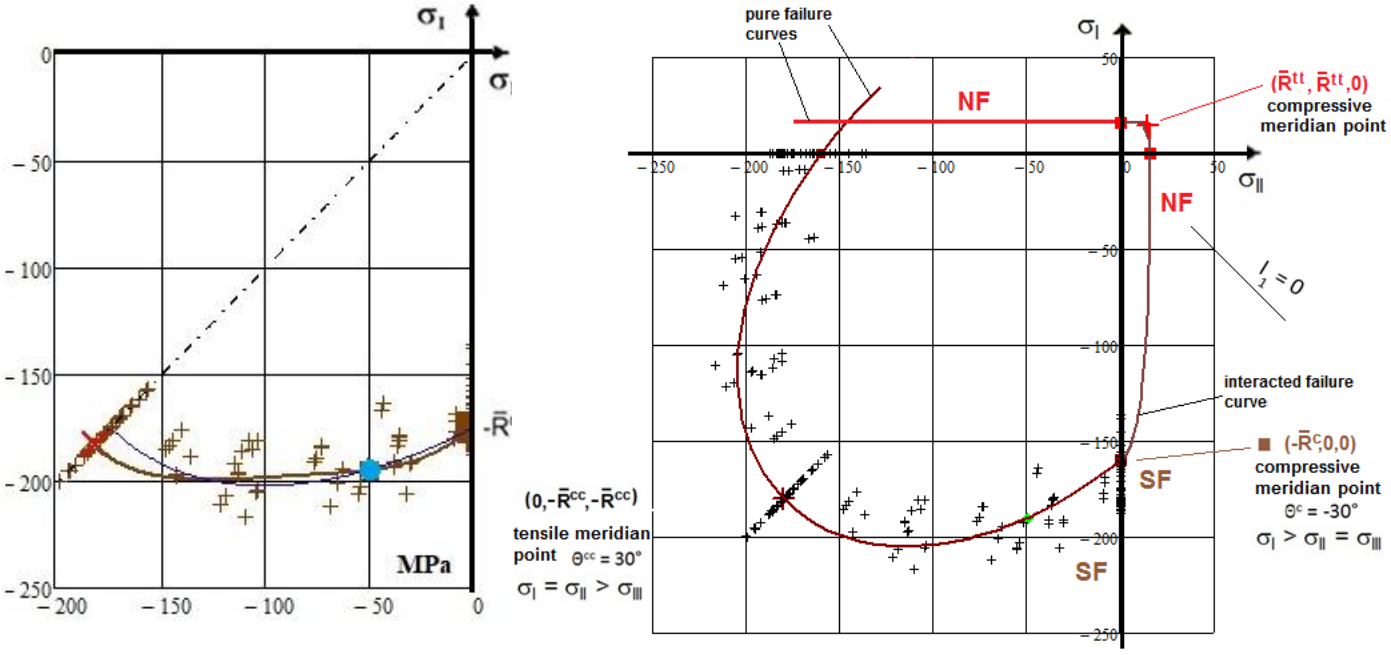

Fig.26-5, UHPC:
(left) Mapping the course of 2D test data in the principal stress plane. The blue fix point serves for friction quantification, mapping course of test data in the SF-domain only (normalization by R^c) *considering the alternating Lode angle* ϑ
(right) Full principal stress plane view, mapping interaction NF with SF in their transition zone (normalization by R^t).

***LL**:*
* *Reliable mapping requires an approach which shall be physically-based and 'practical'. Such an approach should equally well map (1) the course of test data fixing the 3D fracture body, (2) the course of test data in the Principal Stress plane (bias 2D cross-section of the 3D fracture body), and (3) of the test data course along the two 3D-test meridians TM and CM.*
In this context: Engineering mapping has basically to capture physics, must be simple and understandable and shall use measurable parameters. Therefore, concerning all part figures 2D and 3D, these show that SFC-models applied for mapping can be good compromises, only. All theoretical approaches have their applicability limits and the very difficult 3D-testing as well
* *Fracture initiation in solid mechanics is given, if the multi-stress state vector touches the surface of the fracture body which represents the surface of all failure 1D-, 2D- and 3D-failure stress vectors. The fracture body surface is defined by a material stressing effort Eff = 100% = 1.*

* *A display using a confining stress (TM: $\sigma_{II}= \sigma_{III}$, CM: $\sigma_{I}= \sigma_{II}$) as coordinate leads to another mapping figure than the Haigh-Lode-Westergaard coordinates give.*
* *Using just TM or just CM test data cannot result in a reliable physical fracture body.*
* *Of course, general 3D-failure stress states may not lie on TM (30°) or CM (-30°) but on another Lode angle around the hoop.*
* *The fracture planes of TM and CM are different.*
* *Both, the different course of the test data points compared to the also incorporated ellipse in the principal stress plane and the difference of the TM and the CM-curve document the inherent 120°-rotational symmetry of isotropic materials.(360°/3= 120° is given, because all 3 principal stresses are of equal mechanical importance, see Fig.14-9.*

* *The fracture body of a dense isotropic material has an open bottom fracture surface!*

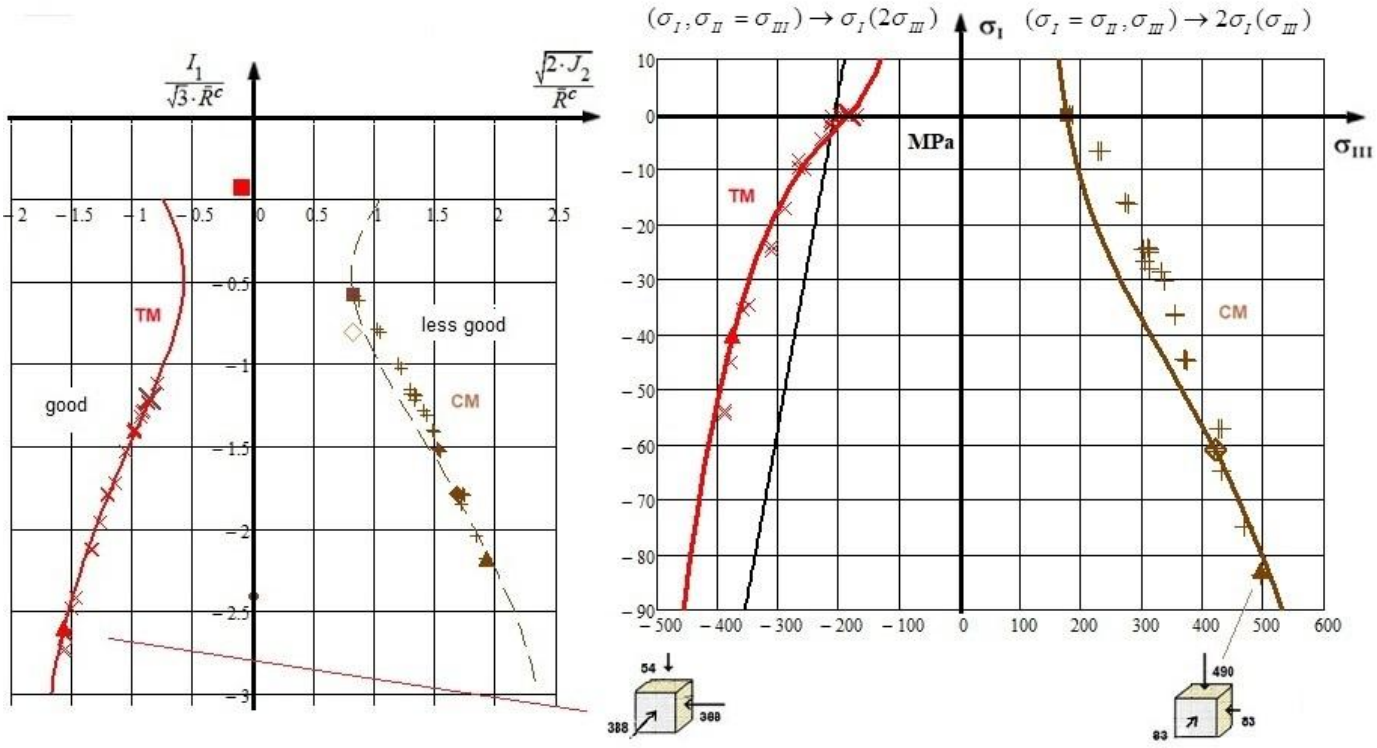

Fig. 26-6, UHPC: (left) mapping display of the two test data sets in Haigh-Lode-Westergaard coordinates. (right) Display using confining stress coordinates.

Eventually, *Table 26-4* presents the determination of the 5 UHPC model parameters.

Table 26-4,UHPC: Determiantion of the SFC model parameters

$$F\tau = \frac{c1 \cdot 6J2 \cdot \Theta\tau}{2Rc^2} + c2 \cdot \frac{I1}{Rc} + c3 \cdot \left(\frac{I1}{Rc}\right)^2 + c4 \cdot \left(\frac{I1}{Rc}\right)^3 = 1$$

$$I1 = \sigma I + \sigma II + \sigma III \qquad J2 = \frac{(\sigma I - \sigma II)^2 + (\sigma II - \sigma III)^2 + (\sigma III - \sigma I)^2}{6}$$

$$J3 = \frac{(2 \cdot \sigma I - \sigma II - \sigma III) \cdot (2 \cdot \sigma II - \sigma I - \sigma III) \cdot (2\sigma III - \sigma I - \sigma II)}{27}$$

$$\Theta\tau = \sqrt[3]{1 + d\tau \cdot 1.5 \cdot 3^{0.5} \cdot J3 \cdot J2^{-1.5}} = \sqrt[3]{1 + d\tau \cdot \sin(3\theta)}$$

$$\Theta\tau TM = \sqrt[3]{1 + d\tau \cdot \sin(3\theta t)} = \sqrt[3]{1 + d\tau} \qquad \Theta\tau CM = \sqrt[3]{1 + d\tau \cdot \sin(3\theta c)} = \sqrt[3]{1 - d\tau}$$

$$\theta = \frac{1}{3} \cdot \operatorname{asin}\left[1.5 \cdot 3^{0.5} \cdot \frac{(2 \cdot \sigma I - \sigma II) \cdot (2 \cdot \sigma II - \sigma I) \cdot (-\sigma II - \sigma I)}{27} \cdot \left(\frac{2 \cdot \sigma I^2 - 2 \cdot \sigma I \cdot \sigma II + 2 \cdot \sigma II^2}{6}\right)^{-1.5}\right]$$

Vorgabe $c1 := 2$

$$c1 \cdot \frac{3 \cdot J2c \cdot \sqrt[3]{1 - 1 \cdot d\tau}}{Rc^2} + c2 \cdot \frac{I1c}{Rc} + c3 \cdot \left(\frac{I1c}{Rc}\right)^2 + c4 \cdot \left(\frac{I1c}{Rc}\right)^3 = 1$$

$$c1 \cdot \frac{3 \cdot J2cc \cdot \sqrt[3]{1 + 1 \cdot d\tau}}{Rc^2} + c2 \cdot \frac{I1cc}{Rc} + c3 \cdot \left(\frac{I1cc}{Rc}\right)^2 + c4 \cdot \left(\frac{I1cc}{Rc}\right)^3 = 1$$

$$c1 \cdot \frac{3 \cdot J2f \cdot \sqrt[3]{1 + 1 \cdot d\tau \cdot \sin(3\theta f)}}{Rc^2} + c2 \cdot \frac{I1f}{Rc} + c3 \cdot \left(\frac{I1f}{Rc}\right)^2 + c4 \cdot \left(\frac{I1f}{Rc}\right)^3 = 1$$

$$c1 \cdot 3 \frac{J2vc1}{Rc^2} \cdot \sqrt[3]{1 - 1 \cdot d\tau} + c2 \cdot \frac{I1vc1}{Rc} + c3 \cdot \left(\frac{I1vc1}{Rc}\right)^2 + c4 \cdot \left(\frac{I1vc1}{Rc}\right)^3 = 1$$

$$c1 \cdot 3 \frac{J2v}{Rc^2} \cdot \sqrt[3]{1 + 1 \cdot d\tau} + c2 \cdot \frac{I1v}{Rc} + c3 \cdot \left(\frac{I1v}{Rc}\right)^2 + c4 \cdot \left(\frac{I1v}{Rc}\right)^3 = 1$$

$A\tau := \text{Suchen}(c1, d\tau, c2, c3, c4)$

Table 26-5 follows with the derivation of the mapping curves in confining stress coordinates from the model parameters for the full UHPV fracture body.

Table 26-5: Relationships to derive mapping with the confining stress coordinates

TM **Transfer to confing stress coordinates** **CM**

$\sigma II = \sigma III$ $\quad J2 = \frac{(\sigma I - \sigma II)^2 + (\sigma II - \sigma III)^2 + (\sigma III - \sigma I)^2}{6}$ $\quad \sigma II = \sigma I$

$(\sigma It - \sigma IIt)^2 + (0)^2 + (\sigma IIIt - \sigma It)^2$ same function $0^2 + (\sigma IIc - \sigma IIIc)^2 + (\sigma IIIc - \sigma Ic)^2$

$J2 = \frac{Rc^2 \cdot x^2}{2}$ $\quad J2 := \frac{\left[(\sigma I - \sigma III)^2 + (\sigma III - \sigma I)^2\right]}{6}$ for TM and CM equal !

$I1t = \sqrt{3} \cdot Rc \cdot yt$ $\quad x^2 = \frac{\left[(\sigma I - \sigma III)^2 + (\sigma III - \sigma I)^2\right]}{3 \cdot Rc^2}$

$I1 = \sigma I + \sigma II + \sigma III$ $\quad yt = \frac{I1t}{\sqrt{3} \cdot Rc} = \frac{\sigma It + 2\sigma IIIt}{\sqrt{3} \cdot Rc}$ $\quad \sigma IIIt = \frac{\sqrt{3} \cdot Rc \cdot yt}{2} - \frac{\sigma It}{2}$ $\quad yc = \frac{\sigma Ic + 2\sigma IIIc}{\sqrt{3} \cdot Rc}$

$$xTM = \sqrt{\frac{\left[\sigma It - \left(\frac{\sqrt{3} \cdot Rc \cdot y}{2} - \frac{\sigma It}{2}\right)\right]^2 + \left(\frac{\sqrt{3} \cdot Rc \cdot y}{2} - \frac{\sigma It}{2} - \sigma It\right)^2}{3 \cdot Rc^2}} = \sqrt{\frac{\frac{1}{2} \cdot \left(3 \cdot \sigma It - \sqrt{3} \cdot Rc \cdot y\right)^2}{3 \cdot Rc^2}}$$

$$xCM = \sqrt{\frac{\left[\sigma Ic - \left(\sqrt{3} \cdot Rc \cdot y - 2 \cdot \sigma Ic\right)\right]^2 + \left(\sqrt{3} \cdot Rc \cdot y - 2 \cdot \sigma Ic - \frac{\sigma Ic}{2} - \sigma Ic\right)^2}{3 \cdot Rc^2}} = \sqrt{\frac{2 \cdot \left(3 \cdot \sigma Ic - \sqrt{3} \cdot Rc \cdot y\right)^2}{3 \cdot Rc^2}}$$

Values for x are given by inserting the y-coordinate into the SFC

$j := 0, 1 .. 40$ $\quad y_j := \frac{-j}{10} - 1$ y runs negative

$$xTM_j = \sqrt{\left[-\frac{2 \cdot \left[c2 \cdot Rc^2 \cdot I1_j - Rc^3 + c3 \cdot Rc \cdot \left(I1_j\right)^2 + c4 \cdot \left(I1_j\right)^3\right]}{3 \cdot Rc^3 \cdot c1 \cdot \Theta\tau TM}\right]} \quad xCM_j = \sqrt{\left[-\frac{2 \cdot \left[c2 \cdot Rc^2 \cdot I1_j - Rc^3 + c3 \cdot Rc \cdot \left(I1_j\right)^2 + c4 \cdot \left(I1_j\right)^3\right]}{3 \cdot Rc^3 \cdot c1 \cdot \Theta\tau CM}\right]}$$

Finally the y-value is inserted into the confing stress version of x xTM, xCM are known

Vorgabe $\sigma It := -100$

$$xTM = \sqrt{\frac{\left[\sigma It - \left(\frac{\sqrt{3} \cdot Rc \cdot y}{2} - \frac{\sigma It}{2}\right)\right]^2 + \left(\frac{\sqrt{3} \cdot Rc \cdot y}{2} - \frac{\sigma It}{2} - \sigma It\right)^2}{3 \cdot Rc^2}}$$

$V(xTM, y) := Suchen(\sigma It)$ $\quad \sigma It_j := V\left(xTM_j, y_j\right)$ $\quad \sigma IIIt_j := \frac{\sqrt{3} \cdot Rc \cdot y_j}{2} - \frac{\sigma It_j}{2}$

Mathcad did not compute σIc_j however the formula can be simplified and σI extracted

$\sigma It_j := \frac{\sqrt{6} \cdot Rc \cdot xTM_j}{3} + \frac{\sqrt{3} \cdot Rc \cdot y_j}{3}$ $\quad \sigma Ic_j := \frac{\sqrt{3} \cdot Rc \cdot y_j}{3} + \frac{\sqrt{2} \cdot \sqrt{3} \cdot Rc \cdot xCM_j}{6}$

$\sigma IIIt_j := \frac{\sqrt{3} \cdot Rc \cdot y_j}{2} - \frac{\sigma It_j}{2}$ $\quad \sigma IIIc_j := \sqrt{3} \cdot Rc \cdot y_j - 2 \cdot \sigma Ic_j$

*25.3 **Rock Material***, example Sandstone

As for concrete the properties for Underground Rock Failure Stress Analysis are also provided by tests on the tensile and the compressive meridian.

Tensile domain:

Also in rock materials in the vicinity of excavations and boreholes tensile stresses will occur. Further, an undesirable brittle sudden failure is to prevent when a bore-hole is drilled. Therefore, a tensile strength proof requires a tensile strength $\bar{R}^t$ for the distinct rock material.

An estimation for the tensile strength value delivers the Brazilian splitting test (*indirect* tensile strength test) because a classical tensile test specimen is merely to obtain. A solid cylinder or disk (short cylinder) test specimens is used for the initially crack-free (intact) material, see *Fig.26-7.* The evaluation is performed via the formula $f_{sp} = \bar{R}^t = 2 \cdot q \,/(\pi \cdot d \cdot \lambda)$, from [*The constructor.org*].

Note: This 'indirect' measurement caused researchers to predict a value by using a Mohr-Coulomb-based SFC but the determined value must be wrong. In this context the author fully supports Mingqing You [*You15*] that a tensile strength R^t is a separate parameter and cannot be estimated by models working in the tensile-compressive transition zone. A real value for $\bar{R}^t$ is only to obtain by a uniaxial tensile stress test $\{\sigma\} = (\sigma^t_{ax} = F^t/A,\ 0,\ 0)^T$

Compressive domain:

Usual test series for concrete material (*see the concrete applications before)* are most often performed along CM and not so often along TM. For the general demonstration of the strength capacity, however, the full fracture failure body is required because all mixed 3D-compressive stress states are principally possible and their failure stress vectors determine the surface of the fracture body.

In rock mechanics the stress situation seems to be normally just linked to stress states along the compressive meridian. This explains why no bi-axial strength $\bar{R}^{cc}$ is provided in rock literature an entity that enables to describe the 120°-symmetry. Mapping just the course of test data along a meridian simplifies the task: Just the functional description of the test meridian remains of interest.

A stress state in a material, formulated in Mohr's *mathematical* stresses, reads

$\{\sigma\} = (\sigma_I,\ \sigma_{II},\ \sigma_{III})^T$ with σ_I becoming the smallest failure stress (most positive)

$\sigma_I > \sigma_{II} > \sigma_{III}$ mathematically and σ_{III} the largest compressive failure stress (most negative).

Tensile stresses must be signed positive in this context, otherwise confusion becomes extreme!

For the tensile meridian follows $\{\sigma\} = (\sigma_I,\ \sigma_{II},\ \sigma_{III} = \sigma_{II})^T$ with $\sigma_I = \sigma^t_{ax} - p_{hyd}$

and the compressive meridian $\{\sigma\} = (\sigma_I = \sigma_{II},\ \sigma_{II},\ \sigma_{III})^T$ with $\sigma_{III} = \sigma^c_{ax} - p_{hyd}$.

TM captures $\bar{R}^{cc}$ (and $\bar{R}^t$, in the domain of the Normal Fracture mode) and CM captures $\bar{R}^c$ (and principally also $\bar{R}^{tt}$ in the domain of the Normal Fracture mode).

In rock mechanics, being one part of civil engineering, hydrostatic pressure is used, when testing concrete and UD material, but is to replace by the term Confining Pressure CP. This makes to introduce some definitions of rock mechanics terms: In construction, tensile stress is usually still negative, but not always. This makes literature interpretations difficult!

- Multi-axial rock compressive strength capacity [*You15*]
  (the stress-sketch in Figure 1 of [Lan19] must be corrected. It does not fit to the provided failure stress states. In Fig.26-7 this is corrected)
  $\sigma_{III} \equiv \sigma_S \equiv \sigma_1$ termed here min or principal stress
- 1D uniaxial strengths: UTS $= \bar{R}^t$, UCS $= \bar{R}^c$

Unfortunately the author found different meanings: In engineering design dimensioning UTS means Ultimate Tensile Strength and not Uniaxial Tensile Strength and UCS ultimate compressive strength *(still also applied in 'geo engineer'! Why is it not generally used in rock mechanics?)* and not for instance Unconfirmed Compressive Strength [*Wikipedia*]. UCS stands for the maximum axial compressive stress that a specimen can bear under zero Confining Pressure (*compressive stress*), which means it is nothing else than the usual simple standardized technical compression strength $\bar{R}^c$ in engineering.

- ✓ Confining pressure CP: maximum level of hydrostatic compression applied in a tri-axial compression test of a concrete, a rock material or a neat resin test specimen defined by

  $\{\sigma\}$ = ($\sigma_{ax}{}^t$ - CP , -CP, -CP) or with $\sigma_{ax}{}^c$ (tensile meridian)

  $\{\sigma\}$ = ($\sigma_{ax}{}^c$ - CP , -CP,, -CP) (*induced by test rig brushes in case of concrete*)

- ✓ Confining lithostatic pressure: CP = p_{hyd} + overlying weight.

The author would like to conclude: *Using usual mathematical stresses it reads*

- Sealed, polished dog-bone test specimens deliver the failure stress points ($-\bar{R}^{ccc}$,$-\bar{R}^{ccc}$,$-\bar{R}^{ccc}$) no pore pressure, ($-\bar{R}^{c}$, 0, 0) , ($\bar{R}^{t}$, 0, 0) and further multi-axial compressive failure stresses on the compressive meridian.
- A bi-axial compressive failure stress ($-\bar{R}^{cc}$,-, 0) is obtainable by the dog-bone test specimen for $\sigma_1 = 0$ or $\sigma_{ax}{}^t = -CP$. However, the author did not find one single bi-axial strength value $\bar{R}^{cc}$ in the papers he examined! However, the UHPC fracture stress data set, thankfully left by IFM Dresden, brought a statistically good base which should have a similar tendency as rock material
- A bi-axial tensile failure stress ($\bar{R}^{tt}$, $\bar{R}^{tt}$, 0) can be obtained by cube test specimens prepared by a good gluing in order to load the needed bi-axial tensile stresses.

Test procedure: The confining pressure CP is achieved and then kept constant during the test. The axial stress σ_1 is increased at a certain rate until the test specimen fails at $_{max}\sigma_1$. It is to consider whether the porosity of the rock or the soil material and the moisture saturation plays a role.
Fig.26-7 presents fracture pictures of the investigated Berea sandstone. Essential is that the fracture angle increases with CP.

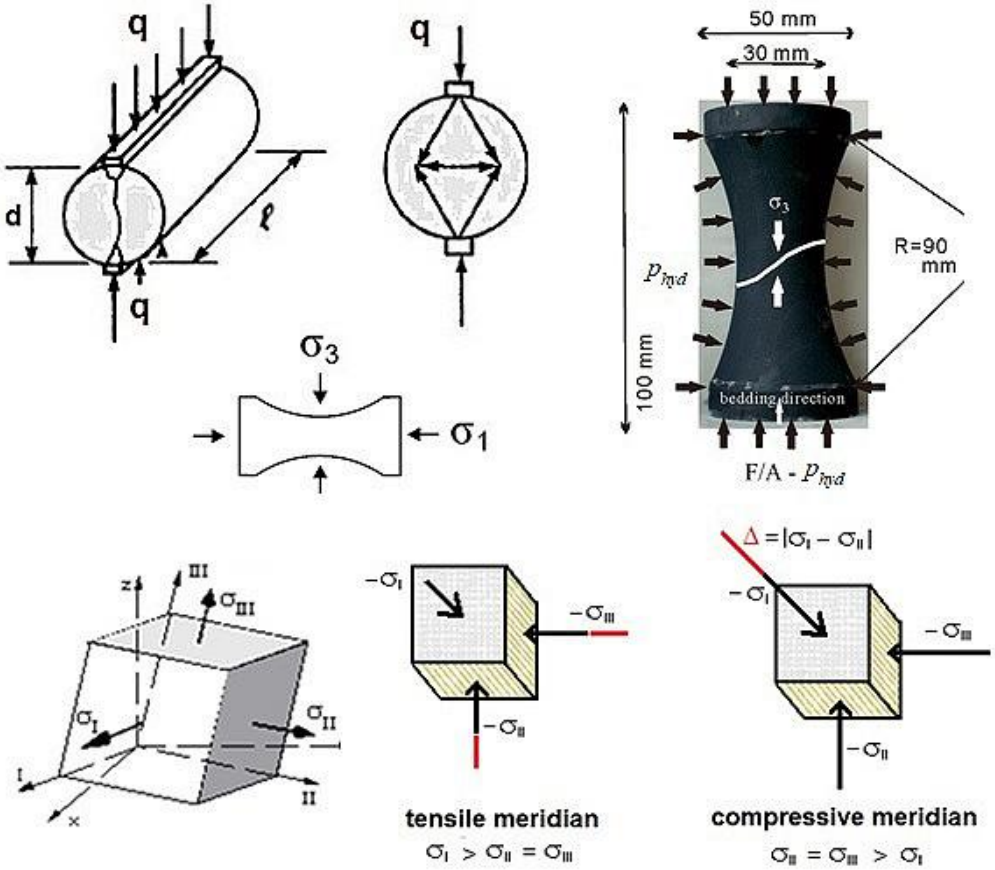

Fig. 26-7: Brazilian cylinder or disk (short length) for an indirect estimation of $\bar{R}^t$ and dog-bone (sealed, highest preparation effort, grinding from solid block with axial bedding layers) test specimen for direct measurement of tri-axial fracture stress states along compressive meridian including the tension-compression domain.
(Δ depicts the differential stress entity causing shear stress with shear deformation)

Similarly to other brittle materials the task always is the full (onset-of-fracture) body surface capturing NF and SF and not by SF just $I_1 < 0$ and thereby not regarding the intrinsic 120°-rotational symmetry. The TM and CM test data points are two oppositely located cross-sections of the body. The classical type of visualization is to use the Haigh-Lode-Westergaard coordinates count equally in all directions. Visualization by using a confining stress cannot lead to the same mapping curve (see Fig. 26.6).

LL:

The interpretation of the concrete-diagrams above leads to the following results for rock materials:

- *Using just TM or just CM test data incorporates a bottleneck concerning the achievement of a reliable physical fracture body*
- *The use of the geo-Mohr-Coulomb Criterion leads to a straight mapping of the course of test data along the tensile meridian. The model of the author captures the curved course*
- *Engineers in other disciplines become pretty stressed because we civil engineers unfortunately use construction design tools which still call tensile stresses negative stresses. This completely disturbs the logic of the well-known 'civil engineer' A. Mohr in context with his use of mathematical stresses!*

Fig.26-8, Sandstone: Fracture pictures of Berea sandstone from [Lan19].

Personal experience

A dangerous cohesive shear strength with an associated critical sliding angle lead to a land slide at the West-East Main road of Bhutan.
A video clip taken by me would show how huge rocks were 'travelling' down.

This dramatic situation, depicted in the figure above, led to my most dangerous car trip, on gravel roads, along gorges up to 1000 m deep, from the Central Himalaya down to the plain and back up into the high mountains. AND, there was the same driver who had to drive from 7 until 23 o'clock on these roads, unbelievable.

27 UD-Strength Failure criteria: Which one should I take?

***Aim**: Assisting the user not to follow the FE Manual recommendation:"Take the worst result of all".*

In the future, we will be forced to compute 3D-based reserve factors in static component Design Verification. The 2D-based Classical Laminate Theory for unidirectional fiber-reinforced matrices is not sufficient for this. For these reasons, the author has tried to compare those SFCs that were 'contributing' to the World Wide Failure Exercises (WWFE) for UD materials, namely Tsai-Wu, Hashin, Puck and Cuntze. The comparison carried out (*generally too little test data is available*) looks at the necessary input, shows the received failure envelopes for three 2D stress combinations and tries to evaluate the results, so that FE Manual recommendations "*Take the worst result of all*" is not to be followed anymore!

Regarding the chapters before, the SFCs of Hashin and Tsai-Wu will be presented, only, and some missing things of Puck's SFC.

27.1 SFC Hashin

* Hypothesis 2, valid for Cuntze's FMC-bases SFC-formulations:

"*For UD-material the SFCs should be invariant under any rotation around the fiber direction*."

Hashin with the Hypothesis 2 also proposed an invariant-based global quadratic approach with two different stress invariants:

$$I_1=\sigma_1,\ I_2=\sigma_2+\sigma_3,\ I_3={\tau_{31}}^2+{\tau_{21}}^2,\ I_4={\tau_{23}}^2-\sigma_2\cdot\sigma_3,\ I_5=4\tau_{23}\tau_{31}\tau_{21}-\sigma_2\cdot{\tau_{31}}^2-\sigma_3\cdot{\tau_{21}}^2).$$

Table 27-1 compiles the four SFCs of Zvi Hashin.

Table 27-1: Four SFCs, for FF1, FF2, IFF1 and IFF2

$\{\sigma\}=(\sigma_1,\sigma_2,\sigma_3,\tau_{23},\tau_{31},\tau_{21})^{\mathrm{T}}$, $\left\{\bar{R}\right\}=(\bar{R}_{\parallel}^{t},\bar{R}_{\parallel}^{c},\bar{R}_{\perp}^{t},\bar{R}_{\perp}^{c},\bar{R}_{\perp\parallel};\ \bar{R}_{23})^{\mathrm{T}}$; 6 strengths, principally

Interaction of the 4 modes necessary.

Hypothesis 1: $F\left(\left\{\sigma^{A}\right\},\left\{\bar{R}^{A}\right\},\theta_{\mathrm{fp}}\right)=1$, Puck's way

Hypothesis 2: $F\left(\{\sigma\},\left\{\bar{R}\right\}\right)=1$, Cuntze's way, *below*

FF1, $\sigma_1>0$: $\left(\frac{\sigma_1}{\bar{R}_{\mathrm{II}}^{t}}\right)^2+\frac{\tau_{31}^2+\tau_{21}^2}{{\bar{R}_{\perp\parallel}}^2}$; FF2, $\sigma_1<0$: $\left(\frac{-\sigma_1}{\bar{R}_{\mathrm{II}}^{c}}\right)^2=1,$

IFF1, $\sigma_2+\sigma_3>0$: $\frac{\left(\sigma_2+\sigma_3\right)^2}{\bar{R}_{\perp}^{t}}+\frac{\left({\tau_{23}}^2-\sigma_2\cdot\sigma_3\right)}{{\bar{R}_{23}}^2}+\frac{\left(\tau_{31}^2+\tau_{21}^2\right)}{{\bar{R}_{\perp\parallel}}^2}=1,$

IFF2, $\sigma_2+\sigma_3<0$: $\left(\frac{\bar{R}_{\perp}^{c\,2}}{4\cdot{\bar{R}_{23}}^2}-1\right)\cdot\frac{\left(\sigma_2+\sigma_3\right)}{\bar{R}_{\perp}^{c}}+\frac{\left(\sigma_2+\sigma_3\right)^2}{4\cdot{\bar{R}_{23}}^2}+\frac{\left({\tau_{23}}^2-\sigma_2\cdot\sigma_3\right)}{{\bar{R}_{23}}^2}+\frac{\left(\tau_{31}^2+\tau_{21}^2\right)}{{\bar{R}_{\perp\parallel}}^2}=1,$

Interlaminar failure: $\sigma_3>0$: $\left(\frac{\sigma_3}{R_3^{t}}\right)^2=1;$ $\sigma_3<0$: $\left(\frac{-\sigma_3}{R_3^{c}}\right)^2=1$.

* Hypothesis 1, valid for Puck's Action Plane IFF formulation:

"In the event that a failure plane under a distinct fracture angle can be identified, the failure is produced by the normal and shear stresses on that plane".

Hashin proposed this modified Mohr-Coulomb IFF approach but did not pursue this idea due to numerical difficulties (*A. Puck succeeded on this way*).

Question: What about the determination of $\bar{R}_{23} \neq \bar{R}_{23}^{\tau}$? *See Technical Terms, please.*

27.2 SFC Tsai-Wu, global SFC

A general anisotropic tensor polynomial expression of Zakharov and Goldenblat-Kopnov with the parameters F_i, F_{ij} as strength model parameters was the basis of the Tsai-Wu SFC $\sum_{i=1}^{6}(F_i \cdot \sigma_i)+\sum_{j=1}^{6}\sum_{i=1}^{6}(F_{ij} \cdot \sigma_i \cdot \sigma_j)=1$. From this tensor formulation, Tsai-Wu used the linear and quadratic terms, see *Table 27-2*:

Table 27-2: 3D SFCs of Tsai-Wu

$\{\sigma\} = (\sigma_1, \sigma_2, \sigma_3, \tau_{23}, \tau_{31}, \tau_{21})^T$, $\{\bar{R}\} = (\bar{R}_{\parallel}^t, \bar{R}_{\parallel}^c, \bar{R}_{\perp}^t, \bar{R}_{\perp}^c, \bar{R}_{\perp\parallel}; \bar{R}_{23})^T$, 6 strengths

$F(\{\sigma\}, \{\bar{R}\}) = 1$. *The* interaction *is global SFC – inert*

$F_i \cdot \sigma_i + F_{ij} \cdot \sigma_i \cdot \sigma_j = 1$ with (i,j = 1,2..6) or executed

$$F_{11} \cdot \sigma_1^2 + F_1 \cdot \sigma_1 + 2F_{12} \cdot \sigma_1 \cdot \sigma_2 + 2F_{13} \cdot \sigma_1 \cdot \sigma_3 + F_{22} \cdot \sigma_2^2 + F_2 \cdot \sigma_2 +$$
$$+ 2F_{23} \cdot \sigma_2 \cdot \sigma_3 + F_{33} \cdot \sigma_3^2 + F_{33} \cdot \sigma_3^2 + F_3 \cdot \sigma_3 + F_{44} \cdot \tau_{23}^2 + F_{55} \cdot \tau_{13}^2 + F_{66} \cdot \tau_{12}^2 = 1$$

with the strength model parameters

$$F_1 = 1/\bar{R}_{\parallel}^t - 1/\bar{R}_{\parallel}^c, \quad F_{11} = 1/(\bar{R}_{\parallel}^t \cdot \bar{R}_{\parallel}^c), \quad F_2 = 1/\bar{R}_{\perp}^t - 1/\bar{R}_{\perp}^c, \quad F_{22} = 1/(\bar{R}_{\perp} \cdot \bar{R}_{\perp}^c) = F_{33},$$
$$F_{13} = F_{12}, \quad F_{55} = F_{66} = 1/\bar{R}_{\perp\parallel}^2, \quad 2F_{23} = 2F_{22} - 1/\bar{R}_{23}^2, \quad F_{44} = 2 \cdot (F_{22} + F_{23})$$

and - *in order to avoid an open failure surface* - the so-called interaction term

$F_{12} = \bar{F}_{12} \cdot \sqrt{F_{11} \cdot F_{22}}$ with $-1 \le \bar{F}_{12} \le 1$; usually applied $F_{12} = -0.5$.

Question, again: What about the determination of $\bar{R}_{23}$ and the value for F_{12} for 3D applications?

27.3 SFC Puck

Some history:

**As early as 1969 A. Puck recognized to separate FF from IFF (not Hashin as is sometimes said). Since the mid-eighties Puck from Uni Kassel, Cuntze from MAN and colleagues of the DLR-Braunschweig looked together for an improved IFF-SFC.*

* *H. Schuermann, Uni Darmstadt, found the article [Has80] with the Hashin Hypothesis 1 which Puck could successfully execute. Cuntze recommended to use the matrix formulation to mathematically simpler convince the reader, which was more successful than his excellently written model description.*

* *Beside several dissertation works, Puck's IFF model was further developed in a founded research project 1994. Results were published in VDI Progress Reports Series 5 Vol.506, VDI-Verlag, Düsseldorf, 1997, [VDI97]. The investigations for this book gave valuable results for Puck's book, 1996.*

* *Due to the still highly established Puck IFF model Cuntze invited Puck to put his SFC into the [VDI 2014] German Guideline, Sheet 3, Development of Fibre-Reinforced Plastic Components, Analysis.*

Puck's so-called Action Plane IFF Conditions (1991) base on Mohr-Coulomb and Hashin.

In his interaction approach for the 3 IFF modes Puck interacted the 3 Mohr stresses σ_n , τ_{nt} , τ_{nl} on the IFF fracture plane, see *Fig.27-4*. He uses parabolic or elliptic polynomials to formulate a so-called master fracture body in the (σ_n , τ_{nt} , τ_{nl}) space. Thereby he assumes that a compressive σ_n cannot cause fracture on its action plane and that the stress σ_1 does not have any influence on the angle of the IFF fracture plane. The stresses on the fracture plane are decisive for fracture: A tensile stress σ_n supports the fracture, while in contrast a compressive stress makes the material 'stronger'. In other words: A compressive σ_n impedes IFF which is caused by the action plane shear stresses τ_{nt} and τ_{n1}, or – in other words - cannot cause fracture on its action plane. Fracture-responsible are only those stresses which act on a common action plane.

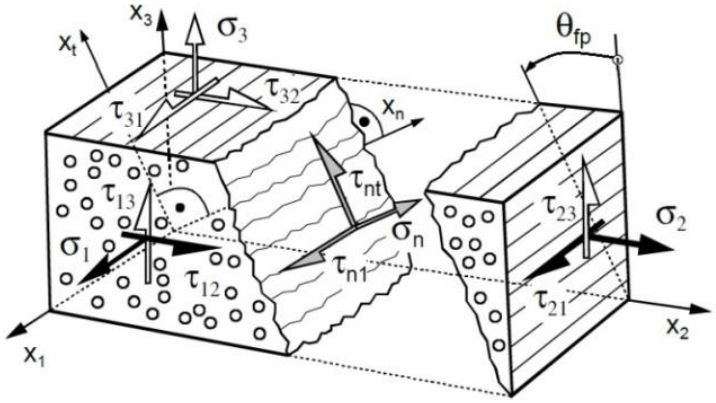

Fig.27-4, UD-composite element: Lamina and action plane stresses at an inclined failure angle θ_{fp} (from [Lut05, SAMPE])

Fig.27-5 presents Puck's 3 IFF modes: mode A (= IFF1), mode B (≡ IFF3), mode C (≡ IFF2. The modes A and B lead to transversal fracture planes with $\theta_{fp} = 0$, whereas in mode C inclined planes occur $O° < \theta_{fp} < 55°$ (for CFRP). The determination of the unknown IFF action plane angle θ_{fp} is

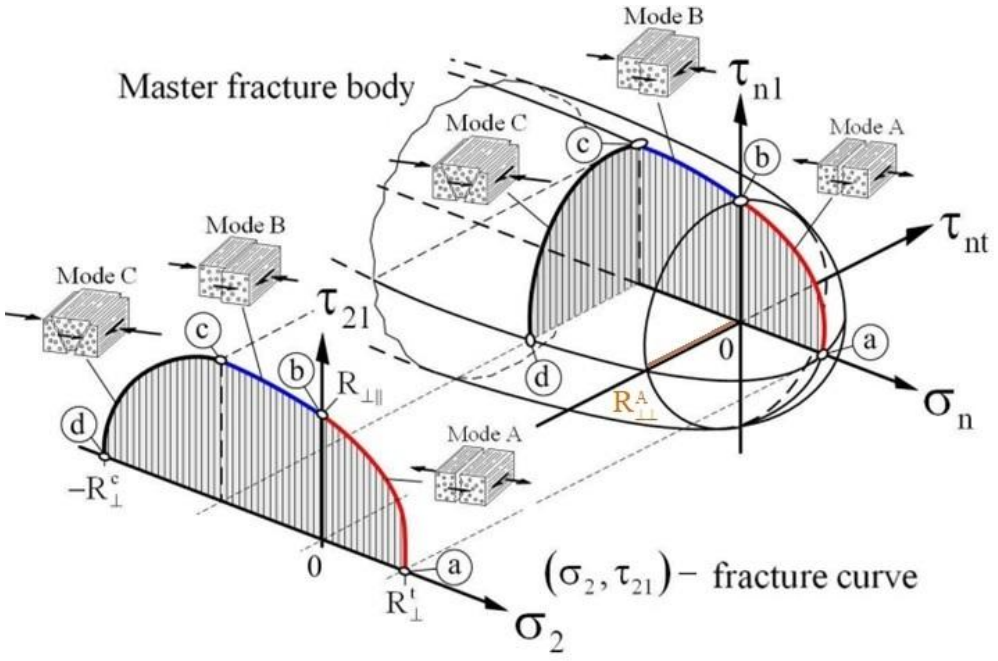

Fig.27-5: Master fracture body with Puck's IFF modes and action plane stresses (σn, τnt, τn1). *(left) Lamina stresses and main IFF cross section of the fracture body in lamina stresses* (σ_2, τ_{21}) *[courtesy H. Schürmann]*

performed by a search process in the domain -90° < θ_{fp} < 90. For the in-plane stress state $\tau_{21}(\sigma_2)$ which is dominant in many structural components, Puck found an analytic solution for the angle of the fracture plane [*Puc02*]: $\cos\theta_{\text{fp}} = \sqrt{\frac{1}{2+2\cdot p^{c}_{\perp\perp}}\cdot\left[\left(\frac{\bar{R}^{A}_{23}}{\bar{R}_{\perp\parallel}}\right)^{2}\cdot\left(\frac{\tau_{21}}{\sigma_2}\right)^{2}+1\right]}$.

In *Table 27-3* Puck's Action Plane Mohr-Coulomb-linked (global) IFF SFCs discriminate 3 IFF domains and are completed by the simple maximum stress modes FF1 and FF2. Two IFF fracture plane resistances (superscript ^{A}) directly are technical strengths.

Table 27-3: SFCs for FF1, FF2, IFF1, IFF2 and IFF3

$\{\sigma\} = (\sigma_1, \sigma_2, \sigma_3, \tau_{23}, \tau_{31}, \tau_{21})^{\mathrm{T}}$, $\{\bar{R}\} = (\bar{R}^{t}_{\parallel}, \bar{R}^{c}_{\parallel}, \bar{R}^{t}_{\perp}, \bar{R}^{c}_{\perp}, \bar{R}_{\perp\parallel};\ \bar{R}^{A}_{23})^{\mathrm{T}}$, 6 strengths, principally

In Mohr's action plane stresses the IFF-SFC reads $F\left(\sigma_n, \tau_n, \bar{R}_{\sigma}, \bar{R}_{\tau}, \theta_{\text{fp}}\right) = 1$,

$F\left(\{\sigma^{A}\}, \{\bar{R}^{A}\}, \theta_{\text{fp}}\right) = 1$ with $\{\bar{R}\} = (\bar{R}^{t}_{\parallel}, \bar{R}^{c}_{\parallel}, \bar{R}^{A}_{\perp} = \bar{R}^{t}_{\perp}, \bar{R}^{A}_{23}, \bar{R}^{A}_{\perp\parallel} = \bar{R}_{\perp\parallel})^{\mathrm{T}}$; *Puck*: $\bar{R}^{A}_{23} \neq \bar{R}_{23}$!

FF1, $\sigma_1 > 0$: $\left(\frac{\sigma_1}{\bar{R}^{\mathrm{t}}_{\mathrm{II}}}\right)^{2}$; FF2, $\sigma_1 < 0$: $\left(\frac{-\sigma_1}{\bar{R}^{\mathrm{c}}_{\parallel}}\right)^{2} = 1$, (maximum stress criteria)

and due to the IFF hypotheses, two different eqations are provided [*Puc* 96, *p.*118]

IFF: $\sigma_n > 0$: $\varepsilon = \left(\frac{\tau_{nt}}{\bar{R}^{A}_{23}}\right)^{2} + \left(\frac{\tau_{n\ell}}{\bar{R}^{A}_{\perp\parallel}}\right)^{2} + \left(\frac{\sigma_n}{\bar{R}^{A}_{\perp}}\right) = 1$, $\tau_n = \sqrt{\tau_{nt}^{\,2} + \tau_{n1}^{\,2}}$

IFF: $\sigma_n < 0$: $\varepsilon = \left(\frac{\tau_{nt}}{\bar{R}^{A}_{23} - p_{\perp\perp}{}^{\mathrm{c}}\cdot\sigma_n}\right)^{2} + \left(\frac{\tau_{n\ell}}{\bar{R}^{A}_{\perp\parallel} - p_{\perp\parallel}{}^{\mathrm{c}}\cdot\sigma_n}\right)^{2} = 1$, [*Puc*96, *p.*143]

$\Rightarrow$ from originally assumed 6 material strengths down to 5 action plane resistancies which capture all 3 sub-modes IFF1, IFF2 and IFF3.

The following transfer relationship is to apply above ($_{fp}$ = failure plane)

$$\begin{Bmatrix}\sigma_n(\theta_{fp})\\ \tau_n(\theta_{fp})\\ \tau_{n\ell}(\theta_{fp})\end{Bmatrix} = \begin{bmatrix} c^2 & s^2 & 2sc & 0 & 0\\ -sc & sc & c^2-s^2 & 0 & 0\\ 0 & 0 & 0 & s & c\end{bmatrix}\cdot\begin{Bmatrix}\sigma_2\\ \sigma_3\\ \tau_{23}\\ \tau_{31}\\ \tau_{21}\end{Bmatrix},\quad c = \cos\theta_{fp} \text{ and } s = \sin\theta_{fp}\ .$$

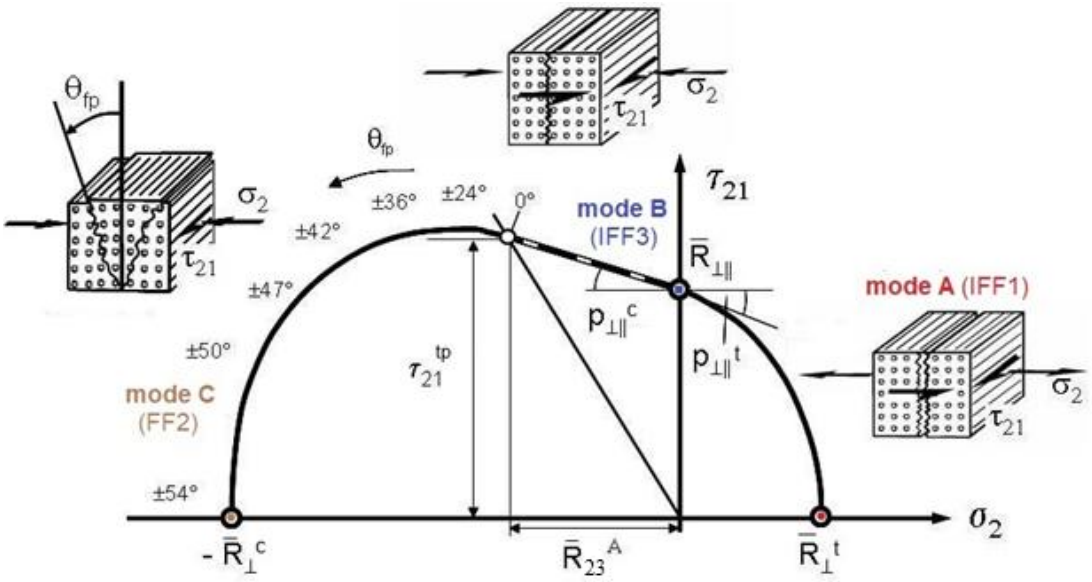

Fig. 27-6: Fracture modes of the (σ_2,τ_{21})-failure envelope; index ^{tp} *marks the touchpoint between mode B and C, [Lut13, Puc96]*

Table 27-4: 2D-IFF [VDI2014]

Mode A (= IFF1) : $\varepsilon = \frac{1}{\bar{R}_{\perp\mathrm{II}}} \cdot \sqrt{\left(\frac{\bar{R}_{\perp\|}}{\bar{R}_{\perp}^{t}} - p_{\perp\|}^{t}\right)^2 \cdot \sigma_2^{\,2} + \tau_{21}^2} + p_{\perp\|}^{t} \cdot \sigma_2;$

Mode B (≅ IFF3) : $\varepsilon = \frac{1}{\bar{R}_{\perp\mathrm{II}}} \cdot \sqrt{p_{\perp\|}^{c\,2} \cdot \sigma_2^{\,2} + \tau_{21}^2} + p_{\perp\|}^{c} \cdot \sigma_2;$

Mode C (≅ IFF2) : $\varepsilon = \frac{\tau_{21}^2}{4 \cdot \left(\bar{R}_{\perp\|} + p_{\perp\|}^{c} \cdot \bar{R}_{23}^{A}\right)^2} \cdot \frac{\bar{R}_{\perp}^{c}}{-\sigma_2} + \frac{-\sigma_2}{\bar{R}_{\perp}^{c}}$

ε is also termed f_E [*Lut*05, *VDI* 2014]

$\tau_{21}^{tp} = \bar{R}_{\perp\mathrm{II}} \cdot \sqrt{1 + 2 \cdot p_{23}^{c}}, \quad \sigma_2^{tp} = -\bar{R}_{23}^{A}, \quad \bar{R}_{23}^{A} = \left[\bar{R}_{\perp\mathrm{II}} \cdot \sqrt{1 + 2 \cdot p_{\perp\mathrm{II}}^{c} \cdot \bar{R}_{\perp}^{c} / \bar{R}_{\perp\mathrm{II}}} - 1\right] / 2 \cdot p_{\perp\|}^{c},$

* The action plane resistance $\bar{R}_{23}^{A}$ depends on the chosen fracture body model such as the parabolic Mohr envelope and not just the linear Mohr approach.

* Assumption on coupling the inclination parameters: $p_{23}^{c} = p_{\perp\|}^{c} \cdot \bar{R}_{23}^{A} / \bar{R}_{\perp\|}.$

R_{23}^{A} is found in the horizontal cross-section of Puck's Master failure body. It is a IFF-Mohr model-linked quantity and consequently a given model strength parameter and not a technical strength. It finally did vanish therefore as a measurable technical strength. Puck's R_{23}^{A} is a model parameter and defined by Puck's Mohr-Model using two strength and the so-called inclination parameters *p*, depicted in Fig.6.

Practically, 5 independent failure activing stresses are left, which would support Cuntze's material symmetry-based 'generic' number of 5 he elaborated for UD materials.

Of course, an interaction of IFF with the two FF modes is also with Puck mandatory in order to capture the combined (joint) failure danger. This procedure is documented in detail in the VDI 2014, sheet 3. One reason to do that is that experiments demonstrate micro-damage activation at the ends of broken filaments. Puck terms this 'weakening of the matrix' and uses a so-called weakening factor. Applying Cuntze's interaction equation *Eff* = 1 this is automatically performed in the foreseen comparison.

27.4 Comparison of the obtained different SFC Failure Envelopes

In consequence of the rare test data sets just **2D**-models of Tsai-Wu, Hashin, Puck and Cuntze could be numerically investigated.

A comparison is only possible if the interaction can be equally performed for each model and the same interaction. This could be realized for the 4 models by a transfer to the single 2D-*Eff*-formulation, example Tsai-Wu:

$$\frac{\sigma_1^2/Eff^2}{\bar{R}_{||}^{\,t}\cdot\bar{R}_{||}^{\,c}}+\frac{\sigma_1}{Eff}\cdot\left(\frac{1}{\bar{R}_{||}^{\,t}}-\frac{1}{\bar{R}_{||}^{\,c}}\right)+\frac{2F_{12}\cdot\sigma_1\cdot\sigma_2/Eff^2}{\sqrt{\bar{R}_{||}^{\,t}\cdot\bar{R}_{||}^{\,c}\cdot\bar{R}_{\perp}^{\,t}\cdot\bar{R}_{\perp}^{\,c}}}+\frac{\sigma_2^2/Eff^2}{\bar{R}_{\perp}^{\,t}\cdot\bar{R}_{\perp}^{\,c}}+\frac{\sigma_2}{Eff}\cdot\left(\frac{1}{\bar{R}_{\perp}^{\,t}}-\frac{1}{\bar{R}_{\perp}^{\,c}}\right)+\frac{\tau_{12}^2/Eff^2}{\bar{R}_{\perp||}}=1$$

The investigation focuses mapping of the curves of test data by SFCs. In these formulations each single strength is an average strength consequently indicated by a bar over.

The following figures present the failure envelopes of investigated three plane stress combinations.

SFC Failure Envelopes

Fig.27-6 visualizes, how the four models map the most interesting cross-section of the UD fracture body, namely $\tau_{21}(\sigma_2)$.

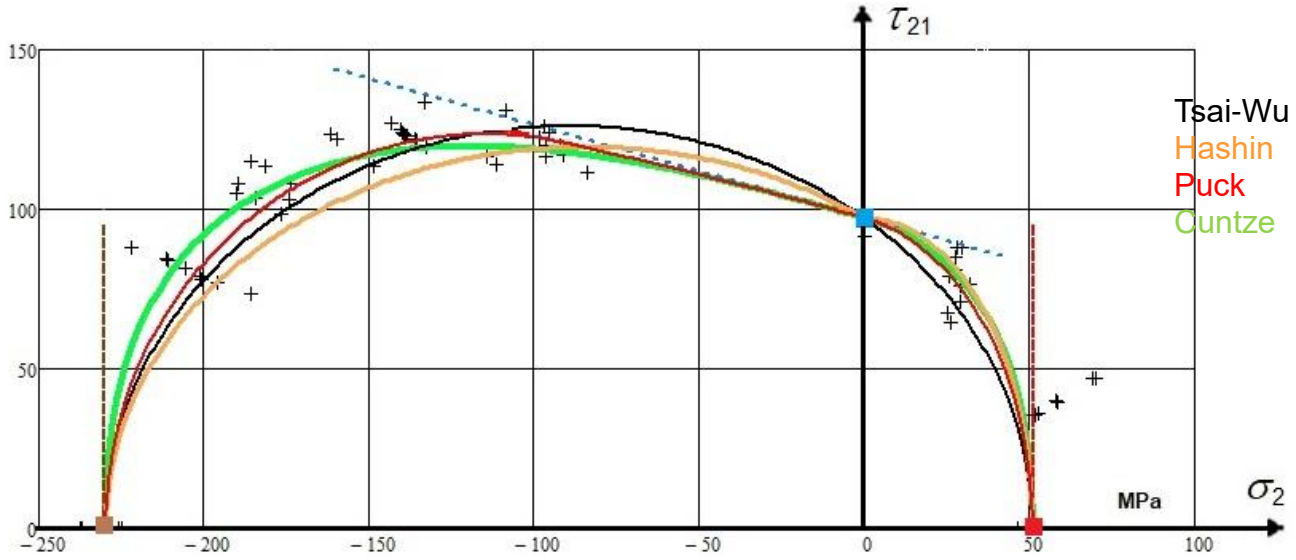

Fig. 27-6: CFRP test results (MAN Technologie research project with A. Puck, IKV Aachen et al.)

$\{\bar{R}\} = (1280,\ 800,\ 51,\ 230,\ 97)^T$ MPa, $\mu_{\perp\parallel} = 0.3$ [*VDI 97*]

Fig.27-7 depicts the failure envelope $\sigma_2(\sigma_1)$, being the WWFE Test Case 3. In this test case below, just the 4 strength values were provided together with the not $R_{\perp}^{c}$ -matching test data of a Russian test data

provider showing a test discrepancy (*passed away, no request possible*) in the fourth quadrant of Fig.27-7. However, the tendency of the two different (*assumed*) test sets can be carefully used for validation. The global Tsai-Wu SFC lies fully outside, which would be of high effect for stability analysis. The test data set in the quadrant III was provided by M.. Knops, IKV Aachen, [*Kno03*].
Mapping tells, that modal modelling is the better choice.

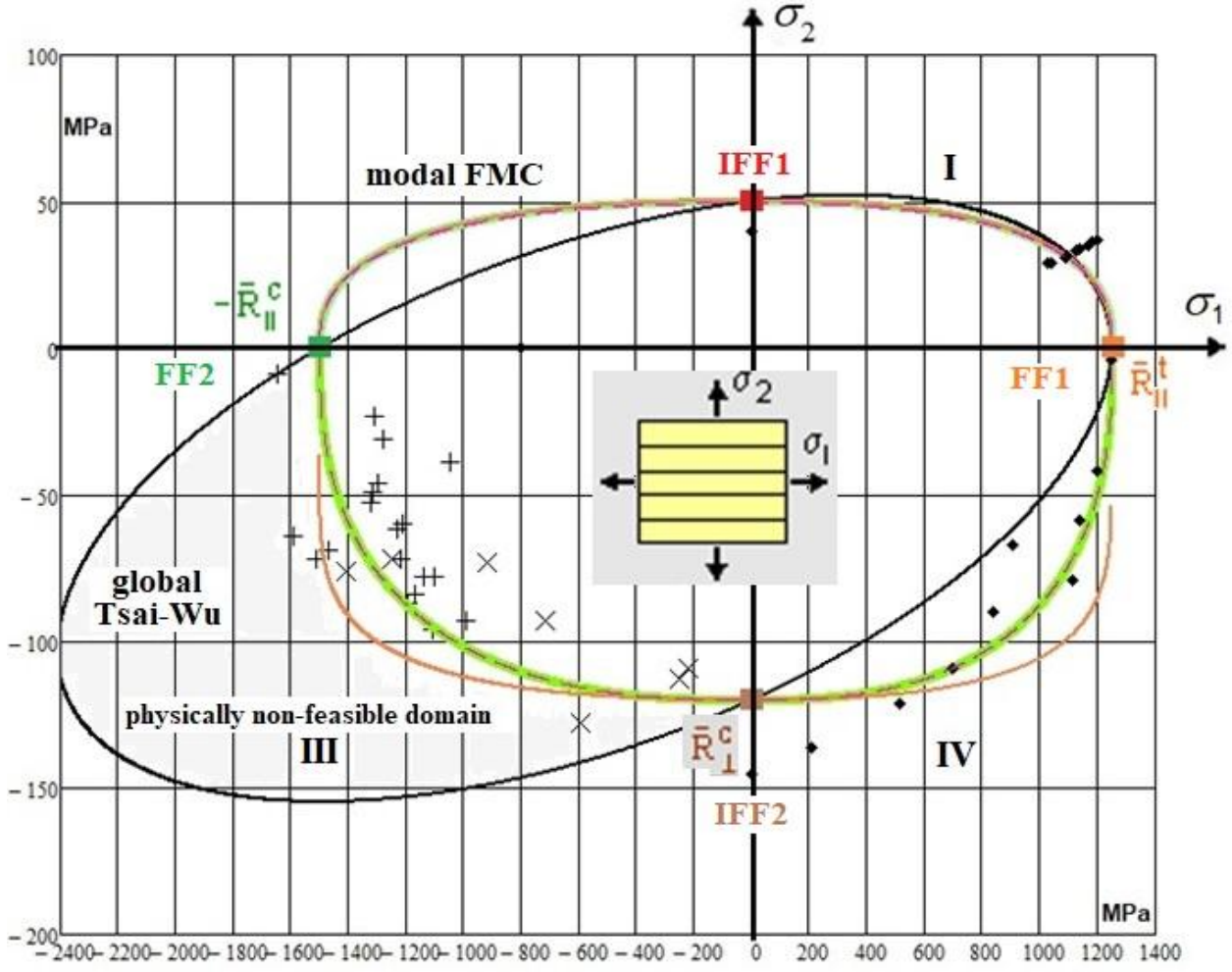

Fig.27-7, WWFE-I, TC3: Hoop wound tube lamina. E-glass/MY750 Ep.

$$\{\bar{R}\} = (1280,\ 800,\ 51,\ 230,\ 97)^T$$

In order to be able to generate above different envelopes the author had to harmonize terminology and to make them to apply his interaction formula for the modal SFC ones.

This limited the amount of further numerical comparisons. $\tau_{21}(\sigma_1)$ could be investigated.

From Fig.27-8 can be concluded that the envelope of Puck and Cuntze lie upon another. Modal Hashin and Global Tsai-Wu are lying inside.

27.5 Computation of a SFC-linked Reserve Factor

Principally, in order to avoid either to be too conservative or too un-conservative, a separation is required of the always needed 'analysis of the average structural behavior' in Design Dimensioning (*using average properties and average stress-strain curves*) in order to obtain optimum structural information (= 50% expectation value) from the mandatory single Design Verification analysis of the

final design, where statistically minimum values for strength and minimum, mean or maximum values for the task-demanded other properties are applied as Design Values. There it is to demonstrate that '*A relevant Limit State is not met yet'*.

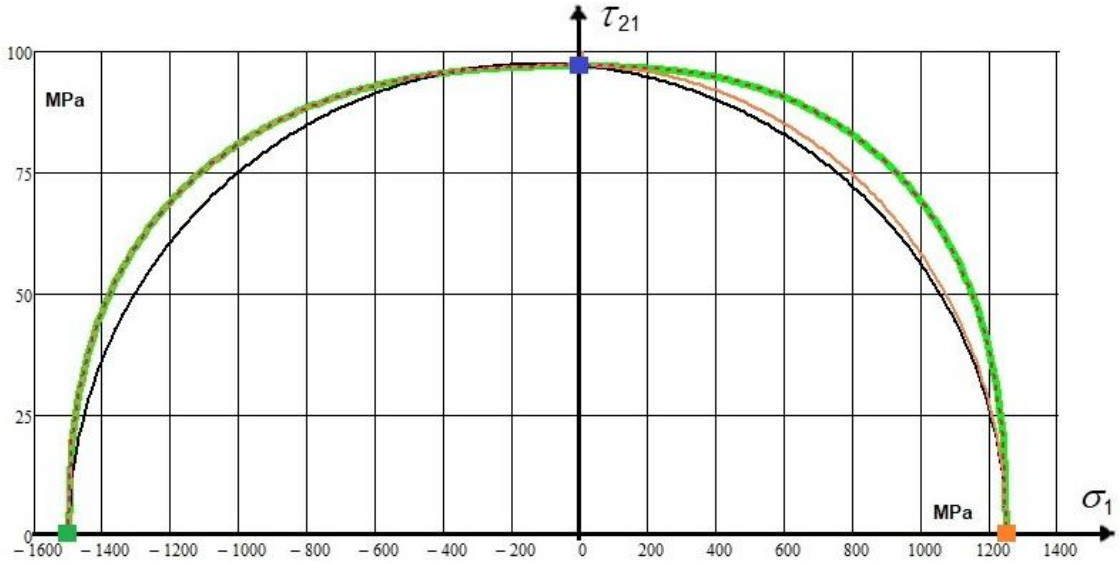

Fig.27-8: $\{\bar{R}\} = (1280,\ 800,\ 51,\ 230,\ 97)^T$

A very simple example of the Design Verification of a critical UD lamina in a distinct wall design was depicted as *RF*-calculation procedure in $13. The certification–relevant load-defined Reserve Factor *RF* corresponds in the linear case to the material reserve factor f_{RF}. Its value here is $RF = 1.25 > 1$ → Laminate wall design is verified!

The multiple Lessons Learned and conclusions are incorporated in the following list:

LL

- ✓ *Considering FE-results and necessary properties: We must more and more 3D-design! However properties, especially for composites is 3D-property data test sets, are seldom sufficiently available*
- ✓ *So-called global SFCs couple physically different failure modes whereas the modal SFCs describe each single failure mode and therefore will better map the course of test data*
- ✓ *First-Ply-Failure (FPF) envelopes are searched by these SFCs, which means determination of 'Onset-of-damage' and includes both Inter Fiber Failure (IFF) and Fiber Failure (FF). Last Ply Failure (LPF) usually requires a non-linear analysis, which can be used to save a design*
- ✓ *Material symmetry seems to require for UD materials a 'generic' number of 5, valid for strengths and elasticity properties and the distinct SFCs.*
- ✓ *In this context: The Standard 3D SFCs of Tsai-Wu and Hashin employ the so-called cohesive (shear) strength* R_{23} *and regard it as a technical strength and not as a general strength quantity. The mystery behind the various interpretations is tried to be unlocked by the author. Because most of the published applications are 2D-ones the employed SFCs do not require* R_{23} *and its determination by tests needed not to be presented*
- ✓ *Often, SFCs employ just strengths and no friction value. This is physically not accurate and the undesired consequence in Design Verification is: RF may be not on the safe side*
- ✓ *SFCs are 'just' necessary but not sufficient for the prediction of strength failure. Basically, due to internal flaws, also an energy criterion is to apply. The novel approach 'Finite Fracture Mechanics (FFM)' offers a hybrid criterion to more realistically predict the stress-based crack initiation in brittle isotropic and UD materials.*

- ✓ *The physically clear-based quantity Eff gives an impressive interpretation of the failure envelope or what 100% strength capacity in 3D stress states physically really means.*
- ✓ *From the nevertheless well performed WWFEs the author had to learn that provided test results can be far away from the reality like an inaccurate theoretical model. Theory creates a model of the reality and one experiment shows 'just' one realization of the reality. Test article analysis is mandatory to interpret the test results and for a simulation-based improvement of the design. Only well-understood experiments can verify the design assumptions made!*
- ✓ *Assuming 6 strength quantities seems to violate material symmetry. Cuntze's SFC set just employs 5 measurable strengths and 2 friction parameters.*

This is a good place to make the reader aware of the World-Wide-Failure-Exercises on UD-material.

Many thanks to the QinetiQ-team, UK, the organizers Mike, Sam and Peter for setting up and survive such a long lasting effortful world-wide exercise.

The SFC models of Puck and Cuntze are most probably those SFC models, which are best validated by 2D and the few 3D UD experiments.

The author did not participate in WWFE-III, the part *Micro-damage Theories*.

Where are the practical results of this WWFE presented ??

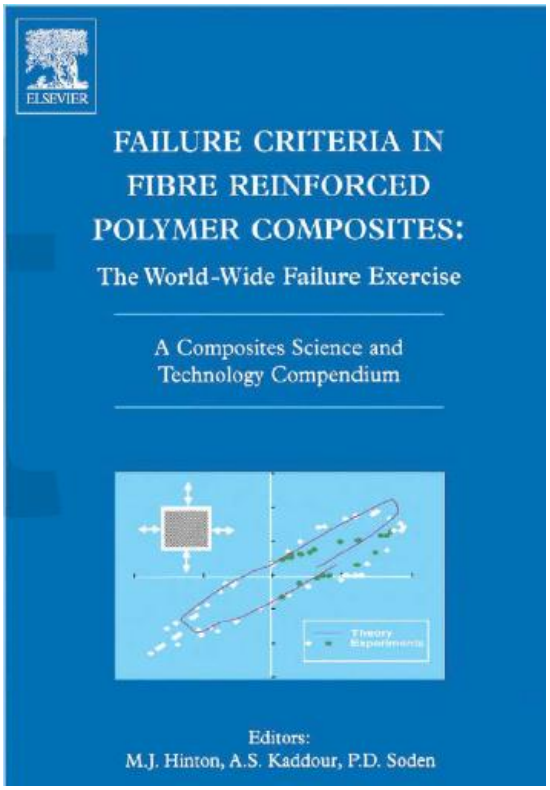

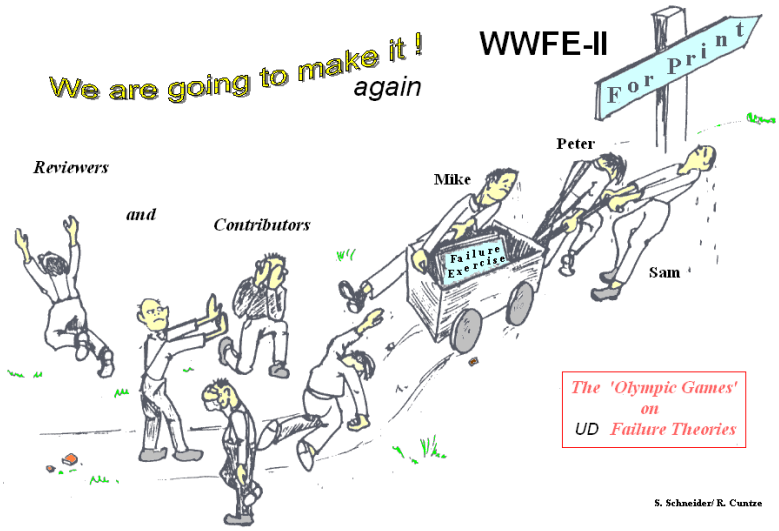

Organizer: QinetiQ , UK, since 1991

[Hinton, Kaddour, Soden, Smith, Shuguang Li]

Aim: For UD materials, only!

'Testing Predictive Failure Theories for Fiber–Reinforced Polymer Composites to the full !'

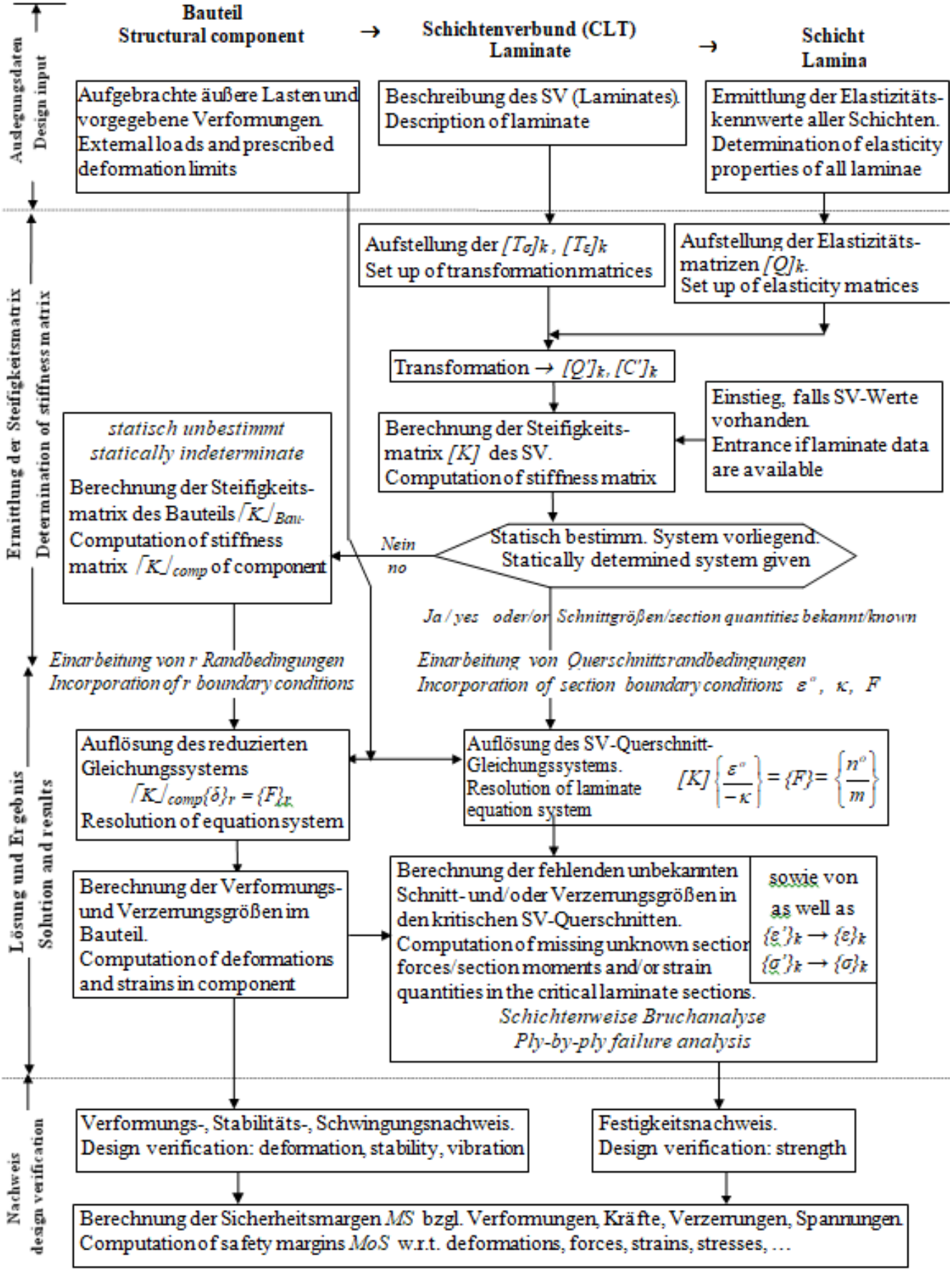

Design verification procedureof a laminate

28 Technical Terms, Laminate Description, Material Stressing Effort *Eff*

***Aim**: Bridging mutual understanding between engineering disciplines.*

28.1 Terms (see Glossary-Cuntze)

Some terms for a better common understanding and for the application of SFCs comparison shall be added. This is the more necessary for composites:

Beschichtung und Beschlichtung

- Analysis: Computation that uses fixed model parameters, such as of the final design
- Fracture body: smoothed surface of the ends of the multi-axial failure stress vectors
- Failure condition: Condition on which a failure becomes effective, meaning $F = 1$ for one limit state
- Failure criterion: Distinctive feature defined as a condition for one of the 3 states F < = > 1
- Failure Mode Concept (FMC)**:** invariant, failure mode-based general concept to generate strength failure conditions (SFCs) for single failure modes. It is a 'modal' formulation in contrast to 'global' concepts where all failure modes are mathematically linked and a concept for materials that can be homogenized (smeared). Applicability of a SFC ends if homogenization as pre-requisite of modeling is violated
- Fracture body: smoothed surface of the ends of the multi-axial failure stress vectors
- First-Ply-Failure (FPF): usually First Inter-Fiber-Failure IFF in a lamina of the laminate. FPF failure envelopes are searched by the SFCs. This means determination of 'Onset-of-damage' and includes both Inter Fiber Failure (IFF) and Fiber Failure (FF)
- Isotropic material: material with identical properties in all directions
- Lamella: specific lamina in construction
- Lamina: Designation of the single UD ply as computational element of the laminate, used as laminate subset or building block for laminate modeling. It might capture several equal plies
- Laminate: multi-ply-composed structure (stack)
- Last-Ply-Failure (LPF) in the laminate: usually requires a non-linear laminate analysis, which can be used to save a design
- Material Stressing Effort $\sigma = R \cdot Eff$ (not material utilization in the usual sense of manufacture waste minimization): artificial term, generated in the UD World Wide Failure Exercises in order to get an English term for the meaningful German term Werkstoffanstrengung. The SCF is stress-based and not strain –based. In the linear case it is directly valid $f_{Res} = RF = 1/ Eff$. (in his book Puck originally used the term effort ε and further exposure). $Eff_{max} = 100\% = 1$
- Macro-Damage: technischer Schaden):
- Micro-Damage (Schädigung):
- Parameters: usually scattering design parameters including material properties
- Ply, layer: Physical element from a winding, tape-laying process etc
- Properties: 'Agreed' values to achieve a common and comparable design basis. Must be provided with average value and coefficient of variation
- Reserve Factor *RF*: load-defined value RF_{ult} = *final failure load / design ultimate load* (*DUL*)
- material Reserve Factor f_{Res}: f_{Res} = *strength design allowable / stress at distinct design load*
- general strength R: strength design allowable for Design Verification;
- average strength $\bar{R}$: in model validation for mapping tasks, marked by the statistical 'bar over'
- Simulation: Process, that consists of several analysis loops and lasts until the system is imitated in the Design Dimensioning process. The model parameters are adjusted hereby to the 'real world'

- Strength quantities: $\{R\} = (R_{\parallel}^{t}, R_{\parallel}^{c}, R_{\perp}^{t}, R_{\perp}^{c}, R_{\perp\parallel};\ R_{23})^{T} \Leftarrow (X, X', Y, Y', S_{12}; S_{23})^{T}$ Tsai
- Stress tensor components: They should not read 'stress components' (*only a shear stress can be composed of a tensile component jointly acting with a compressive stress component*)
- Technical strength, standard-measurable: for UD-clarity symbolically indexed $R_{\perp}^{\ c}, R_{\perp\parallel};\ R^{t}, R^{c}$
- General strength quantity: indexed by numbers like $R_{\perp\perp} \rightarrow R_{23}$.

It seems necessary to again cite for the two different composite domains two long-time used terms:

Material composite (Werkstoffverbund): structural-mechanically a composed 'construction of different materials.

Note: A not smearable 'conglomerate' is usually the Fiber-grid-Reinforced-Concrete.

Composite material (Verbundwerkstoff): combination of constituent materials, different in composition.

For the strength properties it is to discriminate in the English language:

Yield stress (unfortunately termed yield strength, despite of the fact that it is not set as a strength property for Design Verification): material property corresponding to the point at which the material begins to deform plastically (in German Streckgrenze Re), is end of proportionality σ_{prop}

Proof stress: point at which the material exhibits 0.2% of plastic deformation, known as stress at 0.2% strain-offset and set as yield strength property $R_{p0.2}$. (in German Fließgrenze or 0.2% -Dehngrenze).

Repetition: *Shear Strength Quantities in Spatial Analysis of isotropic and anisotropic materials*

These are an essential input with UD materials however also with isotropic mineral materials.

For 3D-analysis two specific shear strength quantities are applied, see *Fig. 28-1*:

* An approach-formalistic τ_{23}/R_{23} linked shear fracture stress $\tau_{23}^{fracture} = R_{23} \le R_{\perp}^{t}$,

used with Tsai-Wu and in the invariant approach of Hashin and further

* A Mohr-based approach linked so-called cohesive strength $R_{23}^{\tau} = \tau_n(\sigma_n = 0)$, used within an

Hashin approach and in consequence, principally also with Puck. Since Puck formulated a full IFF-SFC $R_{23}^{\tau} \Rightarrow R_{23}^{A}$, defined by all 3 IFFs interacting approach, he could model-associated de-dicate his action plane resistance a relation with other model parameters.

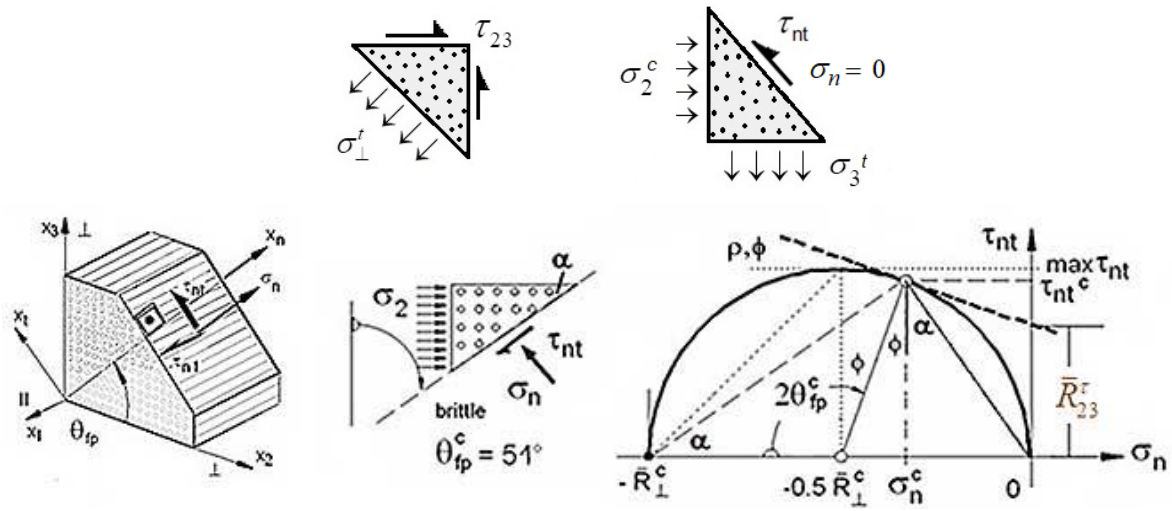

Fig. 28-1: (up) Difference of transversal shear fracture stress and cohesive strength. (below) Mohr-Coulomb curve characteristics

28.2 Indexing and Material Notations

Indexing is a chaos in the disciplines: It seems to be that the author could find (*some years ago for the planned novel ESA –Material Handbook*) a physically clear indexing system for the 3 material family models isotropic, transversely-isotropic UD and orthotropic materials (fabrics etc.). This indexing captures all material properties and allows a switching between.

The author's Glossar on 'Technical Terms' (Springer) hopefully shall be a contribution to a better mutual understanding of 'constructive' engineers from the building industry and engineers from mechanical engineering and further, of engineers from the textile, manufacturing and material discipline as well in order to better manage the more and more interdisciplinary future project tasks.

Notes on designations: As a consequence to isotropic materials (European standardization) the letter R has to be used for strength. US notations for UD material with letters X (*direction 1*, ∥) and Y (*direction 2*, ⊥) confuse with the structural axes' descriptions X and Y. R_m := '*resistance maximale*' (French) = tensile fracture strength (superscript ^{t} is usually skipped because in mechanical engineering design runs in the tensile domain, which is opposite to civil engineering, where fiber reinforcement is coming up viewing carbon concrete). See further [*Cuntze Glossar*].

In the following Table, on basis of investigations of the VDI-2014 Working Group and on investigations for above Materials Handbook, Cuntze proposed internationally not confusing terms for strengths and physical properties. These self-explaining symbolic designations read for UD- materials:

Property type	**UD quantities**	**'generic' number**
fracture strength properties	$\{R\} = (R^t_{\|\|}, R^c_{\|\|}, R^t_{\perp}, R^c_{\perp}, R_{\perp\|\|})^{\mathrm{T}}$,	5
+ friction properties	$\mu_{\perp\|\|}$, $\mu_{\perp\perp}$	2
elasticity properties	$\{E\} = (\mathrm{E}_{\|\|}, E_{\perp}, G_{\mathrm{II}\perp}, \nu_{\perp\mathrm{II}}, \nu_{\perp\perp})$	5
hygrothermal properties	$\{\alpha\} = \mathrm{CTE}\,(\alpha^T_{\|\|}, \alpha^T_{\perp})$; $\mathrm{CME}\,(\alpha^M_{\|\|}, \alpha^M_{\perp})$	2 ; 2

Notes on composites and matrices:

(1) The constituents retain their identities in the composite; that is, they do not dissolve or otherwise merge completely into each other although they act in concert. Composite materials provide improved characteristics not obtainable by any of the original constituents acting alone.
(2) Normally the constituents can be physically identified, and there is an interface between them.
(3) Composites include fibrous materials, fabrics, laminated (layers of materials), and combinations of any of them.
(4) Composite materials can be metallic, non-metallic or a hybrid combination thereof. Carbon concrete is one example.
(5) Approximately homogenizable to a smeared material are short fiber-reinforced FRC, SMC, UD-ply = UD-lamella. The lamella is smearable and therefore it can be modelled as a 'composite material'.
(6) Layered materials and foam materials are also forms of composite materials.

(7) Cement-based mortar is a ‘smearable’ composite material (the construction organization RILEM has a problem here, because they do not discriminate ‘material composite’ from ‘composite material’)

Table 28-1: Notations of material properties

9	general orthotropic	R_1^t	R_2^t	R_3^t	R_1^c	R_2^c	R_3^c	R_{12}	R_{23}	R_{13}
5	UD, ≅ non-crimp fabrics	$R_{\parallel}^t$ NF	$R_{\perp}^t$ NF	$R_{\perp}^t$ NF	$R_{\parallel}^c$ SF	$R_{\perp}^c$ SF	$R_{\perp}^c$ SF	$R_{\parallel\perp}$ SF	$R_{\perp\perp}$ NF	$R_{\parallel\perp}$ SF
6	fabrics	R_W^t	R_F^t	R_3^t	R_W^c	R_F^c	R_3^c	R_{WF}	R_{F3}	R_{W3}
9	fabrics general	R_W^t	R_F^t	R_3^t	R_W^c	R_F^c	R_3^c	R_{WF}	R_{F3}	R_{W3}
5	mat	R_{1M}^t	R_{1M}^t	R_{3M}^t	R_M^c	R_{1M}^c	R_{3M}^c	R_M^τ	R_M^τ	R_M^τ
2	*ductile* isotropic *brittle*	R_m SF	R_m SF	R_m SF	deformation-limited			R_m^τ	R_m^τ	R_m^τ
		R_m NF	R_m NF	R_m NF	R_m^c SF	R_m^c SF	R_m^c SF	R_m^σ NF	R_m^σ NF	R_m^σ NF

9	*general orthotr.*	E_1	E_2	E_3	G_{12}	G_{23}	G_{13}	ν_{12}	ν_{23}	ν_{13}	**comments**
5	*UD, ≅ non-crimp fabrics*	$E_{\parallel}$	$E_{\perp}$	$E_{\perp}$	$G_{\parallel\perp}$	$G_{\perp\perp}$	$G_{\parallel\perp}$	$\nu_{\parallel\perp}$	$\nu_{\perp\perp}$	$\nu_{\parallel\perp}$	$G_{\perp\perp} = E_{\perp}/(2+2\nu_{\perp\perp})$ $\nu_{\perp\parallel} = \nu_{\parallel\perp} E_{\perp} / E_{\parallel}$ 3 *is perpendicular to quasi-isotropic 2-3-plane*
6	*fabrics*	E_W	E_F	E_3	G_{WF}	G_{W3}	$G_{\parallel W3}$	ν_{WF}	ν_{W3}	ν_{W3}	*Warp = Fill*
9	*fabrics general*	E_W	E_F	E_3	G_{WF}	G_{W3}	G_{F3}	ν_{WF}	ν_{F3}	ν_{W3}	*Warp ≠ Fill*
5	*mat*	E_M	E_M	E_3	G_M	G_{M3}	G_{M3}	ν_M	ν_{M3}	ν_{M3}	$G_M = E_M/(2+2\nu_M)$ 1 *is perpendicular to quasi-isotropic mat plane*
2	*isotropic*	E	E	E	G	G	G	ν	ν	ν	$G=E/(2+2\nu)$

9	general orthotropic	α_{T1}	α_{T2}	α_{T3}	α_{M1}	α_{M2}	α_{M3}
5	UD ≅ non-crimp fabrics	$\alpha_{T\parallel}$	$\alpha_{T\perp}$	$\alpha_{T\perp}$	$\alpha_{M\parallel}$	$\alpha_{M\perp}$	$\alpha_{M\perp}$
6	fabrics	α_{TW}	α_{TW}	α_{T3}	α_{MW}	α_{MW}	α_{M3}
9	fabrics general	α_W	α_F	α_F	α_{MW}	α_{MF}	α_{M3}
5	mat	α_{TM}	α_{TM}	α_{TM3}	α_{MM}	α_{MM}	α_{MM3}
2	isotropic for comparison	α_T	α_T	α_T	α_M	α_M	α_M

Table of structural properties

Strength properties: *NF:= Normal Fracture, SF:= Shear Fracture, R:= strength, σ, τ := indicate the fracture responsible normal or shear stress acting on the fracture ‘plane’.*
Hygro-thermal properties*: T:= Thermal, M:= Moisture and Mat. λ , c : not listed.*

Elasticity properties: *E:=Young's modulus, v:=Poisson's ratio, G:=shear modulus. ||:= parallel to the fiber, ⊥ := transversal to the fiber direction; W:= Weft, F:= Fill, M:= Mat .* $\nu_{\|\perp}$ *:= (here!) larger Poisson's ratio. 1:= lamina fiber direction, 2:= lamina transverse fiber direction across the width or the plane, 3:= through-thickness direction; x ,y := principal in-plane laminate directions, z:= thickness direction (interlaminar).*

For non-linear analyses the author recommends the stress-strain curves in Fig.28-2

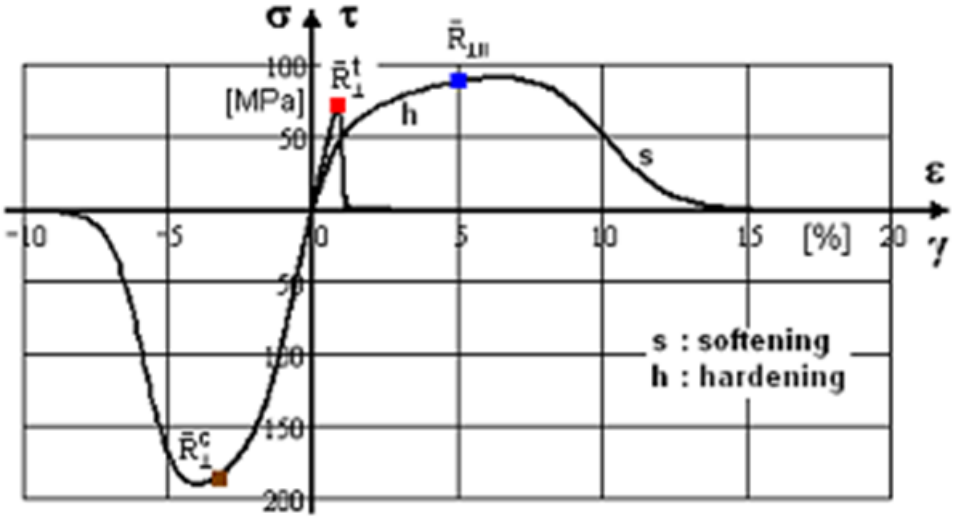

Fig.28-2 UD ply:: Full stress –strain curves with load-controlled hardening and deformation-controlled softeningof the ply (layer)embedded in a laminate

28.3 Upcoming construction standards in Germany with comments

Standards in Germany are finalized, see *Fig.28-3*:

- polymer matrix: BÜV 10 update
- mineral matrix: novel DAfStb-Richtlinie "Betonbauteile mit nicht-metallischer Bewehrung".

Comments of the author after a careful investigation of the two standard proposals, about 2020:

The DAfStb guideline "Concrete components with non-metallic reinforcement" is intended for fiber-reinforced components with concrete matrix.

*For engineers it is confusing not to clearly say which fiber material group the guideline is for. The fiber type CF, GF sets the limits of application.

*Originally for the *open* fiber grid the name lamella for a *dense* non-crimp fabric was used. The lamella however was still intensively used in construction repair of corroding steel-concrete ceilings (see *Fig.28-4*)

*The suffix $_{nm}$ could be replaced by the indices of the polymer matrix world, namely for the pure fiber$_f$ and the cured fiber strand $_{\|}$.

*Why sticking further to the old German-originated letter *f* (strength). Still at the GruSiBau-time (*about 1985, development of the excellent partial safety factor concept*) the author used the international letter *R* for the resistance entity strength in construction. Using the letter *R* – internationally and partly nationally still started - makes life of engineers over the technical fences simpler, internationally at least.

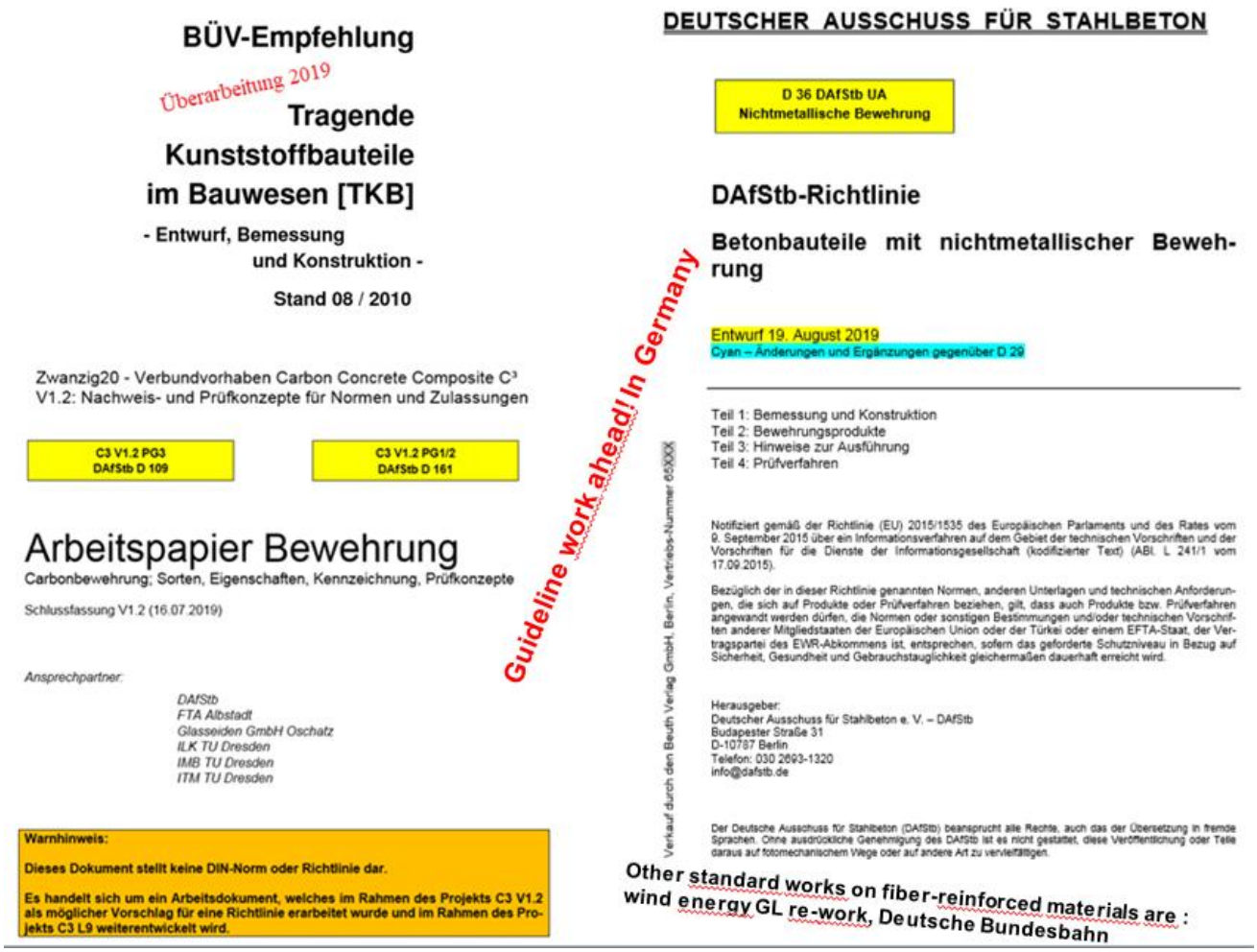

Fig.28-3: Guideline work ahead in Germany, BÜV10 update and D 36 novel

The BÜV-recommendation for load-carrying composite parts in construction is intended for fiber-reinforced components with polymer matrix.

*Above two upcoming standards are not harmonized regarding the designations amongst themselves and w.r.t. terms half a century internationally used in timber construction and also with polymer matrices. This is all the sadder for the author, because he edited the VDI 2014, sheet 3 guideline - initiated by civil engineers !- but not used in construction. The European Codes hopefully will improve this unfortunate situation.

Fig.28-5 presents a proposal for an ordering scheme.

***LL**: Harmonization of denotations remains an urgent on-going task .*

Production of optimal structural components:

It firstly requires an optimum design

which includes connections, joints and applicable materials.

Then the locally best materials are to determine and to sort out - regarding production -

to ensure the required optimum component properties considering sustainability.

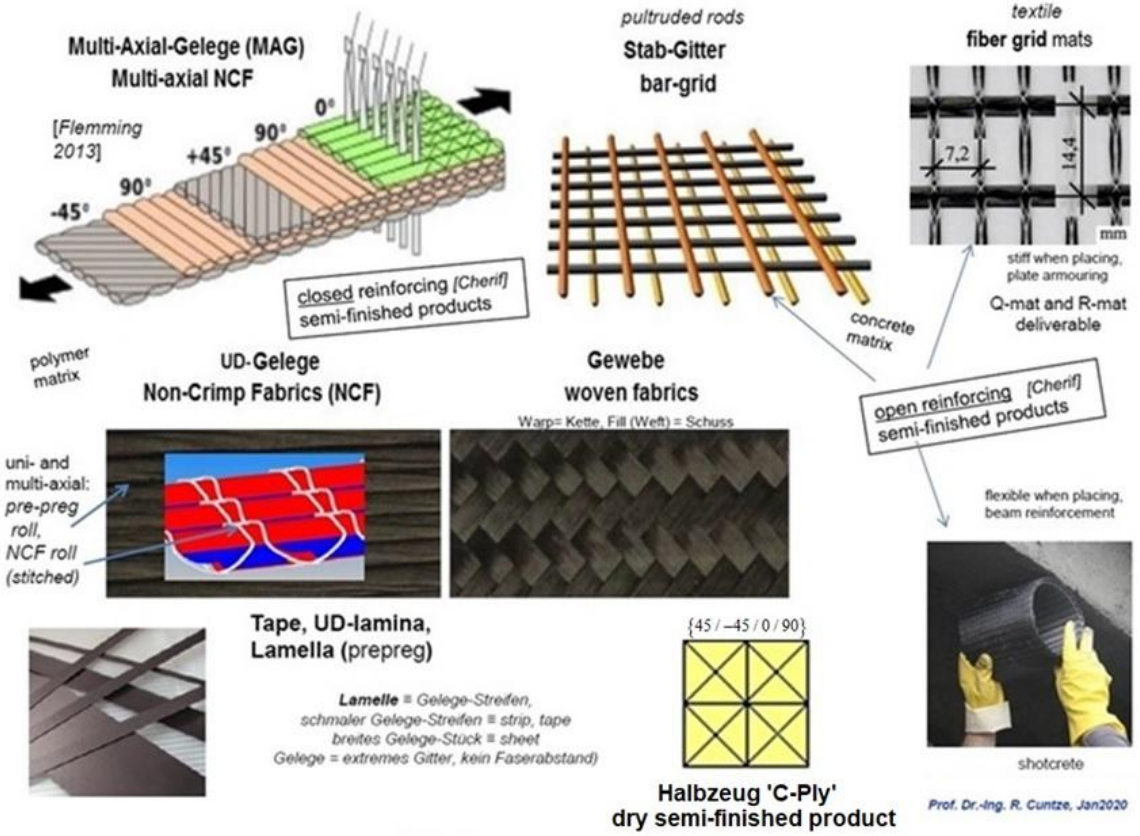

Fig.28-4: Basic fiber-reinforcing products in Engineering

isotropic	Normal-Concrete / Fine [1] Concrete	Concrete matrix	—	water + cement (CEM I, CEM III) + aggregate (sand, gravel) + possibly additives, such as super-plasticiser, retarder					max. grain > 4 mm [1] / max. grain < 4 mm	Fiber [2] Reinforced Concrete: GFRC, CFRC, PPFRC, PBOFRC (F(R)C)	Fiber Composite Materials FCM
			grid-type reinforcing structures **Fiber-Concrete-Composite FCC**								
anisotropic	[3] CRC or CC, GFC or GC (FRC)	Reinforcement Form	**UDRC**		**Textile-Reinforced Concrete TRC**					short fiber, long fiber	
			rope, bar	rebar grid	R-, Q-grid		embroid-ered sandwich	non-woven (randomly oriented, oriented)			
			1D	**2D**	Reinforcement Alignment		**2D**	**2D — 3D**		**2D — 3D**	
			semi-finished products for reinforcements (endless fiber, long fiber)							for matrix improvement	
	CFRP, GFRP, AFP, BsFRP (FRP)		UD ply, lamella strips		NCF lamella sheet		fabric	non-woven (randomly oriented, oriented)			
			Fiber-Polymer-Composite FPC *closed reinforcing structures*								
isotropic	Thermosets, Thermo-plastics	Polymer matrix	Resin Systems: thermosets, thermoplastics, with catalysts etc.							SMC, BMC (FP)	

Fig.28-5: Ordering scheme proposal for Fiber-Composite Materials FCM, construction-linked such as Fiber-Reinforced Polymer FRP, Fiber-Reinforced Concrete FRC, CFRC:= CarbonFiber–Reinforced Concrete, Bi-Directionally Reinforced Concrete BDRC, UHP-(short)Fiber-Reinforced Concrete, HPFRC. Green couloured are still fixed notions.Matrix types of the Reinforcements FRPm = Fiber-Reinforced Polymer matrix, Fiber-Reinforced-Mineral matrix FRMm. International subscipts f = filament, m = matrix; superscripts t = tension, c = compression

29 Miscelleaneous

In this chapter some results of the author's works are collected, which have been discussed in his various working groups (WG).

29.1 WG Construction-linked Additive Fabrication AF

Classification of fabrication processes: Subtractive processes (waste), Formative processes and Additive processes (automatically digitized fabrication now) [*VDI 2403*]. *The term manufacture is not accurate: Manus* and *facere → means made by hand*.

1. In Subtractive processes, the geometry to be created is created by defining the removal of individual volume regions. Typical representatives of this group of manufacturing processes are machining processes such as turning, drilling or milling. (timber construction etc.)
2. Formative processes refer to the production of geometries by forming in compliance with volume constancy. Formative manufacturing processes are deep drawing, forging or primary forming.
3. Additive fabrication processes create a geometry by joining together volume elements (so-called "voxels"), such as the standard processes concreting, bracketing, plastering a wall etc.

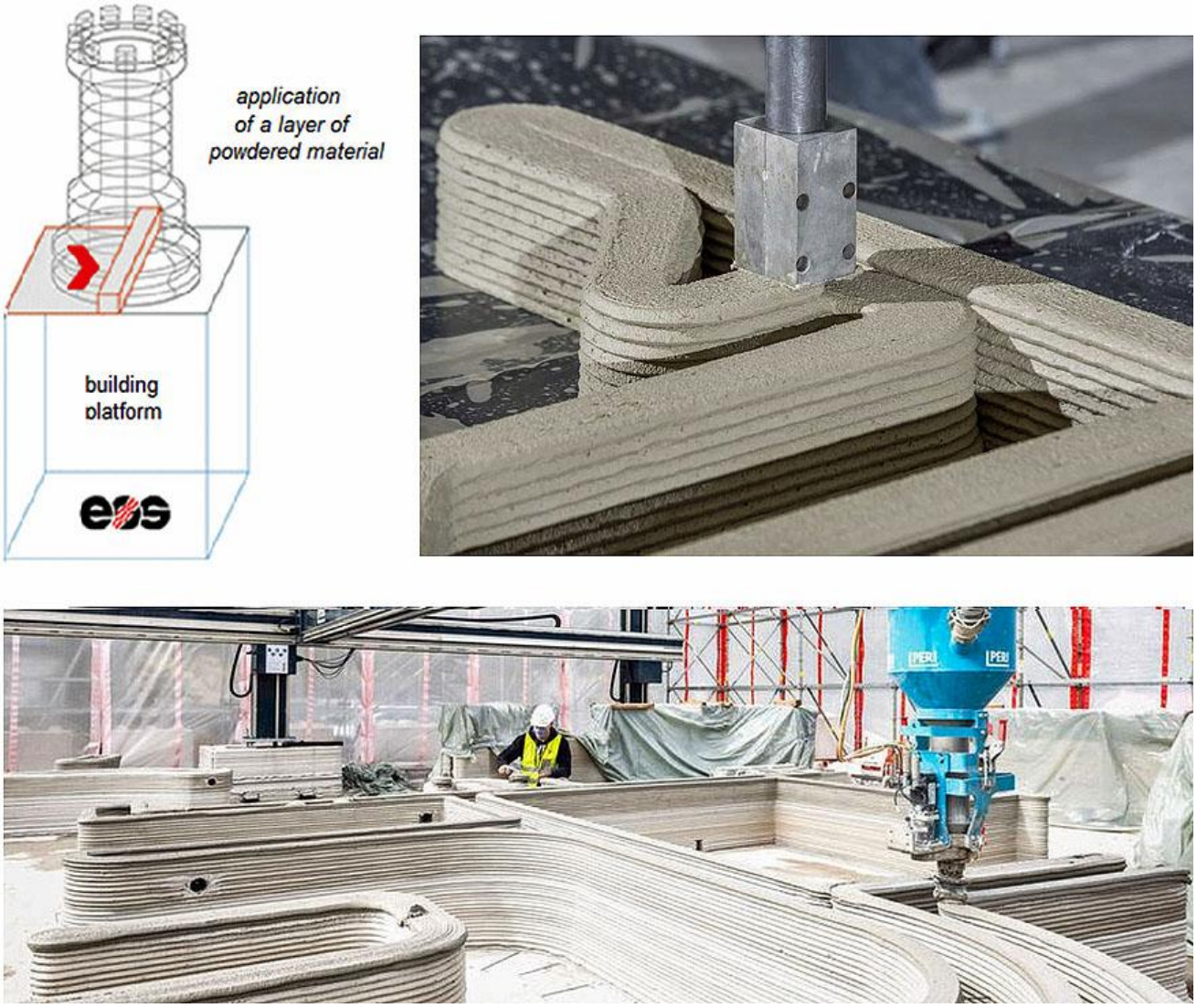

Fig.29-1: Particle-bed technique (up left), Mortar strand depositing technique (up, right); (below) Peri GmbH, building a two-story house in Beckum, 2021

Additive fabrication processes have been an essential part of my CU Construction WG "Automated Fabrication in the Construction Industry including Serial Construction".

Any material that can be glued, welded or melted can be used in AF. For industrial purposes, metals, plastics, sand and ceramics are common materials, but the process is to adapt. The engineer's desire is to obtain accurate process names in the additive fabrication point 3, the term 3D-print does not give a clear process information. Therefore some basic definitions are provided for construction. The two basic digitized additive fabrication processes in construction are to term:

(3a) P**owder bed process:** *true original 3D horizontal slice printing in construction*

Total cross-section including the 'openings' is produced in a powder bed layering process. Layer thickness is usually << 1 mm. (*for formwork production, usually*). Technique Selective Laser Sintering, does pretty well correspond with the printing definition '*Procedure, to apply something by pressure like printing a book'*.

In mechanical engineering, Fused Layer Modeling (FLM) is probably the most widely used 3D printing process. For copyright reasons, Fused Deposition Modeling (FDM) or Fused Filament Fabrication (FFF), a freely usable name for the 'melt layering process' used, has been established. The layer pattern is then the distinguishing feature for FFF-printed parts.

(3b) Extruded (fine) mortar-strand deposit process: is no 3D printing in the original sense

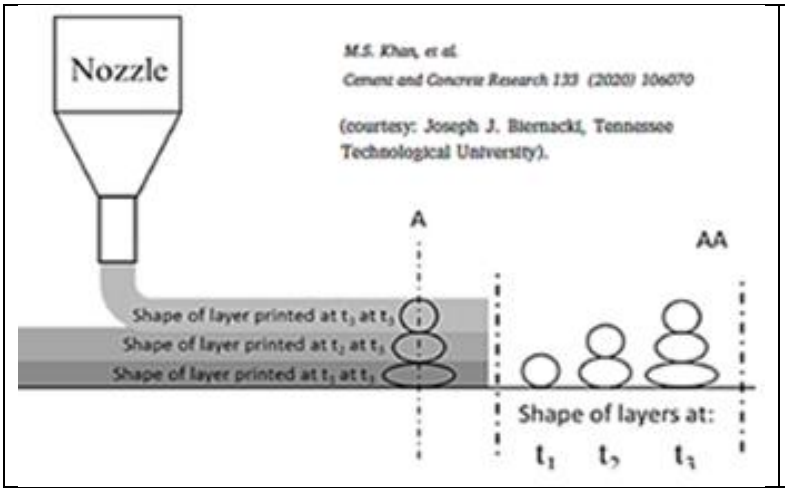

(3a): Technique Extruded mortar strand deposit. Total cross-section including 'openings' is produced in a 'path tracking operation'. Layer thickness is several mm, depending on the strand thickness.

This picture shows very clearly the problem that the mortar has to solve in terms of curing at different times t

Future task will be *"Rethinking construction and relearning".*
Part of this will be "Automated construction with additive fabrication processes", so that we can build cheaper, more sustainably, with better quality, and even faster in the future". The aim is to obtain a force-path-oriented placement of minimal concrete quantity including possible fiber reinforcement (short, long, endless) and thus also to reduce the huge CO_2 backpack of the huge amount of concrete caused by cement production!

***LL**: It is often written that entire buildings are produced with a '3D concrete printer'. The correct wording would be: (only) the walls and other compressed load-bearing building structures are made with the special process 'Extruded mortar-strand deposit'. Cost-effective conventional ceiling slabs are still required.*

29.2 Buckling analysis versus Strength analysis

This chapter provides introductory information about buckling of columns (beams), plates, panels and shells. It shortly addresses just essential features in stability analysis (*speaking stability is more positive than buckling*).

This chapter is just dealing with static stability problems. It covers a very basic background in order to guide the practicing designer to better understand the manuals of commercial analysis software.

The following contents basically stems from the creation of the ESA Buckling Handbook, ECSS-E-HB-32-24A. Cuntze was first convenor and founder of the team as well as a co-author of the later prepared HSB 40100-04] from R. Cuntze and J. Broede.

Noteworthy: In the HSB, section 40000, for a wide spectrum of columns, rods, rings and deep beams design sheets are found. The same is given in the chapter plates where the available design sheets on anisotropic plates provided by J. Broede and colleagues are outstanding sheets.

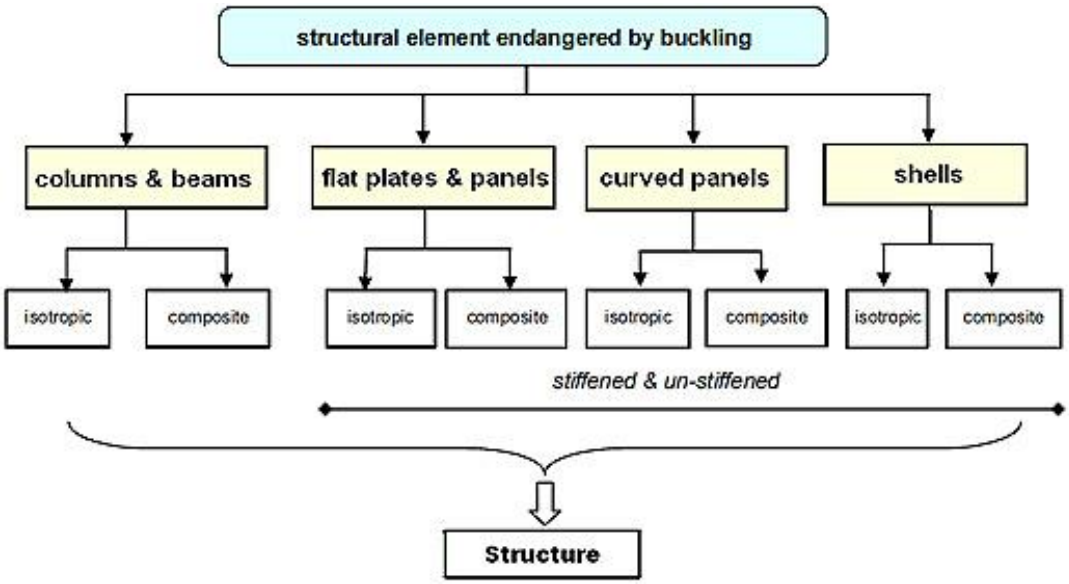

Fig.29-2: Breakdown of buckling of endangered structural elements [Cuntze, ECSS]

Different levels of analysis complexity are treated in the literature above. Going in steps from the lower level of complexity to the higher level of complexity (which will be denoted as a "hierarchical approach") the structural analyst is able to carry out and finally to successfully interpret analyses at the highest level of complexity, typically finite element computations (see [*CUN22*]).

In structural design the following subjects must be demonstrated: *Material* Strength, applying SFCs, strength criteria, and *Structural* Strength, applying buckling resistance conditions. *Fig.23-3* compiles these subjects.

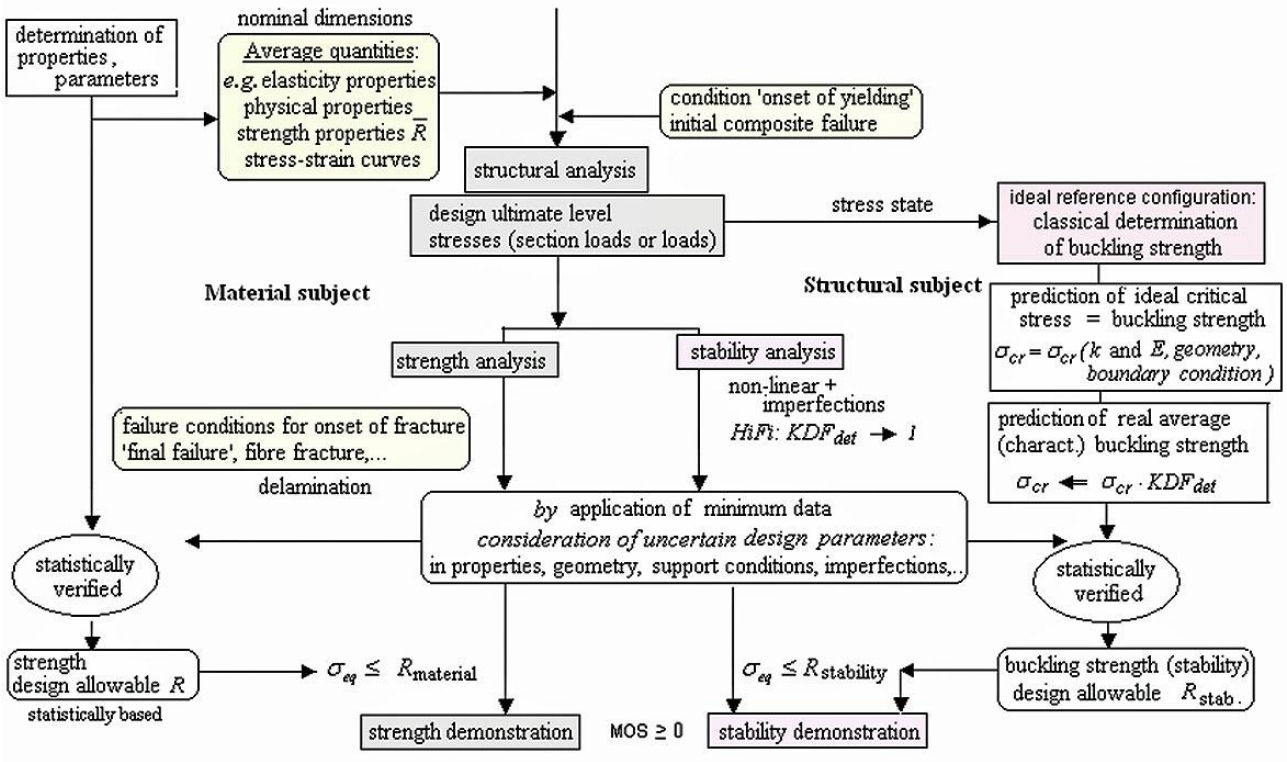

Fig. 29-3: Visualization of the (actually) required deterministic input demands.
KDF usually corrects difference of calculation model to experiment (50% expectance value), k:=buckling factor (from handbook tables), MoS:=Margin of Safety

Using such an engineering procedure the engineer is able to analyze the stability of (large) structures composed of structural elements, also referred to in literature as structural components or structural items. The term structural element includes typical elements such as columns and beams, plates, panels, and shells. In practice these structural elements often contain structural details, e.g. shells containing openings or reinforcements. The associated "basic" structural elements, the elements without structural details are denoted in the ECSS as "Typical Structural Elements".

Non-axial symmetric shells and truss systems are not addressed in the book.

29.3 Some Final Notes from Personal Experience

- ✓ Mechanics remains one very essential basis when developing light-weight structural components and Artificial Intelligence (AI) with its algorithms is a helpful supporting tool
- ✓ Only System Engineering with experienced engineers using mechanics and the necessary other disciplines - together with AI - enables to produce qualified products
- ✓ At the end someone has to sign that the developed structure will work and by that will take over responsibility. This experienced person is the absolutely necessary 'plausibility checker' for the obtained analysis and test results including generic AI-supported results.
- ✓ Bridge disciplines and materials by showing up similarities to simplify engineering life!
- ✓ In the present multi-physics applications product development is the work of several experienced engineers. Otherwise one does not deliver qualified 'Multiple function structural products'.
- ✓ In the case of bending of FRPlastic- and FRConcrete-parts carbon fibers can be only exploited using pre-tensioning and thereby compressing the tension-sensitive matrices Plastic or Concrete

- ✓ Viewing SFCs, one must be careful with conclusions reported in literature (unpleasant personal experience): SFC model *modifications* - created by another author - are used under the name of the originator and then poorly rated, however, the modification was not reported!
- ✓ Experienced engineers know: "Check your test together with test data evaluation. Check your analysis including assumptions."
- ✓ There is a rationale to take a distinct $\sigma - \varepsilon$ curve: From risk analyses and decision theory the best prediction will be achieved by applying the *mean(σ,ε)-curve* = 50% probability !
- ✓ "Certification by Analysis, only": Here, simulation can optimize the output of the usually only permitted minimum number of physical tests, and enabling to better manage risk and improve prediction.

30 Glossary Book, Contributions to Handbooks, Guidelines, Courses, etc

30.1 Glossary Book

“Technical terms for composite components in civil engineering and mechanical engineering”

The construction industry is an industry in which the topic of high-performance fibre composites is not yet established on the one hand, but where there is enormous application potential on the other. Against this backdrop, Carbon Composites e.V. (CCeV) in Augsburg has founded a specialist department in civil engineering "CC Bau (construction)".

For CC Bau, this repositioning meant that Fibre-Reinforced Plastic (FRP) - and the various fiber-reinforced concrete matrices had to be covered, i.e. 'fibre-reinforced concrete'. The latter envolves endless ‘(roving)-Reinforced Concrete’ (RC) as well as ‘(short) Fibre Reinforced Concrete’ (FRC).

The following matrix applications must therefore be captured: *(1) Polymer matrix-related*, such as Glass fibre plastic pipes and containers, wind rotor blades and pedestrian bridges in GlassFRP and CarbonFRP as well, and *(2) Concrete matrix-related*, such as textile ‘fibre grid’ (mat) -reinforced concrete bridges and machine foundations, overhead line masts, industrial floors, multi-storey car parks, silos, prefabricated garages, transformer houses, offshore applications, tubbings, sandwich façade panels, un-tensioned and tensioned bending panels, FRP shells and bridges.
Further, a big topic is the rehabilitation with FRP-‘lamellas’ (tapes, strips) such as the reinforcement of a ceiling plate (slab), because of increased moments, using CFRP-lamellas applied by surface bonding,

Carbon Fibers in the construction industry reduce the concrete amount, which is positive for the CO_2 footprint due to the reduced clinker production required and are sustainable due to their non-corroding behaviour in contrast to steel.”

Purpose of this Glossary:

Borders between engineering disciplines are disappearing, more and more. It can also be noticed that in the different fields of the fiber-using industry there are different "speeches" and that technical terms are sometimes used very differently. Several groups of engineers would therefore have to be connected conceptually so that they understand each other correctly when making decisions. These are 'constructive' engineers from building industry and mechanical engineering and further, engineers from the textile and material range as well as from manufacturing.
This glossary focuses especially on carbon fibers CF and concrete matrices. At the beginning it presents a first scheme of order for the different, interconnected disciplines. At the end, a picture gallery illustrates technological details and applications. This gallery just includes carbon applications from construction industry because these are less known.

30.2 HSF, "Handbook for the German Ministry of Defense on a Safety Concept for Fiber Reinforced Plastic Structures". Koblenz, 1992 (*in German*)

Cuntze R., Rackwitz R., Gollwitzer S., Plica S. and Stoeffler G.

30.3 " VDI 2014 Sheet 1-3" (1980 - 2006):

Development of FRP components (fibre reinforced plastics); concept and design

Me as *Editor of the VDI 2014, sheet 3, (2006) and contributor to sheets 1 and 2

*Presenter of a draft on "Reliability & Safety" , sheet 4 (see later)

The treatment of us contributors, who together have spent many 'man-years' for the development of this guideline, by the VDI is very strange.

Official Information in the Web:

This guideline includes recommendations for the design of components made of fibre-reinforced plastics (FRP) which consist of individual fibre-reinforced laminae in which fibres are embedded in a plastic matrix. It records the state of the art regarding calculation methods for the development of FRP components. To a very great extent the guideline is based on approved methods which have already been tried and tested in practice and does not therefore necessarily reflect the very latest research findings, this affects methods used for strain and stress calculation. **Editor**: VDI-Gesellschaft Materials Engineering (**GME**). Chairman Prof. Dr.-Ing. Christian Hopmann, IKV, RWTH Aachen.
Price: **290 €**, Beuth Publishing.

Reality:

- There was not yet any GME existing.
- After 26 years, the VDI guideline was finally completed. Twice during this time, we thanked the ladies from MAN, who also made time-based documentation possible.
- Having the translation done at our own expense was no obstacle for us compared to the enormous effort before.

Words of thanks from the VDI:

The **VDI** expressed its **gratitude** to the remaining team: by

3 lines to the industrial editor Cuntze **for 2 'man years' of labor in my vacant time during 26 years,**

2 lines to the other remaining tough persistent contributors Huybrechts, Lutz and Puck.

(By the way: one man year was at that time 150 k€ for me when performing offers).

The VDI-director at that time, Dr. Fuchs, told me on the phone:

"*Mr. Cuntze, I have no influence over that*."

(Mr. Fuchs had previously applied to me for a position.)

On top: The names of us contributors are nowhere cited! Hence, we did never exist for the reader.

This perhaps makes it understandable that only a few thank you lines were enough.

The VDI must ask itself whether this was an appropriate way of saying 'thank you'.

I'm waiting now for the announced update in 2026, 4.

Working Group VDI 2014, Meeting members: Moser (founder), Cuntze (editor), Lutz (tough contributor)

All are civil engineers, however the guideline was practically not known in civil engineering for dimensioning! I know, that the price was one obstacle. Why did we not spent 'Beuth Publishing' 100k€, that industry would have purchased a much cheaper guideline and applied the results of the WG, which invested ten times more??

Our efforts and their results have therefore unfortunately not been able to find the desired benefit in the industry.

Members of one of the first WG meetings

1981, at Freudenstadt, AVK conference:
Moser, Krawinkel, Preuß, Niederstadt, Lutz, Conen, Wurtinger, Cuntze

VDI 2014 Focus:

Plenty combinations of material components to be captured in the guideline

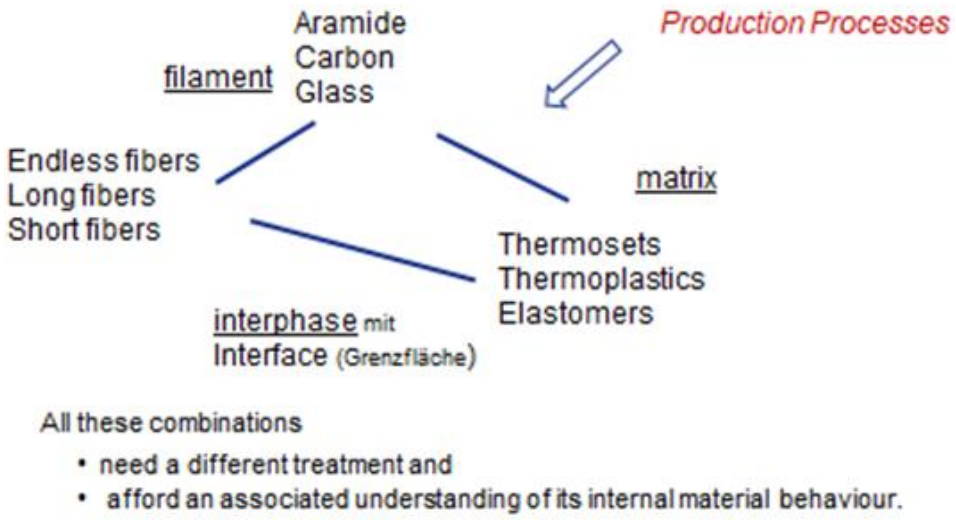

All these combinations

- need a different treatment and
- afford an associated understanding of its internal material behaviour.

A first VDI 2014-dedicated conference at Prof. Knauer at Dresden

Verstärkte Plaste 90 at Dresden University (September 1990), organizer B. Knauer.
Panel discussion:
Einsfeld, Sorry, *Cuntze, Buchs, Lustig, Knauer*

Sondersitzung "Schwingfestigkeit", VDI Richtlinie 2014, Teil 3

Ort:	Institut für konstruktiven Leichtbau und Bauweisen, TU Darmstadt
Datum:	21.6.00, 9:15 bis 16:30
Thema:	**Wie wird der rechnerische Schwingfestigkeitsnachweis für Faser-Kunststoff-Verbund-Bauteile in der Praxis geführt?**

Teilnehmer:	
Prof. Cuntze	MAN-Technologie
Prof. Schürmann	Institut für konstruktiven Leichtbau und Bauweisen, TU Darmstadt
Herr Gerharz	LBF Darmstadt
Dr. Huth	Fairchild Dornier, Oberpfaffenhofen
Herr Osthorst	Aerodyn, ...
Herr Garbe	ehemals TUD und LBF
Herr Denzin	Institut für konstruktiven Leichtbau und Bauweisen, TUD
Herr Scholz	Rolladen-Schneider Flugzeugbau,
Dr. Huybrechts	ABB Forschung, Heidelberg
Prof. Puck	ehemals GH Kassel
Dr. Gaedke	DLR, Braunschweig
Herr Kleinhansl	Aero Dynamik Consult, ...
Dr. Wacker	Germanischer Lloyd, HV Hamburg
Herr Kensche	DLR, Stuttgart
Herr Lutz	IMS, Innsbruck

entschuldigt:	
Dr. Hachenberg	DASA, Hamburg
H. Emmerling	ECD, Ottobrunn

Anlass der Sondersitzung:
Beim Endbearbeiten des Kapitels 'Schwingfestigkeit' kam der Ausschuß überein, nachzuprüfen, ob nicht doch ein paar Vordimensionierungsformeln dem Leser bereitgestellt werden können. Dazu sollte ein Expertenmeeting stattfinden, zu dem vornehmlich Industrieleute eingeladen werden, die solche Nachweise zu führen haben.
Bemerkung:
Die stattfindenden 'Fatigue-Conferences' (s. Anlage) geben höchstens Hilfe, das Thema Ermüdung (Schwingfestigkeit) zu verstehen, bieten aber keine Unterlagen für das Aufstellen von 'Auslegungsformeln'.

1. Ausführungen der einzelnen Teilnehmer

Wacker

Der GL gibt in seiner Windflügelrichtlinie Hinweise zur rechnerischen Durchführung des Schwingfestigkeitsnachweises. Wacker verteilt das diesbezügliche Kapitel der GL-Richtlinie.

Im wesentlichen basiert der rechnerische Schwingfestigkeitsnachweis auf folgenden Grundlagen:

- **Die Zeitfestigkeit des FKV wird durch eine synthetische Wöhlerlinie (sog. Typ 2, d.i. Gerade im doppelt-logarithmischen Maßstab ausgehend von der Kurzzeitfestigkeit bzw. deren charakteristischem Wert) beschrieben für R = -1**
- **Annahme: Gültigkeit des Goodman-Diagramms vorausgesetzt zur Umrechnung auf andere Spannungsverhältnisse R**
- **Annahme: Gültigkeit der Miner Regel**

Die Neigungen k der Wöhlerlinie $N^{1/k}$ sind in der GL-Richtlinie angegeben mit:

- k = 9 für GFK mit UP-Harzen
- k = 10 für GFK mit EP-Harzen
- k = 14 für CFK.

VDI 2014: Meeting on Composite Fatigue in 2000

ICS 59.100, 83.140.20 VDI-RICHTLINIEN September 2006

VEREIN DEUTSCHER INGENIEURE

Entwicklung von Bauteilen aus Faser-Kunststoff-Verbund Berechnungen

Development of FRP components (fibre reinforced plastics) Analysis

VDI 2014

Blatt 3 / Part 3

Ausg. deutsch/englisch
Issue German/English

Frühere Ausgabe: 04.97 Entwurf, deutsch
Former edition: 04.97 Draft, in German only

Zu beziehen durch / Available at Beuth Verlag GmbH, 10772 Berlin – Alle Rechte vorbehalten / All rights reserved © Verein Deutscher Ingenieure e.V., Düsseldorf 2006

Vervielfältigung – auch für innerbetriebliche Zwecke – nicht gestattet / Reproduction – even for internal use – not permitted

Die deutsche Version dieser Richtlinie ist verbindlich.

No guarantee can be given with respect to the English translation. The German version of this guideline shall be taken as authoritative.

Inhalt Seite

Vorbemerkung . . . 3
1 Anwendungsbereich . . . 3
2 Abkürzungen, Begriffe, Symbole, Indizierung . . . 4
3 Berechnungsablauf . . . 12
3.1 Allgemeines . . . 12
3.2 Auslegungsphilosophie . . . 14
3.3 Berechnungsprogramme . . . 15
4 Modellierung der Schicht . . . 16
4.1 Allgemeines . . . 16
4.2 Eben beanspruchte Schicht . . . 18
4.2.1 UD-Schicht (faserparalleles KOS) 18
4.2.2 G-Schicht und M-Schicht . . . 20
4.2.3 Drehung der UD-Schicht in das Laminat-KOS . . . 21
4.2.4 Berücksichtigung der Schubspannungen aus Querkraft bei UD-Schichten . . . 22
4.3 Räumlich beanspruchte Schichten . . . 23
4.3.1 Mechanische Beanspruchung (faserparalleles KOS) . . . 23
4.3.2 Mechanische Beanspruchung einer UD-Schicht (gedrehtes KOS) . . . 25
4.4 Einfluss von Beanspruchungsarten/-dauer 26
4.4.1 Kurzzeitbeanspruchung . . . 26
4.4.2 Ruhende Langzeitbeanspruchung . 26
4.4.3 Schwingbeanspruchung . . . 30
4.4.4 Stoßbeanspruchung . . . 31
4.5 Festigkeitskriterien . . . 31
4.5.1 Allgemeines . . . 32
4.5.2 Bruchbedingungen für UD-Schichten . . . 36
4.5.3 G-Schicht . . . 44
4.5.4 M-Schicht . . . 45
4.5.5 Einzusetzende Festigkeitswerte . . 46
4.6 Anwendung von Berechnungsprogrammen . . . 46
4.6.1 UD-Schicht . . . 46
4.6.2 G-Schicht . . . 48

Contents Page

Preliminary note . . . 3
1 Scope . . . 3
2 Abbreviations, terminology, symbols, superscripts and subscripts . . . 4
3 Analytical procedure . . . 12
3.1 General comments . . . 12
3.2 Design philosophy . . . 14
3.3 Computer programs . . . 15
4 Modelling the lamina . . . 16
4.1 General comments . . . 16
4.2 Two-dimensionally loaded lamina . . . 18
4.2.1 UD lamina (parallel-to-fibre COS) . 18
4.2.2 WF lamina and M lamina . . . 20
4.2.3 Rotation of the UD lamina into the laminate . . . 21
4.2.4 Inclusion of shear stresses from transverse forces in case of UD laminae . . . 22
4.3 Laminae subject to three-dimensional loading . . . 23
4.3.1 Mechanical loading (parallel-to-fibre COS) . . . 23
4.3.2 Mechanical loading of a UD lamina (rotated COS) . . . 25
4.4 Influence of loading type and duration . . 26
4.4.1 Short-term load . . . 26
4.4.2 Long-term static load . . . 26
4.4.3 Cyclic load . . . 30
4.4.4 Impact load . . . 31
4.5 Strength criteria . . . 31
4.5.1 General comments . . . 32
4.5.2 Fracture conditions for UD lamina . . . 36
4.5.3 WF lamina . . . 44
4.5.4 M lamina . . . 45
4.5.5 Strength values to be used . . . 46
4.6 Application of calculation programs . . . 46
4.6.1 UD lamina . . . 46
4.6.2 WF lamina . . . 48

VDI-Gesellschaft Kunststofftechnik

VDI-Handbuch Kunststofftechnik
VDI-Handbuch Konstruktion

VEREIN DEUTSCHER INGENIEURE

Entwicklung von Bauteilen aus Faser-Kunststoff-Verbund
Zuverlässigkeit und Sicherheit

VDI 2014
Blatt 4 (4. Entwurf)
Zusammengestellt
R. Cuntze, MAN

Development of FRP components
(fibre reinforced plastics)
Reliability and Safety

Einsprüche bis ??.??.1995 an
Verein Deutscher Ingenieure
VDI-Gesellschaft Kunststofftechnik
Postfach 10 11 39
40002 Düsseldorf

Inhalt Seite

Vorbemerkung .....

1. Anwendungsbereich, Nutzen .....

2. Abkürzungen, Begriffe, Symbole .....

3. Nachweis .....
- 3.1 Allgemeines zu Rechnerischem und Experimentellem Nachweis .....
- 3.2 Mechanische Modellierung (Grenzzustände)
- 3.3 Experimenteller Nachweis .....

4. Traditionelles Sicherheitskonzept (TSK) .....
- 4.1 Allgemeines, charakteristische Werte .....
- 4.2 Unsichere Eingangsgrößen beim Rechnerischen Nachweis .....
- 4.3 Sicherheitsfaktoren (Auslegung) und Sicherheitsmargen (rechn. und experim. Nachweis)
- 4.4 Kritik am TSK .....

5. Probabilistisches Sicherheitskonzept (PSK) .....
- 5.1 Allgemeines .....
- 5.2 Einwirkungsgrößen, Widerstandsgrößen und stochastische Konstruktionsparameter .....
- 5.3 Teilsicherheitsfaktoren (semiprobabilistische Vorgehensweise) .....
- 5.4 Stochastische Modellierung und Logische Modellierung des Versagenssystems .....
- 5.5 Berechnung von Versagenswahrscheinlichkeit oder Zuverlässigkeit .....

6. Bestimmung von Kennwerten .....
- 6.1 Definition und Verwendung von Dimensionierungskennwerten .....
- 6.2 Ermittlung der statistischen Parameter aus Meßdaten .....
- 6.3 Ermittlung Charakteristischer Werte .....

7. Produktsicherung .....
- 7.1 RAMS-orientierte Entwicklung .....
- 7.2 Qualitätssicherungskonzept und Integritätskontrolle mit Prüfmethoden .....
- 7.3 Versuche zur Erzielung der Strukturzuverlässigkeit des FKV-Bauteils .....

Literatur .....

Anhang 1 Schätzverfahren, Statistische Tests, Updating Verfahren, Bayes .....

Vorbemerkung

Die Richtlinie enthält Empfehlungen für das Entwikkeln von Bauteilen aus Faser-Kunststoff-Verbunden (FKV), die aus einzelnen faserverstärkten Schichten bestehen, bei denen Fasern in einer Kunststoff-Matrix eingebettet sind. Die Bauteilentwicklung wird dargestellt, wobei die Berechnungen eingehender behandelt werden. Die Richtlinie will durch Systematisieren und Vereinheitlichen der Bauteildimensionierung auch die Zulassungsverfahren und die Qualitätssicherung erleichtern. Sie ist in vier Teile gegliedert:

- Blatt 1 Grundlagen
- Blatt 2 Konzeption und Gestaltung .....
- Blatt 3 Berechnung .....
- Blatt 4 Zuverlässigkeit und Sicherheit.

Beispielsammlung: s. VDI Report??

Jakobi, Puck, Voirol

Eckert, Vollrath, Moser

Eckert, Lutz, Haller

Puck, Voirol, Lutz, Moser,

Huybrechts, Knauer

30.4 HSB, "German Aeronautical Handbook" ('*Airbus design folder*') , since 1972

HSB
HANDBUCH STRUKTUR BERECHNUNG

General description

Issue E Year 2018
Page 1 of 21

Luftfahrt-Technisches Handbuch (LTH)

HSB

HANDBUCH STRUKTUR BERECHNUNG

Fundamentals and Methods
for
Aeronautical Design and Analyses

issued by

iasb INDUSTRIE-AUSSCHUSS-STRUKTUR-BERECHNUNGSUNTERLAGEN

Prepared:	Checked:	Date:	
Dr. M. Schagerl	Dr. M. Magin	22.11.2018	IASB / IVW

Digitally signed by Michael Magin
Date: 2020.10.20 00:13:05 CEST

Design sheet contributor 1972-2015

Co- reworker and Co-translator of the 'Airbus' structural handbook into English (2004)

IASB 1972-2024

First paticipation:
July 1972, Session 12.

Last participation:
July 2024,Session 185
at Ottobrunn.

Bansemir, , Hickethier ,(IABG), Spaink,.Schürmann

Bansemir 65 years present at IABG, Ottobrunn

Damping values search attempt

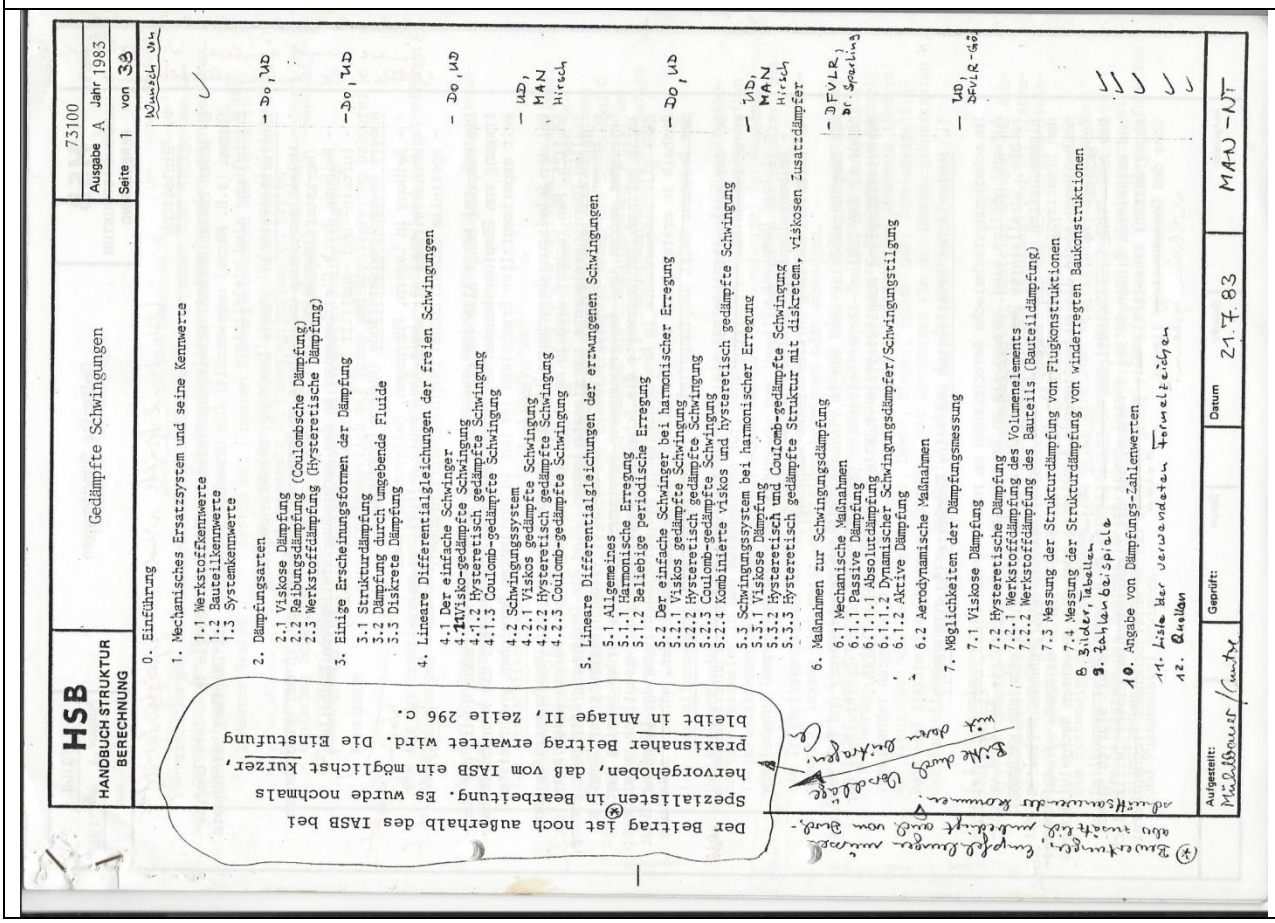

Proposed Structure

Dr.-Ing. habil. RALF CUNTZE VDI

M. A. N. - NEUE TECHNOLOGIE
Dachauer Straße 667
8000 MÜNCHEN 50
Telefon (089) 1480 3279

München, 22.07.1983

Hr. Prof. Dr. Schiehlen, TU-Stuttgart
Hr. Dr.-Ing. Sperling, TU-München
Hr. Dipl.-Ing. G. Hirsch, RWTH-Aachen
Hr. Dipl.-Ing. Kießling, DFVLR-Göttingen
Hr. Dr.-Ing. Rother, Dornier
Hr. Dipl.-Ing. Stolle, VFW
Hr. Dr.-Ing. Bansemir, MBB-UD
Hr. Dipl.-Ing. Bauer, ERNO

Mitarbeit am HSB-Blatt "Gedämpfte Schwingungen"

Sehr geehrte Herren,

der Industrieausschuß für Strukturberechnung (IASB) bemüht sich für sein luftfahrttechnisches "Handbuch für Strukturberechnung" (HSB) um die Aufnahme eines Handbuchblattes "Gedämpfte Schwingungen". Dieses soll einerseits dem Anwender eine schnelle Arbeit erlauben und andererseits auch den physikalischen Hintergrund nebst diversen Dämpfungsarten aufzeigen, damit eine schnelle Kontrolle der, bei Rechnungen getroffenen Dämpfungsannahmen, möglich wird.
Dieser Blattentwurf enthält eine Ausarbeitung, die die verschiedenen, an mich herangetragenen Wünsche berücksichtigt. Leider fehlen noch die 2 Seiten Beispiele (S. 33, 34), da die Zahlenrechnung im Rahmen einer noch fertigzustellenden Semesterarbeit an der TUM erst geliefert wird. Im übrigen konnten aus Zeitgründen nicht alle Korrekturen seitens der DFVLR aber auch der Verfasser bei diesem Entwurf mit eingearbeitet werden.

In Anbetracht der Wichtigkeit dieses Blattes würden der IASB und speziell ich sich freuen, von Ihnen oder Ihren Mitarbeitern Anmerkungen und Verbesserungsvorschläge zu bekommen. Dieses betrifft auch Kürzungen. Beim vorliegenden Entwurf, gegenüber dem letzten, wurden bezüglich des Gesamtinhaltes schon einige Kürzungen durchgeführt.

Herzlichen Dank für Ihre Mühe im voraus

Ihr R. Cuntze

Kopie: Hr. Dr. E. Schreiner, MBB-UF
Vorsitzender des IASB

ä

Verein Deutsc
VDI-Gesellsch

An Verteiler

Prof. Ahrendts (Uni Stuttgart)
Dr. Bansemir (MBB-UD)
Dr. Brunsch (MBB-UF)
Conen (Dornier), z.Hd. H. Dr. Flemmig
Dr. Cuntze (MAN)
Prof. Einfeld (BAM-Berlin)
Prof. Fitzer (UNI Karlsruhe)
Prof. Giencke (Uni Berlin)
Prof. Puck (Universität-Gesamthoch-schule Kassel)
Prof. Moser (Uni Innsbruck)
Dr. Schütz oder Gerharz (Lab. f. Betriebs-festigkeit, Darmst.)
Dr. Schulte (DFVLR-Köln), Mitinitiator
Dr. Stellbrink (DFVLR-Stuttgart)
Dr. Stenzensberger (Technochemie)
Dr. Wurtinger (MAN)
N.N. (DFVLR-Braunschweig), H. Dr. Bergmann
N.N. (ERNO), H. Ludwig
N.N. (VFW), H. Stolle

EINLADUNG

Hiermit bitte ich um Teilnahme an einer ersten Diskussionskreis-Runde mit dem Arbeitstitel

"Spannungsermittlung und Versagensverhalten von Faserverbundstrukturen"

Ort: MAN-München, Neue Technologie, Dachauer Str. 667, 8 München 50

Termin: Anfang Dezember 1983

Einladender: Dr.-Ing. habil. Ralf Cuntze, Tel. 089/1480-3279

ANMERKUNG ZUM DISKUSSIONSKREIS

Ziele: "Intern" berichten, wo der Schuh in Richtung obigen Themas drückt. Diskussion der zugehörigen Probleme. Aufzeigen von Verfahrenswegen. Absprache von Untersuchungen.

Anlaß für die Gründung: Probleme, die sich bei der Bearbeitung verschiedener Aufgaben herausgestellt haben, wie

1. bei der Erstellung der neuen VDI-Ri-2013 (Der Berechnungsingenieur weiß häufig nicht, was er tun soll. Z.B. Ermüdung von MSV)
2. bei verschiedenen Forschungsvorhaben zum Versagensverhalten
3. bei der Bestimmung von Reservefaktoren mehrschichtiger Faserkunststoff-Verbunde bzw. der Spannungsermittlung nach dem Erste-Schicht-Versagen

und etliche Gespräche, die die Notwendigkeit eines solchen Kreises dokumentieren.

Teilnehmerkreis: Statiker, Werkstoff-, Schwingfestigkeits- und Fertigungsleute aus Industrie, Instituten u. Universität

Teilnehmerkreisgröße: Weniger als 20 Personen gewünscht.

Angesprochene Teilnehmer: Siehe Verteiler.

Wunsch bisher schon angesprochener Teilnehmer: Es wird um aktive, konstruktiv Mitarbeit gebeten, da nur dann die zu erübrigende Zeit nutzbringend aufgebracht sein wird.

ANMERKUNG ZUM TREFFEN IN MÜNCHEN

Hauptpunkte der ersten Sitzung:
- Allgemeines zum Diskussionskreis
- Angemeldete Teilnehmerkreisbeiträge. Vortrag und Diskussion.
  Bisher geplant sind
  Kurzvortrag Cuntze: Rechnung zwischen Erste-Schicht-Versagen und Bruchberechnung des Reservefaktors.
  Kurzvortrag Schulte: Versagensverhalten von MSV.
- Schwerpunktvorträge von Fachleuten innerhalb oder außerhalb des Kreises
- Falls Zeit, weitere Beiträge des Teilnehmerkreises

Anmeldungen und Absagen bitte an den Einladenden bis 1. November 1983!
Bitte um Anmeldung von Themen von kurzen Beiträgen bis 1. November 1983!
Spezielle Einladung mit Programm folgen im November durch den Einladenden.

Stress determination and failure behavior of fiber composite structures (1983)

LEHRSTUHL UND INSTITUT B FÜR MECHANIK

TECHNISCHE UNIVERSITÄT MÜNCHEN
DIREKTOR: PROF. DR. K. MAGNUS

8000 MÜNCHEN 2 · ARCISSTRASSE 21 · POSTFACH 202420 · TEL. (089) 2105509

E i n l a d u n g

Am Freitag, den 16. Juli 1976, hält

Herr Dr.-Ing. R. C u n t z e ,

Maschinenfabrik Augsburg - Nürnberg,
Neue Technologie, München

einen Vortrag über das Thema

Die Berechnung eines hochbeanspruchbaren
Bauteils aus Faserverbundwerkstoff, aufgezeigt
am Beispiel eines Satellitenmotorgehäuses.

Der Vortrag findet im Rahmen des Seminars über Fragen der Mechanik statt. Der Vortrag beginnt um 14 Uhr s.t. in der Bibliothek des Lehrstuhls, Zi. 108 (2. Obergeschoß, Luisenstraße 37 a).

HOCHSCHULE DER BUNDESWEHR MÜNCHEN
Fachbereich Bauingenieur- und Vermessungswesen
Wissenschaftliche Einrichtung für Mechanik und Statik

EINFÜHRUNG IN DIE BRUCHMECHANIK IN ANBINDUNG AN DEN KONVENTIONELLEN FESTIGKEITSNACHWEIS

RALF CUNTZE

1981, 82, 83

EINLEITUNG

1. DEFINITIONEN ZUR BRUCHMECHANIK
2. KONVENTIONELLER UND BRUCHMECHANISCHER BAUTEILNACHWEIS
3. KONTINUUMSMECHANISCHE GRUNDLAGEN DER BRUCHMECHANIK
4. SPANNUNGS- UND VERSCHIEBUNGSFELD IM RIßSPITZENBEREICH UND SPANNUNGSINTENSITÄTEN
5. BRUCHMECHANIK-KONZEPTE UND RESTFESTIGKEIT
   5.1 KLASSISCHE BRUCHMECHANIK IDEAL SPRÖDER KÖRPER
   5.2 LINEAR ELASTISCHE BRUCHMECHANIK (LEBM)
   5.3 FLIEßBRUCHMECHANIK (FBM)
6. BRUCHMECHANISCHE KONZEPTE BEI DER RIßAUSBREITUNG
7. BESTIMMUNG BRUCHMECHANISCHER WERKSTOFFKENNWERTE
8. VORGEHENSWEISE BEI BRUCHMECHANISCHER BAUTEIL-AUSLEGUNG UND -NACHWEIS

Lecture: Introduction into Fracture Mechanics (Unu Bundeswehr, München/Neububerg)

MCM-98: Int. conf. on Mechanics of Composite Materials
Riga, April 20-23, 1998. Topic: Strength, Fatigue and Failure

MAN TECHNOLOGIE

Effective Dimensioning of 3D-stressed UD-laminates on Basis of "Fracture-type Strength Criteria"

April 16

(= criteria based on Cuntze's "Failure Mode Concept")

Reasonings for the Investigation:

- Lack of Failure Criteria to *practicably* assess 3D-states of Stress
- Search for an Effective Strength Analysis tool for a reliable (pre-)Dimensioning on basis of Basic Strength Data, only
- To show the Applicability of the presenter's "Failure Mode Concept" to *brittle* UD-material.

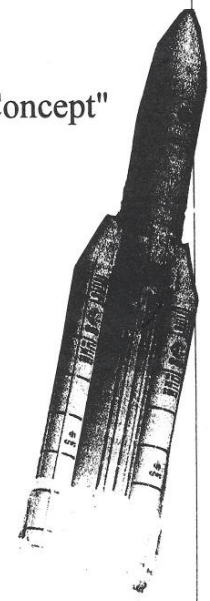

Objectives of the talk: the presentation of

- FEM-Code appropriate Failure Criteria
- Computation of Reserve Factors for the 'Proof of Design'.

Contents of the talk (15 min. incl. discussion)

1. Constraints of Effective Dimensioning
2. General Features of the "Failure Mode Concept"
3. Failure Conditions (criteria) derived by above Concept
4. Determination of Curve Parameters
5. Verification of the Conditions by Curve-fitting of GFRP Test Data
6. Numerical Example: GFRP, 2D-state of stress. Determination of Reserve Factors
7. Application of the S/W-tool to a uniformly loaded Sandwich Plate after implementation into MARC/MENTAT [by G. Sukarie)]

Conclusions and Outlook

Presenter: R.G. Cuntze; MAN Technologie AG, Liebigstrasse 5a, D-85757 Karlsfeld. Tel. 0049-8131-89-1783; Fax -1939; E-mail: Ralf_Cuntze@mt.man.de
Co-author: G. Sukarie

Presented at the Tenth International Conference on the Mechanics of Composite Materials (Riga, April 1998)

First Presentation of my Failure-Mode-Concept

X. INTERNATIONALES
HERMAN F. MARK-SYMPOSIUM

7. und 8. Oktober 1991

Dienstag, 8.10.1991

9.00 Uhr — **Begrüßung**
Prof. O. Hinterhofer
Österreichisches Forschungsinstitut
für Chemie und Technik, Wien, A

Eröffnung
Präs. Komm.-Rat Gen.Dir. Dr. E. Witt
Österreichisches Forschungsinstitut
für Chemie und Technik, Wien, A

THEORIE DER VERBUNDE (MAKRO- UND MIKROMECHANISCHE MODELLE)

Leitung: Prof. U. Einsfeld

9.15 Uhr — Prof. K. Moser
Universität Innsbruck, Innsbruck, A
"Über Modellvorstellungen zu einer Theorie"

10.15 Uhr — Prof. St. Tsai
Stanford University, Stanford, USA
"The Use of Personal Computers in the Design of Composite Materials"

11.00 Uhr — K A F F E E P A U S E

11.15 Uhr — Prof. R. Rikards
Riga Technical University, Riga, Lettland
"Finite Element Analysis of Vibration and Damping of Laminated Composites"

12.00 Uhr — M I T T A G S B U F F E T

BAUTEILENTWURF UND DIMENSIONIERUNG

Leitung: Dr. W. Jessenig

13.30 Uhr — Dr. W. Eichberger
Isovolta, Österreichische Isolierwerke AG
"Temperaturbeständige Epoxid-Glasfaser-Verbundwerkstoffe"

14.15 Uhr — Prof. B. Knauer
Technische Universität Dresden, Dresden
"Konstruktion und Berechnung bei Hochleistungsverbunden"

15.00 Uhr — Prof. G. Nonhoff
Fachhochschule Aachen, Aachen, D
"Berechnung und Überwachung von tragenden Strukturen aus GFK"

CHEMIE UND VERBUNDKOMPONENTEN

Leitung: Dr. O. Seycek

9.30 Uhr — Prof. A. H. Cardon
Free University Brussels, Brüssel, B
"From Micro- to Macroproperties of Polymer Based Composite Systems by Integration of the Characteristics of the Interphase Regions"

10.15 Uhr — Dr. H. Stenzenberger
Technochemie GmbH, Dossenheim, D
"Neue Entwicklungen bei Matrixduromeren"

11.00 Uhr — K A F F E E P A U S E

11.15 Uhr — Dr. J. Hugo
National Research Institute for Materials, Prag, CSFR
"GFR Polypropylene - Creep and Toughness as a Reflection of Time and Temperature Dependent Filler/Matrix Interaction"

12.00 Uhr — Dr. R. Schmid
Ciba Geigy Ltd., Fribourg, CH
"Fundamentale Zusammenhänge zwischen chemischer Struktur, Eigenschaften des Matrix-Harzes und der Festigkeit von Composites"

12.45 Uhr — M I T T A G S P A U S E

WERKSTOFFE UND VERFAHREN

Leitung: Dipl.-Ing. D. Franz

14.00 Uhr — Prof. G. Ehrenstein
Lehrstuhl für Kunststofftechnik, Universität Erlangen,
"Mechanische Bewertung von Verbundkunststoffen bei dynamischer Belastung"

14.45 Uhr — Prof. M.Rätzsch
Institut für Technologie der Polymere, Dresden, D
"Polymerverstärkung durch topologische Überstrukturen"

15.30 UHR — K A F F E E P A U S E

15.45 Uhr — Dr. R. Cuntze, Dr. R. Heibel
MAN Technologie AG, München, D
British Nuclear Fuels Ltd., Chester, GB
"Anhebung der "Einsatzgrenze Rißbildung" eines CFK-Rohrs durch Einbringung von Eigenspannungen"

16.30 — **Podiumsdiskussion und Abschluß des Symposiums**
Moser / Knauer / Rätsch / Ehrenstein
Leitung: Prof. U. Einsfeld

Presenting a process in order to increase the performance of rotating tubes
by micro-crack reduction due to pre-straining

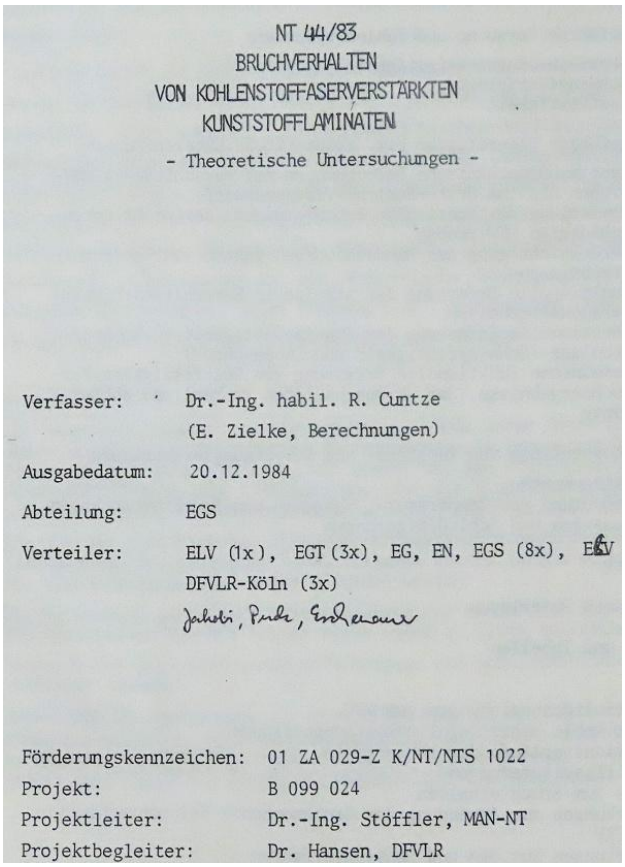

NT 44/83

BRUCHVERHALTEN
VON KOHLENSTOFFASERVERSTÄRKTEN
KUNSTSTOFFLAMINATEN

- Theoretische Untersuchungen -

Verfasser: Dr.-Ing. habil. R. Cuntze
(E. Zielke, Berechnungen)

Ausgabedatum: 20.12.1984

Abteilung: EGS

Verteiler: ELV (1x), EGT (3x), EG, EN, EGS (8x), E[illegible]V
DFVLR-Köln (3x)
Jahoti, Pinke, Enderauer

Förderungskennzeichen: 01 ZA 029-Z K/NT/NTS 1022
Projekt: B 099 024
Projektleiter: Dr.-Ing. Stöffler, MAN-NT
Projektbegleiter: Dr. Hansen, DFVLR

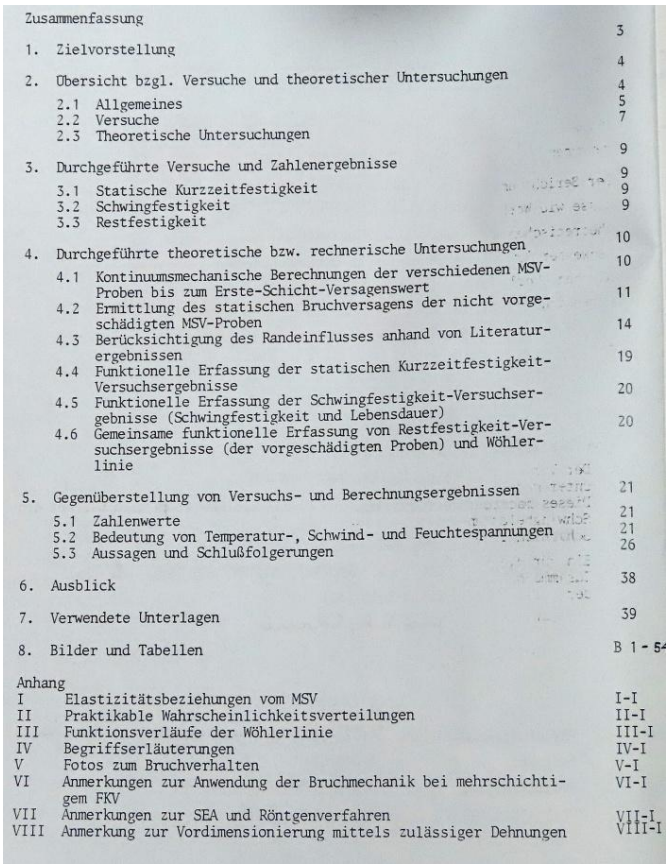

Zusammenfassung 3

1. Zielvorstellung 4

2. Übersicht bzgl. Versuche und theoretischer Untersuchungen 4
   2.1 Allgemeines 5
   2.2 Versuche 7
   2.3 Theoretische Untersuchungen 9

3. Durchgeführte Versuche und Zahlenergebnisse 9
   3.1 Statische Kurzzeitfestigkeit 9
   3.2 Schwingfestigkeit 9
   3.3 Restfestigkeit 10

4. Durchgeführte theoretische bzw. rechnerische Untersuchungen 10
   4.1 Kontinuumsmechanische Berechnungen der verschiedenen MSV-Proben bis zum Erste-Schicht-Versagenswert 11
   4.2 Ermittlung des statischen Bruchversagens der nicht vorgeschädigten MSV-Proben 14
   4.3 Berücksichtigung des Randeinflusses anhand von Literaturergebnissen 19
   4.4 Funktionelle Erfassung der statischen Kurzzeitfestigkeit-Versuchsergebnisse 20
   4.5 Funktionelle Erfassung der Schwingfestigkeit-Versuchsergebnisse (Schwingfestigkeit und Lebensdauer) 20
   4.6 Gemeinsame funktionelle Erfassung von Restfestigkeit-Versuchsergebnisse (der vorgeschädigten Proben) und Wöhlerlinie

5. Gegenüberstellung von Versuchs- und Berechnungsergebnissen 21
   5.1 Zahlenwerte 21
   5.2 Bedeutung von Temperatur-, Schwind- und Feuchtespannungen 21
   5.3 Aussagen und Schlußfolgerungen 26

6. Ausblick 38

7. Verwendete Unterlagen 39

8. Bilder und Tabellen B 1 - 54

Anhang
I Elastizitätsbeziehungen vom MSV I-I
II Praktikable Wahrscheinlichkeitsverteilungen II-I
III Funktionsverläufe der Wöhlerlinie III-I
IV Begriffserläuterungen IV-I
V Fotos zum Bruchverhalten V-I
VI Anmerkungen zur Anwendung der Bruchmechanik bei mehrschichtigem FKV VI-I
VII Anmerkungen zur SEA und Röntgenverfahren VII-I
VIII Anmerkung zur Vordimensionierung mittels zulässiger Dehnungen VIII-I

Fracture behavior of carbon fiber reinforced plastic laminates (1984)

30.5 " Weekly course: Development of Fibre Reinforced Plastic Components" (1986, 1989)

SHORT COURSE

DEVELOPMENT OF FIBRE REINFORCED PLASTIC COMPONENTS

Pretoria

16th to 18th April 1986

repeated 1989

Presented by : Dr R G Cuntze

Course Organizer : P A Coetzer

Organizer P. A. Coetzer

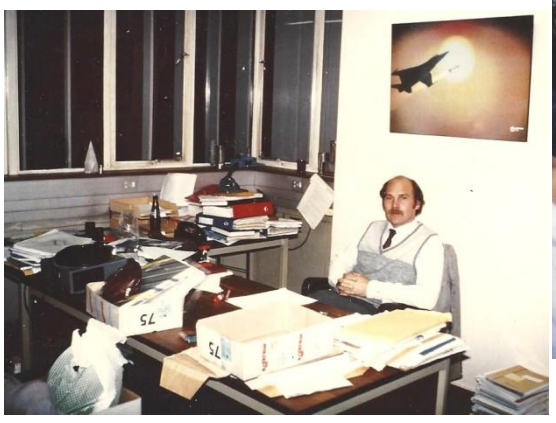

Family invitation:
Inviting person, Prof. Pier Haarhoff, right

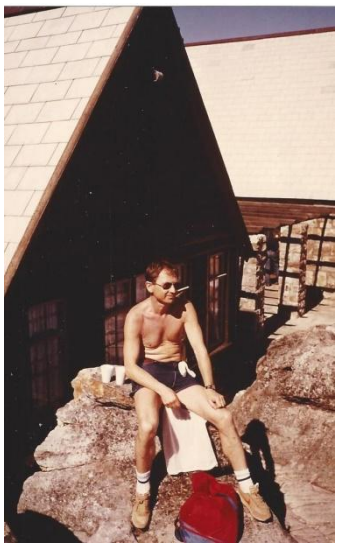

After tackling the Table Mountain alone. Warning: climb through the area of very poisonous snakes

Protea: Blowing for me when getting up (unusual time)

A witch doctor

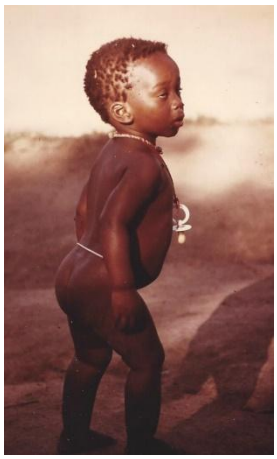

Victoria falls 1986: Being lucky to be the only non-local to attend a performance

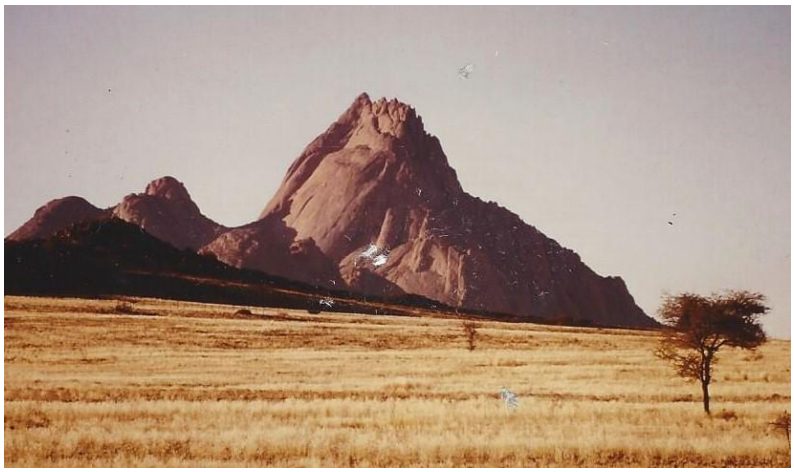

Famous Spitzkoppe

One zebra of a herd of well over 1000 crossing

Etosha Pan 1986. Alone with my two friends in the barely fenced camp.
2016: Full house

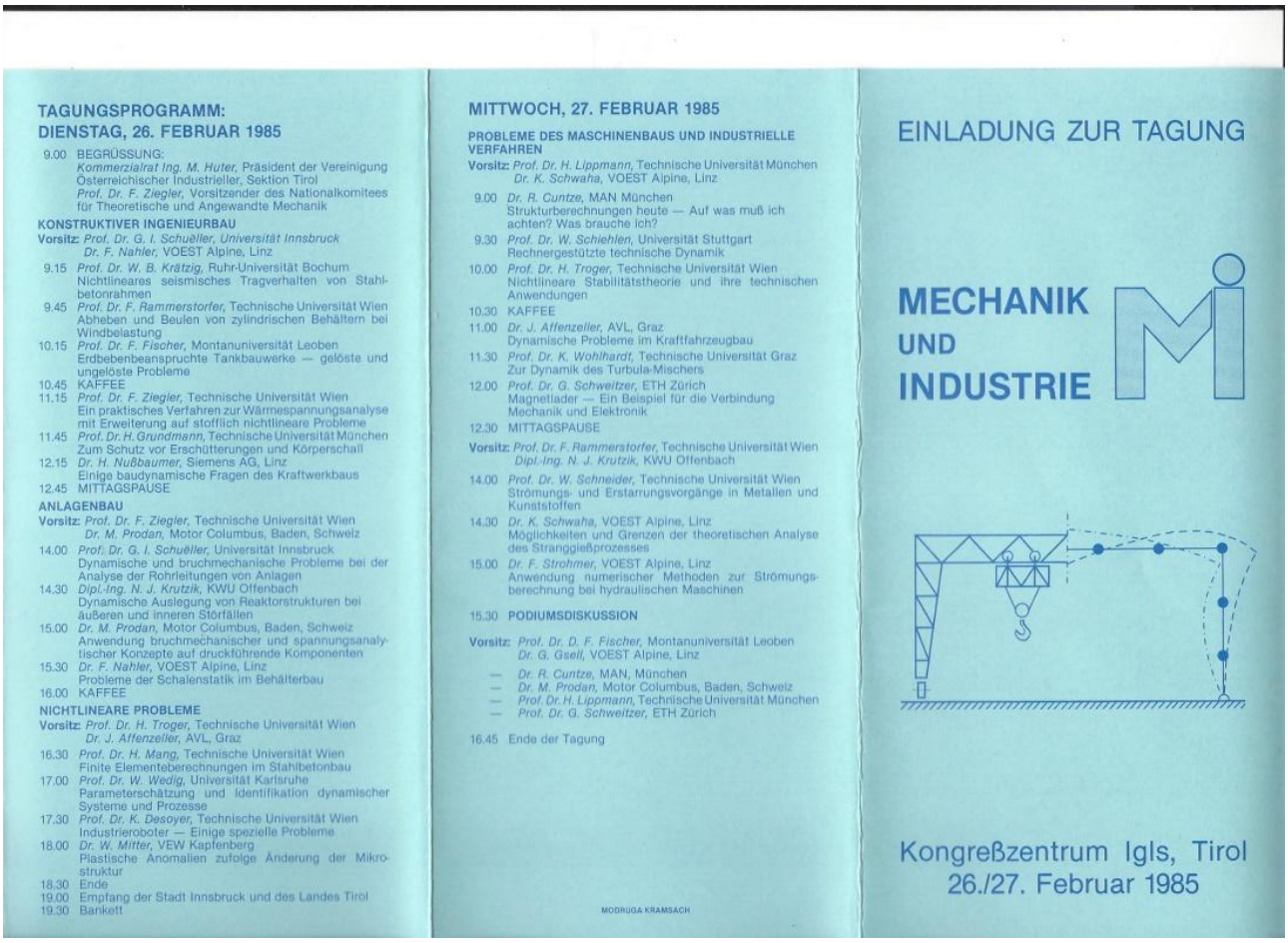

TAGUNGSPROGRAMM:
DIENSTAG, 26. FEBRUAR 1985

9.00 BEGRÜSSUNG:
Kommerzialrat Ing. M. Huter, Präsident der Vereinigung Österreichischer Industrieller, Sektion Tirol
Prof. Dr. F. Ziegler, Vorsitzender des Nationalkomitees für Theoretische und Angewandte Mechanik

KONSTRUKTIVER INGENIEURBAU
Vorsitz: *Prof. Dr. G. I. Schueller, Universität Innsbruck*
Dr. F. Nahler, VOEST Alpine, Linz

9.15 *Prof. Dr. W. B. Krätzig,* Ruhr-Universität Bochum
Nichtlineares seismisches Tragverhalten von Stahlbetonrahmen
9.45 *Prof. Dr. F. Rammerstorfer,* Technische Universität Wien
Abheben und Beulen von zylindrischen Behältern bei Windbelastung
10.15 *Prof. Dr. F. Fischer,* Montanuniversität Leoben
Erdbebenbeanspruchte Tankbauwerke — gelöste und ungelöste Probleme
10.45 KAFFEE
11.15 *Prof. Dr. F. Ziegler,* Technische Universität Wien
Ein praktisches Verfahren zur Wärmespannungsanalyse mit Erweiterung auf stoffllich nichtlineare Probleme
11.45 *Prof. Dr. H. Grundmann,* Technische Universität München
Zum Schutz vor Erschütterungen und Körperschall
12.15 *Dr. H. Nußbaumer,* Siemens AG, Linz
Einige baudynamische Fragen des Kraftwerkbaus
12.45 MITTAGSPAUSE

ANLAGENBAU
Vorsitz: *Prof. Dr. F. Ziegler,* Technische Universität Wien
Dr. M. Prodan, Motor Columbus, Baden, Schweiz

14.00 *Prof. Dr. G. I. Schueller,* Universität Innsbruck
Dynamische und bruchmechanische Probleme bei der Analyse der Rohrleitungen von Anlagen
14.30 *Dipl.-Ing. N. J. Krutzik,* KWU Offenbach
Dynamische Auslegung von Reaktorstrukturen bei äußeren und inneren Störfällen
15.00 *Dr. M. Prodan,* Motor Columbus, Baden, Schweiz
Anwendung bruchmechanischer und spannungsanalytischer Konzepte auf druckführende Komponenten
15.30 *Dr. F. Nahler,* VOEST Alpine, Linz
Probleme der Schalenstatik im Behälterbau
16.00 KAFFEE

NICHTLINEARE PROBLEME
Vorsitz: *Prof. Dr. H. Troger,* Technische Universität Wien
Dr. J. Affenzeller, AVL, Graz

16.30 *Prof. Dr. H. Mang,* Technische Universität Wien
Finite Elementeberechnungen im Stahlbetonbau
17.00 *Prof. Dr. W. Wedig,* Universität Karlsruhe
Parameterschätzung und Identifikation dynamischer Systeme und Prozesse
17.30 *Prof. Dr. K. Desoyer,* Technische Universität Wien
Industrieroboter — Einige spezielle Probleme
18.00 *Dr. W. Mirfter,* VEW Kapfenberg
Plastische Anomalien zufolge Änderung der Mikrostruktur
18.30 Ende
19.00 Empfang der Stadt Innsbruck und des Landes Tirol
19.30 Bankett

MITTWOCH, 27. FEBRUAR 1985

PROBLEME DES MASCHINENBAUS UND INDUSTRIELLE VERFAHREN
Vorsitz: *Prof. Dr. H. Lippmann,* Technische Universität München
Dr. K. Schwaha, VOEST Alpine, Linz

9.00 *Dr. R. Cuntze,* MAN München
Strukturberechnungen heute — Auf was muß ich achten? Was brauche ich?
9.30 *Prof. Dr. W. Schiehlen,* Universität Stuttgart
Rechnergestützte technische Dynamik
10.00 *Prof. Dr. H. Troger,* Technische Universität Wien
Nichtlineare Stabilitätstheorie und ihre technischen Anwendungen
10.30 KAFFEE
11.00 *Dr. J. Affenzeller,* AVL, Graz
Dynamische Probleme im Kraftfahrzeugbau
11.30 *Prof. Dr. K. Wohlhardt,* Technische Universität Graz
Zur Dynamik des Turbula-Mischers
12.00 *Prof. Dr. G. Schweitzer,* ETH Zürich
Magnetlader — Ein Beispiel für die Verbindung Mechanik und Elektronik
12.30 MITTAGSPAUSE

Vorsitz: *Prof. Dr. F. Rammerstorfer,* Technische Universität Wien
Dipl.-Ing. N. J. Krutzik, KWU Offenbach

14.00 *Prof. Dr. W. Schneider,* Technische Universität Wien
Strömungs- und Erstarrungsvorgänge in Metallen und Kunststoffen
14.30 *Dr. K. Schwaha,* VOEST Alpine, Linz
Möglichkeiten und Grenzen der theoretischen Analyse des Stranggießprozesses
15.00 *Dr. F. Strohmer,* VOEST Alpine, Linz
Anwendung numerischer Methoden zur Strömungsberechnung bei hydraulischen Maschinen

15.30 **PODIUMSDISKUSSION**

Vorsitz: *Prof. Dr. D. F. Fischer,* Montanuniversität Leoben
Dr. G. Gsell, VOEST Alpine, Linz
— *Dr. R. Cuntze,* MAN, München
— *Dr. M. Prodan,* Motor Columbus, Baden, Schweiz
— *Prof. Dr. H. Lippmann,* Technische Universität München
— *Prof. Dr. G. Schweitzer,* ETH Zürich

16.45 Ende der Tagung

MODRUGA KRAMSACH

EINLADUNG ZUR TAGUNG

MECHANIK UND INDUSTRIE

Kongreßzentrum Igls, Tirol
26./27. Februar 1985

Above:

One of the traditional meetings of the Bavarian-Tyrol people working in structural mechanics

30.6 ESA/ESTEC Contributions: Since 1970 for the ESA/ESTEC Space Engineering (up) beginning with Material Handbook and down

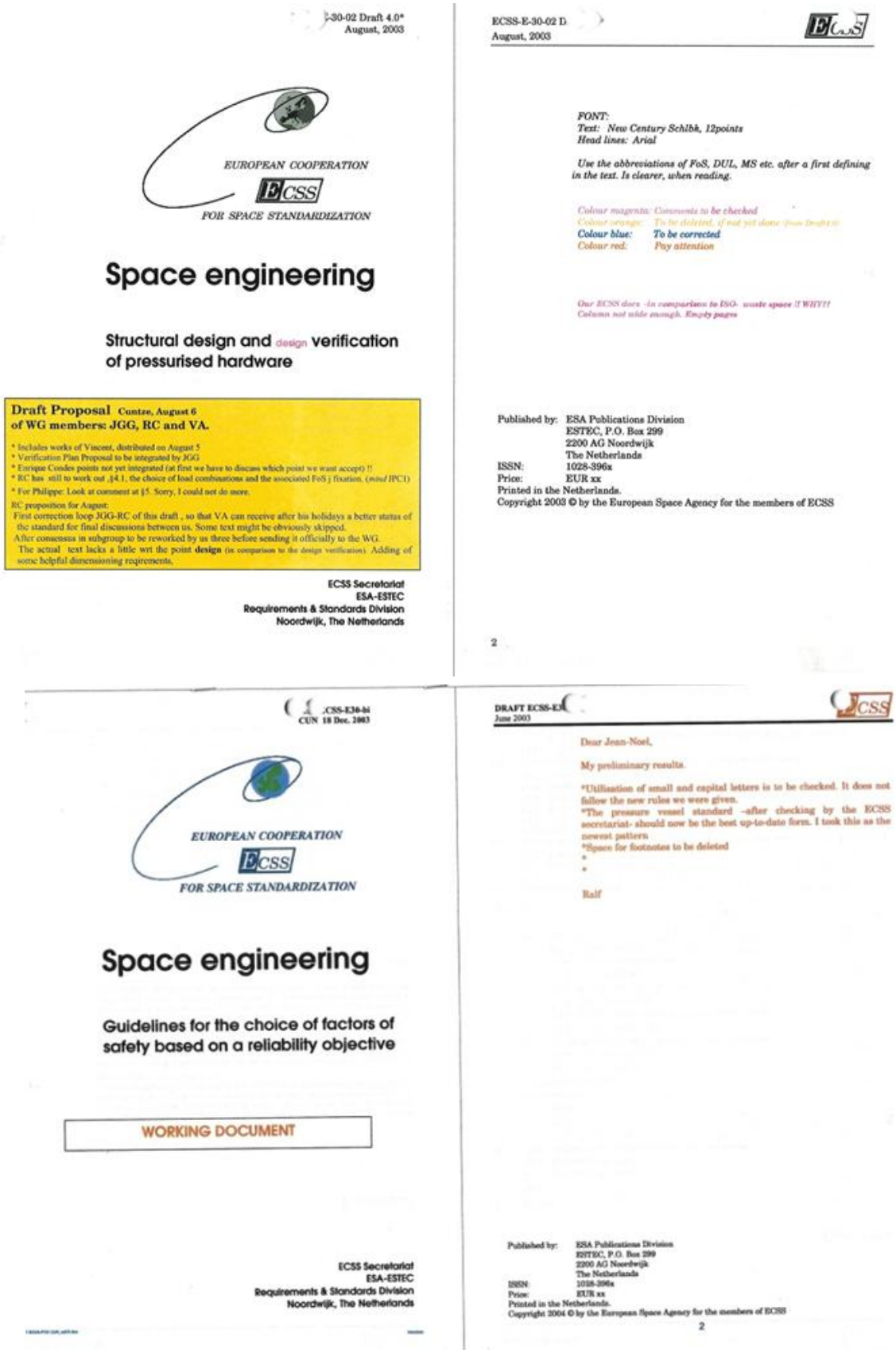

-30-02 Draft 4.0*
August, 2003

EUROPEAN COOPERATION
ECSS
FOR SPACE STANDARDIZATION

Space engineering

Structural design and design verification of pressurised hardware

Draft Proposal Cuntze, August 6
of WG members: JGG, RC and VA.

* Includes works of Vincent, distributed on August 5
* Verification Plan Proposal to be integrated by JGG
* Enrique Condes points not yet integrated (at first we have to discuss which point we want accept) !!
* RC has still to work out §4.1, the choice of load combinations and the associated FoS ∫ fixation. (*mind* IPC1)
* For Philippe: Look at comment at §5. Sorry, I could not do more.

RC proposition for August:
First correction loop JGG-RC of this draft , so that VA can receive after his holidays a better status of the standard for final discussions between us. Some text might be obviously skipped.
After consensus in subgroup to be reworked by us three before sending it officially to the WG.
The actual text lacks a little wrt the point **design** (in comparison to the design verification). Adding of some helpful dimensioning requirements.

ECSS Secretariat
ESA-ESTEC
Requirements & Standards Division
Noordwijk, The Netherlands

ECSS-E-30-02 D
August, 2003

FONT:
Text: New Century Schlbk, 12points
Head lines: Arial

Use the abbreviations of FoS, DUL, MS etc. after a first defining in the text. Is clearer, when reading.

Colour magenta: Comments to be checked
Colour orange: To be deleted, if not yet done (from Draft 4)
Colour blue: To be corrected
Colour red: Pay attention

Our ECSS does -in comparison to ISO- waste space !! WHY!!!
Column not wide enough. Empty pages

Published by: ESA Publications Division
ESTEC, P.O. Box 299
2200 AG Noordwijk
The Netherlands
ISSN: 1028-396x
Price: EUR xx
Printed in the Netherlands.
Copyright 2003 © by the European Space Agency for the members of ECSS

2

-CSS-E30-bi
CUN 18 Dec. 2003

EUROPEAN COOPERATION
ECSS
FOR SPACE STANDARDIZATION

Space engineering

Guidelines for the choice of factors of safety based on a reliability objective

WORKING DOCUMENT

ECSS Secretariat
ESA-ESTEC
Requirements & Standards Division
Noordwijk, The Netherlands

DRAFT ECSS-E
June 2003

Dear Jean-Noel,

My preliminary results.

*Utilisation of small and capital letters is to be checked. It does not follow the new rules we were given.
*The pressure vessel standard -after checking by the ECSS secretariat- should now be the best up-to-date form. I took this as the newest pattern
*Space for footnotes to be deleted
*
*

Ralf

Published by: ESA Publications Division
ESTEC, P.O. Box 299
2200 AG Noordwijk
The Netherlands
ISSN: 1028-396x
Price: EUR xx
Printed in the Netherlands.
Copyright 2004 © by the European Space Agency for the members of ECSS

2

ECSS-E-HB-32-24A
24 March 2010

EUROPEAN COOPERATION
ECSS
FOR SPACE STANDARDIZATION

Space engineering

Buckling of structures

ECSS Secretariat
ESA-ESTEC
Requirements & Standards Division
Noordwijk, The Netherlands

This Handbook has been authored and agreed upon by:

J. Arbocz, TU Delft
C. Bisagni, Politecnico di Milano
A. Calvi, ESA-ESTEC (Convenor)
E. Carrera, Politecnico di Torino
R. Cuntze, formerly MAN-Technologie
R. Degenhardt, DLR Braunschweig and PFH Göttingen
N. Gualtieri, Thales Alenia Space
H. Haller, Intales
N. Impollonia, Università di Catania
M. Jacquesson, CNES
E. Jansen, TU Delft
H.R. Meyer-Piening, ETH Zuerich
H. Oery, RWTH Aachen
A. Rittweger, Astrium EADS
R. Rolfes, Leibniz Universitaet Hannover
G. Schullerer, MT Aerospace
G. Turzo, CNES
T. Weller, Technion, Haifa
J. Wijker, Dutch Space

The valuable contributions of the following persons are acknowledged:
C. Huehne, DLR Braunschweig; D. Petry, Astrium EADS;
H. G. Reimerdes, RWTH Aachen; K. Rohwer, DLR Braunschweig;
R. Zimmermann, DLR Braunschweig.

The ECSS-E-HB-32-24 has been prepared by merging the volunteer contributions of the authors. Comments concerning the technical content of this handbook will be welcomed by the European Cooperation for Space Standardization, Noordwijk, the Netherlands, www.ecss.nl.

Sept. 11, 2001. Planes bomb the World Trade Center and the Pentagon:
Immediately after the news broke, an employee disseminating the news said, "This is a shock to the world. This will change our lives. There is only one chance, and that is for the civilized world to stand together."

And what happened in the last time??

Minutes and Status report

	Bureau Of Lightweight structures **MINUTES OF MEETING**	**Date :** Feb. 02/03 2006

Location **: INTALES at Technical University Innsbruck (A)**

Object : **ECSS-E-30-24 Buckling Handbook (BH): 4th** *meeting*

Meeting Place and Time:

- First day: Start at 9.15 , End at 18.00
- Second day: Start at 9.00 , End at 15.30.

List of Participants:

Name	Acronym	Company	Remark
Full members and supporting members			
Johan Arbocz	JA	TU Delft	-
Paul Arendsen	PA	NLR, Holland	-
Gerd Bertrand	GB	AIRBUS-Germany, Hbg.	no response.
Vincent Billey	VB	EADS-ST LM	02/03-
Chiara Bisagni	CB	Politec Milano	02/03
Adriano Calvi	AC	ESTEC	02/03
Erasmo Carrera	EC	Politec Torino	-
Ralf Cuntze	RC (convenor)	Bureau Cuntze	02/03
Richard Degenhardt	RD	DLR, BS	02/03
Bodo Geier	BG	DLR, BS	-
Nunziatino Gualtieri	NG	ALENIA Spazio	02/03
Herbert Haller	HH (secretary)	INTALES, Innsbruck	02/03
Eelco L. Jansen	EJ	TU Delft	02/03
Marie Jacquesson	MJ	CNES DLA (EVRY)	02/03
Ali Limam	AL	INSA Lyon	-
H. R. Meyer-Piening	HRMP	ETH Zuerich	02/03
Huba Oery	HO	RWTH Aachen	-
Dirk Petry	DP	ASTRIUM EADS	02/03
Hans G. Reimerdes	HGR	RWTH Aachen	-
Michael Rotter	MR	Univ. Edinburgh	02/03
Andreas Rittweger	AR	EADS Bremen	never response
Raimund Rolfes	RR	Uni Hannover	02/03
Günther Schullerer	GS	MT-Aerospace Augsburg	02/03
Guy Turzo	GT	CNES Toulouse	02/03
Jaap Wijker	JW	Dutch Space	-
Rolf Zimmermann	RZ	DLR, BS	retired
New and visiting members			
			-

Diffusion : participants + non-attending WG members + T. Henriksen + Athena Tilson.

Thanks to Herbert for providing us with such a nice weather.

Again, my thanks for the fruitful and effective discussions, for taking over work for the preparation of the BH draft, and to Michael for helping to substantiate 'our' *ECSS* handbook by inputting 'things' from 'his' civil engineering *ECCS* standard/handbook (of mixed type)!

Further Meetings planned:

5th Meeting: End of April, Bremen, EADS (Dr. Rittweger) + AIRBUS (Mr. H. Wellen)
Discussion of *Large Structure Examples,* permitted for being published in our Buckl. Hdbk.
To be fixed by RC with Rittweger and Wellen! Desired: April, 18-20
6th Meeting: planned: June 26-27, Edinburgh (Prof. M. Rotter)
7th Meeting planned: Sept. 21-22, Milano (Prof. C. Bisagni)
8th Meeting planned: first advent week (In 2006 is the latest possible begin!), Dec. 4-8 !, Munich, DP
9th Meeting ….

DISCUSSION POINTS AND RESULTS

1) **Welcome, Introduction of new WG Member** Prof. Michael Rotter

2) **Discussion of MoM, 3rd Meeting, Hannover** No comment.

3) **Discussion on next meetings** Results see above.

4) **Discussion of Action Items List (AIL), 3rd Meeting, Hannover** Status of Actions
- A19: Linked to A46 are linked concerning strategy. A common agreement is suggested. Impact from later presentation by Michael Rotter to be included.
- A49: The tracking of doc: Marking for example by letter "X" and date for the version (whole doc). Result of discussion:
  Name of doc.: (Sub)Chapter Title.(acronym date)
  Example *§1_3 Analysis Methods (NG11oct2005).*
- A62: CB tries further to get agreement from system engineer an input for §3.2
- A64: CB did some analyses and the action is closed for CB. HH tries to do some analyses till next meeting
- A70 RC provides MR and PA with info till 15.2.06
- A77 will be taken over by EJ. RC will inform TW until the next meeting

5) **Discussion of contents of Website Folders of the Buckling Handbook.**
All folders of the BH Website have been looked at and actual uploaded contents discussed.
- Direct actions are directed to the AIL
- The Hdbk draft will be uploaded as .pdf file.

6) **References**
- The reference list will be attached to each chapter
- The references will be handled by full authors name for preparation
- The citation will be changed to numbers after checking procedure of WG, tbc see A91, for final draft to be delivered before Public Review
- Equations, Tables, Figures: follow the referencing system of the other ECSS-handbooks
- Paragraphs: As it is.

7) **Checking/Reviewing of a Working Document = DRR folder** (proposition from NG)
Presentation by RC
- The DRR folder within a chapter folder is the area for submission of review results.
- In order to not forget any correction proposal, comment etc. the official Document Review Record (DRR) form sheet for ECSS Standards shall be taken, see Website: DRR for E-30-24, template and for one example(of RC), see *DRRs folder for corresponding ECSS Standards.*

Procedure if you wish to write a DRR, on chapter 2.3 e.g.,
- Download the template from the *Template Folder*
- Update the completed file named, e.g. ***DRR2_3 FlatPanels (EJ11oct2005)_RC date*** , as seen above, where RC here means the initials of the author of the DRR
- Upload the document to the folder Working Documents
§2.3 Flat Panels
Chapter DRRs.

8) **+ How to get on** BH **Website?** Repetition for PA.
GOOGLE→ECSS→Log in→My Team

9) **Presentation of Company INTALES** by HH

10) **Presentation about Shell Structures** (Analysis, Failure modes, ECCS Handbook) by MR.
Prof. Rotter was invited to present in Innsbruck his institute + past ECCS activities + how ECCS may contribute to ECSS BH.
There are valuable parts/ideas/figures/tables. However, the (legal) possibility of implementation of which will have to be considered by us when taking over something.

11) **Example for BEAM buckling** presented by HRMP
Variable cross section values – Finite Diff. on Excel Sheet
Example transferable to a solid propellant launcher on launch pad

12) **Commitment of RC and RD as compilers for §1.7**

13) **Full TOC urgently needed.**
Therefore, RC needs the not yet structured SUB-TOCs of the respective compilers in order to complete the Handbook TOC

14) **Paul Andresen may take over §2.4 Flat Panels** (information from EJ)

15) **Drafting of §1.8**
To A92: RR encourages JW to begin drafting.
Also ask the contributors to give their statements by 1st march 2006.

16) **Proposal for § 1.7 „Manufacturing Aspects"** (see Website §1.7). Presentation by RC
The proposal, necessary for the upcoming discussions of RC + RG with manufacturing engineers, has been discussed, simplified and uploaded:
New: §1.7 Buckling implications of manufacturing and assembling processes
1.7.1 Sensitive parameters for buckling
1,7.2 Metallic materials

1.7.3 Composite materials.

17) **GT shall provide a presentation on the development of a launcher** for Bremen

18) **Discussion: Should software be annexed to the handbook** for design reasons, only?
* Software: - not certified 'little' programs, no maintenance (author may be addressed)
- Teaching software and checking tools for the more sophisticated FE codes
- Not foreseen for production aspects
* Description of Software: Scope, Theory, Limitations
* Simple Program Structure.

Final Conclusion of Discussion: Decision will be taken at 5th meeting in Bremen. Majority voted for an annex of little programs on EXCEL sheets etc. ..

19) **Lack of support by ECSS Secretariat** (reported by AC)
Due to this lack the WG members are asked to produce the Figures and Tables as far as possible on their own.
Discussion on a support, again, when the preliminary Hdbk draft will be finalized for Public Review.

20) ***Which are the 'design limit states' to be applied in the non-linear buckling analysis?***
Load reached at stop of a numerical computation; deformation or strain as a usability limit state; initiation of global yielding or of local yielding; initiation of inter-fibre fracture in a lamina of the laminate; delamination; or ??
To be discussed at Bremen.

21) **TOC Structure of *Large Examples***
A structure for the body text of the Large Examples was presented by RC (see Website §3.1) and discussed. GT recommends to give Test-Analysis Correlation an own chapter.
This structure may be improved by WG members in order to find a more general structure. Of course, the structure can be tailored by each chapter compiler, if necessary.

22) **Virtual Testing shall be mentioned in the handbook**

23) **TOC Structure of *Structural Element examples***
A structure for the body text of these examples was presented by RC (see Website § 2.5, shared area) and discussed. The application was for a CFRP cylinder at DLR Braunschweig.
This structure may be improved in order to probably find a more generally applicable structure. Of course, the structure can be tailored by each chapter compiler if necessary.

24) **Subgroup fixations**
- Ali Limam, Paul Arendsen and Michael Rotter will take over work.
- Rolf Zimmermann still contributes to the sub chapters he addressed before his retirement.

Best regards, *Ralf & Herbert. 07/02/06*

ECSS-E-30 24 BUCKLING-HANDBOOK (BH) **ACTION ITEMS LIST**
Status: November, 08/09, 2006 at MT Aerospace, Augsburg for next meeting

Action		Description	Actionee	Deadline	Status
1.	**27/04/05 Noordw.**	use of verbs	EG	30/05/05	closed
2.	27/04/05	sketch on validation/verification to Work Docs	RR	15/05/05	closed
3.	28/04/05	putting MoM attachments on website	AT	asap	ongoing
4.	28/04/05	WG BH member list	RC	15/05/05	closed
5.	28/04/05	review of NWI (basis for Work Plan discussion)	all	20/06/05	closed
6.	28/04/05	plausibility check list for analyses	RC	08/07/05	closed
7.	28/04/05	input glossary/definitions from SRUCTURAL	NG	15/07/05	closed
8.	28/04/05	clarification of *Consideration of operational aspects*	AC, MK	20/06/05	closed
9.	28/04/05	clarification of the meaning "Documentation of lessons learned during design, manufacturing, verification and operations	NG, MK	20/06/05	closed
10	28/04/05	copy right problem (we use source data)	EG, AC	20/06/05	response text required
11	28/04/05	recommend. to fill in the date on 1st page of Hdbk ?	RC	20/06/05	closed
12	28/04/05	asking INSA colleagues for their vacant time	RC	20/06/05	closed
13	28/05/05	provision of ASTM website on "council on codes & standards, committee 60"	AC	20/06/05	closed, on website
14	28/04/05	fill in the Report Form for EP	RC	July 05	closed
15	28/04/05	volunteers for contributions, part 1 through 3	all	20/06/05	closed
16	28/04/05	collection: contributions to sub-chapters	all	20/06/05	closed
17	28/04/05	downloading possibility from our website: for members, only	Athena	asap	closed
18	28/04/05	template for handbook from secretariat	EG. AC	20/06/05	**open**
19	28/04/05	flow chart How to run buckling	HH	20/06/05	closed
20	28/04/05	search for further volunteers for checking (especially those which cannot attend the meetings)	all	20/07/05	ongoing
21	**23/06/05 Noordw.**	asking HRMP for a Part 3structure example or a Part 2 structural element example	RC	01/09/05	closed
22	23/06/05	contributions from EADS-ST France (Aerospatiale) required for §3.1	VB	15/09/05	closed
23	23/06/05	issue of an address list incl. acronyms (add to next MOM)	RC	15/09/05	closed
24	23/06/05	does ESTEC perform Structure buckling tests?	AC	15/09/05	closed
25	23/06/05	interviewing Dr. Vollrath, VDI, for taking VDI2014 Guideline as a Reference Doc and its§6.2, Stability, as a Work Doc	RC	01/09/05	closed
26	23/06/05	example Part 3: from Columbus receivable? NO!	NG	15/09/05	closed
27	23/06/05	giving V. Billey and B. Geier full access to website	Athena	asap	closed
28	23/06/05	processing and distributing of a Work Plan draft	RC	01/08/05	closed
29	23/06/05	adding NASA docs to website AC provides link	EJ, AC	21/07/05	closed
30	23/06/05	interviewing Dr. Clormann, MAN Technologie, for examples Part 3 (Lox-Tank, Front Skirt, Booster,..);	RC	15/09/05	Closed and linked to A32
31	24/06/05	interviewing Hr. Wellen, (fuselage shells, composite bulkhead,..), §3.3	RC, GV	15/09/05 **11/2006**	**pending**
32	24/06/05	interviewing Dr. Rittweger, EADS-ST Bremen for examples, Part 3 (link to A 30 !)	RC	15/09/05	closed (AR agreed)
33	24/06/05	interviewing Prof. Schwarmann, Airbus, for examples at Bremen and Hamburg	RC	15/09/05	closed
34	24/06/05	attempting to put GARTEUR results on website: BG checks potential contributions (Nov. Hannover)	BG, RD	15/02/06	closed
35	24/06/05	upload Koiters article on curvature parameter	EJ	01/08/05	closed
36	24/06/05	PDF draft of BH to website before each meeting	RC	10/09/05	ongoing
37	24/06/05	presentation on COCOMAT (design verification, glossary, philosophy,..)	AK	2nd meet.	closed
38	24/06/05	wrt. definitions adding BG article on Structural Behaviour to Work Doc	BG	01/08/05	closed
39	24/06/05	setting up and distributing a list of the Work Docs (although still on website)	HH		closed
40	24/06/05	setting up and distributing a list of the Reference Docs (although on website)	HH		closed
41	24/06/05	finding a specialist incl. compiler for § Manufacturing Aspects (see SMH group)	GT, RC, RD, all	asap **09/2006**	**pending**
42	24/06/05	informing RMP wrt Zürich on meeting requirements	RC	01/08/05	closed
43	24/06/05	implementing *DRD Buckling* as Work Doc	NG	01/08/05	closed
44	24/06/05	wrt "Engin. language": Can we get a PDF of Bush-Almroth?? If yes, add to Reference Docs	EJ	01/08/05	closed
45	24/06/05	wrt accurate property input for all materials (ductile aerospace metals, usually brittle composites, ductile GLARE hybrid composite, etc.): generate a table for the elasticity properties for the strength properties for the hygrothermal properties	 RC RC RC	 01/09/5	 closed
46	**15/09/05 Zuerich**	handbook flow chart at beginning is required	HH	asap	closed
47	15/09/05	checking whether the ECSS ordering terms for the Handbook (not a standard!!): *paragraph, section, chapter* are correctly used ???	EG	asap	closed
48	15/09/05	DRD on Buckling is added to website	RC	01/08/05	closed
49	15/09/05	Tracking of *Buckling HB* draft changes	ECSS + WG, AC	asap 15/01/06	**Still under discussion**
50	15/09/05	Preparation of general list of symbols (collecting from members) as basis for discussions, this list will be enhanced if necessary	RC	1/11/05	closed
51	15/09/05	Input for action 50, Send to RC (nothing received)	all	23/09/05	closed
52	15/09/05	Discussion between NG + RR about §1.1 to finalize this point	NG, RR	30/09/05	closed
53	15/09/05	Ask HGR and HO to make a TOC §1.4 to be discussed at 3rd meeting	RC	15/10/05	closed
54	15/09/05	§1.5.1 (new), §1.5.3 proposal for draft	RC	4/11/05	closed
55	15/09/05	§1.5.2 proposal for draft	CB	4/11/05	closed
56	15/09/05	§1.6.3 proposal for draft (see A100)	JB, RD	15/10/05	closed
57	15/09/05	Ask JB for contribution to §1.7 (JB cancelled membership)	GT	15/10/05	closed
58	15/09/05	Comments about §1.9 to CB	MJ, GT	15/10/05	closed
59	15/09/05	Information from RC to compilers: Tanchum Weller for §2.3 , Bodo Geier for §2.4, Jerome Buffe for several chapters in PARTs 1 to 3.	RC	23/09/05	closed

Pressurized Hardware

Structural meeting 2004
Adriano Calvi, Nuntiatino Gualtieri, Michel Klein

FoS 2004

Förderung: bmb+f

SimMAT SimPRO SimBAU

Projektträger des BMBF und BMWi

Werkstoffe in der Simulation

Produktinnovationen durch
gezielten Einsatz
der Werkstoffsimulation

Berichte von den MaTech - Kompetenzzentren

4. November 2004

Projektträger Jülich
Geschäftsbereich PTJ-NMT
Bearbeiter: Dr. C. Wadewitz, 5.12.2003

Termin, Ort	27. November 2003, Max-Planck-Institut für Polymerforschung, Mainz
Thema	4. Sitzung des Lenkungsausschusses für die BMBF Kompetenzzentren „Materialsimulation“ (FZK: 03N6015), „Prozesssimulation“ (FZK: 03N6016), „Bauteilsimulation“ (FZK: 03N6017)
Teilnehmer	**Mitglieder des Lenkungsgremiums:** Prof. Cuntze (MAN Technologie AG), Prof. Arzt (MPI für Metallforschung), Prof. Suter (ETH Zürich), Prof. Haldenwanger (AUDI AG) **Vertreter der Zentren:** Prof. Kremer (MPI f. Polymerforschung), Dr. Besold (MPI f. Polymerforschung), Prof. Michaeli (IKV Aachen), Herr Franz (IKV Aachen), Dr. Schmitt (Fh IWM Freiburg)

30.6 Author-founded Germany-wide group Betriebsfestigkeits-Nachweis BeNa *(in 2010)*

Considering the high-performance UD lamina-composed laminates the classical fatigue tests are performed on laminates. The idea of the author-founded Germany-wide group BeNa (in 2010) with its members however was to base fatigue life prediction 'embedded lamina-wise' in order to be more general in fatigue life design in the future and to save test costs and time. Associated test specimens shall capture the interface effect of the lamina embedded in the laminate.

„Composite-Fatigue"-Gruppe : 2nd Meeting, at ISD Hannover:

Both, J. (LLB, TUM) , Cuntze, R. (CCeV) , Heislitz, A. (KLuB, TU-Da) , Himmel, N. (IVW, TU-KL) , Horst, P. (IFL, TU-BS) , Jansen, E. (ISD, LUH) , Koch, I. (ILK, TU-DD) , Krüger, H. (ISD, LUH) , Laveuve, D. (LBF, Fraunhofer) , Rolfes, R. (ISD, LUH) , Schürmann, H. (KLuB, TU-DA) , Schulte, K. (TU-HH) , Trappe V. (BAM).

Ana at later meeting at Dresden:

TU Hamburg-Harburg: Prof. Schulte, Herr Kosmann; Uni Hannover: Dr. Jansen; TU Dresden: Prof. Gude, Dr. Koch; TU Braunschweig: Prof. Horst (leader), Herr Greif; IKV Aachen: Herr Marder; IVW Kaiserslautern: Dr. Magin; KLuB Darmstadt: Prof. Schürmann, Frau Heislitz, Frau Feldten; LBF Darmstadt: Prof. Büter, Herr Laveuve; BAM: Dr. Trappe; TU München: Herr Both**.**

30.7 "Project leader of the funded Research on UD Fracture Criteria", meaning on **Puck 's Strength Criteria**

Kopie zur Info.: GHK, IKV, LLK, RWTH, Prof. Puck 30.11.93

FORSCHUNGSZENTRUM JÜLICH GmbH KFA

FORSCHUNGSZENTRUM JÜLICH GmbH · PLR · D-52425 Jülich
Fracht-/Paketanschrift: Leo-Brandt-Straße, D-52428 Jülich

MAN Technologie AG
Hauptabteilung Strukturanalyse
Herrn Dr. R. Cuntze
Postfach 50 04 26

80997 München

Projektträger
Material- und Rohstofforschung
des Bundesministeriums für
Forschung und Technologie
PLR

Ihre Nachricht vom / Zeichen	Bei Beantwortung bitte angeben	Telefon-Durchwahl (02461) 61	Telefax (02461) 612398	JÜLICH
	PLR/3/Dr.Pe/Hp 3A 312551093	5866 Dr. Peter		23.11.1993

Förderung von Forschungsvorhaben im Programm Materialforschung

Ihr Projektantrag "Zum verbesserten Festigkeitsnachweis von FKV-Bauteilen", Aktenzeichen 3A 312551093

Sehr geehrter Herr Dr. Cuntze,

wir haben Ihren o. g. Antrag geprüft und sind der Auffassung, daß das Vorhaben in der vorliegenden, fachlich hochwertigen Fassung dem Gutachterausschuß des BMFT zur weiteren Beurteilung vorgelegt werden kann. Die detaillierte Projektbeschreibung vermittelt uns den Eindruck eines anspruchsvollen, innovativen F+E-Vorhabens, das auch wesentlichen Kriterien eines neuen BMFT-Förderprogramms entspricht.

Bezüglich der zur Zeit resultierenden Gesamtförderquote von 69 % möchten wir aber darauf hinweisen, daß gemäß EG-Beihilferegelung für industrielle Grundlagenforschung eine Förderquote von maximal 50 % eingeräumt wird. In Anbetracht des hohen Institutsanteils und damit des vergleichsweise hohen Anteils an stark grundlagenorientierten Arbeiten, die auch mit einem höheren wissenschaftlichen Risiko verbunden sind, halten wir eine Förderpräferenz von 10 % für möglich, so daß von einer Gesamtförderquote von jedoch höchstens 60 % ausgegangen werden kann. Dies ist zu berücksichtigen.

Hinsichtlich der Anwendungsrelevanz Ihres Vorhabens werden vorwiegend Strukturen für die Luft- und Raumfahrt angesprochen. Wir sind der Meinung, daß die Bedeutung wesentlich breiter zu sehen ist. Das ist vor allem deshalb besonders wichtig, weil im Rahmen der Vorbereitung des neuen BMFT-Programms festgelegt worden ist, daß Werkstofforschung für die Luftfahrt innerhalb dieses Programms nur dann als förderwürdig gesehen wird, wenn auch ein erhebliches Anwendungspotential für bodengebundene Verkehrssysteme gegeben ist. Dies sollte deutlich herausgearbeitet werden. Daraus folgt die Notwendigkeit der Beteiligung eines "terrestrischen Anwenders" als

Vorsitzender des Aufsichtsrates: Parlamentarischer Staatssekretär Bernd Neumann · Vorstand: Prof. Dr. Joachim Treusch (Vorsitzender), Georg v. Klitzing (stellv. Vorsitzender), Prof. Dr. Ernst Pöppel, Prof. Dr.-Ing. Rolf Theenhaus · Sitz der Gesellschaft: Jülich · Eingetragen im Handelsregister des Amtsgerichts Jülich Nr. HR B 57
Bankkonten: Landeszentralbank, Zweigstelle Düren: 39508060 (BLZ 39500000) · Kreissparkasse Düren, Niederlassung Jülich, 40030 (BLZ 39550110) · Westdeutsche Landesbank Köln: 158964 (BLZ 37050000) · Postgiroamt Köln: 1865 31-507 (BLZ 37010050) · Telex-Nr.: 833556 kfa d · Tel.-Sammel-Nr. (02461) 61-0 · Telefax-Sammel-Nr. (02461) 615327

Cardanwelle für Golf - Synchro, Drehfeder, Widerstandsklotz, ...

Anlage 3

Berichtszeitraum von Juli 95 bis Juni 96	PROJEKTBERICHT	
Stand vom:		

Projekt:	Projekt-Nummer:	Projektleiter:	Planung/Kontrolle:
ZFB Kriterium	B 099207	Szelinski	Dr. Cuntze

Auftraggeber:	Laufzeit des Vorhabens:
BMFT / MAN-MT (47 % / 53 %)	von Mai 94 bis Okt. 96

PROJEKTSTATUS:

1. TECHNIK

1.1 Abgeschlossene Arbeiten, laufende Arbeiten:
Die Aufgaben wurden im Laufe des BZ zügig abgearbeitet, und lagen im wesentlichen im Plan. Verschiedene Untersuchungen im Detail waren bei den Standardprobekörpern noch nachzuziehen wie z.B. die Ermittlung der Referenzflächen, die Ausdeutung der Weibull-Effekte und die Erfassung der möglichen Unterschiede zwischen AWV und einsinnig UD-gewickelten Rohren. Bei den Sonderprobekörpern standen die Quetsch-Nut und der gekrümmte Biegebalken zur Bearbeitung an. Beim gekrümmten Biegebalken zeigte sich, daß durch den Einfluß der Schubspannung der Bruch nicht exakt im Scheitelbereich der Trägers erzeugt werden konnte, auch zusätzliche Maßnahmen, die die Schubspannung reduzieren sollten, waren nicht frei von lokalen Störungen. Die Quetsch-Nut, die eine Aussage über die maximale Querbeanspruchung liefern soll, wird noch bearbeitet. Zur besseren Bewertung der Versuchsergebnisse sind noch einige theoretische Untersuchungen, gekoppelt mit FEM-Berechnungen, notwendig.

1.2 Kritische Probleme, Schwierigkeiten:
Auf Anraten der projektleitenden Stelle in Jülich ist ein Aufstockungsantrag gestellt worden, der die Thematik vertiefen und ausweiten sollte. Die Bearbeitung des letztlich doch - aufgrund fehlender Mittel - abgelehnten Aufstockungsantrages, dessen Bewilligung nach den ersten Informationen aus Jülich nur noch eine Formsache zu sein schien, hatte Kosten verursacht und Stunden verbraucht, die zum Ende des Projektes nun leider fehlen.

1.3 Vorgesehene Maßnahmen, Empfehlungen zur Behebung der Schwierigkeiten:
Die abschließenden Aktivitäten müssen so zusammengefaßt und gestrafft werden, daß der zu erwartende Mittelmehrbedarf minimiert wird.

1.4 Fertigstellungsgrad in % (geschätzt): 90 %

2. Zeit

2.1 Sollterminplan: ☒ gehalten ☐ Verschiebung um ..... auf .....

2.2 Erreichte Meilensteine:
sind im Detail nicht spezifiziert.

2.3 Entstandene Berichte: (Kurzfassung beifügen)
3. und 4. Halbjahreszwischenbericht (Kopien beiliegend), zahlreiche Technische Notizen, Entwurf des Technischen Abschlußberichts in der Form eines VDI-Fortschrittsberichtes (zur Veröffentlichung)

3. Kosten

3.1 Kostenstand nach Berichtszeitraum:
(Vergleich: Mittelfreigabe für Projekt und Kostenverlauf)

	Freigabe Soll [TDM]	Kosten Ist [TDM]
Freigabe bzw. Kostenanfall im Berichtszeitraum	945	945
Freigabe bzw. Kostenanfall kumulativ	1.654	1.654
Obligo bis einschließlich Berichtszeitraum		
Gesamtfreigabe bzw. -Kostenanfall einschl. Berichtszeitraum		

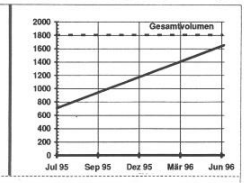

3.2 Mittelmehrbedarf:
☐ nein ☒ wahrscheinlich TDM 40 000 ☐ sicher TDM .....

3.3 angefallene Stunden: eigener Bereich 2960 andere Bereiche 1675

Above very good evaluation of a research proposal was then confirmed by good results and these results were finally published in detail in a VDI booklet ▶

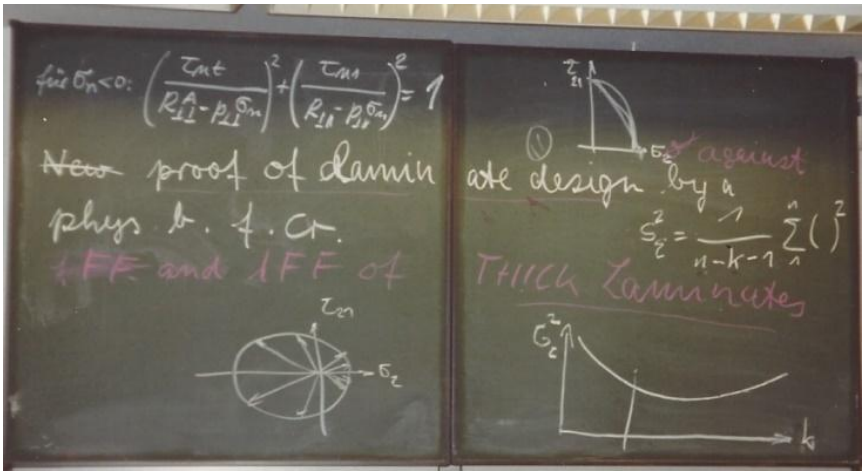

Meckbach,
Rita Jeltsch-Fricker,
RüdigerRackwitz

Lothar Kroll,
Alfred Puck,
Rita Jeltsch-Fricker

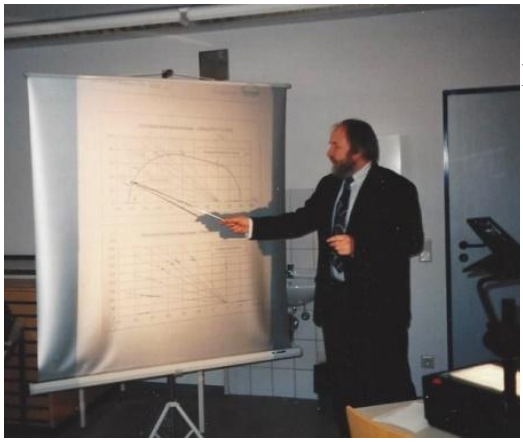

Bernd Szelinski, MAN Part project leader, informing the team.

(right) Our mathematician lady honoured

Gollwitzer, Meckbach, Szelinski , sorry, Kroll

Puck, Jeltsch-Fricker, Rackwitz

Puck, Sorry, Deska, Peter

<u>Below</u>, ICCM 11 "Failure Criteria Panelists" and ESA Exchange Group

TELAC

Technology Laboratory for Advanced Composites
Department of Aeronautics and Astronautics
Massachusetts Institute of Technology
77 Massachusetts Avenue
Cambridge, Massachusetts 02139

Paul A. Lagace, Director
Professor of
Aeronautics and Astronautics
MacVICAR FACULTY FELLOW

ROOM 33-301 (617) 253-3628
TELEX 92-1473 FAX (617) 253-9301
EMAIL pal@mit.edu

MEMORANDUM

To: Participants in the ICCM-11 Failure Criteria Panel
(Chris Chamis, Ralf Cuntze, John Hart-Smith, Michael Hinton, Stephen Tsai)
From: Paul Lagace and Mark Spearing
Date: July 13, 1998
Re: Follow-up on our panel

It is nearly exactly a year ago that we were in Australia for ICCM-11 and we had that very interesting and invigorating panel session and discussion that drew many people that one evening. As we promised then, one of our hopes was to write a paper based on the session. I quote the original "charge/purpose" of the forum which was sent to each of you in preparation for our session:

"The PURPOSE of the forum is to discuss the current status of composite failure criteria with a focus on what we need to do to better our understanding and capability in this regard. Although this clearly begins at the material level, the ultimate objective is to predict failure of composite structures, so we should orient discussion there as well. I should also note that the emphasis should be on what further needs to be done. Clearly each of you needs to indicate where you feel we are now and what approach is proper. But we should not get caught up in a discussion of history. Rather, we need to emphasize the present state and the future. I am further hoping that we may be able to reach some level of consensus on these items by the end of the forum and that this may even lead to a co-authored paper amongst us. But we'll see how things go in the forum before discussing that."

We have, indeed, moved forward in that regard. This has been delayed somewhat by the sabbatical I took during the fall and I apologize for that delay. But we are now ready to send out this material to you, ask you to review it, and get back to us with some comments and answers.

We have reviewed the notes that Mark took at the session and have talked about it extensively. Based on this, we propose the following title and outline for the paper:

"COMPOSITE FAILURE CRITERIA-WHERE WE ARE; WHERE WE NEED TO GO"

1. Introduction
2. Forum (Panel, Charge, etc.)
3. Common themes
4. Key Areas of Disagreement
5. Identified Areas for Further Work
6. Summary

As to the writing of the paper with this outline, Mark and I would write sections 1 and 2 from the material we agreed to prior to the session. After receiving your comments, we would take a first cut at sections 3, 4, and 5 based on the notes that are included with this letter. As previously noted, the first is a set of "minutes" of the session. But of greater importance with regard to writing the paper is an extraction of the "key points" (common themes, key areas of disagreement, identified areas for further work) which we have made from the "minutes". These key points are in the document entitled "ICCM Failure Panel Summary.

The immediate question is whether you are still interested in being a part of this paper jointly authored by all the participants in this panel session. Our hope is that the answer is yes. If so, we ask that you do the following at this point in time:

1. Review the notes and make any corrections.
2. Review the points for sections 3, 4, and 5, in the document titled "ICCM Failure Panel Summary" and make any corrections, additions, etc.

It would help to receive this by mid-September, if not sooner. From there, we will draft the entire paper and send this draft to you for comments and edits. This process will continue until we converge on a paper to which we can all agree. This work up front will make that convergence process easier. We would also like to conduct this by email to make communication easier (we can even send around everyone's comments). So please let us know your current address and any "inabilities" in terms of reading attached documents.

This paper can be a real service to the composites community by enumerating the areas of agreement, disagreement, and further needed work with regard to failure and failure criteria. We hope that you agree and that you do wish to continue to work with us on this paper.

Please contact us by phone or email if you have any immediate questions or thoughts. Both of us look forward to your response.

enc. (2)

PAL/dab

esa

TO: EXCHANGE GROUP MEMBERS and affiliates
Messrs:
R. Cuntze MAN
H. Krings MAN
A. Jimenez CASA
J-P Vialaneix CNES Toulouse
P.Taquet/D.Bouvier SONACA
C.J. Verberne RAUFOSS
P. Fornari ALENIA TORINO
V. Detremmerie SABCA
M. Teare MMS Stevenage
R.W. van der Ven FOKKER LEIDEN
D. Bashford ERA Technology
E. Lettner ICI FIBERITE EUROPE
Ms J. Wilson/R. Hussey RJ Consultants
J. Bolz (DASA-RI Bremen)
D.J. Light (Bae Airbus -Bristol)
H. Aamodt (Kongsberg)
L.J.B Peeters (Stork)

INTERNAL: C. Stavrinides, M. Klein A.Pradier T. Henriksen M. Judd G.Ramusat B.Dunn R. Raynal W. Pinter-Krainer

FROM: D.C.G. Eaton Structural Engineering Section - YME
Fax: +31 71 565 5427
Phone: +31 71 565 3989

DATE: 19 Feb 1997
REF: YME/DCGE/2689

1. FORMULATION OF THE TASK

Requirement:
Meet a specified natural frequency

Reasons:
. To avoid vibration coupling of connected structural parts.
. To fit an eigenfrequency into a poor part of a power spectrum

Model to outline the single Problems:
. Vibrating cantilever, narrow strip of a plate
. Calculation of its lowest natural circular frequency $\bar{\omega}_1$

Visualization of the Task:

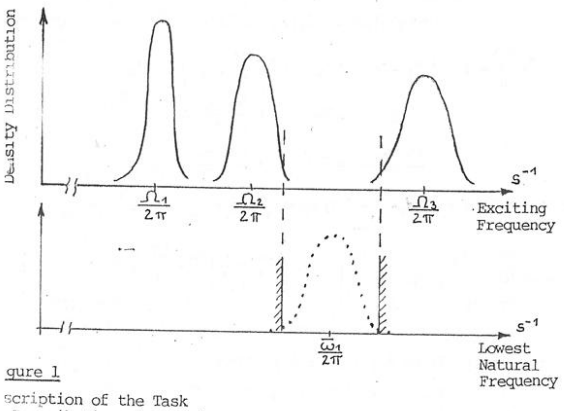

gure 1
scription of the Task
ribution of Exciting Frequencies
Density Distribution of the Stochastic Natural Bending Frequency and Frequency Window to me met

EUROMECH COLLOQUIUM 219 September 23-26, 1986 , Kasse

INFLUENCE OF THE
VARIATION OF STRUCTURAL PROPERTIES ON THE
PROBABILITY OF A COMPOSITE PLATE TO MEET A
TARGET EIGENFREQUENCY

by

Ralf Georg Cuntze and Martin Grimmelt
MAN Technologie GmbH, D 8000 München

OVERALL OBJECTIVE:

Design of structures with respect to specified reliability values (Safety Requirement in Space Craft Vehicles Design Spezification)

SPECIFIC OBJECTIVE OF THIS PAPER:

Determination of the probability that the scattering natural frequency $\bar{\omega}_1$ will lie within a specified window.

CONTENTS OF THE TALK:

1) Formulation of the Task
2) Description of the Mechanical Model with
   . Differential equations of the dynamical model
   . Essential structural parameters of the plate (laminate)
   . Structural properties of a layer (ply)
3) Probabilistic Approach with Description of
   . Stochastic Model
   . Reliability Model
   . Solution procedure
4) Example
   . Description of performed test specimens and properties
   . Results form theory and tests
   . Comparison of results

Conclusions of Investigation

GAMM/IFIP - Workshop on
STOCHASTIC OPTIMIZATION: Numerical Methods and Technical Applications
Neubiberg/München, May 29 - 31, 1990

SCIENTIFIC PROGRAM

The registration and all lectures take place in room 0301, building 33 (see map).
The Reception and the Conference Dinner take place in the Casino (OHG, building 61)

Tuesday, May 29

8.00	- 9.00	Registration	
9.00	- 9.15	Opening Session	
Chairman: K. Marti			
9.15	- 10.00	E.A. McBEAN:	Optimization Modelling for Acid Rain Abatement Decisions
10.00	- 10.30	COFFEE BREAK	
10.30	- 11.15	H.I. GASSMANN:	A Problem of Forest Management under Uncertainty and Numerical Techniques for its Solution
11.15	- 12.00	W. RÖMISCH:	A Stochastic Programming Model for Optimal Power Dispatch: Stability and Numerical Treatment
12.00	- 13.30	LUNCH	
Chairman: P. Kall			
13.30	- 14.15	H. NIEDERREITER:	Lattice Rules for Multiple Integration
14.15	- 15.00	K. FRAUENDORFER:	The Simplicial Approximation Scheme and its Relation to other Approaches for Two-Stage Stochastic Programs
15.00	- 15.30	COFFEE BREAK	
15.30	- 16.15	J. MAYER:	Computational Techniques for Probabilistic Constrained Optimization Problems
16.15	- 17.00	S. FLÅM:	Exact Penalty Functions in Single-Stage Stochastic Programming
18.00		RECEPTION	

Wednesday, May 30

Chairman: H. Eschenauer			
8.30	- 9.15	R.G. CUNTZE:	Structural Design, Optimization and Reliability Justification. A Comparative Study related to the Example: Axially Loaded Strut
9.15	- 10.00	R. RACKWITZ:	Practical Strategies to Identify Local Minima in Reliability Calculations
10.00	- 10.30	COFFEE BREAK	
10.30	- 11.15	A. VASARHELYI:	Collapse Load Analysis and Optimal Plastic Design by Stochastic Programming
11.15	- 12.00	G. PFLUG:	Optimization of Discrete Event Processes
12.00	- 13.30	LUNCH	
Chairman: G.I. Schuëller			
13.30	- 14.15	R. SCHULTZ:	On the Structure of the Objective Function in a Linear Two-Stage Stochastic Integer Program
14.15	- 15.00	N. SIMAKOV:	Adaptive Stochastic Model for the Analysis and Forecast of Energy Consumption
15.00	- 15.30	COFFEE BREAK	
15.30	- 16.15	N. BABA:	Three Approaches for Solving the Noise Corrupted Multiobjective Optimization Problem
16.15	- 17.00	F. KURSAWE:	A Variant of Evolution Strategies for Vector Optimization
18.00		CONFERENCE DINNER	

THURSDAY, May 31

Chairman: J. Mayer			
8.30	- 9.15	N. BABA:	A Stochastic Optimization Approach for Training the Parameters in Neural Network
9.15	- 10.00	E. PLÖCHINGER:	Step Size Selction in Robbins-Monro Processes Considered as a Problem of Stochastic Dynamic Programming
10.00	- 10.30	COFFEE BREAK	
10.30	- 11.15	K.-J. BÖTTCHER:	Efficiency Comparison of Stochastic and Deterministic Search Methods
11.15	- 11.30	CLOSING SESSION	

30.8 European Projects

BRITE/EURAM project 4194, 1991

Sorrs, sorry,,Santos, sorry, Rackwitz, ?,

Szelinski, Gierlinski, Gollwitzer, ?, sorry, Palle Thoft- Christensen , Else Thoft-Cristensen, Nigel?

Out of the Summary from the Tender:

The methodologies and software developed during the project will be specialized to applications in the aerospace industry. However, many aspects of the work have much wider potential application. In general, all industrial sectors which involve high performance as safety critical structures will benefit. The benefits come from improved performance, stemming from reliability-oriented design and shortened development times through the use of interactive optimization.

In the last decade or so the lead times from concept to final design of structural components have been reduced, often dramatically, as a result of CAD techniques. Typical of these benefits are:

- A concurrent flexible design technique has the potential to significantly reduce mass and fabrication costs
- Utilization of an effective design tool, which combines sensitivity and reliability concepts, will promote a better understanding of the influence of essential design parameters on the structural behavior. It also will lead to improved efficiency in the design phase of the development of a structural product
- Gain of a strategic advantage as a result of designing with less risk and with considerable time saving.

"RELIABILITY-BASED OPTIMAL DESIGN METHODOLOGY WITH APPLICATIONS TO ADVANCED AEROSPACE STRUCTURES"

(RELOPT DESIGN)

Contract BREU-CT91-0456 (WNSN)
B/E-4194

B/E-4194/B(0)-1.2 MAN

TABLE OF CONTENTS

Summary

I Requirements for Reliability-based Analysis and Optim. of Aerospace Structures
I1 Introduction
I2 Traditional Design Concept
I3 Modern Design Concept
I4 General Description and Way of Analysis of the Large Example Structures
I5 Requirements for the Development of the Integrated Design SW-product CARBOS
IA Guiding Case Study "Filament wound hollow strut under tension and bending"

II Data Acquisition and Statistical Analysis
II1 Definition of basic variables and data base structure
II2 Data acquisition and evaluation
II3 Statistical analysis procedure

III Design Sensitivity Analysis
III1 Sizing design sensitivity analysis
III2 Shape design sensitivity analysis
III3 Software development

IV Reliability Modelling
IV1 Load models
IV2 Methodology for identification of failure modes and critical points
IV3 Time-invariant and time-variant strength models and failure criteria
IV4 Numerical techniques for time-variant and time-invariant reliability
IV5 Software development

V Interactive Reliability -based Design Optimisation
V1 Reliability-oriented optimisation
V2 Software development

VI Computer System Integration and Case Studies
VI1 Integration of data base with reliability and optimisation software
VI2 Testing and verification of reliability software
VI3 Development of visual aids for control of the computational process
VI4 Setting up model and all necessary data; analysis of test cases

A1 Notions, Abbreviations and Glossary
A2 Literature and Internal Reports
A3 Theoretical Manual
A4 User Guide
A5 Benchmarks for Verification of the Single Modules
A6 Benchmarks for Qualification of CARBOS
A7 Applications

Annexe IA: GUIDING CASE STUDY:

Filament Wound Hollow Strut under Tension and Bending

CONTENTS

1. **Introduction**
2. **Input for the Design**
   - 2.1 Structure Identification
   - 2.2 Design Requirements, Dimensioning Load Cases
   - 2.3 Factors of Safety and Reliability Constraints
   - 2.4 Design Allowables and their Determination
3. **Deterministic Conceptual Design (Phase 0 "Concept" or "Study")**
   - 3.1 Mechanical Model incl. State Functions (MM)
   - 3.2 Definition of Initial Data Set of Design Parameter
   - 3.3 Pre-Dimensioning incl. Material Choice
   - 3.4 RAMS Functional Analysis, FMECA and Critical Points Log
   - 3.5 Reliability Allocation for the Cross Section of the Strut
   - 3.6 Determination of Initial (Deterministic) Design Space
4. **Probabilistic Preliminary Design (Phase I "Prel. Design Development")**
   - 4.1 Elaboration of Prel. Stochastic Data Set (StM) and Prob. Design Space
   - 4.2 Logical Modelling of the Strut's Failure System
   - 4.3 Design Sensitivity Analysis (DSA)
   - 4.4 Plan of Design Development Tests (material, manufacture trial, load)
   - 4.5 Reliability Analysis (REL)
   - 4.6 Reliability based Optimisation (Sizing by OPT)
   - 4.7 Assessment of Results and Choice of Design
5. **Proof (Justification) of Final Design (Phase II "Design Development")**
   - 5.1 Evaluation of Design Development Tests (StA)
   - 5.2 Final Stochastic Data Set
   - 5.3 Design Sensitivity Analysis
   - 5.4 Reliability Oriented Optimisation
   - 5.5 Assessment of Results and Fixing of Final Design
   - 5.6 Justification Computations with Reliability Check
6. **Qualification of Structure by Test (Phase III "Design Verification")**
   - 6.1 Plan and Performance of the Qualification Test
   - 6.2 Test Results and Evaluation of the Qualification Test
   - 6.3 Qualification Document with Compliance Matrix

Figures

Annexe

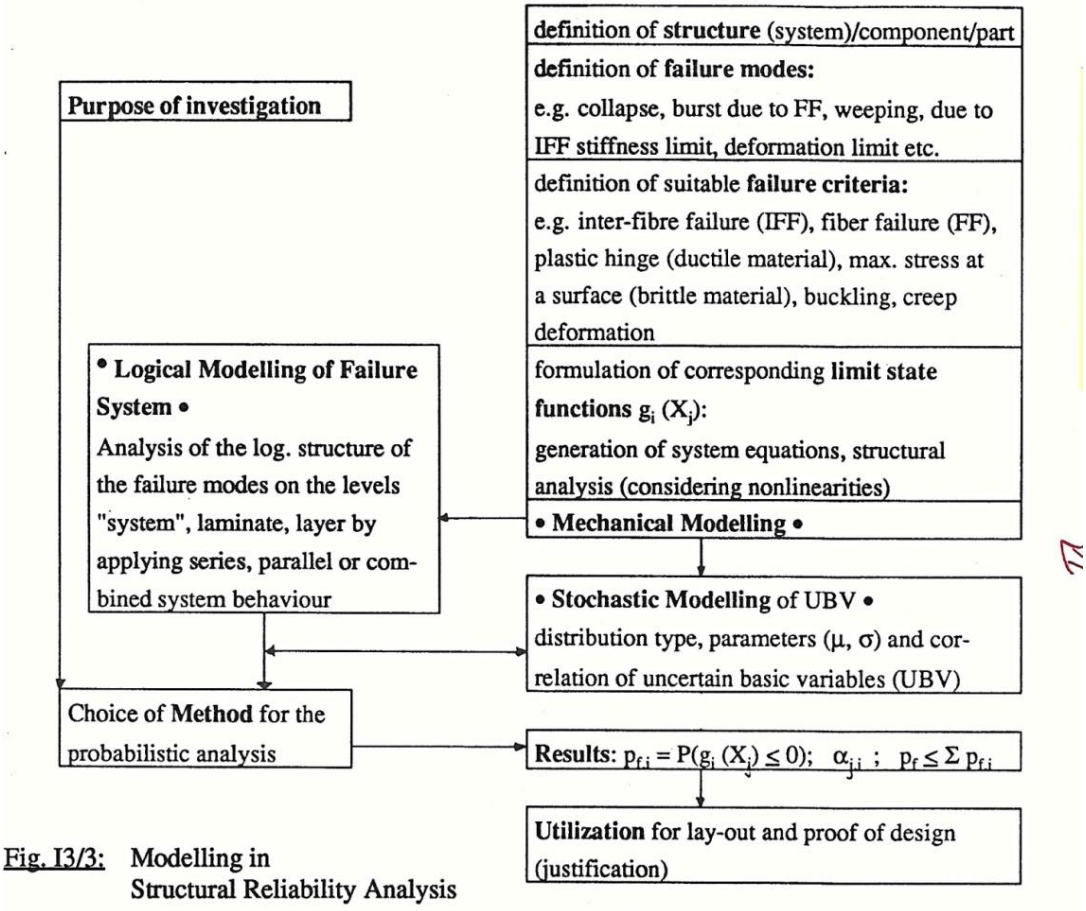

Fig. I3/3: Modelling in Structural Reliability Analysis

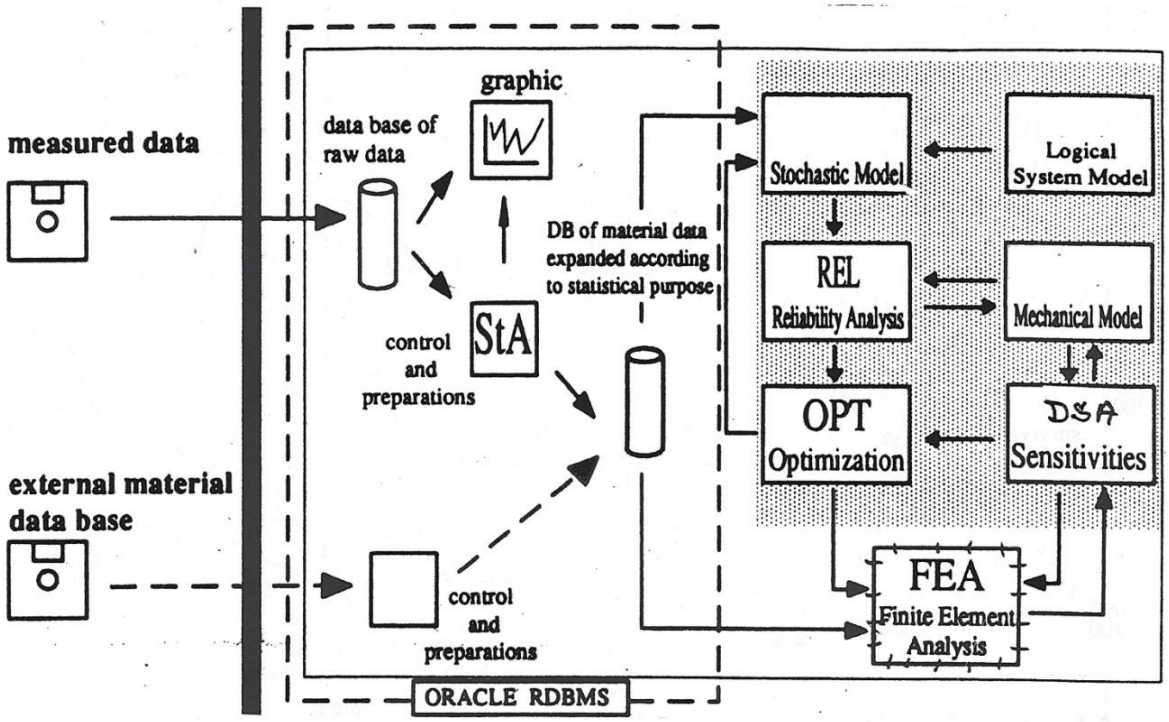

Fig. 4/10: Flow Chart of CARBOS for Reliability Based Optimisation (to be reworked)

8.30	Majela	: Expert Systems in Structural Modelling and Desig
	Moeltzel	: An Interactive Hybrid System Approach to Near Optimal Design of Mechanical Components
9.15	Hartmann	: Application of AI-Tolls for Re-Analysis Within Structural Optimization
	Reitman	: Optimization Problems on the Boundaries of Structural Engineering
10.30	Cuntze	: Reliability - Oriented Optimization With Application
	Mlejnek	: Some Contributions to Optimal Design Using Approximate Explicit Behaviour Models
11.15	Fonseca	: Plastic Limit Design of Shells
	Kaftanoglu	: Computer Aided Design of Power Shafts

NATO/NASA/NSF/USAF

AVDANCED STUDY INSTITUTE

Computer Aided Optimal Design

Structural and Mechanical Systems

SPONSORS

North Atlantic Treaty Organization
The U. S. National Aeronautics and Space Administration
The U. S. National Science Foundation
The U. S. Air Force

Mota Soares

SUPPORTERS

CEMUL: Centro de Mecânica e Materiais
da Universidade Técnica de Lisboa
INIC: Instituto Nacional de Investigação Científica
Secretaria de Estado do Ensino Superior
Comissão Permanente INVOTAN
JNICT: Junta Nacional de Investigação Científica e Tecnológica
Instituto Superior Técnico
Universidade Técnica de Lisboa
MAGUE: Construções Metalomecânicas, S.A.R.L.
PECHINEY
European Research Office, United States Army
SOREFAME: Sociedades Reunidas de Fabricações Metálicas, S.A.R.L.
Escola Náutica Infante D. Henrique
BPA: Banco Português do Atlântico
TAP: AIR PORTUGAL
Companhia Carris de Ferro de Lisboa
Rodoviária Nacional
MAN Technologie Gmbh

Volume 3

TRÓIA, PORTUGAL
June 29 – July 11
1986

……

Munich Lightweight Seminar

continuously since 25 years, beginning

……

30.9 **Last Presentations** 2023-2025 at **Various Conferences on Composites etc**

Presentation in the past:
(the *more complicate time'*:
Hope, that the presentation of
the transparencies will *work*

2025, *less complicated presentation time*. Better?
No. The pointer could not *work* due to a false plugging.

Landshut Lightweight Conference and Talk to my Carbon Composites WG "Engineering"

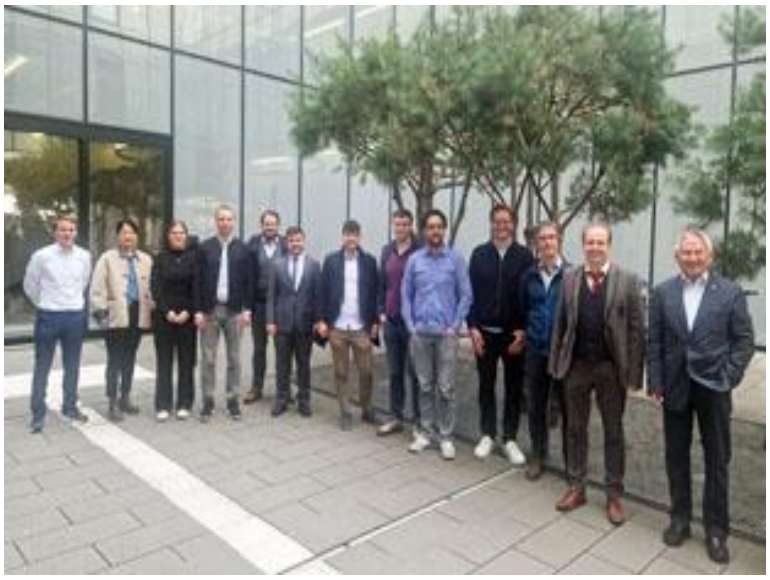

Static 3D-Strength Failure Criteria for the Structural Material Families Isotropic, Transversely–isotropic UD-Lamina and Orthotropic Fabrics.
And? Achievement of a Novel, Simpler Structural Mechanics Building.
on basis of Cuntze's successfully Test Data-linked Failure-Mode-Concept (FMC)

DGM-Fachausschuss Hybride Werkstoffe,
21.2. 2024

31 References, Cuntze since 2000 and Acknowledgement

31.1 References

[Awa78] Awaji H and Sato S: *A Statistical Theory for the Fracture of Brittle Solids under Multiaxial Stresses*. Int. J. of Fracture 14 (1978), R 13-16

[Cun00] *Progressive failure of 3D-stressed laminates*: *Multiple nonlinearity treated by the Failure Mode Concept.* Recent Developments in Durability Analysis of Composite Structures. Balkema, ISBN 90 5809 103 1

[Cun01] *Assessment of Load- and Strain-controlled States of Stress in 'Hot Spots' – on the way to an Industrial Approach for 'Gurson Materials'*. Europ. Conf. on Launcher Technology Strascourg , De1.11-14, 2001

[Cun03] Cuntze R and Memhard D*: Evaluation of the Tension Rod Test for Ductile Material Behavior*. European Conference on Spacecraft Structures, Materials & Mechanical Testing CNES, DLR; ESA, ISU: Toulouse, 11-13 December, 2002. Conference Proceedings

[Cun04] *The Predictive Capability of Failure Mode Concept-based Strength Criteria for Multidirectional Laminates*. Part B, Composites Science and Technology 63 (2004), 487-516

[Cun06] *Failure Conditions for Isotropic Materials, Unidirectional Composites, Woven Fabrics - their Visualization and Links*. https://www.ndt.net › cdcm2006 › papers › cuntze, PDF

[Cun13] *Comparison between Experimental and Theoretical Results using Cuntze's Failure Mode Concept model for Composites under Tri-axial Loadings – Part B of the WWFE-II*. Journal of Composite Materials", Vol.47 (2013), 893-924

[Cun17] *Fracture Failure Bodies of Porous Concrete (foam-like), Normal Concrete, Ultra-High-Performance-Concrete and of the Lamella - generated on basis of Cuntze's Failure-Mode-Concept (FMC*). NWC2017, June 11-14, NAFEMS, Stockholm *

[Cun19] *Technical terms for composite components in civil engineering and mechanical engineering*. Fachbegriffe mit Erklärung und Definition. In: Fachbegriffe für Kompositbauteile – Technical terms for composite parts. 171 pages, Springer Vieweg, Wiesbaden (2019). Pre-print downloadable*

[CUN22] *Life-Work Cuntze - a compilation*. 2022/2023. *The Failure-Mode-Concept FMC, a physical and theoretical Material Symmetry-driven basis to generate Strength Criteria, that gave a reason to look after a 'more closed' Strength Mechanics Building, and in addition Very Much on Structural Materials, Techniques and Design including work-life experiences of the author in many engineering fields*. (about 850 pages), downloadable from https://www.carbon-connected.de/Group/Prof.Ralf.Cuntze

[Cun23a] *Design of Composites using Failure-Mode-Concept-based tools— from Failure Model Validation to Design Verification*. Mechanics of Composite Materials, Vol. 59, No. 2, May, 2023, pp. 263-282*

[Cun23b] *Minimum Test Effort-based Derivation of Constant-Fatigue-Life curves - displayed for the brittle UD composite materials.* Springer, Advanced Structured Materials, Vol.199, 107–146, draft *

[Cun23c] *Comparative Characterization of Four Significant UD Strength Failure Criteria (SFC) with focusing a direct use of Friction Values, use of 'Strength' and 'Proportional Loading'. 54 pages**

[Cun23d] *Gedanken eines faseranwendungserfahrenen Ingenieurs zum Umgang mit Faser-Mikro-bruchstücken und Feinstäuben bei Herstellung und Recycling faserverstärkter Bauteile*. Composites United construction (CU Bau) *

[Cun24b] *Ceramic Strength Models for Monolithic (isotropic), Transversely-isotropic UD and Fabric Materials**

[Cun24c] Cuntze R and Kappel E: *Benefits, applying Tsai's Ideas 'Trace', 'Double-Double' and 'Omni Failure Envelope' to Multiply UD-ply composed Laminates.* 60 pages *

[Cun24a] Cuntze R and Kappel E: *Why not designing multidirectional laminates with in-plane Strength Design Sheets applying the UD criteria of Tsai-Wu and Cuntze*? Part 1, Analytical foundation in Mechanics of Composite Materials (MCM), Vol. 60, No. 5, November, 2024; Part 2 , Application in MCM , Nov., too

[Cun25] *UD-composites Strength Failure Criteria – However, which one should I take* ? Presentation at the 12. Landshuter Leichtbau-Kolloquium, 26./27. Februar 2025 * (to be published by Springer)

[Fla82] Flaggs D L and Kural, MH: *Experimental Determination of the In Situ Transverse Lamina Strength in Graphite Epoxy Laminates.* J. Comp. Mat. Vol 16 (1982), 103-116

[Har93b] Hart-Smith L J: *An Inherent Fallacy in Composite Interaction Failure Curves*. Designers Corner, Composites 24 (1993), 523-524

[Has80] Hashin Z: *Failure Criteria for Unidirectional Fiber Composites*. J. of Appl. Mech. 47 (1980), 329-334

[Hin02] Hinton M J , Kaddour A S and P.D. Soden P D: *A comparison of the predictive capabilities of current failure theories for composite laminates, judged against experimental* ***evidence*** (it would have been very nice). Composites Science and Technology 2002 (62), 1725-97

[Hah15] Hahne C: Zur Festigkeitsbewertung von Strukturbauteilen aus Kohlenstofffaser-Kunststoff-Verbunden unter PKW-Betriebslasten“, Shaker Verlag, Dissertation 2015, TU-Darmstadt, Schriftenreihe Konstruktiver Leichtbau mit Faser-Kunststoff-Verbunden, Herausgeber Prof. Dr.-Ing Helmut Schürmann

[HSB 02000-01] Cuntze R: *Essential topics in the determination of a reliable reserve factor*. 2012, HSB sheet, 20 pages. HSB = (luftfahrttechnisches) Handbuch für Strukturberechnung (*German aerospace handbook*). Edited by the industrial committee (*working group*!) IASB = IndustrieAusschuss für StrukturBerechnung

[Jai20] Jain N and Koch D: *Prediction of Failure in Ceramic Matrix Composites Using Damage-Based Failure Criterion*. J. Compos. Sci. 2020, 4, 183; doi:10.3390/jcs4040183

[Kaw04] Kawai M: *A phenomenological model for off-axis fatigue behavior of uni-directional polymer matrix composites under different stress ratios*. Composites Part A 35 (2004), 955-963

[Kno03] Knops M: *Sukzessives Bruchgeschehen in Faserverbundlaminaten*. Diss. 2003. Aachen, Institut für Kunststoffverarbeitung

[Kow83] Kowaltschuk B.I. and Giginjak F.F.: ..in Russian, Kiew, Naikowa Dumka 1983

[Leg02] Leguillon D: *Strength or Toughness? –A criterion for crack onset at a notch*. Europ. J. of Mechanics A/Solids 21 (2002), 61 – 72 end. Ist. D. sci. Lett., Cl. Mat. Nat.18, 705-714 (1885

[Li24] Li H, Pel L, You Z and Smeulders D: *Stress-dependent Mohr-Coulomb shear strength parameters for intact rock*. Nature.com/scientific reports

[Lut06] Lutz G: *The Puck theory of failure in laminates in the context of the new guideline VDI 2014, Part* 3. NDT.net https://www.ndt.net › cdcm2006 › papers › lutzii, PDF

[Puc96] Puck A: *Festigkeitsanalyse von Faser-Matrix-Laminaten - Modelle für die Praxis.* München, Carl Hanser Verlag, 1996

[Tsa71] Tsai S W and Wu E M: *A General Theory of Strength for An-isotropic Materials*. Journal Comp. Materials 5 (1971), 58-80

[You15] You M: *Strength criterion for rocks under compressive-tensile stresses and its application*. J. of Rock Mechanics and Geotechnical Engineering 7 (2015), 434-439

The CV at hand is to some extent only an excerpt of the document [CUN22].

However, some specific chapters therefrom shall be mentioned below for probably interested readers.

31.2 Annex on other Works of the author

If one might be interested one can find information on the following subjects in the author's compilation [*CUN22*] especially on various projects at MAN the author was involved.

18 Structural Vibration and Work Cases 586

18.1 General on Oscillation/Vibration 586

18.2 Damping and Damped Vibrations 591

18.3 The Influence of Dead Mass and Elastic Clamping on the Bending frequency of a slender Tower with linearly reducing Thickness (1969) 594

18.4 Natural Frequencies of Thin Inclined Isotropic Plates (*Cuntze, 1969*) 598

18.5 Natural Frequencies (eigenfrequencies) of Orthotropic Deep Beams (Dissertation, 1968) 603

18.6 The Influence of Cross-sectional Shear Flexibility and Rotatory Inertia on the Natural Frequencies of Beams with Uniformly Distributed Mass (1983) 616

18.7 Analysis of the Natural Frequencies of Laminated Beams of low 'Shear-rigidity' 624

18.8 Influence of low Cross-sectional Shear Rigidity and Rotatory Inertia on the Critical Speeds of Shafts with Uniformly Distributed Mass *(1984)* 627

18.9 Natural Frequencies of a Cracked Beam for Production Quality-testing of Rotor blades 637

18.10 Equivalent Sinusoidal Acceleration corresponding to an Excitation by Random Vibration 641

19 Some Flywheels and Rotors 643

19.1 Metallic Energy storage Flywheel for the floating crane ship Swartow (1982) 643

19.2 A New concept of a Composite Flywheel due to novel fiber-reinforced materials (1988) 649

19.3 An Axial Energy Storage Rotor, the 'EnWheel' (2015) 653

19.4 Increasing the Limit of Usability of CFRP Tubes by Built-in-Stresses (1993) 664

19.5 The Large Windmill GroWiAn GROWIAN (1977-1982), development and build 678

19.6 Design of a Fiber-reinforced Gas-Ultra-Centrifuge Cylinder, GUZ (1971-1986) 696

20 Some Winding Theory of Filament Wound Pressure Vessels 702

20.1 Introduction 702

20.2 Geometry of the Rotation Shell with Bottom Equilibrium Equations 704

20.3 General Fiber Net-shell 707

20.4 Meridian Shape (contour) of the Vessel Bottom under Internal Pressure 710

20.5 Contour of the Fiber Net-shell Bottom under Centrifugal Loading *(Fig 3f)* 715

20.6 Theoretically Possible and practically Feasible Winding Contours 718

20.7 Winding Patterns 723

20.8 Applications of Winding Theory at MAN Technologie 725

Life-Work *Cuntze* - a compilation Living Document edition 29mar23 12

20.9 Application of winding technology, re-calculation of above AFRP tank (1975) 729

31.3 Thanks and Acknowledgement

Many Thanks to: My parents Helmy and Werner for my *inherited tenacity* to endure this hobby alongside the job, my first wife Jutta and to my second wife Maria for tolerating my private, very time-consuming scientific hobby and work.

The professores

- *Hans Kauderer, E. Doeinck, Theo. Lehmann, Frederick-Henry Schroeder and Kurt Magnus for my knowledge of mechanics, which of course is still imperfect. Theo Lehmann and F-H Schroeder were my doctoral supervisors.*
- *Theo Lehmann, as well as the purple-robed jaguar driver Zerna, especially for the tensor analysis knowledge, which I was later able to use it in fiber laying winding technique*
- *Bodo Heimeshoff and Huba Öry for the self-critical way of working, which is later called 'self-testing' in ISO 9000. Bodo Heimeshoff and Harry Grundmann, who were my habilitation fathers in 1978*
- *Alfred Puck for many valuable discussions and his indirect initiation of my Failure Mode Concept (FMC) idea*
- *Gerhard Schüeller and Rüdiger Rackwitz for the knowledge of structural reliability, later applied in my FMC idea*
- *Karl-Heinz Schwalbe for my fracture mechanics knowledge, in his specific Working Group*
- *Ms. Rita Jeltsch-Fricker for "Getting on the Right Mathematical Path" in a large MAN research project on A. Puck's Action Plane Stress criterion*
- *The honorary professor-reviewers Werner Hufenbach, Hans Eschenauer and finally Mr. Fahlbusch of the Bundeswehr University for the realization of the honorary professorship at the UniBw at Neubiberg.*

Thanks to all those who are not named, especially MAN colleagues and the members of the Aerospace-Technical Industry Committee for Structural Calculation (IASB), who contributed to both my professional and my scientific work.

Without the encouragement of Wilfried (Prof. Becker, TU Darmstadt) I would not have made it through the laborious work in the last two decades.

Yes, and where wouldn't I have gotten stuck everywhere in Mathcad-code calculations if it there would not have been Dipl.-Ing. Bernd Szelinski, who was usually able to eliminate Mathcad-attributable difficulties, such as changed letters, characters or that vectors were no longer read. It's a pity that such a great calculation program has such shortcomings and errors are incorrectly noted or it doesn't calculate and doesn't give a suspicion of error. Sometimes, another solution way could be gone.

Not to forget Dr.-Ing. Andreas Freund, with whose Mathcad skills I was only able to make the numerical entry into WWFE-I, culminating in a joint paper on WWFE-I A. A big thank-you to Bernd and Andreas.

And again to all my scientific friends and partners: arbitrary order

Bodo Heimeshoff, Huba Öry, Alfred Puck, Steve Tsai, Wilfried Becker, Holm Altenbach, Werner Hufenbach, Volker Ulbrich, Rolands Rikards, Lothar Kroll, Klaus Rohwer, Siegfried Schmauder, Gottfried Ehrenstein, Walter Wunderlich, Peter Offermann, Gerd Busse, Urs Meier, Frank Schladitz etc.

31.4 Resume

Life philosophy, experience

A lifelong close friend of Konrad Zuse and my father-friend once told me Zuse's retrospective:

"Looking back on my career, I can only hope that in the future there will be room not only for the specialist in his field, but also for the universally gifted. I believe that versatility in particular is the prescriptive for ideas that are out of the ordinary. Such an idea, an 'infidelity' of technology, if you will, was ultimately the computer".

In this context what I learned:

"Without versatility, I would never have been able to see the invisible bridges between the materials and their disciplines. Test results of related materials provide valuable information for the pre-dimensioning of novel materials". This saves time and money.

As far as new ideas are concerned, T.A. Edison is right: 1 % inspiration, 99% transpiration.

This was about the same with my FMC. Never stop if people want you to give up or my mathematical codes Mathcad.

Further, with my FMC it basically looks similar to the outstanding scientist Max Planck experiences, who said:

"It is one of the most painful experiences of my life that I have never succeeded in bringing a new assertion, for the correctness of which could provide a compelling theoretical proof, to general recognition. New scientific work prevails after the extinction of the opponents".

Where are the discussions in the contact-simple computer time?

Karl Poppers has summarized what is still very close to my heart in his 12 principles for a new professional ethic:

"It is impossible to avoid all mistakes or even all mistakes that are avoidable in themselves. Since we must learn from our mistakes, we must also learn to accept gratefully when others draw attention to our mistakes."

I hope I've always been very grateful for bug reports.

Much Experience is required in Design! But what is experience?

"Experience is not what happens to you; it's what you do with what happens to you".

Aldous Huxley

Final note

Above non-funded work mainly addresses the author's working life in industry with the intension to transfer theory into engineering application.

This 'single authored' work includes:

*Idea finding,
*idea exploitation to generate the FMC-theory,
*text writing of this document,
*extensive numerical analyses with rendering of results like fracture bodies using the programs Mathcad 13 and 15,
*typing of formulas,
*difficult visualizations of the calculation results, sketches, diagrams etc.

All these works have been performed by the author himself.

And, facing the program crashes of Word (twice, per day at least) presumably due to the large document and Mathcad 15 due to complicate computations. And that word corrections were indicated to have been executed but in reality not performed.

A final shock in 2015 was Windows 11, making Mathcad, formula editor (signs vanished like ||, however not regularly!), paint etc not working anymore. Handling such a large document was the major ongoing challenge! I discovered that disabling autosave was the only way to work with the huge document. Of course, I now had to constantly remember to save it myself.

Many thanks are given to those who believed in my work [*W. Becker*] and had some discussions with me on several topics [*Wolfgang Brocks with Fracture Mechanics, Andreas Freund with Mathcad 13 and UD mapping etc, Martin Grimmelt with Statistics, Probabilistics.*]. This thankyou includes the WWFE organizers within the performance of WWFE-I and –II from 1999 through 2013 especially *Sam (Kaddour)* and those that peered my WWFE-contributions. Not to forget are all those which delivered a basis for some body texts. *B. Szelinski* helped not to despair of Mathcad versions.

To my wife Maria: *"My heartfelt thanks for allowing me to devote so much time of 'our time together' to my time-consuming hobby* ".

Dedication to all the people who have guided me to the wide variety of technical fields during my 60-years working life.

This was challenging but also difficult and at the same time beautiful. Never giving up was the motto.

Personal desire of the author:

"*It were good for both the dicsciplines mechanical and civil engineering to act side-by-side such as croco and hippo document below*".

Surprising picture, Sambia 2011.

31.2 Thanks and Acknowledgement

Many Thanks to: My parents Helmy and Werner for my *inherited tenacity* to endure this hobby alongside the job, my first wife Jutta and to my second wife Maria for tolerating my private, very time-consuming scientific hobby and work.

The professores

- *Hans Kauderer, E. Doeinck, Theo. Lehmann, Frederick-Henry Schroeder and Kurt Magnus for my knowledge of mechanics, which of course is still imperfect. Theo Lehmann and F-H Schroeder were my doctoral supervisors.*
- *Theo Lehmann, as well as the purple-robed jaguar driver Zerna, especially for the tensor analysis knowledge, which I was later able to use in the fiber laying winding technique*
- *Bodo Heimeshoff and Huba Öry for the self-critical way of working, which is later called 'self-testing' in ISO 9000. Bodo Heimeshoff and Harry Grundmann, who were my habilitation fathers in 1978*
- *Alfred Puck for many valuable discussions and his indirect initiation of my Failure Mode Concept (FMC) idea*
- *Rüdiger Rackwitz for the knowledge of structural reliability, applied in my FMC idea*
- *Karl-Heinz Schwalbe for my fracture mechanics knowledge*
- *Ms. Rita Jeltsch-Fricker for "Getting on the Right Mathematical Path" in a large MAN research project on A. Puck's Action Plane Stress criterion*
- *The honorary professor-reviewers Werner Hufenbach, Hans Eschenauer and finally Mr. Fahlbusch of the Bundeswehr University for the realization of the honorary professorship at the UniBw at Neubiberg*

Thanks to all those who are not named, especially MAN colleagues and the members of the Aerospace-Technical Industry Committee for Structural Calculation (IASB), who contributed to both my professional and my scientific work.

Without the encouragement of Wilfried (Prof. Becker, TU Darmstadt) I would not have made it through the laborious work in the last two decades.

Yes, and where wouldn't I have gotten stuck everywhere in Mathcad-code calculations if it there would not have been Dipl.-Ing. Bernd Szelinski, who was usually able to eliminate Mathcad-attributable difficulties, such as changed letters, characters or that vectors were no longer read. It's a pity that such a great calculation program has such shortcomings and errors are incorrectly noted or it doesn't calculate and doesn't give a suspicion of error. Sometimes, another solution way could be gone.

Not to forget Dr.-Ing. Andreas Freund, with whose Mathcad skills I was only able to make the numerical entry into WWFE-I, culminating in a joint paper on WWFE-I A. Thank you Bernd and Andreas.

And finally not to forget: Many thanks to my IT-friend, the problem solver Peter Keller.

And, to my scientific friends and partners:

Bodo Heimeshoff, Huba Öry, Alfred Puck, Steve Tsai, Wilfried Becker, Holm Altenbach, Werner Hufenbach, Volker Ulbrich, Rolands Rikards, Lothar Kroll, Klaus Rohwer , Siegfried Schmauder, Gottfried Ehrenstein, Walter Wunderlich, Urs Meier, Holger Theilig, Frank Schladitz.

"Theory is the Quintessence of all Practical Experience" (A. Föppl)

"Quid quid agis, prudenter agas, et respice finem" (*a slogan of my school class*)
Whatever you do, do it wisely and remember where it leads to. *(*from *Gesta Romanorum).*

I hope that I followed this saying.

If I had known beforehand how much time this work would take, I probably would not have done it.

"Si enim alicui placet mea devotio, gaudebo. Si autem nulli placet, memet ipsam tamen iuvat quod feci"
(A letter from Hrotsvit, nun of Gandersheim, 950 anno domini

If my work pleases anyone, I will be happy,
but if it pleases no one, it will nevertheless be good that I did it.

I am grateful that I was able to do all this.

Multi noscunt multa, omnes aliquid, nemo sati.
Many know a lot, everyone knows something, no one knows enough.
The above Latin saying is for me the basis for hopefully coming valuable discussions.

Finally, a word about the future.

Our famous Bavarian comedian Karl Valentin, who starved to death in 1948, once said:
"*The future was better in the past*"! Is that really true?

In any case, I can say for myself:
"*The future was longer for me in the past*"!

In addition to very good experience in working life, negative experience should not be forgotten:

- *The belittling of company employees in the event of non-achievement of goals, so that many give up inwardly in the end and prefer to take care of a change of company with the associated deterioration in efficiency.*
- *Reorganize, but do not check whether this measure has led to an improvement in this situation.*
- *The Not-Invented-Here syndrome: It derogatively describes the disregard of already existing knowledge by companies or institutions due to the place of origin [https://de.m.wikipedia.org/wiki/Not-invented-here-Syndrom].*
- *And recently, because the available information on the web is not used actively enough, will AI help here?*
- *Based on my experiences with my Failure-Mode-Concept and from my travels, I can only fully agree with Mark Twain:" "How long it takes for one part of the world to adopt the useful ideas of another part is surprising and inexplicable. This form of stupidity is not limited to any community, no nation; it is universal."*

  Concerning my idea of the existence of a material-symmetry-based 'Generic Number' for Structural materials: Here I fully feel like the great scientist Max Karl Ernst Ludwig Planck, when stating: „It is one of the most painful experiences of my scientific life that I have rarely, yes, I would like to say, never succeeded, in bringing a new assertion, for the correctness of which I could provide a complete, compelling, but only theoretical proof, to general recognition."
- *No blocking of information and workflow between the areas in the companies pursuing a joint project is absolutely necessary*
- *Fighting with Closed Minds people*
- *ARIANE development: Good progress of the projects by the French system managers, but often cost-intensive, unfortunately blocked by the fact that new French project engineers - without the necessary project knowledge and thus without any decision-making authority - were our discussion partners. And, 'bureaucratic' people partly checked the contract fulfilment of the contractors*
- *The preservation of a company's knowledge is targeted by the experienced. One should not say "What, you've been with the company for so long? Our human resources department has done a bad job there." Just motivating instead of threatening alone creates an improvement.*

Hope for my Friends:

I eat finest dark chocolate for becoming milder with my progressing age!

What worries me deeply as a structural engineer from industry:

An acquaintance recently said to me: Less than 10% of my students only come to my basic mechanics lecture. Too demanding? That would be bad for German industry. We cannot remain competitive like this! The valuable tool AI helps us to get suggestions for solutions. But who is supposed to judge them without corresponding knowledge of mechanics?

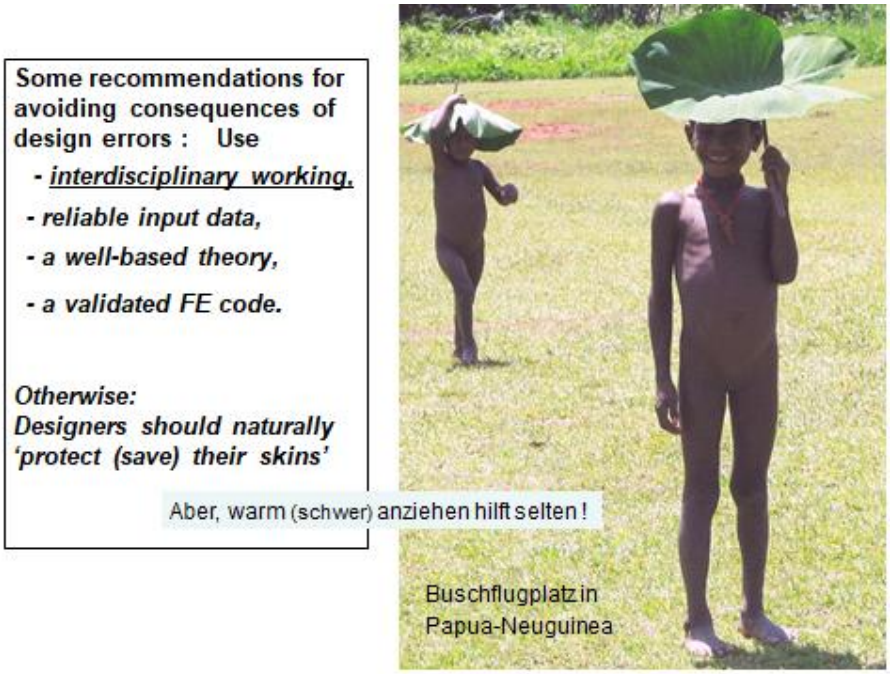

'Dressing warmly' (thickening) rarely helps to get a good design!

And now a few very different things that I did not understand during my life:

• Why did I, alone on March 30, 1945, bend down in a ditch and walked 300 meters into the woods to my parents, away from my grandparents?

• Why did my uncle's property at Erfurt-Bergstromweg no longer officially exist after reunification? Now it officially exists again, but all of his immediate family members and heirs have died.

• Why was there no internationally useful greenback-like euro note from 2000 onwards, but only a heavy, difficult-to-exchange coin?

• Why was conscription (armed forces service) suspended and social service abolished in 2011?

• As someone affected, who nevertheless supported the shutdown of nuclear power plants along with the German majority at the time, I had imagined a sensible phasing out. It appalls me that politicians would have preferred to shut down the power immediately, but after the final shutdown, these same politicians are now clamoring for expensive restarts.

• It is really surprising that China is better than us in several industrial areas? We sold them the latest equipment. They further have to work more.

* Why is it not mandatory for a government - as is normally the case in industry - to plan for the necessary basic materials for the country and its economy as a primary task?

Some other affiliations:

Member of :

***VDI (Association of German Engineers). > 50 years**

***DGLR (German Society for Aircraft and Spacecraft). > 40 years**

- **Member of DVM-WG "Characteristic Value Determination and Application of Fracture Mechanics". *Headed by K.-H. Schwalbe (*1980)**

- **Member of the Probability Working group of *G. Schueller (1986)***

- **Founder and organizer of 4 Working Groups at Composites United e.V.**
  - Engineering, *aerospace, mechanical engineering*
  - Composites Fatigue, *aerospace, mechanical engineering*
  - Design Dimensioning and Design Verification, *civil engineering*
  - Automated fabrication in construction including serial production

  Including Extrusion-based Additive Fabrication (*'~~3D Printing~~'*) , *civil engineering.)*

ANHANG C

Mitgliederverzeichnis der für die Merkblatterstellung verantwortlichen DVM-Arbeitsgruppe "Kennwertermittlung und Anwendung der Bruchmechanik"

Das vorliegende DVM-Merkblatt wurde in einer Gemeinschaftsarbeit von der Arbeitsgruppe "Kennwertermittlung und Anwendung der Bruchmechanik" innerhalb des "Arbeitskreises Bruchvorgänge", integriert im "Deutscher Verband für Materialprüfung e. V. (DVM)", unter der Federführung der beiden Leiter der Arbeitsgruppe, A. Cornec, J. Heerens, beide GKSS-Forschungszentrum Geesthacht, ausgearbeitet. An diesem DVM-Merkblatt waren nachfolgend aufgeführte Institute und Firmen und deren Mitarbeiter maßgeblich beteiligt:

Bundesanstalt für Materialforschung und -prüfung (BAM), Berlin	K. Wobst
Fraunhofer-Institut für Werkstoffmechanik (IWM), Freiburg	B. Voß
GKSS-Forschungszentrum Geesthacht GmbH	A. Cornec J. Heerens
Institut für Eisenhüttenkunde (IEHK), Aachen	A. Heuser D. Dormagen
Interatom, Bergisch-Gladbach	H. Huthmann
Kernforschungszentrum Karlsruhe (KfK)	A. Brückner
Kraftwerk Union AG, Erlangen	A. Gerscha
Kraftwerk Union AG, Mülheim	F. Vahle
MAN-Technologie, München	R. Cuntze
Messerschmitt-Bölkow-Blohm (MBB), Bremen	K. Blomeier L. Schwarmann
Rheinisch-Westfälischer TÜV, Essen	B. Reimann M. Remke
Staatliche Materialprüfungsanstalt (MPA), Universität Stuttgart	U. Eisele E. Roos
TÜV-Hannover	E. Boroske
Universität Karlsruhe	W. Ehl

The **Engineering Working Group: Focus on Parameters** *[CCeV News 2010, second]*

The Engineering Working Group in the CCeV has been in existence since spring 2009. After the kick-off meeting with a keynote speech on the topic "Design and Verification", further theme days with user contributions dealt with the topics of "general optimization", "targeted additions to optimization" (such as hybrid CFRP-metal composites, efficient rotor blade design with ANSYS, robust design optimization taking into account manufacturing tolerances) as well as the formulation of strength-failure conditions.

In spring 2010, a joint, coordinated event took place with the NDI working group "Materials and Component Testing". Within the framework of the topic "Tools in Damage Tolerance Design", the NDI Block in production (determination of defect sizes) and then the Block Requirement of the Approval Authorities, Evaluation of Defects and Verification Methods were dealt with.

The Engineering working group has set itself the task of bringing together practically and theoretically oriented engineers. These come from smaller and large companies as well as from the university and institute sector. The exchange of experience between users and researchers at the university is one of the goals of the working group. In addition, it aims to promote thinking in the component process chain from design to verification, provide appropriate knowledge, convey analysis tools with their applicability limits and integrate the findings of other more practically oriented CCeV working groups.

In principle, the CCeV attaches great importance to the fact that the working groups learn from each other, strive for cross-connections and optimise processes. In this sense, the meeting of the Engineering Working Group always takes place together with that of the NDI Working Group. The above-mentioned lecture series provide a framework for the exchange of experiences. The presentations held together with the minutes of the meeting can be downloaded from the CCeV website (Carbon Composites -> Range of Services -> Working Groups/Groups -> Engineering). For this desired cross-linking, a sub-working group "Evaluation of NDI" is planned with the topics of maintenance, repair, inspectability, damage tolerance, and later recycling.

Another important sub-working group on the "Evaluation of new engineering software products" has already started its work. For this purpose, members are asked to list their software tools according to a fixed scheme, to submit evaluations and to formulate wishes. Some of the criteria to be applied here are: result quality, robustness, reliability, user-friendliness, cost, etc. The software companies are already involved in order to then specifically address the problems of the users.

For the next event, which will take place on 22.10.2010, the topic "Material characteristics and material characterization" was requested. For the members of the Engineering Working Group, the lack of reliable material characteristics (elasticity variables, strength parameters, etc.) for design and verification is also a major problem. In addition, validated strength conditions for the representation of multiaxial fracture stress states of the unidirectional (UD) layer are only available to a limited extent.

In this context, it is regrettable that the huge expenditures and valuable validation results of participants and organizers of QinetiQ (UK) in the implementation of the World Wide Failure Exercises-I and -II are unknown to many designers, but also to materials characterizers and test center employees in industry and institutes. WWFE-I had as its topic the validation of UD strength conditions with biaxial fracture stress states, while the WWFE-II, which is currently being phased out, is trying to do the same with provided 3D fracture stress states. The author was successfully involved in WWFE-I, and has experienced the difficulties of providing reliable test data - especially in WWFE-II: Test specimens, test benches, measurements and evaluation offer many possibilities for error. A test result is always experimental evidence, but almost never the complete experimental proof. A sensible balance of theory and experiment, in addition to good cooperation in both areas, is therefore imperative.

The CCeV strives to pass on experience so that some wheels are not reinvented by expensive experiments, but gaps are closed. For this purpose, contributions are also uploaded to the CCeV website, which help, for example, to determine the necessary multiaxial strength data.

Some Meetings of the author-founded Working Groups of

Carbon Composites e.V. (CCeV, Augsburg) and Composites United (CU, Berlin)

„Automatisierte Fertigung im Bauwesen von Bauteilen mit Polymermatrix und Betonmatrix"

- Was gibt es Neues? –

2. Thementag 'Automatisierte Fertigung'

DACH-Veranstaltung von allen CC Bau-AG´s, speziell AG 'Robotergestützte Fertigung'

Zielgruppen: Bauwirtschaft, Architekten, Planer, Handwerker, Auftraggeber, Zulassungsstellen

am **13. Juni 2019 an der Uni Innsbruck, Technikerstrasse 21, A 6020 Innsbruck**
Institut für Konstruktion und Materialwissenschaften, Arbeitsbereich für Massivbau und Brückenbau: Univ.-Prof. Dr.-Ing. Jürgen Feix
Institut für Experimentelle Architektur, Arbeitsbereich Hochbau: Univ.-Prof. Dr. M. Colletti,
DI G. Grasser 0043 650 441 9086
CCeV-Kontakt Bernhard Jahn (Bernhard.Jahn@carbon-composites.eu).
Thementag: 95 € für Nicht-Mitglieder, frei für Vortragende, Presse.
Folien: englisch, deutsch. Vorträge: 25 + 5 min Diskussion.

8:30	Registrierung der Teilnehmer mit Kaffee, Brezeln, Getränke
9:00	**Einführende Worte.** *R. Cuntze*
9:15	**Vorstellung des Instituts.** *M. Colletti, J. Feix*
.9:30	3D Concrete Printing - **from Lab to Practice**. *F. Bos, Uni Eindhoven Holland*
10:00	**Eine mögliche zukünftige Bauweise für den Hoch- und Brückenbau unter den Gesichtspunkten von Lebensdauerkosten, Qualität, Erhaltung der Flexibilität des Ortsbetonbaus und BIM.** *J. Kurath, ZHAW Winterthur*
10:30	*Kaffeepause*
11:00	**Entwurfs- und Bemessungsstrategien für den Faserverbundpavillon auf der BUGA in Heilbronn 2019**. *V. Koslowski, ITKE (Knippers) Uni Stuttgart*
11:30	**Integration der Bewehrung in die additive Betonfertigung**. *V. Mechtcherine, Institut für Baustoffe, TU Dresden*
12:00	**Material und Prozess - adaptive Strategien in der Baurobotik mithilfe von Assistenzsystemen**. *S. Brell-Cokcan, Lehrstuhl für Individualisierte Bauproduktion, RWTH Aachen*
12:30	*Mittagspause*
13:30	**Technische Umsetzung des 3D-Betondrucks in praxisgerechte Fertigung.** *E. Artner, O.Balog, Baumit GmbHTextile*
14:00	**Modulares bauen bei Max Bögl**. *J. Schaffrath, Max Bögl, Neumarkt in der Oberpfalz*
14:30	**COEBRO - Additive Fabrication of Concrete Elements by Robots – Technologie und Anwendungsbeispiele.** *A. Trummer, TU Graz*
15:00	*Kaffeepause*
15:30	**Textile Bewehrung für den 3D Druck mit Beton**. *J. Konzilia, G. Grasser, Uni Innsbruck*
16:00	**Resümee, Abschlussdiskussion zur Inhaltsbelegung der AG "Robotergestützte Fertigung"**
16:15	**Institutsbesichtigung mit "Techn. Umsetzung des 3 D Betondrucks in praxisgerechte Fertigung"**
	Get Together

Ihre Ralf Cuntze und G. Grasser

Hinweis:
CC Bau, Fachabteilung des CCeV, besteht aus 4 AGs: Bemessung und Nachweis (Prof. Dr.-Ing. habil. Ralf Cuntze, Augsburg), Faserverbundarmierter Beton (Dr.-Ing. Ingelore Gaitzsch, texton Dresden), Faserverstärkte Kunststoffe (Prof. Dr.-Ing. Jens Ridzewski, IMA Dresden), Robotergestützte Fertigung (Dipl.-Ing. Otto Kellenberger, AlphaTeck)
Nächste Termine der CC-Bau-AGs:
13. November 2018: CC Bau-Abteilungsversammlung mit 4 Fachvorträgen bei der HWTK Leipzig. März 2019: AG „Faserarmierter Beton" bei Neviges. Oktober 2019 AG „Bemessung und Nachweis – vom Werkstoff bis zur Zulassung für Bauteile mit Polymermatrix und Betonmatrix" bei der Uni Weimar

2. Thementag 'Automatisierte Fertigung im Bauwesen'_RC_13juni19_final

CC BAU

COMPOSITES UNITED

CU-Thementag

„Vom Werkstoff bis zur Zulassung von Bauteilen aus Polymermatrix und Betonmatrix“

22. Oktober 2019 beim Institut für Angewandte Bauforschung Weimar gGmbH, Über der Nonnenwiese 1, 99428 Weimar

Zielgruppen: Bauwirtschaft, Architekten, Planer, Handwerker, Auftraggeber, Zulassungsstellen
Veranstaltung der CC Bau-AGs „Bemessung und Nachweis“ und „Faserverstärkter Kunststoff“

CCeV-Kontakt: Bernhard Jahn (Bernhard.Jahn@carbon-composites.eu).
Teilnehmergebühr: 95 € für Nicht-Mitglieder, frei für CCeV-Mitglieder, Vortragende und Presse.
Folien: englisch, deutsch. Vorträge: 25 + 5 min Diskussion.

8:30	Registrierung der Teilnehmer, Begrüßungskaffee
8:45	**Einführende Worte mit Ausrichtung CC Bau.** *R. Cuntze / J. Ridzewski*
9:00	**Vorstellung Institut:** *Dr.-Ing. Barbara Leydolph, IAB Weimar*
9:15	**Verwendete Baustoffe mit Schwerpunkt Carbonbeton:**. *M. Butler, Institut für Baustoffe, TU Dresden*
9:30	**Fertigungsverfahren: Bauteile mit Polymermatrix.** *J. Ridzewski, IMA Dresden*
10:00	**Fertigungsverfahren: Bauteile mit Betonmatrix**. *G. Eisewicht, BCS Natur- und Spezialbaustoffe GmbH Dresden*
10:30	*Kaffeepause*
11:00	**Festigkeitsmodellierung der Baustoffe Beton und Lamelle**. *R. Cuntze, CC Bau Augsburg*
11:30	**Lasten, Sicherheitskonzept und Zulassungsaspekte.** *S. Rempel, Solidian Albstadt*
12:00	**Dimensionierungsbeispiel, GFK-Behälter** (nach BüV 2010). *M. Oppe, Büro Knippers-Helbig Stuttgart*
12:30	*Mittagspause*
13:30	**Dimensionierungsbeispiel, Faserbetonbauteil.** *B. Wielek, Sistrans, Tirol*
14:00	**Dimensionierungsbeispiel, CF-Textilbeton-Bauteile**: *S. May, Carbocon-GmbH. Dresden*
14:30	**Dimensionierungsbeispiel, CLT-Modellierung und Bemessung einer Textilbeton-Schale.** *D. Franitza, FE-Union GbR, Chemnitz*
15:00	*Kaffeepause*
15:30	**Abteilungsversammlung - CC Bau**
16:30	**Get Together**

Wir freuen uns auf Ihre Beiträge Ihr Ralf Cuntze und der weitere CC Bau-Vorstand

Hinweise: CC Bau, ehemals CC TUDALIT, Fachabteilung des CCeV, besteht ab 1.1. 2018 aus den 4 AGs: Bemessung und Nachweis (Prof. Ralf Cuntze), Faserverbundarmierte Betone (Dr. Ingelore Gaitzsch), Faserverstärkte Kunststoffe (Prof. Jens Ridzewski), Automatisierte Fertigung im Bauwesen (Ralf Cuntze)
Termine 2020: Workshop am 19. Februar, Ulmer Betontage bzgl. „Wie bekomme ich Carbonbeton-Anwendungen auf die Baustelle“?; CC Bau-AGs-Sitzung, 17. März bei der Universität Siegen.

COMPOSITES UNITED

BETONTAGE CONCRETE SOLUTIONS

COMPOSITES UNITED

CC Bau-Forum

“Carbonbeton-Anwendungen in der Praxis
- ***auf der Baustelle und im Fertigteilwerk“***
Transformation von praktischem Anwendungswissen.
Zielgruppe: Hersteller, Sanierer, Vertreter der Betonbranche
am 19. Februar , integriert bei den
Ulmer Betontage vom 18. - 21. 2. 2020

10:30	***Kaffeepause – Networking***
10:55	**Einführende Worte** *Prof. Dr.-Ing. habil. Ralf Cuntze - Composites United e.V.(former Carbon Composites e.V.)*
11:00	**Verwendete Baustoffe** *Dr.-Ing. Marko Butler - Institut für Baustoffe, TU Dresden*
11:20	**Mehrfach gekrümmte Schalentragwerke aus Carbonbeton :** **Entwicklung wirtschaftlicher Betontechnologien zur Herstellung von Fertigteilen** *Dr.-Ing. Gerald Eisewicht - BCS Natur- und Spezialbaustoffe GmbH Dresden* **Entwicklung einer Spritzbetontechnologie am Beispiel der „TWIST“-Schale des Ergebnishauses CUBE** *M.A., Dipl.-Wirtsch.-Ing. (FH) Matthias Tietze - Institut für Massivbau, TU Dresden*
12:00	**Einsatzbereiche von C³ – Carbon Concrete Composite aus Sicht einer mittelständischen Bauunternehmung** *Dr.-Ing. Frank Jesse - Hentschke Bau GmbH, Bautzen*
12:30	*Mittagspause und Besuch der Ausstellung*
14:00	**Carbon-bewehrte Parkhausdeckenplatten: Von der Idee zur industriellen Fertigung** *Dipl.-Ing. Oliver Heppes - GOLDBECK Bauelemente Bielefeld SE*
14:30	**Ökobilanz der Carbonbeton-Brücke in Albstadt-Ebingen** *Dr.-Ing. Sergej Rempel - solidian GmbH, Albstadt*
15:00	**Carbonbetontechnologie in der Sanierung** *Diplom-Ingenieur Ammar Al-Jamous - Carbonbetontechnologie und Tragwerksplanung, Dresden*
15:30	*Kaffeepause*
16:00	**Die wirtschaftliche Carbonbeton-Wertschöpfungskette - am Beispiel der Vorzugsanwendung Carbonbeton-Fertigteilwand** *M.A., Dipl.-Wirtsch.-Ing. (FH) Matthias Tietze - Institut für Massivbau, TU Dresden*
16:25	**Projektkostenabschätzung – eine realisierbare Vision?** *Dr.–Ing. Arne Ostermann - 4 cost, Hamburg*
16:45	**Praxisbericht: Wann rechnet sich Carbonbeton – und wann ist seine Verwendung nachhaltig?** *Dr.-Ing. Frank Jesse - Hentschke Bau GmbH, Bautzen*
17:15	„Der besondere Beitrag“ als Ulmer Tagesabschluss – Info wurden angefordert (Frau Blank)

Ihr Ralf Cuntze und der weitere Vorstand CC Bau

Weitere Termine 2020 der CU-Fachabteilung CC Bau:

- **17.03.2020** AG-Faserarmierter Beton bei der Uni Siegen
- Juli 2020 AG-Sitzung bzw. CU-Thementag-Automatisierte Fertigung im Bauwesen, Ort noch offen
- **10.09.2020** AG-Sitzung bzw. Thementag aller AG´s / TU-Chemnitz

*Agenda Carbonbeton_Ulmer Betontage_19feb20_Cuntze_Stand 30sep19_*

CC Bau-Forum

"Carbonbeton-Anwendungen in der Praxis - auf der Baustelle und im Fertigteilwerk"

Transformation von praktischem Anwendungswissen.

Zielgruppe: Hersteller, Sanierer, Vertreter der Betonbranche

am 25. Februar, Donnerstag, als Podium integriert bei den Ulmer Betontagen vom 23. - 26.02.2021

25 min Vortrag + 5 min Diskussion. Folien: deutsch oder englisch. Vortrag: falls möglich möglich deutsch

08:30	*Kaffeepause – Networking*
09:00	**Einführende Worte** *Prof. Dr.-Ing. habil. Ralf Cuntze, CU Bau, Augsburg. Composites United e.V. CUeV (formerly CCeV)*
09:15	**Digitale Entwicklung – von der Faser zum textilen Gelege.** *Roy Thyroff, rothycon – Roy Thyroff Consulting, Naila*
09:30	**Carbonbeton: Zwischen Theorie & Praxis.** *Dipl.-Ing. Oliver Heppes, GOLDBECK Bauelemente Bielefeld SE*
12:10	**Größer, stärker, wirtschaftlicher - Carbonbewehrungen in neuen Dimensionen.** *Dipl.-Ing. Stephan Gießer, Solidian, Albstadt*
12:40	***Mittagspause und Besuch der Ausstellung***
14:00	**Tragwerksplanung des C³–Ergebnishauses „CUBE" – Bemessung, Nachweisführung und Zulassung im Einzelfall.** *Dipl.-Ing. Hendrik Ritter, Assmann Beraten und Bauen, Dresden*
14:30	**Modulare Brückenbauwerke aus Carbonbeton** *M.Sc. Sven Bosbach, Lehrstuhl und Institut für Massivbau, RWTH Aachen*
15:00	**Bauen mit CPC-Carbonbetonplatten, einer komplett neuen Bauweise in Beton – Verfahren, Konstruieren, Bemessen.** *Prof. Joseph Kurath, ZHAW Winterthur, Schweiz*
15:30	**Stadtbahnbrücke Stuttgart: CFK-Zugglieder finden Akzeptanz.** *Prof. Dr. Urs Meier, EMPA, Dübendorf, Schweiz*
16:00	**Ausgewählte Ingenieurbauwerke - nachträgliche Bauteilverstärkung mit Carbon-Faser-Kunststoffen „CFK" (geklebte Lamellen).** *Dr.-Ing. Horst Peters, HPTL Carbon GmbH, Ditzingen*

Ihr Ralf Cuntze und der weitere Vorstand des Netzwerks CU Bau

Weitere Termine 2020 / 2021 des Netzweks CU Bau:

- 19.11. 2020: CU Thementag „Richtlinien, bauaufsichtliche Zulassungen und Bauartgenehmigungen für die potenziellen Anwender Architekten, Tragwerksplaner und Bauherrn". Zoom-Konferenz
- 17.03.2021: Thementag aller Arbeitsgruppen des Netzwerks CU BAU mit TU Chemnitz. Zoom-Konferenz?
- 30.03.2021: 4. Thementag der AG „Automatisierte Fertigung im Bauwesen inkl. Serielles Bauen". Zoom-Konferenz?

Das Netzwerk CU Bau, besteht aus 4 Arbeitsgruppen: Bemessung und Nachweis (Prof. Ralf Cuntze), Faserverbundarmierter Beton (Dr. Ingelore Gaitzsch), Faserverstärkte Kunststoffe (Prof. Jens Ridzewski), Automatisierte Fertigung im Bauwesen inkl. Serielles Bauern (Cuntze)

Agenda Carbonbeton-Forum Ulmer Betontage Cuntze 21okt20

CARBON COMPOSITES

Gemeinsame Sitzung der 3er-CCeV-AG

Engineering, Zerstörungsfreie Werkstoff- u. Bauteilprüfung, Kleb- und Verbindungstechnik,

am **9. 3. 2018 beim CCeV, Am Technologiezentrum 5, D 86159 Augsburg**
CCeV-Kontakt Bernhard Jahn (Bernhard.Jahn@carbon-composites.eu).

Agenda (Folien deutsch oder englisch, 25 + 5 min)

9:00	**Begrüßung**
9:15	Vortragstitel. *NN, LCC, München (Kümmerer Dr. Hartmann)*
9:30	**Betrachtungen zur Betriebsfestigkeit von CFK-Triaxialgeflechten.** *F.Herrla, Institut für Leichtbau, UniBw, Neubiberg*
10:00	**Novel Lifetime Prediction for UD-materials**. *R. Cuntze, CCeV Augsburg*
10:30	*Kaffeepause*
11:00	**Schwingfestigkeit von Klebverbindungen unter multiaxialer Schwellbelastung**. *C. Nagel, IFAM Bremen*
11:30	**Festigkeitssimulation in Klebverbindungen**. *R. Sachse, DLR Stuttgart*
12:00	**Einbeziehung geklebter Fensterbänder und Glasfronten in die Festigkeit von Schiffen**. *O. Klapp, IFAM Bremen*
12:30	*Mittagspause*
13:30	**Carbon Fiber Armored Polymer – a novel economic process?** *R. Müller, Kube GmbH Ingenieurbüro, Plochingen*
14:00	**Konzentrierte Lasteinleitung in CFK-Strukturen unter Anwendung der lokalen Metall-hybridisierung**. *E.Petersen, DLR Braunschweig*
14:30	**Faseroptische Prüfmethoden zur Inspektion von CFK-Komponenten.** *D. Samiek, Polytec GmbH*
15:00	*Kaffeepause*
15:30	**Koppelmittelfreie Prüfung von CFK und CFK-Metall-Klebeverbindungen mit Hilfe von Luftultraschall.** *R. Steinhausen, Forschungszentrum Ultraschall*
16:00	**Einsatz des Nichtlinearen Ultraschalls für die Untersuchung geklebter CFK-Strukturen.** *M. Kreutzbruck, Institut für Kunststofftechnik, Uni Stuttgart*
16:15	**Resumee, Abschlussdiskussion**
	Get Together

Wir freuen uns auf eine rege Beteiligung und interessante Vorträge

Ihre Ralf Cuntze (08136-7754), Marc Kreutzbruck und Markus Brede

Hinweise: Sitzungstermine: 16. 11. 2018, gemeinsam mit CC Austria, FH OÖ Campus Wels (Österreich), Dr. R. Hinterhölzl (Leiter Studiengang Leichtbau und Composite-Werkstoffe); 8. 3. 19 UniBw, Neubiberg (Institut für Luft- und Raumfahrt, Prof. H. Rapp)

Thementag der AG Engineering
"Ermittlung strukturmechanischer Kennwerte und Modellparameter *unter Beachtung von Auslegung, Nachweis und Zulassung*"

- *Betrachtung von Schicht, Laminat, Festigkeitsmodell etc.* –

Zielgruppe: Berechnungsingenieure in Anwendung und Forschung

Donnerstag, 6. November. Beginn: 9:00 Uhr, Ende: ca. 16 Uhr
Atrium-Saal der HWK Schwaben, Siebentischstraße 52-58, 86161 Augsburg
(Unkostenbeitrag Thementag: 95 € + MwSt für Nicht-Vortragende und Nicht-CCeV-Mitglieder)
Am 7.11. ist eine Veranstaltung der 3 AGs Engineering, NDI und Kleben. IHK-Schwaben, Stettenstr., 9 Uhr
Münchner Leichtbauseminar: "Werkstoff- und Bauteildaten für Simulationsmodelle im Leichtbau" 29.10., 12.11., 26.11.

Begrüßung *R. Cuntze (CCeV) , H. Bansemir (vormals Eurocopter)*

Vorträge (5 min Diskussion), Folien, englisch oder deutsch

1. (9.05) **SURVEY: Material Properties and Model Parameters, necessary for the Analysis of Static & Cyclic Stress States.** *R. Cuntze, CCeV-AGs Engineering Maschinenbau* und *Faserverstärkung im Bauwesen*
2. (9.45) **Beitrag zur korrekten Bestimmung der Quer-Längsschubsteifigkeit und Festigkeit und von Pucks Modellparametern zur Erfassung interner Werkstoffreibung.** *A. Bleier, Karl Mayer Textilmaschinenfabrik, Obertshausen; vormals KLuB TU-Darmstadt*
3. (10.15) **Normen und Standards, Normungsportal der Composites Germany.** *F. Fendt, CCeV-AG Normung und Standardisierung*

Kaffee-Pause: (10.45)

4. (11.15) **Prüfmethoden und Werkstoff-Probekörpergestaltung.** *H. Bansemir, vormals Eurocopter)*
5. (11.45) **„Bessere Methoden für bessere Werte", Verbesserungsvorschläge u.a. am Beispiel der Modul-Degradationsmethode.** *T. Haberle, RUAG*

Mittagsbuffet: (12.15)

6. (13.00) **Ermittlung von UD-Kennwerten und Cuntzes Reibungsparametern beim DLR-Braunschweig.** *E. Petersen, DLR-Braunschweig*
7. (13.30) **Welche Baustoffkennwerte benötigen die Textilbetonbauer?** *F. Schladitz, IfM TU-Dresden*
8. (14.00) **Establishing an in-house Process for Composite Testing – an overview.** *J. Bold, Johnson Controls, Burscheid*

Kaffee-Pause: (14.30)

9. (15.00) **Digimat Multi-Scale Modeling Platform. A Paradigm Shift in the Optimal Engineering of Composite Materials & Structures.** *R. Assaker, X-stream, Munich*
10. (15.30) **Neue Prüfmethoden zur Ermittlung temperatur- und dehnratenabhängiger Kennwertfelder für die Luftfahrt- und Automobilindustrie.** *R. Bochynek, Leichtbau-Zentrum Sachsen, Dresden*
11. (16.00) **Diskussion:** Wo drückt der Schuh am meisten? **mit Ausklang im Foyer, Abendbuffet**

Es freuen sich auf eine rege Beteiligung und inhaltsreiche interessante Vorträge

Ihre Ralf Cuntze und Horst Bansemir

CARBON COMPOSITES	*MINUTES OF MEETING (MOM)* THEMENTAG ERMÜDUNG	Februar 14, 2013

Gemeinsame Sitzung mit „Deutsche Arbeitsgruppe BeNa (Betriebsfestigkeits-Nachweis)
Ermüdung von Bauteilen aus Faserverbundwerkstoff (FVW)
- Vertiefte Betrachtung von UD-Laminaten mit Ausblick Textile Composites –

Ort: IHK Schwaben, Stettenstrasse 1+3, 86150 Augsburg, Hans-Liebherr-Raum. Zeit: 8.00 bis 17.00.
Vorträge: 20 min + 5min Diskussion
Begrüßung: *(P. Horst, TU-Braunschweig, Leiter AG BeNa)*; einführende 'Folien' *(R. Cuntze, CCeV*
Vorstellung und Ziele der AG BeNa. *P. Horst, TU-Braunschweig*

1. Vom Ermüdungsverhalten von Metallen zu dem von FVW. *G. Kress, ETH Zürich*
2. Ein Lebensdauervorhersagemodell für langfaserverstärkte Laminate. *R. Cuntze, CCeV*
3. ZfP und Festigkeit/Ermüdung. *V. Trappe (BeNa), BAM Berlin*
4. Ein neues physikalisch basiertes Ermüdungs-Schädigungsmodell für Faser-Kunststoff-Verbunde. *R. Rolfes (BeNa), ISD, TU-Hannover*
5. FE-Analyse der Ermüdungsschädigung von FKV. *M. Magin (BeNa), IVW Kaiserslautern*
6. Anforderungen und Herausforderungen an die Betriebsfestigkeiten für Faserverbund strukturen bei der A350XWB. *D. Hartung, Premium Aerotec Augsburg*
7. Composite Fatigue Approach in Airbus. *W. Göbel / L. Ratier, Airbus*
8. Ermüdet Textilbeton? *F. Jesse, BTU-Cottbus*
9. Fatigue Life Simulat. and Verification of Wind Turbine Rotorblades. *E. Eyb, Re-Power*
10. Betriebsfestigkeitsbewertung von Faserverbundwerkstoffen – Übersicht und Ausblick. *M. Hack, LMS Kaiserslautern*
11. Methods for life predict. of comp. materials and adhesively-bonded composite joints. S. *Vassilopoulos, EPFL Lausanne, CH*, editor *"Fatigue life prediction of composites and comp. structures"*, 2010
12. Lebensdauervorhersage bei BMW. *P. Wagner, BMW München*
13. Zur Festigkeitsbewertung von CFK-Strukturen unter PKW-Betriebslasten. *C. Hahne/ U. Knaust, Audi Ingolstadt*
14. Praxiseffekte bei der Schwingfestigkeitsanalyse orthotroper Faserkunststoffverbunde. *Ch. Enke / J. Eulitz / R. Grothaus, EAST-4D Carbon Technology Dresden*
15. (I) Geschichte der Fatigue-Nachweisführung bei Eurocopter (seit 1965). *H. Banzemir.* (II) Vorgehensweise bei dem Fatigue-Nachweis mit der Bestimmung der Wöhlerkurven und Arbeitskurven. *E. Ahci, Eurocopter Donauwörth .* (III) Die dynamische Festigkeit von Kohlefaser-Verbundstrukturen. *A. Weinert, Eurocopter*

Aufnahme von interessierten Industrie- und Behördenmitgliedern in die AG BeNa. :
Laut Teilnehmern (>120) ein erfolgreicher Thementag mit der richtigen Mischung.

1. Workshop "Composite Fatigue",6.2.2014: Bitte um Vortrags-Vorschläge bis zum 1. 9. 2013 an mich.
2. Thementag "Industrielle Anwendbarkeit der Schädigungsmechanik – Schwerpunkt FVW", 24.10.2013, ganztägig in Augsburg vor der Herbstsitzung der AG "Engineering ", Fr.25.10.13
3. Fazit : Die Abschätzung der Lebensdauer von FKV-Bauteilen unter Betriebsbeanspruchung ist eine wichtige Aufgabe, weil man sich nur begrenzten Testaufwand erlauben kann. Generell kann man sagen: Es ist keine allgemein anwendbare Lebensdauervorhersagemethode für Laminate vorhanden und das erst recht für textile Laminate. Ermüdungsgefahr besteht auch seitens der Textilbetonindustrie.

Meinen allerbesten Dank an alle Vortragenden für die gelungenen Vorträge.

Ihr Ralf Cuntze

PS: Nur Mitarbeiter von CCeV-Mitgliedern haben vollen Zugriff auf alle PDFs auf der CCeV-Website.

Experience Composites 2016 – Symposium/Congress, Sept. 21-23

Augsburg Messezentrum **Thementag**

1. (10.00) **Introduction Design and Design Verification.** *R. Cuntze, CCeV, Augsburg*
2. (10.30) **Novel Material models and multi-scale simulation methods for composite materials.** *R. Boehm, ILK Dresden*
3. (11.00) **Simulation of Manufacturing Processes.** *C. Huehne, DLR-Braunschweig*
4. (11.30) **MAI-Cluster, Impacts from Section Design Results.** *R. Hinterhoelzl, LLC, TU-München*

Lunch Break (12.00)

5. (13.30) **Load Introduction in Monolithic and Hybrid Leightweight Structures.** *H. Rapp, UniBw München*
6. (14.00) **Fatigue, BeNa's View State–of-the-Art**: *I. Koch, ILK TU-Dresden (member of German fatigue working group BeNa, Betriebsfestigkeits-Nachweis)*
7. (14.30) **Strength and Curing Simulation of Thick-walled Composites with ANSYS WB 17.0.** *R. Roos, ANSYS Switzerland*
8. (15.00) **Impacts from the NAFEMS Composites Group.** *C. Huehne, DLR-Braunschweig, NAFEMS Steering Committee*

Coffee Break (15.30)

9. (16.00) **The German Aeronautical Handbook HSB: Current contributions and research activities on fundamentals and methods for structural design and analyses.** *M. Schagerl, JKU-Linz, Austria*
10. (16.30) **First-Ply Failure and what then? – Solutions for a detailed simulation of failure.** *Matthias Hörmann, CADFEM GmbH, Grafing*
11. (17.00) **Certification Aspects.** *H. Bansemir, formerly Eurocopter Germany, München.*

Thementag "Industrielle Anwendbarkeit der Schädigungsmechanik"

- *Betrachtung von UD Laminaten bis zu textilen Composites – Grundlagen und Anwendung*

Zielgruppe: Berechnungsingenieure in Anwendung und Forschung

Donnerstag, 24. Oktober. Beginn: 8:15 Uhr, Ende: 16.00 Uhr

A1-01-A1.02-Saal der HWK Schwaben, Siebentischstraße 52-58, 86161 Augsburg

(Am 25. 10. ist die gemeinsame Veranstaltung der 3 AGs Engineering, NDI, Kleben. Hierzu sind alle Teilnehmer ebenfalls eingeladen. Zwei Schädigungsmechanik-Vorträge werden dann nachgeholt. Unkostenbeitrag: 95€ für Nicht-Vortragende und Nicht-CCeV-Mitglieder)

Begrüßung *R. Cuntze (CCeV), R. Böhm (ILK Dresden)*

Vorträge (25 min + 5 min Diskussion): *Betonung: Was gelt? Wo drückt der Schuh?*

1. (8.30) **Einführung in die Schädigungsmechanik von Werkstoffen.** *Dr. U. Weber, Prof. S. Schmauder (IWMF Uni Stuttgart), in English or German*
2. (9.00) **Schädigungsmechanik für Faser-Kunststoff-Verbunde: Phänomenologische Ansätze.** *Dr. R. Böhm (ILK Dresden)*
3. (9 .30) **Virtuelle Werkstoffentwicklung mit Multi-Skalen-Simulationen am Beispiel von Leichtbau-Flugzeugturbinen.** *A. Freund (LZS Dresden).*

Kaffee-Pause: (10.00)

4. (10.30) **Modellierung der Schädigungsmechanismen bei keramischen Faserverbundwerkstoffen.** *Dr. S. Hofmann, (DLR Stuttgart)*
5. (11.00) **3D-XFEM-Modellierung des Schädigungsverhaltens von Faser-Kunststoff-Verbunden.** *Dr. M. Kästner, S. Müller, Prof. V. Ulbricht (IFKM Dresden)*
6. (11.30) **A link between damage initiation thresholds in static loading and fatigue strength of textile composites.** *Prof. S. Lomov, MTM Leuven*

Mittagsbuffet: (12.00)

7. (13.00) **Entwicklung der Schädigungsmechanik für Faser-Kunststoff-Verbunde (FKV) von 1970-2013.** *Prof. A. Matzenmiller (Uni Kassel)*
8. (13.30) **Anforderungen an die Schädigungsmechanik von FVK-Laminaten für die virtuelle Fahrzeug Crash-Auslegung.** *Dr. M. Nossek (BMW AG)*
9. (14.00) **Failure Analysis at Airbus.** *Dr. Anja Wetzel (Airbus, Hamburg)*

Kaffee-Pause: (14.30)

10. (15.00) **Mechanism-based Three-dimensional Constitutive Model for Anisotropic Damage in Fiber-reinforced Composites.** *M. Chatiri (CADFEM)*
11. (15.30) **Diskussion zur erreichten Anwendbarkeit der schädigungsmechanischen Ansätze**

Ausklang im Foyer, Abendbuffet, Zeit für Gespräche

Freitag, 25.10. Nachläufer (Vortragende vorlesungsmäßig am 24. belegt) im Rahmen der AG *Engineering*:

1. **Modellierung von Material- und Strukturschädigung des Verbundwerkstoffs Stahlbeton.** *Prof. V. Petryna (TU-Berlin)*
2. **Schädigungsmechanik für Faser-Kunststoff-Verbunde – Mikromechanisch basierte Ansätze.** *Prof. R. Rolfes (ISD Uni Hannover),*

Bitte Herrn Jahn (CCeV) mitteilen: (1) Wegen Catering, Teilnahme an welchen Buffets; (2) Übersendung des Vortrag-PDFs

Es freuen sich auf eine rege Beteiligung und inhaltsreiche interessante Vorträge

Ihre Ralf Cuntze und Robert Böhm

CC BAU

CARBON COMPOSITES

Bemessung und Nachweis

- *vom Werkstoff bis zur Zulassung von Bauteilen aus Polymermatrix und Betonmatrix* -

Veranstaltung von allen CC Bau-AGs

Zielgruppen: Bauwirtschaft, Architekten, Planer, Handwerker, Auftraggeber, Zulassungsstellen

22. Oktober 2019 in Weimar, beim Institut für Angewandte Bauforschung Weimar gGmbH

Örtlicher Kontakt: Frau Schalling, 03643 8684 148, k.schalling@iab-weimar.de>

CCeV-Kontakt Bernhard Jahn (Bernhard.Jahn@carbon-composites.eu).

Thementag: 95 € für Nicht-Mitglieder, frei für Vortragende, Presse.

Folien: englisch, deutsch. Vorträge: 25 + 5 min Diskussion.

8:30	Registrierung der Teilnehmer, Kaffee und Brezeln o.ä.
8:45	**Einführende Worte mit Ausrichtung CC Bau.** *R. Cuntze / J. Ridzewski*
9:00	**Vorstellung Institut:** *Dr.-Ing. Barbara Leydolph, IAB Weimar*
9:15	**Verwendete Baustoffe mit Schwerpunkt Carbonbeton:**. *M. Butler, Institut für Baustoffe, TU Dresden*
9:30	**Fertigungsverfahren: Bauteile mit Polymermatrix.** *J. Ridzewski, IMA Dresden*
10:00	**Fertigungsverfahren: Bauteile mit Betonmatrix**. *G. Eisewicht, BCS Natur- und Spezialbaustoffe GmbH Dresden*
10:30	*Kaffeepause*
11:00	**Festigkeitsmodellierung der Baustoffe Beton und Lamelle**. *R. Cuntze, CC Bau Augsburg*
11:30	**Lasten, Sicherheitskonzept und Zulassungsaspekte.** *S. Rempel, Solidian Albstadt*
12:00	**Dimensionierungsbeispiel, GFK-Behälter** (nach BüV 2010). *M. Oppe, Büro Knippers-Helbig Stuttgart*
12:30	*Mittagspause*
13:30	**Dimensionierungsbeispiel, Faserbetonbauteil.** *B. Wietek, Sistrans, Tirol*
14:00	**Dimensionierungsbeispiel, CF-Textilbeton-Bauteile**: *S. May, Carbocon-GmbH. Dresden*
14:30	**Dimensionierungsbeispiel, CLT-Modellierung und Bemessung einer Textilbeton-Schale.** *D. Franitza, FE-Union GbR, Chemnitz*
15:00	*Kaffeepause*
15:30	**Abteilungsversammlung**
16:00	**Get Together**

Wir freuen uns auf Ihre Beiträge Ihr Ralf Cuntze und weiterer CC Bau-Vostand

Hinweise: CC Bau, ehemals CC TUDALIT, Fachabteilung des CCeV, besteht ab 1.1. 2018 aus den 4 AGs: Bemessung und Nachweis (Prof. Ralf Cuntze), Faserverbundarmierte Betone (Dr. Ingelore Gaitzsch), Faserverstärkte Kunststoffe (Prof. Jens Ridzewski), Automatisierte Fertigung im Bauwesen (kommissarisch: Ralf Cuntze)

Termine 2019: 22. Februar, AG „Faserarmierter Beton", Uni Dresden, 13. Juni, AG „Automatisierte Fertigung im Bauwesen", Uni Innsbruck

Termine 2020: Workshop am 19. Februar, Ulmer Betontage bzgl. „Wie bekomme ich Carbonbeton-Anwendungen auf die Bausstelle"?; CC Bau-AGs-Sitzung, 24. Februar, Siegen (weitere Sitzungsplanung mit Möglichkeiten Aachen, Dresden,

Carbonbeton – die Zukunft des Bauens hat begonnen

Foto: Silvia Statt mayer

Prof. Dr.-Ing. Ralf Cuntze

Als sich 1970 zum ersten Mal Carbonfasern (CF) in meine Fingerspitzen bohrten, wusste ich noch nicht, wie schmerzhaft erst der weitere Weg in Richtung Anwendung sein würde. Die damals gegenüber heute hundertfach teurere Carbonfaser fand praktisch nur Einsatz in Raumfahrt, Luftfahrt oder ultraschnellen Zentrifugen, also im Maschinenbau, und sie war eingebettet in eine Kunststoffmatrix. So waren Ende der 1970er Jahre Diskussionen mit Prof. Rupert Springenschmid, damaliger Institutsleiter „Zentrum Baustoffe und Materialprüfung" der TU München, über den Einsatz von Carbonfasern im Bauwesen schlicht visionär. Erst als ich etwas später bei Prof. Urs Meier, eidgenössische Materialprüfanstalt EMPA, einen sechs Meter langen Biegeträger aus Glasfaserkunststoff bei einem erfolgreichen Langzeit-Ermüdungstest bewundern konnte, bekamen Gedanken bzgl. der Verwendung von Faserkunststoff und Faserbeton im Bauwesen wieder einen Nährboden. An einen Einsatz der immer noch sehr teuren Carbonfasern im Bauwesen war aber noch nicht zu denken.

Der Einsatz z. B. von Kurz-Glasfasern in Faserbeton zur Erhöhung der Zugfestigkeit war ein erster Schritt in Richtung Fasereinsatz, allerdings darf dieser derzeit nicht als anrechenbarer Anteil von tragender Bewehrung gesehen werden, sondern als eine signifikante räumliche Erhöhung lokaler Festigkeit, die sonst zusätzlich durch „händisch" zu armierende Lasteinleitungsstellen abgedeckt wird. Für solche Fälle könnten mm-lange Carbonfasern, hergestellt aus „gemahlenem" rezykliertem Carbonfaser-Gewölle, räumlich verteilt in trockenen Zement, sicherlich ihren Einsatz finden. Erst als es gelang, Stahlstäbe in Stahlbewehrungsmatten durch textile Gelege aus polymermatrixbeschichteten alkaliresistenten Glasfaserrovings und später auch Carbonfaserrovings zu ersetzen (entspricht einem Faser-Kunststoff-Verbund), war der Startschuss für professionelle Anwendungen gegeben und der sogenannte Textilbeton geschaffen. Natürlich ist die Betonmatrix an die jeweilige Faserverstärkung anzupassen. Zulassungen für Bewehrungsstäbe gibt es für Glas.

Durch die im Vergleich zum Stahlbeton kleinere Maschenweite der Carbon-Bewehrungsmatte und die feinere Betonmatrix werden die lokale Rissbildung und somit das Eindringen von Feuchtigkeit stark verringert. Damit wird das gefürchtete Beton-Abplatzen (stahlkorrosionsbedingtes Abplatzen gibt es nicht mehr) nach einigen Jahren als Folge der sogenannten Alkali-Aggregat-Reaktion behindert und die Dauerhaftigkeit des Bauteils erhöht. Bauwerke mit der immer noch relativ teuren Carbonfaser „rechnen sich", wenn man die minimale Wartung, die geringere Betonmasse sowie den niedrigeren Montageaufwand lebenszyklusbezogen kostenkalkuliert. Dies gilt speziell für den anstehenden riesigen Aufwand zur Bauwerkserhaltung und -verstärkung!

Energieverbrauch und CO_2-Erzeugung sind wesentlich geringer als bei Betonstahl, wobei die Einsparpotenziale noch nicht ausgeschöpft sind. Carbonbeton, diese neue Art des Bauens, wird somit sicherlich einen wesentlichen Innovationsschub im Bauwesen auslösen. Leichtere und filigranere Konstruktionen bis hin zu einem neuen Möbeldesign werden Wirklichkeit. Bauen wird ressourcenschonender, nachhaltiger und effizienter werden. Wünschenswert wäre es, wenn die langwierige Zulassungsprozedur weniger Hürden hätte, aber auch die Planung von Bauten mehr auf der Basis von Nachhaltigkeit durchgeführt würde.

Lassen Sie sich durch die Beiträge in diesem Heft begeistern. Besonders möchte ich Ihnen dabei die Vorstellung der sogenannte Planermappe ans Herz legen, mit der die notwendige Überzeugungsarbeit bei Architekten, Baufirmen und Zulassungsstellen einfacher wird.

Ihr Ralf Cuntze
(R C = Reinforced Concrete)

By the way: I almost forgot, but I met Prof. Springenschmid (now 95) in November 2024:
As early as 1977, I (*MAN-Technologie*) often discussed with him and co-workers (*Center for Building Materials and Materials Testing at the Technical University of Munich*) in detail about reinforcing finer concrete with CF k-filament rovings (now applied are tows containing 50k filaments).

CC BAU CC AUSTRIA CC SCHWEIZ CARBON COMPOSITES

DACH-Veranstaltung aller Arbeitsgruppen der CCeV-Fachabteilung „CC Bau“

am 21.06.2018, Raum MY 01.09, bei der
ZHAW Architektur, Gestaltung und Bauingenieurwesen,Gebäude MY, Lagerplatz 21, 8400 Winterthur,
Frau Sydow, 0041 58 934 69 82, CCeV-Kontakt: Bernhard Jahn (Bernhard.Jahn@carbon-composites.eu).

Das Bauwesen ist eine Branche, bei der das Thema Hochleistungsfaserverbund einerseits noch nicht etabliert ist, andererseits jedoch ein enormes Anwendungspotential besteht. Vor diesem Hintergrund hat sich der Carbon Composites e.V. (CCeV) entschieden, das Thema für seine Mitglieder weiter aufzubereiten, zu vertiefen und gemeinsam voranzutreiben. Am 28. September 2017 wurde daher „CC Bau“ als CCeV-eigene Fachabteilung gegründet. CC Bau knüpft direkt an die bisherige Gemeinschaftsabteilung CC Tudalit von CCeV und Tudalit e.V. an. Auch in Zukunft wird die Fachabteilung CC Bau zum Mehrwert der Mitglieder eng mit anderen Netzwerken wie Tudalit e.V. und C^3 – Carbon Concrete Composite e.V. kooperieren. Die Fachabteilung CC Bau bietet mit ihren Arbeitsgruppen eine Plattform für Kontakte, Wissenstransfer und Erfahrungsaustausch auf dem Gebiet leichter faser- und textilverstärkter Verbundstrukturen für Anwendungen im Bauwesen. Eingeladen sind Vertreter aus Wissenschaft, Forschung und Lehre, Unternehmer aus der gesamten Wertschöpfungskette von textilverstärkten Verbundstrukturen sowie Planer, Vertreter von Behörden und interessierte Bauherren. Die Arbeitsgruppen unterstützen mit Vortrags- und Gesprächsangeboten die Entwicklung neuer Projekte und innovative Zusammenarbeit.

CCeV-Thementag: CCeV-Mitglieder und Vortragende frei, Nicht-CCeVler 95€ (zzgl. 19%MwSt)

Programm (Folien deutsch oder englisch, 25 + 5 min),

9:15	**Begrüßung** - *Prof. Cuntze, Prof. Kurath*
9:30	**Mit Carbon stark vorgespannte, sehr dünne Betonplatten CPC** - *Prof. J. Kurath, ZHAW Winterthur, Architektur, Gestaltung und Bauingenieurwesen*
10:00	**3D Carb.** - *Prof. P. Ermanni/ 3D Carb-Beteiligter, ETH Zürich*
10:30	*Kaffeepause*
11:00	**22 Jahre Forschung über mit Karbonfasern vorgespannten Beton an der EMPA.** - *Prof. G. Terrasi, EMPA, Dübendorf*
11:30	**Faserverbundwerkstoff-Visionen der 1970er und 80er Jahre: Update 2018.** - *Prof.. U. Meier, EMPA, Dübendorf*
12:00	**Eigenschaften und Anwendungsfelder gestickter textiler Bewehrungen.** - *Prof. J. Feix / M. Egger, Institut Massivbau und Brückenbau, Uni Innsbruck*
12:30	*Mittagspause*
13:30	**Stickerei als Fertigungstechnologie für die Bautechnik.** - *Prof. T. Bechtold, Textilchemie, Uibk Vorarlberg*
14:00	**Zur Bemessung von Brücken und Dächern aus Faserverbundwerkstoffen.** - *Prof. T. Keller, EPFL-ENAC-CCLAB, Lausanne*
14:30	**CFK- Verstärkungen in Deutschland.** - *Dr. H. Peters, Büro HPS (Carbon for Civil Engineering Stuttgart / T. Lepinski, Entecsol, Wittstock,*
15:00	*Kaffeepause*
15:30	**Die TUDALIT-Planermappe.** *(Autoren: U. Assmann /. P. Offermann, TUDALIT e.V. - Dresden) - Prof. Cuntze*
16:00	**ZHAW-Besichtigung**
	Get Together

Ihr Ralf Cuntze (08136-7754) mit Ingelore Gaitzsch, Jens Ridzewski, Otto Kellenberger

Hinweise: Nächste Veranstaltungen aller Arbeitsgruppen der CCeV-Fachabteilung CC Bau ist am 09.11.2018 in Stuttgart (DLR Stuttgart, Pfaffenwaldring 38-40, Hörsaal, 70569 Stuttgart, Campus Vaihingen).
10. Carbon- und Textilbetontage, 25.-26.9. 2018 in Dresden.

4. Thementag der AG 'Automatisierte Fertigung im Bauwesen inklusiv Serielles Bauen'

Dienstag, 30.03.2021
Zoom-Videokonferenz

CUeV-Kontakt: Bernhard Jahn (Bernhard.Jahn@carbon-composites.eu).
Teilnehmergebühr: 55 € für Nicht-Mitglieder, frei für CU-Mitglieder, Vortragende und Presse.
Folien englisch, deutsch. Vorträge: 25 + 5 min Diskussion, in Deutsch, falls möglich .

08:30	**Registrierung der Teilnehmer**
09:00	**Begrüßung.** *CU BAU* (Cuntze und Dr. Thomas Heber für Roy Thyroff)
09:10	**Kurzvorstellung Composites United mit CU Bau + Einführung.** *Prof. Dr.-Ing. habil. Ralf Cuntze*
09:30	**Industrieller 3D-Druck im Bauwesen – Anwendung des Powder-Binder-Jettings.** *Dipl.-Ing. Tobias Grün; Voxeljet AG, Friedberg*
10:00	**'3D-Druck' in der Baupraxis – Erfahrungen der ersten zugelassenen Gebäude in Deutschland.** *Dr. Fabian Meyer-Brötz, Leitung 3D Construction Printing, Peri GmbH, Weissenhorn*
10:30	**Additive Fertigung im Bauwesen: Neue Herausforderungen für numerische Simulations-methoden.** *M.Sc. Alexander Paolini, Lehrstuhl für Computergestützte Modellierung und Simulation, TU München*
11:00	*Kaffeepause*
11:30	**Klassifizierung digitaler Fertigungsverfahren im Betonbau.** *Prof. Dr.-Ing. Viktor Mechtcherine, Institut für Baustoffe, TU Dresden*
12:00	**Connecting Value Chains – Status Quo der Robotik im Bauwesen .** *Dipl.-Ing. Thomas Adams, Individualized Production in Architecture/RWTH Aachen University*
12:30	*Mittagspause*
13:30	**Automatisierung im Bauwesen – Robotereinsatz auf der Baustelle (Mauerwerksrobotik).** *M.Sc. Adrian Fehrle, Lehrstuhl für Fertigungsautomatisierung und Produktionssystematik, FA-Uni Erlangen-Nürnbg*
14:00	**Additive Fertigung im Bauwesen durch selektive Zementaktivierung.** *M.Sc. Daniel Talke, Lehrstuhl für Holzbau und Baukonstruktion, TU München*
14:30	*Kaffeepause*
15:00	**Produktion individueller Teile für Decken und Träger bei ersten Praxisprojekten.** *Dipl. Ing. Eduard Artner, BauMinator / '3D Druck', Baumit GmbH, Wopfing, Österreich*
15:30	**3D-Welding - WAAM im Bauwesen.** (Auftragsschweißen) *Dipl.-Ing. Christoph Holzinger, Assoc.-Prof. DI. Dr.nat.techn. Andreas Trummer, Technische Universität Graz*
16:00	**Virtuelle Besichtigung der 3D-Druck-Einrichtungen des IGCV-Neubaus in Augsburg.** *Dipl.-Ing. M. Binder, IGCV Fraunhofer Augsburg, Additive Fertigung – Werkstoffe und Prozessentwicklung*
16:45	**Schlusswort / Get Together**

Programmgestaltung: Ralf Cuntze

Letzte und kommende Termine der Fachabteilung CU BAU:
20.10. 2020: CU-Bau AG Faserverbundarmierter Beton. Zoom-Videokonferenz
19.11. 2020: CU Bau-Thementag „Richtlinien, bauaufsichtliche Zulassungen und Bauartgenehmigungen für die potenziellen Anwender Architekten, Tragwerksplaner und Bauherrn"
25. 02. 2021: CU Bau-Forum „Carbonbeton-Anwendungen in der Praxis – auf der Baustelle und im Fertigteilwerk". Ulmer Betontage.

Definition: ISO/ASTM 52900 defines (digitized) Automatic Fabrication (Fertigung, nicht 'Manufaktur') as "Process of joining materials to make parts from 3D model data, usually layer upon layer". 3D-Druck ist ein Verfahren innerhalb AF, nicht korrekt oft noch immer *Manufacturing* genannt, obwohl automatisiert
'3D-Druck' bedeutet laut VDI-Ri 3405 „Kaltes Extrusionsverfahren, wobei der Baustoff über eine Düse strangweise abgelegt wird" oder baubezogen "Extrudierte Ablage von Betonsträngen". 3D-Druck ist im Wesentlichen ein "Pulverbett-basiertes Verfahren", wie es z.B. Voxeljet für die Herstellung von Schalung benutzt.

Theme day of the WG 'Automated production in construction including serial construction'

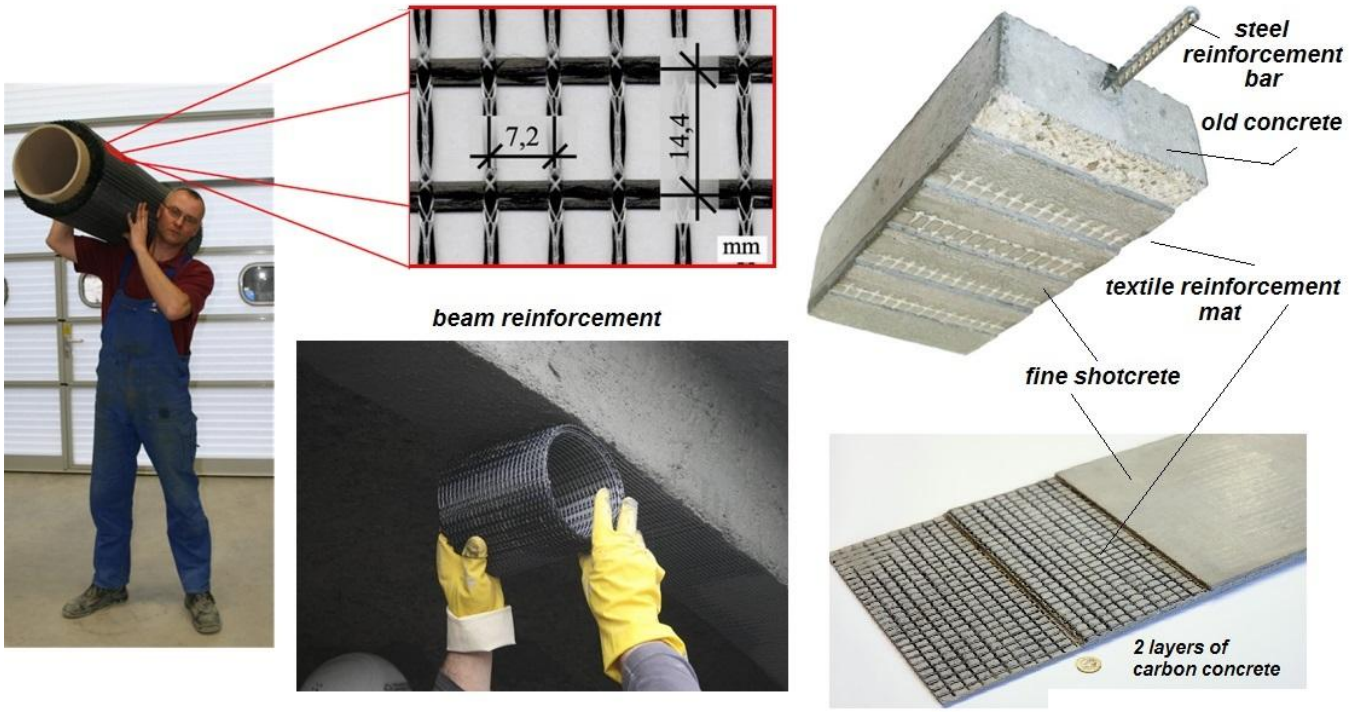

Fig.: For Rehabilitation, retrofitting of a slab. Fiber grid in detail and wrapped on a roll during application. As an example 2 applied fiber grid lattice layers of CF yarns. [IfM Dresden]

Fig: Erected over night!
First, purely CF-reinforced concrete bridge in the world. Albstadt-Ebingen. 2015, using a solidian GRID Q95-CCE-38 fiber grid (mat) [christian.kulas@solidian.com, www.solidian.com]
Thanks to Christian.

Citation of the (civil engineer) Mayor of Albstadt, Udo Hollauer:

*"**The bridge pays off, and is sustainable"!!***

Some project disappointments after a relatively large effort

MAN-Technologie (MT):

- **Stop of the Uranium Enrichment Multi-body Centrifuges in Steel and CFRP after having achieved a speed record with the CFRP rotor version**
- **MT stopped the wind energy business after GrOWIAN, WKA 60 etc**
- **Ariane 5-Hermes after some ESA-driven effort**

{{Information |Description ={{fr|1=Projet de navette spatiale Hermès.
 "Olympus OM10 + Kodachrome 100 ASA"}} |Source ={{own}} |Author =Daniel Villafruela |Date =1992-05-05 |Permission = |other_

From WIKIPEDIA: Hermes was originally a project of the French Space Agency (CNES) for a manned space shuttle to supply flights into low Earth orbit (LEO) and continued by the European Space Agency (ESA). The project was discontinued in November 1992 after a change in financial and political conditions. Hermes was to be launched into space at the top of an Ariane 5 and consisted of two modules: the resource module, which will be separated before re-entry into the atmosphere, and the space shuttle itself, which would land in the same way as the Space Shuttle. In the last planning version, before the end of the project, Hermes was supposed to transport three astronauts and three tons of payload. The total mass at launch would have been 21 tonnes, which was considered the maximum payload of an Ariane 5 Plus

Private projects :

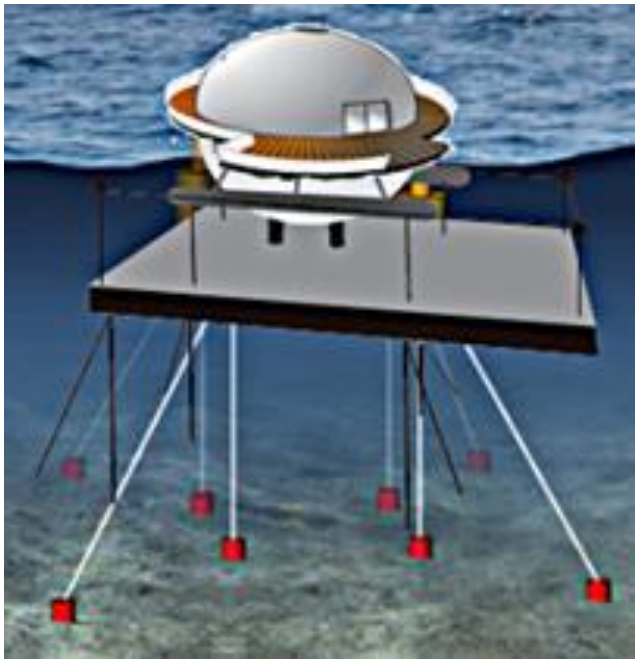

Project Idea, ArcOval, 2015

Purist-Engineering bureau:
(*Martin Maria Daum & Elis Heck, Karlsruhe*)
"Development of new concepts for the water habitat"

Floating House on a 'Tension Leg' Platform (TLP)

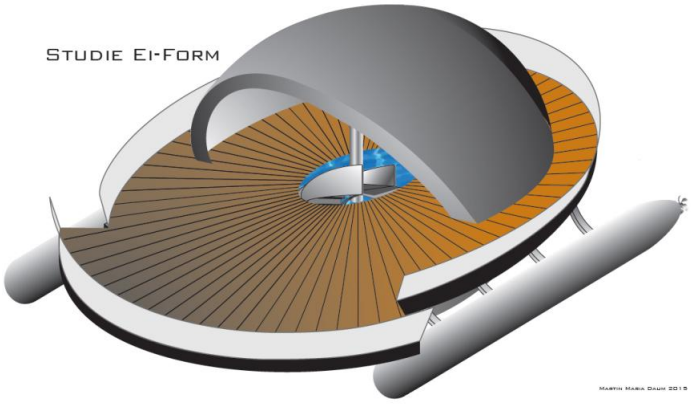

Humans have always dreamed of making the oceans habitable, but a colonization of open sea areas with artificial islands firmly fixed to the seabed is still pending. The project described below shows which possibilities can already be realized. Young developments in the field of materials such as carbon concrete, constructive developments in the construction of marine structures, as well as progress in solar energy generation and energy storage enable the construction of the floating and mobile building described below:

The floating building consists of a coated, corrosion-free textile carbon-reinforced concrete shell. Inside, there are residential and functional units on two levels. With a volume of approx. 500 m^3, the ArcOval is comparable to a small single-family house:

* Architect Martin Maria *Daum*, Karlsruhe: The idea
* Civil Engineer Ralf *Cuntze*, head of the working group "Fiber Reinforcement in Construction" at Carbon Composites e.V. Augsburg:
  The composition of further consortium members
  Prof. Dr.-Ing. Frank *Dahlhaus*, TLP, Uni Freiberg
  Dr.-Ing. habil. Sandra *Gelbrich*, Research area 'lightweight construction in construction' with Uni Chemnitz
  Dr.-Ing. Peter *Strangfeld*, BTU Cottbus
  Prof. Dr.-Ing. Frank *Hülsmeier*, Uni Leipzig
  with preparation of the template for funding.

A 75 m^2 photovoltaic system is used for self-sufficient energy supply. The solar-generated electricity is stored by lithium-ion batteries. To reduce unnecessary electricity consumption through electricity conversion, there is both an alternating current grid and a low-voltage supply.

The principle of the Tension Leg Platform was developed for anchoring large oil rigs and offshore wind turbines. At sea depths of over 30 meters, this anchoring method offers significant cost advantages over conventional steel constructions. The enormous buoyancy of the 400 m^3 ArcOval buoyancy body is

compensated by the ballast bodies placed on the seabed. A stiffening rope construction combines ballast and buoyancy. The platform, which floats below the surface of the water, is almost immune to wave movements due to this construction, i.e. like a solid island.

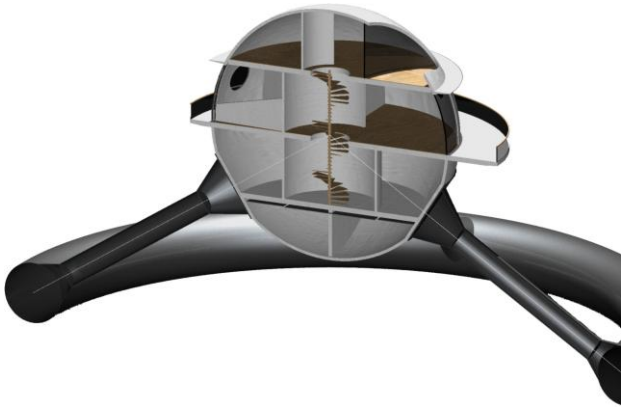

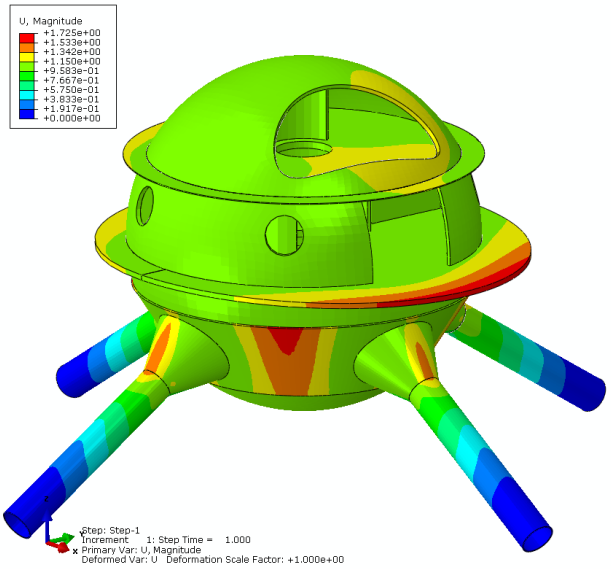

Design studies
above: ***Living space concept,***
*right****: preliminary statics***

Andreas Ehrlich, Sandra Gelbrich (*TU-Chemnitz*)
Professur Strukturleichtbau und Kunststoff-verarbeitung (*L.Kroll*), FB Leichtbau im Bauwesen

Tension-leg Platform

Frank Dahlhaus (*TU Bergakademie Freiberg*)

Counterweight on the seabed.
Toroidal floating ring is held under
the water surface (*horizontal line right*) with ropes.
Stabilization by buoyancy of the ring.

Unfortunately,
after the completion of this preparatory work,
Mr. Daum fell pretty ill and the project had to be stopped
before submission as a real research project with a diverse
combination of new tasks.

Project Idea

High Performance Concrete (HPC) optimized with Carbon Nano Tubes (CNT) and nano-structured cement, with and without fiber reinforcement, 2014/15

Basic ideas of the project application manager Ralf Cuntze:

1. Basic idea of the project application manager R. Cuntze: Concrete matrix: Dispersion of multi-k roving snippets, so that a stochastic spatial distribution of the very light individual fibres homogeneously reinforces the concrete matrix, fibre volume content approximately 1%. This helps to strengthen stress concentration loci avoiding the introduction of locally necessary, time-consuming reinforcement at these local stress concentration points, such as edges, load applications, boreholes.
   → main project goal: High tensile strength UHPC concrete 'matrix' through evenly distributed insertion of mm-sized individual fibers in an optimized cement mixture for the concrete matrix. Good for local stress peaks, force application points of highly stressed components such as railway sleepers, etc.
2. Load-carrying components: Replacement of the steel reinforcement mats in the planned demonstrators with carbon and possibly very inexpensive basalt fibre mats (alkali resistance!), called fiber grids. Weight reduction is directly given, as no rust protection cover of about 2 cm is necessary.

The short version of the research proposal reads:
The aim is to develop a dense, ultra-high-strength concrete in order to use short-fibre and long-fibre reinforcements to produce components with optimum weight, strength, fracture toughness and wear, with a long service life. In addition to the use of specially activated CarbonNanoTubes (CNT), the use of nanostructured cement (CO_2 savings by avoiding energy-intensive clinker burning due to the use of blast furnace slag) helps to achieve this.

*In the project, the flooring manufacturing partner KLB (Kötztal) is responsible for mixing the concrete matrix components and producing the standard test specimens required for certification.
*The KMU Zoz activates the blast furnace slag as well as dry dispersion CNTs and creates the concrete matrix composition with Uni-Augsburg and KLB.
*Uni-A creates, tests and analyzes small test specimens as part of matrix optimization.
*Construction company Kalchschmid lays out and manufactures the transformer house demonstrator achieving a reduction of wall thickness and of the about 35% steel reinforcement with its difficult armoring
*Technical University of Munich determines relevant hardened concrete properties.

Compilation of the future consortium partners and preparation of the project documents by R. Cuntze.

Project winning chance was very high.
Nevertheless, two SME partners dropped out and could not be replaced, so that further application efforts became pointless.

Probably the first World-Wide Conference on Wind Energy (1978)

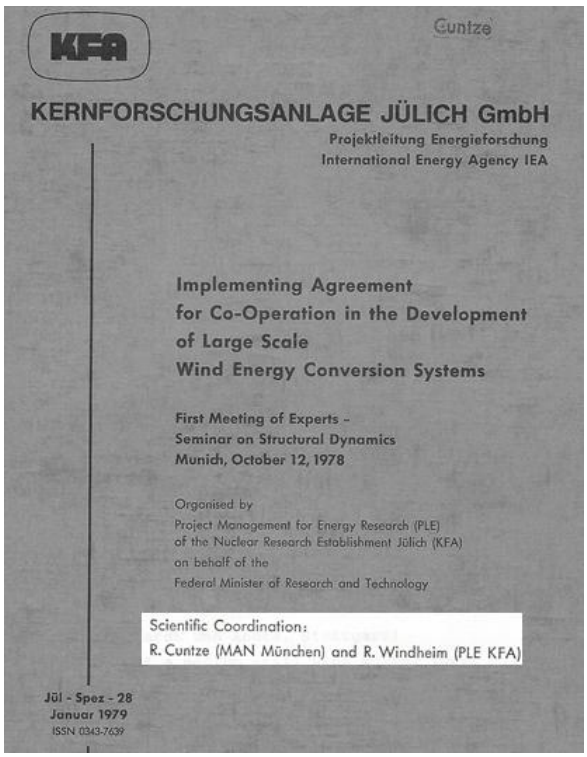

KFA

Cuntze

KERNFORSCHUNGSANLAGE JÜLICH GmbH

Projektleitung Energieforschung
International Energy Agency IEA

Implementing Agreement
for Co-Operation in the Development
of Large Scale
Wind Energy Conversion Systems

First Meeting of Experts –
Seminar on Structural Dynamics
Munich, October 12, 1978

Organised by
Project Management for Energy Research (PLE)
of the Nuclear Research Establishment Jülich (KFA)
on behalf of the
Federal Minister of Research and Technology

Scientific Coordination:
R. Cuntze (MAN München) and R. Windheim (PLE KFA)

Jül - Spez - 28
Januar 1979
ISSN 0343-7639

Bau, Test und Entwicklung großer Windenergieanlagen

Seminar über Arbeiten im Rahmen des Programmes Energieforschung und -technologien des Bundesministers für Forschung und Technologie 23./24. März 1981

Durchgeführt von der
Projektleitung Energieforschung PLE
in der Kernforschungsanlage Jülich GmbH KFA
im Auftrag des
Bundesministers für Forschung und Technologie BMFT

Leitung: R. Windheim (PLE) in Zusammenarbeit mit
R. Cuntze (MAN-Neue Technologie, München)

(left) International wind energy conference at MAN (1978),
(right) Seminar Research project from KFA Jülich GmbH (1981)
(below) contributors

C O N T E N T S

	Page
C.J. CHRISTENSEN, P. LUNSAGER (Research Est. Risø) Investigations of structural dynamics on the Gedser WTG and new Danish wind turbines	1
P. LUNSAGER (Research Est. Risø) Measurements of performance and structural response of the Danish 200 kW Gedser windmill	51
O. FABIAN (Dept. for Fluid Mechanics, Techn. Univ. DK) A strategy for aeroelastic analysis of WECS	95
D. PETERSEN (DFVLR Braunschweig) Modes and frequencies of GROWIAN rotor blades	105
D. LUDWIG (DFVLR Göttingen) Dynamics of wind turbine rotor blades	139
F. KIESSLING (DFVLR Göttingen) Aeroelastic modelling of the coupled wind turbine rotor tower system	161
I. KOVACS (Leonhardt und Andrä, Stuttgart) Dynamic design of a medium stiff wind energy tower ..	181
R. CUNTZE, I. ZAUN (MAN - NT, München) Calculation of the natural frequencies of the braced GROWIAN tower with dead head mass	197
S.E. THOR (FFA, Stockholm) Computer methods for structural weight optimization of fiber reinforced plastics	215
D.A. SPERA (NASA, USA) Structural dynamics analysis of large wind turbines in the USA	239

Peculiarities addressing Strength and Composites

From a presentation to the working group members of the
Kurt A. Körber Stiftung on "Innovationsfaktor Mathematik"

"How presenting mathematics to industry people".

Standing in the medieval tradition of pictorial expression, the so-called phrenologists created a map of the brain by inscribed the abundance of mental qualities and tendencies of the human being – called organs – in the form of air bubbles in the skull. Phrenology is the study of the size and shape of people's heads in the belief that you can find out about their characters and abilities from this.

How much do you think this 'organ' is weighing?
About 15 g of about 1.3kg brain → extreme lightweight !

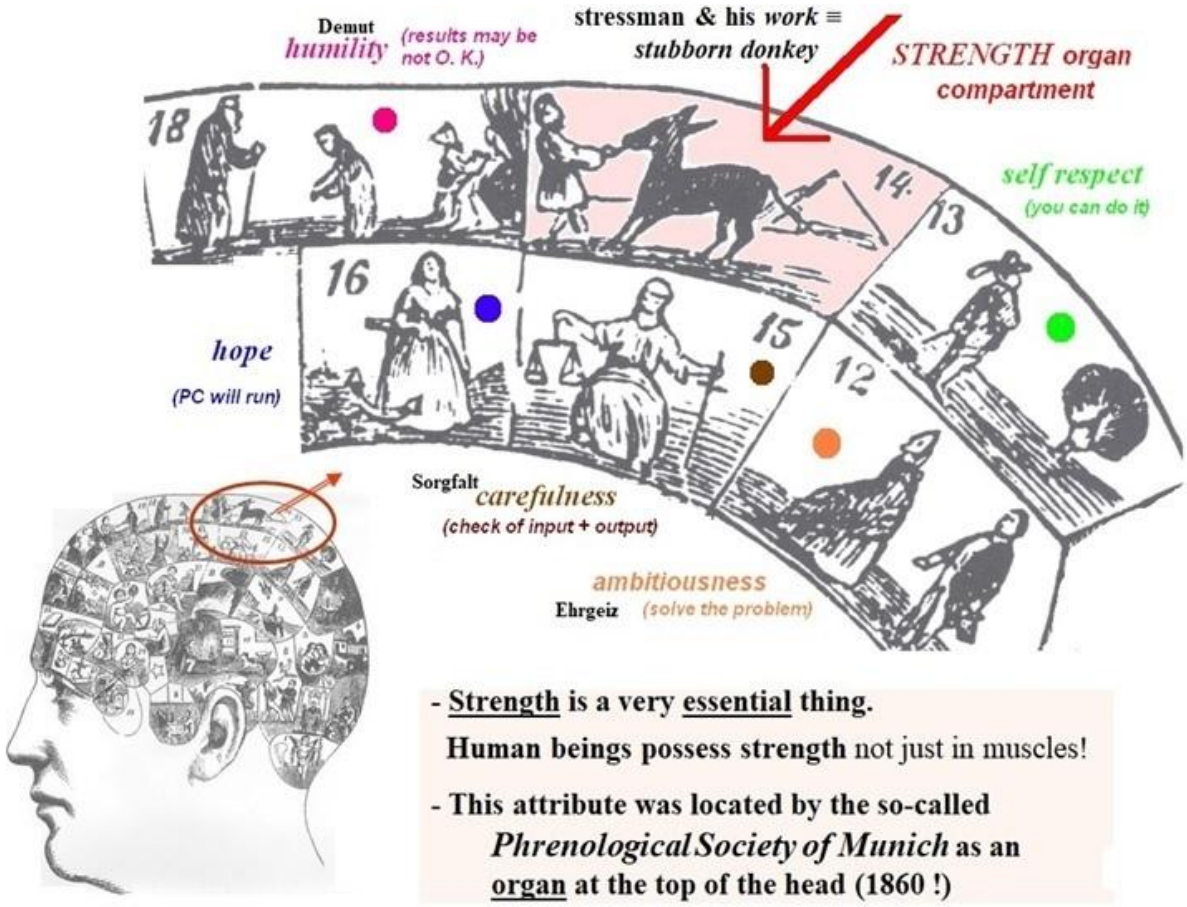

(For us Southern Germans: This has nothing to do with the well beloved 'white-blue' soccer club 1860 Munich *(Bayern Munich are the Reds)* but it might stimulate more club success in future, hopefully).

The phrenological theory of localization places the

- Strength organ' in an excellent position of the skull, as a Stubborn donkey, which the strength man (14) has to tame namely a position between the 'organs'
- Self-respect (13), that one dares to approach a thing
- Ambitiousness (12), to solve the problem
- Carefulness (15), to check the computational output
- Hope (16), that hardware and software work
- Humility (18), when something was wrong.

-
-

Innovation Factor Mathematics

Wissenschaftszentrum Nordrhein-Westfalen

Reichsstr. 45
40217 Düsseldorf
Telefon: 0211/38 790-0
Telefax: 0211/370586

Herrn
Dr. Georg Cuntze
MAN Technologie AG
Main Dept. Struct. and Thermal Analysis
Bauschingerstraße 20

80997 München

Düsseldorf, den 21. Oktober 1993

Buchpublikation "Innovationsfaktor Mathematik"
hier: Protokoll der Beiratssitzung vom 29. September 1993
in Heidelberg

Sehr geehrter Herr Cuntze,

ich übersende Ihnen in der Anlage das Protokoll der Beiratssitzung vom 29. September 1993 in Heidelberg.

Kurz gesagt, es wurde bei der Sitzung beschlossen, das Buch auf der Basis von "success stories" aufzubauen. Alle Beiratsmitglieder sind gebeten, mir einen Entwurf **bis zum 15. Dezember 1993** zuzuschicken.

Weitere Details finden Sie im Protokoll. Bei Rückfragen können Sie sich gern jederzeit an mich wenden.

Mit freundlichen Grüßen

Dr. Simon Golin M.Sc.

Anlagen
Protokoll

Protokoll

der Beiratssitzung
zur Buchpublikation "Innovationsfaktor Mathematik"
am 29. September 1993 in Heidelberg

Anwesend waren die Herren Bock, Bulirsch, Cuntze, Engl, Golin, Grien, Heinze, Huber, Janßen, Königs, Minnemann, Neunzert und Stoyan.

Zu Beginn des Treffens stand die Diskussion über die Zielgruppe und die Abgrenzung zu anderen bestehenden Buchprojekten. Es wurde Einvernehmen darüber erzielt, daß auf der Basis des im folgenden skizzierten Konzepts die geplante Publikation

- sich von existierenden bzw. geplanten Büchern genügend abhöbe
- sinnvoll und wünschenswert sei
- unter Mitwirkung der Beiratsmitglieder (als Autoren und/oder in beratender Funktion) machbar sei
- und sich finanzieren ließe.

Buchkonzept

Zielgruppe des geplanten Buches sind in erster Linie die sog. Entscheidungsträger in Industrie und Wirtschaft (definiert als "diejenigen, die für Projekte, Forschung und/oder mathematische Anwendungen Geld ausgeben können"). Ebenfalls erreicht werden sollen die Entscheidungsträger in Politik und Administration, wie auch zu erwarten ist, daß darüber hinaus Abiturienten, Lehrer, Studenten in Anfangssemestern sowie Studien- und Berufsberater das Buch lesenswert finden werden.

Inhaltlich wird angestrebt, bei dieser Zielgruppe Aufmerksamkeit für die **anwendungsorientierte** Mathematik zu wecken und ein korrektes Bild von ihrem ökonomischen Nutzen zu erzeugen. Nicht **die gesamte anwendungsorientierte** Mathematik, sondern ihre **Bedeutung**, aktuelle Veränderungen und typische Anwendungen sollen repräsentativ dargestellt werden. Kurz gesagt, es geht um "eine Werbebroschüre in Form eines Buches" (Herr Engl).

Es wurde beschlossen, das Buch anhand von "Geschichten" in angenehm lesbarer Form aufzubauen. Jede dieser Stories soll eine allgemeine "Botschaft" über die anwendungsorientierte Mathematik zum Ausdruck bringen und die Gliederung

- Fallbeispiel / "success story" (unter Einbezug von Hinweisen, wie es zu Mißerfolgen kommen kann)
- das Instrumentarium der anwendungsorientierten Mathematik
- allgemeine "Botschaft" zur Bedeutung und/oder der Situation der anwendungsorientierten Mathematik

(in dieser Reihenfolge!) aufweisen.

Lesson Learned here as engineer:

The Applied Mathematicians in this WG were better understandable
than most of my mechanics scientist colleagues in engineering!

Famous *COMPOSITES:* Looking at the *combination of skills*

(multi-functionality)

The Wolpertinger the most famous Bavarian 'Composite', is a Bavarian mythical creature whose exact origins are unclear. It is depicted as a hybrid creature in various forms, including a squirrel with a duck's beak (Schnabel).

The platypus (Schnabeltier) is an egg-laying mammal from Australia. Animals like the platypus have already realized the highly valued multi-functionality in design to a very large extent.

By the way, Wolpertinger and platypus have in common that they are very shy and nocturnal.

This does not predestine them as models for multifunctional strength criteria, because these are used unrestrainedly during the day without checking the special applicability limit.

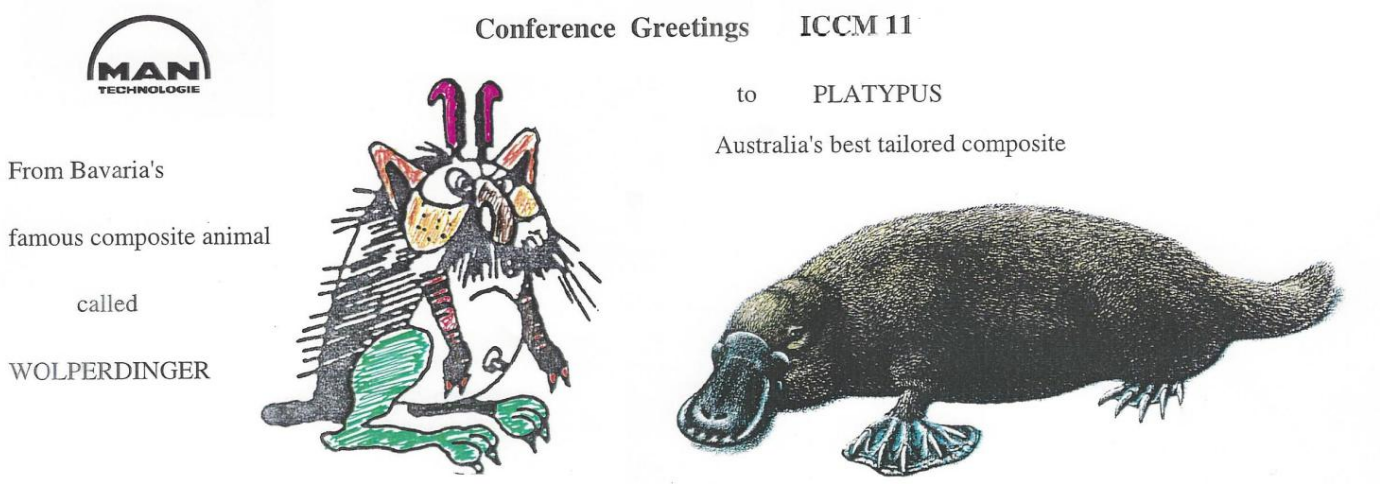

32 Affiliations, professionally and privately

32.1 German Society of Aeronautical Engineers (DGLR), for more than 40 years

32.2 IASB 1972-2024

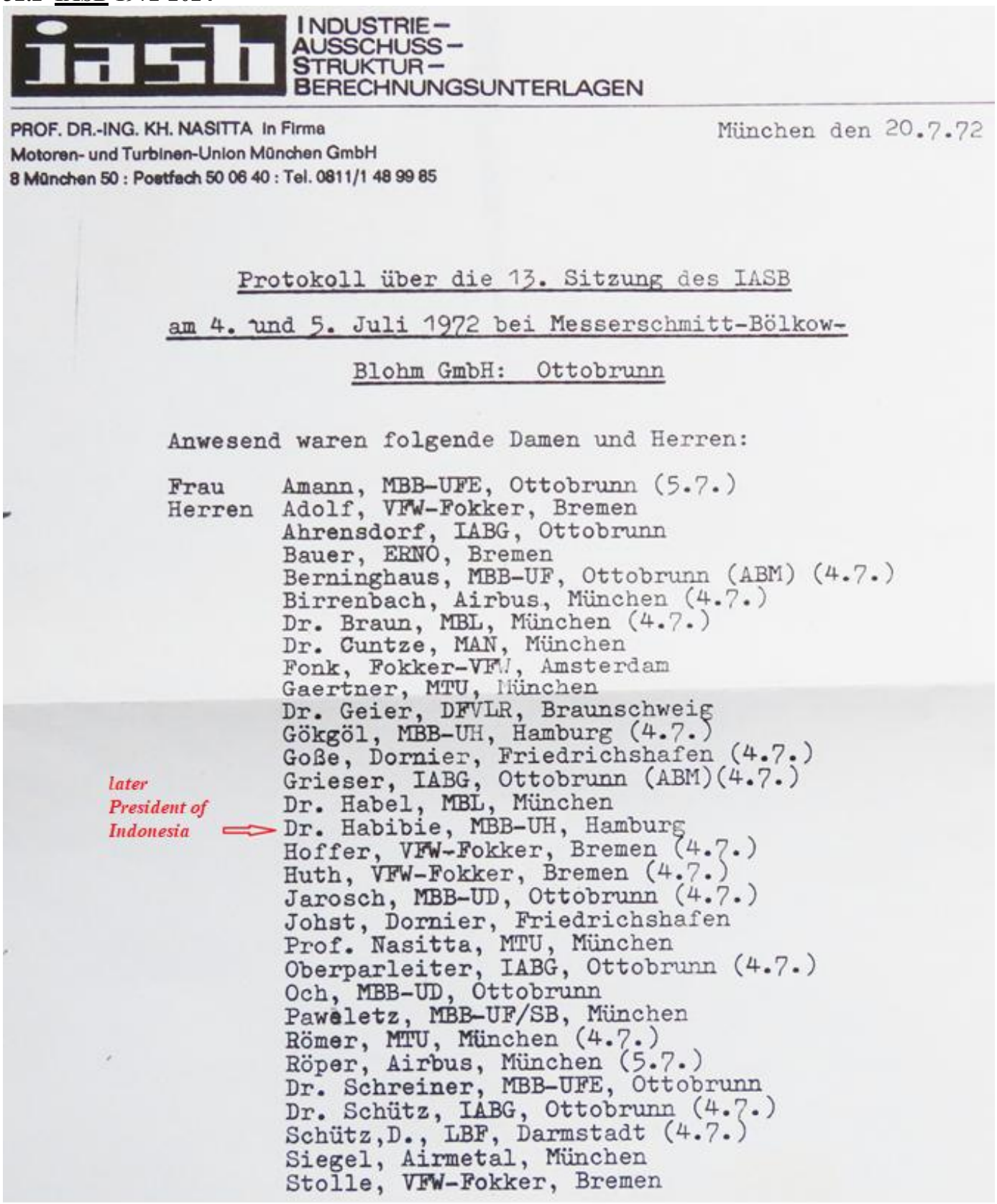

iasb INDUSTRIE-AUSSCHUSS-STRUKTUR-BERECHNUNGSUNTERLAGEN

PROF. DR.-ING. KH. NASITTA In Firma
Motoren- und Turbinen-Union München GmbH
8 München 50 : Postfach 50 06 40 : Tel. 0811/1 48 99 65

München den 20.7.72

Protokoll über die 13. Sitzung des IASB

am 4. und 5. Juli 1972 bei Messerschmitt-Bölkow-

Blohm GmbH: Ottobrunn

Anwesend waren folgende Damen und Herren:

Frau Amann, MBB-UFE, Ottobrunn (5.7.)
Herren Adolf, VFW-Fokker, Bremen
Ahrensdorf, IABG, Ottobrunn
Bauer, ERNO, Bremen
Berninghaus, MBB-UF, Ottobrunn (ABM) (4.7.)
Birrenbach, Airbus, München (4.7.)
Dr. Braun, MBL, München (4.7.)
Dr. Cuntze, MAN, München
Fonk, Fokker-VFW, Amsterdam
Gaertner, MTU, München
Dr. Geier, DFVLR, Braunschweig
Gökgöl, MBB-UH, Hamburg (4.7.)
Goße, Dornier, Friedrichshafen (4.7.)
Grieser, IABG, Ottobrunn (ABM)(4.7.)
Dr. Habel, MBL, München
Dr. Habibie, MBB-UH, Hamburg
Hoffer, VFW-Fokker, Bremen (4.7.)
Huth, VFW-Fokker, Bremen (4.7.)
Jarosch, MBB-UD, Ottobrunn (4.7.)
Johst, Dornier, Friedrichshafen
Prof. Nasitta, MTU, München
Oberparleiter, IABG, Ottobrunn (4.7.)
Och, MBB-UD, Ottobrunn
Pawèletz, MBB-UF/SB, München
Römer, MTU, München (4.7.)
Röper, Airbus, München (5.7.)
Dr. Schreiner, MBB-UFE, Ottobrunn
Dr. Schütz, IABG, Ottobrunn (4.7.)
Schütz,D., LBF, Darmstadt (4.7.)
Siegel, Airmetal, München
Stolle, VFW-Fokker, Bremen

later President of Indonesia ⇨

32.3 Former private affiliations

10 years 'L'Ordre des Coteaux de Champagne'

30 years 'Chaine de Rotisseurs'

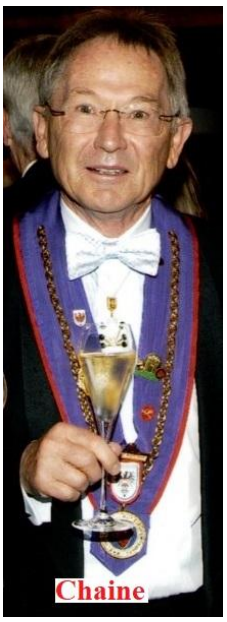

My godfather for joining the Chaine was Prof. Dr. Wolfgang von Stetten, the German head of the order and cousin of my friend Helmut Hermann

<u>German Mauritious Association</u>.

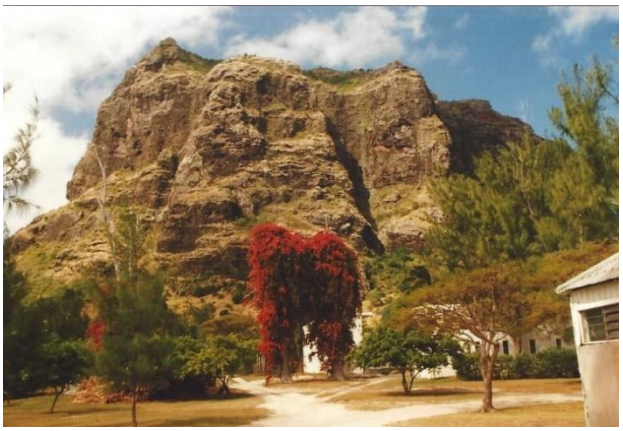

(left) Final Meeting of the German Mauritius Association, 25 years.
founded by my friend Consul General Prof. Dr. Dr. Johannes Kneifel (left)

(right) Famous hill 'Le Morne', which I could still climb in 1986 with the hill-owning farmer. Now closed.

32.4 DAV = *German Alpine Club* > 50 Years

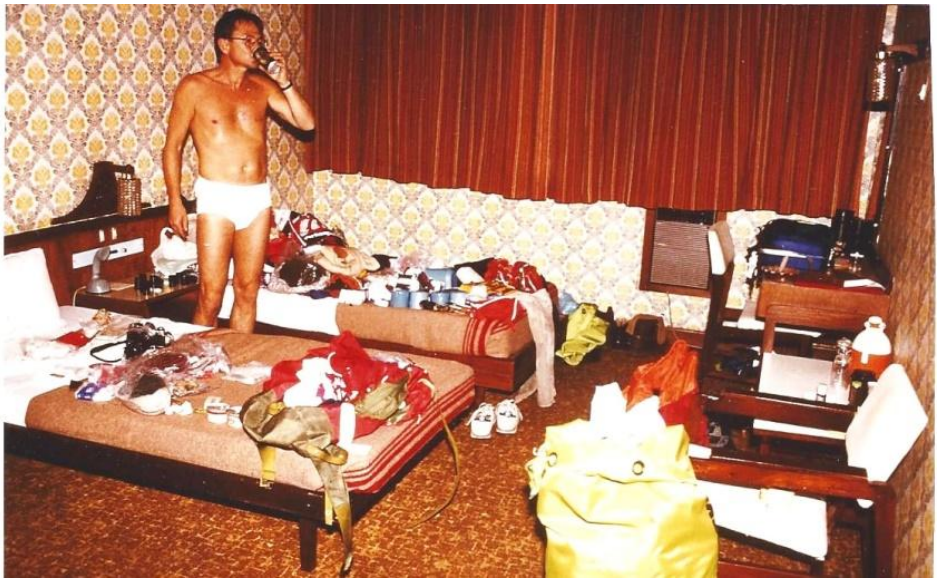

Equipment

Double shoe for the high mountains

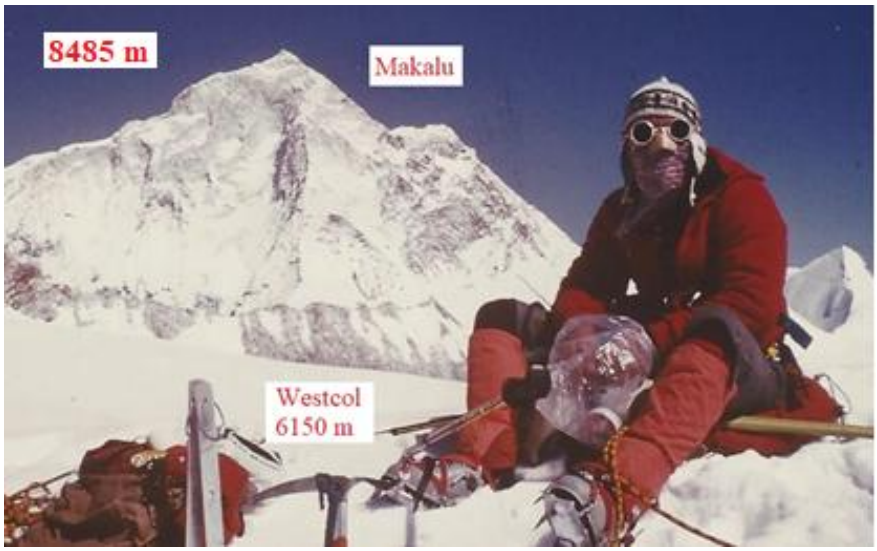

Equipment, missing:

Since the porters with the equipment were missing, we had to take spare clothes.

Consequence:
You take what you have..
Because much is possible
if a goal is pursued

Abseiling from the Mingbo La pass, 5800 m, impressive life event:

Arrival 9 a.m. Abseiling together with a fearful sherpani (with rubber boots in the ice!) to take over the intermediate station at 10 o'clock.

Then for 8 hours let down the trekking participants, equipment and Sherpas descending in the ice channel secured to the rope and then pull this heavy rope up again and again. From 4 p.m. sunlight gone and freezing cold. I had the to go down the ice channel with the last person, our cook – tied up in front of me. When we were downstairs, he untied himself and then disappeared downstairs with a last cry in the dark.
Now my exhausted colleague from the high station slowly came down with his headlamp. I gave him my ice pick, because I still had an ice axe and then we crossed the steep slope extremely carefully. After about an hour, someone came towards us. It was the guide who told us that he had met the cook on the ascent. Great joy.
For me, the only thing left was to drink, wrap myself in the two sleeping bags and sleep on a mat between boulders.

Notes:

**Sherpas can carry twice as much of us at great height, but could not help pull the heavy rope.*
**All the pictures my colleague took of this event from above were developed incorrectly. Grief.*

32.5 Hiking & Mountain friends Club "Glonntal-Indersdorf e.V."

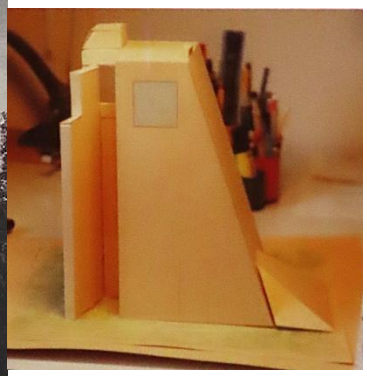

model

1980, inauguration of 'my' climbing garden
With the administrative officer of the County Dachau and the world well-known climbers
M. Dacher, O. Wiedemann and S. Geschwendner

und des back ma a no . . .

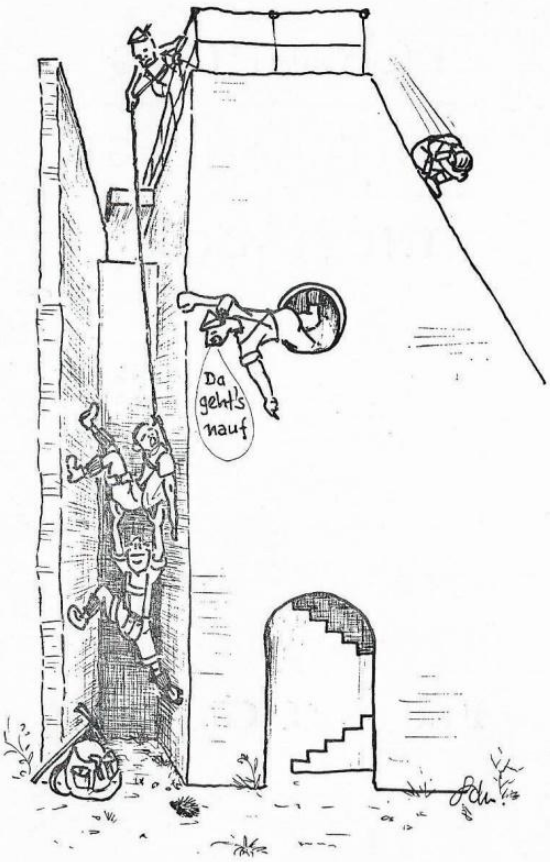

Programm

Veranstaltungsort: Kletteranlage-Indersdorf am Sportplatz in Markt-Indersdorf

Beginn: 10.00 Uhr

Begrüßung der Gäste

Ansprachen von Landrat H.-J. Christmann und vom Schirmherrn der Veranstaltung Hans Strixner

Turmweihe

Klettervorführungen durch:

Michael Dacher	*(4 Achttausender)*
Otto Wiedemann	*(einer der schnellsten Kletterer der Welt)*
Sepp Gschwendtner	*(einer der extremsten Deutschen Freikletterer)*

Bergvorführungen durch:

die Bergwacht München

Den Stand der neuesten Ausrüstungen zeigen die Firmen Scheck, Hanwag und Salewa.

Für Ihr leibliches Wohl sorgt ein Festzelt mit diversen Schmankerln,
Bierpreis DM 3,90 je Maß

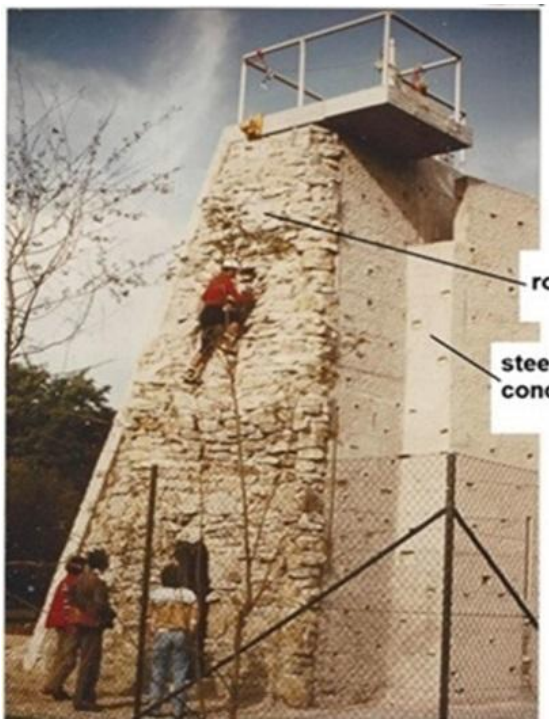

5th German 'climbing garden'

Designed,
concrete casted,
one side masoned with
rock stones from the alps
by the author

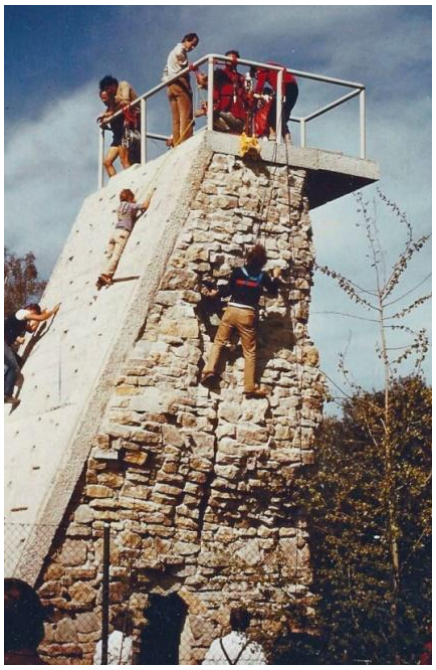

Cleaning up at the Climbing garden. 2023

Catholic Mass on a mountain
(left: our mayor Hans Strixner)

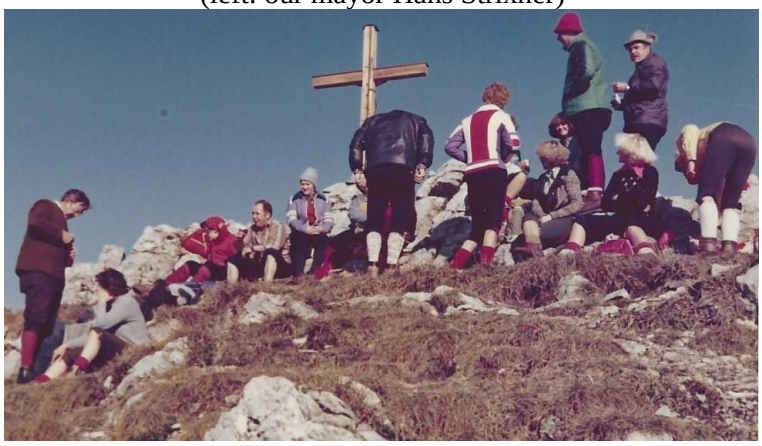

Indoor sports during winter time

Hiking tour

with Hans Rieger in the mountains: my Birthday 66

Music band on top

Hiking Theme:

Isar

From the source until running into the river Danube

In the mountains with my neighbour.
Our highlight: In the early morning by car to the Zugspitze carpark at Ehrwald. Then up to 2962 m, followed by 25 km down to the olympic ski jumping ramp and home in the evening.

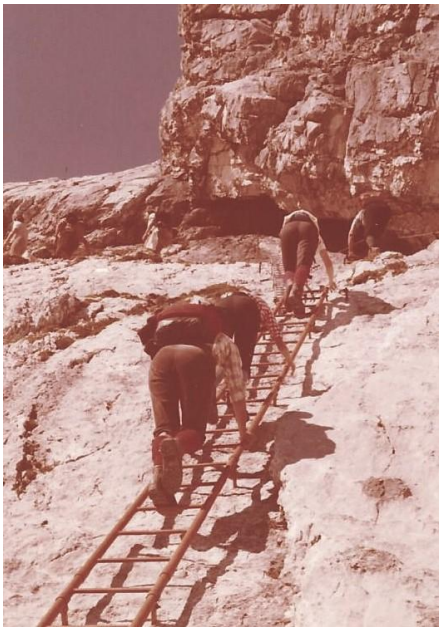

Via ferrata

Below: our traditional Christmas Hiking Tour, Dec.26

Christmas Hike, Dec 26: Usually GREEN

Maria presents a Christmas gift

120 decorative pieces

Usually: Eastern is more snow than at Christmas

Saying Good Bye at MAN

Before clearing out the office

Surprisingly, it was not clear under German law who would have to pay the remaining days of the month after the 65th birthday;
i.e. from September 9 until retirement on October 1.

MAN kindly took over the payment of this amount.

32.6 Good-Old-Boys and a Good–Girl, former members of MAN-Technologie

One of our yearly trips, 2010, 2015 and below at our former company

"Scientists are researching what is,
engineers create what never existed."
Theodore von Kármán

32.7 Some specific scientific Conferences

Tuesday, July 30, PM

Mechanical Properties of Composites I
ROOM: Council/Chamber

Chairman: Dr. Steven Tsai, Chief, Mechanics & Surface Interactions Br., AFWAL, Wright-Patterson AFB, OH 45433

Vice Chairman: Dr. R. Cuntze, MAN - Nene Technologie, AbC, EGS, Dachaner Str. 667, Post fach 500620, D-8000 Munich 50, West Germany

Lightweight Progress:
At least in conference material weight:

Transport of symposium documents: ICCM Hawai 1985
(books, 11kg, post office, received after 5 months), NAFEMS (0.? kg, direct home)

Conference at Leeuven with giving a presentation

When Ignaas Verpoest changed his activities from metal to composites

SIXTH INTERNATIONAL CONFERENCE ON COMPOSITE MATERIALS

ICCM & ECCM

SECOND EUROPEAN CONFERENCE ON COMPOSIT MATERIALS

IMPERIAL COLLEGE, LONDON, UK, JULY 20-24, 1987

SCIENTIFIC PAPERS SELECTION COMMITTEE

Australia
J. R. Inglis

Belgium
A. H. Cardon
N. Sprecher
I. Verpoest

Canada
K. N. Street

Denmark
H. Lilholt

France
A. R. Bunsell
F. X. de Charentenay
R. Naslain

Germany (Federal Republic)
R. Cuntze
K. Friedrich
H. Kellerer
K. Schulte

Italy
I. Crivelli-Visconti

Japan
T. Hayashi
H. Miyairi

Netherlands
P. Bristoll
A. Cervenka
D. A. Cliffe
J. B. W. Morsink
P. Sheard
J. L. Thomason
C. P. Valkering

A. W. van Breen
G. Walton

Sweden
R. Warren

Switzerland
E. Anderson

UK
R. D. Adams
M. G. Bader
W. M. Banks
A. Bennett
M. J. Bevis
S. M. Bishop
B. J. Briscoe
N. C. Buskell
W. S. Carswell
P. Cawley
T. W. Clyne
F. N. Cogswell
T. A. Collings
P. T. Curtis
M. W. Darlington
A. G. Gibson
J. S. Higgins
J. M. Hodgkinson
P. J. Hogg
D. Hull
F. R. Jones
A. Kelly
D. Kewley
A. J. Kinloch
P. A. Lloyd
A. Marchant
I. H. Marshall
F. L. Matthews
J. Morton

N. A. Payne
L. N. Phillips
R. T. Potter
R. D. Rawlings
G. Scowen
R. L. Smith
K. A. Stevens
G. Turvey
I. M. Ward
J. G. Williams

USA
P. Beardmore
H. F. Brinson
T.-W. Chou
L. J. Cohen
J. H. Crews
H. Dharan
A. K. Dhingra
D. A. Dillard
S. G. Fishman
C. T. Herakovich
M. W. Hyer
W. S. Johnson
R. M. Jones
F. A. Kulacki
J. K. Lees
K. Liechti
R. B. Pipes
D. Post
K. M. Prewo
Y. Rajapakse
R. Rowlands
R. A. Signorelli
G. S. Springer
S. W. Tsai
J. M. Whitney
J. F. M. Wiggenraad
D. J. Wilkins

TITLE: Interlaminar Stresses VENUE: Huxley 340
CO-CHAIRMEN: Dr. R. Cuntze, MAN-Neue Technologie, Munich, W. Germany
Prof. R.M. Jones, Virginia Polytechnic Institute, Blacksburg, USA

TIME	PAPER
10.00	On the finite element calculation of failure modes in laminated CFRP specimens – an engineering approach *by K. Ickert and J. Argyris, ICA, University of Stuttgart, W. Germany*
10.25	Analysis of suppression of free-edge delamination by introducing adhesive layer *by S.R. Soni, Adtech Systems Research Inc, Fairborn, OH, USA and R.Y. Kim, University of Dayton Research Institutes, OH, USA*
10.50	Efficient three-dimensional finite element failure analysis of compression loaded angle-ply plates with holes *by S.W. Burns and C.T. Herakovich, Virginia Polytechnic Institute, Blacksburg, VI, USA*
11.15	A simplified approach for interlaminar stresses around a hole in $[\theta/-\theta]_s$ laminates *by Zhang Kai-da, Northwestern Polytechnical University, Xian, Shaanxi, China and C.E.S. Ueng, Georgia Inst of Technology, Atlanta, GA, USA*
11.40	The analysis of deformations and strains in composites by Moiré interferometry *by D. Post Virginia Polytechnic Institute, Blacksburg, VI, USA*
12.05	Studies of delamination growth and final failure under tensile loading *by P.A. Lagace and J.C. Brewer, Massachusetts Institute of Technology, USA*

On the Occasion of
the 6th International and 2nd European Conference
on Composite Materials

HER MAJESTY'S GOVERNMENT
in the United Kingdom of Great Britain and Northern Ireland
request the honour of the company of

Herr Dr RG Cuntze

at a Reception at Lancaster House St James's SW1
on Monday 20 July 1987 from 6.30 pm to 8 pm

Mr Robert Atkins MP
Parliamentary Under Secretary of State
at the Department of Trade and Industry
will receive the guests

Cars to approach Lancaster House by way of Cleveland Row

Please reply to: Government Hospitality
8 Cleveland Row St James's SW1A 1DH

UK, to be well-dressed for the welcome dinner
Stan Matthews let us enter the room of the celebratory event after knocking with a stick and saying our name

LINK setzen

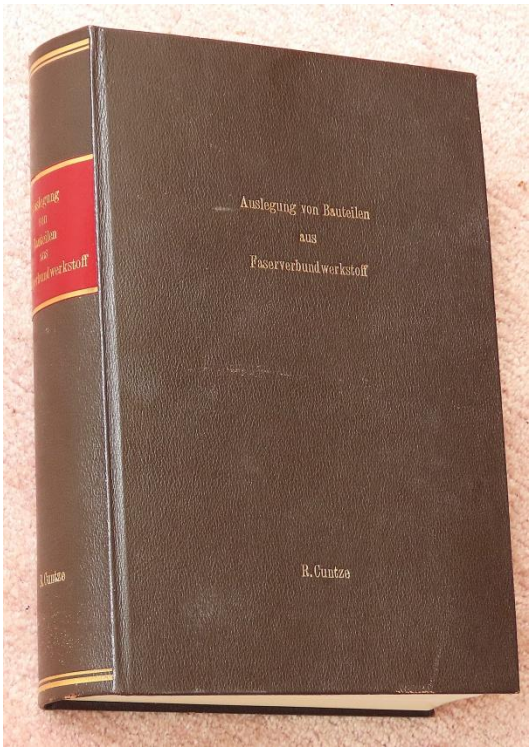

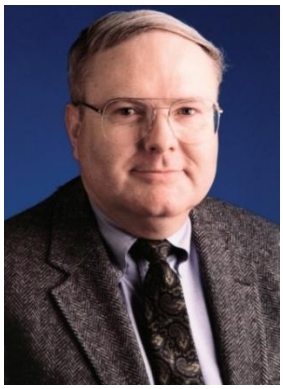

Mechanics of Composites masterials 1975.

left: My book idea (*600 pages on composites, of course in German, next picture between others*)

I could directly stop when Bob presented his book on composites

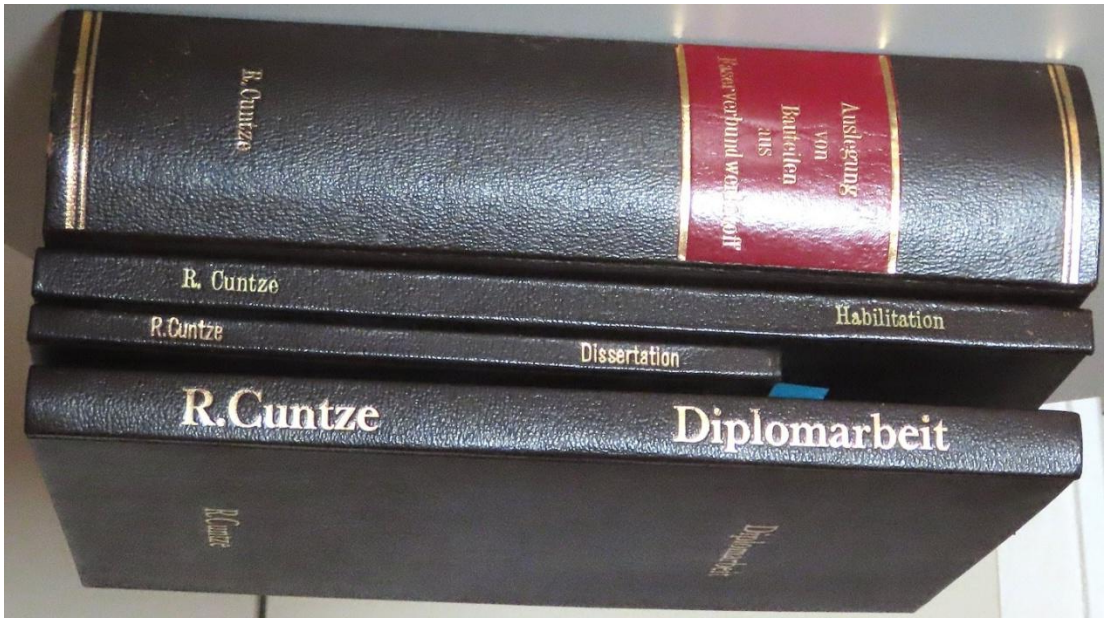

Ralf, Holger, Klaus Friedrich with Ignaas visting
Rolands (central behind) at his conference MCM 1998

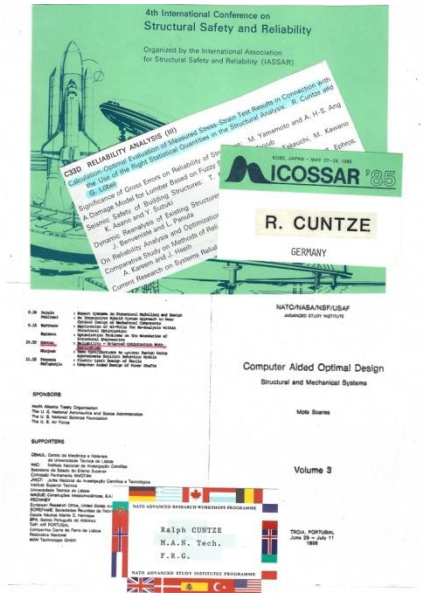

Cinference at Osaka
Japan

World fair at Tsukuba

Conferences at Paderborn

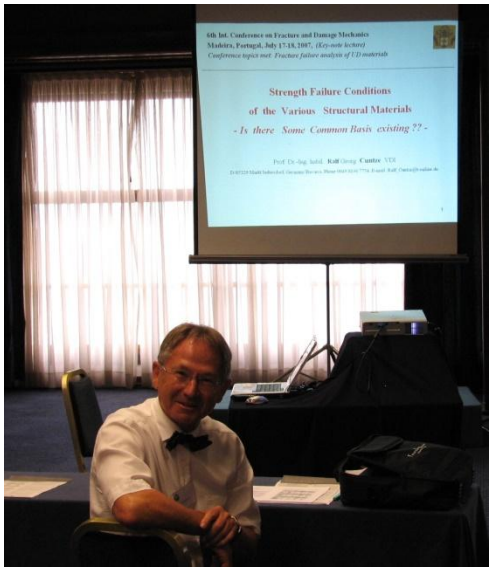

Madeira

Wolfgang, Holger with wife, Ralf and Fritz

On the Way with Friends

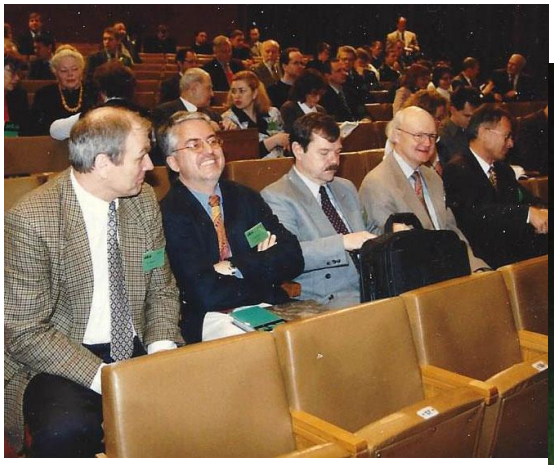

Rolands Rikards, Holm Altenbach, Holger Theilig, Klaus Rohwer, Ralf Cuntze

Mechanics meetings with Wilfried Becker, Holm Altenbach and Vladimir Kulupaev

My school friend Walter Fischer: How to make twig brooms?

Huba Öry with Heinrich Wellen (Airbus Bremen, 2008

Again Paderborn, in the monastery

Rikards, Kumosa, Theilig, Cuntze, Richard

Fritz from behind, Ralf, Rolands

Over the years with:

Anatolyi Levin

Helmut Hermann

Alois Albrecht

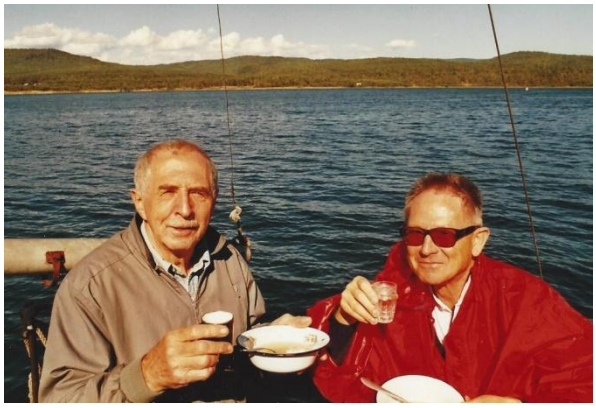

With my friend Anatol. Enjoying the Baikal Sea, just before an extreme gust of wind put the sailing ship to the water *(we had luck*)

Anatol, Walter and two Ladies friends of them

Eating and drinking with friends at Moscow

Anatol was invited to visit the solar observatory high above Lake Baikal. (His friend was the director.) I was allowed by her to look at the sun and was then given a stunning photo of the sun.

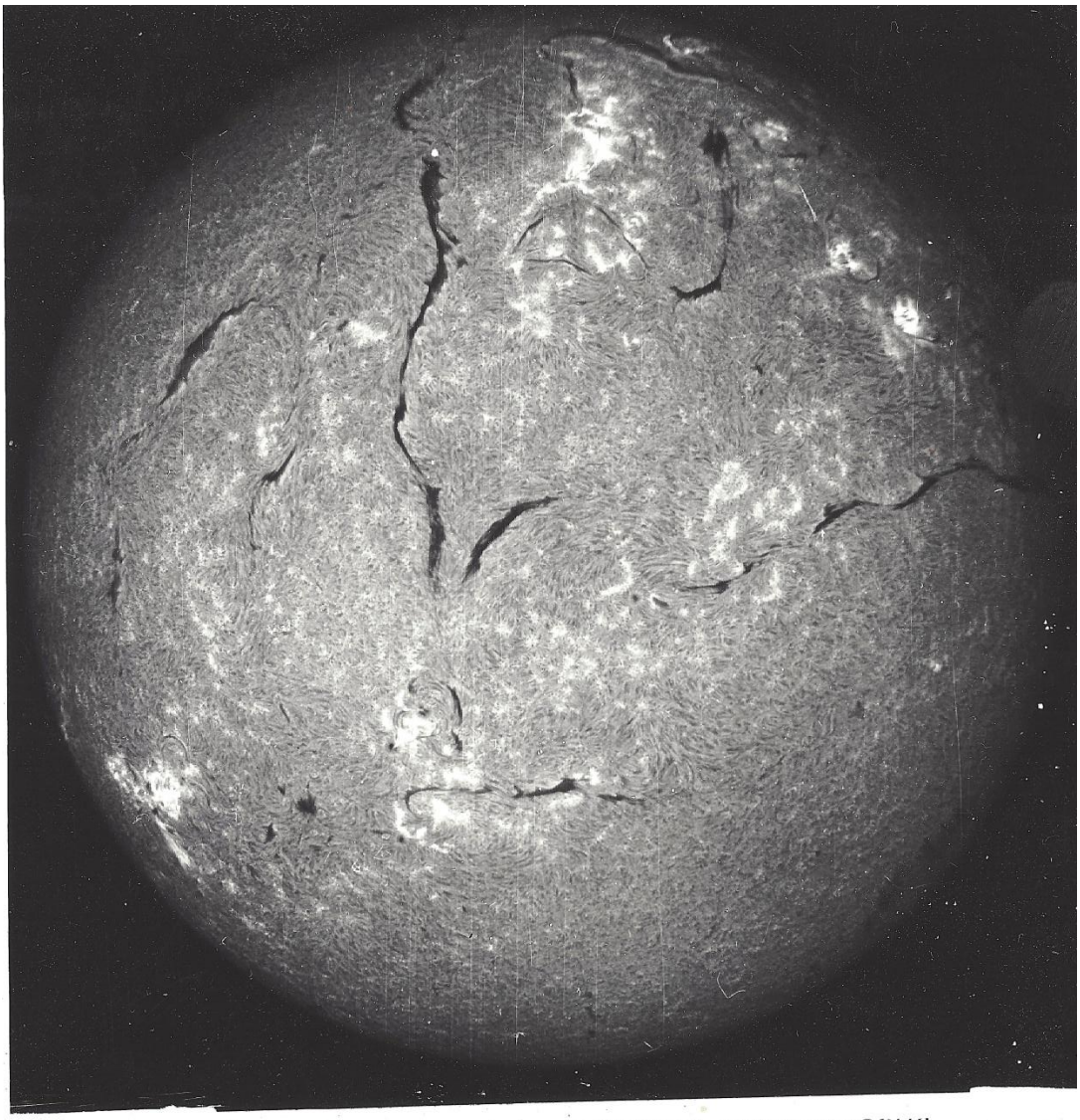

Meetings at the house of Walter Wunderlich (*common SAP 4 FEM-memories*) and Rotraud Wunderlich

Knittel, Cuntze,
and Obermeyer, Ramm, Pfeiffer, Heimeshoff

Pfeiffer, Cuntze, Heimeshoff

Visit of Mausi in my working room at home

Relaxing when Ralf works in a complicated position

Mausi, an optical checking of my results

Yakutsk Conference: On the Lena Rocks

КРЕЧЕТ
Авиационно-туристическая компания

Свидетельство

RALF
CUNTZE

является почетным гостем,
посетившим "9" июля 2001 года Долину Гейзеров,
один из уникальнейших уголков планеты Земля
Почетный гость располагает приятными воспоминаниями
и незабываемыми впечатлениями.

Yakutzk conference on a ship .

Talk but much wodka-encouraged recreation on the boat necessary

Celebration of the old customs

On the Lena rocks, 2001

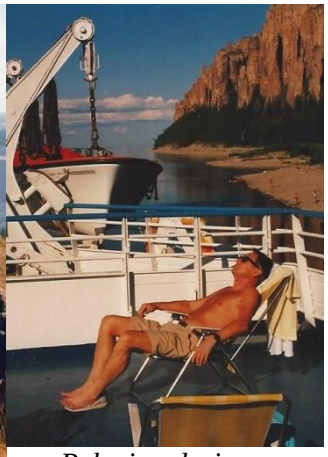

Relaxing during conference

Forbidden during the strong Soviet time: Revival of the ancient customs of the Yakuts. Totem Poles, equal to the attaching North-America Inuit

Setting a Totem pole

Untypical minimalized breakfast

with the witch doctor at the Lena beach

Bath in the cold Lena river

Excursion Kamtchatka, Wladiwostok, 2001

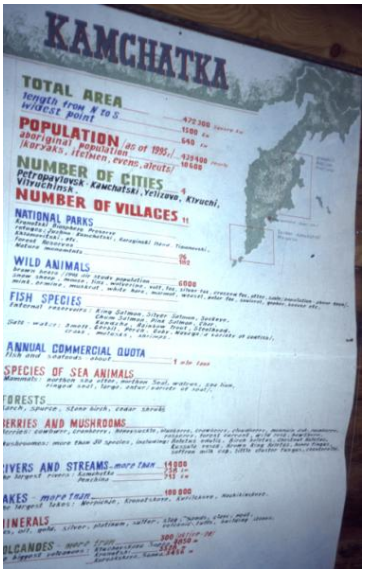

In front of the institute

me with the Institute leader

The target, reached: our volcano with lava flow

Leaving Petropawlows-Kamchatsk for a research excursion of the volcanic institute. (below) Institute leader of the corresponding institute on the island Sachalin

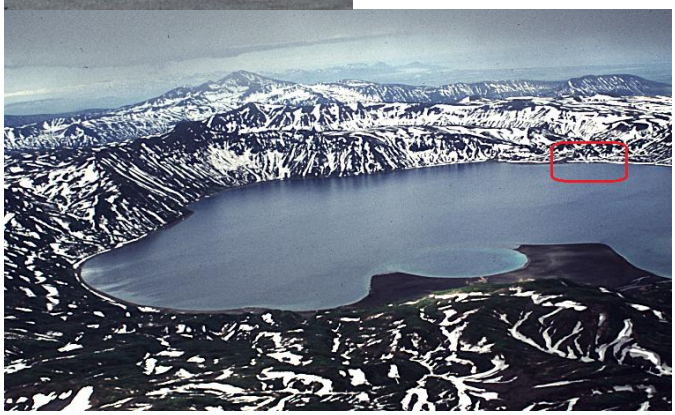

Our camp at the volcano Semjachik

Excursion to the Geysers land

By pure chance, a ZDF team from St. Petersburg was invited to the institute. Quite by chance, I was able to watch this short film on television.

Good vodka and cake are the key to a good meeting result

Crossing the dead volcano lake, no fish. Good for us, because no huge Kamchatka bears had been there anymore

(up) in the Valley of Vapors

(left) Somehow a pretty narrow living

(right) last day no food anymore, waiting for the heli

Our volcano in the background

No food anymore

Food available:Dining again, with Anatol & friends

Back to Moscow

Cuntze Ralf

Von: Malyshev [forum2001@mail.rcnet.ru]
Gesendet: Donnerstag, 07. Dezember 2000 14:57
An: ??? Technologie ??; Cuntze ?.

Forum-en.ZIP

Dear Colleague,

The 40-year anniversary of the first manned space flight in the history of mankind will be celebrated on April 12, 2001. We would like to inform you about Forum 2001, which will be held on April 11 -13 next Year in Moscow in honor of that event. You can find the detailed information into Attach File.

It would be great pleasure for us if you participate in this Forum.

Organizing Committee

All Russian spacecraft conference

Viewing ***Star City*** with inviting colleague Alifanov

Invitation of Dr. Alifanov (right) to below anniversary at Moscow, being the first ***All*** Russian spacecraft conference , bringing together – for the first time - all Russian engineers and a few western engineers.
In the Hotel Cosmos, for two hours in the noon break all spacecraft engines were presented for the first time !

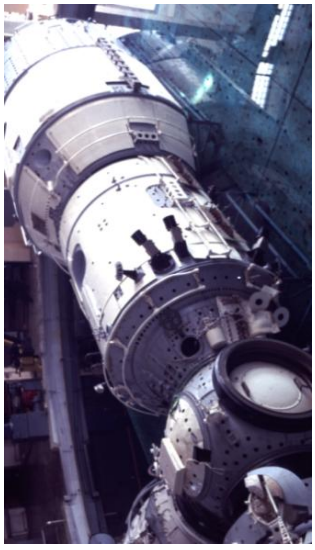

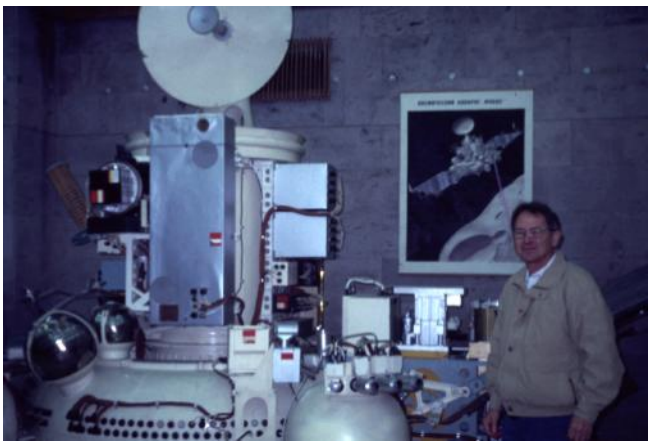

Visiting MIR (peace) at Star City

An orthodox patriarch and soldiers

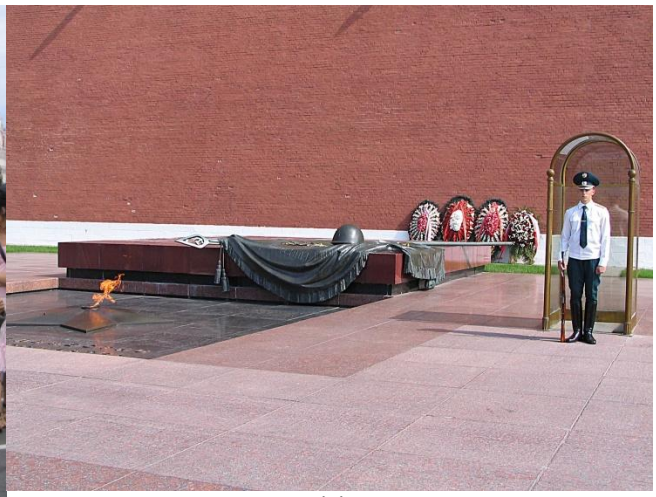

waiting

Industrial & Scientific Advisory Committee (ISAC) Mission letter

Dear MAAXIMUS ISAC Members. Welcome on MAAXIMUS board !

Dominique GUITTARD as Technical Coordinator, myself as Project Coordinator and the whole Management Committee are really proud to have you in our MAAXIMUS Advisory Board. We all thank you again for accepting to support us.

Maaximus	***MORE AFFORDABLE AIRCRAFT THROUGH EXTENDED, INTEGRATED AND MATURE NUMERICAL SIZING*** **** Project month M1,M2, starting from the 1st April 2008.***

My Travelling Friends

Eddi: Look the excellent fish!

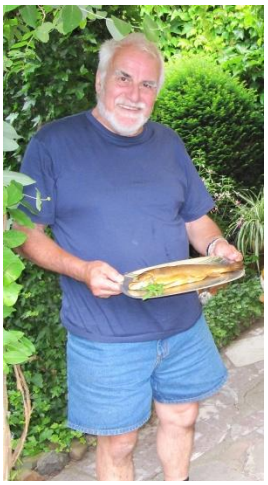

Julius: up a pyramid

Marian:
Mango SUPER FAN

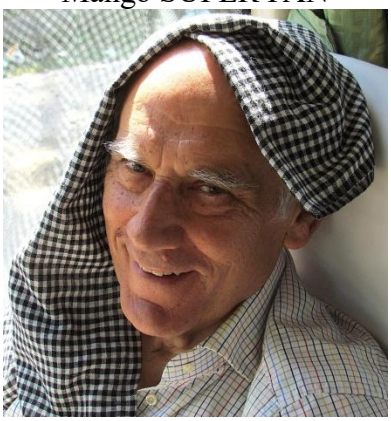

Ralf (enjoys double)& Otmar (teetotaler, thanksfully)

Vinzenz: We were thirsty

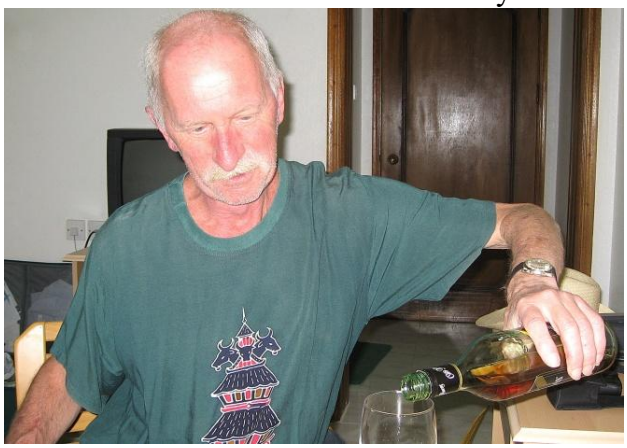

32.8 Rotel Tours with Begin of Digital Photography

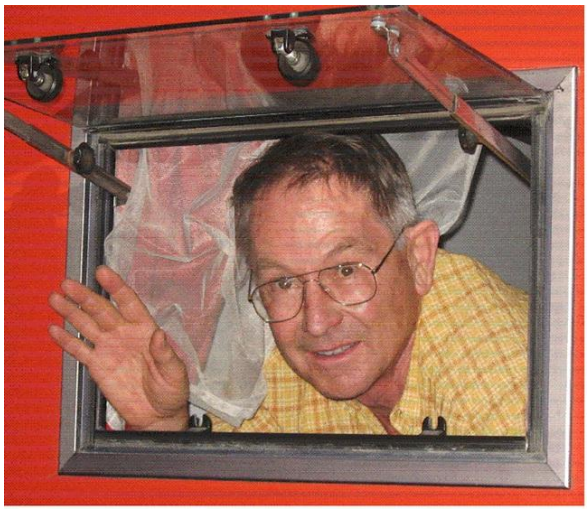

Cabin: 80cm x 80cm x 210cm

The relative narrowness of a ROTEL sleeping cabin helped the author to explore the wide world of nature and his good basic engineering education helped him to widely explore the world of engineering.

daily cleaning job, Ralf

Digital time onset

* Taking photos on a long vacation with a camera: Previously, 30 rolls of film were expensive and bulky, and the price was about the same as a camera later on.

* Discussion about: Digital SLR replacement cameras: Not yet practical as long as projectors and TVs don't have the same quality as the projector! >10 M pixels, image stabilizer for large zoom, 12x zoom, 4 x 512 MB memory cards.

* Advantageable photography since 2001*: I saved more and more transport volume and money.*

* My Canon SX 70 HS now: *zoom 21-1365* (35 mm equivalent)

my begin with 8 MB, next size above

following size of
Secure Digital (SD) Memory Card

+ adapter

present small ones

corresponds to 5 billion punch cards

5,000,000

Elastic string around the neck for safety reasons during difficult use

DIGIC 8 4K-Video

65fach 20,3

optischer Megapixel

Zoom

Dreh- und

schwenkbares

7,5cm LCD

Canon SX 70 HS (used since 2019)
after several SX pre-runners

32.9 New engagement, 2015

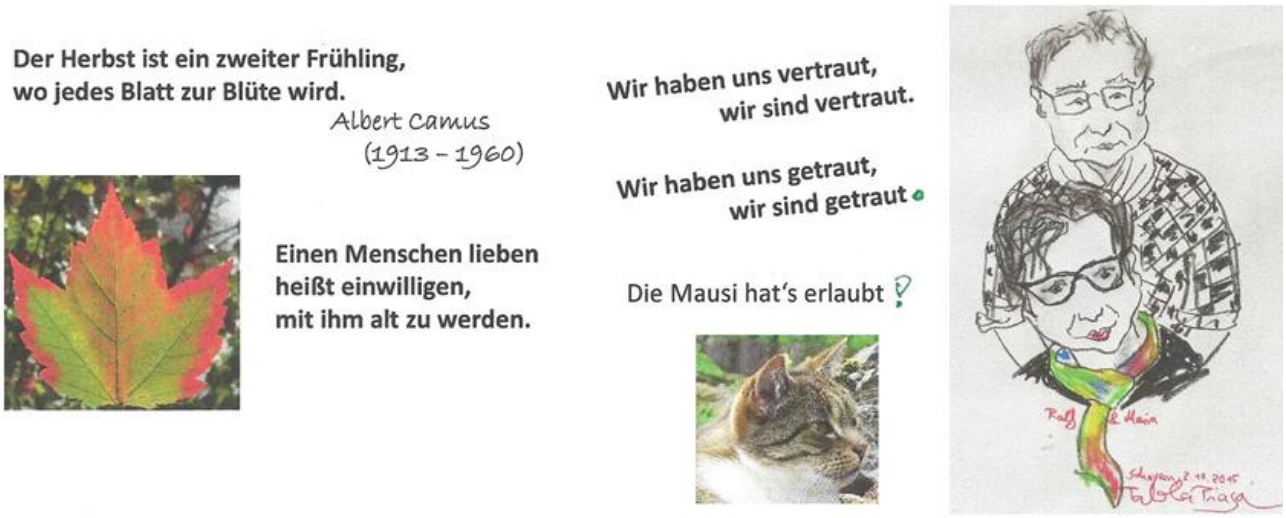

Ralf & Maria.

Becoming 75 years

My friends, in front Karin & Toni. My hiking friend Hands Rieger played on

80 Years: Birthday Celebration

This is a friendly Bavarian family music-band

This is not a suitcase
but a birthday cake

Bavaria meets South-Tyrol

Maria,
hiking with her South-Tyrol relatives

A good view and a good picture

(up)The novel farmhouse of Hilda
(right) the photographer

Hilda, Maria, Waltraud

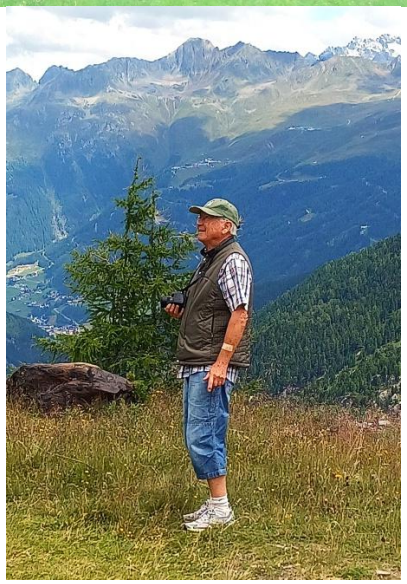

Who is the king??

youth

Covid Pandemie

Covid Pandemie in D
27. 1. 2020 - 7. 4. 2023
2 x Astra Zeneca , 1 x Moderna.
Have not been affected.

Measurement tool:

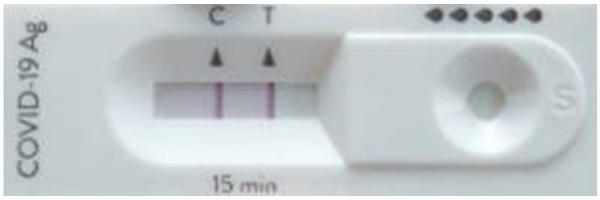

Hair: 7µm, fine dust 10 µm, corona virus 0.1 µm

In mid-April 2020, I sent an email (unanswered, of course) to Prof. Streeck, asking why we weren't properly informed about the physical requirements:

Requirement: 1.5 m distance. Why?

"The risk to a person depends on the amount of virus ingested and that person's resistance."

This leads to the conclusion: No breathing on them, but don't chase two men away from a train station park bench at night. The fact that medical professionals with additional training in statistics have long publicly claimed that the risk of spread is exponential is simply outrageous: With exponential spread, theoretically all 81 million Germans would have been affected after 21 days.

At the end of February 2020 we flew to Island for a winter trip. With us flew some Icelanders which had been skiing at Ischgl, Tyrol.

After 3 days we were put in quarantine in a nice landscape. However, good food from a good hotel kitchen is not so good if it is cold.

CORONA: Very *Bad* but also a little *Good* for me.
The good thing of the Covid time was: I could concentrate on my CV parts.

Sportsmanship of the author

After I had to say goodbye to soccer at the age of 55 because I couldn't see the football on the ground quickly enough due to a weakness of the upper eyelid muscle, mountain hiking, cycling and jogging remained for the time being. From the age of 75 on, there are 2x circle training, cycling per week and a special type of so-called 'slow jogging ', protecting the knees, on Sunday morning (*60 min +*), plus swimming in summer and gymnastics in winter. 10 more or less big hikes are added per year. More then 40 swims in our Mückensee lake.

I do not take much care of energy consumption: 60 min cycling at 160 Watt = 1570 kcal (1 kcal = 4.19kJ), eating 100 g apples = 50 kcal and 100 g butter = 717 kcal. We poor cyclists and 'Slow joggers' can never do that much!

My last day-trip with my neighbor Elmar: By car 120 km (about 2 hours) to the car park. There up at 7:50. (*The Alpspitze could not be managed due to fresh autumn snow*). Another trail was gone passing the famous Höllental. Back to the car and 17:10 back to Markt Indersdorf, a little exhausted however proud and happy.

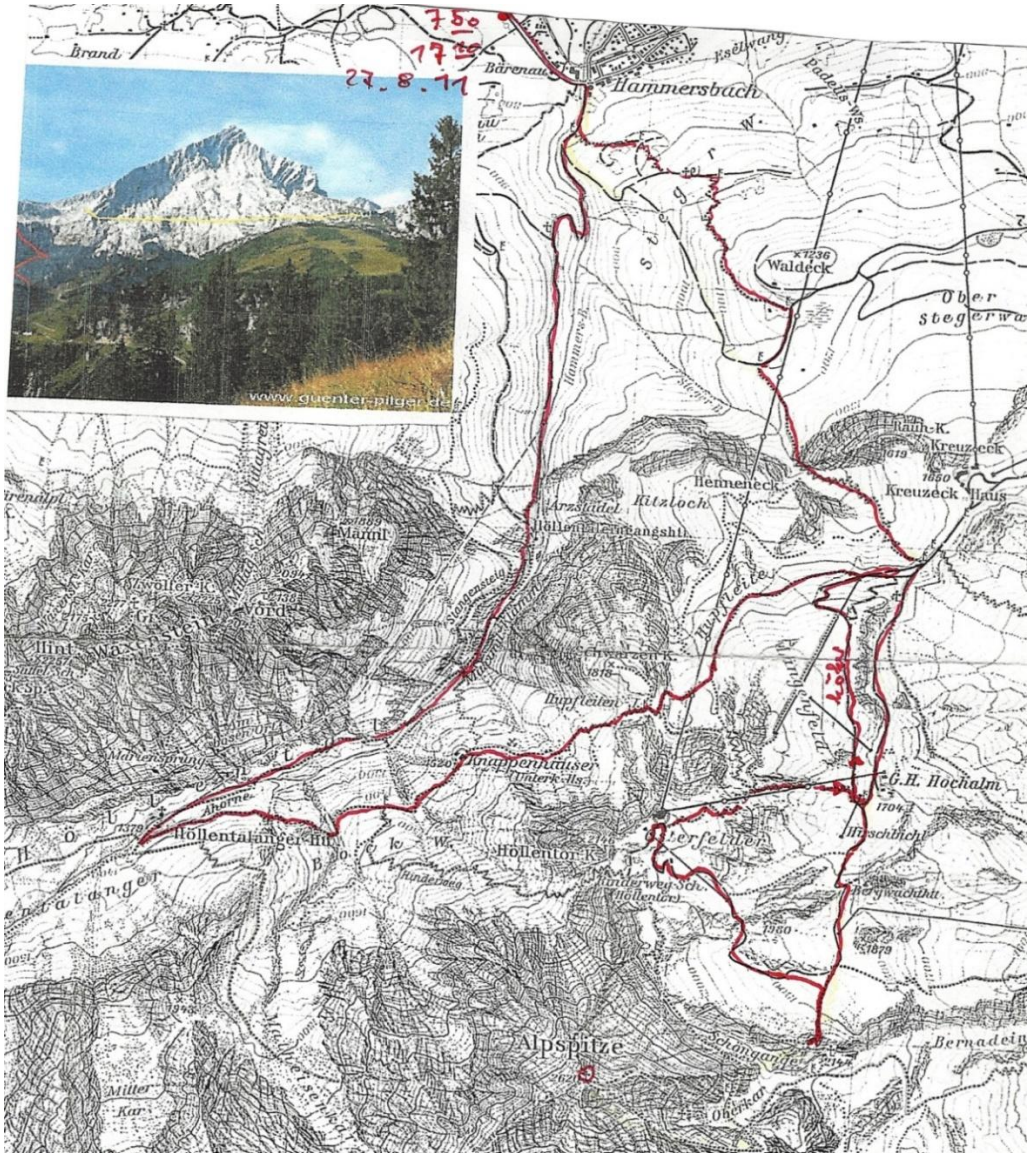

Ischgl 1973

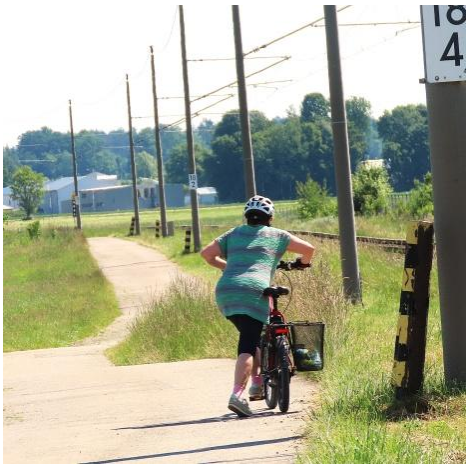

Biking with Maria:

More than 50 times

Where did this happen??

The Car Driver

Ford M15

Opel Manta with my mum

Mercedes Coupe 230

BMW 230

BMW 3 compact

BMW 125

At our beloved Mückensee Lake

dragon fly couple sink eggs

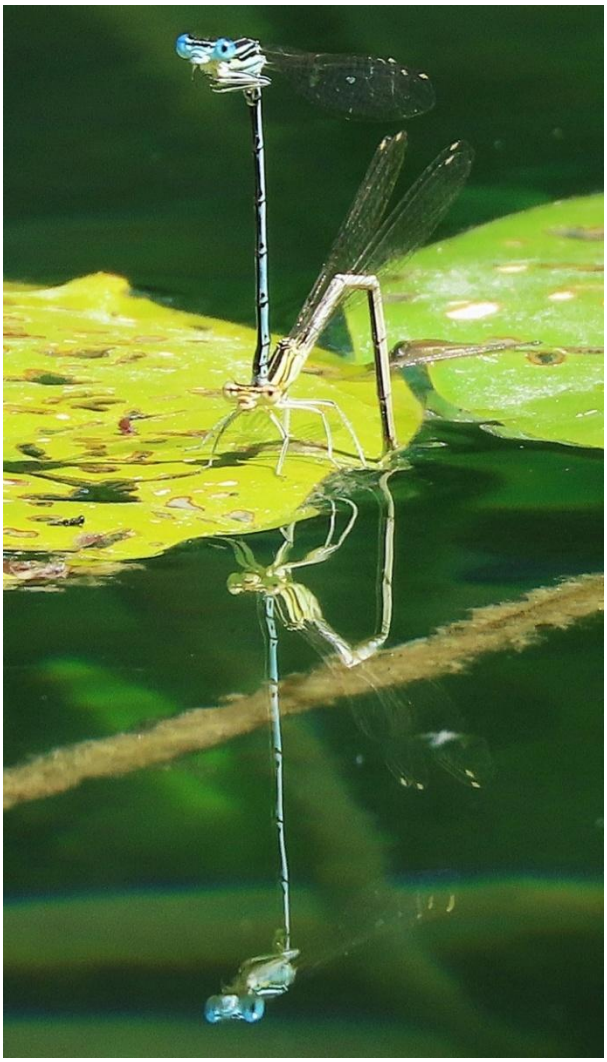

swimming with my coot family

Me too

dragon flies above

dragonfly on floating leaf

Carp species weighing several kg

great crested grebe

33 Documenting Hobbies: Globetrotter, Hiking, Photography, Sparrows & Alpine-cyclamen ‘Breeding’

Flowers and Flower Curiosities faced at home

big gentiana

lime-loving alpine rose

garden orchid

Edelweiss

alpine roses

(left,
first time
found)

Real
Moonwort

(right)

lichen plant

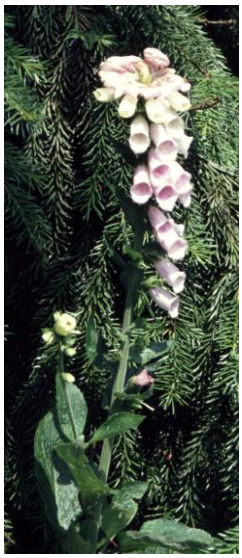

seldom foxglove hybrid and
right a blossom sensation

Edelweiss flower on November 30, 2024,
in the snow. 8 months too early!

winter alpine lilies

shrub gentian

leave in winter

daisy from the back

Water roses in my garden ‘lake’

Who will win in 2025?
The big fern or the summer alpine lilies?

anemone

anamone

Holy place of the trolls

Beautyful Gentiana: 35 years old flower

3 different wood anemones
pink, white, yellow

Nature loves diversity: Cornflowers

Roses, January 1, 2020.

winter flower

Yellow & red thimble

stone carnation

Which butterfly caterpillar is this in my garden pond?

Orchid

What is this ??
⇔

Swallowwort gentian

autumn gentian

crocus

Silver thistle

Gentian

Daphne (red)

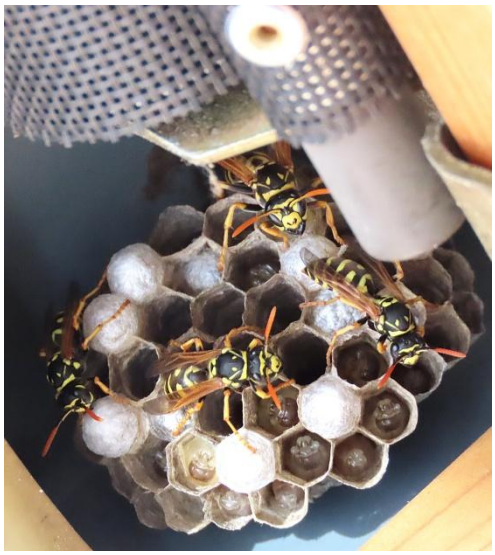

wasp nest

Feeding sparrow mum: Stuff in

elegance

Butterfly: hummingbird hawk-moth wild bee

Learning from the tits

Three different butterflies at a time

approaching bumblebee

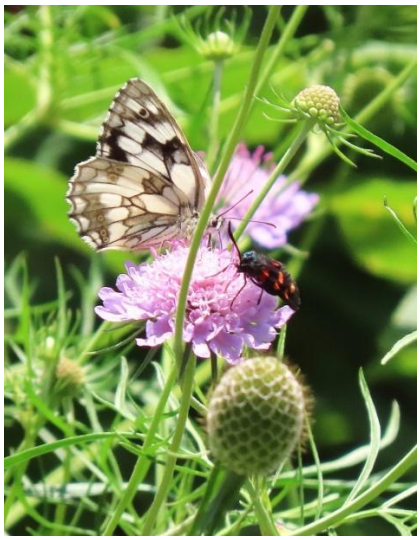

At our beloved Mückensee Lake

dragon fly couple sink eggs

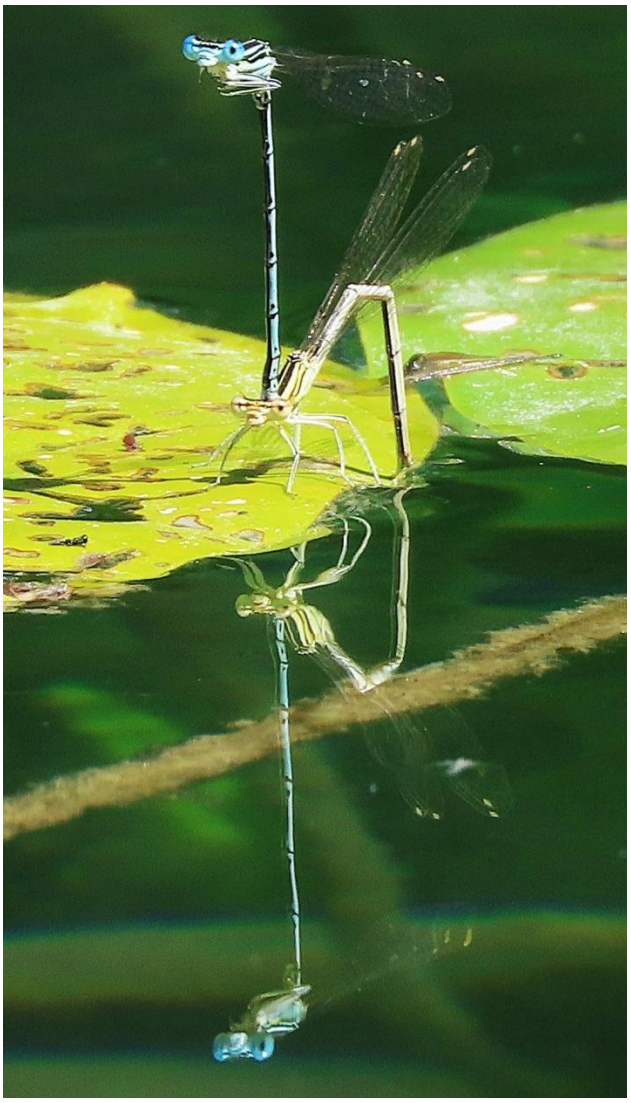

swimming with my coot family

Me too

dragon flies above

dragonfly on floating leaf

Carp species weighing several kg

great crested grebe

Pets in House and Garden

Chinchi

Mausi, completely asleep

(left) relaxing.
(right) Maria and Mausi, both deep-sleepers

In our Garden and somewhere nearby

two deer from our pack

Hedgehog in the garden

pheasant

marsh tit

Bathing makes fun

carrion crow

My amphibians at the wedding dance

Beautiful mouse
In my garden

What is this??

mind

A nice young frog couple in love (*a year later I saw when she ran away from him*!)

Slugs suck out a dead frog. I catch them with a mixture of oat flakes and wheat beer

Copulation of snails

various butterflies

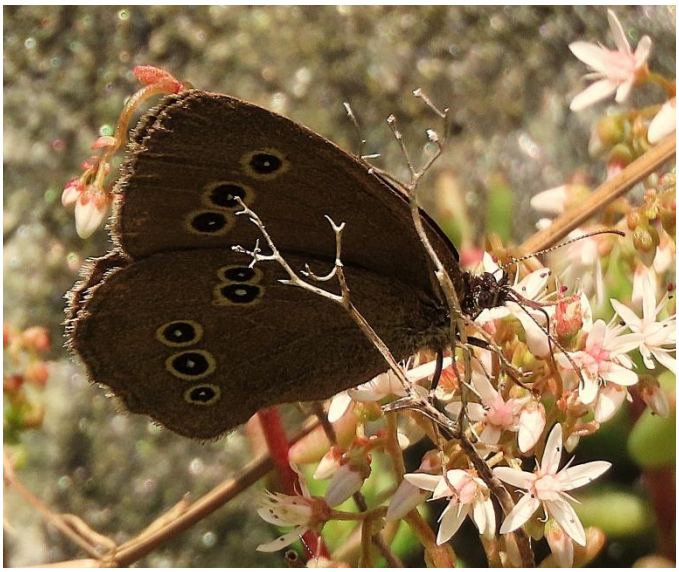

beautiful

What is this?

.. and this?

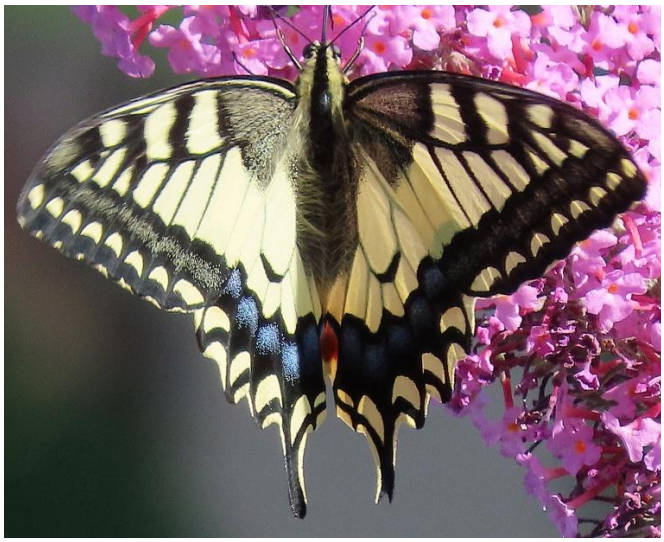

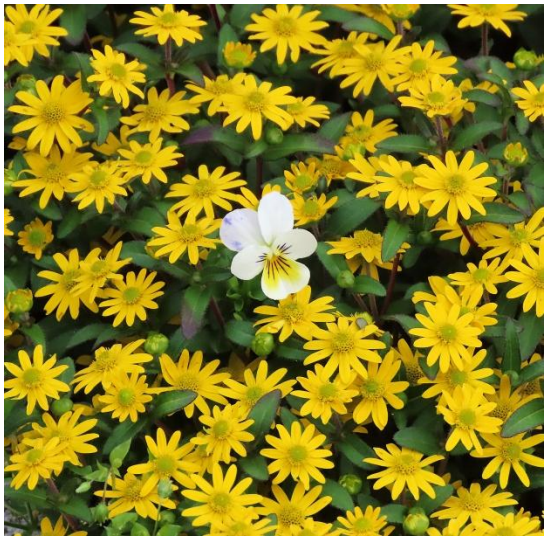

I am here

Garden view 2010

sparrow and great tit at the tit feeder

Family discussion

Greeting guests

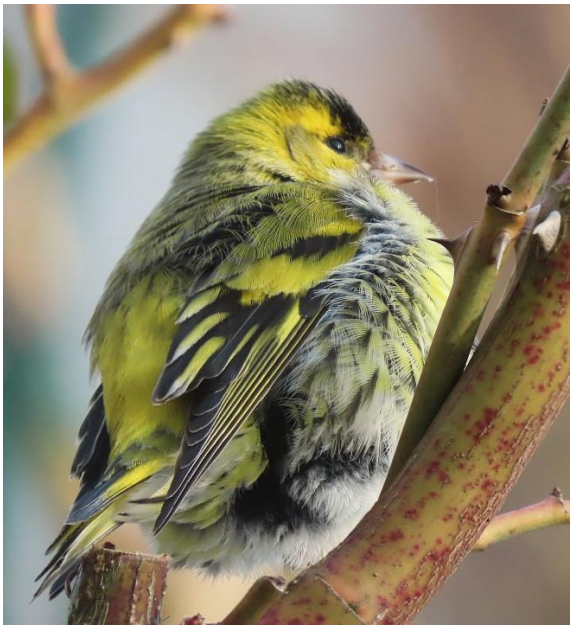

Young birds

Pictures from around the world

marmot

chameleon

largest Moth & Tarsier, the smallest ape

echidna

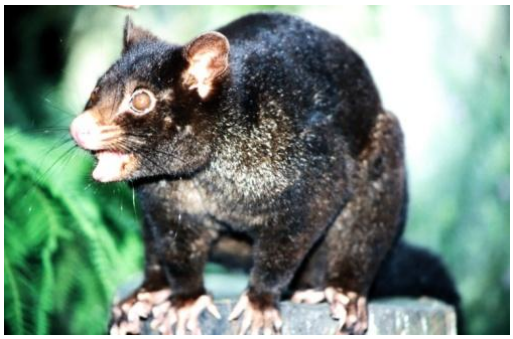

Wombat and Tasmanian devil

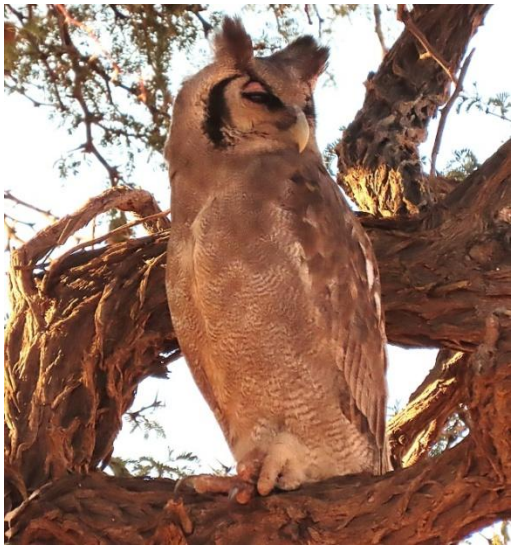

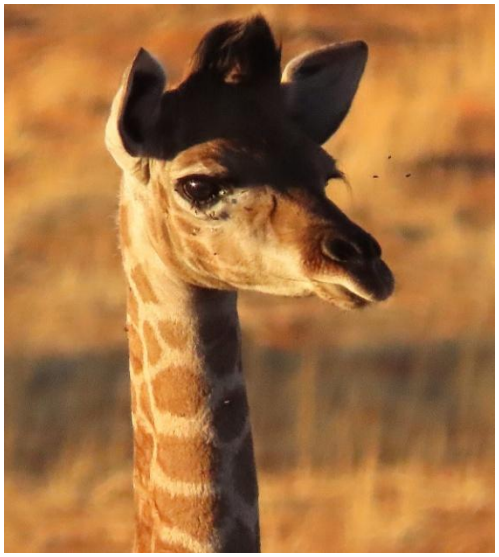

Dreaming of Visiting the World and its Mountains and of photographing

Pay attention, seagull

The photographer, some years later

Climbing Exercises as first preparations

First climbing skills experienced with Brian in the Dales, UK, summer 1957 !

Note, please:

Slide presentation sets of the time with my first wife Jutta are fully missing, just some collected paper pictures could be scanned and included.
These journeys were Peru, Ladakh, Nepal (1983), Alaska, Japan 1986, south East Asia in the first month after opening they could be visited (Myanmar, Laos, Cambodia, Saigon with Thailand, 1991), Australia, Tasmania, New Zealand, Pacific Islands (Hawai, Fidji, Tonga, Aitutaki, Bora Bora, Tahiti), Emirates-Oman, Patagonia, South America DAV-Anden trekking, ..

With my friend Alois †:
Relaxing after having climbed my first mountain above 3000 m, the Acherkogl in the Ötz-valley, under bad weather conditions,1958, and 1988 again.

(right) Mother does not look to the top!!

Saas Fee

Learning by doing
and recreation.
4000 m plus, Dom etc.

Taschachferner, 1977
Ice climbing course

Since 2013 the last place of Alois however he can view his Acherkogl, 3008 m

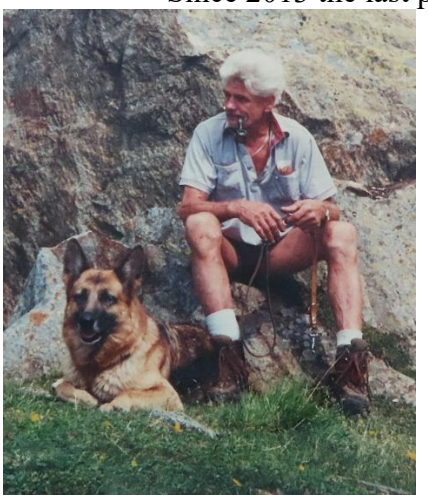

Gentiana nivalis

Alpine rose

Most interesting Private Journeys

Iran 1975, mountain tour Demavend (4667m), Teheran, Caspian Sea, Isfahan, GOM

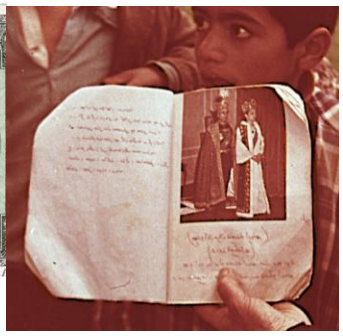

Swinging Minarett

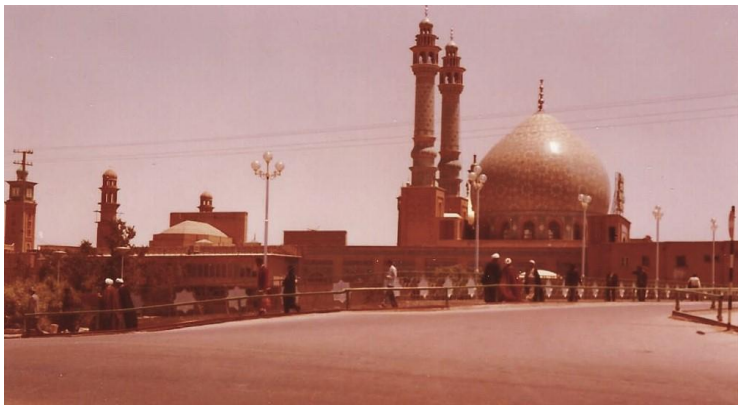

Finding the priceless ancestors of today's tulips in red and yellow

Before Khomeini, not to forget: The “Shaw” sent busses to the mountains to get children to school !

I did not reach the top,

LL: The mules could not go through the too high snow, so I also pulled a trekking bag up the mountain with the mountain guide. Even if you are very strong. Never overexert yourself on the mountain !!

It was 3 hours too late when I was fit again

From Caspean Sea back through the mountains and then to Isfahan

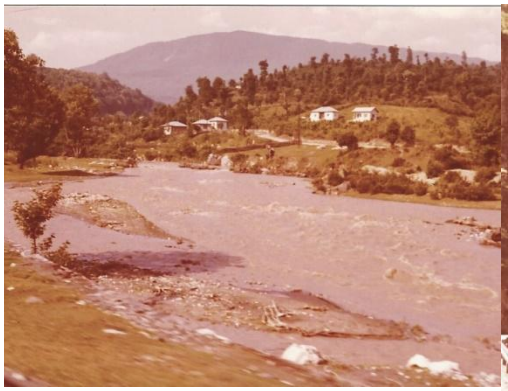

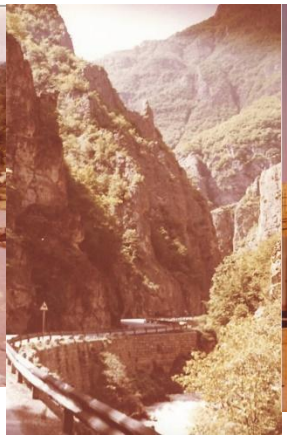

Tunesia 1972

Peru 1979

no high-up mountain pictures saved

After a birth under a rock-roof dwelling in the Andes

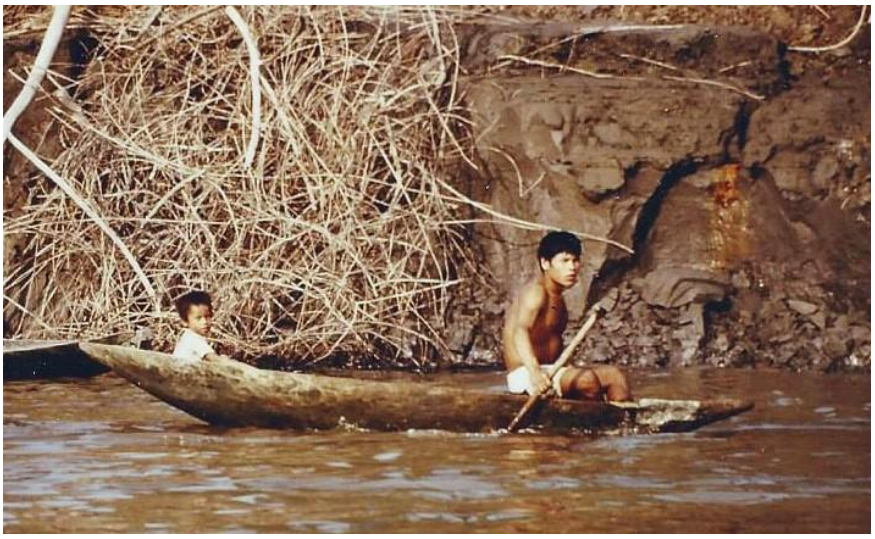

Amazon

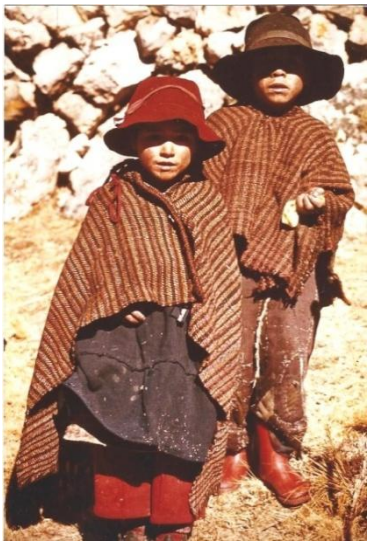

These children had never seen a ball and did not know what to do!

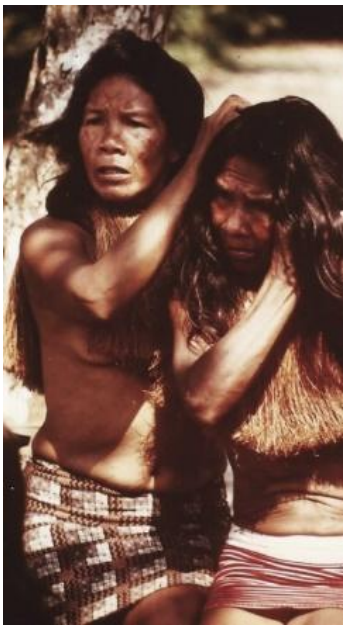

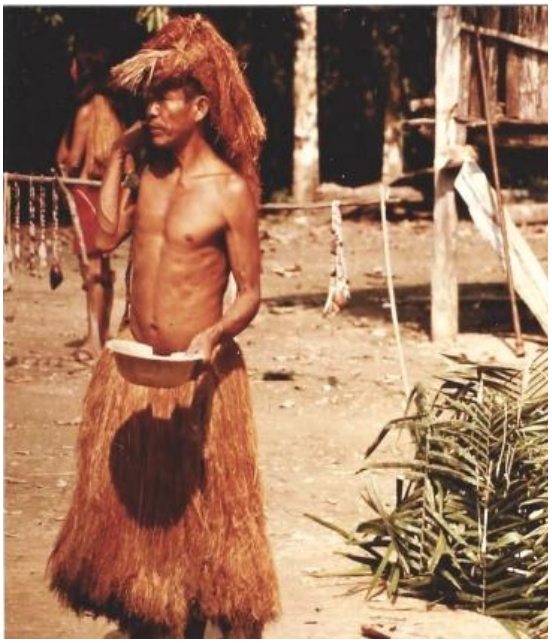

Ladakh 1981

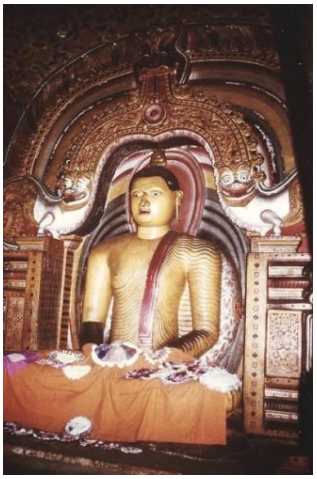

Invitation in to the house of a yak herd owner
(with my first wife Jutta)

The unimaginable value of 5 cm pasture grass in Ladakh

.

As you can see from the photos above, the grass is very short and therefore about 5 cm large pasture grass is extremely valuable for the mountain farmers:

The path led our trekking group into the valley of the neighboring community, which then led to a serious threat situation for us by the mountain farmers living there. Our problem was quickly solved the next day, when a judge was 'called', who arrived on foot - walking under a parasol of the assistant - after many hours of walking. He immediately convicted the leader in a court hearing at an altitude of 4500 m and immediately had him taken to prison. When we descended again a few days later, the prisoner's relatives asked us to help them get him released. A major reason for this was that the relatives had to bring food to the detainee. Living 10 km away and having to take care of it *on foot* was a very big problem for them.

An invitation from a dealer in Leh, with whom I had also talked a lot:

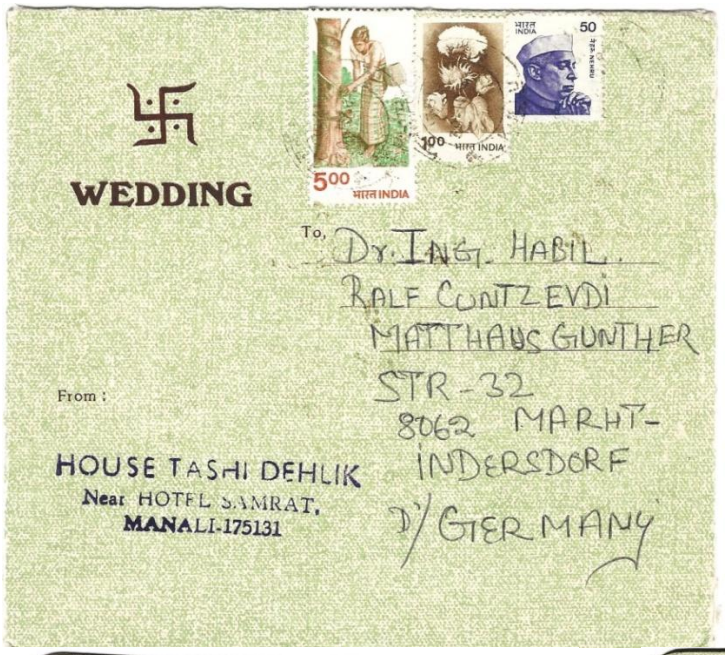

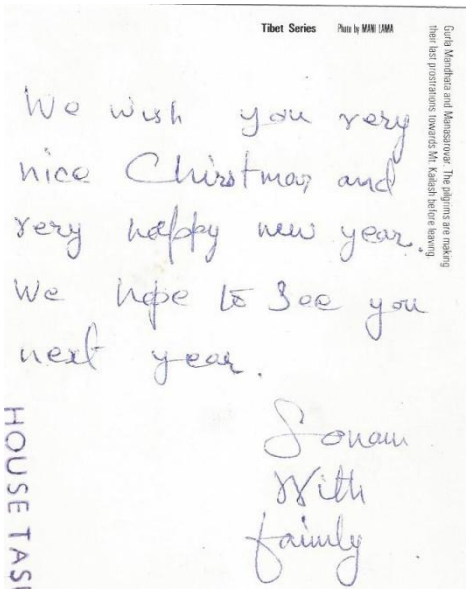

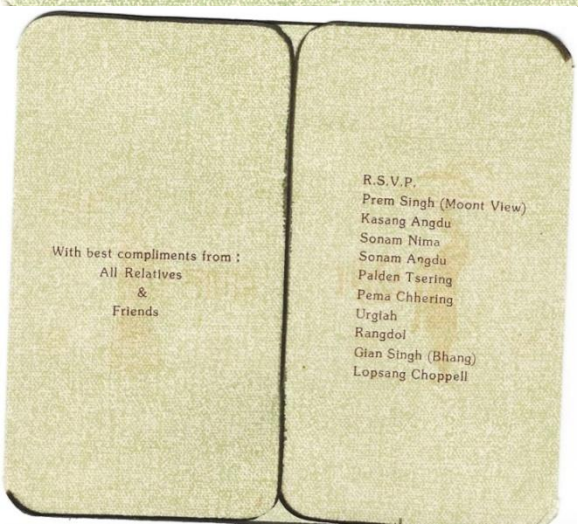

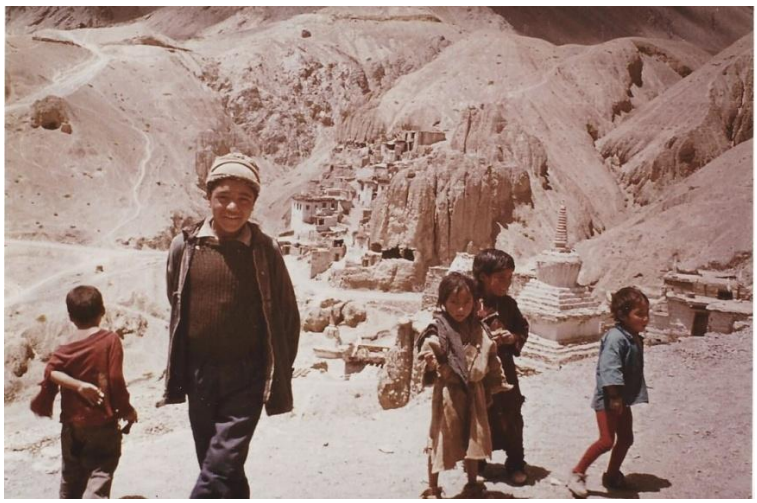

(right): This woman on a mountain pasture high in the mountains needed painkillers. But after she repeatedly shook her head, it didn't seem to be enough, and we all searched for more pills. What we didn't know: shaking her head meant thank you!

Himalayan Trekking, Nepal 1983

Difficult Himalayan
high altitude tour,
31 days.

Destinations: Westcol 6153 m, Naulekh 6363, Mera Peak 6461m. Mera La Pass 5415 m. Base Camp: 4600 m at Baruntse 7220m. Over the Mingbo La Pass, 5817 m, back to Lukhla via Pangpoche, Tengpoche Khumjung

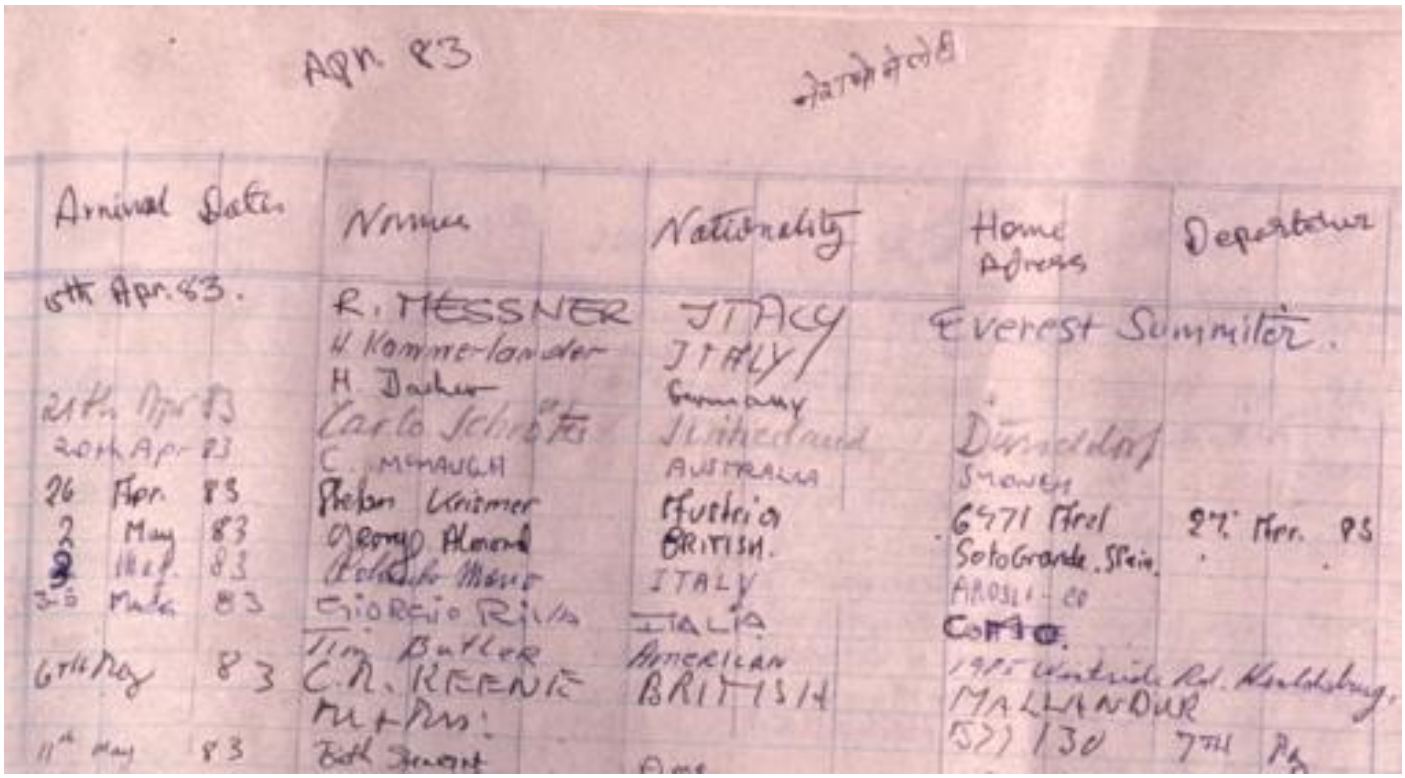

4 days waiting: Getting-up early, airport Kathmandu, back to hotel etc.
After 4 days arrival at Lukhla airport

Lukhla airfield at almost 3000m: Very dangerous landing and starting

The airfield is served from Kathmandu fully depending on weather and visibility conditions. The slope of the 527 m long runway is around 12 %, and it can only be landed uphill and taken off downhill. The end of the runway then abruptly breaks off about 600 m deep to the Dudh Kosi River. After landing, we noticed the good fencing of the former airfield garden. As we marched past: The fence was constructed from over 280 propeller blades.

Previous, down: The Mount Everest Log Book: Messner, Kammerlander, Dacher (*followed my invitation and opened 'my' climbing garden'*). Successful ascent via a variant of the normal route in alpine style.

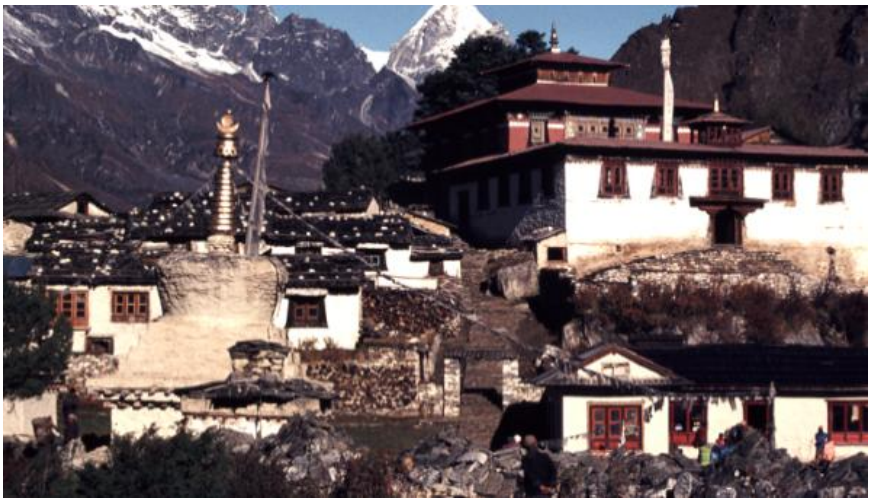

(left) Ama Dablam, 6800 m. Namche Basar

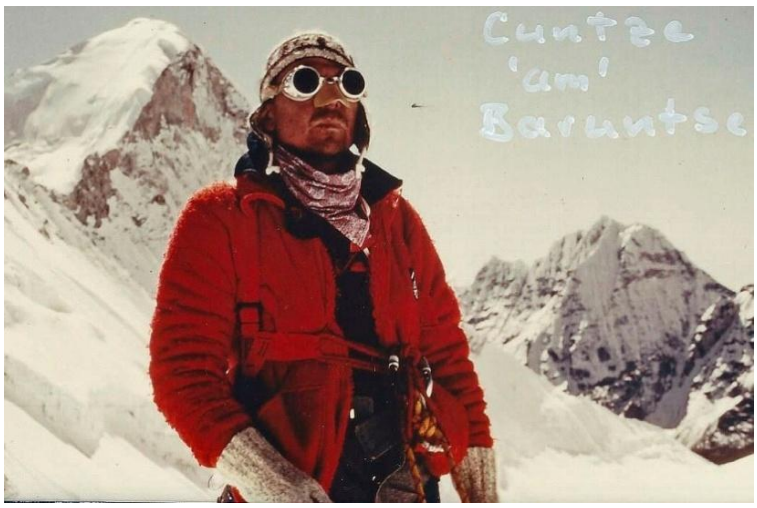

C*untze* (6150 m) in front of the Bar*untse* (7150 m) with the 'spare' clothes I had carried (*number of sherpas not fully available*)

At home all is much better!!!

Grand view

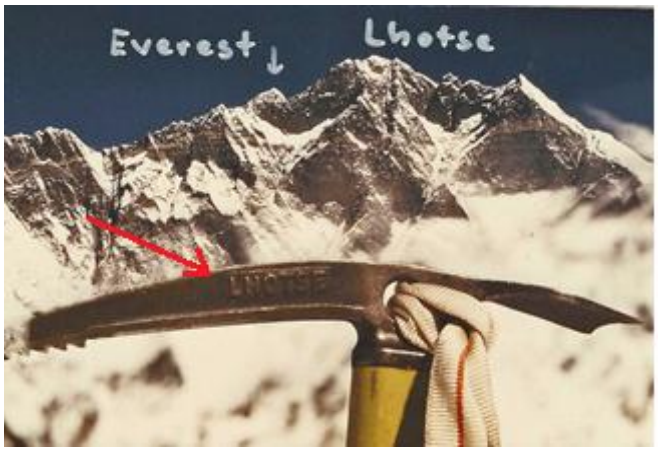

(up): heavy snowfall. (left): Lhotse ice-pick in front of the Lhotse (8516 m)

Mountain experience

After waking up in the morning: opening the 4 zippers inner sleeping bag, outer sleeping bag, inner tent, outer tent. Great view: Half a meter of fresh snow. Ascent of Mera La? Too strenuous!

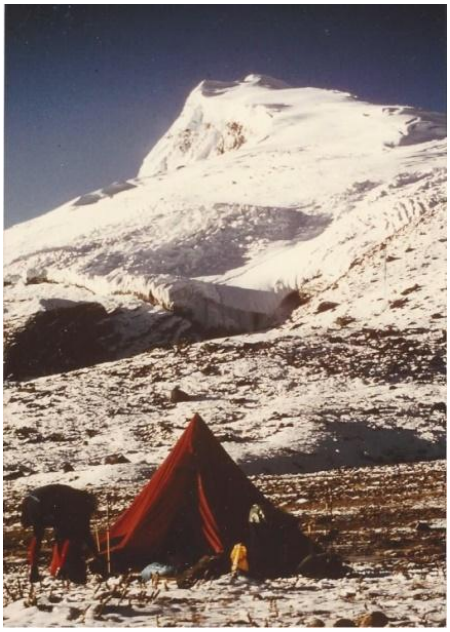

left:
A yak manure place keeps warm when having breakfast. Mind the dog!

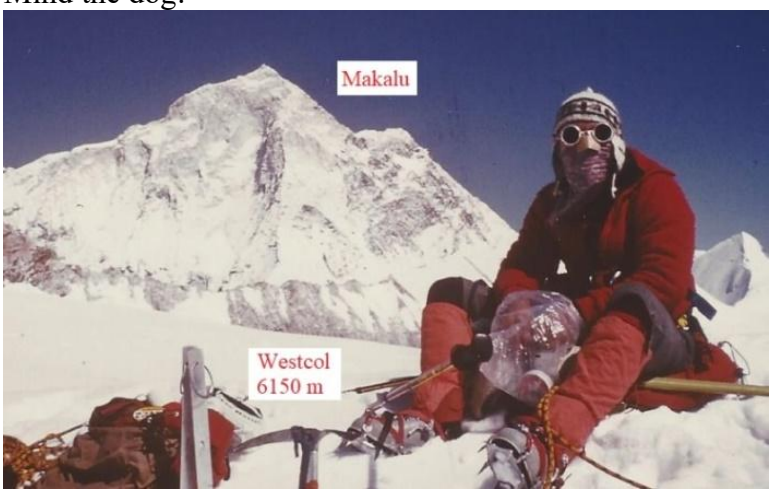

Camp, high up

after all efforts

At the end, gifts are distributed to the sherpas

relaxing

Alaska 1986 etc

Bed & breakfast at the Venice-like
Fairbanks near the polar circle.

Together with a trapper and a bush pilot
And Grandma with grandson

A Story from the railway-trip to Fairbanks

On the train from Anchorage to Fairbanks (venice of the north), you usually stand outside the carriage on the platform. When I returned to the carriage after a longer stay, part of my seat was simply taken. Never mind the amount of space. Upon returning after my second stay, the group was sitting comfortably together, chatting. I recognized the language: Bavarian! It turned out that the elderman was the chief physician of the hospital located 300 meters as the crow flies from my home.

Surprise for me as wheat beer drinker:
At the reception dinner in a Kodiak restaurant my favorite wheat beer at that time, Moy Beer, was served in the small town Kodiak, a *good flying distance south of Anchorage*

(right) Riding an ATV in the Kodial mountains:
Here the All-Terrain Vehicle, not to be confused with our Automated Transfer Vehicle for the space station

My relatives.
Together with the family

Bear hunting at Kodiak Island: 1986
Number of Kodiak bears to be shot: 50 at about 50 dollars each.
Mass, possible: > 600 kg. Grizzly > 400 kg.
Shooting is cheap however the preparation costs 100-fold.
This did not enjoy the wife of my relatives neighbor!
Kodiak bears in Alaska are predominantly carnivores. They are active during hunting seasons and are voracious salmon eaters all year, especially during the period regarded as 'salmon spawning season'. This must be due to their coastal diet, which slowly accumulates into their huge mass.
The Kamtschatka bear is of the same size.

Since I happened to be in Kodiak during salmon season, we naturally went fishing. There was no fishing luck, just like the schoolboys next door!

Nome: end of Iditarod sled race

Patagonia: trekking Cerro Torre (left) & Fitz Roy, 1987

Lago Argentino

Hiking in the El Paine parque

Slipper flowers

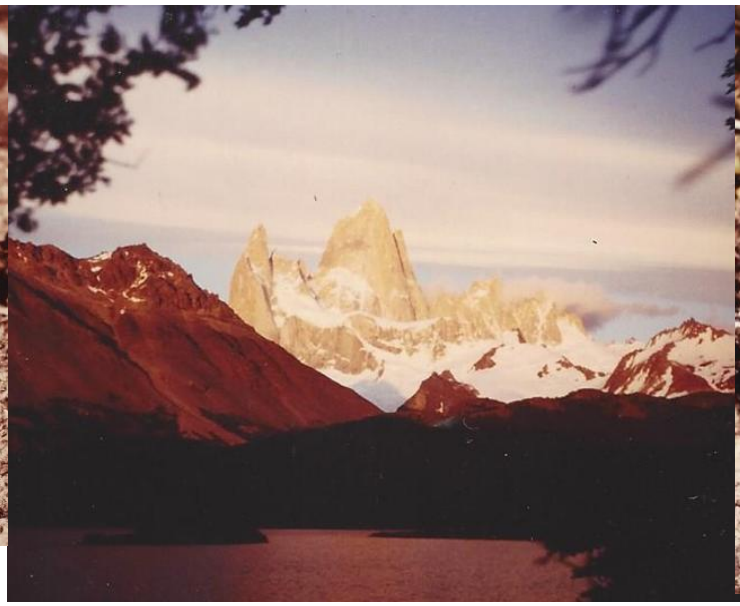

super-difficult Cerro Torre and right Fitz Roy (3406m)

DAV-tour, 1994:
Trekking with climbing.

Holy mountain of the Inka
Licancabur (5921 m)
and the famous flamingo lake
at 4000 m height

Lago Argentino

Breaking off a glacier wall

into the lake

Moon pictures with my Canon,
taken by hand

Some Special Digital Photography's from trips all over

Venezuela
Me and the guide

Venezuela

"Challenging tasks strengthen!

2013
Venezuela

Komodo waran, 80kg

At Fiji,

in the house of a retired Hindhu sugar engineer:

Look and feeling is like that one I had when I walked with my Grandma for spinning and crocheting in 1944.

People are almost the same in the world.

The world is small.

Australia 1997

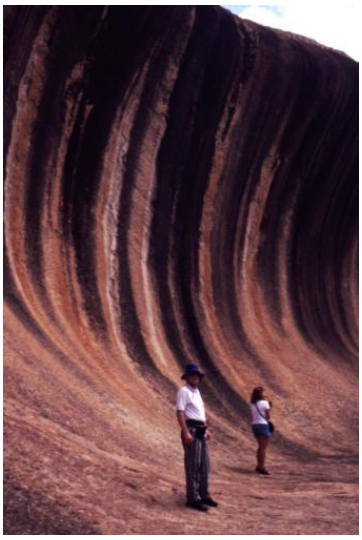

aborigines

looking from Ayer's Rock

Namibia , 2020

The highest sand dune of the world.
Fast sand surfing downward

walking along the sand ridge:
3 steps forward, 2 steps back

fashion photography in front of the big dune

Leopard, neglecting the photographer

Best fruits are up

Don’t come here!

Carneval at Windhoek

Alone in the Etosha Pan, 1986.
2020 : crowd of tourists

Crossing

Polar Circle

and

equator

Wiilll

Oman 2023

Desert rose

Frankincense and dromedaries

a white young dromedar

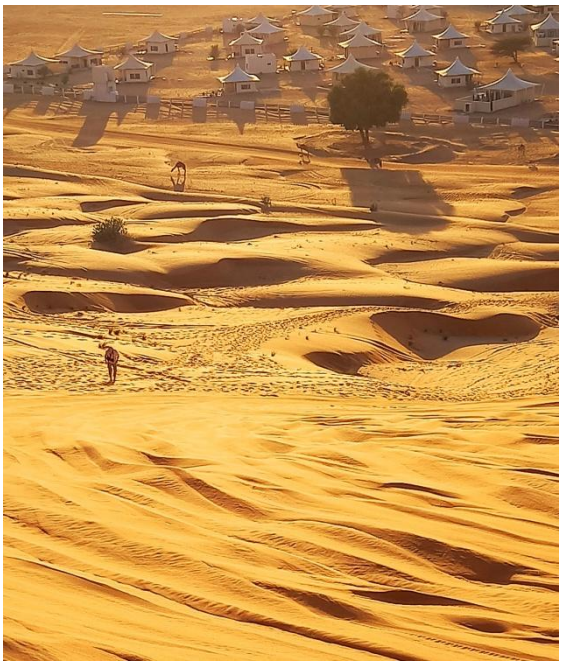

Person left: Thats' me. *For sunset*

One step up, half a step down again

A lake in the dry Oman

Seagull: Pay attention!!

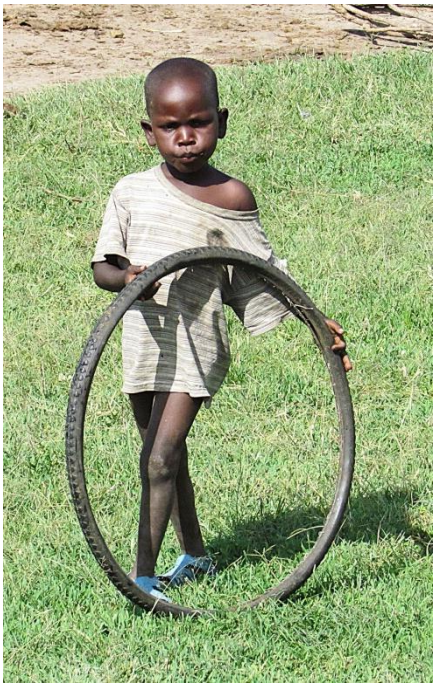

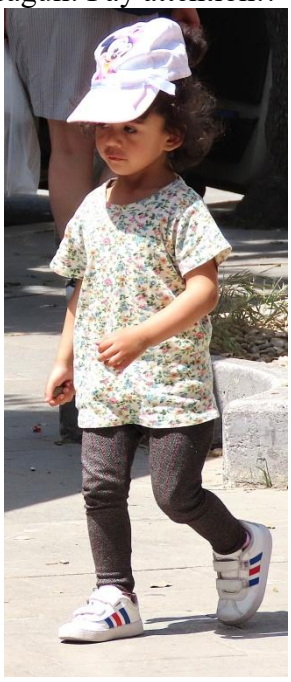

Ethiopia

Stone of languages

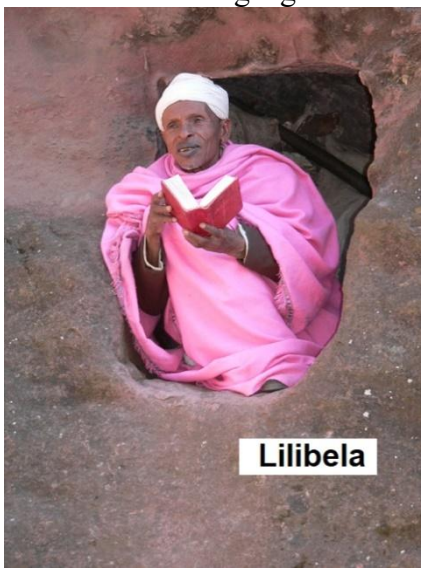

Lilibela: Church, cut out of the mountain rock

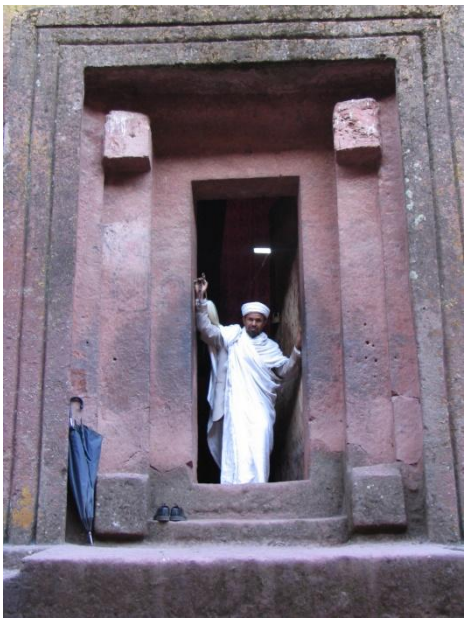

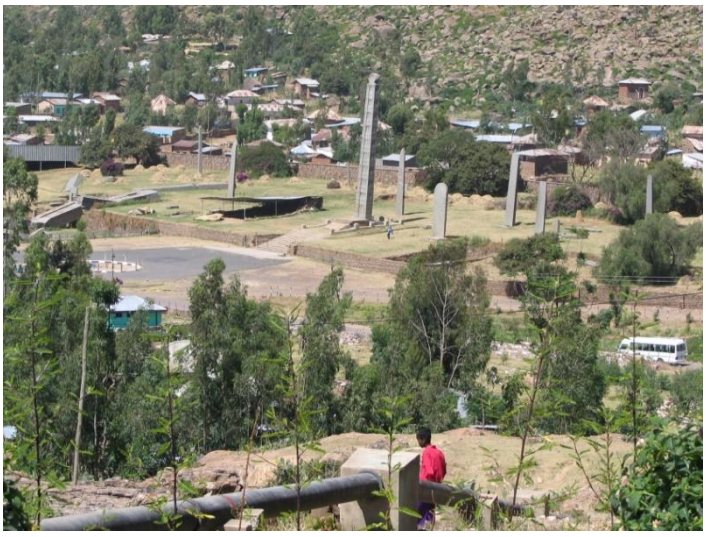

Defending the group

refurbishing

Ras Dashen, 4550 m (a gunman took care of the group)

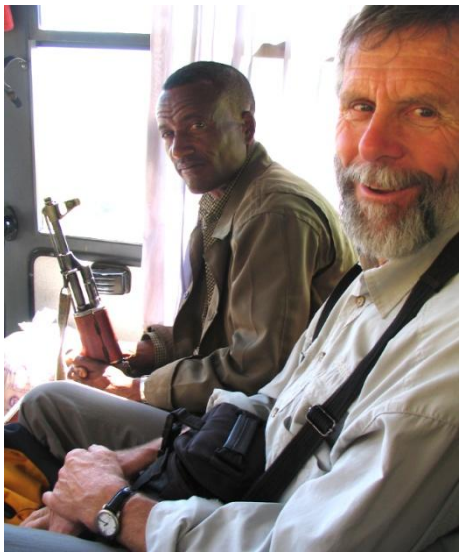

with Sigi Hupfauer, our
experienced alpine tour guide
(*8 peaks of the 14 over 8000 m*)

Transport of dromedars

Incredible for me: **Kairo**
The moon, taken by hand on a ship !!

A nice lady in the National Museum

India: (above) Blessing by a Hindu priest
(left) Carpet weaving by children, helping her parents due to their small fingers

Friend or lazy beneficiary, **Columbia**

hyacinth

Indonesia

Feeding an Oran-Utan

Uyghur

Crossing China from Kasakstsn, 2005

Greening the road
through the desert Taklamakan

no Dromedar but Tramp Animal

Chinese family on the wall (2005!)

equator

Albtraum einer Brückenüberfahrt

Cuntze: Sikkim, 2012

2 nightmares of crossing a bridge

encounters

Darjeeling, Sikkim, Bhutan

Dancing festival

On the hike to the Tiger Nest

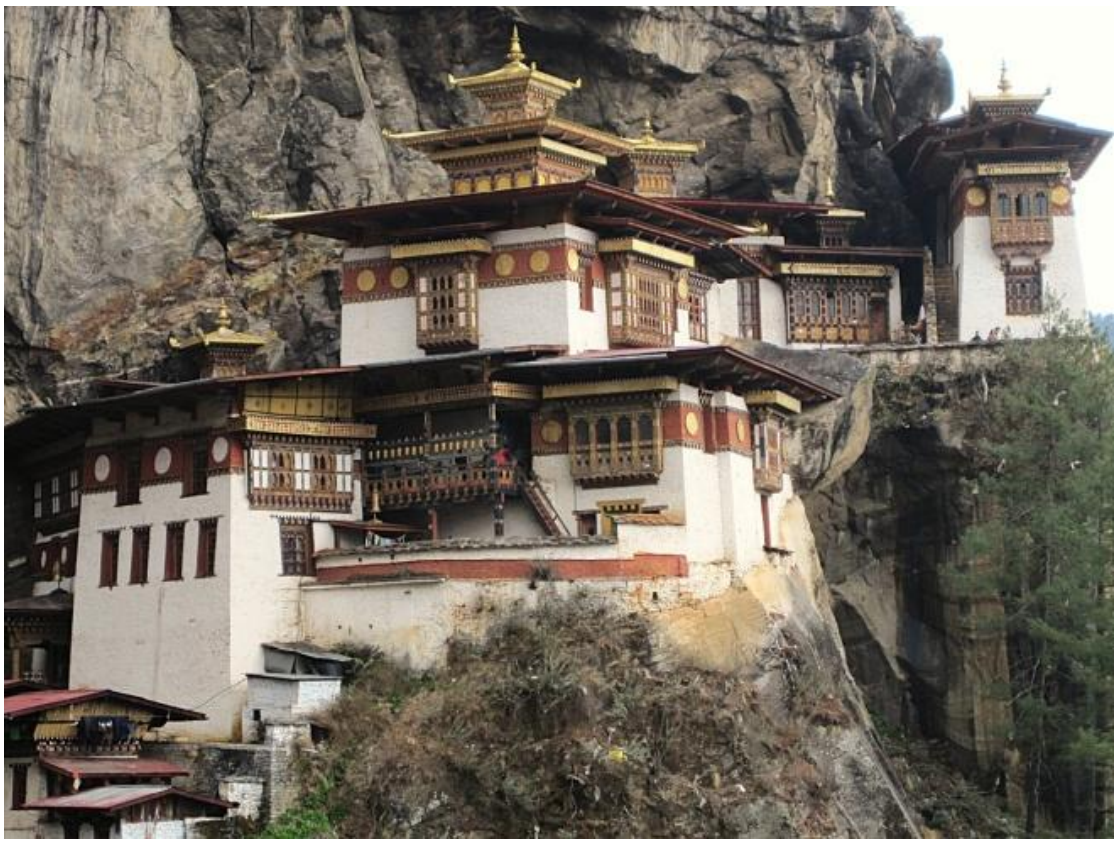

Tiger Nest

in Bhutan

high up

Banana with beautiful bird

Ama Dablam

Ralf, Maria, Christian & Biggi

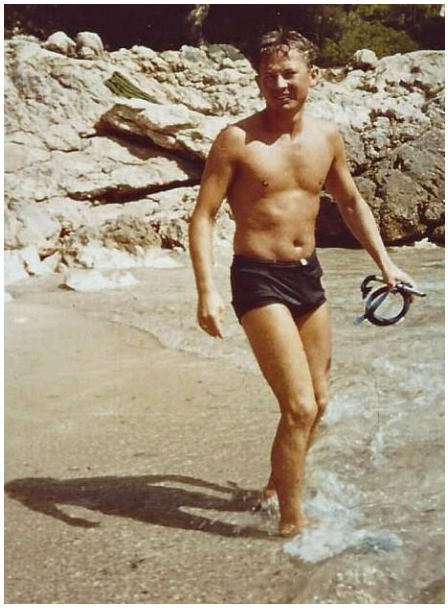

My shortening by 3 cm and 1kg more mass
- over the decades –
became balanced by a thickening of the belly!
This is nature.

The family tree needed to be updated again:

My cousin, an IT specialist, wanted to do this. I had sent him all my documents for this purpose. Unfortunately, he died suddenly.

Who will take over this work??

There are no other family members left to care for the Cuntze grave.

More than 400 km away, I had to decide to abandon the grave.

Some memorabilia, with their special experiences, always look at me on the way to my study.

Flying back:
One astonishing way back to Munich airport

If flying will be not possible anymore:
Then I can comfortably watch from my balcony the landing planes on the southern Munich runway and the taking off on the northern

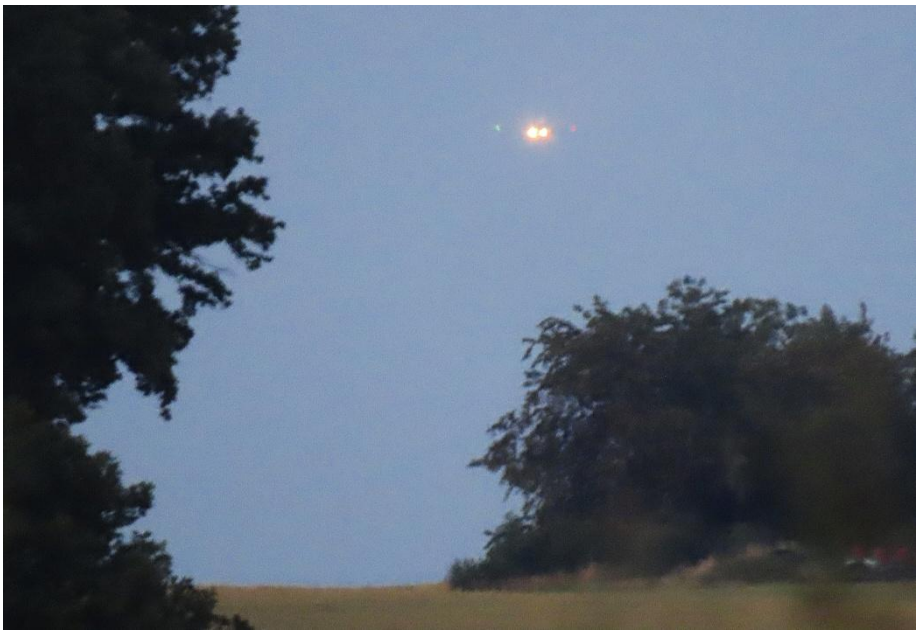

Munich Airport view from my balcony, 30 km west

Indersdorf ⇔ Scheyern

Maybe I can do this long hike of 44 km in 2025 for a last time.

I'm very Thankful for all

From my balcony:

Isn't this picture from at home not also very beautiful ??

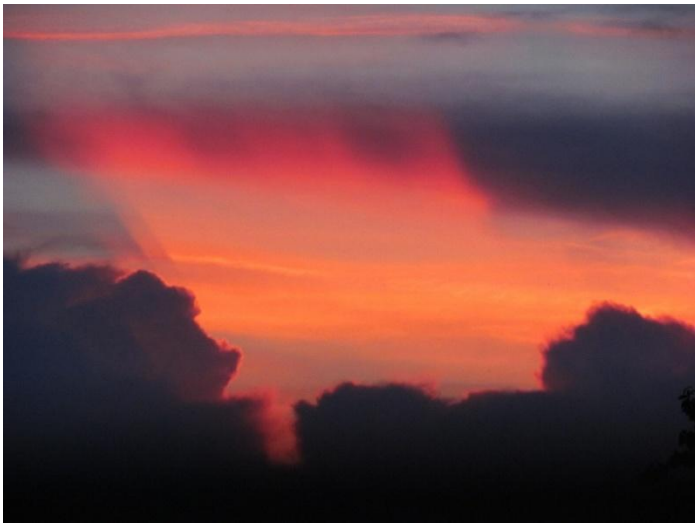

Those, who might be interested in the following rarely available videoclips-rich PPTs, click at the links:

carbon-connected.de/Group/Prof.Ralf.Cuntze

A photography preview is attached below, practically just for Papua-Guinee.

Due to the 520 MB-limit in WORD some specific Tours are attached as PPTs:
namely Papua-New Guinee (also Word, as folows), North-Corea and Yemen (not safe anymore)

Papua-New Guinee

August
2006

mit
Ikarus

SING-SING
in Papua-Neu-Guinea

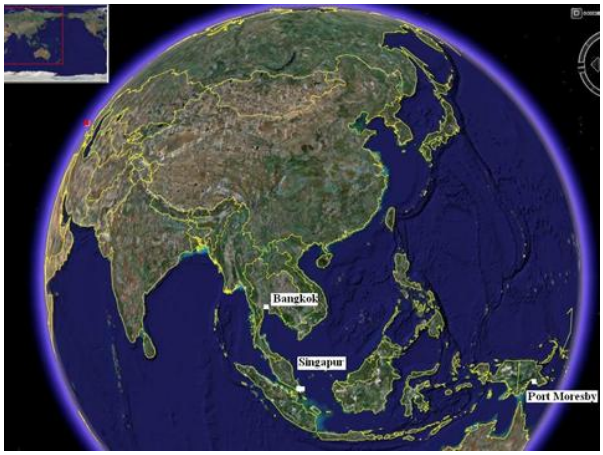

not a safe country anymore

Schau mal, wer
da schaut!

Papua
Las Vegas

sugar cane +
betel nut

photo-
shot

What is this on their backs?
Child care !

winter or summer

airport in the
bush

transport to lodge

world record
moth

wig maker

At night to save the wig

15 months life to obtain the high-valued wig from the wig maker

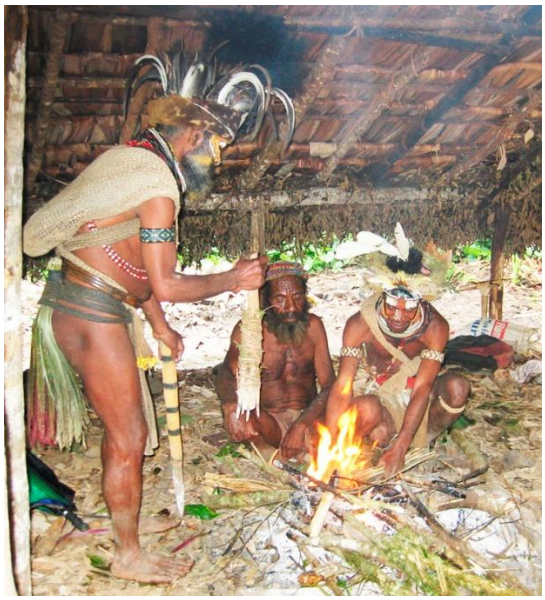

witch doctor

entrance to Tari settlement

manufacture of ropes

Mi laik Kaikai = have hunger

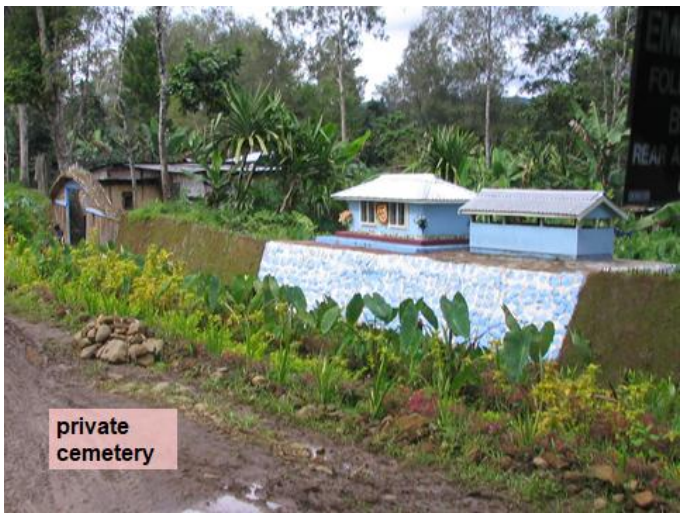
private
cemetery

potatoe

the village
elder and
his wife

in the flash-
enlighted
hut

purchase price for the bride is probably okay

Saying good-bye at the Ambua-Lodge

Nearby the 4000 peaks to Timbukte

4000 m high

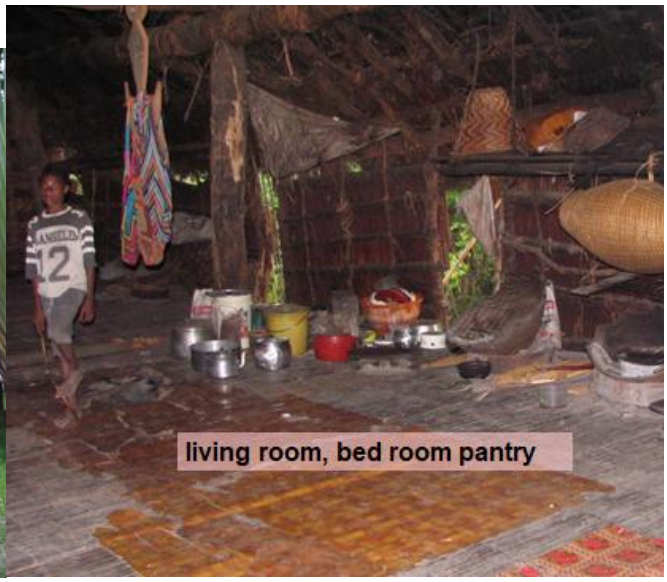
living room, bed room pantry

Vanilla

palm fertilization

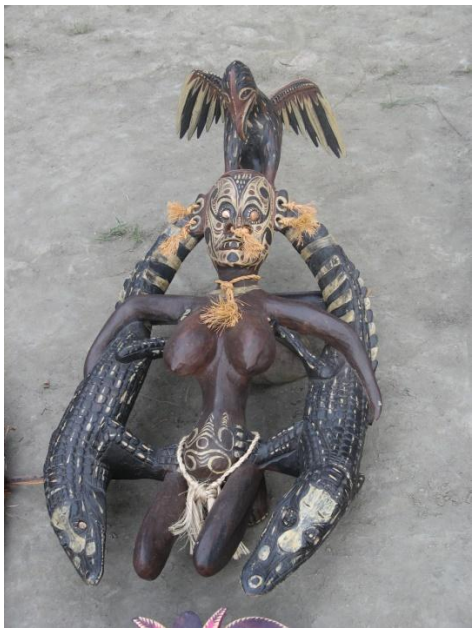

SCHOOL RULES:
Wash before coming to school
Comb your hair before come to sch
Eat before comming to school.
Come to school at all times.
No fighting in school ground.
Do not in the school ground.
Do not spoil school propeties.
Look after school propeties.
CLASS RULES
Do not steal inside the classroom
Do not swear inside the classroom
Do not fight inside the classroom
Do not play inside the classroom
Do not eat inside the classroom
Do not break classroom rules.
Listen to the teacher at all time

Nothing can disfigure a beautiful fellow

no rope
20 m

North Corea (without video-clips)

Singing North-Korea

Pyongyang

Kim Il Song, Mother of Korea !!

Excellent subway

Grown-up at the German nation separating border, now visiting the internal Corean border.

Room of Space peace treaty with the USA.

Accident as everywhere

Organized trip in North-Corea

Taking a trip

Travel colleague from Cottbus, formerly Eastern Germany celebrating thr team rise into the common first German Bundesliga

Yemen

Beautiful, Sanaa and ...

visiting a family